Characterization of Galectin-1 in Pancreatic Cancer:

A sweet target for a bitter disease

Neus Martínez Bosch

Director – **Dr. Pilar Navarro Medrano**

Tesi Doctoral UPF / 2011

Pilar Navarro
(Director)

Neus Martínez
(PhD candidate)

Ricardo Gutiérrez
(Tutor)

Cancer Research Program

(IMIM, Institut de Recerca Hospital del Mar)

Department of Experimental and Health Sciences, UPF

Barcelona, June 2011

Cover design:

Josep Martínez Bosch

Fernando Arias

A l'Albert

Als meus pares

PREFACE AND ACKNOWLEDGEMENTS

L'èxit en ciència consisteix en la resistència al fracàs. Començo el final d'una etapa amb una frase que va marcar-ne l'inici. Just arribar a l'IMIM, aterrant d'un entorn totalment diferent i sense tenir massa idea de com funcionava la ciència, em van sorprendre aquestes paraules d'en Paco Real. Suposo que no en comprenia el significat. Suposo que em faltava completar aquesta etapa com a estudiant de doctorat per poder entendre-ho en totes les seves dimensions.

Fer un doctorat és un privilegi. Jo no me n'he adonat del tot fins que he trobat el moment per parar experimentalment i resumir tota la feina feta amb aquests quatre anys. Per aquells de nosaltres que no tenim unes aptituds excepcionals per l'escriptura, se'ns brinda la oportunitat única de deixar la nostra empremta, d'expressar-nos d'una forma tan personal. Escriure la teva tesi, detallar tot el que has après en aquesta etapa, el coneixement que has recollit i el més important, afegir-hi el teu granet de sorra. Parar per uns instants el temps, ordenar tota la feina per convertir-la en una història coherent, comprensible i omplir-la de significat. Això és quelcom que no gaires professionals tenen el luxe de fer, i n'hem d'estar agraïts.

M'agradaria començar agraint a la Pilar tot el suport que m'ha donat aquests anys. Per creure en una estudiant de Química acabada de llicenciar amb curiositat per un tema totalment diferent. Gràcies per deixar-me participar en tants projectes interessants i per donar-me tantes oportunitats per descobrir la millor vessant del món de la ciència. Gràcies per formar-me d'una manera tan

completa i per donar suport a la meva vida personal, també. Com una vegada et vaig dir, és un plaer treballar amb persones. Voldria també agrair molt efusivament al Ricardo Gutiérrez, qui m'ha ajudat moltíssim amb tota la part bioquímica, ha revisat la tesi detingudament i amb qui he tingut la sort de compartir reptes, experiments i resultats en primera persona.

M'agradaria donar les gràcies a tots i cadascun dels membres del nostre gran petit grup. Al David, per la seva forma senzilla de ser, per la seva gran generositat i ajuda desinteressada en qualsevol moment. Perquè entenc i m'identifico molt amb la seva filosofia de la vida i per totes les estones boniques que hem viscut. A l'Elena, gràcies per ensenyar-me mil coses al laboratori, per discutir els resultats i aportar noves idees i suggeriments. I pels nostres bons moments, que no han estat pocs. M'agradaria agrair molt especialment a la Mireia tot el suport que m'ha donat al llarg de la tesi. La part *in vivo* és sense dubte la més interessant del projecte però també és, sense cap dubte, la que m'ha donat més dificultats, tan tècnicament com ètica. Gràcies Mireia per ajudar-me tant amb els ratolins, per ensenyar-me a treballar amb ells sempre amb un somriure d'orella a orella. Agrairé al Ram per internacionalitzar el nostre grup. M'agradaria donar les gràcies també a tots amb els qui hem compartit laboratori i que han fet que venir a treballar cada dia fos tan agradable. Gràcies a la Tania per ser una persona tan positiva i alegre i al seu valuós suport amb el micròtom. Gràcies també a l'Amaya per realitzar molts dels talls dels blocs de parafina. Durant aquests quatre anys i mig han passat moltes persones pel laboratori amb qui he tingut la sort d'interactuar i aprendre'n cosetes. Gràcies a la Paola, la meva primera estudiant

de pràctiques, que va haver de patir la meva inexperiència com a "mentora". Merci beaucoup Fabien, pel teu humor tan francès i la teva dedicació. Gràcies a la Coral, el Carles, la Vane, l'Andreia, el Nuno, el Tibor, l'Aina, el Mohammad, l'Almu, l'Ada, la Carme, la Konstantina, la Sílvia, la Conchi, el Madriles, l'Amado i la Raquel. Però el meu agraïment no té fronteres restringides a les sortides d'emergència del laboratori i s'estén molt més enllà. Per començar m'agradaria donar les gràcies al grup de Snail, un equip de persones dinàmic i vital que es complementa amb la gran personalitat de cada membre. Moltíssimes gràcies a tots però molt especialment a la Jordina, sempre apunt per escoltar i disposada a ajudar amb tota naturalitat. Gràcies també amb molt afecte a la Rosa, Raul, Niko, Gabri, Montse, Manolo, Estel, Núria, Alícia, Alba, Sandra, Natàlia, Patri i Víctor. Al programa de recerca en Càncer tenim la sort de ser un grup força nombrós i m'agradaria també donar les gràcies a membres del laboratori 4 com la Mercè, amb qui he compartit la recta final de la tesi, la Laura, el Ramon, la Lara, la Marta, la Kathi i a membres entranyables del grup de Cèl·lules Mare i Càncer, com la Mari, la Leonor, la Júlia, la Vero, l'Erika, la Teresa i el Pol. I després de dir tants noms estic segura que encara me'n deixo un bon grapat. Voldria també donar les gràcies als IPs del programa de Càncer, per les discussions en els seminaris de la unitat i col·laboracions. Gràcies especialment al Paco Real, la Inma i l'Anouchka, al Xavi, l'Anna, el Lluís, l'Antonio, el Jepi, el Gabriel, la Clara i la Carme. Gràcies també al Jose Yélamos per la seva col·laboració amb el projecte de PARP-1. I com no, al suport administratiu infalible de la Lorena i la Sílvia. Agrair també al comitè de tesi, format pel Ricardo Gutiérrez, l'Anna Bigas i la Pura Muñoz. Encara a l'edifici del PRBB em queden moltes persones per

agrair i sense les quals aquesta tesi no hagués estat possible. Gràcies a l'Esther Llop i als companys de "Fàrmaco". Agrair també al personal de l'estabulari, tant de direcció, com de gestió i cura dels animals. Moltes gràcies al Juan Martín Caballero, la Mireia, la Begoña, el Pep, la Sara, la Marta, la Vicen i a l'Olga. Moltes gràcies a la Núria Somoza i a la Piedad del servei científico-tècnics de l'IMIM, a l'Eulàlia i la Lara del SAM, al servei de genòmica de la UPF, al de microscopia UPF/CRG i a l'Òscar i al Patxi de manteniment, per fer possibles els meus somnis amb el reciclatge. Gràcies també al programa Intervals i a tot el seu equip, per l'oferta formativa i de qualitat que ens ofereixen. I com no, moltíssimes gràcies a l'excepcional personal de cuina i de neteja amb qui tenim la sort de treballar: moltes gràcies Paqui, Sílvia, Montse, Carme i Jose per mantenir aquest ordre tan necessari i al Carlos i al Juan per repartir-nos els paquets amb tanta alegria. Però com deia, encara fora del PRBB em falta molta gent que no puc pas deixar de mencionar. En primer lloc voldria donar les gràcies a les persones que em van introduir desinteressadament en el món de la recerca: al Josep Maria LLuch i a l'Àngels Gonzàlez de la UAB per confiar en mi i a l'Anna Aragay per obrir-me les portes a la Biomedicina amb una més que interessant estada a Bergen. Gràcies als col·laboradors com el Pablo Fuentes al IIB Sant Pau, la Mar Iglesias i la Jèssica Munné de l'Hospital del Mar, al grup de la Cristina Fillat al CRG i l'Èlia Zafra al PCB. I parlant de col·laboracions no puc oblidar agrair profundament al grup de l'Steve Leach, a la Megan Cleveland i molt especialment a la Meritxell Rovira, qui em va fer viure una estada immillorable a Baltimore.

Però qui m'ha donat el més gran suport, ja no només aquests anys de doctorat sinó durant tota la meva formació, ha estat la meva família. M'agradaria donar-vos les gràcies per ser sempre tan entusiastes amb la meva carrera i sobretot per oferir-me el millor que uns pares poden oferir a uns fills: l'amor. Val, d'acord, aquí m'he posat una mica massa sentimental però és que es tracta d'un moment molt especial per a mi. M'agradaria recompensar-vos tot l'esforç que heu fet per donar-me els millors estudis possibles, per seguir-me d'aprop al cole, a la universitat i durant el doctorat. Tot agraïment seria poc per dirigir-me a l'Albert, el meu nòvio de tota la vida quan vaig començar el doctorat, el meu marit per tota la vida quan l'acabo. Sense el teu suport i la il·lusió de compartir amb tu cada moment, aquest esforç no hauria tingut sentit. Gràcies per escoltar tots i cada un dels seminaris, per inventar-te les preguntes més enginyoses, per ajudar-me infinitament amb la tesi i per respectar la meva feina d'una forma tan gran. Gràcies també als meus dos estimats germans, Quim i Pepe (a qui es deu el dibuix de la portada d'aquesta tesi), a la Maica, i a la família Flotats Pozo al complet: a la Puri, l'Albert, la Marta, el Jordi, l'Anna, el Marc, el petit Artur, a la petita que està en camí i als més que vindran. Gràcies per fer tan interessant la meva vida i per omplir-la de significat. Moltes gràcies també als avis: la Paquita, la Núria, l'abuela, la Nuri i el Francisco, així com un record ben especial pel meu avi Josep, sempre tan orgullós dels seus néts, pel Francisco, la tieta i la senyora Carme. Voldria també agrair a la Kanen i a totes les companyes de dansa perquè ens uneix un sentiment de respecte i admiració per aquesta disciplina, que per uns instants ens fa no tocar de peus a terra. I ja per acabar, donar les gràcies als meus amics, per compartir tantes i tantes estones i per distreure'm en

moments no gaire fàcils. Gràcies a la Laia, la Cris, la Ro, la Blanca, la Marta, la meva cosina Anna i la seva petita Aina, la Tena, la Núria, la Gemma, la Marisa, la Cris, l'Adriana i la Samanta.

Tots i cadascun de vosaltres heu fet que aquests anys hagin estat els millors de la meva vida i heu contribuït en l'escriptura d'aquest manuscrit final. Així que acabaré tornant-vos a donar LES GRÀCIES perquè sense vosaltres això no hagués estat possible.

Además, quería agradecer al tribunal por su dedicación en el análisis de este manuscrito, su presencia en el día de la defensa y su interés para dar forma a la discusión. Quería también agradecerles enormemente su tiempo invertido y excusarme por adelantado por no dominar el arte de la brevedad.

Agradecer también a la Fundación Ramón Areces que ha dado el soporte económico a la realización de la tesis doctoral durante cuatro años.

Voldria donar les gràcies a la Fundació IMIM i a la Universitat Pompeu Fabra per les ajudes de publicació de tesis doctorals.

I ja només em resta desitjar-vos que gaudiu llegint aquesta història d'aventures, amors i guerres tant com jo he gaudit escrivint-la. Un plaer.

Bé, suposo que tinc tants amb qui compartir aquest treball que val més que comenci a donar explicacions abans que comenci a fer-se massa tard...

x

Life is like riding a bicycle.
To keep your balance you must keep moving.

Albert Einstein

ABSTRACT

Pancreatic cancer is nowadays one of the neoplasms with worst prognosis, so research towards the discovery of new molecular targets for therapy and diagnosis is more than urgent. In this direction, we have deeply evaluated the role of Galectin-1 (Gal-1) - a protein that is highly overexpressed in the tumor stroma- in pancreatic tumor progression. Interestingly, we have found that Gal-1 interacts with tissue plasminogen activator (tPA) and that this interplay seems to be involved both in pancreatic tumor epithelial cells and fibroblasts migration, Erk1/2 activation and invasion, suggesting its importance in the tumor/stroma crosstalk *in vitro*. We have also focused on the biochemical identification of tPA/Gal-1 interaction domains. Furthermore, we have studied Gal-1 role in pancreatic tumor progression *in vivo*, using murine (xenografts and transgenics) and zebrafish models. We have found that Gal-1 participates in proliferation, angiogenesis, stroma formation and necrosis in Ela-1-myc pancreatic tumors, as well as in the acinar to ductal metaplasia. Importantly, these effects result in an overall significant increase in the survival of Ela-1-myc mice with reduced Gal-1 levels. We have also analyzed Gal-1 role in mouse embryonic pancreatic development, finding interesting parallelisms with tumors. Finally, the molecular mechanisms involved in Gal-1 driving tumor pancreatic progression have been addressed through a transcriptome analysis. All together, our data support Gal-1 as a new molecular target to fight against pancreatic cancer.

RESUM

Avui en dia, el càncer de pàncrees representa un dels tumors amb més elevats índex de mortalitat, per la qual cosa la recerca dirigida a la identificació de molècules per teràpia i diagnosi són més que necessàries. Amb aquest objectiu, hem avaluat el paper que juga Galectina-1 (Gal-1) - una proteïna altament sobreexpressada en l'estroma tumoral- en la progressió tumoral pancreàtica. Hem trobat que Gal-1 interactua amb l'activador tissular del plasminògen (tPA), participant en la migració, l'activació de Erk1/2 i la invasió, tant en cèl·lules tumorals pancreàtiques com en fibroblasts *in vitro*, suggerint una importància caudal d'aquesta interacció en la comunicació entre el tumor i l'estroma. Així mateix, ens hem centrat en la identificació bioquímica dels dominis d'interacció entre Gal-1 i tPA. A més, el paper de Gal-1 en la progressió tumoral pancreàtica ha estat adreçat *in vivo*, utilitzant models murins (xenografts i transgènics) i el peix zebra. Així doncs hem trobat que Gal-1 participa en la proliferació, angiogènesi, formació de l'estroma i la necrosi dels tumors pancreàtics dels ratolins Ela-1-myc, així com en la metaplasia acinar-ductal. De forma significativa, aquests efectes es tradueixen en un increment important en la supervivència dels ratolins Ela-1-myc amb nivells reduïts de Gal-1. Hem també analitzat el paper que juga Gal-1 en el desenvolupament pancreàtic embrionari murí, trobant paral·lelismes interessants amb els tumors. Finalment, hem volgut ocupar-nos dels mecanismes moleculars involucrats en els efectes produïts per Gal-1 durant la progressió tumoral pancreàtica mitjançant microarrays. Les nostres dades presenten Gal-1 com una nova diana terapèutica per lluitar contra el càncer de pàncrees.

CONTENTS

1 INTRODUCTION

The most incomprehensible thing about the world is that it is comprehensible.

Albert Einstein

1.1 THE PANCREAS

1.1.1 Anatomy, Physiology and Development

Mammalian pancreas is a mixed endocrine and exocrine gland that is in charge of glucose metabolism and food digestion. The exocrine pancreas (80% of the tissue mass of the organ) is composed of acinar cells organized into functional units termed acini that produce and secrete zymogens, which upon later activation in the duodenum give rise to trypsin, chymotrypsin, carboxypeptidase, amylase and lipase.

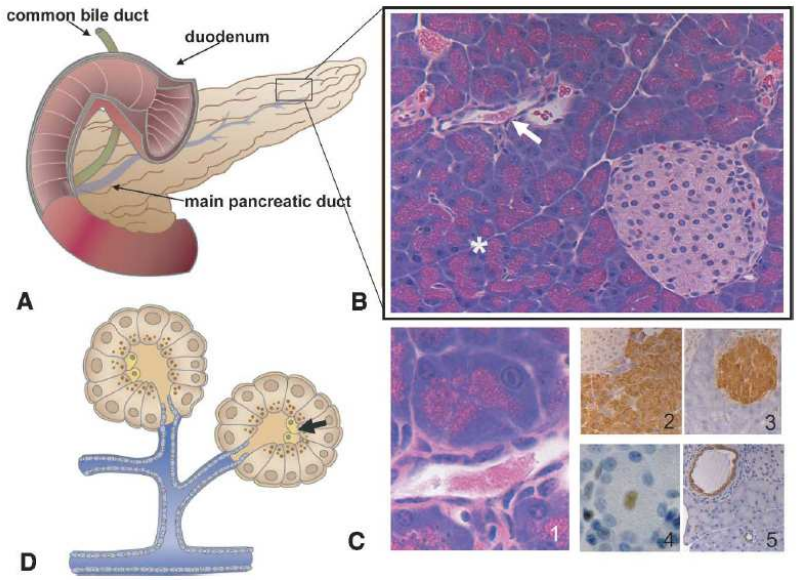

Figure 1. Pancreas anatomy. A) Gross anatomy of the pancreas highlighting its relationship with the duodenum and the common bile duct. B) Hematoxylin and eosin (H&E) staining of the pancreas with its major components: an islet of Langerhans, acini (asterisk), and a duct (arrow). C) Pancreatic tissue sections showing an acinar unit and a duct (panel 1), amylase staining of acinar cells (panel 2), insulin staining in β-cells in an islet of Langerhans (panel 3), Hes1 staining in a centroacinar cell (panel 4) and cytokeratin-19 (CK19) staining in ductal cells (panel 5). D) Representation of the relation between different cell types of exocrine pancreas (the arrow shows centroacinar cells). Extracted from [1].

Ductal cells add mucous and bicarbonate to the enzyme mixture and form a network responsible for bringing enzymes from acinar cells to the gastrointestinal tract. Centroacinar cells are found at the interface of ducts and acini and their detailed function is still a matter of study[2], having proposed to be adult stem cells for exocrine pancreas. The endocrine part of the pancreas is organized in the islets of Langerhans that consist of clusters of four specialized cell types: α- and β-cells regulate the usage of glucose by producing glucagon and insulin, respectively, whereas δ- and PP cells secrete somatostatin and pancreatic polypeptide, which modulate the secretory properties of the other pancreatic cell types (Fig.1).

During development, mammalian pancreas appears as two separate buds, through evagination of the early gut endoderm on the dorsal and ventral site of the duodenum[3,4]. In humans, the pancreas appears around the 26th day of gestation whereas in mice around embryonic day 9.5 (E9.5)[5]. Repression of sonic Hedgehog (Shh) within the endoderm is one of the earliest events being critical for pancreas specification[6] as well as Pdx1 expression (in mouse at E8.5), which is required for further pancreatic development[7]. Ptf1a/p48 is expressed slightly later (E9.5) and it is required to commit cells to a pancreatic fate[8] (Fig.2). The expanding pancreatic epithelium branches into the surrounding mesenchyme and buds fuse together to form a single mixed gland by E12.5[4]. A secondary transition in pancreas development occurs following Notch repression at E13.5, when progenitors are able to differentiate into distinct mature pancreatic cell types[9,10], through the fine tuned regulation of many transcription factors (TFs)[11] (Fig.2).

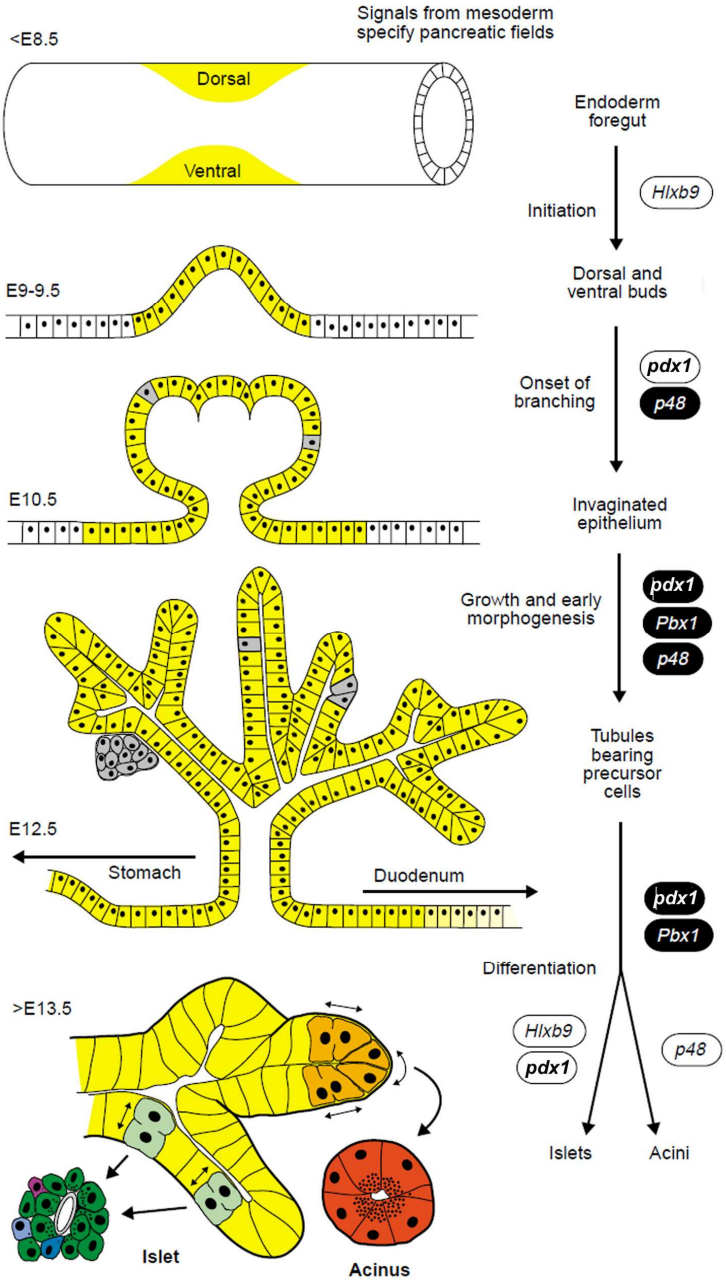

Figure 2. Mice pancreatic development and differentiation is driven by a hierarchical and combinatorial network of TFs. Yellow shading corresponds to Pdx1 positive areas and grey indicates early-differentiated endocrine cell clusters. Adapted from [4].

Signals driving pancreatic development first come from several sources such as the notochord[12], the aorta or the cardiogenic mesoderm[4]. Later in time, the main source of stimuli is the mesenchyme[13,14], highlighting the importance of epithelial/ mesenchymal interactions for pancreatic morphogenesis, ramification proliferation, and differentiation[5]. The mesenchyme seems to be important for regulating relative amounts of endocrine and exocrine pancreatic tissue[14,15] probably involving Notch signaling, FGFs and TGF-β, among others[5].

1.2 PANCREATIC CANCER

1.2.1 Statistics, Treatment and Cell of Origin

The cellular diversity of the pancreas is translated into an extensive heterogeneity of pancreatic malignancies. The most common type of pancreatic cancer, accounting for more than 85% of the cases, is pancreatic ductal adenocarcinoma (PDAC), which is twice as frequent in the head of the organ as in the body or tail (Tab.1).

TUMOR TYPE	I (%)	Immunohistology markers	Main features
Ductal adenocarcinoma	90	CK7,8,18,19, CEA, MUC1	Forming glands embedded in stroma High metastasis rate
Intraductal papillary-mucinous neoplasm, intestinal type	3-5	CK7,8,18,19, CEA, MUC2	Excessive mucin production, which dilates pancreatic ducts
Mucinous cystic neoplasm	6	CK7,8,18,19, CEA, MUC1	Mucin producing epithelial cells with an ovarian-type of stroma
Serous cystic neoplasm	1	CK7,8,18,19	Most benign Glycogen-rich cells forming small cysts
Acinar cell carcinoma	1-2	CK8,18; CK7,19 (70-80%), TRYP	Cytoplasm with a lot of zymogen granules Large nodular lesions
Pancreatoblastoma	<1	CK7,8,181,19, MUC1, TRYP	Childhood tumor (25% of pancreatic tumors)
Endocrine tumor	1-2	CK8,18,19, NSE, SYN, CG	Hormonal hypersecretion
Solid-pseudopapillary neoplasm	1-2	**NSE**	Affecting girls and young women Progesterone receptor immunostaining

Table 1. Pancreatic different tumor types. Their overall incidence among pancreatic cancer (I(%)), immunohistology markers and main features are shown. CK (cytokeratin), CEA (carcinoembryonic antigen), MUC (mucin), TRYP (trypsin), NSE (neuron specific enolase), SYN (synaptophisin), CG (chromogranin A) Data have been summarized from [16] and [17].

PDAC is one of the deadliest of all solid malignancies[18]. The five-year survival rate is just around 6%[19]. Mortality rate is so high because of the absence of sensitive and specific tools to achieve diagnosis at earlier stages, as the disease shows no overt symptoms

before metastasis occurs[20] and also because of high resistance to conventional treatments[21]. Distant metastases are frequent in PDAC, and although they have been found almost in every organ site, the most common ones are the liver, peritoneum, lung, pleura, bones and adrenal glands[22-24]. Recently, novel insights into the genetic features underlying pancreatic cancer metastasis have been identified[25,26], defining a broad time window of opportunity for early detection. Although 10-15% of patients have potentially resectable tumors, many of them experience recurrence of disease after surgery[27]. Erlotinib (an EGFR tyrosine kinase inhibitor) and gemcitabine (a nucleoside analogue)[27,28] have been approved by the FDA for advanced pancreatic cancer therapy. However, treatment results in a modest benefit consisting of an increase in survival of only few months as pancreatic cancer cells seem to be chemotherapy-resistant[21]. Many other agents have been tested in clinical trials[29]. Combinations of gemcitabine with cetuximab (anti-EGFR antibody)[30] and with bevacizumab (anti-VEGF antibody)[31] have also been analyzed without reaching successful results. Thus, there is an urgent need to better understand the molecular mechanisms controlling formation and progression of PDAC and its precursor lesions, in the direction of identifying new molecules suitable for being targeted[32]. Very recently, folfirinox (a pyrimidine analog) shed some light in the field by significantly improving overall survival in phase III studies[33-35]. Several strategies directed to the tumor microenvironment have also appeared by targeting factors produced by stromal cells that are known to stimulate cancer cell growth or endothelial cell (EC) proliferation, although they are still in preliminary studies[36-39].

The unknown cell of origin of PDAC remains one of the most important opened areas of research, constituting a subject of high controversy in the field as the developmental plasticity of the pancreas enables transdifferentiation between cell lineages[40,41]. It has been proposed that different cell types can give rise to PDAC: it may originate from poorly differentiated ductal cells [42-45] but also from de-differentiated acinar[46,47], centroacinar[48], islet[49-51] or progenitor[52] cells. Transgenic mouse models targeting genes under different cell type specific promoters have brought some evidence into the cell of origin dilemma, although discrepancies are still apparent. Direct *K-Ras* expression (the most frequent genetic alteration in PDAC) under acinar (elastase)[53] or ductal (CK19)[54,55] promoters fails to generate PDAC. In contrast, expression of the oncogene during early embryonic pancreatic development succeeds in generating PanINs and PDAC[56,57], suggesting that PDAC might originate from early precursors. Nevertheless, different data support alternative hypotheses regarding the source of PDAC. For instance, metaplasic conversion from acinar cells to duct-like cells occurs in culture and under a variety of stresses both *in vitro*[58,59] and *in vivo*[53,60]. Indeed, targeting oncogenes (like *Tgf-α*[61], *c-Myc*[62]) under the control of an acinar specific promoter as elastase-1 has proven to induce acinar to ductal metaplasia (ADM)[61] and neoplasms with ductal features[62]. These animal models and their usefulness to better understand PDAC cell origin will be described in more detail in section *1.2.4.2.2. Genetically Engineered Mouse Models*.

1.2.2 PDAC Genetic Alterations and Precursor Lesions

Known risk factors for suffering pancreatic cancer include advanced age, smoking, long-standing chronic pancreatitis, diabetes and obesity[63-67]. Approximately 10% of patients demonstrate a familial predisposition to develop tumors in the pancreas[68,69]. Multiple alterations in genes important in pancreatic cancer progression have been identified, including tumor suppressor genes like *p16/CDKN2A (INK4A)*, *TP53*, *DPC4* (*SMAD4*) and *BRCA2*, oncogenes such as *K-RAS* and c-*MYC* and genome maintenance genes as the telomerase[70,71] (Fig.3).

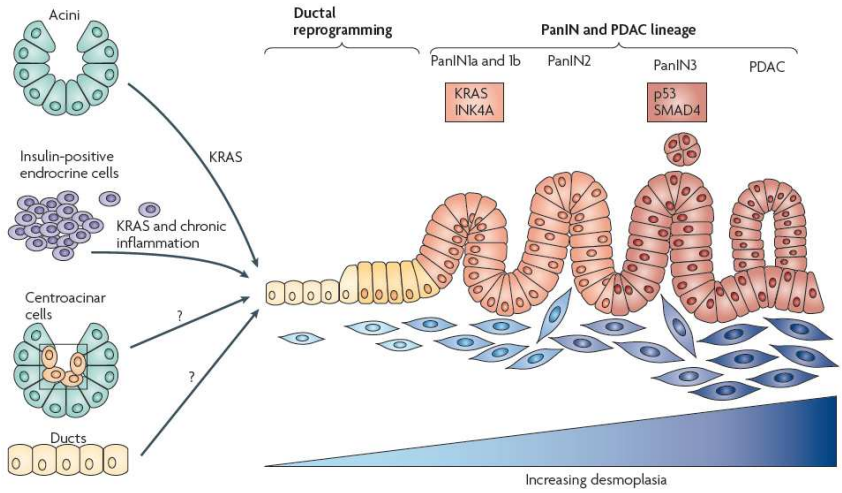

Figure 3. Genetic events, precursor lesions and possible cell of origin in PDAC. PanINs are arranged in three steps of increasing cellular atypia and accumulation of mutations (common mutations appear in boxes), which are also accompanied by changes in the stroma. Mouse models in which *K-Ras* is activated in some adult cell type lineages have shown that both acini and insulin-positive cells can give rise to PanINs and sometimes to PDAC, requiring reprogramming into a ductal cell lineage. Centroacinar and ductal cells might also be the source of PDAC. Extracted from [72].

Moreover, non invasive precursor lesions have also been characterized, which have enabled linking the multi-step progression of pancreatic cancer with the subsequent genetic alterations.

Histologically, these precursors can be classified into microscopic lesions, such as pancreatic intraepithelial neoplasia (PanIN)[73,74] (Fig.3), and macroscopic ones like the intraductal papillary mucinous neoplasm (IPMN) and the mucinous cystic neoplasm (MCN)[75,76].

PanINs are the best characterized precursor lesions at the pathological and molecular level[77,78]. In PanIN lesions, the normal cuboidal flat epithelium lining of the ducts is replaced by columnar mucinous cells with various degrees of dysplasia. PanIN-1 lesions have a flat (PanIN-1A) or papillary (PanIN-1B) mucinous epithelium with minimal cytonuclear atypia. PanIN-2 lesions show increasing cellular atypia and loss of polarity consistent with low grade dysplasia, whereas PanIN-3 refers to high-grade dysplasia or carcinoma *in situ*, being still confined within the basement membrane. Progression from minimally dysplastic epithelium (PanIN-1A and 1B) to more severe dysplasia (PanIN-2 and 3) and finally to invasive carcinoma is paralleled by the successive accumulation of mutations[1,40]. *K-RAS* mutation is found in more than 90% of pancreatic cancers[79,80] and it is one of the first genetic events seen in human PanIN progression[81]. The mutation always takes place in codon 12 and results in constitutive activation of the protein. The high frequency of *K-RAS* mutations suggests that this can be considered an initiating event, and genetically engineered animal models targeting this gene and resulting in pancreatic cancer formation confirm this hypothesis[72,82]. Loss of *CDKN2A* gene expression occurs in 80-95% of pancreatic adenocarcinomas[83], disrupting both the retinoblastoma (Rb) and p53 tumor-suppression pathways through loss of function of *INK4A/p16* and *ARF/p14*, respectively. In later-stage PanINs, *TP53* tumor suppressor gene is found to be mutated in

50% of cases[84], whereas loss of *SMAD4* occurs in 30% of pancreatic cancers[85,86].

In addition to these well known altered genes, pancreatic cancer seems to be genetically very complex and heterogeneous. Importantly, a comprehensive genetic analysis has revealed that a large number of genetic alterations (an average of 63) affect only a core set of 12 signaling pathways and processes that are genetically altered in 67-100% of cases of pancreatic cancer[87] (Tab.2). The specific genes altered in each pancreatic tumor are largely different. Thus, this type of global studies has enabled fishing universal alterations in important signaling pathways such as TGF-β, Wnt/Notch and Hedgehog (Hh)[72], which had not been previously found in the absence of analysis of functional gene groups.

Pathway	Fraction of tumor (%)	Representative altered genes
Apoptosis	100	CASP10, VCP, CAD, HIP1
DNA damage control	63	ERCC4, ERCC6, EP300M RANBP2, TP53
Regulation of G1/S phase transition	100	CDKN2A, FBXW7, CHD1, APC2
Hedgehog signaling	100	TBX5, SOX3, LRP2, GLI1, GLI3, BOC, BMPR2, CREBBP
Homophilic cell adhesion	79	CDH1, CDH10, CDH2, CDH7, FAT, PCDH15, PCDH17, PCDH18, PCDH9, PCDHB2, PCDHGA1, PCDHGA11, PCDHGC4
Integrin signaling	67	ITGA4, ITGA9, ITGA11, LAMA1, LAMA4, LAMA5, FN1, ILK
JNK signaling	96	MAP4K3, TNF, ATF2, NFATC3
KRAS signaling	100	KRAS, MAP2K4, RASGRP3
Regulation of invasion	92	ADAM11, ADAM12, ADAM19, ADAM5220, ADAMTS15, DPP6, MEP1A, PCSK6, APG4A, PRSS23
Small GTPase-dependent signaling	79	AGHGEF7, ARHGEF9, CDC42BPA, DEPDC2, PLCB3, PLCB4, RP1, PLXNB1, PRKCG
TGFβ signaling	100	TGFBR2, BMPR2, SMAD4, SMAD3
Wnt/Notch signaling	100	MYC, PPP2R3A, WNT9A, MAP2, TSC2, GATA6, TCF4

Table 2. Core signaling pathways and the genes altered in most pancreatic cancers. The first column defines the regulatory process or pathway altered. The second column represents the percentage of tumors with genetic alterations in at least one of the genes from the mentioned pathway and the last column gives some examples of the genes altered. Adapted from [87].

1.2.2.1 Hedgehog Signaling and PDAC

In Hh canonical signaling pathway, a secreted ligand (Shh, Ihh or Dhh) binds to Patched (Ptch) transmembrane receptor, releasing Ptch mediated Smoothened (Smo) inhibition. Active Smo induces nuclear translocation of Gli2 and Gli3 transcription factors, which results in activation of their target genes, including Gli1, Ptch1, D-type cyclins, Bmi1 and Bcl2[88,89]. Evidence supports a non-canonical pathway leading to Gli activation in pancreatic cancer, regulated by TGF-β and K-Ras[90,91] (Fig.4).

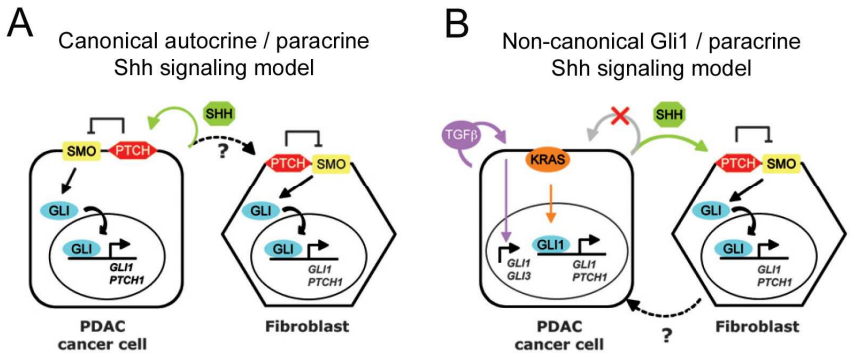

Figure 4. Canonical and non-canonical Gli activation in autocrine/paracrine signaling. A) Canonical Hh dependent Gli activation is involved in autocrine signaling in pancreatic cancer. B) Non-canonical Gli activation in pancreatic cancer cells is unconnected to Hh and it is induced by K-Ras or TGF-β. Paracrine canonical Shh signaling would be affecting fibroblasts. Adapted from [92].

Shh signaling pathway is not observed in normal pancreas but it is misregulated in PDAC and PanINs, in which overexpression of Hh ligands, Ptch and Smo has been reported[93]. Gli1 levels are also upregulated not only in human pancreatic cancer[87], but also in its metastasis[94]. *In vitro* and *in vivo* studies have emphasized Hh importance in PDAC genesis and progression[93,95]. Interestingly, several reports have proposed a paracrine mechanism to explain Hh

induced tumorigenesis, in which tumor cells would secrete Hh ligand that would activate several target genes in stromal cells[96,97]. Importantly, Shh has been reported to contribute to the desmoplastic event in pancreatic cancer, regulating the tumor microenvironment[98,99] and it's inhibition has been considered to successfully overcome PDAC chemotherapy resistance[100].

1.2.3 Role of the Stroma in PDAC

Although the importance of the tumor microenvironment was already highlighted more than 100 years ago[101], it has not been until recently that the interaction between tumor cells and the stroma has been widely analyzed[102-104]. Furthermore, in pancreatic cancer, this issue takes even more relevance as desmoplasia is one of pancreatic cancer hallmarks[105-107].

Desmoplasia is the term used to define the accumulation in the tumor microenvironment of an altered extracellular matrix (ECM) and a variety of non-epithelial cell types including fibroblasts, immune and inflammatory cells (lymphocytes, macrophages and mast cells) and cells comprising vasculature ECs, pericytes and smooth muscle cells)[108,109]. Cancer cells can alter their surrounding stroma to form a supportive tumor environment by secreting growth factors (like bFGF, VEGF, PDGF, EGFR and TGF-β[110]) and proteolytic enzymes[111,112]. At the same time, activated fibroblasts (also referred to as myofibroblasts or carcinoma-associated fibroblasts (CAFs)), secrete growth factor and cytokines[113] (like SDF-1[114], IGF1, HGF) and upregulate the expression of serine proteases[115] and matrix

metalloproteinases (MMPs)[116]. These molecules act on an autocrine and paracrine fashion to remodel the ECM and promote tumor cell proliferation, survival, migration, invasion and angiogenesis[117] (Fig.5). Moreover, the stroma can directly act as a "mutagen" being able to convert non-tumorigenic cell populations to tumorigenic ones[118-120]. The interaction between tumor epithelial cells and the stroma seems to be key in cancer progression[121] as this unique microenvironment harbors and nourishes cancer cells, improving their invasive and metastatic potential[119,122].

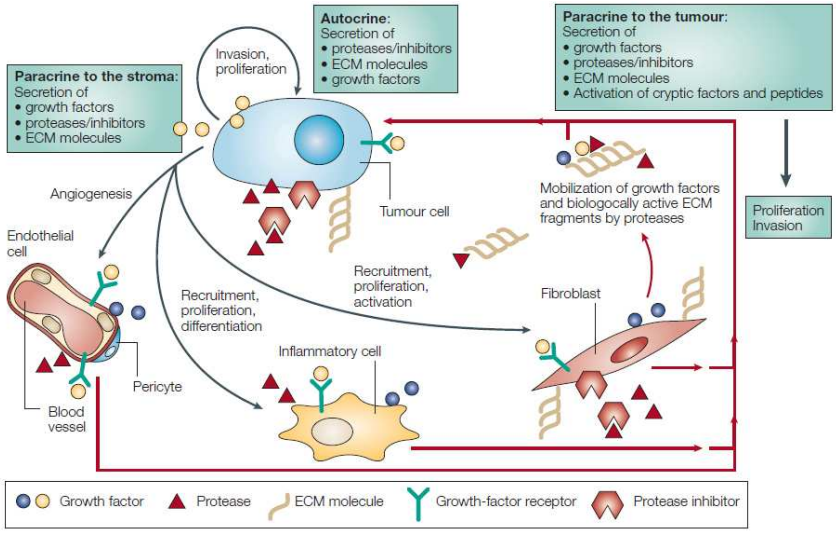

Figure 5. Interactions between tumoral and activated stromal cells. Tumor cells secrete growth factors and proteases that exert an autocrine and paracrine effect leading to ECM degradation, angiogenesis and recruitment of inflammatory cells and fibroblasts, which amplify these signals. Extracted from [108].

As mentioned above, desmoplasia is very prominent in PDAC[123] and deeply influences tumor progression. Indeed, the bulk of PDAC tumor volume consists of a collagen-rich ECM and non-neoplastic fibroblastic, vascular and inflammatory cells. As in other tumor types[124], a close correlation between inflammation and cancer exists

in the pancreas, being pancreatitis a major risk factor for PDAC[125,126]. Pancreatic stellate cells (PSC)[127] have emerged as the main contributor to fibroblastic proliferation and fibrosis in both chronic pancreatitis and PDAC[128]. Activated PSCs[129,130] produce large amounts of collagen, thrombospondin, MMPs and their inhibitors (TIMPs), and release inflammatory mediators, including TGF-β[131]. PSCs enhance tumor cell growth, invasion[132,133] and tumor progression[134,135], while tumor cells activate stellate cells, generating a positive feedback loop resulting in the extensive desmoplastic reaction and PDAC subsequent fatal aggressiveness.

Targeting tumor-associated stroma in therapy has emerged as an interesting issue[31,136-141] as its functions seem to be critical for neoplastic cell growth. Besides, in contrast to tumoral cells, stromal cells are genetically stable and thus less susceptible to drug resistance. Therefore, any tyrosine kinase inhibitor interfering with growth factor receptor signaling might be useful to suppress stromal cell proliferation. In pancreatic cancer for instance, specific antagonists of HGF can block enhanced invasiveness of pancreatic carcinoma caused by irradiated fibroblasts[132]. Different putative therapeutic strategies include VEGF Trap, which may act inhibiting VEGF-A induced angiogenesis by stromal cells[37] and a monoclonal antibody against CTGF, which can attenuate tumor growth, metastasis and angiogenesis *in vivo*[38]. Inhibitors directed to Cox-2, a well known mediator of inflammation, can also decrease invasiveness[39].

1.2.4 Animal Models of PDAC

1.2.4.1 Hamster and Rat Animal Models of PDAC

Carcinogen administration was one of the first strategies used to model pancreatic cancer in animals, typically in hamster or rat[142,142-149] (Tab.3). Despite the fact that some of the pancreatic neoplasms developed in these models histologically resembled their human counterpart, clear disadvantages have relegated chemical carcinogenesis in pancreatic cancer research. The major problems of these models are that specific tumors in the pancreas are rarely formed, and when formed, they do not always contain the molecular alterations typically found in human pancreatic tumors. Moreover, the lack of genetic definition in these systems impairs validating neither the role of specific genetic lesions nor the interrelation of biochemical signaling pathways. Thus, alternative animal models and strategies have been faced in PDAC research[150].

	TUMOR			
CARCINOGEN	**Acronym**	**Animal**	**Phenotype**	**Refs**
N-nitrosobis(2-oxopropyl)amine	BOP	Hamster	Ductal	*Pour PM, 1991*
Azaserine		Rat	Acinar	*Longnecker DS, 1981*
7,12-dimethylbenz(a)anthracene	DMBA	Rat	Ductal	*Bockman DE, 1981*
4-(methynitrosoamino)-1-(3-pyrdidyl)-1-butanone	NNK	Rat	Acinar, ductal	*Rivenson A et al, 1988; Pour PM et al, 1989*
		Hamster	Ductal, acinar	*Schüller HM et al, 1993*
N-nitrosol(2-hydoxypropyl)(2-oxopropyl)amine	HPOP	Hamster	Ductal	*Pour PM, 1991*
		Rat	Acinar	*Longnecker DS et al, 1985*
N-mehyl-N-nitrosourea	MNU	Guinea pig	Ductal	*Reddy JK et al, 1975*
		Hamster	Ductal	*Furukawa F et al, 1992*

Table 3. Pancreatic neoplasms generated through animal carcinogen administration. Adapted from [151], were detailed references can be found.

1.2.4.2 Mouse Models of PDAC

Pancreatic adenocarcinoma is rarely observed spontaneously or following carcinogen administration in mice, but different strategies have allowed modeling PDAC in mice, such as xenogeneic cell

transplantation and genetic engineering[150,152]. Mouse models provide diverse strategies and genetic systems to study the complexity of cancer pathogenesis in a physiological whole animal context[153], thus mimicking the environment in which human disease occurs. Although tumorigenic pathways in human and mouse are pretty conserved[154], special care must be taken when extrapolating results from mouse to human, being conscious of the system limitations[155].

1.2.4.2.1 Xenograft Models

Xenograft models can be generated by injecting cultured or primary pancreatic cancer cells under the skin or implanting them orthotopically in the pancreas of immunodefficient mice. Both nude mice[156] (which lack a functional thymus due to *Foxn1* gene disruption, and thus present T-lymphocyte deficiencies) and severe combined immunodeficiency mice (SCID, which lack functional B and T-lymphocytes[157]) have been widely used in pancreatic cancer studies[158] and are still often the chosen strategy for studying pancreatic cancer metastasis[159-162], molecular biology aspects and therapy efficiency in PDAC[163,164]. Xenografts present some interesting advantages over different animal models as they are rapidly established without the need for time-consuming and expensive breeding. Moreover, disease develops rapidly and latency is much more reproducible compared to genetically engineered models. Another important fact is that in orthotopic implantation models, host pancreatic cells are not genetically altered and tumors can eventually invade to this normal parenchyma, similar to what occurs in human pancreatic cancer. However, a drawback in

the use of xenografts is intrinsic in its definition: the lack of an intact immune system in the host animal significantly alters the tumor microenvironment. Thus, differences in the tumor-supporting stroma and microvasculature of immunodefficient mice can affect cancer progression and treatment efficiency, setting a difference from its human counterpart[27,100]. Xenograft models have also failed to develop tumors in the typical stepwise progression of preinvasive stages (PanINs) and do not usually reproduce human tumors at the histological level. In an attempt to overcome some of these issues, several alternative strategies have been used. For example, co-injection of pancreatic tumor cells and stellate cells[134,135,165-167] has partly covered the stromal contribution, proving the importance of the tumor/stroma interactions in pancreatic cancer. Implantation of tumor cell lines derived from genetically engineered mouse models into immunodefficient mice has also been used[100,168].

1.2.4.2.2 Genetically Engineered Mouse Models

Genetic engineering strategies have allowed the generation of many different mouse strains that develop PDAC and recapitulate the human disease in several ways[169,170]. First animal models established, used the tissue-specific promoter/enhancer elements in the rat elastase-1 locus[171] to drive activated *H-Ras* or *SV40 T-antigen*[172,173], which resulted in pancreatic acinar tumor formation. In contrast, the expression of c-*Myc* transgene under the same regulatory elements led to mixed acinar/ductal neoplasms, supposing a major improvement as a PDAC model[62] (see section *1.2.4.2.3. Ela-1-myc Transgenic Model*). When TGF-α was overexpressed, acinar cells transdifferentiated into duct-like cells

and premalignant lesions were observed[61,174-176], although PDAC was just occasionally seen at advanced stages. Crossbreeding with p53 null mice accelerated tumor development dramatically[175,177]. Another different strategy was proposed by generating a transgenic line in which TVA expression (the receptor for avian leukosis sarcoma virus subgroup A) was restricted to the pancreas by the elastase promoter. Penetrant acinar/ductal or endocrine tumors appeared after infection with viruses encoding mouse polyoma virus middle T antigen or c-Myc, respectively[178]. Outcome differences comparing Ela-1-myc to RCAS/TVA/c-Myc might be due to the distinct time expression window as c-Myc expression occurs since embryogenesis in the first case, or 2 days after birth in the second. Differences in c-Myc levels due to viral infection efficiency might also offer a possible explanation. Other PDAC models have been generated by misexpression of Gli2[95] or loss of Pten[48], resulting in pancreatic neoplasms, though classical mPanINs are absent in these pancreata.

Most models though, have been based on the expression of *K-Ras* oncogene, consistent to what is found in human PDAC[79,80]. Both ductal (CK19[54,55]) and acinar (elastase-1[53]) driven oncogenic K-Ras expression fail to recapitulate the signature features of PDAC. Knock-in of the *K-Ras* oncogene in *Mist1* locus induces invasive and metastatic pancreatic tumors[179], which still do not resemble human PDAC.

Very interestingly, mice expressing oncogenic K-Ras^{G12D} during the early stages of embryonic pancreatic development (Pdx1-Cre;LSL-K-Ras^{G12D} and p48$^{+/Cre}$;LSL-K-Ras^{G12D}) recapitulate the full spectrum

of PanIN lesions, although they show prolonged latencies and incomplete PDAC penetrance[56]. This model has been improved by combining oncogenic K-Ras expression with tissue-specific deficiency of Ink4a/Arf[180], p53[181,182], Pten[183], Smad4/Dpc4[184-186], TGFBR2[187] or by Notch upregulation[188], which accelerate tumor progression and induce invasion and metastasis, so common in PDAC. In a similar manner, expression of K-Ras^{G12V} oncogene in embryonic cells of acinar/centroacinar lineage results in pancreatic tumoral lesions mimicking human pancreatic tumor development[57]. Highlighting the importance of non-genetic events, if expression is activated in adult acinar tissue, mice have to be challenged with chronic pancreatitis in order to recapitulate whole disease progression[57], although PanIN formation can be spontaneously observed[189].

1.2.4.2.3 Ela-1-myc Transgenic Model

c-Myc is found to be overexpressed and/or amplified in many neoplasms promoting transformation[190]. Although in pancreatic cancer, c-Myc is not one of the universal gene alterations, consistent data suggest that its role in this pathology may have been underestimated[191]. Its gene amplification and/or overexpression has been found in 54% of a pool of 31 pancreatic cancer cell lines[192] and in around 30% of human tissue samples, metastatic tumors and even in some PanIN lesions[193-197]. Finer analysis have reported much higher levels of overexpression[198]. Increased c-Myc mRNA and protein level appears in 70% of cases in human PDAC[193,197,199], correlating with the histopathological tumor grade. These data underline c-Myc as an important mediator in pancreatic tumor development and progression. *In vivo* studies have also proven the

relevance of c-Myc in this context, as carcinogen administration in rat also induces increased c-Myc expression[200,201]. Still, a more convincing evidence for a critical role of c-Myc in pancreatic cancer comes from the fact that transgenic mice overexpressing this protein develop 100% penetrance pancreatic tumors.

Ela-1-myc transgene contains murine c-*Myc* gene cloned between the rat elastase-1 promoter and enhancer and the 3' untranslated and poly(A) addition sequences of the human growth hormone (GH), conferring higher protein stability to the product mRNA[62] (Fig.6).

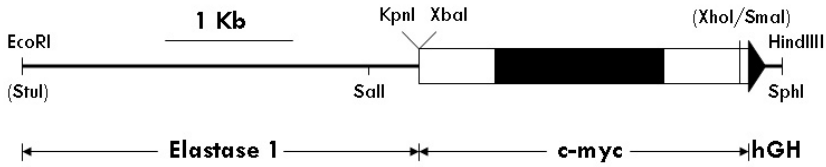

Figure 6. Ela-1-myc transgene. The construct is formed by the rat elastase 1 promoter, c-*Myc* murine gene and the human growth hormone 3' UTR and poly(A) sequences (hGH). Adapted from [62].

Ela-1-myc transgenic mice develop pancreatic cancer between 2 and 7 months of age with 100% incidence[62]. One half of these tumors are acinar cell carcinomas whereas the rest are mixed acinar/ductal pancreatic adenocarcinomas embedded in a dense desmoplastic reaction, so typical of human PDAC (Fig.7). The importance of this model resides in that, although it is based on a single transgene, it gives rise to some ductal pancreatic tumors in a short latency period. Moreover, Ela-1-myc mice are among the few animal models presenting spontaneous metastases to the liver[202,203], another feature commonly found in human PDAC and which is responsible for most of pancreatic cancer deaths in patients[25,204].

Thus, this transgenic model has also been used to identify genes involved in pancreatic cancer liver metastasis[205].

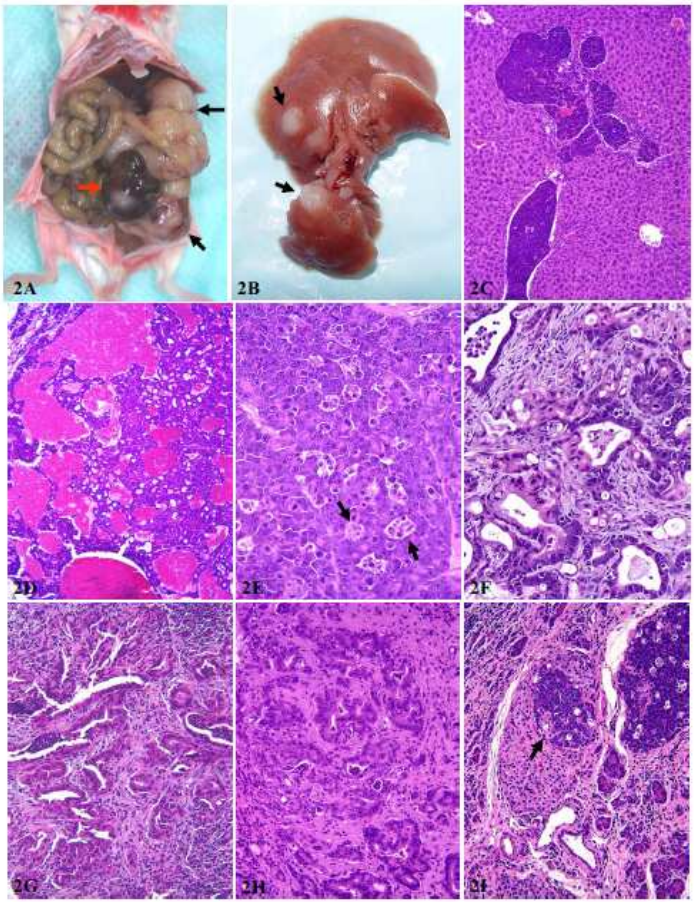

Figure 7. Pancreatic tumors in Ela-1-myc mice. 2A) Macroscopic nodules in the peritoneal cavity can be red or white. 2B) Focuses of liver metastases (arrows). 2C) H&E staining of liver metastasis confirming its pancreatic origin. 2D and 2E) acinar cell carcinomas. 2F) Mixed acinar and ductal adenocarcinomas. 2G and 2H) PDAC with its typical desmoplastic reaction. 2I) acinar cell carcinoma within an islet (arrow). Extracted from [202].

1.2.4.3 Zebrafish Models of PDAC

Zebrafish (*Danio rerio*) has emerged as a new animal model to study cancer biology[206] due to some interesting advantages that allows complementing other *in vivo* systems. Pancreas anatomy and histology is pretty conserved among zebrafish and mammals and several signaling pathways and ortholog transcription factors regulate pancreas development in both families, suggesting that zebrafish can be a suitable model for pancreatic cancer studies[207].

A zebrafish model developing pancreatic cancer has also been reported[82]: ptf1a:eGFP-K-Ras^{G12V}. In this system, oncogenic K-Ras expression under the control of Ptf1a regulatory elements results in impaired differentiation of the pancreatic progenitor pool of cells, which finally leads to pancreatic cancer formation. Although these tumors are very heterogenic concerning histological patterns of differentiation, some of them resemble human pancreatic tumors displaying dense stromal reaction, invasion sites and even sharing abnormal signaling pathway activation such as Hh. Another zebrafish model developing pancreatic cancer that has not yet been reported (Ptf1a:GAL4/VP16 UAS:eGFP-K-Ras^{G12V}) consists of K-Ras activation using the GAL4/UAS system, in which the transcription factor GAL4 activates UAS-fused genes (in this case oncogenic K-Ras). Ptf1a regulates GAL4 expression and VP16 is used to increase K-Ras activation levels (Leach SD. Unpublished data).

1.3 TISSUE PLASMINOGEN ACTIVATOR

1.3.1 The Plasminogen System

The plasminogen system is a delicately balanced system comprised of the protease plasmin, its inactive precursor (plasminogen), its activators (tPA and uPA), their receptors (uPAR, AnnexinA2 and others) and inhibitors (α_2-antiplasmin, α_2-macroglobulin, PAI-1 and PAI-2) (Fig.8).

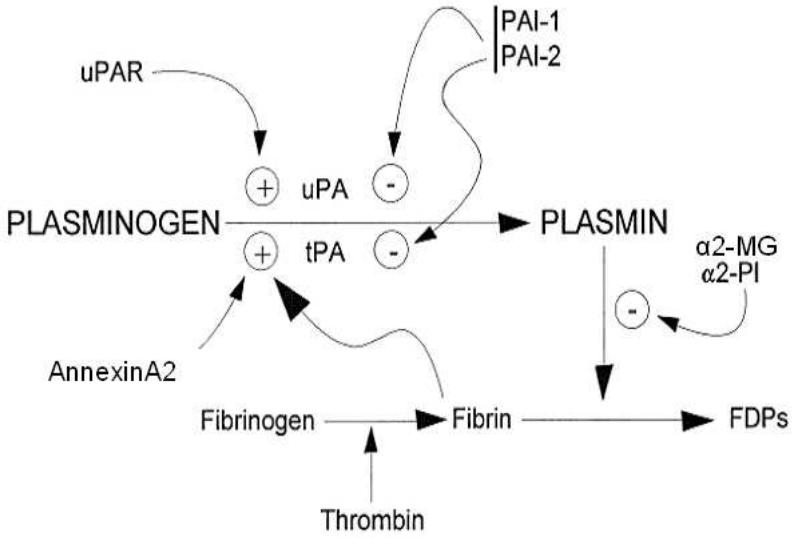

Figure 8. The plasminogen system. uPA and tPA can convert plasminogen into plasmin, which degrades fibrin clots generating fibrin degradation products (FDPs). Fibrin itself is understood as a plasminogen activator receptor as well as uPAR and AnxA2. The negative regulators of the system include PAI-1, PAI-2 at the plasminogen activator level and α_2-antiplasmin and α_2-macroglobulin at the plasmin level. Adapted from [208].

Plasminogen (Pg), which is synthesized in the liver[209] in its circulating Glu-Pg form (Glu1-Asn791), is converted to Lys-plasminogen (Lys77-Asn791) by plasmin[210]. Lys-Pg shows higher fibrin affinity[211] and it is activated 10-20 times more readily by tPA[212]. Lys-Pg is converted

to plasmin after plasminogen activator mediated proteolysis[213] of Arg561-Val562. Both chains are held together by a disulphide bond. Plasmin active site is based on three residues: His602, Asp645 and Ser740[214].

Two human plasminogen activators (PAs) exist, both consisting in serine proteases: tissue plasminogen activator (tPA) and urokinase plasminogen activator (uPA). Due to its fibrin specificity[212], tPA-mediated plasmin generation has been classically involved in fibrin dissolution in circulation[215], whereas uPA has been more linked to pericellular proteolysis via ECM degradation[216] and activation of growth factors and latent proteases[217]. uPA is a glycoprotein[218,219] consisting of 4 autonomous protein domains: a signal peptide, an EGF domain, a kringle and a serine protease (SP) domain. uPA is released in a single-chained form that is rapidly converted into a two-chain form by kallikrein or plasmin[220,221]. It is secreted by kidney[222,223] and ECs[224], as well as by tumor cells[225]. uPA mediated plasminogen activation is greatly enhanced by its binding to uPA receptor (uPAR)[226,227], which is also involved in the activator clearance by endocytosis in the liver[228,229]. tPA characteristics and functions will be described later (see section *1.3.3. Tissue Plasminogen Activator and tPA Receptors*).

Fibrinolysis and other plasminogen system functions are tunely regulated by controlled EC synthesis and release of PAs but also through plasminogen activator inhbitors (PAIs), which usually belong to the family of serine proteinase inhibitors (serpins) and can act by directly targeting plasmin or plasminogen activators. tPA and uPA are rapidly inactivated in human plasma by PAIs, among which PAI-

1 is the physiologically most important one[230]. Other proteins are also able to inhibit tPA and uPA[231], like PAI-2[232], PAI-3[233], neuroserpin[234], proteinase nexin-1[235] and procarboxipeptidase B[236], yet their activities are significantly lower or their specificity broader. Inhibitors directly blocking plasmin are also physiologically relevant. α_2-antiplasmin (produced by the liver) is the main plasmin inhibitor and it is involved both in the rapid inactivation of the free protease by blocking its active site[237], as well as in its slow inhibition when plasmin is formed at the fibrin surface[238]. α_2-macroglobulin, which is produced by ECs and macrophages, does not belong to the serpin family and although its activity is ten times lower compared to α_2-antiplasmin, it neutralizes plasmin when excessively produced[239]. Thrombin activatable fibrinolytic inhibitor (TAFI) also inhibits plasmin as well as both tPA and uPA[240].

Many of the plasminogen system functions require protease localization over fibrin for fibrinolysis or over the cellular membrane. This can be mediated by plasminogen receptors like α-enolase[241,242], AnnexinA2 (AnxA2)[243], glyceraldehyde 3-phosphate dehydrogenase[244], amphoterin[245], LRP-like protein[246] or gangliosides[247]. However, the interaction with the cell membrane is more frequently mediated by plasminogen activator receptors, which increase PA activity, protect them from their inhibitors and localize plasmin activity where required.

1.3.2 Plasminogen System Functions

The plasminogen system is involved in a wide variety of physiological and pathological functions. Plasmin displays a wide

range of targets including fibrin as its classical substrate but also MMP precursors, ECM proteins like laminin or fibronectin and growth factors like latent TGF-β1, bFGF and VEGF[248-254] (Fig.9). Still, the main function of the plasminogen system is the degradation of blood clots after thrombosis[215,255] and indeed tPA is currently being used for the treatment of acute vascular diseases like myocardial infarction or stroke[256,257]. Nevertheless, the plasminogen system is also involved in ECM degradation and remodeling[251,258] and even in cell signaling events[259], which widens its potential in therapy but also makes the study of tPA secondary effects a very important issue[260-262].

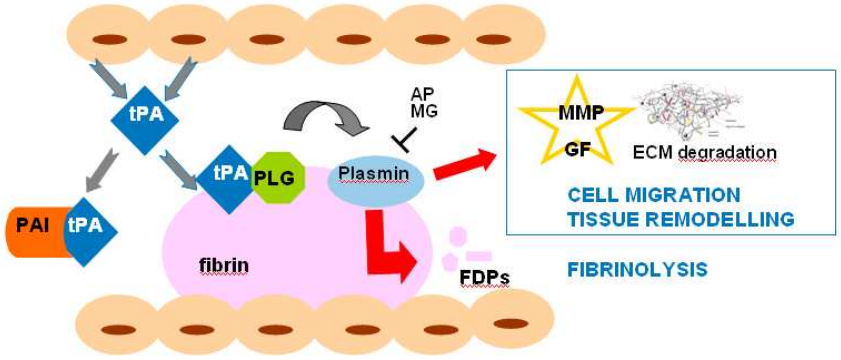

Figure 9. tPA physiological functions. The best documented role for tPA is the activation of the zymogen plasminogen into plasmin, which degrades fibrin clots in blood vessels after thrombosis. Moreover, tPA is also involved in activation of MMPs and growth factors and in the ECM degradation, participating in cell migration and tissue remodeling events.

The generation of transgenic mice with altered members of the plasminogen system has enabled establishing its role in several biological processes[263] such as in cell migration and adhesion[264,265], wound healing[266], nervous system development[267-269], ovulation and embryogenesis[270], trophoblast invasion[271] and macrophage migration[272]. Importantly, the plasminogen system has also been linked to several pathologic conditions such Alzheimer[259],

atherosclerosis[273], myocardial ischemia[274], angiogenesis[275], tumor growth and metastasis[276,277], inflammation[278] and infection[272].

Single deficiencies of tPA or uPA in mice are not severe and animals develop normally, are fertile and have a normal life span. tPA knockout (KO) mice present reduced thrombolytic potential and uPA KO mice occasionally develop spontaneous fibrin deposits, both animals showing increased incidence of endotoxin-induced thrombosis[279]. Nevertheless, combined deficiency of tPA and uPA in mice markedly affects general health, producing extensive intravascular and extravascular fibrin deposits in several organs and multi organ dysfunction[279,280], resembling the phenotype of plasminogen loss in mice[270,281].

1.3.3 Tissue Plasminogen Activator and tPA Receptors

1.3.3.1 Tissue Plasminogen Activator (tPA)

Tissue Plasminogen activator is a glycoprotein of 527 aminoacids (AAs) and around 70 KDa, depending on specific glycosylation. tPA is synthesized as a single-chain protein but it is quickly hydrolyzed at Arg275-Ile276 by plasmin, forming a two-chain structure maintained together by a disulfide bond[282]. Structurally, apart from a typical signal peptide and a prosequence, tPA is formed by 5 different autonomous domains (Fig.10), which are encoded by separate exons or sets of exons[283,284]: 1) The fibronectin type I domain in the amino terminus, which mediates fibrin affinity (FN1: residues Ser1 to Lys49); 2) An EGF-like domain (EGF: residues Ser50 to Asp87), which is probably involved in cell surface receptor binding; 3) Two

kringle regions (K1 and K2: residues Thr88 to Gly176, and Asn177 to Cys261, respectively) with a triple looped structure, with a high degree of homology with plasminogen kringle domains and 4) A serine protease domain (SP: residues Ser262 to Pro527) with the active site residues His322, Asp371 and Ser478, whose X-ray crystal structure is available both for single-chain and two-chain tPA.

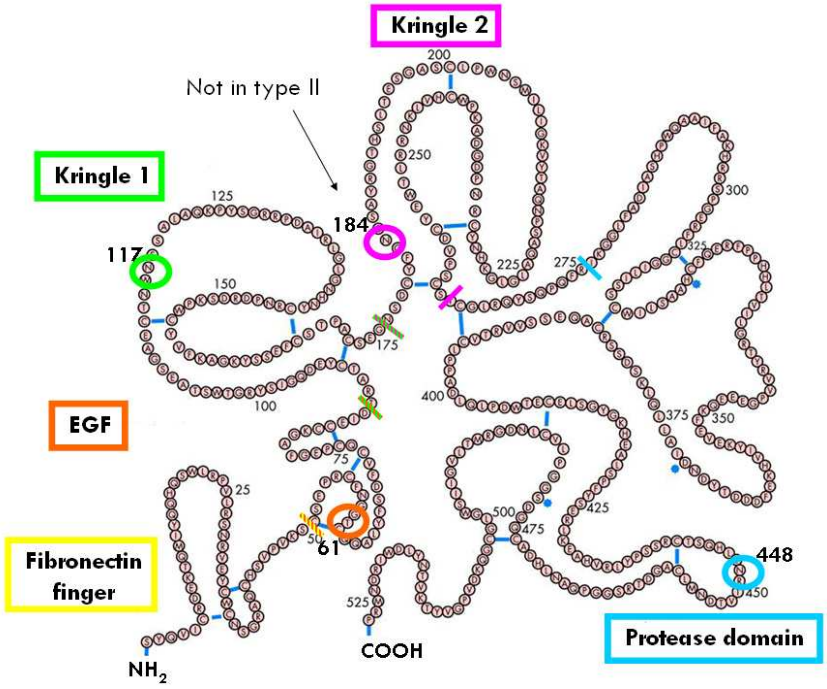

Figure 10. tPA structural domains and its glycosylation sites. tPA consists of a fibronectin finger domain, an EGF-like domain (containing an O-glycosylation site at T61), two kringle domains (with N-glycosylation sites at Asn117 and Asn184) and the protease domain (which harbors the third N-glycosylation at Asn448). Adapted from [285].

Due to the size of tPA and the presence of glycosylated chains in the molecule, the complete structure of the protease remains still undetermined. However, the detailed structure has been revealed for some of the domains by NMR or X-Ray diffraction as for FN1[286], EGF[287], K2[288-290] and the catalytic domains[291-293] (Fig.11).

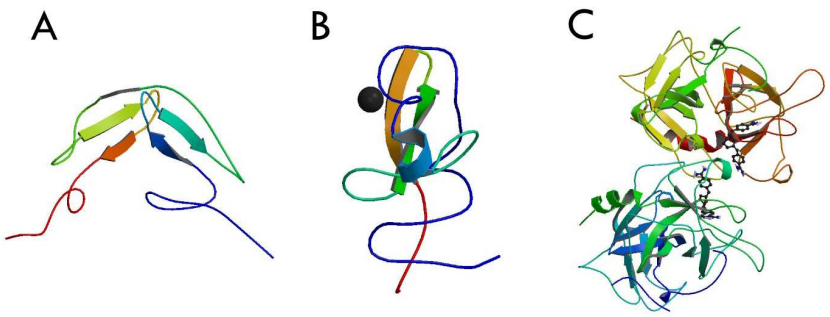

Figure 11. Structure of independent domains of tPA. A) NMR determined structure of FN1 and EGF domains[287]. B) Crystal structure of the K2 domain at 2.40 Å resolution[290]. C) Catalytic domain of two chain-tPA complex of a bis-benzamidine determined by X-Ray diffraction at 2.90 Å resolution[292].

Glycosylation differences describe two different tPA isoforms (type I and type II), displaying species, cell and site-specific patterns of this post-translational modification[294-296]. In type I tPA 4 glycosylation sites are occupied in separate domains, which play a role in different biological and pathological tPA functions[251,295,297-300]: an O-linked fucose in Thr61[301] (EGF domain) and three N-linked carbohydrate chains; an oligomannosidic structure highly conserved between species at Asn117 (in K1)[298], and two complex and hybrid type structures at Asn184 (in K2) and Asn448 (in SP)[294,295,302]. Type II tPA lacks the glycosylation at Asn184 and this absence allows the conversion of single-chain to two-chain tPA, through plasmin mediated cleavage of the polypeptide backbone between Arg275 and Ile276. The presence of glycan chains at site Asn184 affects the structure of the glycan population at Asn448, being two-chain tPA a more active tPA regarding clot lytic activity and fibrin-binding capacity[297,303-305].

tPA resting plasma level is around 5 ng/mL but large amounts can be quickly released under different circumstances. It is mainly

synthesized by ECs[306], but it has also been detected in the central nervous system[307-309], being secreted by neurons and glial cells[310,311] and it can also be produced by keratinocytes[312,313], melanocytes[314] and various tumor cells[315-317].

1.3.3.2 tPA Receptors

tPA does not have an exclusive receptor but it is able to bind to several proteins that are involved in its clearance, in its localization on the cell surface or even in mediating intracellular signaling[318].

tPA clearance takes place rapidly in the liver[319] resulting in an initial half life of only a few minutes[320]. LDL-receptor related protein (LRP) is the main tPA scavenger[321], both in its free form or bound to PAI-1. The FN1 and EGF domains[322] of tPA are key in LRP recognition. The mannose receptor is responsible for tPA elimination in ECs[323] and it does so by interacting with the oligomannosidic structures present in the K2 domain, whereas the α-fucose receptor is involved in tPA clearance in other cell contexts[324].

As a way to localize plasmin where needed, avoiding undesired secondary effects, fibrin is able to greatly enhance tPA activity[212], being its main receptor in fibrinolysis. Although K2 and FN1 domains of tPA are important for fibrin binding[325], multiple interactions within tPA and fibrin may play a role in regulating tPA activity[326], resulting in a complex mechanism of binding[327]. Other plasmin substrates such as fibronectin[328] and laminin[329] can also interact with tPA as well as with plasminogen, regulating tPA activity[330,331].

tPA is also able to bind to cell surface receptors, which localize the protease, increase its proteolytic activity towards plasminogen and are also involved in cell signaling transducing, highlighting an interesting role for tPA independently of its catalytic activity[318]. tPA binds to different cell types like fibroblasts[332], ECs[333-335], smooth muscle cells[336], melanoma cells[337] and neurons[245], mainly involving its kringles[338], but also the FN1 and SP domains[339].

The main tPA receptor in the endothelium is AnxA2[243,340], which 60-fold enhances tPA mediated plasmin generation[243]. AnxA2 is not only found in the endothelium but also in neurons, fibroblasts, macrophages, keratinocytes and even in tumoral cells[340-346]. It is involved in plasmin induced fibrinolysis as well as in cellular migration and tissue remodeling events[347,348]. The interaction between AnxA2 and tPA depends on the receptor N-terminal region, although the mechanism is not yet fully understood[349-351]. Amphoterin is tPA best characterized receptor in neurons and it is able to bind both plasminogen and its activator, increasing its catalytic activity specifically in the filopodia[245,352]. Other tPA binding proteins include EGFR[318,353], cytokeratin-8 and 18[354,355], α-enolase[356] and CKAP4[357].

Most of these receptors are overexpressed in different cancers, correlating with more aggressive phenotypes. For instance, AnxA2 is overexpressed in acute promyelocytic leukemia[358] and pancreatic cancer[359,360], as well as cytokeratin-18[361]. Amphoterin is involved in cell migration in neuroblastoma cells[245,352] and cytokeratin-8 is expressed in different tumoral cell lines[362].

1.3.4 Plasminogen System in Cancer

As the plasminogen system is pretty complex, having different substrates and being controlled at different levels, so it is its relationship with tumor biology[276,277,363]. This family of proteins might influence tumor progression in different steps through plasmin formation, degrading the ECM[251], activating latent growth factors[364] and metalloproteinases[252] or even directly triggering cell signaling events, independently of plasmin generation[318,365]. All these steps result in changes in cell proliferation, apoptosis, cell migration, invasion and angiogenesis[366,367].

Classically, uPA has been more commonly related to plasminogen activation for ECM degradation, linking it to cancer invasion[368,369], whereas tPA activation has been proposed to be more involved in fibrinolysis[251], pointing out its importance in thrombolysis[370] and neurobiology[371]. Thus, uPA has been extensively studied in cancer[372] being proposed as an interesting target for anticancer therapy[373-375], whereas tPA mechanisms in neoplasia have been less characterized.

1.3.4.1 uPA and uPAR in Cancer and Pancreatic Cancer

High levels of uPA and its receptor are associated with advanced metastatic cancers[277,376-378]. uPA interaction with uPAR is functionally participating in most of the pathological events driving tumor progression[379] such as cell migration, invasion[366], proliferation[380,381], angiogenesis[382,383] and metastasis[225,384,385]. Interestingly, in many different human cancers, uPA and uPAR are not only expressed by

tumoral cells but also by stromal cell types, such as fibroblasts or macrophages in breast[377,386,387], colon[388] and prostate[389] cancer.

In pancreatic cancer, high uPA and uPAR levels are observed and correlate with increased aggressiveness and poor survival[390-394]. uPA is also found in PanIN lesions and can be detected by serum analysis[392] due to its presence in tumor associated blood vessels, which emphasizes its putative importance in diagnosis. In contrast, it has also been reported that uPA is faintly expressed in tumors (yet uPAR is consistently found to be overexpressed[395]), being more important in areas of tumor associated pancreatitis[360,396]. I*n vitro* studies have found that uPAR inhibits apoptosis and promotes proliferation, adhesion and migration of pancreatic cells through Erk/p38 regulation[397,398]. In the same direction, uPA induces dissociation of cell colonies, promoting invasion and metastasis both *in vitro*[399] and *in vivo*[400] and uPAR is important for hypoxia-induced metastasis[401]. Furthermore, the uPA system is also involved in desmoplasia as the interaction between cancer cell integrins and uPAR of stromal fibroblasts has been reported to be relevant for pancreatic cancer metastasis via MMP-2 activation[402].

1.3.4.2 tPA and Receptors in Cancer and Pancreatic Cancer

tPA overexpression correlates with poor prognosis in several cancers, including melanoma[331,337,403], neuroblastoma[316,404,405], acute non-lymphocytic leukaemia[358,406], hepatocellular carcinoma (HCC)[407], ovarian[408], uterine[409] and pancreatic ductal adenocarcinoma[360,361,410]. Notwithstanding, in breast[411,412] and endometrium carcinoma[413], high tPA levels are observed during

hyperplasia whereas a decrease occurs at advanced stages of tumor progression.

In pancreatic cancer studies, tPA is found to be highly expressed in well differentiated human pancreatic cancer cultures and overexpressed in 95% of pancreatic ductal adenocarcinomas, being absent in normal pancreas[360,361,410] (Fig.12). However, our group has found that tPA mRNA is also present in normal pancreas. Studies towards deciphering the mechanism driving tPA translational control and its relevance in pancreatic cancer have been performed[414].

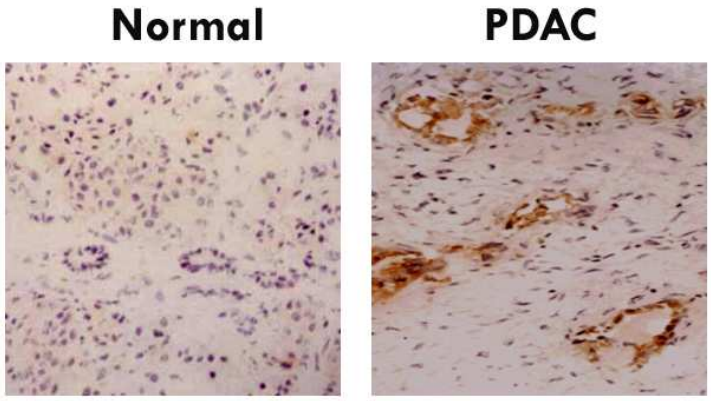

Figure 12. tPA is overexpressed in human pancreatic cancer. tPA expression assessed by immunohistochemistry (IHC) in normal pancreas (normal), showing no tPA expression, whereas in human PDAC, high expression levels of tPA are detected in ducts.

In vitro studies have determined that tPA contributes to pancreatic cancer cell invasion[360], via its interaction with AnxA2[415]. tPA is responsible for mediating Erk1/2 phosphorylation and cell proliferation[416], involving AnxA2 and EGFR[318,353]. However, several molecular mechanisms have been postulated for tPA functions in cancer. Our group points at tPA driving proliferation as a cytokine, in a plasmin independent fashion[318], as it has also been reported in

neurons[259] and kidney fibroblasts[417]. In contrast, others have suggested a proteolytic activity requirement for tPA involving MMP-9 and EGF expression[353], which would favor ECM degradation and subsequent invasion and tumor progression. In athymic mice, pancreatic cancer cells with low tPA levels generate less proliferative and angiogenic tumors[416]. More importantly, Ela-1-myc mice developing pancreatic tumors in a null tPA background, show an increase in survival, with less angiogenic and mitogenic tumors[418]. This effect is clearly dependent on the tumor histological characteristics, being predominant in ductal tumors resembling human PDAC, where tPA is found to be overexpressed.

AnxA2, tPA best known receptor, is also overexpressed in 70% of cases of human pancreatic cancers[359,360] and in ductal transgenic mice tumors[418], whereas its expression in normal pancreas is low and mainly found in pancreatic islets[419]. This receptor has been clearly involved in tPA mediated pancreatic cancer cell invasion[415] and proliferation by both increasing tPA catalytic activity and by triggering tPA cytokine-like effects[318]. Nevertheless, AnxA2 does not seem to be the only functional tPA pancreatic cancer receptor as its interaction with the protease only explains part of the tPA found in the cell membrane[318,415]. These data and the fact that AnxA2 seems to be inappropriate as a target for pancreatic therapy due to its important physiological functions in blood coagulation homeostasis (being the main endothelial tPA receptor), moved our group to identify new tPA receptors that were pancreas specific.

Protein name	Lysate	Raft	p/	Mass (kDa)	Localization	Function
Enolase$^{\Psi}$	+	+	7.0	47	Membrane, cytoplasm,	Metabolism
Galectin-1$^{\Psi}$	+		5.3	15	Membrane, cytoplasm, nucleus	Receptor binding; immune response
Cortactin$^{\Psi}$	+		5.2	61	Cytoskeleton	Structural component
Cytokeratin 8$^{\Psi}$	+	+	5.5	53	Cytoskeleton	Structural component
Tubulin$^{\Psi}$	+	+	5.0	50	Cytoskeleton	Structural component
ARP3$^{\Psi}$	+	+	5.6	47	Cytoskeleton	Structural component
Enigma proteins with LIM and PDZ domains$^{\Psi}$	+		6.6	36	Cytoskeleton	Receptor signaling complex scaffold
Chaperonin (acute related morphine dependence protein)$^{\Psi}$	+		6.2	58	Cytoplasm	Chaperone activity; metabolism
Thioredoxin peroxidase$^{\Psi}$	+		5.4	22	Cytoplasm, nucleus	Peroxidase activity; metabolism
ERK 1$^{\Psi}$	+		6.5	42	Cytoplasm, nucleus	Kinase activity; signal transduction; cell communication
Valosin containing protein$^{\Psi}$	+		5.1	90	Cytoplasm, ER, nucleus	ATPase activity
Elongation factor Tu, mitochondrial precursor$^{\Psi}$	+		7.3	46	Mitochondria	Translation regulator activity

Table 4. Pancreas specific tPA interactors identified by peptide mass fingerprint. Proteins overrepresented in PANC-1 pull-down with tPA-Sepharose compared to HUVEC. Adapted from [420].

In this direction, a proteomic approach was performed by pulling down human pancreatic cancer cell line extracts with tPA bound to sepharose[420]. Putative candidates were separated by 2D-electrophoresis and identified by peptide mass fingerprint. Some of the candidates found had already been described, such as AnxA2, enolase, cytokeratin-8 and 18 or tubulin, but others were described for the first time like Galectin-1 (Gal-1) and valosin containing protein. Considering that tPA is physiologically expressed in the endothelium and looking for specific tPA receptors in the pancreas, these results were compared to the ones obtained with a human EC line, getting a final list of 12 pancreas specific tPA interactors (Tab.4).

Thus, our group identified Gal-1 as a putative specific pancreatic receptor[420]. However these data did not prove whether tPA/Gal-1

interaction was direct or mediated through other proteins. Validating the former of these two possibilities, recombinant Gal-1 was pulled down with tPA[421] (Fig.13A). The dissociation constant of the complex was measured by surface plasmon resonance (SPR), which confirmed tPA specificity for Gal-1, as the lectin displayed similar values for tPA binding as AnxA2, a well known tPA receptor (Fig.13B). Furthermore, Gal-1 was able to increase tPA mediated plasmin generation, suggesting interesting functional outcomes from their interaction[421] (Fig.13C).

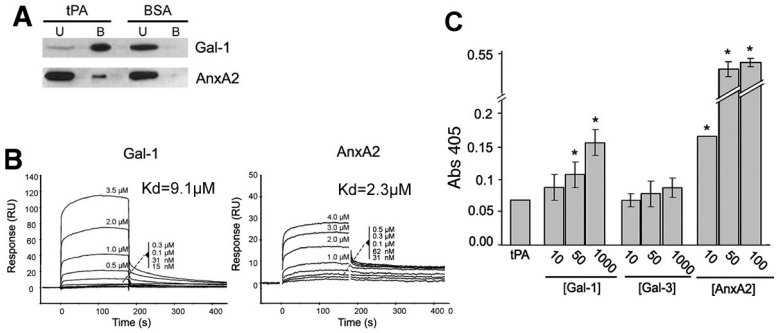

Figure 13. Gal-1 interacts directly *in vitro* with tPA and increases its proteolytic acvivity. A) Pull-down assay with tPA or BSA sepharose beads. Recombinant Gal-1 and AnxA2 were identified by Western blot (WB) in the bound fraction (B) when using tPA-Sepharose beads. B) Gal-1 and AnxA2 dissociation constants with tPA calculated by SPR analysis. tPA was immobilized in an SPR chip and Gal-1 or AnxA2 at different concentrations were flowed through. SPR responses were used to calculate dissociation constants, which appeared to be of the same order of magnitude. C) Gal-1 and AnxA2 increased tPA catalytic activity in a dose dependent manner, assessed by changes in absorbance at 405 nm due to a plasmin chromogenic substrate. Adapted from [421].

1.4 GALECTIN-1

1.4.1 The Galectin Family: Main Features

Galectins belong to the lectin family of proteins, which are highly evolutionary conserved[422] finding their members in all animal kingdoms and even in plants, fungi and viruses[423]. All the proteins of the family share two main features: high affinity for β-galactosides and a well conserved carbohydrate recognition domain of 130 AAs[424]. However, each galectin has a specific carbohydrate binding preference[425], as a result of their ability to accommodate different saccharides attached to galactose[426,427].

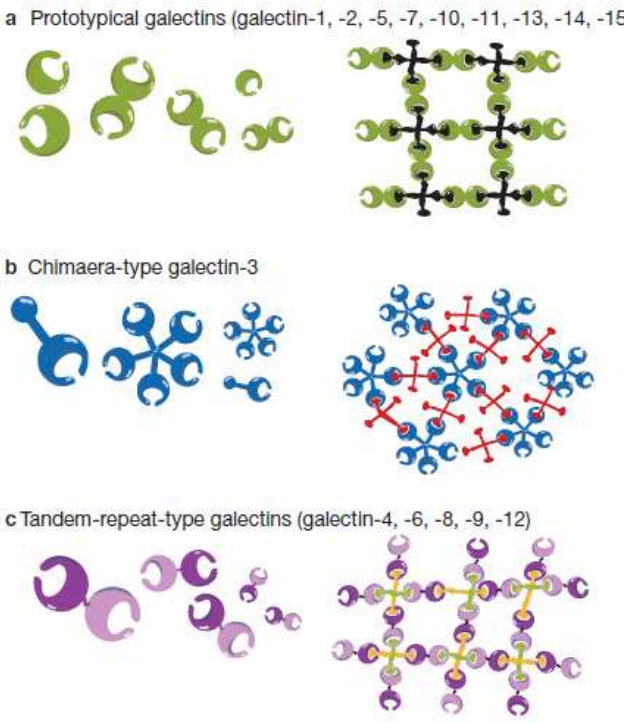

Figure 14. Galectin structural classification. Prototype galectins (Gal-1,2,5,7,10,11,13,14,15) have one carbohydrate recognition domain. The only chimaeric galectin (Galectin-3) has an extended N-terminal domain. Tandem repeat galectins (Gal-4,6,8,9,12) are composed of two different CRD. Extracted from [428].

15 galectins have been described in mammals (11 of which are expressed in humans) and they can be structurally clustered in three groups[423,427,429] (Fig.14): 1) Prototype galectins (1, 2, 5, 7, 10, 11) consist of a single carbohydrate recognition domain (CRD) with a short N-terminal sequence; 2) Tandem galectins (4, 6, 8, 9) are composed of two differents CRDs joined by a short linker peptide sequence; and 3) Chimaeric galectins (Gal-3) have an extended N-terminal tail containing a consensus nine AA residue-repeat rich in Pro, Tyr and Gly.

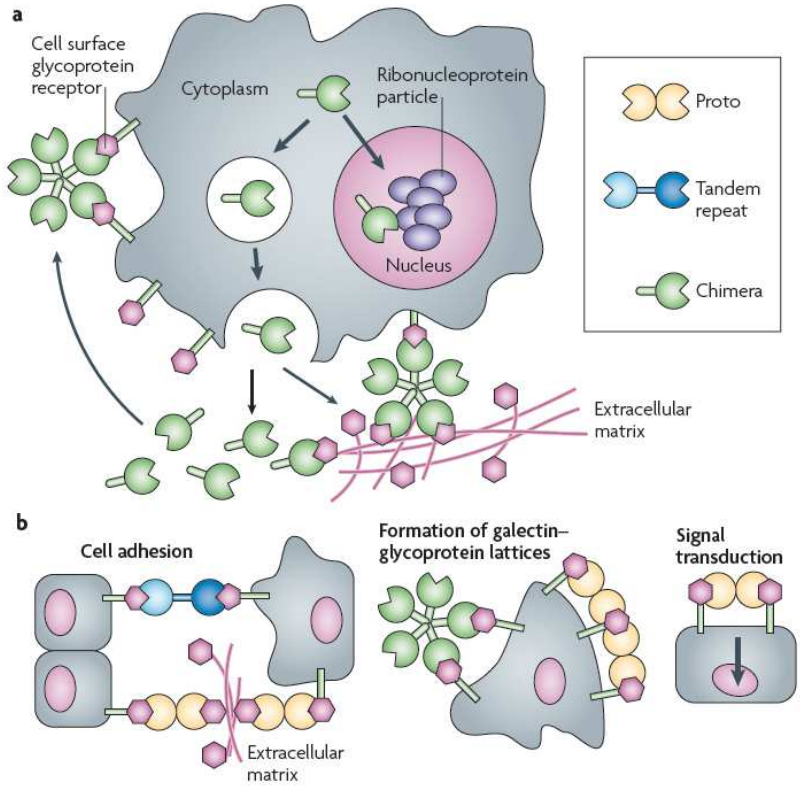

Figure 15. Galectin localization and biological functions. Galectins in the extracellular space can bind to glycans at the cell surface and crosslink them to the ECM. Galectins can also form lattices involved in signaling pathway activation. Extracted from [430].

Galectins are differently distributed in animal tissue and its expression is modulated during differentiation and tissue development, changing in some physiological and pathological conditions[428], such as in cancer[431-433]. Galectins are secreted by a non-canonical pathway[434-436] and display a wide variety of intra and extracellular functions[437-439] (Fig.15).

The galectin family has also been extensively characterized in zebrafish. This animal model is very appropriate to study galectin biological roles due to the presence of a very limited repertoire of galectins[440], which avoids redundancy problems, so frequent in murine models[441]. Members of the three different galectin families are present in zebrafish[442]: three protogalectins (Drgal1-L1, Drgal1-L2 and Drgal1-L3), a chimera galectin (Drgal3) and one tandem-repeat galectin (Drgal9-L1). Among them, Drgal1-L2, structurally and functionally resembles mammalian Gal-1, being also composed of four exons with intron boundaries conserved and maintaining the nine residues present in the CRD as well as the spatial position of the lateral chains of these AAs[443] (Fig.16).

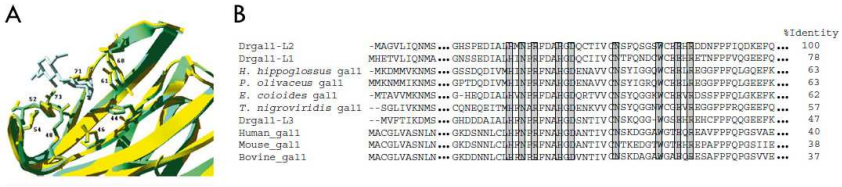

Figure 16. Homology of Drgal1-L2 with Gal-1. A) 3D structure of Drgal1-L2 (yellow) and bovine spleen Gal-1 (green), showing the sidechains of 9 conserved binding site residues of mammalian Gal-1. B) AA sequence comparison (alignment using ClustalW program: (clustalw.genome.ad.jp/) of Drgal1-L2 with mammalian Gal-1 or Gal-1 like proteins from lower vertebrates. Grey residues correspond to the ones interacting with *N*-acetylactosamine. Adapted from [440] and [444].

Studies analyzing Drgal1-L2 deficiency during development have found muscle fiber and blood vessel disorganization, suggesting a possible role for the lectin in skeletal muscle differentiation[444] and angiogenesis[445].

1.4.2 Gal-1: Structure and Functions

The first protein discovered in the human galectin family was Gal-1[446-448], which is encoded by *LGALS1* gene located in chromosome 22q12-13.1[449]. Splicing of its four exons results in a 0.6 Kb transcript that is translated into a protein of 135 AAs, without suffering any post-translational modification. The transcriptional activity of the mouse *Lgals1* gene is basically controlled by the region spanning the transcription start site (-63/+45)[450]. An Sp1 site (-57/-48) and a consensus initiatior element drive RNA synthesis from both the canonical start site as well as an additional one, mapped at position -31[451], which is responsible for more than 50% of Gal-1 mRNAs. Other characterized regulatory elements are the CAAT box, the NF-κB site and the retinoic acid and sodium butyrate response sequences[452], suggesting that Gal-1 expression might be modulated by histone acetylation[453]. The methylation status of Gal-1 promoter is also a very important mechanism of control of gene expression[454-456].

Gal-1 is a symmetrical dimer[424,443,457,458] of 14,5 KDa subunits and it has a β-sandwich "jelly-roll" conformation involving two parallel β-sheets, which form a central hydrophobic core holding both amino and carboxy-terminus of each monomer[459]. Gal-1 CRD has a

binding grove that allows the presence of a tetrasaccharide[427] (A, B, C and D). C site includes the eight conserved AAs responsible for galactose binding (Fig.17), and this is common among all galectins. The rest of the sites are involved in galectin recognition specificity. Both Gal-1 and Gal-3 typically lodge a terminal LacNAc in site C-D but binding is inhibited by the presence of NeuAcα2-6 in the galactose located in B. Functional differences and binding avidities between Gal-1 and Gal-3 suggest the existence of additional determinants of binding specificity[460,461].

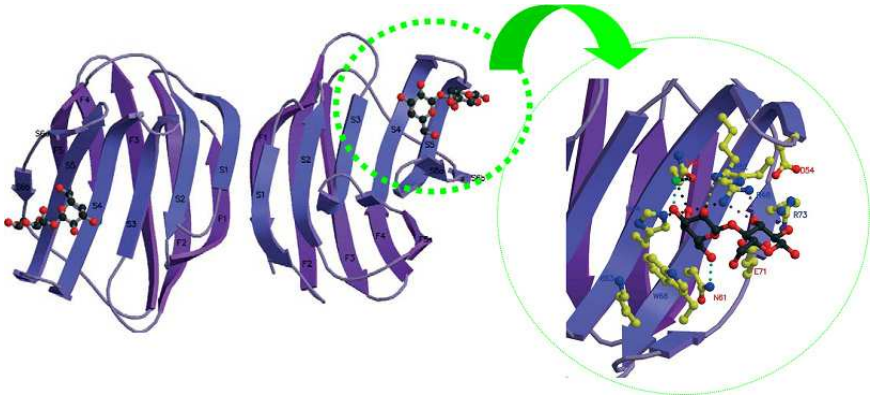

Figure 17. Human dimeric Gal-1 jelly-roll structure complexed with lactose. Ribbon diagram prepared with MOLSCRIPT. Five-stranded (F) and six-stranded (S) sheets of each monomer are labeled in the image and the AAs involved in lactose binding are highlighted in the enlargement (His44, Asn46, Arg48, His52, Asn61, Trp68, Glu71 and Arg73). Adapted from [459].

Gal-1 is found in the cytoplasm, membrane, ECM and nucleus[462], being involved in a wide variety of cellular functions through its ability to recognize many different proteins[463] (Tab.5). Extracellular functions depend on Gal-1 lectin activity whereas intracellular functions are usually independent and involve protein/protein interactions. Indeed, some of the domains involved in non-lectin interactions have also been identified, as the growth inhibitory site,

which consists of a surface loop involving 5 AAs, close to the N-terminus domain[464].

1.4.2.1 Gal-1 establishing Protein/Glycan Interactions

Gal-1 interactions involving its CRD domain and lectin activity are involved in many of Gal-1 important functions. Dimeric Gal-1 preferentially binds to *N*-acetylactosamine units (Gal-β1,4GlcNAc or LacNAc) arranged in multiantennary repeating chains[461,465,466]. Gal-1 interaction with glycans is greatly enhanced when it is surface-bound to cell membranes or to the ECM[467], reaching dissociation constants around 5 μM[468]. Actually, Gal-1 is involved in microdomain (lattice) formation within membranes by crosslinking ligands in a "glycoside cluster effect" that greatly increases its affinity[469-474]. Homodimeric Gal-1 dissociates at low concentrations (7 μM), and its monomers can still bind to carbohydrates but with lower affinity[466,475]. Gal-1 oxidized form lacks lectin activity[476].

In the ECM, Gal-1 displays high affinity for laminin[477], fibronectin[478], thrombospondin, vitronectin, osteopontin and glycosamine glycans such as heparan sulfate or chondroitin sulfate[479,480]. Depending on the cell type and cell activation status, these interactions finally lead to a pro-adhesive or an anti-adhesive effect.

Binding partners	Monomeric/ dimeric Gal-1	Binding type (P–C, P–P)	Cell/tissue types	Biological functions
β1 integrin	Dimeric			
α1β1, α7β1		P–C	Skeletal and vascular SMC	Adhesion, FAK activation
α5β1		P–C	Epithelial carcinoma cells	Inhibit ras-MEK-ERK pathway, increase p21 and p27, and growth inhibition
$\alpha_M\beta2$ integrin		P–C	Macrophage, neutrophils (?)	NS activation
1B2 glycolipid	NS	P–C	Olfactory axon in olfactory bulb	↑ cell–cell and cell–laminin adhesion
Actin	NS	P–P	Brain	NS
		P–C (?)	MOLT-4 T cells	
CA-125	NS	P–C	HeLa cells	Gal-1 export (?)
CD2/CD3	Dimeric	P–C	Jurkat T cells	Membrane redistribution, induction of cell death
CD4	Dimeric	P–C	T cell	NS
CD43	Dimeric	P–C	T cells	Membrane redistribution, induction of cell death
CD45	Dimeric	P–C	T, B cells	Membrane redistribution, induction of cell death
CD7	NS	P–C	T cells	Induction of cell death
Carcino embryonic antigen (CEA, CD66e)	NS	P–C	KM12 colon carcinoma cells	NS
Cytochrome oxidase subunit III	NS	P–P (?)	HeLa cells	NS
Fibronectin	NS	P–C	Ovarian carcinoma, placenta	↑ adhesion
Genim-4 nuclear and (?) cytoplasmic	NS	P–P	HeLa cells	preRNA splicing, RNA interference
Glycoprotein 90K (MAC-2BP)	NS	P–C	A375 melanoma cells	↑ cell aggregation
Glycosaminoglycan (chondroitin sulphate B, heparan sulfate)	NS	P–C	VSMC	Modulation of ECM assembly, ↓ adhesion
GM1 ganglioside	Dimeric	P–C	SK-N-MC neurobastoma cells	↓ growth
HBGp82	NS	P–C	Brain	NS
H-ras	Dimeric	P–P	HeLa, HEK293, Rat-1, 293T cells	↑ ras activation with selective activation of Raf-1/ERK pathway
Laminin	NS	P–C	Melanomas, myoblasts, ovarian carcinomas, Leydig cells, placenta	↑ adhesion
LAMP-1 (CD107a), LAMP-2 (CD107b)	NS	P–C	Ovarian, colon carcinomas	↑ adhesion
Mucin	NS	P–C	Epithelial glycocalyces of gastric and intestinal mucosa	NS

Table 5. Gal-1 binding partners. Description of the best characterized Gal-1 interactors, detailing Gal-1 quaternary structure (dimeric or non-specified (NS)), if it consists in a protein/protein interaction (P-P) or Gal-1 acts through its glycan recognition capacity (P-C), the cell and tissue type in which the interaction has been identified, and the consequent biological functions. (Adapted from [452], where detailed references can be found).

Gal-1 has many cell surface interactors resulting in very different effects (Tab.5). Glycosylated cell surface receptors are closely linked to the adhesive properties mediated by Gal-1. For instance, Gal-1 interaction with $\alpha_7\beta_1$ integrin interferes with integrin/laminin binding and controls cell adhesion[481]. Gal-1 interaction with neuropilin-1 (NRP-1) has been involved in migration and adhesion of ECs[482]. Gal-1 can also function as a regulator of the immune response through its interaction with CD7[483], CD45[468,484-486] and CD43[487]. Moreover, Gal-1 has also been involved in cell growth inhibition through its interaction with $\alpha_5\beta_1$ integrin[488], GM1 ganglioside[489,490] or the glycoprotein 90K/MAC-2BP[491]. Gal-1 can also recognize HBGp82[492] in the brain, CA125[493] in ovarian cancer cells, LAMP-1, LAMP-2 and CEA in colon carcinoma cells[494] and 1B2 glycolipid in olfactory axons[495].

1.4.2.2 Gal-1 establishing Protein/Protein Interactions

Regarding Gal-1 interactions independent of its lectin activity, protein/protein interactions occur intracellularly and involve Gal-1 in a set of very different functions. Gal-1 is able to bind to Gemin4, participating in splicing[496,497] and to pre-B cell receptor resulting in pre-BCR triggering[498]. Gal-1 also binds to H-Ras-GTP[499], promoting its membrane anchorage and subsequent cell transformation, an event that has been tightly linked to tumor progression (see section *1.4.3.1. Gal-1 in Tumor Progression*).

1.4.2.3 Gal-1 Knockout Mice

All these Gal-1 partners depict a very wide distribution of important physiological functions[452,500]. Nevertheless, animals that lack its expression are apparently normal, viable and fertile[501]. Gal-1 shows a broad pattern of expression during mouse embryogenesis[502] and it has been reported to be relevant in embryo implantation[502,503] and in the differentiation of the muscle cell lineage[504,505]. Yet, unexpectedly, mice development does not seem to be overtly affected by Gal-1 deficiency. However, detailed analyses have found that Gal-1 KO mice exhibit a major defect in primary olfactory neuron outgrowth and guidance[506], as expected considering its selective expression in the central nervous system development[507]. Moreover, careful examination of null-mutant mice has found that, although fetal survival is unaffected in syngeneic matings, Gal-1 KO mice show higher rates of fetal loss in allogeneic ones[508]. Other cellular abnormalities in Gal-1 KO mice have been observed under specific experimental conditions, like impaired B-cell development[509], more severe autoimmune neuroinflammation[460], alterations in peritoneal macrophages when recruited in response to inflammatory stimuli[510], greater Th1 and Th17 responses as well as increased trafficking of T cells to mesenteric lymphoid organs and inflamed tissues[511]. Gal-1 KO mice have also proven that Gal-1 binding to developing thymocytes can influence the strength of TCR signaling[512,513].

Two different theories are possible to explain the lack of an important phenotype in Gal-1 deficient animals: either Gal-1 is dispensable for embryogenesis, or redundancy with other galectins compensate for Gal-1 depletion. Gal-3 CRD shares considerable AA

sequence with Gal-1[514], and has very similar glycoconjugate binding specificities[515]. Nevertheless, Gal-1/Gal-3 double KO mice do not show major abnormalities[441], discarding Gal-3 as the galectin overlapping Gal-1 functions in development. Gal-5 remains a feasible candidate as, like Gal-1 and Gal-3, Gal-5 is also expressed at early stages of embryogenesis and share protein expression sites at the time of implantation[441].

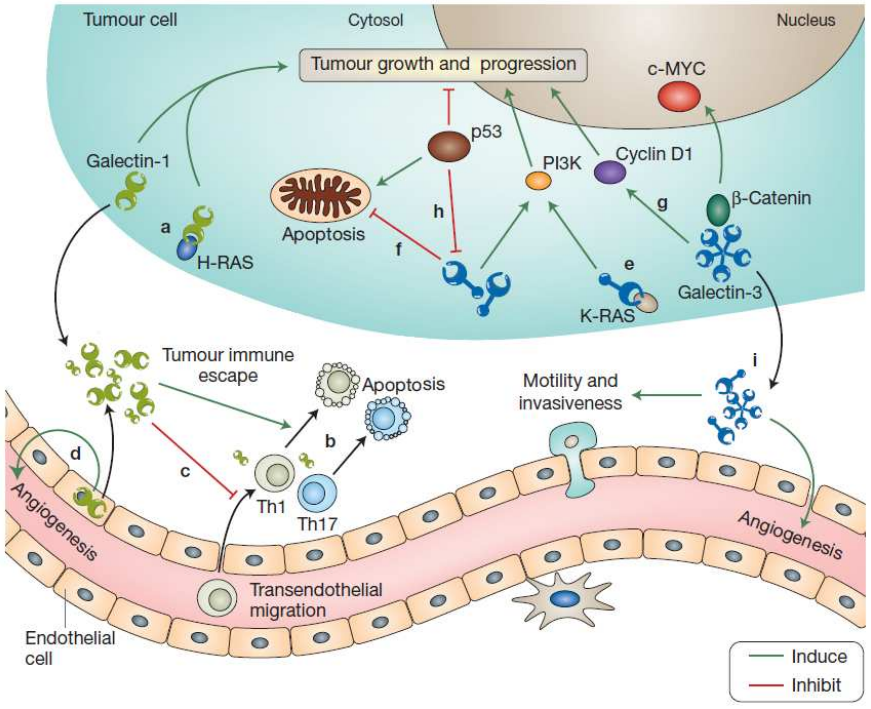

Figure 18. Galectins are involved in several aspects of tumor development both intracellulary and extracellularly. a) Gal-1 promotes H-Ras anchorage to the plasma membrane. b) Gal-1 induces apoptosis in activated T cells, modulates the Th1-Th2-Th17 cytokine balance and thus contributes to the tumor immune escape. c) Gal-1 impairs transendothelial migration of tumor-targeting T cells. d) Gal-1 promotes angiogenesis. e) Gal-3 interacts with K-Ras and promotes neoplastic transformation. f) Gal-3 is antiapoptotic. g) Gal-3 modulates the levels of regulators of cell cycle progression and proliferation such as cyclin-D1, c-Myc and β-catenin. h) p53 mediated apoptosis involves Gal-3 suppression. i) Gal-3 promotes cell migration, invasion and angiogenesis. Extracted from [428].

1.4.3 Galectins and Cancer

Galectins have been reported to be clear modulators of tumor progression[516,517] and their elevated expression usually correlates with tumor clinical aggressiveness and metastasis[432,518]. In particular, Gal-1, Gal-3 and Gal-9 are the best characterized members of the family, displaying important functions in several aspects of cancer biology including cell adhesion, migration, tumor transformation, apoptosis, cell cycle progression, angiogenesis and immune response regulation[516] (Fig.18). Indeed, galectin inhibitors have been well considered in cancer therapy[519-521].

1.4.3.1 Gal-1 in Tumor Progression

Gal-1 involvement in tumor progression is focused on different aspects[516]: neoplastic transformation, tumor cell proliferation and survival[522], angiogenesis, metastasis (through its role in adhesion, migration and invasion regulation[523]), and evasion from the immune response (Fig.19).

Inhibition of Gal-1 expression impairs **transformation** in glioma cells[524]. Among all Gal-1 partners, H-Ras could be the one closer linked to tumor transformation[499]. Gal-1 is involved in facilitating H-Ras-GTP presence on the cell membrane resulting in its stabilization and clustering in non-raft microdomains[525,526]. The subsequent binding of Raf-1 and Erk1/2 activation results in increased cell transformation[527,528]. This interaction is lectin independent and involves Gal-1 hydrophobic pocket[529]. Gal-1 is also very important in fibroblast activation in different tumor settings[530-533], and indeed,

Gal-1 knockdown (KD) in CAFs inhibits *in vivo* tumor progression in oral squamous cell carcinoma (OSCC) xenografts[531].

Gal-1 effects in **cell proliferation** are controversial. It is mitogenic in several cell types, such as in mammalian vascular cells[534] and hepatic stellate cells[535], but it is also able to hamper cell growth in other cell types, such as in stromal bone marrow cells[536]. Intracellular Gal-1 can induce not only cell cycle arrest but also **apoptosis** in cancer cells[537]. Gal-1 concentration seems to be key when deciding the final outcome: high doses (μM) of Gal-1 inhibit cell proliferation independently of its lectin activity whereas low doses (nM) are mitogenic through its ability to recognize carbohydrates[538,539]. Apart from this dose response effect, the cell type and cell activation status[540], the distribution of monomeric versus dimeric forms and Gal-1 compartmentalization might be also affecting the overall result on cell cycle progression.

Gal-1 has been actively involved in the long range dissemination of tumoral cells or **metastasis**[452], as it participates in adhesion, migration, motility and invasion[437,541,542]. Gal-1 can decrease tumor cell adhesion to the ECM, resulting in cell detachment from primary sites and invasion. Alternatively, the dimeric nature of Gal-1 allows crosslinking integrins on the cell surface of tumoral cells to proteins on the ECM[543,544], mediates tumoral cell/cell interactions favouring aggregation[491] and their interaction with ECs[545,546], facilitating tumor cell dispersion on the blood stream and establishment at distal sites during metastasis. In addition, Gal-1 has been also involved in invasion through adhesion independent mechanisms by upregulating well known ECM degradators like MMP-2, MMP-9 or by

reorganizing the actin cytoskeleton through Cdc42[542] or RhoA[541] upregulation.

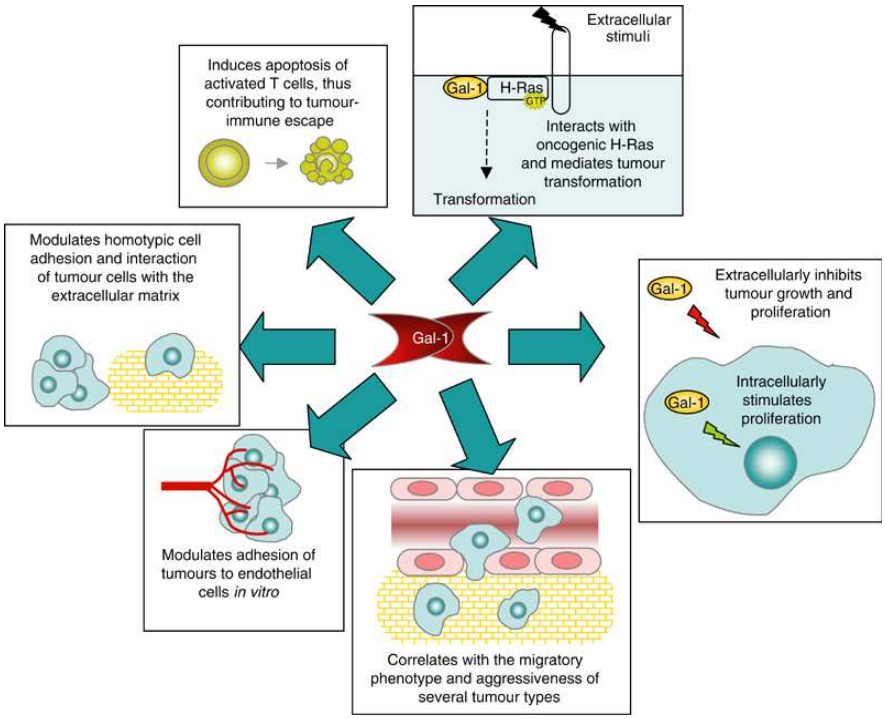

Figure 19. Gal-1 is involved in many different tumor progression events. Gal-1 interacts with oncogenic H-Ras and contributes to its membrane anchorage and tumor transformation. In addition, Gal-1 modulates cell growth, cell adhesion, cell migration and the immune response, thereby affecting the process of tumor metastasis. Extracted from [547].

Gal-1 also plays a key role in **angiogenesis** as it is able to stimulate the growth of vascular ECs[534]. The lectin is overexpressed in activated tumor endothelium[548] and it is involved in EC function[445] (by NRP-1 interaction and VEGFR-2 activation[482]). Gal-1 deficiency impairs tumor growth and angiogenesis *in vivo*[445,549]. Moreover Gal-1 modulates the expression of BEX2[549] and several hypoxia related genes involved in angiogenesis[550]. Paracrine mechanisms involving the uptake by ECs of Gal-1 secreted from tumoral cells have been

linked to EC activation and tumor angiogenesis stimulation[540], through Ras and Erk1/2 activation.

Finally, Gal-1 is involved in the **tumor immune response** promoting an immunosuppressive environment at tumor sites[551] by inhibiting full T-cell activation[552], triggering T cell growth arrest[553] and apoptosis[467,484,554] and protecting the tumor by negatively regulating Th1[460] and proinflammatory cytokines[508,555,556]. These effects are mediated by Gal-1 recognition of cell surface glycoproteins present on T cell membranes such as CD2, CD3, CD7, CD43 and CD45[487,557].

Taking into account Gal-1 functions as a master regulator of the immune response, targeted overexpression or Gal-1 delivery could be considered for inflammation-related diseases, whereas its inhibition should be promising in **cancer therapy**[547,558]. Indeed, downregulating Gal-1 expression inhibits migration and restores susceptibility to apoptosis and so to cytotoxic drugs[559,560], making the search for anti-galectin compounds a topic of high interest[521,561,562]. Moreover, Gal-1 also appears as a feasible **prognosis** and **diagnosis marker**[563]. Serum levels of the lectin have been reported to be useful to monitor tumor progression and clinical severity in patients with head and neck squamous cell carcinoma (HNSCC)[564] and ovarian carcinoma[565], for instance.

1.4.3.2 Gal-1 Expression in Tumors

Gal-1 expression has been identified as a prognostic factor for tumor progression in many different neoplasms[566], such as in

neuroblastoma[490], lymphoma[567], melanoma[554], glioma[541,568], astrocytoma[569], cholangiocarcinoma[570], HCC[455], OSCC[571], colon[572,573], thyroid[574], endometrium[575], HNSCC[576], lung[577], bladder[578], breast[579], prostate[580], ovary[581] and pancreas[582] carcinomas. Moreover, high Gal-1 expression correlates with poor tumor pathologic differentiation grades in OSCC[583]. Gal-1 overexpression is often linked to the stromal compartment of tumors such as in HCC[584], cholangiocarcinoma[570], HNSCC[576], OSCC[571] and in prostate[580], breast[579], pancreas[582], colorectal[585] and ovary carcinoma[581].

Not much is known about Gal-1 expression regulation in tumors. In HCCs, promoter hypomethylation is responsible for Gal-1 overexpression[455], and HIF-1α is able to drive Gal-1 protein expression by directly interacting with its promoter in colorectal cancer cells[586]. In neuroblastoma, TrkB is able to induce Gal-1 upregulation[587].

1.4.3.3 Galectins in Pancreatic Cancer

In pancreatic cancer, Gal-1 and Gal-3 are found to be overexpressed[582,588-590].

Gal-3 expression is faint in ductal cells of normal pancreas but it is high in IPMN[591], chronic pancretatitis, cancerous pancreatic tissue[582] and metastatic cells[592], suggesting its role in cancer cell proliferation and metastasis formation. However, decreased Gal-3 expression has been linked to advanced stage, tumor de-differentiation and metastasis in ductal adenocarcinomas[593], implying a fine tuned

regulation of its levels in different steps of tumor progression. Gal-3 secreted by pancreatic cells plays a role in PSC proliferation and in pancreatic cancer cell proliferation and invasion *in vitro*[594]. A negative correlation between anoikis and Gal-3 presence has been established, too[595]. Besides, the interaction between Gal-3 and Muc4 has been proven to be functional to dock tumor cells to the endothelial surface, what might present a possible mechanism to explain Gal-3 involvement in metastasis[592].

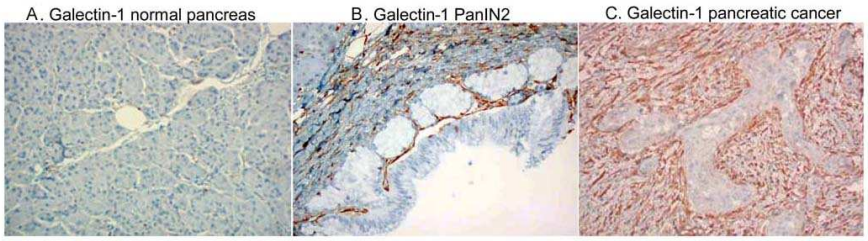

Figure 20. Gal-1 is overexpressed in precursor lesions and pancreatic cancer. Gal-1 IHC in human pancreatic normal tissue (A), in PanIN-2 lesions (B) or in pancreatic cancer tissue (C). Adapted from [596].

Gal-1 has found to be overexpressed in pancreatic tumors compared to normal tissue[582,589,597,598] (Fig.20), correlating with tumor histology and stage[590]. Interestingly, Gal-1 expression by immunohistochemistry (IHC) analysis has been reported to be mainly restricted to ECM and fibroblasts in and around the cancer mass, but not to pancreatic cancer cells[582,598], suggesting its importance in the so characteristic desmoplastic reaction. Gal-1 is also found in the stroma of pancreatic precursor lesions[596] (PanIN-2 and PanIN-3) and in chronic pancreatitis[599] (Fig.20).

Gal-1 could be involved in tumor progression in pancreatic cancer by remodeling the ECM in the formation of the desmoplastic reaction. Indeed, Gal-1 is able to induce activation (increased

collagen synthesis), proliferation and chemokine production (MCP-1 and CINC-1) of PSCs, through Erk1/2, Jnk, NF-κB and AP-1 activation. At the same time, activated PSCs secrete Gal-1, which can be acting autocrinely and might be also regulating the tumor immune response[532,533].

As it has been described above, Gal-1 displays a wide variety of biological functions which bring up a high degree of complexity when trying to understand its involvement in cancer. Thus, Gal-1 might not always tilt the balance in the same direction. In pancreatic cancer cells, for example, stable transfection of the tumor suppressor p16/Ink4a can induce Gal-1 expression and its affinity for the fibronectin receptor, resulting in increased susceptibility towards anoikis[600]. Another Gal-1 antitumoral role is presented by the fact that it is downregulated in gemcitabine resistant pancreatic cancer cells[601]. The ability of Gal-1 to induce opposite effects regarding proliferation and adhesion[437,522,538], as well as its reduced expression found in some tumors[602], hint at Gal-1 as a double side coin and question its nature as a pro-tumoral molecule. Many variables might be influencing the final outcome such as cell type and activation status, Gal-1 levels and localization, as well as its quaternary structure (see *Discussion,* section *3.2.1. Gal-1: a Dice with Many Faces*).

1.5 GLYCOSYLATION IN CANCER

1.5.1 Glycans: General Features and Synthesis

Glycosylation is one of the most common post-translational modifications and nearly half of all proteins in eukaryotes are glycosylated[603,604]. Glycans (oligosaccharides from glycoproteins) are classified considering their linkage to the protein backbone in N-Glycans (*N*-acetylglucosamine bound to the amide side chain of Asn) and O-Glycans (*N*-acetylgalactosamine bound to the hydroxyl of Thr or Ser). Their structural diversity is very complex taking into account the number and nature of monomeric units, their position, anomeric configuration and branching. Glycosylation of proteins can affect their folding, enhance solubility, intracellular trafficking, localization, secretion and rate of degradation[605]. Apart from conferring specific properties to proteins themselves, glycans significantly affect protein/protein interactions, preventing the non-specific ones. In this direction, they mediate accurate cell/cell communication and signal transduction as well as the interaction between a cell and the extracellular milieu and soluble signaling molecules[606-608]. Carbohydrate structures are key in many cell biological functions and indeed eighteen different types of congenital disorders of glycosylation (CDG) have been genetically defined[609].

N-glycans are synthesized in the endoplasmic reticulum (ER)-Golgi Apparatus (GA) compartment and are initiated by en-bloc transfer of a precursor glycan bound to dolichol phosphate ($Glc_3Man_9GlcNAc_2$-Asn-X-Ser, where X is not Pro). Glycosidases in

ER remove 3 glucose residues and a mannose. Further mannoses are removed in the GA until $Man_5GlcNAc_2$-Asn is generated, which suffers the addition of 2 GlcNAc and the elimination of two additional mannoses to generate the core of all complex glycans ($GlcNAc_2Man_3GlcNAc_2$-Asn). The trans-Golgi is responsible for glycan maturation by adding sugars to the core (fucose α1-6 to the first GlcNAc) or extending the branching to form polyLacNAc or capping elongated branches with sialic acid, for example[610,611]. Depending on the structure and location of oligosaccharides to the core, N-glycans can be classified into three groups: complex, high mannose and hybrid types (Fig.21). O-glycans, on the other side, are initiated by the addition of individual monosaccharides followed by extension, being a different enzyme in charge of each glycosidic linkage[612] (Fig.22).

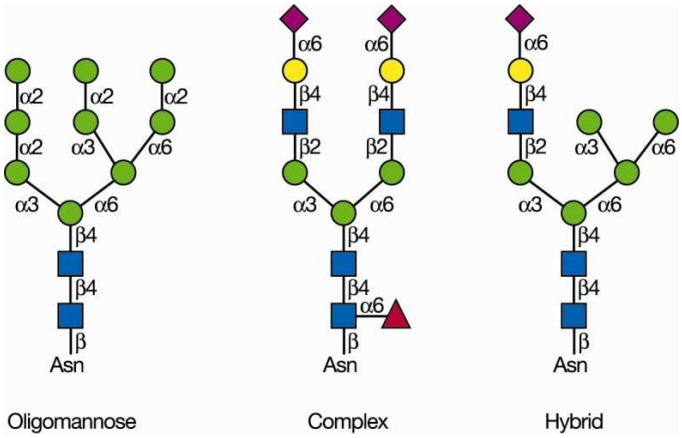

Figure 21. N-glycan classification. The core $Man_3GlcNAc_2$-Asn is fixed in all N-glycans but diversity appears according to the nature and localization of attached oligosaccharides. Oligomannosidic structures are exclusively composed of mannoses added to the core. Complex structures are formed by GalNAc in the antennae. Hybrid structures have mannose residues in the Manα1-6 arm and one or two GalNAc antennaes on the Manα1-3 arm. Extracted from [613].

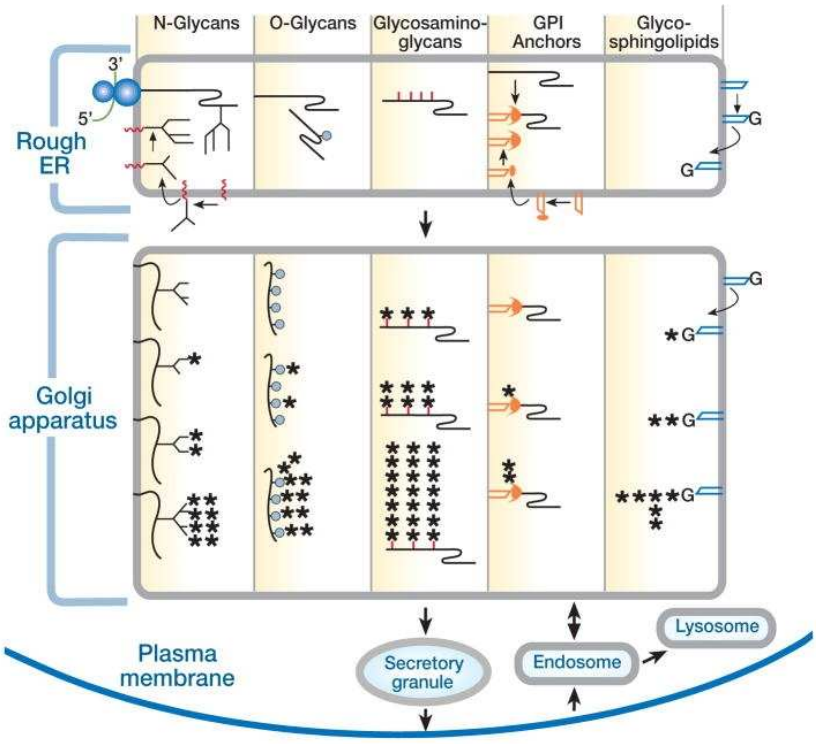

Figure 22. Eukaryotic glycosylation in the ER-GA system. Mechanisms responsible for initiation, trimming and elongation of the most common glycan structures in eukaryotes. Asterisks denote the addition of outer sugars to glycans. Extracted from[613].

Glycoproteins display site-occupancy heterogeneity (macroheterogeneity), which refers to the diversity on the presence or absence of glycan chains in specific AAs. Moreover, not all N-linked glycan sites are occupied[613]. Apart from this source of variation, glycoproteins also present site-specific heterogeneity (microheterogeneity), which describes differences found regarding the carbohydrate content and structure present in a single glycosylation site[614]. This diversity depends on enzyme kinetics but also on the metabolic flux[615,616].

1.5.2 Glycosylation in Cancer

Typically, cancer has been associated with gain-of-functions in oncogenes or loss-of-function in tumor suppressor genes. However, there are many other mechanisms responsible for orchestrating all the events triggering cancer stepwise progression. Aberrant glycosylation is one of cancer cell hallmarks[613], and certain structures are well-known markers of tumor development[605,617-619]. In fact, serum glycoproteins constitute the most frequent family of current tumor markers[620] and glycan-based therapies have been well considered in cancer treatments[621,622] (Tab.6).

Some of the best characterized glycan specific alterations in cancer are a general increase in sialic acid content[623-625], an increase in glycan branching[616,626-628] and overexpression of specific carbohydrate antigens like sialyl Lewis antigens (SLe^a and SLe^x)[629,630] (Fig.23). As mentioned above, the tight regulation of enzymes during protein glycosylation is crucial[631,632] and indeed, the populations of sugars attached to each glycosylated site depends on the cell type in which the glycoprotein is expressed and in the physiological status of the cell. Inflammatory cytokines and growth factors such as IL-1β, TNF-α, IL-6 and EGF[633-635] mediate changes in concentration of glycosyltransferases and glycosidases, altering the proportion of the glycoforms present in a particular glycoprotein.

Glycan involved	Proposed major function(s)	Possible therapeutic targeting	Examples of neoplasms
Growth and proliferation			
N-glycans	Suppress apoptosis; growth-factor signalling	Alkaloid inhibitors of N-linked processing	Breast, melanoma, Ewing's sarcoma
O-glycans	Mucin (MUC4)-mediated activation of ERBB2 receptors	Immunotherapy targeting MUC4 (similar to other mucin-targeting immunotherapy)	Breast
O-glycans	Suppress apoptosis (possibly through galectin-3 binding to tumour *O*-glycans expressing terminal galactose)	Galectin-3 inhibitors (β-galactosides)	Colon, pancreatic
Glycosphingolipids	Control of signalling through lipid rafts	Ceramide glycosylation inhibitors; ganglioside-targeted vaccines	Breast
Heparan-sulphate proteoglycans	Coreceptors for tumour growth factors	Heparin derivatives as heparan-sulphate competitors; sulphotransferase inhibitors	Pancreatic, ovarian, renal, hepatic
Hyaluronan	Signaling through hyaluronan receptors (for example, CD44)	Hyaluronan oligomers; adenoviral delivery of hyaluronan-binding protein genes	Colon, breast
O-GlcNAc	Modify oncogene phosphorylation	*O*-GlcNAc transferase inhibitors	Pancreatic
Tumour invasion			
N-glycans	Alter E-cadherin-dependent tumour adhesion	Alkaloid inhibitors of *N*-glycan processing	Breast, colon
N-glycans	Tumour repulsion (for example, polysialylation)	Sialyltransferase inhibitors	Neuroblastoma, lung (small cell)
O-glycans	Stimulate migration; potentiate migration of tumour cells through inhibition of cell–cell contacts (for example, sialyl Tn on mucins)	Vaccines (for example, conjugated sialyl Tn)	Breast, gastric, ovarian
Glycosphingolipids	Tumour repulsion (for example, G_{M3})	Glycosphingolipid inhibitors; ganglioside-targeted vaccines	Melanoma, neuroblastoma, breast
Heparan-sulphate proteoglycans	Matrix growth factor storage (heparanase substrate)	Heparin fragments and analogues; sulphotransferase inhibitors; xylosides; antisense RNA to perlecan	Breast, colon, hepatic, lymphoma, melanoma
Chondroitin-sulphate proteoglycans	Modulate tumour–matrix attachment	Xylosides	Melanoma, glioma, lung
Hyaluronan	Coordinate tumour growth signalling with cytoskeletal events during migration	Target tumour hyaluronan receptors (for example, gene silencing of CD44)	Breast
Tumour metastasis			
O-glycans	Facilitate tumour adhesion during haematogenous metastasis (SLe^X, SLe^A and other selectin ligands);	Disaccharide primers of glycosylation (reduce tumour SLeX); competition by intravenous heparin	Colon
N-linked and *O*-linked glycans	Promote tumour aggregation (galectin-3 binding)	Galectin-3 inhibitors (β-galactosides)	Melanoma
Glycosphingolipids	Tumour adhesion (sulphated selectin ligands)	Disaccharide primers; competition with heparin	Colon
Tumour angiogenesis			
N-glycans	Promote migration of endothelia	Alkaloid inhibitors of *N*-linked glycosylation	Prostate
Heparan-sulphate proteoglycans	Co-receptor for growth factors; matrix growth factor storage; co-receptor for matrix proteins	Heparin fragments and analogues; sulphotransferase inhibitors; xylosides; antisense RNA to perlecan	Colon, renal, melanoma, breast
Tumour immunity			
Glycosphingolipids	Immune 'silencing' (ganglioside shedding)	Ganglioside vaccines	Melanoma, neuroblastoma, breast

O-GlcNAc, *O*-linked N-acetylglucosamine; SLe, sialyl Lewis.

Table 6. Effects in tumor progression induced by different glycan families and possible therapy strategies associated to them. Adapted from [621], where detailed references can be found.

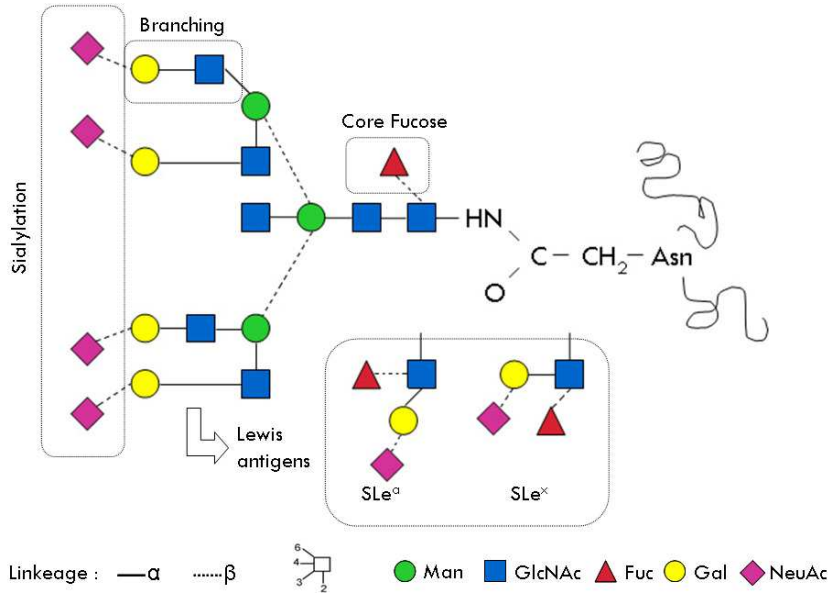

Figure 23. Most frequent N-glycan alterations found in tumors. Common features of cancer glycosylation include sialylation, increased β-1,6-branching, core fucosylation and sialyl-Lewis antigens. Adapted to Consortium for Functional Glycomics symbolism from [636].

Glycan alterations are functionally important in cancer progression by affecting cell proliferation and survival[637,638], adhesion and migration[639-642], angiogenesis and metastatic capability[643-646], as well as the immune escape[647]. A very common feature in cancer is the increased activity of β1-6-*N*-acetylglucosaminyltransferase V[648] (GlcNAcT-V or MGAT5), which is in charge of β1-6 branching of both O and N-glycans[628,630]. As a functional example of this fact, increased branching in the β_1 subunit of $\alpha_5\beta_1$ integrin due to enhanced MGAT5 expression, inhibits integrin clustering, reducing the attachment of cancer cells to fibronectin and thus inducing migration[642]. This enzyme is also involved in enrichment of the SLe^x group, which confers cells the ability to extravasate and metastasize. *In vivo*, progression of mammary tumors in $MGAT5^{-/-}$

mice is significantly impaired[649,650]. Various factors including oncogenes as Src, Her-2/neu, H-Ras, and V-sis and known cancer altered signaling pathways as Ras-Raf-Ets regulate MGAT5 transcription[651-653].

What still remains to be determined is whether changes in glycosylation are a cause or a consequence of transformation. Cytokine regulation of glycosyltransferase activity suggests that signaling from the tumor microenvironment can be the responsible for cancer-associated glycosylation.

1.5.2.1 Glycosylation in Pancreatic Cancer

Specific alterations in pancreatic cancer glycoproteins have been described, such as increased N-glycan branching and increased fucosylation and sialylation[654]. Importantly, some of the aberrantly glycosylated proteins have been suggested as biomarkers[636,655,656]. Lectin antibody microarrays have been used to detect unique glycosylation patterns in pancreatic cancer serum in high-throughput strategies[657,658]. These assays proved efficient specificity and sensitivity and shed some light in distinguishing between pancreatic cancer and chronic pancreatitis, a matter that has been for long unresolved[659]. Major alterations in glycan-associated gene expression associated to pancreatic cancer epithelial to mesenchymal transition (EMT) *in vitro* have been recently reported[660].

Data proposing some of the causes of altered glycosylation have emerged. Proinflammatory stimuli such as IFNγ, TNFα and IL-1α in

pancreatic cancer cells are responsible for altering Muc1, Muc5AC and Muc16 glycosylation in a cell type specific manner[658], and indeed cytokine secretion has also been considered in pancreatic cancer diagnosis[661,662].

One of the current pancreatic tumor markers is the monoclonal antibody CA19-9[663-666], whose epitope is the SLe^a antigen in gangliosides and mucins[667]. SLe^a physiologically functions in the extravasation of lymphocytes from the bloodstream by interacting with selectins on ECs. In accordance with these data, its expression on the surface of pancreatic cancer cells has been linked to metastasis spread to other tissue sites[668,669]. Nevertheless, CA19-9 generally does not have the specificity and sensitivity required for general screening[670-672], being frequently restricted to monitor patient's progress after surgery[673].

RNase-1 was long ago proposed as a tumor marker in pancreatic cancer[674] but both its levels and its activity in serum failed in diagnosis[675,676]. However, differences in glycosylation in this protein exist, finding neutral structures in healthy pancreas whereas charged structures (such as SLe^x and SLe^a antigens) and a significant increase in core fucosylation and sialylation[636,677-679] are observed in pancreatic cancer. Increased core fucosylation is a general cancer feature and it is also common in pancreatic cancer. Serum haptoglobin and acute phase proteins (APP) are also found to be more core fucosylated specifically in pancreatic cancer[655,680].

2 RESULTS

There are only two ways to live your life.
One is as though nothing is a miracle,
The other is as though everything is.

Albert Einstein

2.1 BIOCHEMICAL CHARACTERIZATION OF GAL-1/tPA INTERACTION

As referred in the Introduction, blocking tPA binding to specific pancreatic receptors would represent a new therapeutic strategy to abolish tPA "pro-tumoral" functions in the pancreas without altering blood coagulation homeostasis. Evidences that will be later shown in this manuscript clearly involved Gal-1 in tPA induced pathological events in pancreatic cancer, highlighting the lectin as a promising candidate for therapy (see section *2.2. Study of tPA/Gal-1 Interaction in vitro*). To establish the viability of this novel therapeutic strategy and thinking in the design of inhibitors, we focused our attention on the characterization of tPA/Gal-1 interaction domains.

2.1.1 Glycans are Involved in tPA/Gal-1 Interaction

Galectins are proteins from the lectin family, which display high affinity for β-galactosides. Gal-1 binds galactose, and lactose with even higher affinity, through its carbohydrate recognition domain (CRD). Tissue plasminogen activator is a glycoprotein, with 4 glycosylation sites. Thus, our first hypothesis was that tPA and Gal-1 interaction was N-glycan mediated. In order to know whether that was the case, surface plasmon resonance (SPR) was used to determine if carbohydrates were able to interfere with this interaction. Galactose (in a dose dependent manner) and lactose (with even higher effectiveness), inhibited tPA/Gal-1 interaction[421]. Proving galactose specificity, neither glucose nor cellobiose was able to do so. These data demonstrated that the Gal-1 CRD was involved

in tPA interaction and as expected, pointed at galactose in a β-anomeric position as its high affinity epitope.

We next wanted to carefully analyze the glycosylation sites involved, and identify the protein domains from tPA and Gal-1 that could be of relevance. X-Ray diffraction studies on tPA/Gal-1 crystals would allow mapping the interaction domains but the dimensions of this complex and the presence of glycosylation, made this possibility technically unfeasible, so alternative approaches were explored.

We started by reconfirming the involvement of tPA N-glycosylation in Gal-1 interaction by removing asparagine (Asn)-linked glycan chains with PNGaseF and checking for Gal-1 interaction. As mentioned in the Introduction, recombinant tPA is a mixture of two differently glycosylated isotypes. Type I tPA presents 4 glycans (Thr61, Asn117, Asn184 and Asn448) whereas type II tPA lacks the glycosylation present in the kringle 2 (K2) domain (Asn184). Proper N-deglycosylation was assessed by mass spectrometric (MS) analysis before and after the enzymatic reaction (Fig.23). The presence of a double peak before PNGaseF digestion was due to the two tPA isoforms, which differed on the presence of an additional glycan in type I tPA. As expected, those two peaks became one after N-glycosylation removal, rendering the crude protein with one single O-glycan.

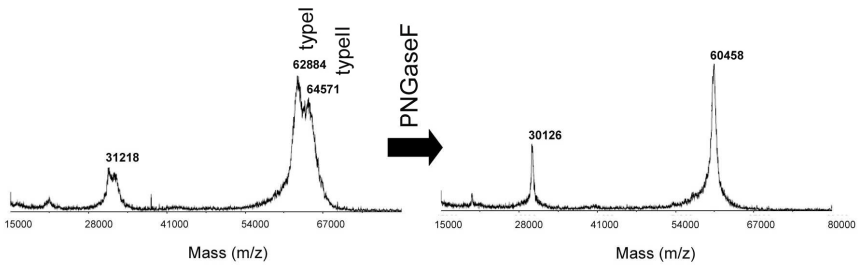

Figure 23. MALDI-TOF mass spectrum of tPA and de-N-glycosylated tPA. Mass spectrometric analysis of recombinant tPA (left) showed two peaks corresponding to type I (64,6 KDa, with 3 N-glycans) and type II (62,9 KDa, with 2 N-glycans). After de-N-glycosylation with PNGaseF (right), tPA showed a single and more narrow peak due to the lack of N-glycosylation, which converted the two type isoforms into a single molecule. The peaks found around 30 KDa corresponded to the double charged molecule.

Gal-1 interaction with recombinant tPA could be monitored by SPR experiments (Fig.24). However, tPA N-deglycosylation resulted in total absence of Gal-1 binding (Fig.24), what was in agreement with the sugar competition experiments previously mentioned[421].

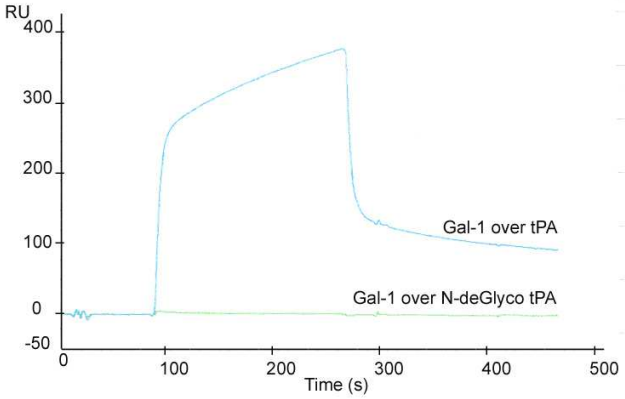

Figure 24. Role of N-glycosylation in Gal-1/tPA interaction assessed by SPR. Gal-1 (500 nM) differential response (relative to BSA) over immobilized tPA (with or without N-glycosylation (N-deGlyco)). During association phase (100-280 s), a mass increase over tPA surface was translated into a positive slope in the sensorgram. During dissociation phase (280-480 s), only buffer was flushed over tPA surface, what resulted in washing of non-specific binding. tPA/Gal-1 interaction was impaired in the absence of Asn-linked glycosylation.

2.1.2 Asn148 is Important for Gal-1/tPA Interaction

The fact that de-N-glycosylated tPA (still containing the single O-glycosylation site at Thr61) could not interact with Gal-1, discarded this O-glycosidic chain as being responsible for Gal-1 interaction. These data brought evidences towards the relevance of one or some of the three remaining N-glycosylation sites.

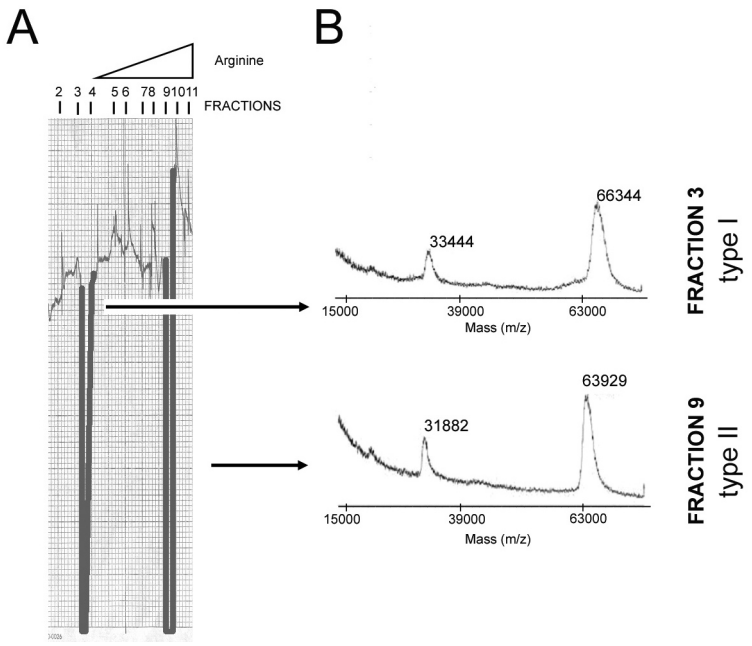

Figure 25. Type I/II tPA separation by Lys-sepharose chromatography. A) Signal obtained from a UV-visible detector and a recorder coupled to the Lys-sepharose column during affinity chromatography. An arginine gradient was applied from fraction 4 to 11 (0.025-0.2 M). 11 fractions were collected and subsequently analyzed for tPA presence. B) MALDI-TOF spectrometric analysis from the two fractions containing isolated tPA type I (fraction 3) and type II (fraction 9).

In order to elaborate on the analysis of the role of N-glycan chains in tPA/Gal-1 interaction, we took advantage of the existence of type I and type II tPA isoforms. To selectively assess the involvement of the glycosylation at Asn184 (only present at type I tPA), we separated both tPA isoforms and compared their ability to interact

with Gal-1 by SPR. This separation had been previously described by using affinity chromatography with a Lys-sepharose 4B resin[305,681]. We achieved proper tPA type I/II isolation and examined the presence of tPA isoforms in each fraction with a UV-visible detector and a recorder coupled to the chromatographic column (Fig.25A). Type II presented increased affinity for the column as retention of tPA to Lys-sepharose was mediated by K2 domain[682,683] and the presence of glycosylation in this site hampered interaction with the resin. MALDI-TOF mass spectrometric analysis of individual fractions allowed identification of type I/II isoforms and confirmed proper separation efficiency (Fig.25B).

We immobilized purified type I and type II tPA on a Biacore sensor chip to check for Gal-1 interaction. Recombinant tPA (the isoform mixture) was also used as a positive control. Type I tPA interacted with Gal-1 with approximately double affinity than type II, as it can be observed in the association and dissociation curves (Fig.26). Recombinant tPA showed intermediate affinity, just above type II tPA, suggesting that our mixture could be highly enriched in this isoform, as it had been previously observed in different contexts[681]. These data suggested that the glycosylaton at Asn184 was important for tPA interaction, although the fact that type II tPA was still able to bind Gal-1 outlined the participation of a second glycosylated site.

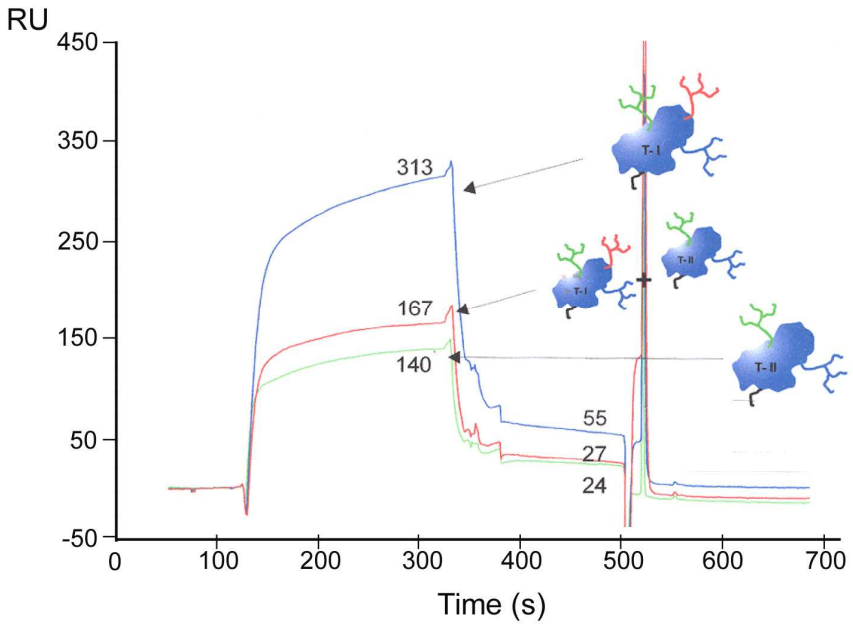

Figure 26. Type I and type II tPA/Gal-1 interaction assessed by SPR. Sensorgram showing the different binding affinities of isolated type I (blue; T-I) and type II (green; T-II) tPA, as well as the commercial recombinant mixture (red). Type I tPA (with an additional N-glycosylation at N184) showed double affinity for Gal-1 compared to type II tPA.

The differential glycosylation between type I and type II tPA isoforms seemed to affect its interaction with Gal-1. Therefore, we performed some preliminary studies to check whether this fact would be translated into a distinct *in vitro* behavior when Gal-1 was presented with the two different tPA isoforms. As will be later presented, Gal-1 was involved in tPA induced Erk1/2 activation in fibroblasts (see section 2.2.2.3. *Gal-1 Involvement in tPA Induced Erk1/2 Activation and Proliferation in Fibroblasts*). In that case, a commercial recombinant mixture of type I and II isoforms was added to cells. This time, we decided to assess the response when type I or type II tPA were individually added to F88.2. Consistent to what we had seen in SPR experiments, Western blot (WB) analysis showed that type I tPA was able to induce a much stronger Erk1/2 activation

compared to type II tPA (Fig.27), suggesting that glycosylation at Asn184 was key for Gal-1/tPA interaction. Comparable levels of Erk1/2 phosphorylation within rtPA and type I tPA suggested that it was probably this fraction I the responsible for Gal-1 interaction and Erk1/2 activation in the recombinant mixture. These data highlighted the importance of the glycan chains in tPA/Gal-1 functional outcomes.

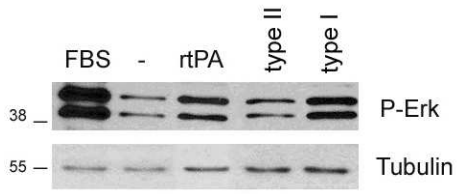

Figure 27. Erk1/2 activation induced by type I and type II tPA in F88.2 cells. WB of Erk1/2 phosphorylation (P-Erk) induced by 2% FBS, recombinant tPA (rtPA) or type I and type II tPA purified through affinity chromatography. Basal activation levels are shown in the negative control (-), in which no stimulus was added. Tubulin is shown as a loading control.

2.1.3 Kringle 2 and Serine Protease Domains of tPA and their Interaction with Gal-1

Glycosylation present at Asn184, which is exclusively present in type I tPA, contains complex and hybrid-type structures, very similar to the ones found at Asn448[295,302]. This similarity made us hypothesize that both Asn184 and Asn448 could be responsible for Gal-1 binding, albeit to a different extend. Besides, glycosylation at Asn117 contains oligomannosidic structures and lacks the galactose moiety to interact with a lectin[298]. Intringuingly, the fact that Gal-1 does not interact with all proteins containing terminal β-galactose residues and that Gal-1 affects tPA catalytic activity[421], suggested that modifications around the proteolytic active center could also

occur upon Gal-1 binding. Therefore, our hypothesis was that protein/protein interactions could also contribute to strengthen the interplay. In this regard, we focused our attention on the glycoprotein regions harboring Asn184 and Asn448, K2 and SP domains, respectively.

We generated two constructs containing tPA fragments with the key N-glycosylation sites. Kringle 2 (htPA-K2) domain (Asn184) and the serine protease (htPA-SP) domain (Asn448) were cloned in the mammalian expression vector pcDNA3/His. This vector contains a His-Tag that is fused to the N-terminal site of the protein of interest, allowing its detection by anti-His antibodies and its purification by Ni-agarose resine. CHO cells were chosen for expression because they were easily transfected and their glycosylation signature closely resembles the one found in man^{684}. In addition, this cell line has also been used to produce recombinant tPA for the clinic. CHO transfected with htPA-K2 or with htPA-SP domains in pcDNA3/His were first assessed at the RNA level by PCR analysis (Fig.28).

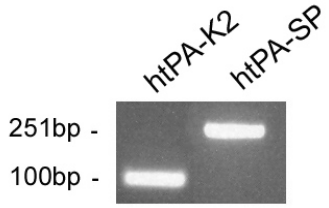

Figure 28. CHO cells expressing K2 and SP tPA domains. CHO cells were transfected with an expression plasmid (pcDNA-HisA) containing K2 or SP domains, which were detected at the RNA level by PCR.

We next aimed to detect htPA-K2 or htPA-SP at the protein level in order to purify these protein fragments and assess their ability to interact with Gal-1 by SPR. However, we are currently working on the purification of protein fragments from CHO cell extracts, where

we have encountered several problems. As previously mentioned, protein fragments were fused to a His-Tag in order to facilitate protein purification and identification but so far we have been unable to detect protein expression. The His-Tag antibody used is very non-specific and our attempts to detect fragments after Ni affinity column isolation have been in vain. Some reports have previously described limitations for His-Tag antibodies intrinsic to their nature [685], but our specific tPA antibodies were not specifically raised towards these K2 or SP fragments, which discarded them for recognition. Our efforts at the moment are directed to optimize culture conditions and the amount of protein produced.

If interaction with Gal-1 was clearly detected with some or both of tPA domains, we would consider their individual crystallization with the lectin and X-Ray diffraction. This technique would offer information to decipher protein conformation upon interaction and would help us identifying the aminoacids (AAs) which might be clue mediating protein/protein recognition. All these data would finally bring precious information towards the design of small peptides targeting tPA to avoid its interaction with Gal-1.

2.1.4 tPA Glycosylation Pattern in Pancreatic Cell Lines

The glycosylation profile of recombinant tPA has been previously described[686-688] but tPA glycosylation is reported to be cell line specific[295]. Differences in glycosylation have been associated to distinct physiologic and pathologic events, cancer among them[605,618].

Therefore, once proven that glycosylated chains from tPA were key for Gal-1 interaction, we wanted to determine the structure and composition of tPA produced and secreted by different tumoral and non-tumoral pancreatic cell lines. Serum free conditioned medium from cell supernatants was harvested and concentrated. tPA was detected by WB and several mobility differences were observed among different pancreatic cell lines (Fig.29). Interestingly, the cell line that presented an apparent significantly altered tPA mobility was HPDE, the only analyzed non-tumoral pancreatic cell line, which has been reported to resemble normal ductal cells[689,690].

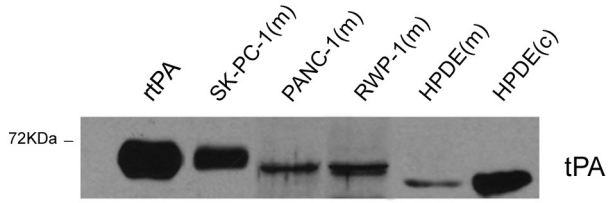

Figure 29. WB detection of tPA in pancreatic cell lines. rtPA (7 µg) and concentrated pancreatic cell conditioned mediums (m) or cell extracts (c) were analyzed for tPA expression.

tPA could be obtained from serum free cell supernatants or cell lysates. tPA glycosylation profiles determined from conditioned medium in RWP-1 cell line were compared to cell extracts and no overt differences were observed (data not shown), suggesting that both sources should provide the same structural information. Nevertheless, if possible, conditioned medium was prefered over lysates to reduce possible sources of protein contamination. HPDE cells produced high amounts of tPA but did not secrete the protein (see section *2.2.1.1. tPA and Gal-1 Expression in Pancreatic Cell Lines*, Fig.33), so cell extracts had to be used in this case. Recombinant tPA produced in CHO cells was used as a control, as their glycan structures had been previously described[686]. Proteins from lysates or

supernatants were separated by 2D-electrophoresis and detected by silver staining. According to the molecular weight observed by WB analysis, gel bands putatively containing tPA were isolated.

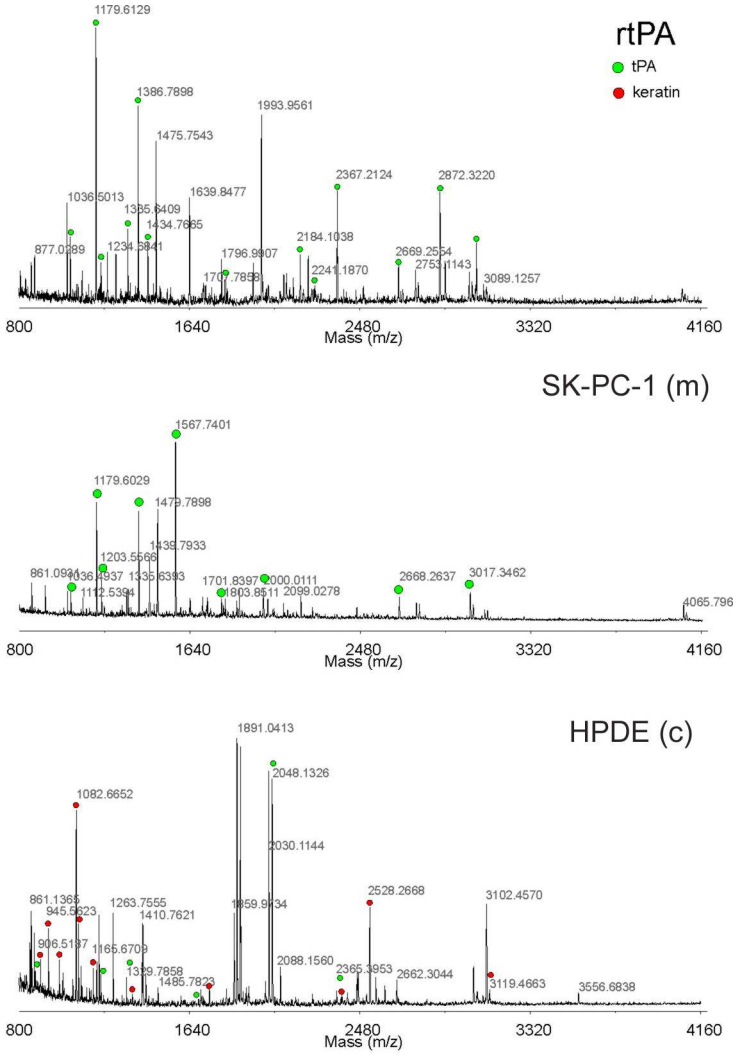

Figure 30. MALDI-TOF MS of peptides released by trypsin digestion from samples subjected to glycan analyses. Recombinant tPA (rtPA) or tPA from SK-PC-1 conditioned medium (m) or HPDE extracts (c), were analyzed by MALDI-TOF MS. Those peaks whose mass coincided with the theoretically predicted after trypsin digestion were identified as tPA peaks (green dots). Peaks matching with cytokeratins are also shown (red dots).

Glycosylated chains were released by in gel PNGAseF digestion and purified carbohydrates were fluorescently labeled and structurally analyzed by HPLC-FLD and MALDI-TOF MS. Protein digestion with trypsin and peptide MALDI-TOF MS was used to identify the proteins whose glycan fraction was subjected to analysis. tPA presence in the samples was confirmed by identifying several predicted tPA peptides (Fig.30). However, several cytokeratin peptides were also identified by MS, although their lack of Asn-linked glycosylation discarded them as a source of carbohydrate contamination.

Quantitative HPLC data collected from different pancreatic cell lines provided the type and relative amounts of each glycosylated chain present (Fig.31). Pancreatic cell chromatograms were compared to a partially hydrolyzed dextran matrix to determine the number of glucose units of each structure. Besides, several different control proteins with well established glycosylation profiles were used to gather information regarding the type of gycan chain corresponding to each chromatographic peak (see *Materials & Methods*, *Fig.119*). In this way, oligomannosidic and complex type glycan structures were identified. HPLC-FLD after sialidase and mannosidase treatment and ion-exchange chromatography (see *Materials & Methods*, *Fig.120*) brought additional knowledge regarding monosaccharide content and linkage, which enabled hypothesizing different structures for each glycosylated chain (Fig.31).

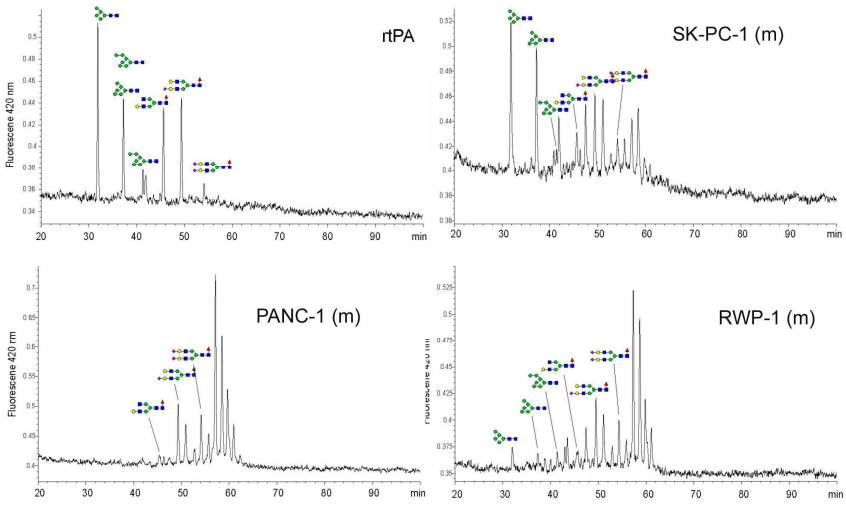

Figure 31. HPLC analyses from fluorescently labeled tPA glycans. Recombinant tPA (rtPA) or tPA from SK-PC-1, PANC-1 and RWP-1 conditioned medium (m) were analyzed by HPLC.

Although MALDI-TOF MS is not a quantitative technique, it provided the overall mass of each glycosylated chain, enabling assigning its exact composition and structure (Fig.32). Joint data collected from both techniques was merged, allowing a description of tPA glycan structures. Several structures previously described for tPA were recognized in pancreatic cancer cell lines. Nevertheless, for HPDE, MS analysis described the presence of several glycosylated chains lacking core fucosylation, a structure that was repetitively found in all other tumoral cell lines. These data were interesting considering that α1-6 fucosylation of the core *N*-acetylglucosamine is most commonly found in cancer compared to normal situations (see *Introduction*, section *1.5.2. Glycosylation in Cancer*).

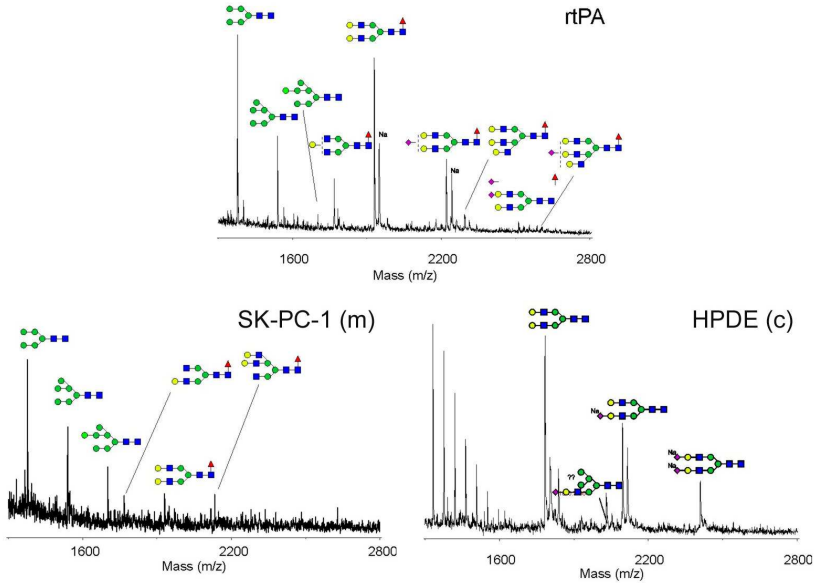

Figure 32. MALDI-TOF MS of glycans from tPA. Recombinant tPA (rtPA) or tPA from SK-PC-1 conditioned medium (m) or HPDE cell extracts (c) were analyzed by MALDI-TOF MS. Peaks were assigned to possible structures according to their mass.

These data are still incomplete and considered preliminary as technical problems due to low sample availability, result in low reproducibility and hamper final structural analysis. Thus, further experiments will be required to clearly identify the pattern of glycosylation of tPA from different pancreatic cell lines and to establish whether the presence of a cancer specific glycosylation profile exists for this protease.

2.2 STUDY OF tPA/GAL-1 INTERACTION IN VITRO

2.2.1 tPA & Gal-1 in the Pancreatic Tumor Epithelium

2.2.1.1 tPA & Gal-1 Expression in Pancreatic Cell Lines

Gal-1 has been previously reported to be overexpressed in pancreatic tumors[589,598], although immunohistochemistry (IHC) data are few and mainly restrict its expression to the stroma[582]. In contrast, tPA is found in ducts of human PDAC lesions[360]. To find a convenient *in vitro* system, we analyzed Gal-1 and tPA expression in a panel of different ductal pancreatic cell lines: HPDE, SK-PC-1, SK-PC-3, PANC-1, BX-PC-3, Hs766t and RWP-1. Cell lysates were prepared and analyzed for Gal-1 and tPA expression by WB (Fig.33).

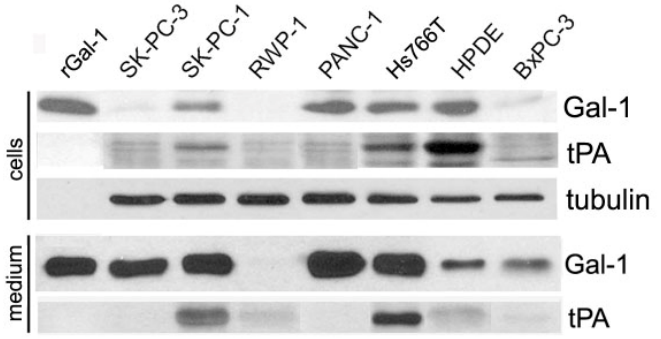

Figure 33. Pancreatic epithelial transformed cells expressed and secreted tPA and Gal-1. WB analysis of endogenous Gal-1 and tPA (cells) and secreted (medium) levels in different pancreatic cell lines. Protein levels were normalized with tubulin. 40 ng of recombinant Gal-1 (rGal-1) were loaded in the first lane.

Moreover, and taking into account that both proteins can be secreted, we also assessed their levels in serum free conditioned medium (CM) obtained from the same cell lines. We found that tPA was expressed at high levels in SK-PC-1, HPDE and Hs766T cells, whereas RWP-1 cells expressed the protease in lower amounts. For

Gal-1 expression, we found that all of them but RWP-1 did secrete the lectin in high levels (Fig.33). tPA interaction with endogenous Gal-1 from PANC-1 and SK-PC-1 cells was confirmed by immunoprecipitation experiments[421].

To further clarify whether secreted Gal-1 was bound to the membrane of pancreatic cell lines, biotinylation experiments were performed, confirming that Gal-1 was not only found intracellularly and in supernatants, but also bound to the cell surface[421].

2.2.1.2 Gal-1 Involvement in tPA Induced Migration

Tissue plasminogen activator is a protease involved in ECM degradation by plasmin activation and it has been reported to be localized in the migration front of pancreatic tumoral cell lines[360]. To determine whether Gal-1 could be involved in tPA induced cell migration in pancreatic cancer, wound healing experiments were performed in PANC-1, SK-PC-1 and HPDE cells (Fig.34).

Gal-1 was nearly undetectable in confluent monolayers by immunofluorescence (IF). However, it clearly redistributed to be localized in the cell migration front after a wound stimulus (Fig.34, arrows).

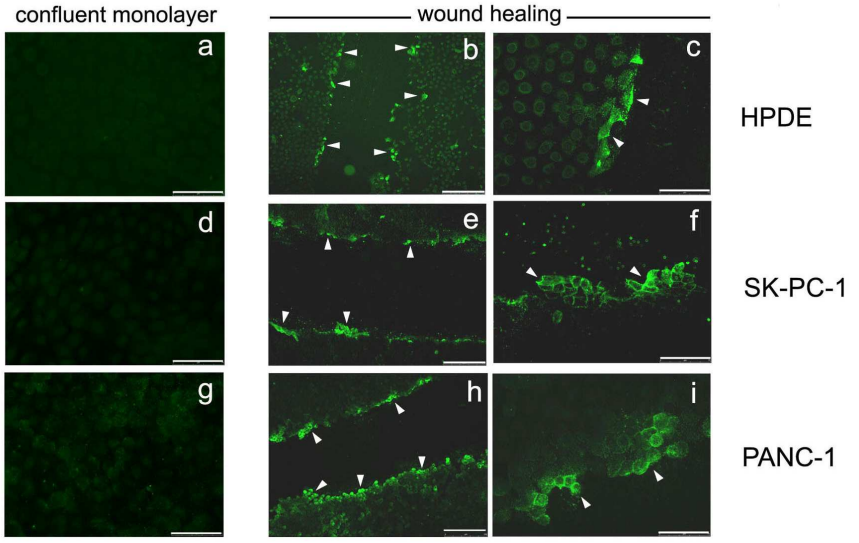

Figure 34. Gal-1 detection in a confluent monolayer and in the migration front in pancreatic cell lines. Immunocytofluorescence images from a confluent monolayer in HPDE (a), SK-PC-1 (d) and PANC-1 (g) cells, showing no overt detectable expression. However, Gal-1 seemed to be redistributed and localized in the migration front in HPDE (b,c), SK-PC-1 (e,f) and PANC-1 (h,i). Scale bars represent 75 μm (a,c,d,f,g,i) and 250 μm (b,e,h).

Concerned about the fact that artifacts are commonly found in edges of IF preparations, we performed two negative controls to ensure signal specificity. On one hand, competition experiments were carried out by preincubating the antibody with the recombinant protein (1:5 ratio, respectively) before adding the mixture into living cells (Fig.35b). In this case, no signal was observed, validating proper antibody recognition. On the other hand, no Gal-1 redistribution was observed if cells were immediately fixed after wounding the confluent surface, without allowing time for the protein to arrange at the migration front, which further confirmed signal specificity (Fig.35c).

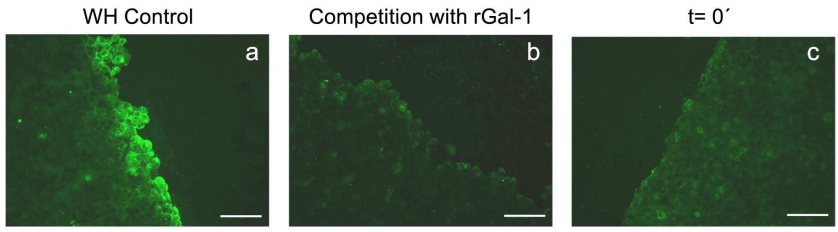

Figure 35. Wound healing controls in PANC-1 cells. Gal-1 was clearly detected at the migration edge during wound healing experiments (a). Signal was competed when the antibody was pre-incubated with human rGal-1 (1:5 ratio, respectively) (b) or when cells were immediately fixed after scratching the confluent monolayer (c). Scale bars represent 100 µm.

To check if the lectin distribution under a migration stimulus agreed with that of tPA, we performed double IF in SK-PC-1 cells, which expressed and secreted high amounts of both proteins (Fig.33). tPA was also observed in the migration edge, although it showed a wider distribution all over the confluent monolayer. Confocal microscopy images showed colocalization of tPA and Gal-1 in some areas of the migration front, suggesting that their interaction could be important in tPA induced migration (Fig.36, arrows).

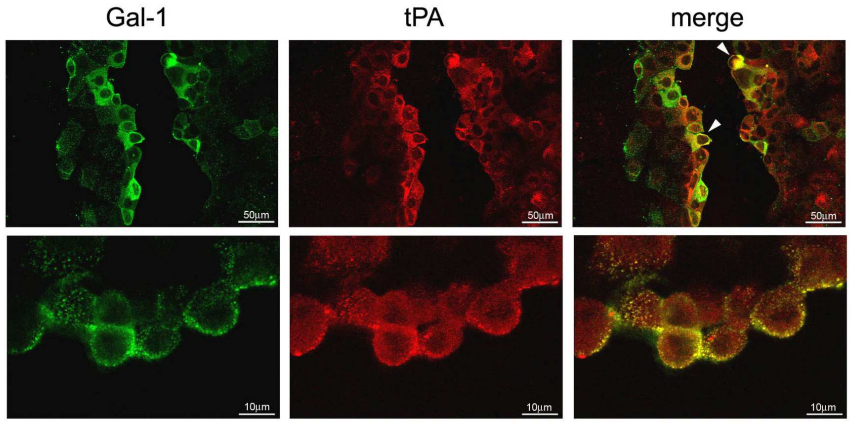

Figure 36. Gal-1 and tPA colocalized at the migration front. Double IF detection of Gal-1 (green) and tPA (red) by confocal microscopy, showing colocalization (yellow) areas in the membrane of cells located in the migration edge. Scale bars are indicated in the figure.

2.2.1.3 Gal-1 Involvement in tPA Induced Erk1/2 Activation and Proliferation

tPA has been previously reported to be mitogenic in pancreatic cancer *in vitro*[416] and *in vivo*[418] and our group has demonstrated that these effects are independent of its proteolytic activity and are mediated by Erk1/2, involving AnxA2 and EGFR[318]. tPA addition to pancreatic cells induced rapid Erk1/2 activation (2-5 min), which was maintained for at least 15 min[318]. To verify whether Gal-1 could also be involved in tPA induced activation of Erk1/2 signaling pathway, we knocked down Gal-1 expression by siRNA mediated silencing in pancreatic cells, achieving a 90% reduction in total Gal-1 cellular levels up to 5 days after transfection (Fig.37A). Erk1/2 phosphorylation was assessed in cells with low Gal-1 levels and compared to non-transfected (-siRNA) or cells transfected with an irrelevant siRNA (+siCtrl)). Cells with low Gal-1 levels showed a strong decrease in Erk1/2 activation (Fig.37B), whereas transfection with an irrelevant siRNA did not affect Erk1/2 phosphorylation levels. Interestingly, Gal-1 reduction did not affect the ability of these cells to respond to other growth factor stimuli (+), indicating that Gal-1 effects were specific for tPA. These data demonstrated that Gal-1 was clearly involved in tPA induced Erk1/2 activation in pancreatic epithelial transformed cells.

Previous data from our group had shown that tPA induced Erk1/2 activation was responsible for the proliferative effects mediated by tPA in pancreatic cancer. Interestingly, our group found that the increase in proliferation induced by tPA in PANC-1 and HPDE cells was impaired when cells displayed low Gal-1 levels, suggesting that

the lectin was also involved in tPA induced proliferation in pancreatic transformed cells[421].

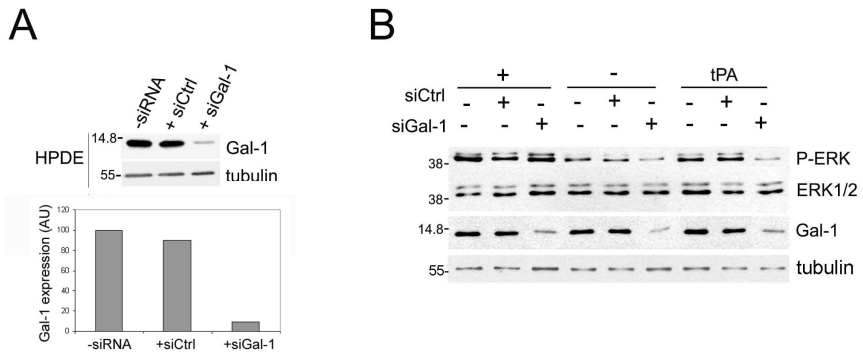

Figure 37. Gal-1 was involved in tPA induced Erk1/2 activation *in vitro*. A) siRNA for Gal-1 (siGal-1) efficiently reduced its protein levels. HPDE cells were transiently transfected with siRNA and Gal-1 levels were assessed by WB 5 days afterwards. Non-transfected cells (-siRNA) or cells transfected with an irrelevant siRNA, were used as controls (+siCtrl). Protein levels were normalized with tubulin. Protein quantification is shown in the lower panel. B) Gal-1 deficiency impaired proper tPA induced Erk1/2 activation. Non-transfected cells or cells tranfected with the irrelevant siRNA (siCtrl) showed increased Erk1/2 activation when treated with growth supplements for 5 min (+) or tPA at 20 μg/mL for 10 min.

2.2.1.4 Gal-1 Involvement in tPA Induced Invasion

tPA has been linked to pancreatic cell invasion *in vitro*[360,416]. In order to determine if Gal-1 was mediating this process, we performed invasion assays over matrigel coated transwells. Three cell lines with different invasive capabilities were used: SK-PC-1 and HPDE (with high tPA levels) and PANC-1 (without tPA). To evaluate Gal-1 importance in invasion, we reduced its levels using the siRNA technique, obtaining efficient reductions of 90% in HPDE, 70% in SK-PC-1 and 60% in PANC-1 (Fig.38A). siRNA transfection procedure *per se* did not alter the invasive capability as untransfected cells behaved similarly as cells transfected with an irrelevant siRNA (siCtrl). However, cells with low Gal-1 levels displayed impaired

invasion ability over matrigel (Fig.38B), corroborating Gal-1 previously reported role in this process in other cell systems[568,691]. To link Gal-1 mediated invasion and tPA, PANC-1 cells were used. In this cell line, recombinant tPA was able to exert a significant increase in invasion, but this phenotype could be completely reverted in the absence of Gal-1 (Fig.38B). These data clearly demonstrated that Gal-1 was involved in tPA-mediated invasion in pancreatic transformed cells.

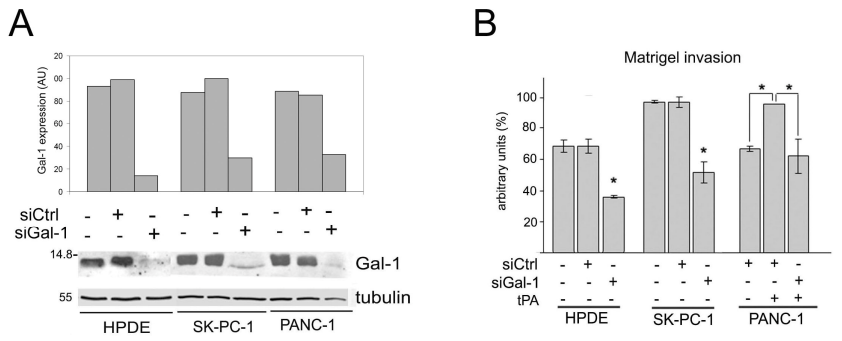

Figure 38. Gal-1 and tPA in pancreatic cell invasion *in vitro*. A) Gal-1 knockdown efficiency by siRNA technique assayed by WB (lower panel) and its quantification 5 days after transfection. HPDE cells showed a 90% reduction, SK-PC-1 cells 70% reduction and PANC-1 60%. B) Untransfected cells or cells transfected with an irrelevant siRNA (siCtrl) showed similar 72 h invasion values over matrigel coated transwells, determined using crystal violet staining. However, siRNA for Gal-1 (siGal-1) impaired invasion in HPDE and SK-PC-1. tPA at 20 µg/mL was able to induce an increase in PANC-1 invasion but this increase was ablated when cells had low Gal-1 levels, suggesting that Gal-1 was involved in tPA induced invasion in vitro. *$p<0.05$ (unless specified, statistics are calculated with t test analysis, see *Matherials & Methods*, section *5.5. Statistical Analysis*).

2.2.2 tPA & Gal-1 in Desmoplasia

2.2.2.1 tPA & Gal-1 Expression in Fibroblasts

Gal-1 and tPA expression were also analyzed in normal pancreas and in tumors from Ela-1-myc mice[421]. tPA was overexpressed in

ductal cells, as it had already been reported before[418], resembling its pattern of expression found in human PDAC[318]. Gal-1 in Ela-1-myc mice was sometimes observed in ductal tumoral cells but repeatedly in the stromal compartment[421], where its overexpression in human PDAC seems to be predominant[582]. Neither tPA nor Gal-1 were expressed in normal acinar or ductal cells[421].

Epithelium/stroma interactions are crucial in tumor progression and in particular in pancreatic cancer, which is characterized by an extensive desmoplastic reaction. This event is so commonly found in PDAC that it has been described as one of its hallmarks, whose functional relevance is not yet well understood. Considering that tPA is a secreted molecule and the vast expression of Gal-1 in the stroma, we wondered whether their interplay could be functionally relevant in the tumor microenvironment.

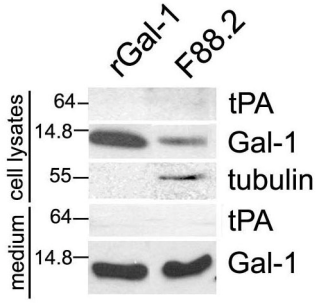

Figure 39. tPA and Gal-1 expression in F88.2 cell line. Intracellular (cell lysates) and secreted (medium) tPA and Gal-1 levels assessed by WB analysis. tPA was not expressed in F88.2 whereas Gal-1 was clearly detected both in its cell lysates and in a secreted manner. Tubulin is shown as an endogenous protein control and 40 ng of recombinant Gal-1 were loaded in the first lane.

We first studied Gal-1 and tPA expression in the F88.2 fibroblastic cell line. Gal-1 was detected in high levels, both intracellulary and also in a secreted manner, while no tPA expression was found (Fig.39).

In vitro interaction between exogenous tPA and endogenous Gal-1 from F88.2 cells was successfully detected by pull-down experiments using recombinant tPA over F88.2 lysates[421].

2.2.2.2 Gal-1 in Fibroblast Migration

To determine whether Gal-1 was important for fibroblast migration, we performed wound healing experiments and checked Gal-1 expression by IF. As described for pancreatic cell lines, Gal-1 in F88.2 was undetected in a confluent monolayer of cells but it redistributed to appear in the migration front, corroborating its known general importance in the migration event (Fig.40).

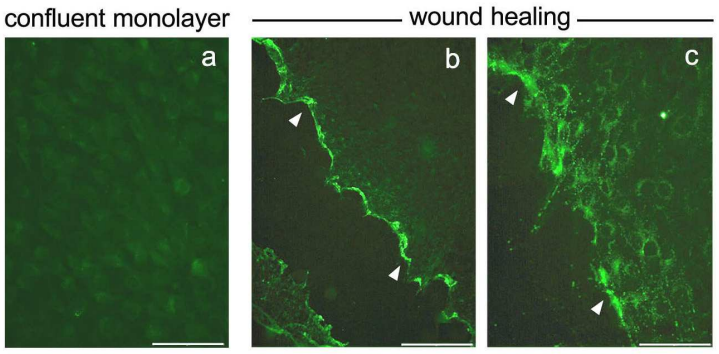

Figure 40. Gal-1 expression in fibroblasts during migration. Gal-1 was almost undetectable by IF in a confluent monolayer of F88.2 cells (a) but it was rapidly rearranged in the migration front after wounding (b,c). Scale bars represent 75 µm (a,c) and 250 µm (b).

2.2.2.3 Gal-1 Involvement in tPA Induced Erk1/2 Activation and Proliferation in Fibroblasts

Recombinant tPA was able to exert a panel of effects over fibroblasts similar to those triggered in pancreatic transformed cell

lines. For example, exogenous tPA was responsible for increased Erk1/2 phosphorylation in fibroblasts *in vitro* (Fig.41). To decipher whether Gal-1 was involved in tPA induced Erk1/2 activation in F88.2, we knocked down the lectin using siRNA mediated silencing. Specific Gal-1 targeting with siRNAs induced up to 70% protein downregulation (Fig.41A). tPA induced Erk1/2 phosphorylation was markedly impaired in the absence of Gal-1, whereas this depletion did not affect FBS mediated signaling pathway activation, indicating that the effects were tPA specific (Fig.41B). These data demonstrated that Gal-1 was involved in tPA triggered Erk1/2 activation not only in pancreatic cell lines but also in fibroblasts.

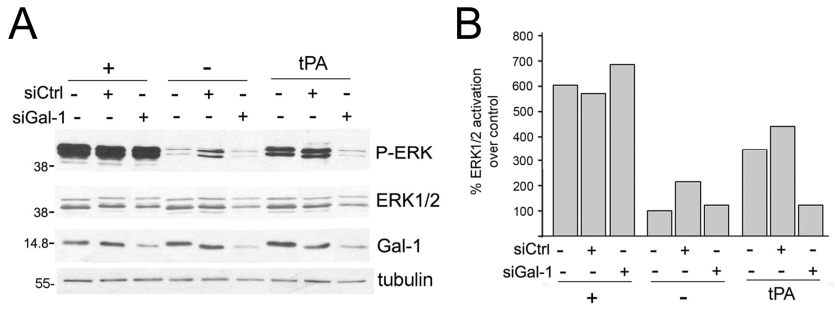

Figure 41. Gal-1 participation in tPA induced Erk1/2 activation in fibroblasts. A) Erk1/2 phosphorylation levels assessed by WB analysis. Erk1/2 was induced 2 min after exogenously adding 5% FBS (+) and 10 min after tPA addition (20 µg/mL, 10 min) in control cells (untransfected or transfected with an irrelevant siRNA (siCtrl)). However, siRNA mediated downregulation of Gal-1 specifically impaired tPA induced Erk1/2 activation. Total Erk1/2 and tubulin levels were used as loading controls. B) Quantification of the WB data.

Thymidine incorporation analysis performed in our group revealed that tPA induced proliferation was also blocked when cells displayed low Gal-1 levels, suggesting that this protein was mediating tPA mitogenic effects in fibroblasts[421].

2.2.2.4 Gal-1 in tPA Induced Invasion in Fibroblasts

Exogenous tPA was able to increase the moderate basal invasive capacity of F88.2 cells (Fig.42B). In order to find out if Gal-1 was involved in tPA induced invasion in fibroblasts, we downregulated the lectin and assessed the ability of these cells to invade through matrigel coated transwells. Protein depletion of 70% using siRNA (Fig.42A), reverted F88.2 invasion levels to the basal situation (without tPA stimulation) (Fig.42B). This fact suggested that Gal-1 was clearly essential for fibroblastic cells to invade upon tPA addition.

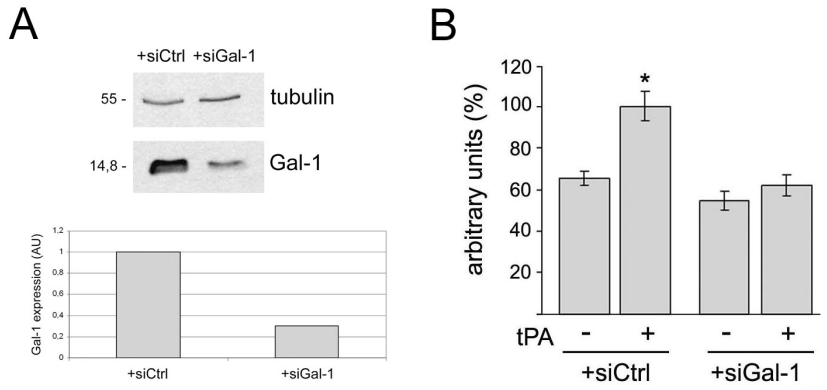

Figure 42. Gal-1 was involved in tPA induced invasion in fibroblasts. A) Gal-1 downregulation after siRNA transfection assessed by WB analysis. Tubulin levels are shown as the loading control. Protein levels were reduced in 70%. B) Recombinant tPA at 20 µg/mL was able to increase F88.2 invasion over matrigel coated transwells significantly. However, upon Gal-1 downregulation, tPA induced invasion was impaired. Invasion levels were quantified through crystal violet staining of cells that invade through matrigel and absorbance was read at 550 nm. *$p<0.05$.

2.2.3 tPA/Gal-1 Interaction in the Interface Between Epithelial Cells and Fibroblasts *in vitro*

Double IF analysis of tPA and Gal-1 in Ela-1-myc tumors showed focal colocalization at the interface of epithelial cells and stromal fibroblasts[421].

As tPA is absent in fibroblasts *in vitro* as well as in the stroma *in vivo*, we hypothesized that the possible source of tPA triggering its pathological effects in mesenchymal cells could be epithelial cells. These data suggested a new epithelial/stroma crosstalk that had never been reported before in pancreatic cancer, nor in any other neoplasm, whose relevance could be huge in the desmoplastic reaction.

In an attempt to reproduce the epithelial/fibroblast crosstalk *in vivo* and to examine the putative Gal-1 involvement in this scenario, we analyzed the effects of pancreatic CM over fibroblast invasion, using cells with normal (siRNA Ctrl) or downregulated (siRNA Gal-1) levels of Gal-1.

Pancreatic cancer cell supernatants were used as chemoattractants in fibroblast invasion assays over matrigel coated transwells (Fig.43). SK-PC-1 supernatants, which secrete tPA in high amounts, induced a significant increase in basal fibroblast invasion. This effect could be reverted by adding the tPA inhibitor PAI-1, suggesting a catalytic requirement for tPA mediated invasion. To further identify tPA as the secreted factor mediating invasion, PANC-1 cells (which do not produce tPA) were used. Addition of PANC-1 conditioned medium

did not have any impact on fibroblast invasion. However, supplementing this supernatant with recombinant tPA, led to a clear increase in fibroblast invasion, which was once again ablated by PAI-1 (Fig.43).

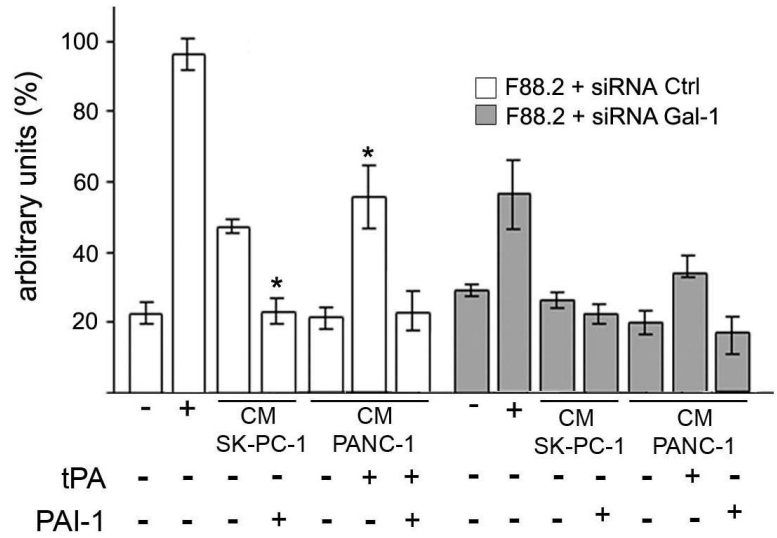

Figure 43. Fibroblast invasion influenced by pancreatic tumoral cell conditioned medium and Gal-1 importance in this crosstalk. Matrigel coated transwell invasion was measured after crystal violet staining, acetic acid extraction and absorbance reading at 550 nm. Basal (-) and 10% FBS induced (+) invasion levels are shown. The addition of SK-PC-1 supernatant (CM SK-PC-1 (containing high tPA levels)) to control cells (siCtrl; white bars), induced an important increase in invasion, which was reverted upon PAI-1 addition. PANC-1 supernatants (CM PANC-1; without tPA) *per se* did not increase fibroblast invasion, but exogenous tPA significantly did. PAI-1, as expected, reduced invasion to basal levels in an analogue manner as to what was observed with SK-PC-1 CM. To study Gal-1 involvement in all these situations, siRNA for Gal-1 was used (siGal-1; grey bars). The increase in fibroblast invasion that occurred upon SK-PC-1 supernatant addition was unobserved after Gal-1 siRNA transfection. Proving Gal-1 specificity for tPA, the increased invasion triggered by adding the protease exogenously in PANC-1 CM, was completely ablated after Gal-1 downregulation.

To decipher to what extent Gal-1 was taking part in all these events, we compared how fibroblasts with normal or downregulated Gal-1 levels responded to the effect of supernatants on invasion (Fig.43). Gal-1 downregulation impaired SK-PC-1 CM induced invasion as well as the increase observed upon tPA addition over

PANC-1 CM. These data emphasized Gal-1/tPA interaction importance in epithelial/fibroblast crosstalk during such an important pathological event as invasion.

Altogether, our *in vitro* results suggested that Gal-1 and tPA could be functionally interacting in pancreatic cancer cell migration and that the lectin was actively involved in tPA induced Erk1/2 activation and invasion not only in pancreatic transformed cells but also in fibroblasts. In addition, we proved that tPA/Gal-1 interaction was relevant in the epithelial/fibroblast crosstalk *in vitro* (see *Discussion*, Fig.116).

2.2.4 tPA & Gal-1 in Angiogenesis

Gal-1 deficiency hampers angiogenesis in different tumor models and recent data have identified some of the putative interplayers in this process[482,540]. Targeting tumor vasculature appears as a promising strategy in the treatment of many neoplasms but unfortunately up to date, very few suitable targets have been identified[692]. Anginex is a specific angiostatic designed β-peptide that has been shown to impair tumor growth and angiogenesis, by specifically targeting activated endothelial cells (ECs) and preventing their adhesion and migration, as well as inducing apoptosis[693-696]. Interestingly, a yeast two-hybrid screening identified Gal-1 as the Anginex molecular target on tumor ECs and indeed, administered Anginex was unable to decrease tumor growth in a null Gal-1 background, although the functional molecular mechanism remained unknown[445].

Considering that tPA is involved in the process of angiogenesis in pancreatic cancer[416,418] and that we had clearly demonstrated its interaction with Gal-1, we hypothesized that Gal-1 could be participating in tPA proangiogenic effect and Anginex could be interfering with this interaction, resulting in its antiangiogenic effect. To approach this possibility, we used SPR, which allowed us analyzing tPA/Gal-1 interaction in the presence or absence of Anginex. Moreover, Gal-1/Anginex interaction had been previously monitored using the same technique revealing a 1:1 stoichiometry and their binding kinetics[445]. tPA was immobilized in a chip and AnxA2, uPA and BSA were used as controls. If preincubation of Gal-1 with Anginex impaired Gal-1 binding to tPA, no signal would be observed in the sensorgram, whereas if Anginex and tPA binding occurred in distinct Gal-1 domains, Anginex preincubation should not alter Gal-1 binding to tPA (Fig.44).

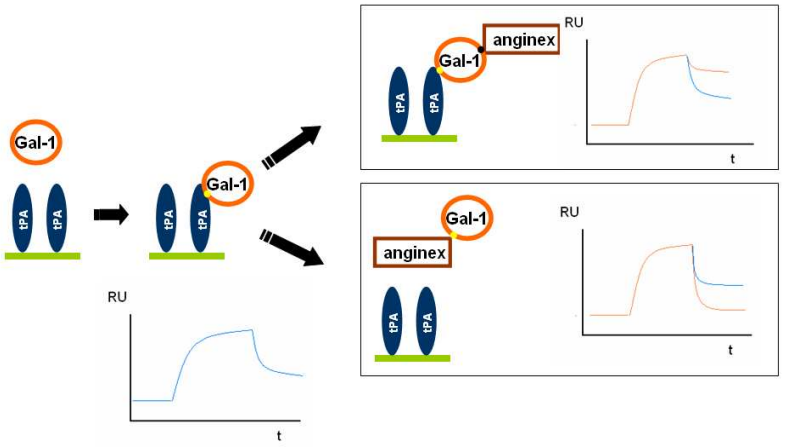

Figure 44. Theoretical predictions of SPR responses when analyzing tPA interaction with Gal-1 preincubated with Anginex. The green surface represents dextran chips, which contain tPA immobilized. When Gal-1 was flushed over tPA surface, a clear response was detected, which was proportional to the mass increase at the surface (blue sensorgram). If Gal-1 was preincubated with Anginex and passed over the surface, two possibilities appeared. Either the response would be higher due to increased mass bound to tPA (higher panel, red sensorgram) or the response could be ablated (lower panel, red sensorgram) if Anginex impaired Gal-1 binding to tPA.

Gal-1 was preincubated with Anginex for 15 min and the mixture was analyzed for tPA interaction. A BSA surface was used as a control for non-specific binding and differential curves (tPA signal - BSA signal) were obtained. Interestingly, a dose dependent decrease in Gal-1 interaction with tPA was observed with increasing Anginex concentration (Fig.45). This would be indicative of Anginex competing with tPA for Gal-1 binding, which would support our second hypothesis (Fig.44). When Anginex concentrations reached 16 μM, the signal was half ablated. However, the strange shape of the sensorgram when using Anginex at higher concentrations (32 and 64 μM) made us reevaluate the interaction more carefully.

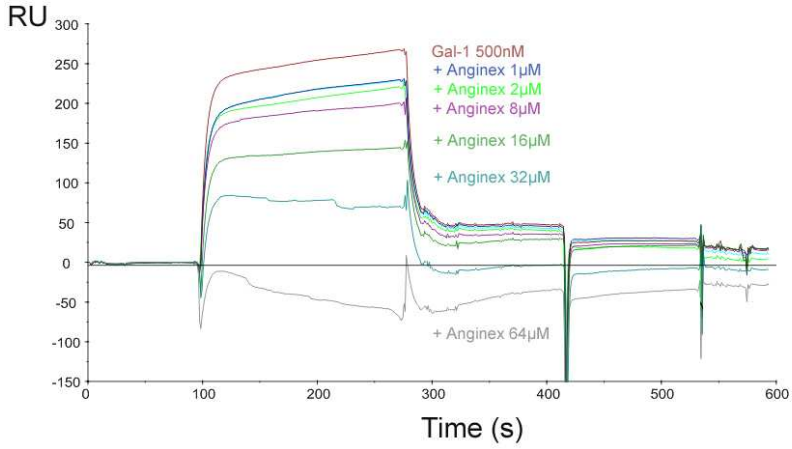

Figure 45. Anginex decreased Gal-1 binding to tPA in a dose dependent manner. Deep red sensorgram corresponds to Gal-1 (500 nM) interaction over immobilized tPA. Increasing Anginex concentration reduced the signal, indicative of less Gal-1 binding to tPA surface. However, Anginex at 32 and 64 μM displayed very strange sensorgrams. All sensorgrams shown are differential (tPA signal - BSA signal).

When individual instead of differential curves were analyzed, we realized that the BSA surface could not be used as a control for non-specific binding, because Gal-1 preincubated with Anginex was binding to it (Fig.46). At low concentrations, tPA signal was higher than the BSA one, resulting in reasonable differential curves,

whereas at increased Anginex concentrations, the BSA signal surpassed the tPA one, offering negative differential curves.

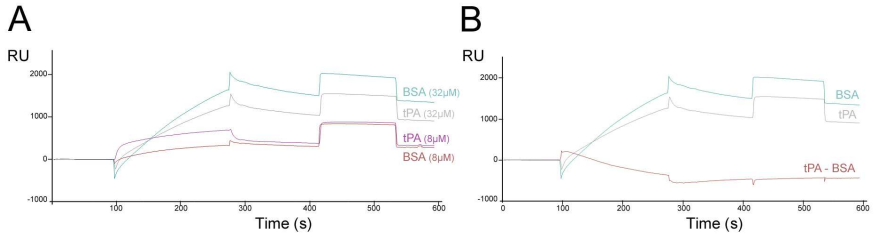

Figure 46. Differential and independent curves recording Gal-1/Anginex interaction with tPA. A) Gal-1 (500 nM) preincubated with Anginex (8 and 32 μM) was analyzed for its interaction with tPA and BSA, which had been previously immobilized at the chip surface. Gal-1 and Anginex displayed high interaction with both tPA (grey (32 μM), purple (8 μM) sensorgrams) and BSA (blue (32 μM), deep red (8 μM) sensorgrams). B) Gal-1 preincubated with Anginex at 32 μM presented higher signal for BSA than for tPA resulting in an overall negative differential curve (deep red sensorgram (tPA-BSA)).

Anginex and Gal-1 were tested over available AnxA2, uPA, tPA and BSA surfaces to check binding selectivity. Gal-1 showed specific interaction with tPA, whereas Anginex was binding to all surfaces in a dose dependent manner (more available surface, more signal; see *Materials and Methods*, section *5.2.9. Protein Immobilization over Surface Plasmon Resonance Chips*). Besides, Anginex dissociation from these surfaces to achieve signal recovery to basal levels was very hard to accomplish (Fig.47).

After finding that Anginex was binding to all of the tested surfaces irrespectively of the protein immobilized, and that the signal was dependent on the free matrix available, we suspected a possible direct interaction of Anginex with the dextran matrix. We examined this possibility by directly passing the angiostatic peptide over a raw chip without any immobilized protein, finding a direct and specific interaction (sensorgram not shown).

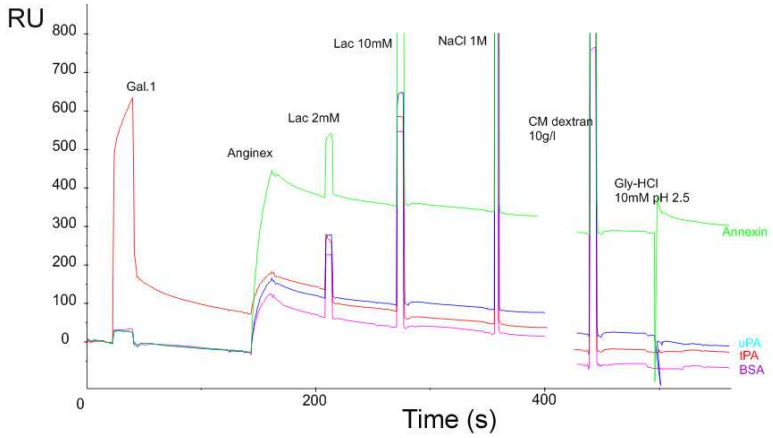

Figure 47. Gal-1 specifically bound to tPA whereas Anginex bound to all surfaces. Gal-1 (500 nM) displayed specificity for tPA binding (red sensorgram, 40 s) while other channels remained unaffected. Anginex (1 μM) bound to all surfaces in a dose dependent fashion depending on the amount of dextran matrix available. In an attempt to recover the surface, different strategies were used: lactose at increasing concentrations (Lac), NaCl, carboxymethylated dextran (CM dextran), Glycine-HCl pH 2.5 (Gly-HCl). All sensorgrams shown correspond to individual curves.

Moreover, Anginex bound at the dextran matrix was able to recruit not only Gal-1 but most of the proteins that were passed over the retained β-peptide (Fig.48). These data discarded SPR as a proper technique to study Anginex interactions. We repeated the same experiments with β-peptide28, a synthetic peptide very similar to Anginex[697] that has been used as a negative control when describing Anginex antiangiogenic properties[693]. The same ambiguous binding pattern was observed with β-peptide28 (data not shown) implying that this non-specificity seemed to be an intrinsic feature of these type of peptides. These data demanded special caution when interpreting the previously published results regarding Gal-1/Anginex direct interaction using SPR.

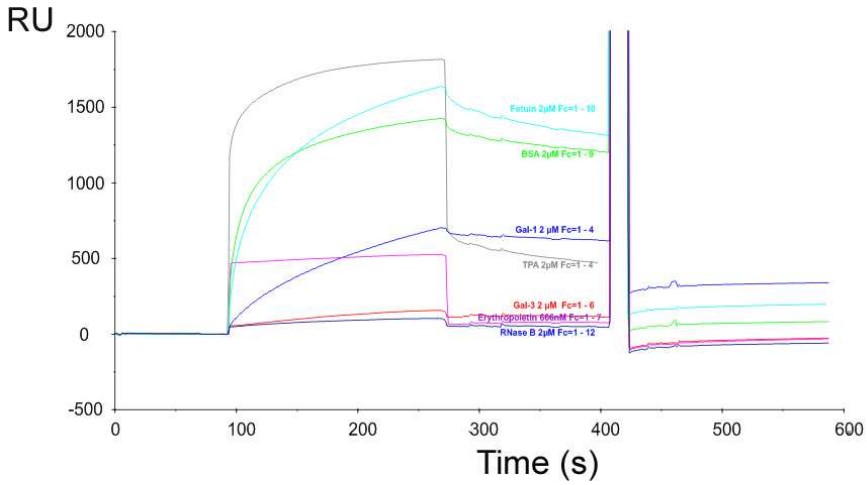

Figure 48. Effect of different proteins over Anginex surface. A panel of 7 available proteins at 2 µM were passed over a dextran matrix which had retained Anginex. 4 of them bound to Anginex displaying high signals during dissociation stage (Fetuin, BSA, Gal-1 and tPA), whereas 3 of them showed weaker interactions (Gal-3, Erythropoietin and RNaseB).

2.3 STUDY OF GAL-1 RELEVANCE IN PDAC IN VIVO

Once proven that Gal-1 was clearly involved in tPA induced pathological effects in pancreatic cancer *in vitro*, we wanted to characterize its involvement in this pathology *in vivo*. To do so, we designed several strategies using different pancreatic cancer animal systems, assessing tumor progression in the presence of distinct Gal-1 levels. We used three major approaches: 1) As an interface with the *in vitro* data, we used xenografts by injecting pancreatic human cancer cell lines with altered Gal-1 levels into nude mice. 2) In a more sophisticated system, and in order to achieve complete Gal-1 depletion, we crossed the transgenic mouse model Ela-1-myc (developing pancreatic tumors) with Gal-1 knockout (KO) mice and 3) We also gathered some data regarding Gal-1 expression in a zebrafish transgenic model of pancreatic tumorigenesis.

2.3.1 *In vivo* Role of Gal-1 in Pancreatic Cancer using Xenograft Models

After observing that reducing Gal-1 levels in pancreatic cell lines *in vitro* impaired many of the pathological events driving pancreatic cancer progression, we wanted to reproduce these data *in vivo*. In this regard, we stably downregulated Gal-1 by infecting PANC-1 cells with lentiviral particles carrying shRNA for Gal-1. These cells were subsequently injected in BALB/c nude mice and tumor progression was followed.

2.3.1.1 Gal-1 Stable Downregulation

In order to perform xenograft studies enabling monitoring tumor progression *in vivo* by bioluminescence detection, we knocked down Gal-1 in the PANC-1_LUC cell line, which stably expressed the luciferase enzyme. To do so, we used Hek293T cells to generate lentiviral particles carrying shRNA sequences targeting Gal-1. The efficiency of five different shRNA sequences targeting Gal-1 was checked in PANC-1 cells (see section *2.4.1. Upregulation or Downregulation of Gal-1 Levels in Cultured Pancreatic Cells*, Fig.101). The most effective shRNAs were used in the PANC-1_LUC cell line. After puromycin selection, Gal-1 protein levels were examined and downregulation confirmed. Different sequences were picked-up for *in vivo* nude mice injection to exclude off-target effects: shGal-1_1, shGal-1_2 and shGal-1_5, which reduced endogenous Gal-1 levels to 10%, 24% and 13%, respectively (Fig.49). As a control to later assess the effects of infection *per se*, parental non-infected cells were used (wt), which were compared to cells infected with an irrelevant shRNA sequence (shCtl or shCtl*).

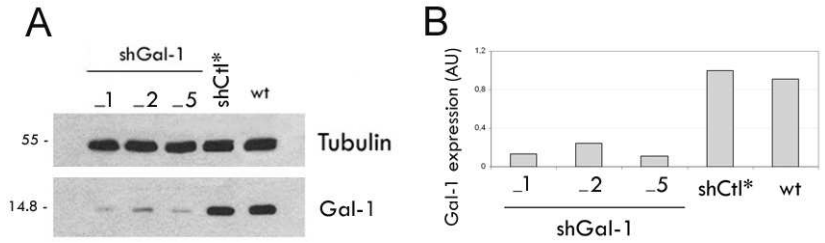

Figure 49. Gal-1 downregulation in the PANC-1_LUC cell line. A) WB detection of Gal-1 protein levels after downregulation. Untransfected (wt) or control transfected cells (shCtl*) showed high levels of Gal-1 whereas cells transfected with three different specific shRNA for Gal-1 displayed very low levels of the lectin (shGal-1_2, shGal-1_3 and shGal-1_5) B) Downregulation quantification. Gal-1 expression was reduced to 10%, 24% and 13%, respectively.

2.3.1.2 *In vitro* Characterization of PANC-1_LUC Cells

Before injecting these cells into nude mice, we characterized their proliferation, invasion and tumoral capacities.

Proliferation of PANC-1_LUC cells with different Gal-1 levels was analyzed through cell culture addition of MTT, a substrate of mitochondrial enzymes associated with metabolic activity. Stable Gal-1 depletion did not affect cell growth rate (Fig.50).

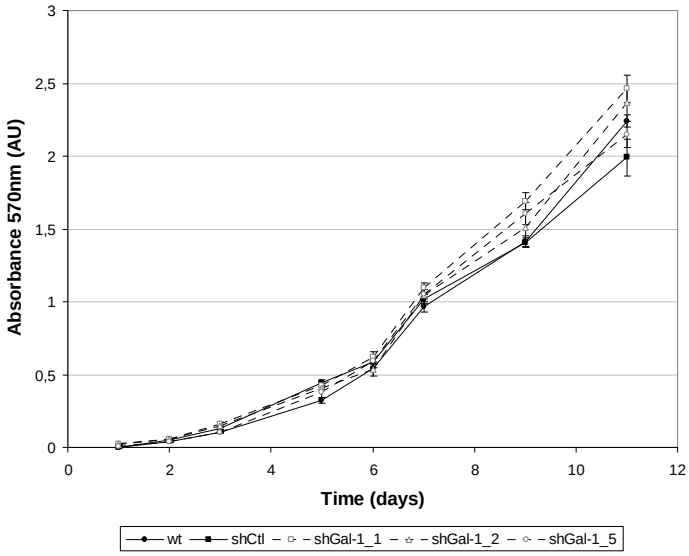

Figure 50. PANC-1_LUC proliferation was independent of Gal-1 levels. Non-infected cells (wt), cells infected with a scramble shRNA (shCtl) and cells with depleted Gal-1 levels (shGal-1) through infection with three different sequences targeting the protein, showed very similar proliferation rates by MTT proliferation assay. Proliferation was quantified by measuring absorbance at 570 nm. One representative experiment out of three has been selected.

Invasion over matrigel coated transwells was also analyzed *in vitro* (Fig.51). Although a trend seemed to be observed as Gal-1 depleted cells showed lower invasion levels, no significant differences were detected ($p=0.18$ by Kruskal Wallis test).

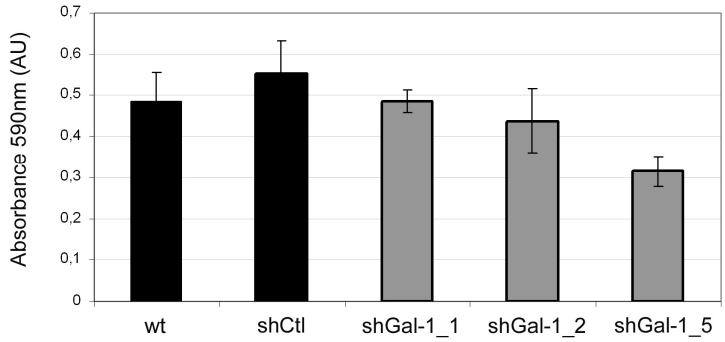

Figure 51. PANC-1_LUC *in vitro* invasion over matrigel coated transwells with cells with basal or low Gal-1 levels. Non-infected cells (wt), cells infected with a scrambled shRNA (shCtl) and cells with low Gal-1 levels (shGal-1) achieved through three different shRNA sequences targeting Gal-1, showed no significant differences regarding invasion (p=0.18 by Kruskal Wallis test). One representative experiment out of three has been selected.

Anchorage independent growth experiments were performed in order to measure the tumorigenic capacity of these cells (Fig.52).

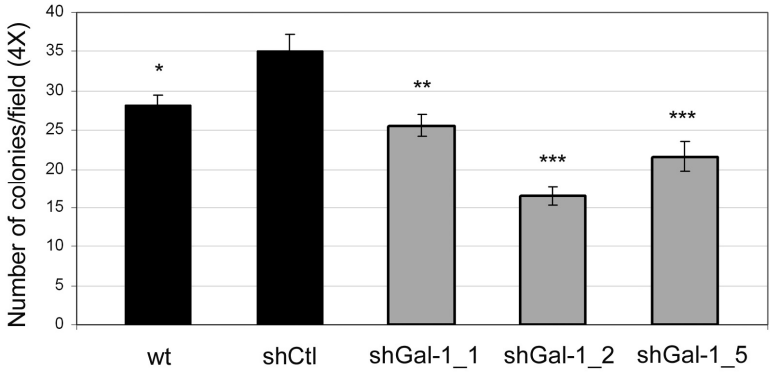

Figure 52. Anchorage independent growth in PANC-1_LUC cells. All shRNA against Gal-1 reduced the substrate independent growth of cells comparing to cells infected with a shCtl (***p<0.0001 and **p=0.007). Nevertheless significant differences were also detected comparing parental uninfected cells and cells harboring a shCtl (*p=0.03, by Mann Whitney test).

Intringuingly, all cells with low Gal-1 levels showed reduced substrate independent growth compared to cells infected with an shCtl (***p<0.0001 for shGal-1_2 and shGal-1_5 and **p=0.007 for shGal-1_1, by Mann Whitney test). However, unexpected

significant differences were also seen when comparing shCtl and non-infected cells (*p=0.03) (Fig.52).

2.3.1.3 Nude Mice Injection of PANC-1_LUC Cells

In order to observe the effects of Gal-1 in tumor progression, four different PANC-1_LUC cell types were used: on one hand, basal levels of Gal-1 were represented by both non-infected parental PANC-1_LUC cells and cells infected with an irrelevant shRNA (shCtl or shCtl*). On the other hand, cells with low Gal-1 protein levels were obtained through 2 different shRNA sequences in order to observe the specific consequences of Gal-1 downregulation and exclude off-target effects. 2 million cells per flank were injected subcutaneously (SC) or intraperitoneally (IP) into nude mice. In the SC implantation and with the objective of assessing Gal-1 importance in tumor formation in exactly the same host environment, we implanted control non-infected cells in the left flank of the animal and infected cells (with shCtl or shGal-1) in the right flank (Fig.53).

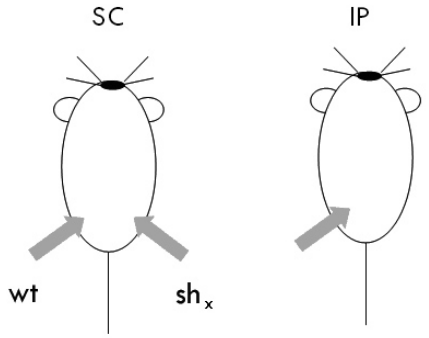

Figure 53. Subcutaneous (SC) and intraperitoneal (IP) injection of PANC-1_LUC cells in nude mice. 2 million of non-infected parental PANC-1_LUC cells (wt) were SC injected in the left flank of the animals whereas infected cells (control: shCtl or shCtl* or Gal-1 depleted: shGal-1_2 and shGal-1_5) were implanted in the right side of the animal. In the IP injection, 2 million cells were used. 4 animals per group were used in both cases. For the IP injection, duplicate experiments were performed.

2.3.1.3.1 Subcutaneous Injection

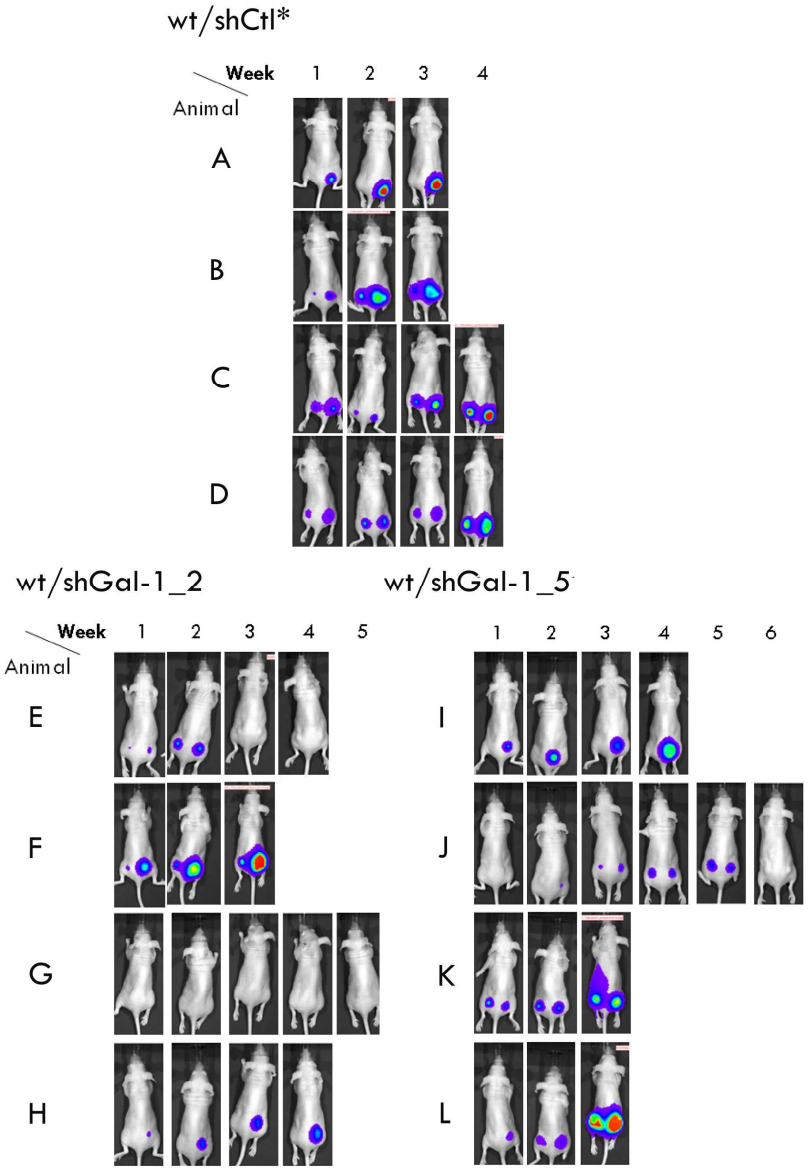

Figure 54. PANC-1_LUC cells with different Gal-1 levels injected SC in nude mice. 2 million cells were implanted in each posterior flank of BALB/c nude mice. Control, non-infected PANC-1_LUC cells (wt) were injected in the left flank whereas infected cells (with shCtl* or with shGal-1 (2 different sequences: shGal-1_2 and shGal-1_5)) in the right flank. Lumininscent images after 5 min exposure were weekly obtained. 4 animals per group were used. Some luciferase measures were unconnected due to possible incorrect IP luciferin injections[698].

2 million cells per flank were subcutaneously injected into nude mice and luciferase signal was recorded weekly as a way to follow tumor progression (Fig.54). Because of the very high variability, an overall effect on tumor development due to Gal-1 downregulation could not be determined. Besides, in this experiment and for unkown reasons, non-infected parental cells presented a very different behavior regarding cell growth, being unable to generate tumors in most animals, so they could not be used as controls. Still, if we compared cells infected with a control shRNA (shCtl*) to cells with low Gal-1 levels, we could observe a slight increase in the bioluminescent signal acquired in control flanks (for instance, this group was the only one displaying saturated images as soon as 2 weeks after cell injection).

Necropsies were performed between 3 and 6 weeks after injection, when tumors reached one centimeter. Hematoxylin & eosin (H&E) staining of subcutaneous tumors revealed their low differentiation grade nature, consisting of solid and compact tumors with necrotic areas in central parts (Fig.55).

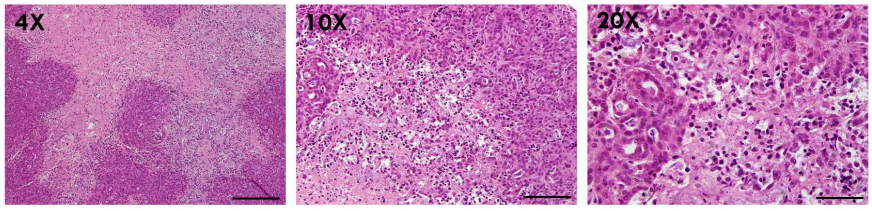

Figure 55. Histologic analysis of SC tumors. H&E staining of a representative subcutaneous tumor with big necrotic central regions. Scale bars represent 500 μm (4X), 200 μm (10X) and 100 μm (20X).

In most cases, the tumor was maintained in the subcutaneous region, although muscle and bone infiltration were sometimes observed in random animals, being unable to establish a relationship between infiltration and Gal-1 levels (Tab.7).

Tumor type	wt	shCtl*	shGal-1_2	shGal-1_5
SC	5	2	1	1
INM	1	1	1	2
INB	1	1	1	1

Table 7. Classification of tumors according to localization. Injected cells on posterior flanks generated subcutaneous tumors (SC) or tumors that infiltrated to the muscle (INM) or the bone (INB). Note that wt cells presented a reduced proportion of bone and muscle infiltrations because their growth was severely impaired for unkown reasons.

2.3.1.3.2 Intraperitoneal Injection

PANC-1_LUC cells were also injected intraperitoneally and *in vivo* tumor progression was followed by weekly luciferase measures (Fig.56 and 57). Although once again, variability was very high, we could also detect a slight tendency towards decreased tumor development when Gal-1 levels were reduced. For instance, in the first IP experiment, half of the shGal-1 mice reached 6 weeks of life and none of them showed signal saturation 3 weeks after injection. In contrast, none of the control mice exceeded a month and 3 of them displayed saturated images after 3 weeks (Fig.56). However, we found important differences among individuals within the same group and less clear results in the second experiment (Fig.57).

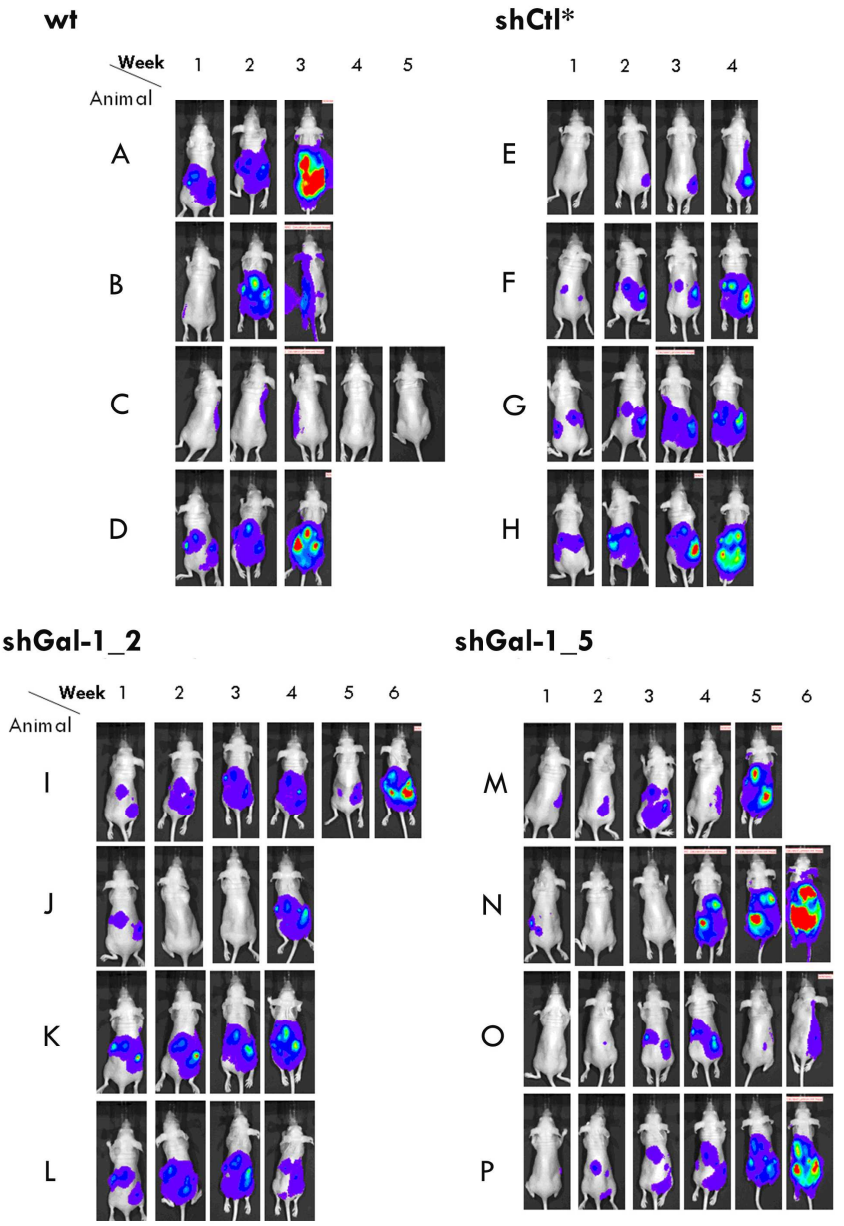

Figure 56. First IP injection of PANC-1_LUC cells with basal or depleted Gal-1 levels. Control mice were injected with 2 million of non-infected cells (wt) or cells infected with the irrelevant shRNA (shCtl*). Cells with low Gal-1 levels (shGal-1_2 and shGal-1_5) were also injected and luciferase measures recorded weekly. 4 animals per group were used and necropsies were performed between 3 and 6 weeks after injection, when mice displayed overall bad state symptoms. Cells were not correctly injected in animal C, as it never presented luciferase positive measures.

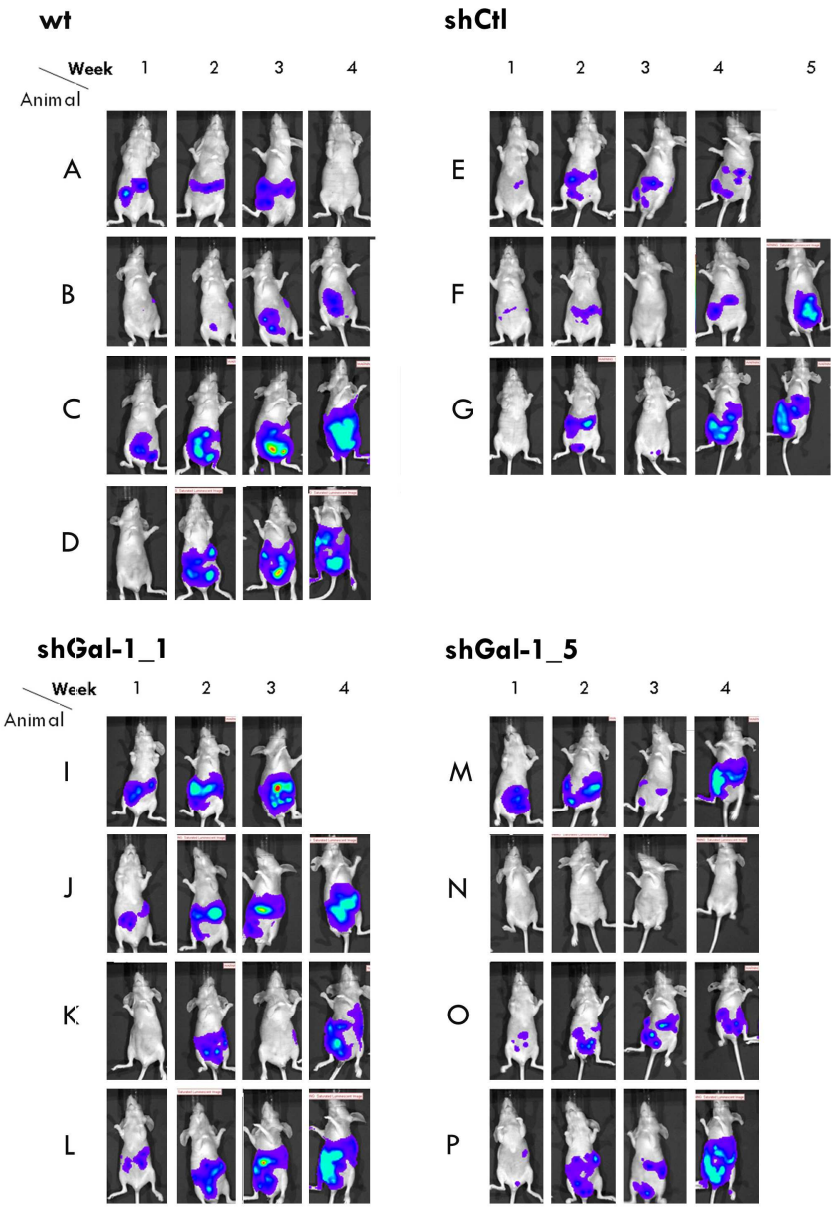

Figure 57. Second IP injection of PANC-1_LUC cells with basal or depleted Gal-1 levels. Control mice were injected with 2 million of non-infected cells (wt) or cells infected with the scrambled shRNA (shCtl). Cells with low Gal-1 levels (shGal-1_1 and shGal-1_5) were also injected and luciferase measures recorded weekly. 4 animals per group were used and necropsies were performed between 3 and 5 weeks after injection, when mice displayed overall bad state symptoms. Cells were not correctly injected in animal N, as it never presented luciferase positive measures. In this case, images were taken with the animal facing up to optimize image intensity.

In order to get a general picture of Gal-1 importance in xenograft tumor progression, all animals were gathered in just two groups for survival analysis. On one side, we grouped animals forming tumors with high Gal-1 levels (which included mice injected with non-infected cells (wt) or infected with an irrelevant shRNA (shCtl* or shCtl)). On the other side, we grouped mice with cells injected with decreased Gal-1 levels (shGal-1), irrespectively of the sequence used (shGal-1_1, shGal-1_2 and shGal-1_5). The lack of a very strong phenotype due to Gal-1 altered levels, added to the low number of animals used and the very high variability, did not allow reaching statistically significant results when analyzing overall survival (p=0.077 by log-rank statistics) (Fig.58).

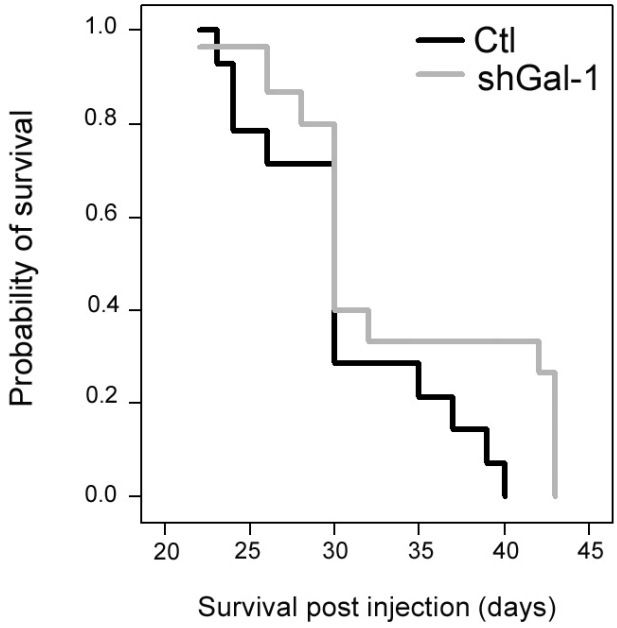

Figure 58. Kaplan Meier survival analysis of IP injected mice. The control group (Ctl) included mice injected with non-infected cells (wt) or infected with an irrelevant shRNA (shCtl* or shCtl). The group with low Gal-1 levels (shGal-1) comprised all mice injected with any of the shRNAs targeting Gal-1 (shGal-1_1, shGal-1_2 and shGal-1_5). Although there seemed to be a trend linking increased survival with decreased Gal-1 levels, differences did not reach statistical significance (p=0.077 by log-rank statistics).

At the histological level, IP tumors were more glandular compared to the SC equivalents, and they could be referred to as adenocarcinomas (Fig.59).

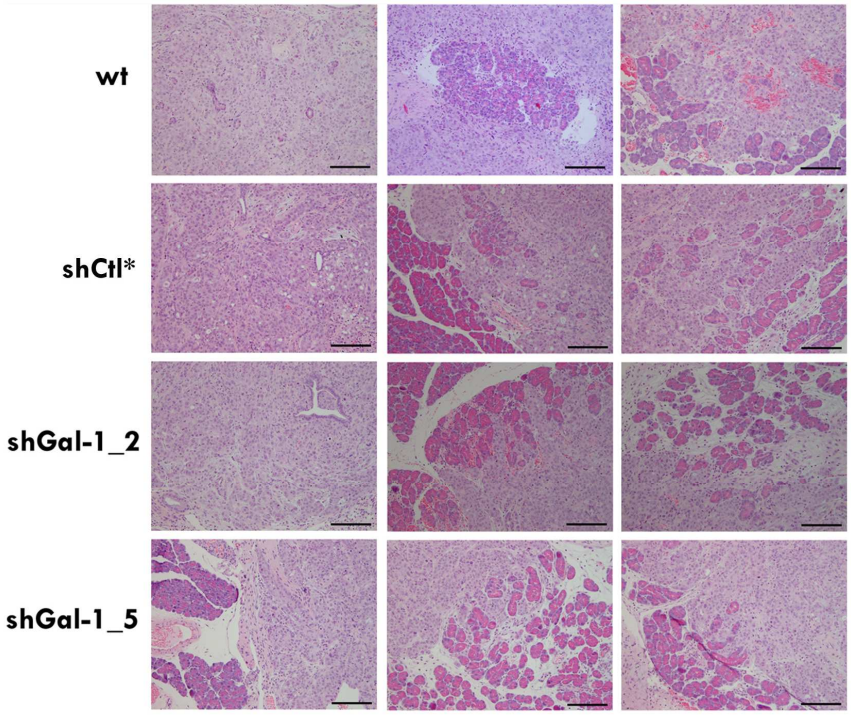

Figure 59. Histologic analysis of IP tumors. H&E staining of representative IP tumors of each group displaying its glandular characteristics and several areas of normal pancreas invasion. Scale bars represent 200 μm (10X).

Very interestingly, although cell injection was performed intraperitoneally and not orthotopically in the pancreas, all animals showed tumor foci in the pancreatic area. These data was confirmed in our group with different pancreatic cancer cell lines[414], and suggest preferential homing of tumoral pancreatic cell lines to its organ of origin. Very interestingly, infiltration into normal pancreas occurred (Fig.59).

Bioluminiscent images in different focuses observed during *in vivo* tumor progression, made us suspect of tumor localization in different sites. These data became evident when analyzing luciferase signal after necropsy in individual organs (Fig.60).

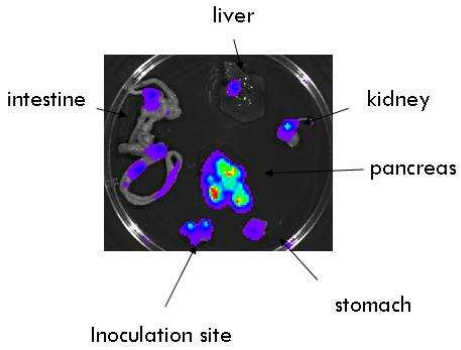

Figure 60. Tumor localization in IP injected xenografts observed by luciferase activity. Bioluminescence was used to detect tumoral sites in mice post necropsy.

	Pancreas	Injection	Liver	Ovary	Intestine	Iliac	Biliar v.	Kidney	Urethra	Spleen	Stomach
Ctl	x		x								
	x										
	x	x									
shCtl*	x	x		x		x	x				
	x	x	x		x						
		x									
	x			x		x					
shGal-1_2	x			x	x			x			
	x	x	x			x					
	x		x						x	x	x
	x	x	x	x		x		x		x	
shGal-1_5	x	x	x	x		x			x		
	x	x	x				x		x		
	x	x							x		

Table 8. Affected organs with tumoral nodules in IP injected mice (first experiment). Xenografts injected with PANC-1_LUC cells with low and high Gal-1 levels showed tumors in different sites. Each row corresponds to one animal.

The major tumor mass was found in the pancreas, though nodules were frequently observed in intestine, kidney, liver, stomach, ovary and in the inoculation site. The frequency of these non-pancreatic localizations was independent of Gal-1 levels of expression (Tab.8 and 9).

	Pancreas	Injection	Liver	Ovary	Intestine	Bladder	Biliar vesicule	Kidney	Stomach
Ctl	x						x		
	x	x			x				
	x	x							
	x	x			x				
shCtl	x	x				x			
	x		x	x		x		x	
	x	x				x			
shGal-1_1	x			x				x	
	x	x							
	x	x							
	x	x		x					x
shGal-1_5	x	x		x				x	
	x		x						
	x	x			x				

Table 9. Affected organs with tumoral nodules in IP injected mice (second experiment). Xenografts injected with PANC-1_LUC cells with low and high Gal-1 levels showed tumors in different sites. Each row corresponds to one animal.

2.3.1.3.3 Immunohistological Analysis of Xenograft Tumors

We first analyzed Gal-1 expression in xenografts tumors in order to determine whether reduced Gal-1 levels were maintained during *in vivo* tumor growth. Gal-1 efficient downregulation was stable *in vivo* in both SC and IP mice, as shown by Gal-1 IHC (Fig.61). Luciferase detection by IHC allowed identification of injected human tumoral

epithelial cells. Pancreatic tumoral cells interfered with Gal-1 shRNA, showed much reduced Gal-1 levels after necropsy (Fig.61). As expected, fibroblasts within tumors showed high Gal-1 levels in all groups, as this cell population belonged to the host animal (confirmed by luciferase negative signals) (Fig.62).

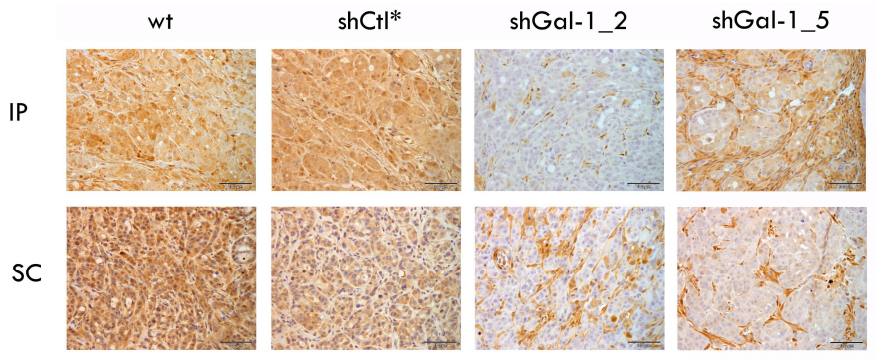

Figure 61. IHC analysis of Gal-1 downregulation *in vivo* in IP and SC tumors. Non-infected (wt) cells or cells infected with an irrelevant shRNA (shCtl*) showed high Gal-1 staining, whereas cells with Gal-1 interference (shGal-1_2 and shGal-1_5) showed clearly lower levels. Positive cells around tumoral epithelial cells corresponded to fibroblasts from the host mice, which had high endogenous Gal-1 levels. Scale bars correspond to 100 μm.

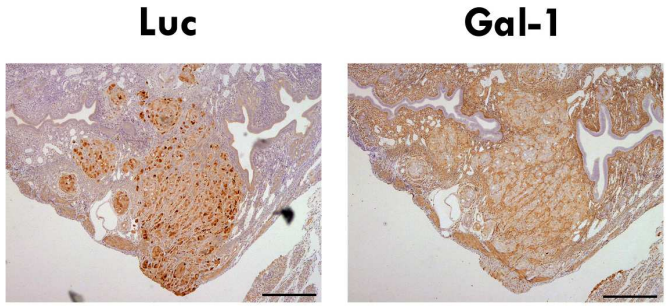

Figure 62. Identification of injected cells by luciferase staining. Injected human tumoral pancreatic cells were identified by IHC taking advantage of their luciferase staining using an antibody against luciferase (Luc). In this example, taken from an IP injected mice with cells interfered with shGal-1_5, a link could be established between positive luciferase cells and negative Gal-1 ones, whereas mice fibroblasts were positive for Gal-1 and negative for luciferase. Scale bars correspond to 500 μm.

We characterized Gal-1 effects in tumor development by analyzing tumor cell proliferation rate, stroma formation and angiogenesis by IHC.

Regarding tumor proliferation, Ki67 detection was assessed, whose expression is high in all active states of the cell cycle (G1, S, G2 and M phases) while it is absent in quiescent cells (G0). In all SC tumors, proliferation rates were almost 100% so quantification was not performed (Fig.63)

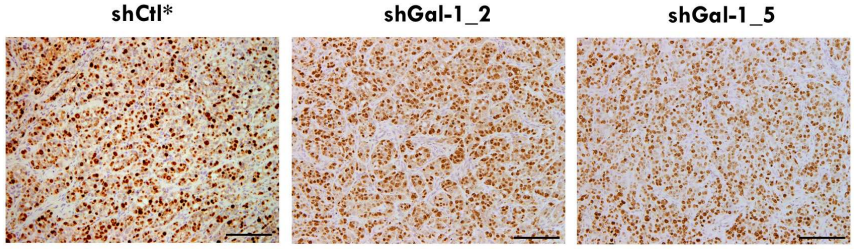

Figure 63. Proliferation in SC tumors. Ki67 IHC to assess and compare proliferation rates in high and low Gal-1 expressing SC tumors. Almost all epithelial cells were proliferating. Scale bars correspond to 200 μm. Note that control tumors (wt) are not shown because they presented growth problems and were almost unobserved (see Fig.54).

In contrast, IP tumors, which reproduced a more physiologic tumor context because of their pancreatic location, showed lower proliferation rates (Fig.64). The percentage of cells proliferating was quantified in each group (Fig.65). We could not find significant differences in proliferation among tumors from cells with high Gal-1 levels and those raised from Gal-1 knockdown cells (Fig.65). However, we must bear in mind that variability in data was pretty high and that the experiment was performed with only four mice, what could be hiding a possible difference, if it existed.

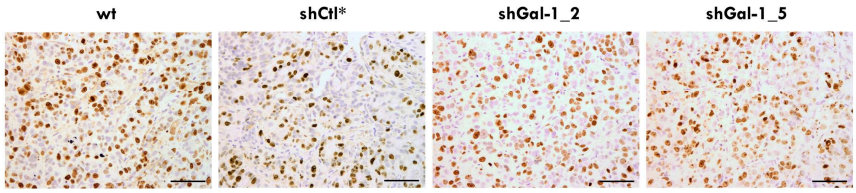

Figure 64. Proliferation detection in IP tumors. Ki67 IHC in tumors with high Gal-1 levels (wt and shCtl*) or with depleted Gal-1 levels (shGal-1_2 and shGal-1_5). Scale bars correspond to 100 µm.

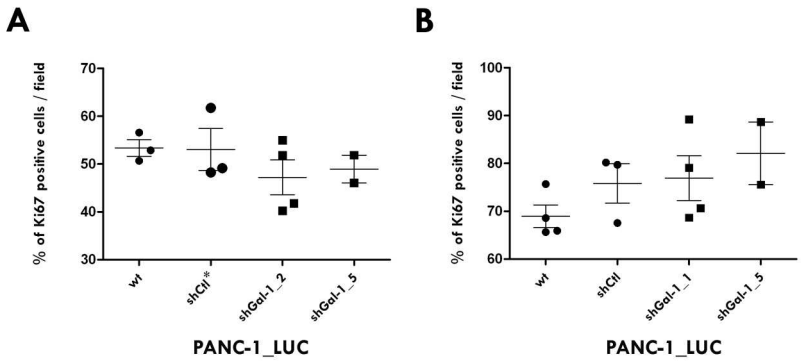

Figure 65. Proliferation rate quantification in IP xenografts. Scatter plots of both experiments showing the percentage of Ki67 positive cells per field. p=0.58 (A: first experiment) and p=0.24 (B: second experiment), by Kruskal Wallis analysis.

Gal-1 is highly expressed in the stroma of pancreatic tumors and *in vitro* experiments demonstrated that Gal-1 was involved in Erk1/2 activation, proliferation, invasion and migration not only in pancreatic tumoral cells but also in fibroblasts (see section *2.2. Study of tPA/Gal-1 Interaction in vitro*). Although in xenograft experiments, the tumor stroma came from the host mice (with high Gal-1 levels in all cases), we wanted to determine whether Gal-1 different levels in tumoral epithelial cells could be influencing the amount of activated fibroblasts in the tumor microenvironment. To analyze this, we assessed α-SMA levels by IHC (Fig.66) and positive tumor areas were quantified (Fig.67). We centered our analysis on IP tumors as the SC equivalents were much more compact and with significantly

less desmoplastic reaction. No overall differences in the amount of stroma present were found, irrespectively of Gal-1 levels (Fig.67).

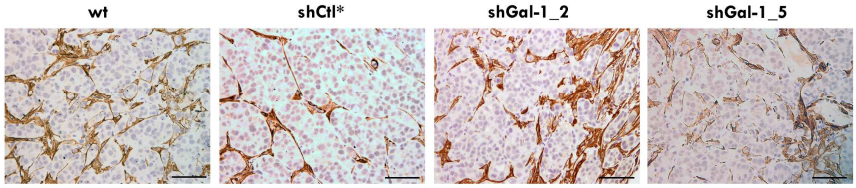

Figure 66. Stroma presence in IP xenografts. α-SMA IHC was used to detect the amount of stroma present in tumors with different Gal-1 levels. Scale bars correspond to 100 μm.

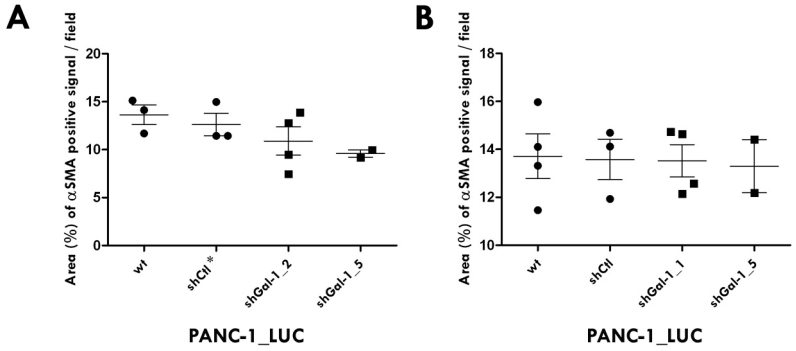

Figure 67. Quantification of the stroma present in IP tumors. Scatter plots from the two experiments performed showing the percentage of positive α-SMA area per field. p=0.18 (A: first experiment) and p=0.99 (B: second experiment) by Kruskal Wallis analysis.

Gal-1 has also been extensively involved in tumor angiogenesis[445,534,540]. In order to compare blood vessel formation depending on Gal-1 presence in tumors, we performed IHC against von Willebrand factor (vWF). Macroblood vessels (>100 μm), medium vessels (50-100 μm), and microvessels (25-50 μm), as well as individual ECs were quantified (Fig.68). We did not detect significant differences regarding tumor angiogenesis depending on Gal-1 levels of injected cells (according to Poisson statistical analysis

considering blood vessel size and tumor localization (center or periphery of the tumor).

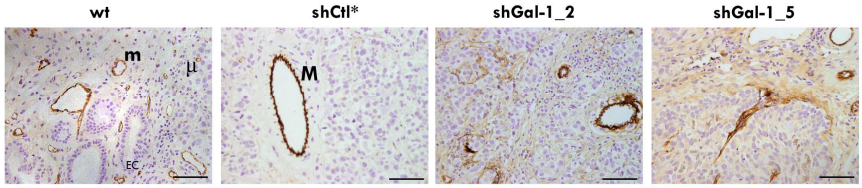

Figure 68. Angiogenesis in IP tumors. IHC against vWF, which allowed identification of blood vessels in tumors. Scale bars correspond to 100 μm. M: macroblood vessel; m: medium blood vessel; μ: microblood vessel; EC: ECs.

2.3.2 *In vivo* Role of Gal-1 in Pancreatic Cancer using Transgenic Models: Ela-1-myc:Gal-1$^{-/-}$

2.3.2.1 Ela-1-myc Pancreatic Tumors

Ela-1-myc transgenic mice develop pancreatic tumors between 2 and 7 months after birth (see *Introduction*, section *1.2.4.2.3. Ela-1-myc Transgenic Model*). Approximately half of these tumors are acinar pure carcinomas with different degrees of differentiation, whereas the second half correspond to mixed or ductal adenocarcinomas, being able to observe areas of acinar to ductal metaplasia (ADM). These transgenic mice general features were confirmed by H&E staining (Fig.69). In general, necrotic areas were sometimes observed, almost invariably linked to the acinar compartment (Fig.69b).

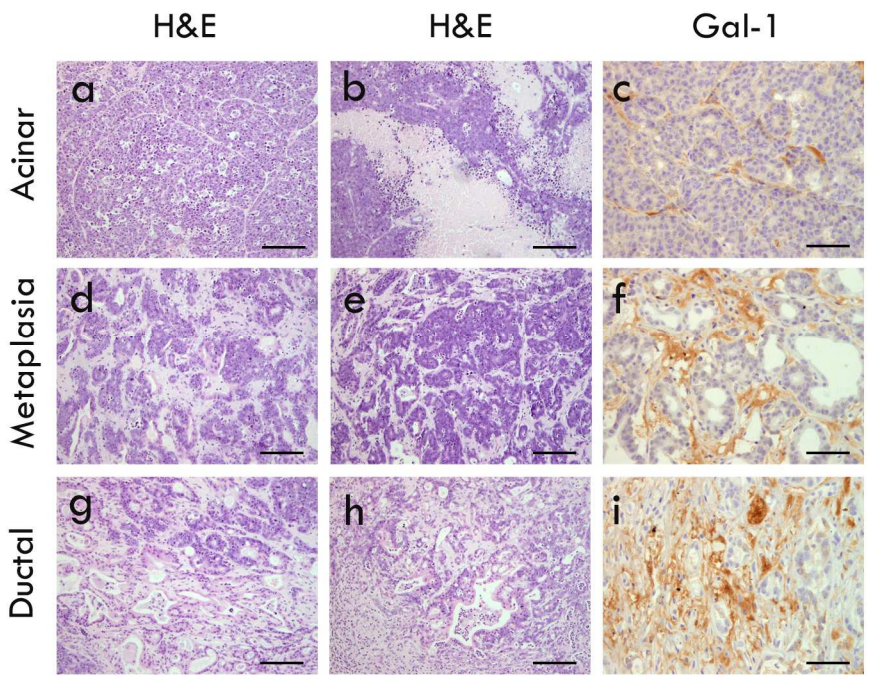

Figure 69. Type of tumors found in Ela-1-myc transgenic mice. H&E staining of pure acinar tumors (a) with necrosis (b), areas of acinar to ductal metaplasia (d,e) and ductal lesions (g,h). Gal-1 staining detected by IHC in the stroma of all kind of tumors (c,f,i). Scale bars correspond to 200 µm for all H&E sections (a,b,d,e,g,h) and 100 µm for Gal-1 IHCs (c,f,i).

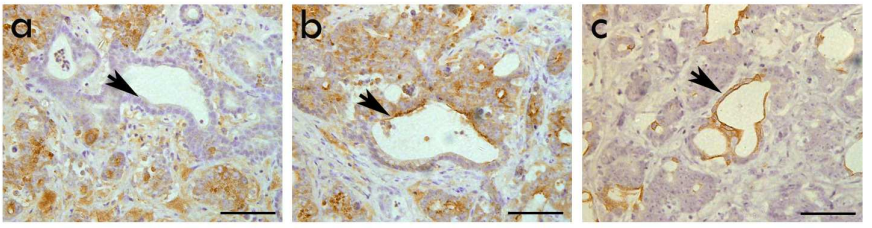

Figure 70. Assessment of Ela-1-myc tumor acinar-ductal differentiation by IHC. (a,b) Amylase detection in mixed focal lesions. Amylase was normally positive in acinar cells, whereas its presence was negative (arrow) in ductal ones (a). However, in Ela-1-myc tumors, we frequently observed ducts that were positive for amylase (arrow), suggesting that they derived from acinar cells. (c) CK19 staining was clearly and exclusively detected in ducts (arrow). Scale bars represent 100 µm.

To examine tumor cell differentiation in Ela-1-myc tumors, we performed cytokeratin-19 (CK19) and amylase staining. As it had

been previously observed in other transgenic mice tumors[47], acinar to ductal metaplasia was identified by the fact that amylase staining (typically found in acinar cells) could be focally observed in some ducts (labeled with CK19) (Fig.70).

2.3.2.2 Ela-1-myc:Gal-1$^{-/-}$ Mice Breeding

Gal-1 is highly overexpressed in the stroma in human pancreatic cancer and so it was in the Ela-1-myc mouse model (Fig.69). These data were also confirmed at the RNA level by *in situ* hybridization (ISH) (data not shown).

In order to better assess Gal-1 role in pancreatic cancer development, we decided to use a system in which total protein depletion could be achieved. To do so, we crossed Ela-1-myc mice with Gal-1 KOs (Fig.71). To optimize crossing efficiency, Ela-1-myc expressing mice were always males. To generate F1, Ela-1-myc male mice were crossbred with female Gal-1$^{-/-}$ to obtain Ela-1-myc heterozygous for Gal-1 (Ela-1-myc$^{+/-}$:Gal-1$^{+/-}$, which represented 50% of the progeny). For the F2, Ela-1-myc$^{+/-}$:Gal-1$^{+/-}$ males from F1 were paired with Gal-1$^{-/-}$ female mice to obtain transgenic mice KO for Gal-1 (Ela-1-myc$^{+/-}$:Gal-1$^{-/-}$, corresponding to 25% of the progeny). To generate the amount of animals required and work with Gal-1 pure genotype populations, we mated Ela-1-myc$^{+/-}$:Gal-1$^{-/-}$ F2 mice with Gal-1 KO or with wild type C57BL/6 females (Ela-1-myc$^{-/-}$:Gal-1$^{+/+}$) to obtain the homozygous (Ela-1-myc$^{+/-}$:Gal-1$^{-/-}$) and heterozygous (Ela-1-myc$^{+/-}$:Gal-1$^{+/-}$) F3 mice, respectively.

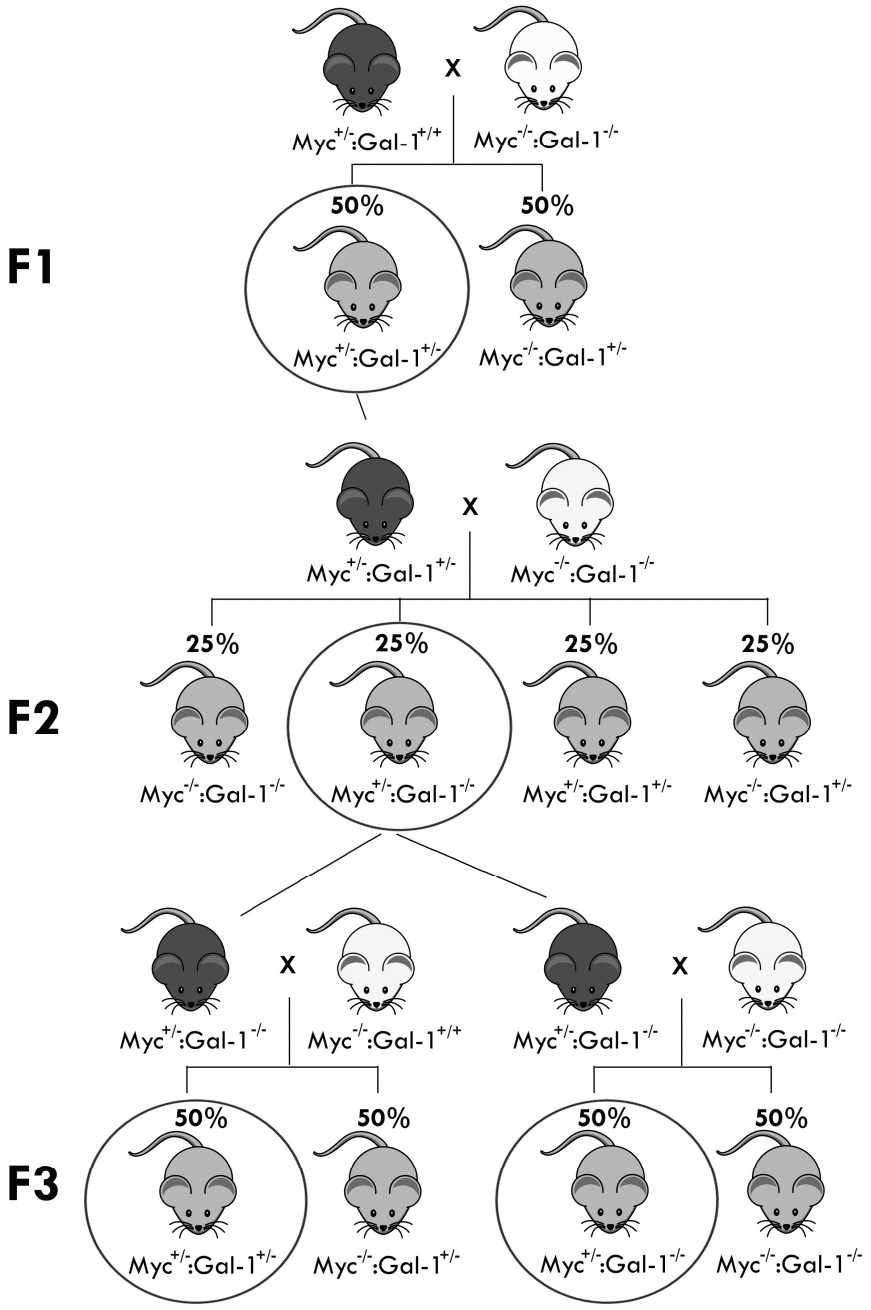

Figure 71. Crossings to obtain the different transgenic mice populations. Dark grey mice represent males, white mice represent females and pale grey mice represent general mice, irrespectively of their sex. Mice required for further crossbreeding or for the final experiment are encircled in the scheme.

Hereafter, Ela-1-myc$^{+/-}$ animals will be referred to as Myc mice in order to simplify nomenclature.

2.3.2.3 Ela-1-myc:Gal-1$^{-/-}$ Mice Tumor Formation and Survival

Our study included 80 Myc:Gal-1$^{+/+}$, 64 Myc:Gal-1$^{+/-}$ and 54 Myc:Gal-1$^{-/-}$ that were born in the same time window (during 7 months). Animals were sacrificed when one of the following direct or indirect signals of pancreatic tumorigenesis appeared: enlarged abdomen, inflammation, palpable abdominal masses, ascites, weakness, decreased activity, weight loss, antalgic position or jaundice. Macroscopically, acinar tumors were white or red, due to hemorrhage within the tumor, whereas ductal lesions were consistently white. Many animals showed more than one tumoral nodule, suggesting that the tumor might have different origins.

Kaplan Meier survival analysis and log-rank statistics found significant differences comparing Ela-1-myc wild type animals and animals lacking one or both Gal-1 alleles ($p<0.0001$) (Fig.72). Whereas the first group showed a mean survival of 124 days (4 months and 4 days), animals with targeted Gal-1 (both heterozygous and KO mice) increased this survival time to 149 days (4 months and 29 days) (Tab.10 and Fig.73). Remarkably, this improvement represented a 20% of the animal life span. Moreover, the importance of these data was highlighted when survival time was evaluated carefully. While only the 19% of Myc:Gal-1$^{+/+}$ exceeded 5 months of age, around 50% of Myc:Gal-1$^{+/-}$ and Myc:Gal-1$^{-/-}$ did. Focusing our attention on long term survivors, only

4% of Myc:Gal-1$^{+/+}$ lived beyond 6 months, whereas this percentage significantly climbed to 17% in Myc:Gal-1$^{+/-}$ and to 22% in Myc:Gal-1$^{-/-}$ (Tab.10 and Fig.73). These data suggested that Gal-1 was important in Ela-1-myc pancreatic tumoral progression and that a significant increase in animal survival could be achieved by targeting its expression. Interestingly, we found that heterozygous and KO mice for Gal-1 showed a similar life-span. Thus, the loss of a single allele of the gene was enough to deeply affect survival time and induce a phenotype change, an event known as haploinsufficiency (see *Discussion*, section *3.5.3.1. Gal-1 Haploinsufficiency in Pancreatic Cancer*).

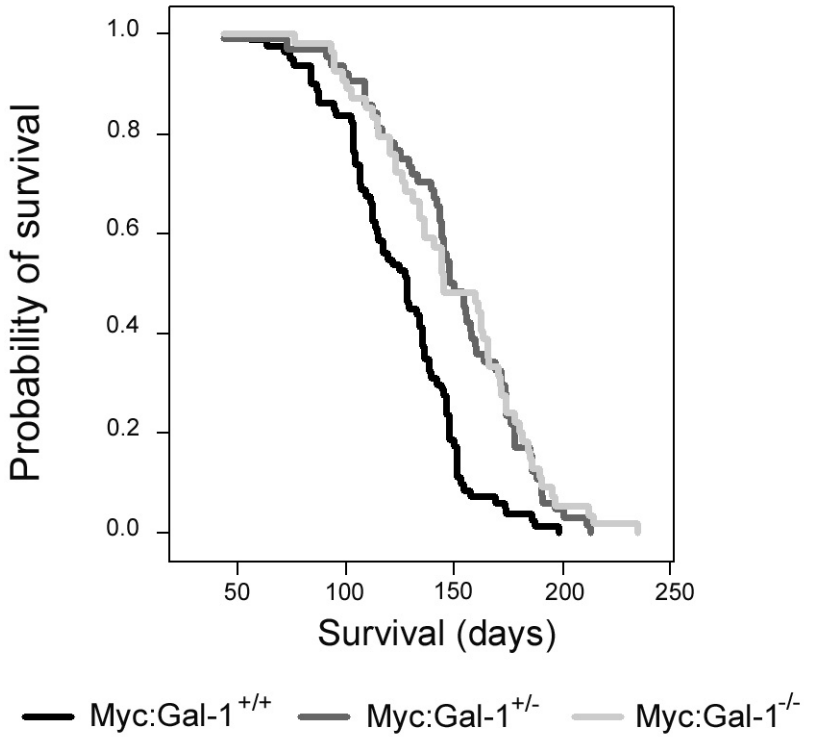

Figure 72. Kaplan Meier survival curves from Myc:Gal-1$^{+/+}$, Myc:Gal-1$^{+/-}$ and Myc:Gal-1$^{-/-}$. Heterozygous and KO mice showed a significant increase in survival time compared to Myc:Gal-1$^{+/+}$ ($p<0.0001$ by log-rank test).

Genotype	n	Survival (days)	Survival (< 4 months)	Survival (4-5 months)	Survival (5-6 months)	Survival (>6 months)
Myc:Gal-1$^{+/+}$	80	124.5	45	36	15	4
Myc:Gal-1$^{+/-}$	64	148.9	20**	30	33*	17*
Myc:Gal-1$^{-/-}$	54	149.4	20**	32	26	22**

Table 10. Survival analysis of Myc:Gal-1$^{+/+}$, Myc:Gal-1$^{+/-}$ and Myc:Gal-1$^{-/-}$. "n" details the number of animals included in the analysis. Mean survival is shown in days. The last four columns show the percentage of animals (~) that died before four months, between the 4th and 5th month, between the 5th and the 6th, or those animals that survived more than 6 months, respectively. Significant differences compared to Myc:Gal-1$^{+/+}$ are denoted by (*) when $p<0.05$ or by (**) if $p<0.005$ (by Chi square test).

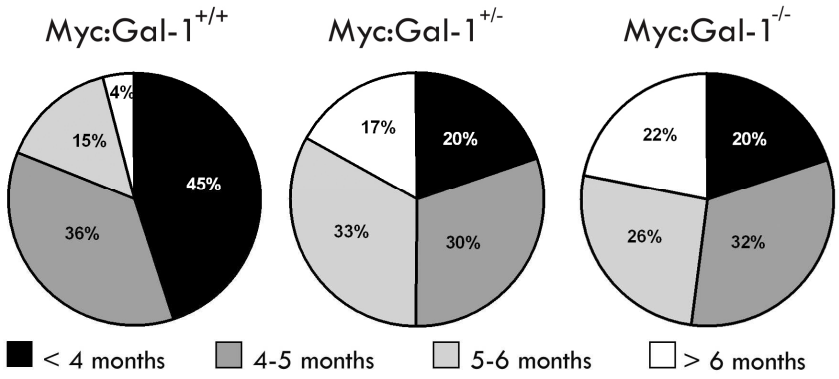

Figure 73. Pie chart analyzing survival of Myc:Gal-1$^{+/+}$, Myc:Gal-1$^{+/-}$ and Myc:Gal-1$^{-/-}$. Percentage of animals that died before four months (black), between the 4th and 5th month (dark grey), between the 5th and the 6th (pale grey) or those animals that survived more than 6 months (white). 80, 64 and 54 of Myc:Gal-1$^{+/+}$, Myc:Gal-1$^{+/-}$ and Myc:Gal-1$^{-/-}$ respectively, were analyzed.

The already dramatic increase in survival in heterozygous animals moved us to assess Gal-1 levels in each group. However, this issue required special attention in order to take into account that Gal-1 was not represented equally in all type of tumors. Qualitatively, Gal-1 IHC indicated that the protein was basically expressed in the stromal compartment of ductal tumors, as well as in ducts and blood vessels (Fig.74). Thus, Gal-1 was found in much higher levels in ductal tumors compared to acinar ones.

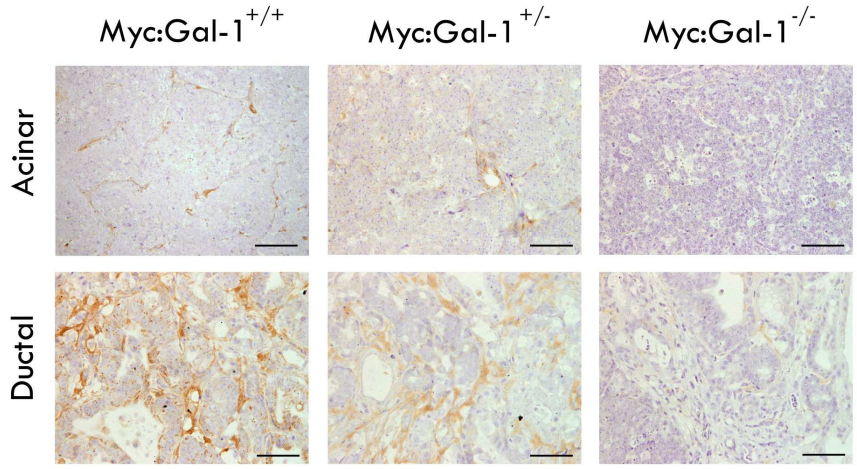

Figure 74. Gal-1 expression in tumors from Myc:Gal-1$^{+/+}$, Myc:Gal-1$^{+/-}$ and Myc:Gal-1$^{-/-}$ mice. IHC was used to detect Gal-1 protein in acinar and ductal tumors. Gal-1 was found to be mainly expressed in fibroblasts, ducts and ECs and for this reason, it was found in much higher levels in ductal tumors, where stroma was much more abundant. Scale bars represent 100 μm.

Therefore, with the intention to quantify the effects of genetic Gal-1 heterozygosis upon protein expression amounts, a loading control to ensure comparison of equivalent cell type populations was required. As we did rarely find pure ductal tumors to compare, we decided to equilibrate protein extracts using a mesenchymal marker such as desmin[127] (Fig.75). Three different ductal enriched tumors from each genotype were chosen and WB analysis confirmed the absence of Gal-1 in Myc:Gal-1$^{-/-}$, but more interestingly, it showed that Gal-1 levels fell to 10% in Myc:Gal-1$^{+/-}$ compared to Myc:Gal-1$^{+/+}$. Consequently, the increased survival observed in heterozygous mice was already due to important protein depletion when one allele was absent.

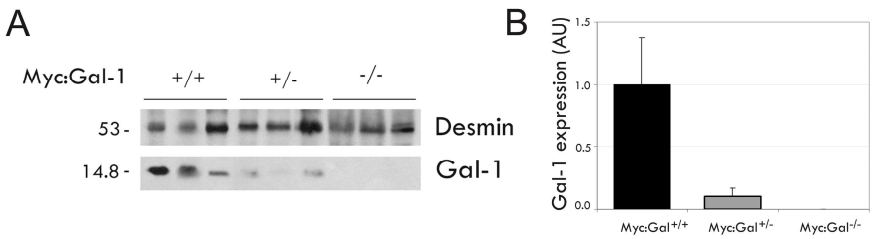

Figure 75. Detection of Gal-1 protein levels in tissue extracts derived from Myc:Gal-1$^{+/+}$, Myc:Gal-1$^{+/-}$ and Myc:Gal-1$^{-/-}$ tumors. A) WB analysis of three different ductal enriched tumors from each group. B) Quantification of the protein levels showing that Myc:Gal-1$^{+/-}$ mice reduced Gal-1 levels to 10% and Myc:Gal-1$^{-/-}$ showed no Gal-1 levels at all, as expected. Desmin was used as the loading control equilibrating mesenchymal populations in heterogeneous tumors.

44 Myc:Gal-1$^{+/+}$, 55 Myc:Gal-1$^{+/-}$ and 43 Myc:Gal-1$^{+/-}$ tumors were histologically analyzed. Regarding metastasis, we observed several macroscopic tumoral foci in organs different from the pancreas, such as in the diaphragma, kidney, liver, intestine, stomach and spleen, although rarely could we observe real invasion after histologic analysis (Fig.76). Instead, tumor was attached to the organ probably because of contiguity rather than real spread through the blood stream. Exceptionally did we find alterations in the organ structure, except for peripancretic lymph nodes (Fig.76g-i). No correlation within genotype and frequency of metastasis could be derived ($p>0.05$ by Chi square), and both acinar and ductal features were observed in metastatic sites (Fig.76).

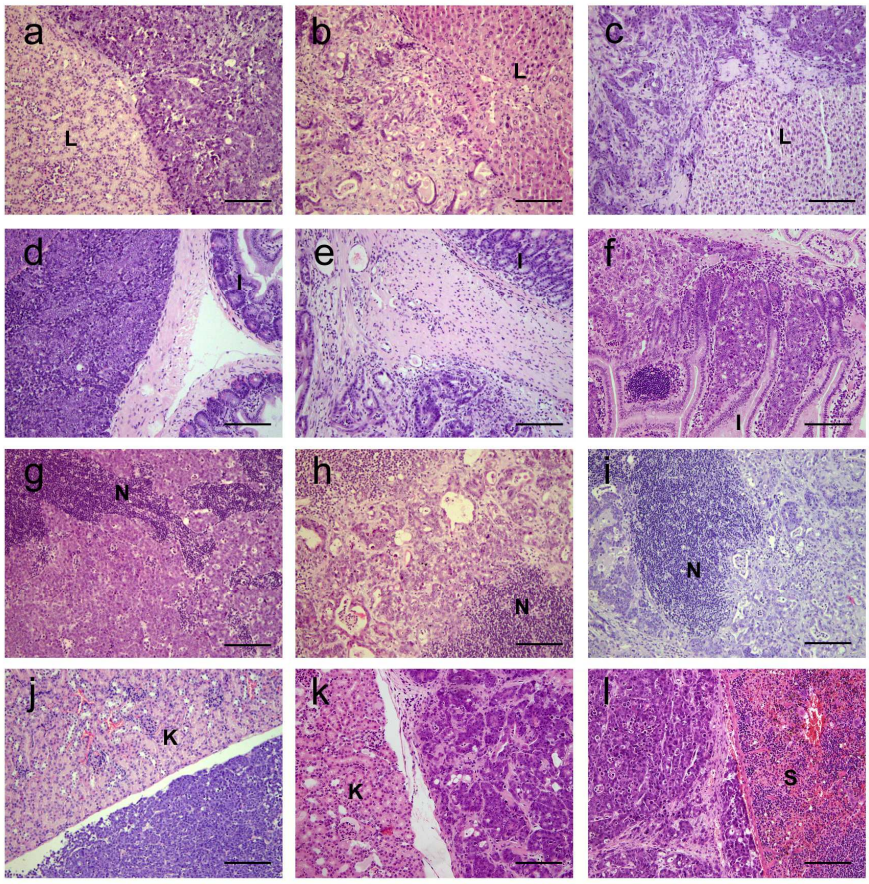

Figure 76. Tumor sites different from pancreas observed in Myc:Gal-1$^{+/+}$, Myc:Gal-1$^{+/-}$ and Myc:Gal-1$^{-/-}$ mice. (a-c) H&E staining from tumors adjacent to liver (L), (d-f) duodenum lamina propria and intestine (I), (g-i) nodes (N), (j,k) kidney (K) and (l) spleen (S). Tumors were usually in contact with these organs without altering their structure except for peripancretic lymph nodes, in which both acinar (g) and ductal (h,i) tumors showed frequent infiltration, still by contiguity. Liver invasion could also be detected (b). Scale bars correspond to 200 μm.

For lymph nodes, a trend towards decreased invasion in heterozygous and KO mice could be observed (Fig.77). Whereas 31.8% of Myc:Gal-1$^{+/+}$ animals presented nodes that had been invaded by pancreatic tumors by contiguity, this percentage was reduced to 27.3% and 27.9% in Myc:Gal-1$^{+/-}$ and Myc:Gal-1$^{-/-}$ mice, respectively.

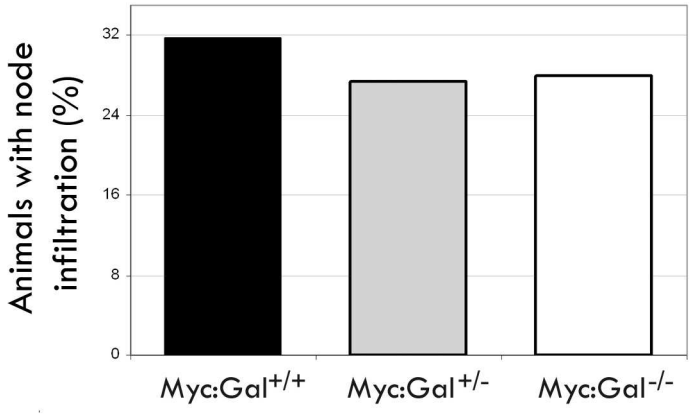

Figure 77. Percentage of animals with peripancreatic lymph node infiltration in Myc:Gal-1$^{+/+}$, Myc:Gal-1$^{+/-}$ and Myc:Gal-1$^{-/-}$ mice. 44, 55 and 43 animals were analyzed from which the 31.8%, 27.3% and 27.9% of Myc:Gal-1$^{+/+}$, Myc:Gal-1$^{+/-}$ and Myc:Gal-1$^{-/-}$ respectively, showed nodes that had been invaded by pancreatic tumors by contiguity. These percentages were not significantly different by Chi square analysis ($p>0.05$).

Tumor size and weight information were collected during the necropsy procedure (Fig.78). No differences on tumor weight were observed comparing animals with both Gal-1 intact alleles, heterozygous and KO mice (2.67, 2.63 and 2.66g, respectively), suggesting that animal welfare was maybe compromised when the tumor reached approximately the same determined dimensions in all groups. The size of each tumor was determined by measuring the 3 largest perpendicular diameters of the tumoral mass. These data were less reliable due to measuring limitations and the irregular shape of tumoral masses. Mean tumor volume was of 4.3 cm^3 for Myc:Gal-1$^{+/+}$, whereas it increased to 5.6 and 5.5 cm^3 for Myc:Gal-1$^{+/-}$ and Myc:Gal-1$^{-/-}$, respectively. Although volume differences among groups did not reach statistical significance, an increase in tumoral size in animals with low Gal-1 levels (heterozygous and KOs) was observed (Fig.78). These data seemed to be contradictory to weight measures but in fact it was just

describing the fact that tumors in heterozygous and KO mice for Gal-1 were much more necrotic and less compact. Thus, their size was bigger although the net weight was comparable (Fig.78).

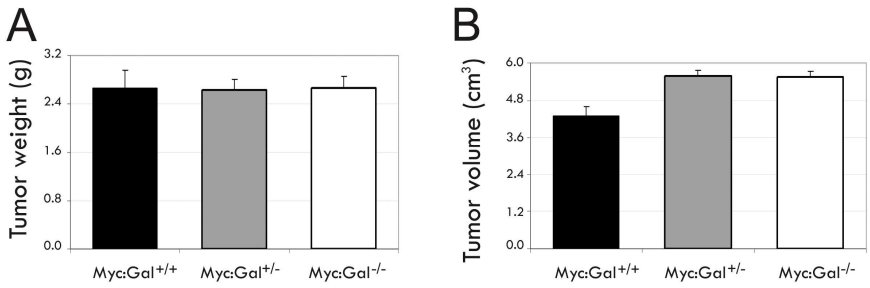

Figure 78. Tumor weight (A) and volume (B) of Myc:Gal-1$^{+/+}$, Myc:Gal-1$^{+/-}$ and Myc:Gal-1$^{-/-}$. The mean values for tumor weight were 2.67, 2.63 and 2.66 for Myc:Gal-1$^{+/+}$, Myc:Gal-1$^{+/-}$ and Myc:Gal-1$^{-/-}$, respectively. Mean tumor volumes were of 4.3, 5.6 and 5.5 cm^3, respectively. Data did not reach statistical significance ($p>0.05$ by Kruskal Wallis analysis).

2.3.2.4 Gal-1 is Involved in Acinar to Ductal Metaplasia

Basic histologic features of the tumors were assessed by H&E staining in 44, 55 and 43 Myc:Gal-1$^{+/+}$, Myc:Gal-1$^{+/-}$ and Myc:Gal-1$^{-/-}$ tumors, respectively. Acinar to ductal metaplasia is frequent in the Ela-1-myc transgenic model[62], an issue that makes this model very appealing for human pancreatic cancer research as it raises the still open debate around pancreatic cancer cell of origin. The abundance of ductal versus acinar component was quantified in tumors from Myc:Gal-1$^{+/+}$, Myc:Gal-1$^{+/-}$ and Myc:Gal-1$^{-/-}$. Tumors were classified among acinar (>80% of acinar component), ductal (>80% of ductal component) or mixed tumors (20-80% of each component) and the number of animals from each group was calculated (Fig.79). Strikingly, a dramatic and Gal-1 dose dependent increase in the number of ductal versus acinar

tumors was found. 43% of Myc:Gal-$1^{+/+}$ animals presented pure or almost pure acinar cell carcinomas, similar to what has been previously reported[62,202]. This number increased to 57% in Myc:Gal-$1^{+/-}$ but significantly rose until 79% in Myc:Gal-$1^{-/-}$ animals. The number of mixed and ductal tumors significantly decreased accordingly, finding a dramatic reduction from 18% of ductal tumors in Myc:Gal-$1^{+/+}$ to a 5% in Myc:Gal-$1^{+/-}$ and a 2% in Myc:Gal-$1^{-/-}$.

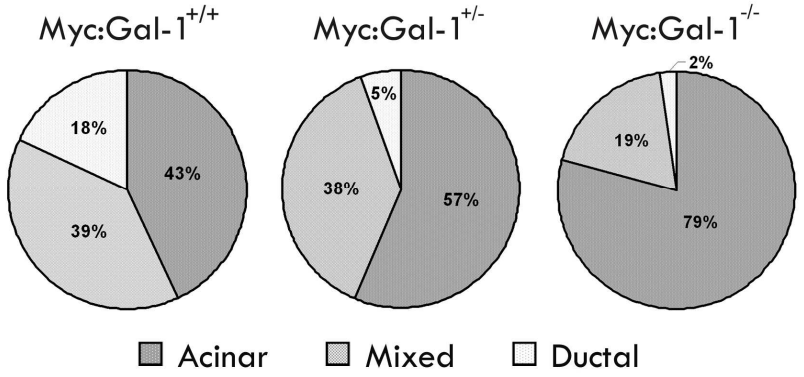

Figure 79. Classification of tumors from Myc:Gal-$1^{+/+}$, Myc:Gal-$1^{+/-}$ and Myc:Gal-$1^{-/-}$ mice among acinar, mixed and ductal. According to their histologic appearance tumors were classified among acinar tumors (>80% of acinar component), ductal tumors (>80% of ductal component) and mixed tumors (tumors bearing both acinar and ductal structures in intermediate percentages, between 20-80%). 44, 55 and 43 tumors were analyzed for each group, respectively. Myc:Gal-$1^{-/-}$ animals showed a significant increase in the number of acinar tumors formed ($p=0.018$ compared to Myc:Gal-$1^{+/-}$ and $p<0.001$ compared to Myc:Gal-$1^{+/+}$). Accordingly, Myc:Gal-$1^{-/-}$ animals showed decreased number of mixed tumors ($p=0.035$ compared to Myc:Gal-$1^{+/-}$ and $p=0.039$ compared to Myc:Gal-$1^{+/+}$). Ductal tumors were also decreased in the heterozygous population ($p=0.045$ compared to Myc:Gal-$1^{+/+}$) and in the KO one ($p=0.015$ compared to Myc:Gal-$1^{+/+}$). Chi square analysis was used for comparisons.

To elaborate on this issue and to examine the nature of mixed tumors in detail, we gathered the data of the percentages of each component from all tumors and studied these pooled results. The above mentioned Gal-1 effect on acinar-ductal phenotype was confirmed and statistically analyzed. A strong correlation between Gal-1 presence and the percentage of ductal component present in

tumors was identified (Fig.80). An average of 40% of the tumor displayed ductal features in Myc:Gal-$1^{+/+}$. Significantly, this percentage was reduced to 23% in Myc:Gal-$1^{+/-}$ ($p=0.016$, by Mann Whitney analysis), and declined to 10% in Myc:Gal-$1^{-/-}$ ($p<0.0001$ comparing to Myc:Gal-$1^{+/+}$ and $p=0.025$ comparing to Myc:Gal-$1^{+/-}$, by Mann Whitney analysis).

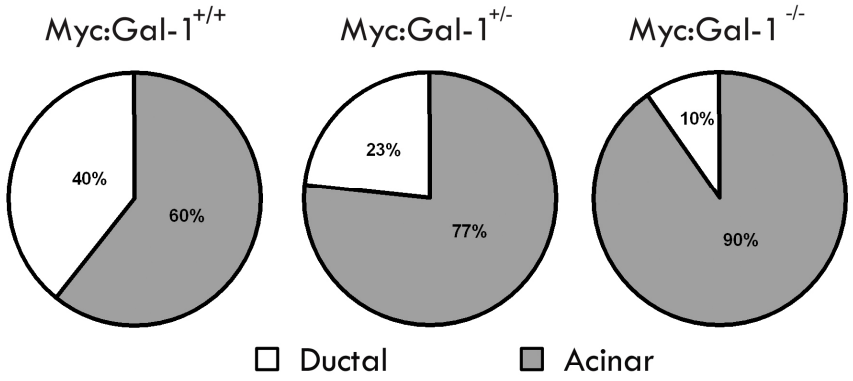

Figure 80. Percentage of ductal versus acinar component from Myc:Gal-$1^{+/+}$, Myc:Gal-$1^{+/-}$ and Myc:Gal-$1^{-/-}$ tumors (44, 55 and 43 tumors were analyzed for each group, respectively). The presence of Gal-1 clearly correlated with an increase in the ductal fraction of tumors. Statistical Mann Whitney values ($p=0.016$ for Myc:Gal-$1^{+/+}$ versus Myc:Gal-$1^{+/-}$; $p<0.0001$ for Myc:Gal-$1^{+/+}$ versus Myc:Gal-$1^{-/-}$; $p=0.025$ for Myc:Gal-$1^{+/-}$ versus Myc:Gal-$1^{-/-}$).

Therefore, the absence of Gal-1 impaired the formation of ductal lesions in the Ela-1-myc transgenic model. These data interestingly suggested that Gal-1 could be actively involved in the acinar to ductal metaplasia in pancreatic cancer, which could be of relevance taking into account that most of the human pancreatic cancer lesions are of ductal appearance and that this event is understood as one of the putative stepwise processes leading to advanced pancreatic adenocarcinoma.

We also characterized the abundance of necrosis in acinar tumors and a direct relation between Gal-1 absence and increased necrosis

was traced (Fig.81). Many Myc:Gal-1$^{-/-}$ animals presented tumoral foci with extensive regions of necrosis inside very compact acinar tumors, which represented the 12.7% of the acinar tumor on average. This percentage was significantly reduced to 7.8% in the Myc:Gal-1$^{+/-}$ (p=0.047 by Mann Whitney) and dropped to 6.0% in Myc:Gal-1$^{+/+}$ (p=0.022 by Mann Whitney). Although reducing Gal-3 levels has been linked to increased apoptosis in several tumoral cell types[699-702], no previous data referred to Gal-1. Moreover, necrosis patches were consistently found inside acinar nodules and seemed to be consequence of asphyxia, hypoxia or hyperproliferation rather than programmed cell death, as no evident morphological images of apoptotic cells were found.

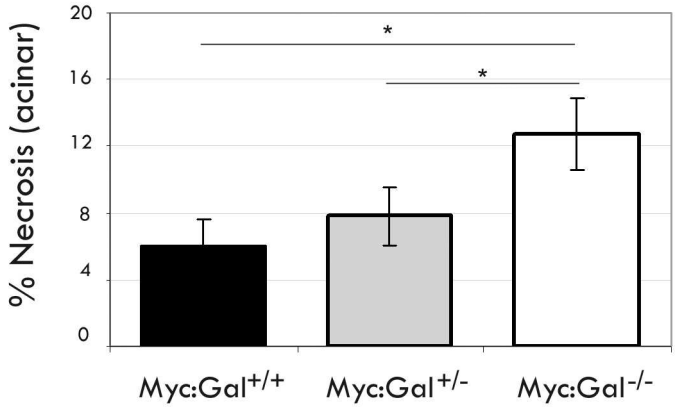

Figure 81. Necrosis indexes in acinar tumors from Myc:Gal-1$^{+/+}$, Myc:Gal-1$^{+/-}$ and Myc:Gal-1$^{-/-}$ mice (44, 55 and 43 tumors were analyzed for each group, respectively). The absence of Gal-1 correlated with increased necrosis in acinar tumors. Myc:Gal-1$^{+/+}$ mice showed 6.0% of necrosis, whereas Myc:Gal-1$^{+/-}$ showed 7.8% and Myc:Gal-1$^{-/-}$ mice had 12.7% of necrosis. *denotes statistical significance by Mann Whitney test (p=0.047 comparing Myc:Gal-1$^{+/-}$ and Myc:Gal-1$^{-/-}$ and p=0.022 for Myc:Gal-1$^{+/+}$ and Myc:Gal-1$^{-/-}$).

In summary, tumors in Myc:Gal-1$^{-/-}$ mice were much more acinar and presented higher necrosis indexes, while heterozygous mice displayed an intermediate phenotype.

2.3.2.5 Ela-1-myc:Gal-1$^{-/-}$ Mice Tumor Characterization

We analyzed tumor characteristics by IHC, assessing proliferation, stroma formation and angiogenesis.

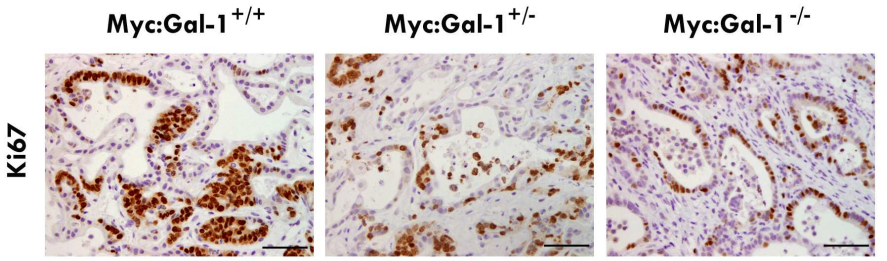

Figure 82. Proliferation in pancreatic ductal tumors in Myc:Gal-1$^{+/+}$, Myc:Gal-1$^{+/-}$ and Myc:Gal-1$^{-/-}$ mice by Ki67 IHC. Scale bars correspond to 100 μm.

Division rates of normal pancreatic epithelial cells are very low[703], but increased cell proliferation is one of the main forces driving pancreatic tumorigenesis. As Gal-1 was basically expressed in the stroma of ductal tumors and proliferation rates were almost 100% in acinar regions, we quantified proliferation only in ductal areas. 15 animals of each group were examined (Fig.82). Myc:Gal-1$^{+/+}$ tumors showed 61.0% of proliferating cells, whereas this percentage was reduced to 43.7 and 38.8% in Myc:Gal-1$^{+/-}$ and Myc:Gal-1$^{-/-}$ mice, respectively (Fig.83). Thus, Myc:Gal-1$^{+/+}$ pancreatic ductal tumors grew at significantly faster levels than heterozygous and KO Gal-1 animals did ($p<0.001$ by Mann Whitney analysis in both cases). These data validated our previous *in vitro* results and indicated that Gal-1 was involved in pancreatic cell proliferation *in vivo*.

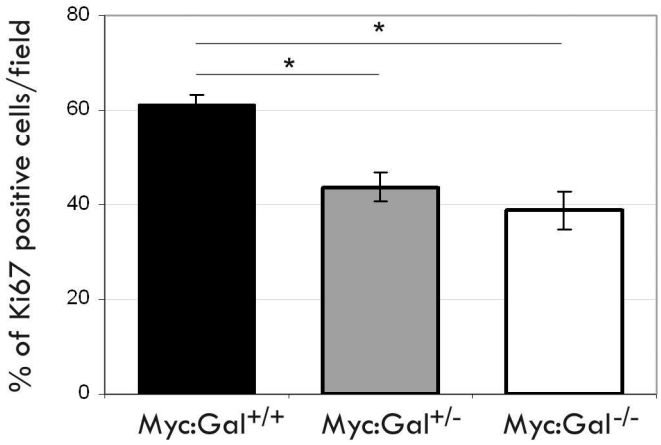

Figure 83. Proliferation rate quantification in pancreatic ductal tumors from Myc:Gal-1$^{+/+}$, Myc:Gal-1$^{+/-}$ and Myc:Gal-1$^{-/-}$ mice, by showing the percentage of Ki67 positive cells. 15 animals of each group were examined. 61.0, 43.7 and 38.8% of cells were proliferating in Myc:Gal-1$^{+/+}$, Myc:Gal-1$^{+/-}$ and Myc:Gal-1$^{-/-}$ mice, respectively. *p<0.001 (by Mann Whitney analysis).

Gal-1 is highly overexpressed in the stroma in pancreatic cancer[582] and its contributions to the desmoplastic event have been reported *in vitro*[421,532,533]. Thus, we decided to analyze stroma formation in ductal lesions. 15 animals of each group were examined (Fig.84).

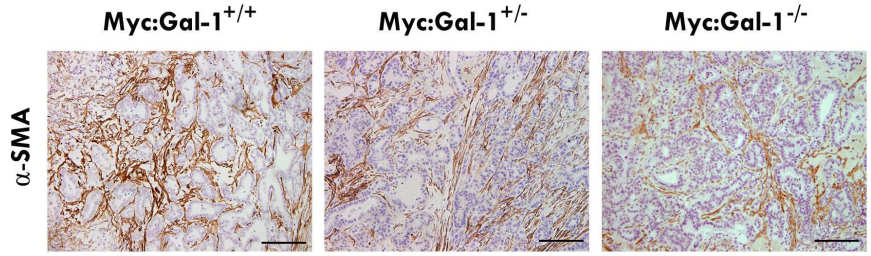

Figure 84. Stroma presence in pancreatic ductal tumors from Myc:Gal-1$^{+/+}$, Myc:Gal-1$^{+/-}$ and Myc:Gal-1$^{-/-}$ mice. α-SMA IHC to detect the amount of stroma present in tumors. Scale bars correspond to 200 μm.

Myc:Gal-1$^{+/+}$ and Myc:Gal-1$^{+/-}$ mice displayed a 14.3% and a 14.6% of the tumoral area identified as stroma, respectively. Nevertheless, this percentage was reduced in Myc:Gal-1$^{-/-}$ tumors to

12.1% (Fig.85A). Although KO animals presented a slight decrease in the amount of α-SMA positive cells, differences did not reach statistical significance by Mann Whitney test.

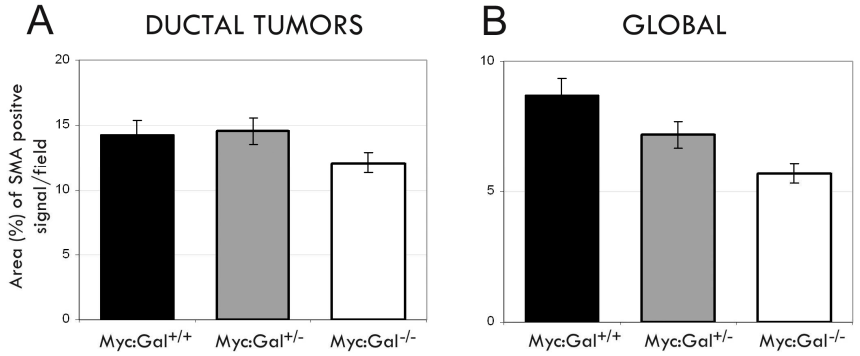

Figure 85. Quantification of the stroma present in pancreatic tumors from Myc:Gal-1$^{+/+}$, Myc:Gal-1$^{+/-}$ and Myc:Gal-1$^{-/-}$ mice, by showing the percentage of positive α-SMA area per field. 15 animals of each group were examined. A) Percentages of stroma present in ductal tumors were of 14.3, 14.6 and 12.1% in Myc:Gal-1$^{+/+}$, Myc:Gal-1$^{+/-}$ and Myc:Gal-1$^{-/-}$ tumors, respectively. Differences did not reach significance by Mann Whitney statistical test. B) Global stroma analysis considering the percentage of acinar and ductal tumors in each genotype.

Yet, we must take into account that the amount of ductal lesions (enriched with the stromal compartment) were much more abundant in Myc:Gal-1$^{+/+}$ (40%) compared to Myc:Gal-1$^{+/-}$ mice (23%), whereas these areas only represented the 10% in Myc:Gal-1$^{-/-}$ tumors (see section *2.3.2.4. Gal-1 is Involved in Acinar to Ductal Metaplasia*, Fig.80). Therefore, a global stroma percentage could be calculated in tumors from wild type, heterozygous and KO animals for Gal-1, considering the percentage of stroma present in each tumor type and the proportions of ductal versus acinar tumor areas. Although the decrease of the amount of stroma in ductal areas was not dramatic, the overall tumoral decrease of the mesenchymal population was markedly observed upon Gal-1 depletion. Whereas in Myc:Gal-1$^{+/+}$ tumors, the stroma represented the 8.7%, this

percentage was reduced to 7.2% in Myc:Gal-1$^{+/-}$ and to 5.7% in the case of Myc:Gal-1$^{-/-}$ mice. These data proved that Gal-1 regulated the amount of stroma formed in pancreatic tumors.

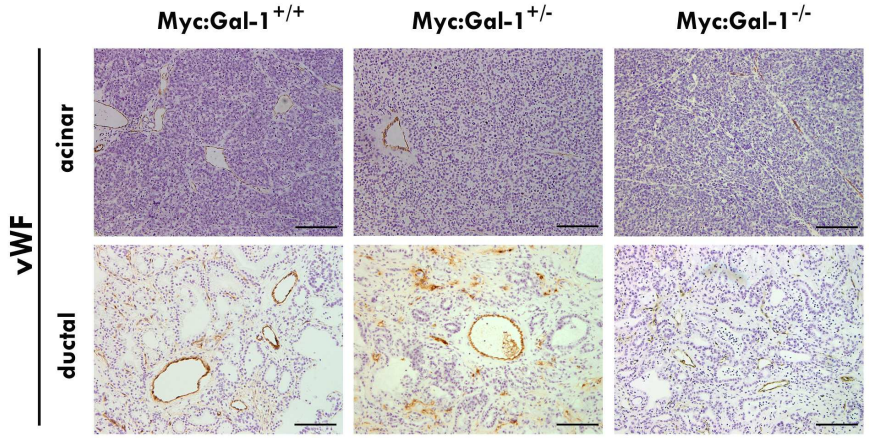

Figure 86. Angiogenesis in pancreatic acinar and ductal tumors from Myc:Gal-1$^{+/+}$, Myc:Gal-1$^{+/-}$ and Myc:Gal-1$^{-/-}$ mice. IHC against vWF to detect blood vessels and ECs present in tumors. Scale bars correspond to 200 μm.

Gal-1 has been repeatedly linked to angiogenesis[445,482,540,550] but none of the previous reports referred to pancreatic cancer. In order to face the importance of the lectin in this tissue context, we characterized angiogenesis in 15 tumors from each group: Myc:Gal-1$^{+/+}$, Myc:Gal-1$^{+/-}$ and Myc:Gal-1$^{-/-}$ mice (Fig.86). In general, acinar tumor masses were rarely vascularized except on their periphery. Still, microscopic histological analysis of tumors revealed that blood vessel formation was severly impaired in Myc:Gal-1$^{-/-}$, where intratumoral blood vessels were smaller and very difficult to be found and instead, individual ECs were detected (Fig.86). By vWF immunostaining, we quantified vascularization in these acinar tumors, which was of 0.9, 0.6 and 0.2% for Myc:Gal-1$^{+/+}$, Myc:Gal-1$^{+/-}$ and Myc:Gal-1$^{-/-}$ mice, respectively (Fig.87A). A significant decrease was detected in the presence of intratumoral blood vessels

in Myc:Gal-1$^{-/-}$ acinar tumors compared to wild type and heterozygous mice ($p<0.005$ by Mann Whitney). Although there seemed to be a reduction in angiogenesis with the single loss of one Gal-1 allele, differences did not reach statistical significance in this case.

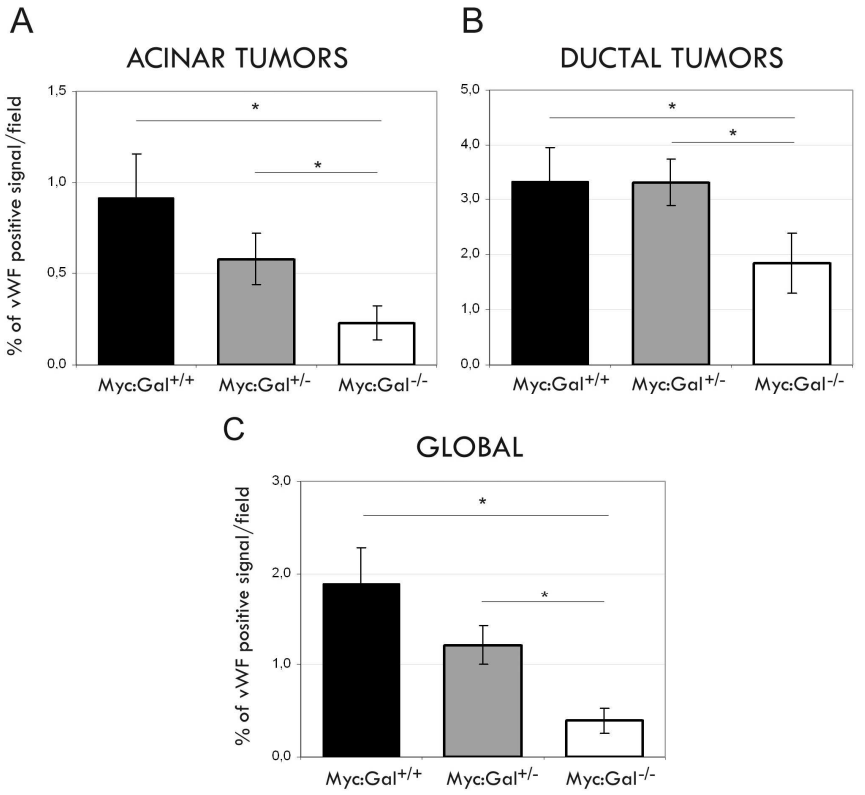

Figure 87. Quantification of angiogenesis in pancreatic acinar and ductal tumors from Myc:Gal-1$^{+/+}$, Myc:Gal-1$^{+/-}$ and Myc:Gal-1$^{-/-}$ mice. IHC against vWF to detect blood vessels and ECs present in tumors. 15 animals of each group were examined. A) The percentage of positive vWF signal per field was of 0.9, 0.6 and 0.2% in acinar tumors from Myc:Gal-1$^{+/+}$, Myc:Gal-1$^{+/-}$ and Myc:Gal-1$^{-/-}$, respectively. B) These values were of 3.3, 3.3 and 1.9% for ductal tumors, respectively. C) For overall tumor analyses, angiogenic values were of 1.9, 1.2 and 0.4, respectively. *denotes $p<0.005$ in both comparisons in the global analysis and in acinar tumors whereas *corresponds to $p=0.04$ (Myc:Gal-1$^{+/+}$ versus Myc:Gal-1$^{-/-}$) and $p=0.01$ (Myc:Gal-1$^{+/-}$ versus Myc:Gal-1$^{-/-}$) by Mann Whitney test. Scale bars correspond to 200 μm.

Regarding ductal tumors, a clear significant decrease in blood vessel formation was also detected in Myc:Gal-1$^{-/-}$ tumors (1.9%) compared to wild type and heterozygous mice (3.3% for both of them) (Fig.87B). Besides, once again we must bear in mind that ductal lesions (which were by far much more vascularized) were more abundant in Myc:Gal-1$^{+/+}$ tumors compared to Myc:Gal-1$^{+/-}$ and the effect was even more pronounced compared to Myc:Gal-1$^{-/-}$. Therefore, if we quantified the global rate of angiogenesis for each genotype, taking into account the proportion of each tumor type and its angiogenic rate, Gal-1 involvement in angiogenesis was even highlighted. Myc:Gal-1$^{+/-}$ tumors showed a 37% reduction of angiogenesis compared to Myc:Gal-1$^{+/+}$ tumors. Significantly, this decrease fell until a 79% when Myc:Gal-1$^{-/-}$ tumors were compared to Myc:Gal-1$^{+/+}$ ones (Fig.87C).

In line with these results, the number of animals that presented intraperitoenal hemorrhage at necropsy was also quantified, finding a significant decrease when pancreatic tumors developed with low or no Gal-1 levels (Fig.88). Whereas 37.8% of Myc:Gal-1$^{+/+}$ animals presented abdominal hemorrhage, this percentage dropped to 13.0% in Myc:Gal-1$^{+/-}$ and fell to 9.5% in Myc:Gal-1$^{-/-}$ mice ($p=0.01$ by Chi square in both cases). This macroscopic evidence confirmed the IHC data obtained from intratumoral masses and validated Gal-1 importance in angiogenesis. Considering low Gal-1 expression in heterozygous mice, there seemed to be a significant correlation between protein levels and hemorrhage risk. According to histological analysis (Fig.89), we believe this kind of hemorrhage could be due to tumoral cell infiltration to blood vessels, which was frequently observed in Myc:Gal-1$^{+/+}$ animals. Besides, the increased

intraperitoneal hemorrhage detected in Myc:Gal-1$^{+/+}$ animals could be explained by the fact that ductal tumors, much more frequent in this animal group, were far more vascularized than acinar ones.

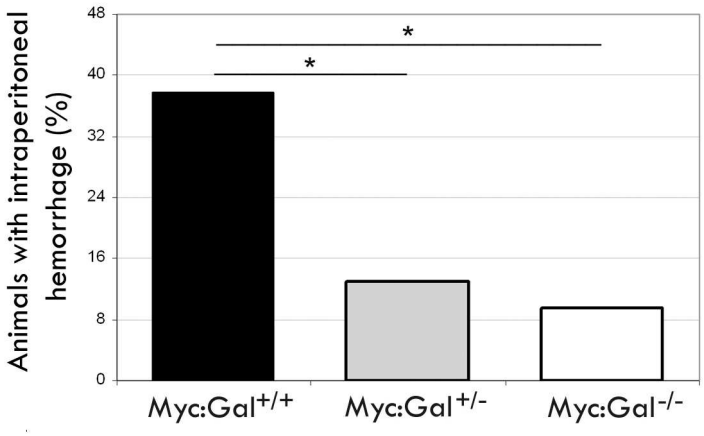

Figure 88. Percentage of animals with IP hemorrhage in tumors from Myc:Gal-1$^{+/+}$, Myc:Gal-1$^{+/-}$ and Myc:Gal-1$^{-/-}$ mice. 37.8% of Myc:Gal-1$^{+/+}$ showed abdominal hemorrhage at necropsies wheres only 13.0% and 9.5% of Myc:Gal-1$^{+/-}$ and Myc:Gal-1$^{-/-}$ respectively showed this distinctive feature. *corresponds to p=0.01 (for Myc:Gal-1$^{+/+}$ versus Myc:Gal-1$^{-/-}$ and for Myc:Gal-1$^{+/+}$ versus Myc:Gal-1$^{+/-}$) by Chi square analysis.

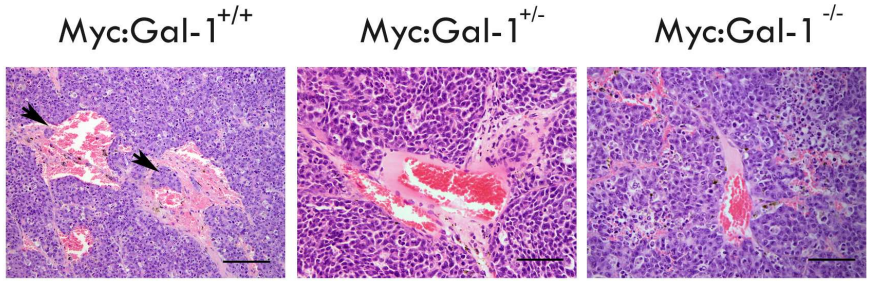

Figure 89. Blood vessel infiltration by tumoral cells in Myc:Gal-1$^{+/+}$, Myc:Gal-1$^{+/-}$ and Myc:Gal-1$^{-/-}$ tumors. Histologic analysis of the angiogenic network in Myc:Gal-1$^{+/+}$, Myc:Gal-1$^{+/-}$ and Myc:Gal-1$^{-/-}$ tumors. Tumoral cells were sometimes found inside the vascular system (arrows). Scale bars represent 100 µm.

Altogether, our data using Ela-1-myc:Gal-1$^{-/-}$ transgenic model demonstrated that Gal-1 was actively involved in several pathological effects driving pancreatic tumor progression *in vivo*. One of the major findings from the study was Gal-1

haploinsufficiency in controlling pancreatic tumor growth and animal survival time. Moreover, we found that Gal-1 was markedly participating in acinar-ductal transdifferentiation of pancreatic tumors, necrosis, stroma formation and angiogenesis, supporting an overall major involvement of Gal-1 in this carcinogenic process *in vivo* (see *Discussion*, Fig.118).

2.3.3 *In vivo* Role of Gal-1 in Pancreatic Cancer using Zebrafish Models

As referred in the Introduction, ptf1a:eGFP-K-Ras^{G12V} emerged as a *bona fide* pancreatic cancer model (see *Introduction*, section *1.2.4.3. Zebrafish Models of PDAC*). Therefore, we wanted to study DrGal1-L2 expression (Gal-1 ortholog in zebrafish) in normal and tumoral pancreas to establish Gal-1 role in zebrafish pancreatic tumor progression.

We set up the ISH protocol in zebrafish paraffin sections using a trypsin probe. Trypsin RNA was specifically detected in acinar cells, confirming the ISH technique protocol (Fig.90).

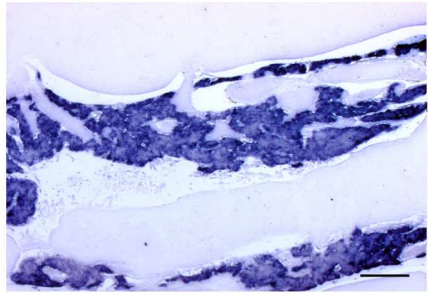

Figure 90. Trypsin detection by ISH in zebrafish paraffin embedded sections. Scale bar corresponds to 200 μm.

We analyzed Gal-1 expression in normal pancreas, both at RNA and protein level. The antisense DrGal1-L2 probe showed a faint and diffuse signal in zebrafish normal pancreas, suggesting low or no expression in intestine and pancreas (data not shown). Protein data was obtained by IHC with a specific anti-DrGal1-L2 antibody. However, in this case, a basal low expression in the pancreas was observed, detecting some cells (probably mesenchymal) with higher protein levels (Fig.91).

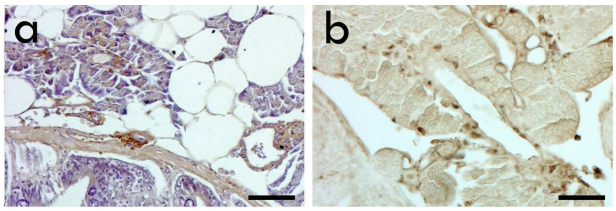

Figure 91. DrGal1-L2 expression in adult zebrafish normal pancreas detected by IHC (a,b: with and without hematoxylin counterstaining). Scale bars correspond to 50 µm.

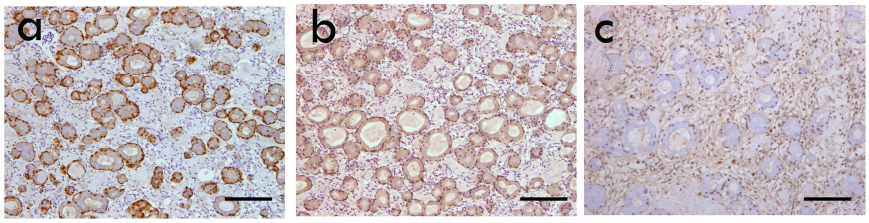

Figure 92. Gal-1 IHC with three different antibodies on zebrafish ptf1a:eGFP-K-Ras^{G12V} transgenic model. a) Goat anti-Gal-1 antibody (R&D Systems). b) Rabbit anti-Gal-1 antibody (Sigma). C) Rabbit anti-Gal-1 antibody (kindly provided by Dr. Gabius). Scale bars correspond to 200 µm (a,b) and 100 µm (c).

We next studied Gal-1 pattern of expression in zebrafish pancreatic tumors of the ptf1a:eGFP-K-Ras^{G12V} transgenic model. In a first approximation, polyclonal antibodies raised against the human Gal-1 protein were used, hoping that the homology between human and zebrafish orthologs would be enough to detect DrGal1-L2. Three different Gal-1 antibodies were used, two of which

displayed a ductal pattern of expression (Fig.92a,b) whilst the third one basically stained the tumoral stroma (Fig.92c).

To confirm protein localization in tumoral zebrafish pancreas, we used a specific antibody raised against zebrafish Gal-1 ortholog. DrGal1-L2 appeared to be found exclusively in the stroma around ducts in zebrafish ductal tumors, reproducing the pattern of expression observed in human and murine pancreatic tumors. This similarity pointed at ptf1a:eGFP-K-Ras^{G12V} as a proper animal system to further analyze the functional role of Gal-1 during pancreatic tumoral progression. In addition, we could reproduce the same results in another zebrafish double transgenic model that was developed in Dr. Leach laboratory: ptf1a:GAL4/VP16 UAS:eGFP-K-Ras^{G12V} (Fig.93). Although tumors formed had a greater acinar component in general, some of them were characterized by an important desmoplastic reaction. Antibody specificity was confirmed by competition experiments with the recombinant protein (Fig.94).

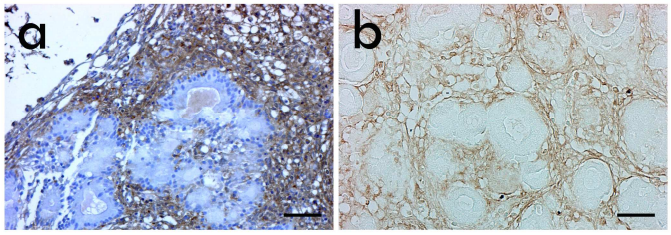

Figure 93. DrGal1-L2 expression in two different adult zebrafish ductal tumors from the ptf1a:eGFP-K-Ras^{G12V} transgenic model. Gal-1 detection by IHC using a specific antibody for DrGal-1-L2. (a) was counterstained with hematoxylin whereas (b) was not. Scale bars correspond to 100 μm.

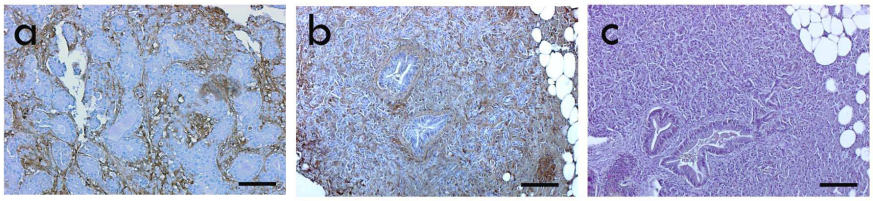

Figure 94. DrGal1-L2 detection in two different adult zebrafish tumors from the ptf1a:GAL4/VP16 UAS:eGFP-K-Ras^{G12V} transgenic model. a,b) DrGal1-L2 IHC in two adult ductal (a: 7 months; b: 2 months) tumors, showing the protein to be localized in the stroma. c) Serial cut from (b) in which competition with the recombinant DrGal1-L2 protein was performed, almost completely depleting the signal. All images were counterstained with hematoxylin. Scale bars correspond to 25 μm (a) and 50 μm (b,c).

Therefore, it seemed that zebrafish transgenic models engineered to generate pancreatic adenocarcinoma could represent a very interesting tool to analyze Gal-1 involvement in tumor progression. Inhibitory strategies had been previously developed to reduce or completely deplete DrGal1-L2 levels *in vivo*. On one hand, morpholinos (MO) specifically designed against Gal-1 zebrafish ortholog could interfere with translation initiation (ATG-MO) or with the splicing process (splice-MO) in one cell embryos. This strategy was previously used and proven to work very well[442,445] but it was restricted to developmental studies, as depletion was only efficient during the first days of the zebrafish development. Pancreatic tumors in the zebrafish models appeared after 2 months, when DrGal1-L2 levels would have already been recovered and so would remain unaffected. Conditional Gal-1 KOs in zebrafish emerged as the alternative, though this technology was still being set up and it was thus unavailable.

2.3.4 Gal-1 in Mouse Pancreas Development

Tumoral transformation has been reported to recapitulate genetic programs involved in early development. For this reason, we decided to assess the relevance of Gal-1 in pancreatic development to see whether we could observe any parallelism to pancreatic tumorigenesis. Indeed, in mice, Gal-1 expression during pancreatic development seemed to be restricted to the stroma surrounding the branching epithelium, resembling what happens in human pancreatic cancer (Fig.95).

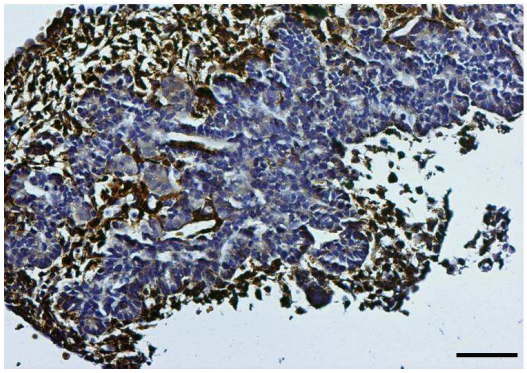

Figure 95. Gal-1 detection by IHC in E13.5 mouse embryo pancreas. Scale bar corresponds to 50 μm.

As mentioned in the Introduction, when pancreatic epithelium becomes enveloped in the mesenchyme, this compartment is the main source of stimuli driving differentiation, proliferation and ramification of pancreatic epithelium[5,13,14] (see *Introduction*, section *1.1.1. Anatomy, Physiology and Development*). Indeed it is the mesenchyme that seems to be responsible for controlling the relative proportion between endocrine and exocrine populations in the pancreas[14,15]. The mechanism driving this process is not fully understood, although it seems clear that the lack of mesenchyme participates in epithelial proliferation by tilting the balance towards

endocrine differentiation. As Gal-1 expression was found in the mesenchyme surrounding pancreatic developing epithelium, we wondered whether it could be actively involved in this event.

In a first approach, we dissected E13.5 mice pancreas and downregulated Gal-1 in these dorsal bud explants through siRNA transfection. IF was used to follow *in vitro* pancreatic development in the presence or absence of the lectin. Although these data are preliminary, we observed a steady increase on the amount of epithelial tissue in low Gal-1 expressing pancreas. In line with this, an increase in the amount of endocrine tissue was also observed, presenting many more islets than usual and of higher size, labeled with insulin/glucagon staining (Fig.96). These islets appeared, as expected, to be positive for E-cadherin, although its intensity was lower than epithelial tissue.

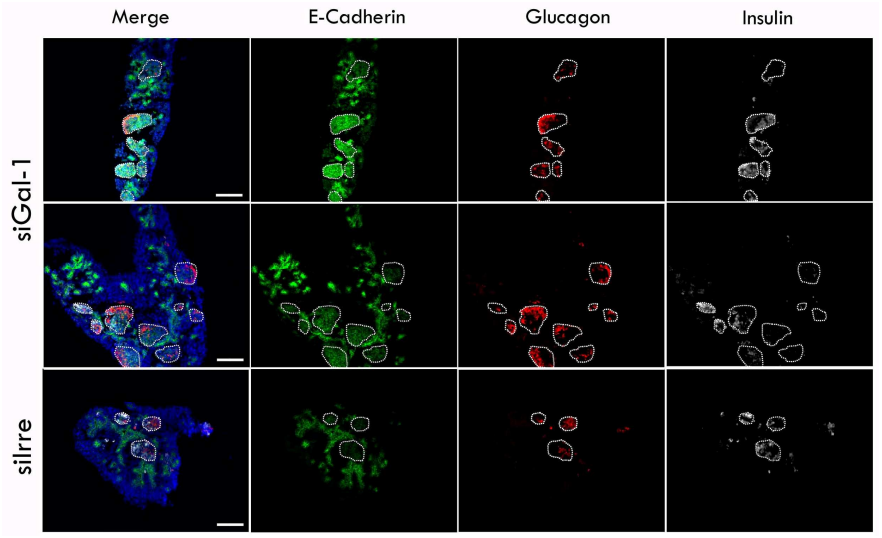

Figure 96. E13.5 dorsal bud explants transfected with Gal-1 siRNA (siGal-1) or transfected with an irrelevant siRNA (silrre). IF staining for E-cadherin (green), DAPI (blue), glucagon (red) and insulin (white) in pancreatic embryonic populations after 6 days of *in vitro* culture is shown. Islets are encircled in white. Scale bars correspond to 100 μm.

Interestingly, higher proportion of stroma was also detected in control pancreas whereas this mesenchymal component seemed to be underrepresented when Gal-1 levels were reduced (Fig.97).

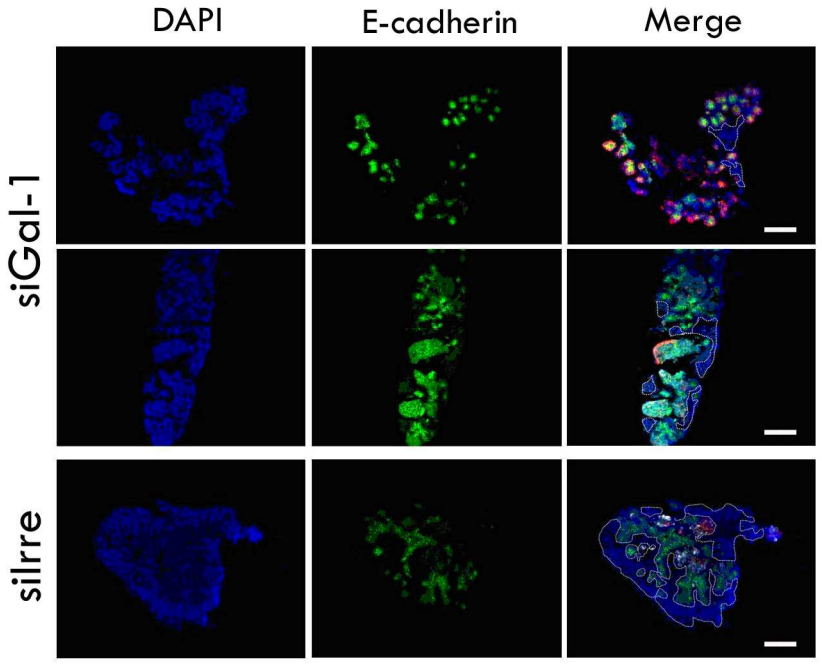

Figure 97. E13.5 dorsal bud explants transfected with Gal-1 siRNA (siGal-1) or transfected with an irrelevant siRNA (siIrre). IF staining for E-cadherin (green) and DAPI (blue) was performed to show the epithelial proportion in developing pancreas. The stroma (negative for E-cadherin) is encircled in white in the merge image. Scale bars correspond to 100 μm.

These preliminary data could be indicating that pancreas with low Gal-1 levels showed increased epithelial proliferation rates and endocrine differentiation was favored, unbalancing the usual proportions of cellular populations. Moreover, the amount of stroma in this case was diminished. We had previously shown that Gal-1 absence impaired tumoral fibroblast proliferation[421] and that Gal-1 modulated the amount of stroma in pancreatic tumor progression *in vivo* (see section *2.3.2.5. Ela-1-myc:Gal-1$^{-/-}$ Mice Tumor*

Characterization). Thus, it seemed that the lectin was controlling the amount of stroma present in the pancreas, both in development and in cancer, influencing in this manner, neighbor epithelial cells. These data presented once again a situation in which both embryogenesis and tumor progression displayed common traits.

To validate these conclusions in a finer system, we performed pancreas dissection from wild type C57BL/6 mice or Gal-1 KO mice at different stages of development and analyzed pancreatic populations. Although these data are also preliminary and need further confirmation, it seemed that Gal-1 KO pancreas showed higher acinar cell marker levels (carboxypeptidase (CPA) and amylase) (Fig.98 and Fig.99) and probably higher endocrine markers too (insulin). No differences were observed regarding E-cadherin expression during development or any overall difference at stage E19.5 (Fig.100).

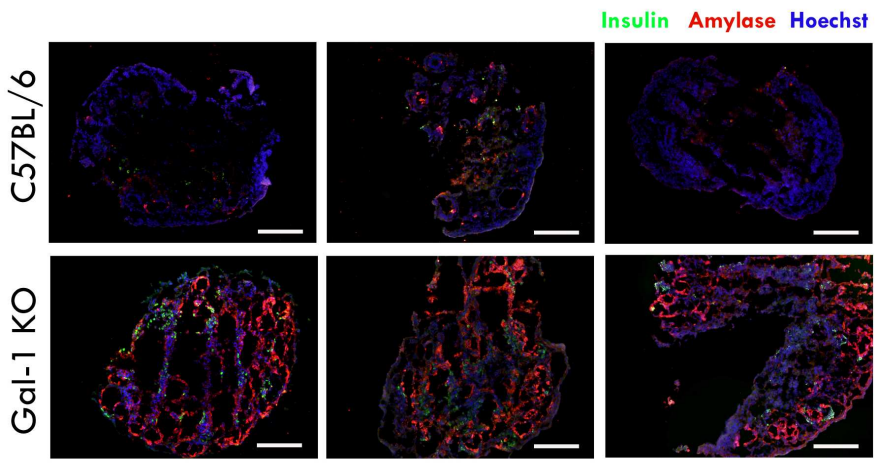

Figure 98. E14.5 dorsal bud explants from wild type C57BL/6 mice and Gal-1 KO mice. IF against insulin (green), amylase (red) and Hoechst (blue) is shown. Scale bars correspond to 200 μm.

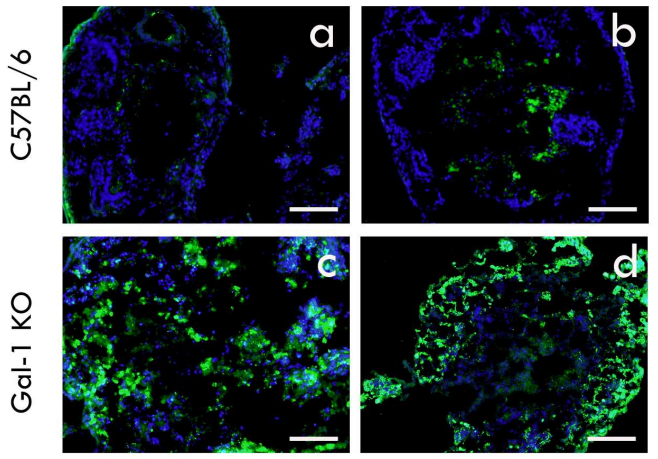

Figure 99. Carboxypeptidase IF in E13.5 (a,c) or E14.5 (b,d) dorsal bud explants from wild type C57BL/6 mice or Gal-1 KO mice. CPA (green), DAPI (blue). Scale bars correspond to 100 µm (a-c) and 200 µm (d).

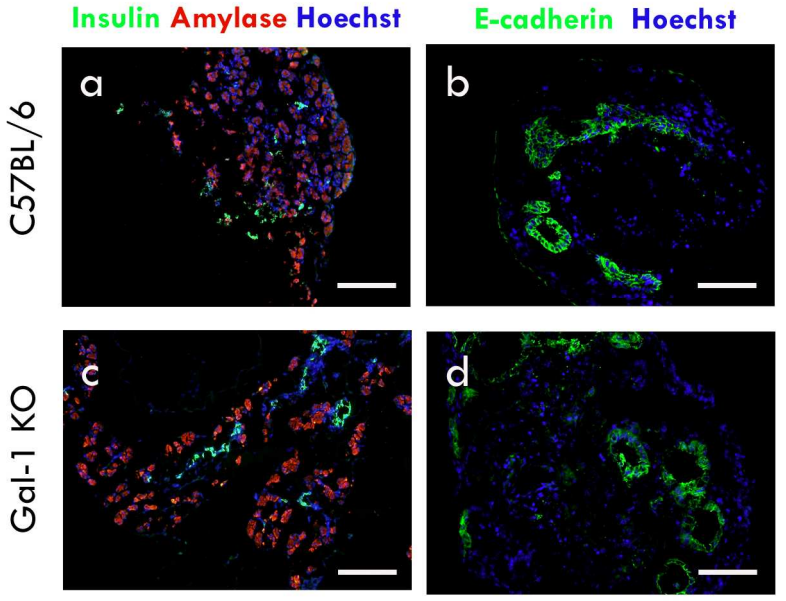

Figure 100. E19.5 and E13.5 dissected pancreas from wild type C57BL/6 mice (a,b) and Gal-1 KO mice (c,d). IF staining of amylase (red) and insulin (green) in E19.5 dissected pancreas (a,c) and E-cadherin in E13.5 dorsal bud explants (b,d). Scale bars correspond to 200 µm.

2.4 DECIPHERING GAL-1 MOLECULAR MECHANISMS: TRANSCRIPTOME ANALYSIS

2.4.1 Upregulation or Downregulation of Gal-1 Levels in Cultured Pancreatic Cancer Cells

We have previously shown that Gal-1 was functional in many pathological events in pancreatic cancer *in vitro* and *in vivo* (see section *2.2. Study of tPA/Gal-1 Interaction in vitro* and *2.3. Study of Gal-1 Relevance in PDAC in vivo*). In order to analyze in depth the molecular mechanisms involved in all these processes, we decided to compare the transcriptome of cells with altered Gal-1 levels by microarray studies. With the aim to design a rigorous analysis and filter as much as possible the results obtained from this high-throughput approach, we worked with two complementary methodologies: Gal-1 downregulation and upregulation.

On one hand, we downregulated Gal-1 through infecting PANC-1 cells (expressing high levels of Gal-1) with lentiviral particles carrying shRNA. We first set up the efficiency of Gal-1 downregulation using 5 different shRNA sequences targeting Gal-1. As a control to later assess the effects of infection *per se*, parental non-infected cells were used and compared to cells infected with an irrelevant shRNA sequence. After puromycin selection, Gal-1 protein levels were assessed (Fig.101). All shRNAs directed to Gal-1 mRNA were significantly active. Proper downregulation was maintained after several passages and also after freeze/thaw cycles (data not shown).

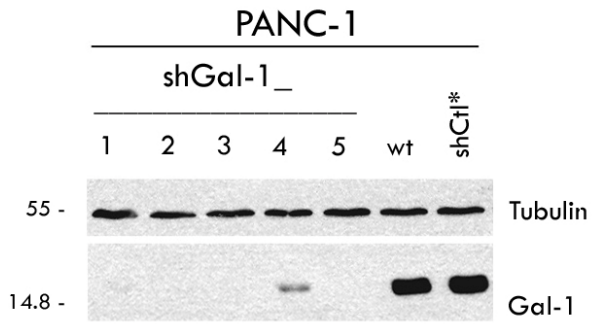

Figure 101. Gal-1 downregulation achieved by shRNA targeting Gal-1 in PANC-1 cells. Protein levels showing Gal-1 depletion 17 days after PANC-1 lentiviral infection carrying 5 different shRNA for Gal-1 (shGal-1_1, shGal-1_2, shGal-1_3, shGal-1_4 and shGal-1_5). Cells were cultured with puromycin in order to achieve selection of positively infected cells. Downregulation was successfully achieved in all cell lines. Tubulin levels are shown as the loading control.

Two different shRNA sequences were selected to exclude off-target effects: shGal-1_2 and shGal-1_5, whose efficiency proved to be slightly better than the rest of the sequences assessed. Gal-1 protein levels were reduced to more than 90% with both shRNA constructs targeting Gal-1 RNA (Fig.102).

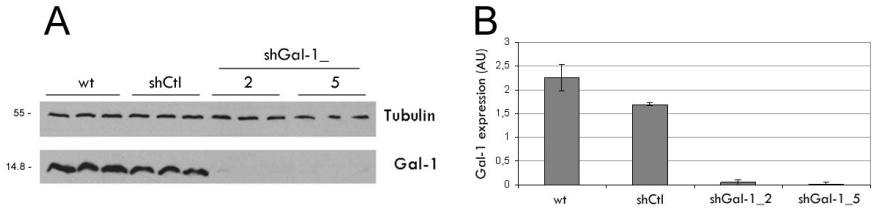

Figure.102. Gal-1 protein expression levels in PANC-1 after shRNA lentiviral infection. A) Protein Gal-1 levels examined by WB in non-infected PANC-1 cells (wt), cells infected with a scrambled shRNA (shCtl) or cells infected with two different shRNA for Gal-1 (shGal-1_2 and shGal-1_5). Triplicates used for the microarray experiment are shown. Tubulin levels were used as the loading control. B) Quantification of the WB analysis showing a significant downregulation of more than 90% from basal Gal-1 levels, with the two shGal-1 sequences.

On the other hand, we selected the RWP-1 cell line, with very low Gal-1 levels, to stably overexpress the lectin. After selection with G418 and cell cloning, we picked a control clone (RWP-1

transfected with empty pcDNA3) and one RWP-1 clone that displayed a fivefold increase of Gal-1 expression (Fig.103).

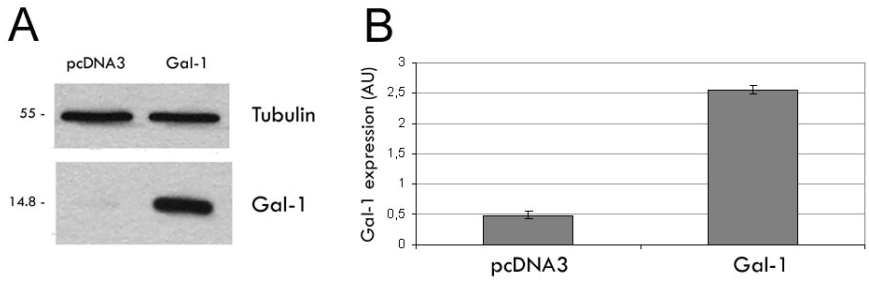

Figure 103. Gal-1 protein levels of expression of RWP-1 clones selected for microarrays analysis. A) Protein expression levels by WB analysis. RWP-1 control clone (pcDNA3) and an RWP-1 clone that overexpressed Gal-1 (Gal-1) are shown. Tubulin was used as a loading control. B) Quantification of the WB data finding quintuplicated expression of the lectin in the RWP-1 Gal-1 clone.

2.4.2 Functional Effects of the Modulation of Gal-1 Levels in Cultured Pancreatic Cancer Cells

In order to characterize these cells with stably altered Gal-1 levels before microarray studies, we checked whether shRNA mediated downregulation or Gal-1 overexpression significantly affected some of the typical Gal-1 related phenotypes.

2.4.2.1 *In vitro* Cell Proliferation

We assessed whether proliferation was altered in pancreatic cells after stable Gal-1 downregulation (PANC-1) or overexpression (RWP-1) by quantifying BrdU incorporation levels (Fig.104A). We found that Gal-1 alteration levels *per se* (in whichever direction), did

not affect proliferation rates (Fig.104B). These data were in agreement with our previous data showing that transient Gal-1 downregulation by siRNA had no effect in HPDE and PANC-1 cell growth[421].

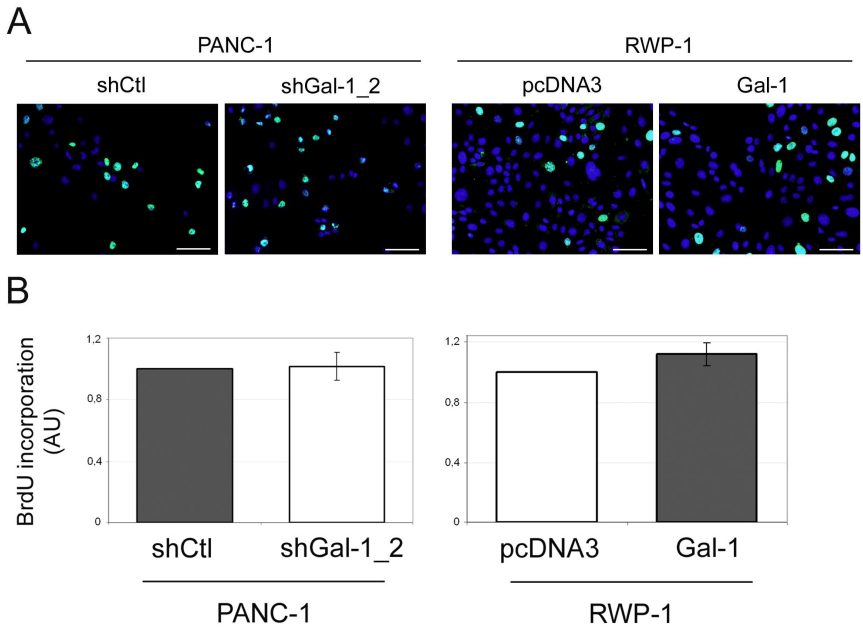

Figure 104. Proliferation remained unaffected upon Gal-1 levels modulation. A) IF examples of proliferation in PANC-1 and RWP-1 cells with endogenous (shCtl, pcDNA3), downregulated (shGal-1_2) or overexpressed (Gal-1) Gal-1 levels, assessed by BrdU incorporation. Scale bars correspond to 100 μm. B) Quantification of proliferation assessed by BrdU incorporation in PANC-1 and RWP-1 cells. No significant differences were observed within groups ($p>0.05$).

2.4.2.2 *In vitro* Cell Adhesion

Secreted Gal-1 plays a very important role mediating cell/ECM interaction through its recognition of many glycosylated cell membrane receptors and ECM glycoproteins[437,477,481]. We decided to analyze whether downregulation or overexpression of Gal-1 levels in PANC-1 and RWP-1 pancreatic tumoral cells resulted in

changes in ECM/cell adhesion. We analyzed adhesion over matrigel in these cells with altered Gal-1 amounts and failed to detect significant differences (Fig.105). Similarly, no effect of Gal-1 levels was observed when performing trypsin lift up experiments (data not shown).

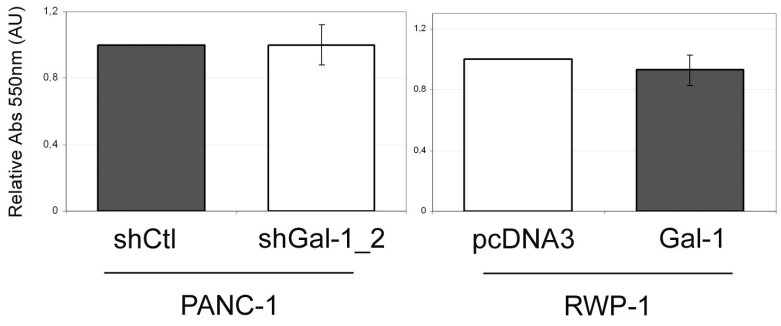

Figure 105. Adhesion over matrigel in PANC-1 and RWP-1 cells with Gal-1 altered levels of expression. Relative adhesion values assessed through MTT staining and absorbance measure at 550 nm of PANC-1 and RWP-1 with endogenous (shCtl, pcDNA3), downregulated (shGal-1_2) or overexpressed (Gal-1) Gal-1 levels. All cells, regardless of their Gal-1 levels displayed similar adhesion levels. No significant differences were observed ($p>0.05$).

2.4.2.3 *In vitro* Cell Mobility

Gal-1 has been described to play a key role in cell migration[541,543,549]. We analyzed whether modulation of Gal-1 expression levels was related to cell motility using wound healing (Fig.106A) and time-lapse video microscopy (Fig.107A).

Migration assessment by wounding a confluent monolayer of cells depicted a controversial scenario. Whereas in PANC-1 cells downregulation of Gal-1 levels resulted in a reduction of the wound closure, in RWP-1, cells overexpressing Gal-1 also showed the same

deficiency (Fig.106B). These data indicated that Gal-1 could exert a positive or negative modulation of cell migration depending on protein levels and/or cellular contexts.

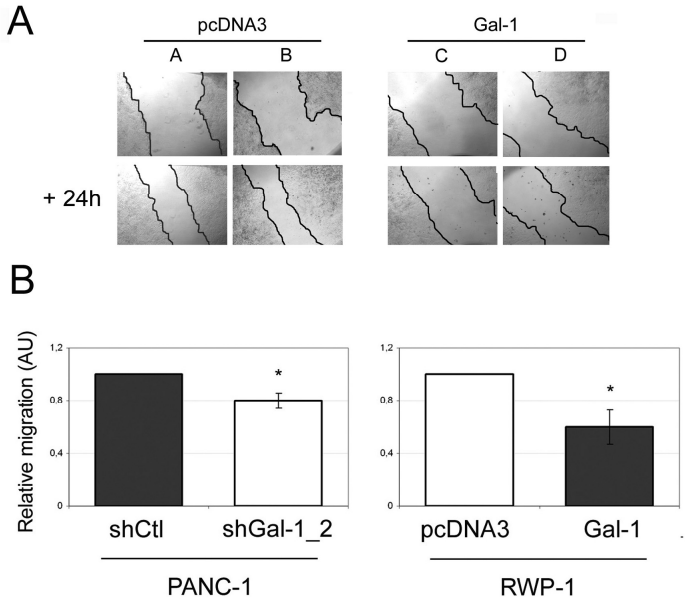

Figure 106. Migration assessed after wounding a confluent monolayer of pancreatic tumoral cells in which Gal-1 levels had been downregulated (PANC-1) or upregulated (RWP-1). A) Wound healing in RWP-1 cells. Two independent fields are shown for each condition. The migration front is highlighted to clarify images. Images were taken with the 4X objective. B) Quantification of migration in PANC-1 and RWP-1 cells after 72h in low FBS conditions. The percentage of empty area was quantified using ImageJ analysis. Graph bars represent migration (1/empty area) of cells relative to the control (shCtl in PANC-1 or pcDNA3 in RWP-1) of five independent experiments. Surprisingly, whereas in PANC-1, Gal-1 deficiency significantly impaired migration (*p=0.005), Gal-1 overexpression produced the same effect in RWP-1 cells (*p=0.01).

Mobility experiments using time-lapse video microscopy were performed to clarify migration results (Fig.107A). Cell tracking was followed during a 10 hour time-frame, which revealed that Gal-1 deficiency significantly reduced PANC-1 cell mobility in a 60%, confirming previous data (Fig.107B). We could not quantify mobility

in the RWP-1 cell line, as isolated cells did not move significantly (data not shown).

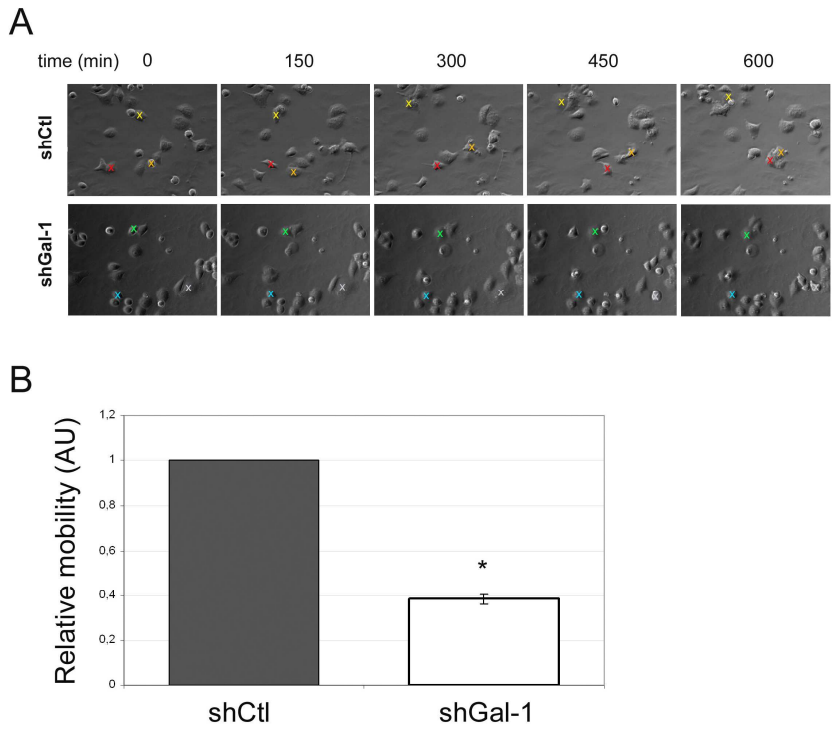

Figure 107. Effect of Gal-1 downregulation over mobility in PANC-1 cells with different Gal-1 levels. A) PANC-1 control cells infected with a control shRNA (shCtl) or with a shRNA targeting Gal-1 (shGal-1) were followed by time-lapse video microscopy. Three different cells of each group were tracked as examples. B) Quantification of the mobility from control or PANC-1 cells infected with shGal-1_2 (shGal-1). Gal-1 depleted cells showed a 60% reduction in their mobility. The graph represents the relative values (mobility shGal-1/mobility shCtl) of two independent experiments. *p=0.001.

2.4.3 Gene Expression Regulation by Gal-1: Microarray Analysis

Microarray expression profiles were obtained for both cellular systems with altered Gal-1 expression levels: PANC-1 cells (with

high endogenous or downregulated Gal-1 levels) and RWP-1 cells (with low endogenous or overexpressed Gal-1 levels). For this transcriptome analysis, a human exon array was used, which allowed analyzing 18708 genes from the human genome and enabled detection of genetic variants due to alternative splicing.

In PANC-1 group, 4 different type of cells were used: non-infected parental PANC-1 cells (wt), cells infected with a control shRNA (shCtl), or cells infected with two different shRNA targeting Gal-1 (shGal-1_2 and shGal-1_5). First of all, preliminary data analysis was done by comparing genes differentially expressed between the non-infected group (wt) and the shCtl, with the aim of filtering those genes altered by the infection protocol. The final outcome of this intersection was compared to both knockdowns (see *Supplementary information,* Tab.S1 and Tab.S4). After all, genes consistently affected by Gal-1 downregulation were summarized in a final list (see *Supplementary information,* Tab.S6).

In RWP-1 group, direct comparison between the two cell populations was performed (a control clone transfected with an empty pcDNA3 vector or a clone markedly overexpressing Gal-1) (see *Supplementary information,* Tab.S7 and Tab.S9). In order to have a global picture about Gal-1 effects in gene expression, we tried to summarize gene data after Gal-1 downregulation or upregulation by intersecting both RWP-1 and PANC-1 lists (see *Supplementary information,* Tab.S10 and Tab.S11). Importantly, Gal-1 gene expression (*LGALS1*), appeared as the third most significantly altered gene in the final list, confirming technique efficiency (Tab.11). Other important gene families whose importance had been

directly or indirectly reported in pancreatic cancer were also revealed, such as *TGFBR3*[704], *NFAT*[705], *ERBB2*[706], *TNF-α*[707] and *NF-κB*[708], among others.

Downregulated in low Gal-1
Overexpressed in low Gal-1

Comp1 4 logFC	Comp13 logFC	Comp65 logFC	AveExp	F	PVal	AdjPVal	Symbol	Description
1,55	0,17	0,25	5,86	139,39	3,00E-011	6,91E-009	TGFBR3	transforming growth factor, beta receptor III
1,37	0,31	0,31	5,55	116,20	1,12E-010	1,90E-008	CACNA1D	calcium channel, voltage-dependent, L type, alpha 1D subunit
1,18	**1,98**	**0,81**	**9,90**	**90,13**	**6,99E-010**	**7,50E-008**	**LGALS1**	**lectin, galactoside-binding, soluble, 1**
1,58	0,32	0,08	6,25	78,95	1,80E-009	1,73E-007	ATP6B1	ATPase, class I, type 8B, member 1
1,51	0,25	0,07	8,20	76,67	2,21E-009	1,98E-007	OPN3	opsin 3
1,30	0,21	0,13	7,78	76,12	2,32E-009	1,98E-007	PRKAA2	protein kinase, AMP-activated, alpha 2 catalytic subunit
1,69	0,08	0,14	6,44	74,33	2,75E-009	2,26E-007	NFATC2	nuclear factor of activated T-cells, cytoplasmic, calcineurin-dependent 2
0,99	0,13	0,90	5,67	72,89	3,16E-009	2,43E-007	SYTL2	synaptotagmin-like 2
1,66	0,38	0,02	5,41	58,38	1,49E-008	8,83E-007	PLEKHH2	pleckstrin homology domain containing, family H (with MyTH4 domain) membe
0,95	0,05	0,14	8,21	57,88	1,58E-008	9,13E-007	TOB1	transducer of ERBB2, 1
-0,56	-0,64	-3,11	7,84	431,81	6,94E-015	3,20E-011	CXCL1	chemokine (C-X-C motif) ligand 1 (melanoma growth stimulating activity, alpha)
-0,25	-0,15	-2,78	5,36	280,24	1,74E-013	2,78E-010	TNFAIP3	tumor necrosis factor, alpha-induced protein 3
-2,63	-0,15	-0,02	4,91	278,88	1,81E-013	2,78E-010	PRSS2	protease, serine, 2 (trypsin 2)
-0,42	-0,21	-2,95	5,48	209,52	1,50E-012	1,03E-009	CXCL2	chemokine (C-X-C motif) ligand 2
-0,61	-0,15	-3,42	6,03	194,20	2,63E-012	1,21E-009	LCN2	lipocalin 2
-0,51	-0,29	-2,05	5,96	173,77	5,97E-012	2,29E-009	CXCL3	chemokine (C-X-C motif) ligand 3
-0,09	-0,02	-2,79	5,91	134,01	3,99E-011	8,77E-009	HLA-DPA1	major histocompatibility complex, class II, DP alpha 1
-0,20	-0,24	-1,87	8,43	112,42	1,43E-010	2,19E-008	NFKBIA	nuclear factor of kappa light polypeptide gene enhancer in B-cells inhibitor, alpha
-2,06	-0,11	-0,56	6,09	101,66	2,95E-010	4,00E-008	ANKRD1	ankyrin repeat domain 1 (cardiac muscle)
-0,08	-0,05	-1,93	6,03	94,43	5,01E-010	5,92E-008	IL32	interleukin 32

Table 11. Top 10 upregulated and downregulated mRNAs in PANC-1 and RWP-1 group intersection list. 10 genes whose expression was decreased more significantly when Gal-1 was downregulated or accordingly, were found upregulated when Gal-1 was overexpressed, are shown in green. 10 genes that were upregulated on low Gal-1 conditions (and downregulated when Gal-1 was overexpressed) are shown in red. Gal-1 appeared as one of the altered genes, confirming technique efficiency and some other interesting genes in pancreatic cancer appeared. See *Supplementary information,* Tab.S10 and Tab.S11 for complete information.

We focused our attention on genes that could actively be participating in pancreatic tumor development due to its involvement in invasion, adhesion, cell signaling, proliferation, angiogenesis or apoptosis, among others (Fig.108).

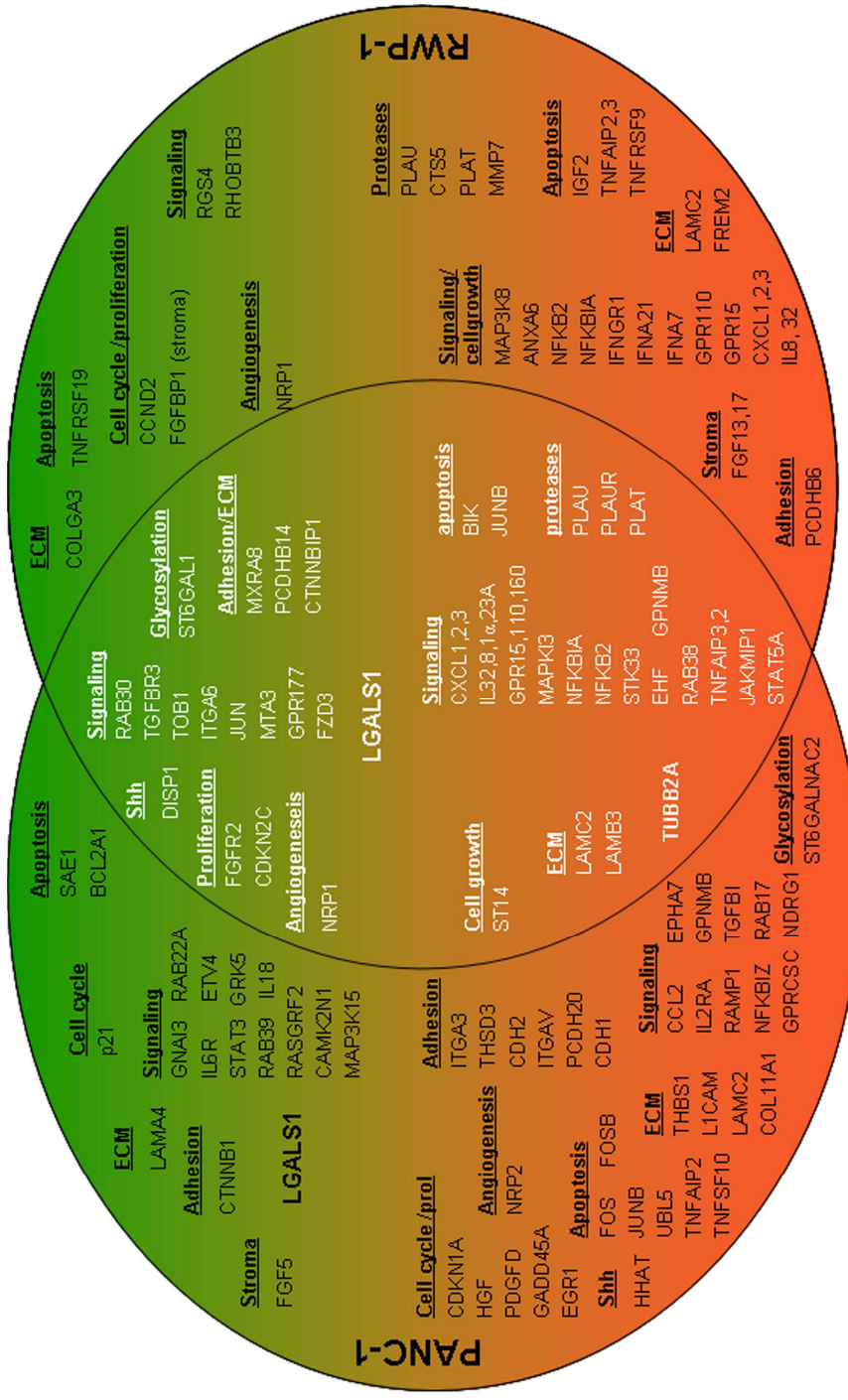
PANC-1
RWP-1
LGALS1
ECM
LAMA4
Adhesion
CTNNB1
Stroma
FGF5
LGALS1
Cell cycle /prol
CDKN1A
HGF
Angiogenesis
PDGFD
NRP2
GADD45A
EGR1
Apoptosis
Shh
FOS
FOSB
HHAT
JUNB
UBL5
TNFAIP2
TNFSF10
Cell cycle
p21
Signaling
GNAI3
RAB22A
IL6R
ETV4
STAT3
GRK5
RAB39
IL18
RASGRF2
CAMK2N1
MAP3K15
Apoptosis
SAE1
BCL2A1
Shh
DISP1
Proliferation
FGFR2
CDKN2C
Angiogeneseis
NRP1
Adhesion
ITGA3
THSD3
CDH2
ITGAV
PCDH20
CDH1
ECM
THBS1
L1CAM
LAMC2
COL11A1
Signaling
CCL2
IL2RA
RAMP1
NFKBIZ
GPRC5C
EPHA7
GPNMB
TGFBI
RAB17
NDRG1
Signaling
RAB30
TGFBR3
TOB1
ITGA6
JUN
MTA3
GPR177
FZD3
Cell growth
ST14
ECM
LAMC2
LAMB3
TUBB2A
Glycosylation
ST6GALNAC2
Glycosylation
ST6GAL1
Adhesion/ECM
MXRA8
PCDHB14
CTNNBIP1
Signaling
CXCL1,2,3
IL32,8,1α,23A
GPR15,110,160
MAPKI3
NFKBIA
NFKB2
STK33
EHF
GPNMB
RAB38
TNFAIP3,2
JAKMIP1
STAT5A
apoptosis
BIK
JUNB
proteases
PLAU
PLAUR
PLAT
Adhesion
PCDHB6
Stroma
FGF13,17
ECM
COLGA3
Apoptosis
TNFRSF19
Cell cycle /proliferation
CCND2
FGFBP1 (stroma)
Angiogenesis
NRP1
Signaling/
cellgrowth
MAP3K8
ANXA6
NFKB2
NFKBIA
IFNGR1
IFNA21
IFNA7
GPR110
GPR15
CXCL1,2,3
IL8, 32
Signaling
RGS4
RHOBTB3
Proteases
PLAU
CTSS
PLAT
MMP7
Apoptosis
IGF2
TNFAIP2,3
TNFRSF9
ECM
LAMC2
FREM2

(*In previous page*) **Figure 108. Schematic representation of genes appeared in microarrays with biologic interest in the context of tumor development.** Scheme with the genes significantly altered in PANC-1 (left circle), RWP-1 (right circle) or in both cell lines (intersection). The red area corresponds to genes that were downregulated when Gal-1 was overexpressed or upregulated when Gal-1 levels were decreased. The green area contains those genes whose expression followed the same pattern as Gal-1 did: upregulated when Gal-1 was overexpressed or downregulated when Gal-1 was knocked down. Selected genes participated in cell cycle, growth, proliferation, adhesion, angiogenesis, apoptosis, signaling, glycosylation, or they were present in the stroma and ECM. Plasminogen proteases were also found, among them tPA.

Ingenuity Pathway Analysis was used to perform functional analysis of the results by clustering altered genes into biological pathways (see *Supplementary information,* Tab.S2, Tab.S5 and Tab.S8). Confirming Gal-1 known importance in several pathological functional events, the altered pathways that appeared in the top list included ECM adhesion molecules (see *Supplementary information,* Tab.S3), ECM/receptor interaction, signal transduction, and several pathways directly linked to cancer and metastasis.

2.4.3.1 Validation of Microarray Data by RT-qPCR Analysis: Gal-1 Modulates Cancer Related Genes

Microarray data at the mRNA level was validated by quantitative real time PCR analysis (RT-qPCR), focusing our attention on several gene groups. We underlined some of the genes related to pancreatic cancer or tumor progression (including the plasminogen activator family), some of those involved in functions previously reported to be controlled by Gal-1 (as cell mobility and adhesion), as well as those already found in previous Gal-1 microarray analysis in other cellular systems[523].

First of all, as a control, we checked Gal-1 levels by RT-qPCR in PANC-1 and RWP-1 cells in which Gal-1 expression had been modulated. Gal-1 mRNA levels were significantly downregulated in PANC-1 cells infected with shGal-1 to more than 80%. Upregulation in RWP-1 cells, markedly increased Gal-1 levels more than 6 fold (Fig.109).

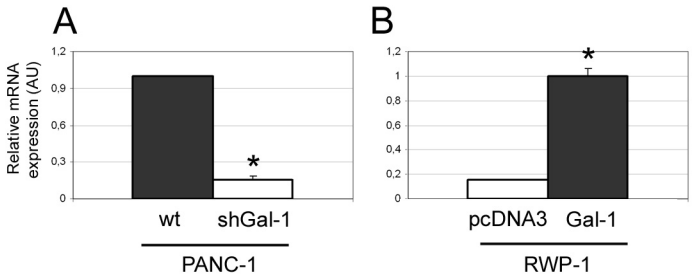

Figure 109. RT-qPCR validation of Gal-1 level alteration in PANC-1 and RWP-1 groups. A) Gal-1 was significantly ($p<0.001$) downregulated (to 0.16) in PANC-1 shGal-1 compared to control (non-infected and shCtl). B) Gal-1 was upregulated after Gal-1 transfection in RWP-1 cells more than 6 fold compared to mock transfected cells (pcDNA3) (*$p<0.001$).

To further confirm our microarray analysis, we validated by RT-qPCR, several genes with well established functions in cancer such as *ERBB2*[709-712] , *CDH1*[713,714], *FGFR2*[715] and *TGFBR3*, although the latter's involvement in PDAC is controversial[704,716-718]. RT-qPCR data showed that TGFBR3 levels were downregulated to 0.5 after Gal-1 interference in PANC-1 cells and overexpressed to 1.21 in RWP-1 Gal-1 overexpressing cells (Fig.110). FGFR2 levels were significantly reduced to 0.7 after PANC-1 stable downregulation. E-cadherin was downregulated after Gal-1 transfection in RWP-1 cells to 0.7 fold compared to mock transfected cells (pcDNA3), though differences did not reach statistical significance. ErbB2

showed almost a two fold increase when Gal-1 levels were upregulated in RWP-1 cells (Fig.110).

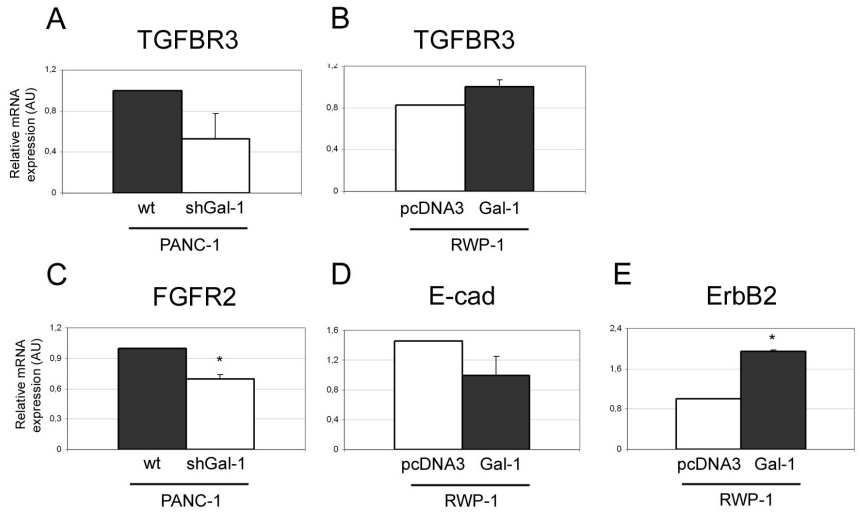

Figure 110. RT-qPCR validation of genes important in cancer. A) TGFBR3 levels were downregulated (to 0.53) in PANC-1 shGal-1 compared to control cells, though differences did not reach significance. B) TGFBR3 was upregulated after Gal-1 transfection in RWP-1 cells to 1.21 fold compared to mock transfected cells (pcDNA3) ($p=0.057$). C) FGFR2 levels were downregulated (to 0.69) in PANC-1 shGal-1 (both interferences) compared to control (non-infected and shCtl) ($p=0.02$). D) E-cadherin (E-cad) was downregulated after Gal-1 transfection in RWP-1 cells to 0.7 compared to mock transfected cells (pcDNA3), though differences did not reach statistical significance. E) ErbB2 showed almost a two fold increase when Gal-1 levels were upregulated in RWP-1 cells ($p<0.001$).

2.4.3.2 Validation of Microarray Data by RT-qPCR Analysis: Gal-1 Modulates Adhesion/Migration Related Genes

We have previously described that Gal-1 was involved in cell migration in our PANC-1 cells (see section *2.4.2.3. In vitro Cell Mobility*). Moreover, pathway analysis stressed that Gal-1 regulated the expression of genes involved in ECM adhesion (see

Supplementary information, Tab.S2 and Tab.S3). Therefore, we validated by RT-qPCR some genes related to ECM/cell adhesion or migration. In addition to the already validated E-cadherin (Fig.110D), whose role in cell adhesion is crucial, we also validated other cell adhesion related genes like fibronectin-1 (Fn-1), integrin α_5 or thrombospondin-1 (Tsp-1). Accordingly, these genes had been previously reported to be upregulated when glioblastoma cells were depleted of Gal-1[523]. All Fn-1, integrin α_5 and Tsp-1 were found to be significantly upregulated around the 50% in PANC-1 cells with low Gal-1 expressing levels (Fig.111).

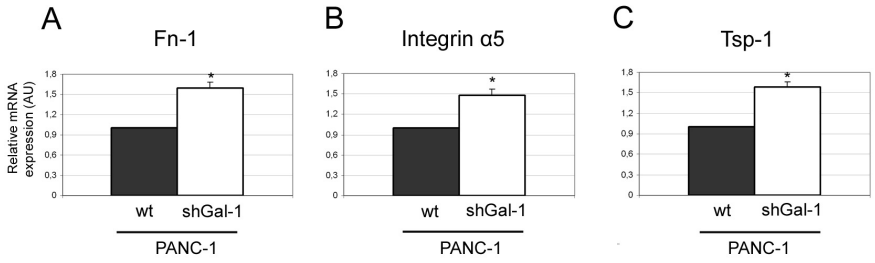

Figure 111. RT-qPCR validation of genes related to cell/ECM interaction in PANC-1 cells with altered Gal-1 levels. Fibronectin-1 (Fn-1) (A), integrin α_5 (B) and thrombospondin-1 (Tsp-1) (C) levels were upregulated in PANC-1 shGal-1 compared to control (non-infected and shCtl). The increases corresponded to 1.60 (A), 1.48 (B) and 1.58 (C), being all of them statistically significant (*p=0.022 (A), *p=0.006 (B), *p=0.002 (C)).

Interestingly, we found that genes from the plasminogen system, in particular tPA, uPA and uPAR, displayed a differential gene expression pattern in the absence or presence of Gal-1. The expression of all these genes has been shown to favor cell invasion through plasmin generation in pancreatic cancer[360,719]. Nevertheless, tPA, uPA and uPAR levels were found to be downregulated when Gal-1 was overexpressed in our microarray data (see *Supplementary information,* Tab.S7, Tab.S9 and Tab.S11). We

confirmed this inverse correlation between Gal-1 and tPA, uPA and uPAR expression at the mRNA level by RT-qPCR. tPA, uPA and uPAR transcripts were reduced to 0.13, 0.3 and 0.51 respectively when Gal-1 was overexpressed in RWP-1 cells (Fig.112).

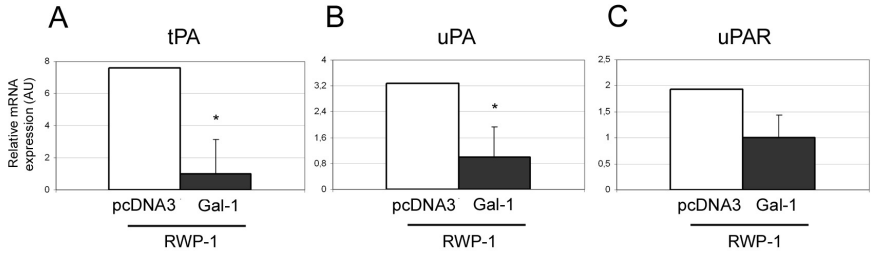

Figure 112. Validation of the members of the plasminogen family whose expression was found to be altered when Gal-1 levels were changed in RWP-1 cells. A) tPA transcripts were reduced to 0.13 when Gal-1 was upregulated (p=0.02). B) uPA transcripts were reduced to 0.3 (p=0.05) and C) uPAR transcripts went to 0.51 (p=0.09).

For those proteins for which an antibody was available, protein level assessment was performed by WB analysis (Fig.113). tPA and uPA from pancreatic cancer cell supernatants were analyzed and were found to be significantly upregulated in low Gal-1 levels conditions, confirming gene data obtained by microarray studies.

Altogether, these data indicate that the plasminogen system family seemed not to be playing a relevant role in Gal-1 mediated increase in pancreatic cell migration found in PANC-1 cells. Nevertheless, the overexpression of these proteases might explain why parental RWP-1 cells (with low Gal-1) presented higher migration levels in wound healing assays compared to cells overexpressing the lectin (Fig.106).

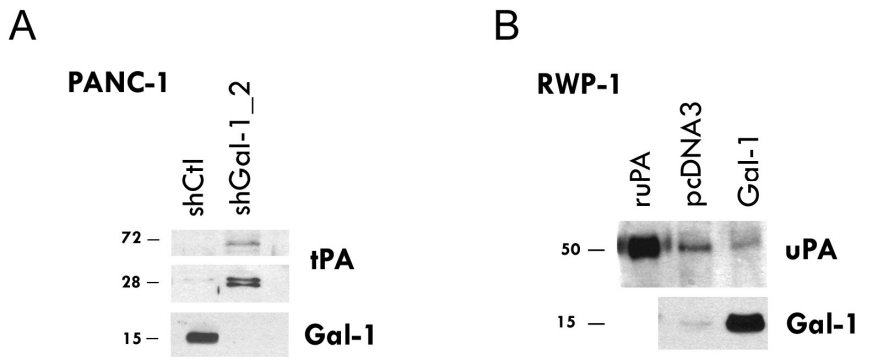

Figure 113. Protein confirmation by WB analysis. A) PANC-1 cells with low Gal-1 levels showed significantly higher tPA levels, confirming gene data obtained by microarray analysis. B) RWP-1 cells overexpressing Gal-1 showed reduced uPA protein expression. Gal-1 levels are shown confirming protein downregulation for PANC-1 and protein overexpression in RWP-1. No loading control is shown as samples analyzed were PANC-1 and RWP-1 supernatants.

2.4.3.3 Validation of Microarray Data by RT-qPCR Analysis: Gal-1 Modulates Shh Pathway Related Genes

Among the genes differentially up and down regulated by Gal-1 in our PANC-1 and RWP-1 microarray studies we identified several proteins from the Hh family. Taking into account that both Gal-1 and Shh pathway are very important for the desmoplastic reaction, and considering its importance in tumor progression, we wanted to study whether the expression of these proteins could be somehow related. Dispatched homolog 1 (Disp1), which is involved in Hh ligand secretion and paracrine signaling[720,721], appeared significantly altered when intersecting PANC-1 and RWP-1 lists ($p<0.001$) (see *Supplementary information,* Tab.S10). Hedgehog acetyltransferase (Hhat), which catalyzes required N-terminal palmitoylation of Shh,

appeared upregulated in PANC-1 cells with low Gal-1 levels (see *Supplementary information,* Tab.S6).

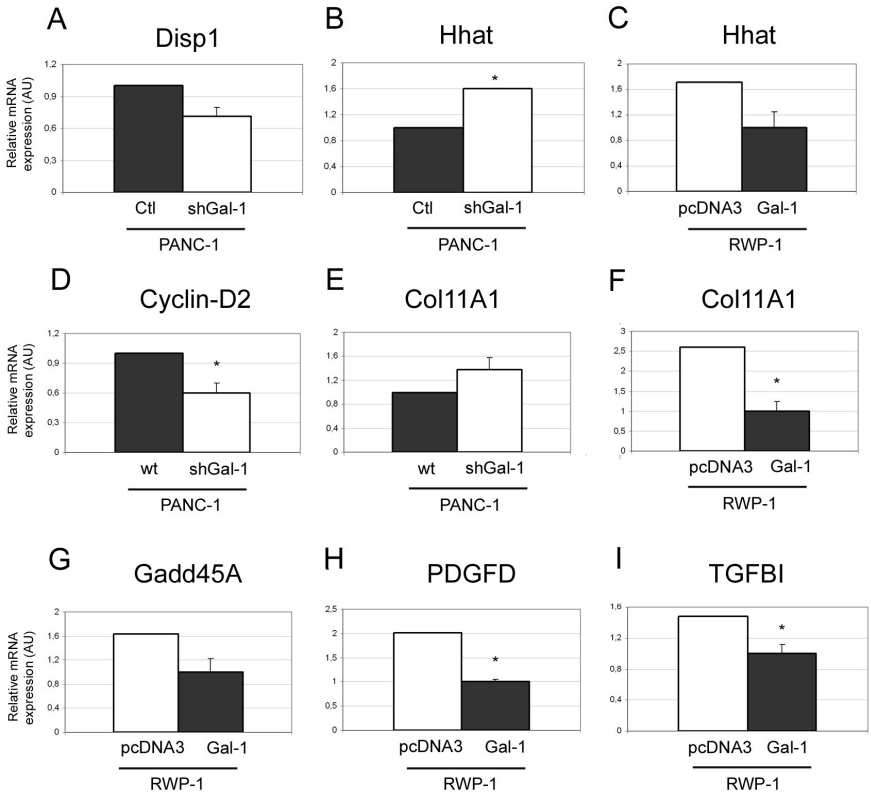

Figure 114. RT-qPCR validation for members of the Hh family and Gli target genes. A) Disp1 levels were reduced in a 28% when Gal-1 levels were depleted ($p=0.07$). B) Hhat experienced a 60% increase when Gal-1 was downregulated in PANC-1 (*$p<0.0001$) and C) a 42% decrease when Gal-1 levels were forcely enhanced in RWP-1 (though differences did not reach significance). D) Cyclin-D2 levels were reduced to 60% when Gal-1 levels were depleted in PANC-1 cells (*$p=0.016$). E) Col11A1 levels were increased 1.37 fold when Gal-1 levels were depleted in PANC-1 (though differences did not reach significance). F) In concordance with E, Col11A1 levels were reduced to 40% when Gal-1 was overexpressed in RWP-1 (*$p=0.0005$). G) Gadd45A levels were reduced in a 40% when Gal-1 was overexpressed in RWP-1 (though differences did not reach significance). H) PDGFD levels were reduced to the half when Gal-1 was overexpressed in RWP-1 (*$p<0.0001$). I) TGFBI levels were reduced to the 67% when Gal-1 was overexpressed in RWP-1 (*$p=0.02$).

We also identified several previously reported Gli1 target genes such as *CCND2*[722] and other new putative partners as *COL11A1*, *GADD45A*, *PDGFD* or *TGFBI* (M.E Fernández-Zapico, personal communication). Therefore, we validated by RT-qPCR analysis the expression levels of Disp1, Hhat, Cyclin-D2, Collagen type11 α1 (Col11A1), PDGFD, Gadd45A, and TGFBI in PANC-1 and RWP-1 cells with altered Gal-1 levels (Fig.107). Disp1 levels in PANC-1 cells were reduced in a 28% when Gal-1 levels were downregulated, whereas Hhat experienced a 60% increase in this situation. Accordingly, Hhat levels decreased in a 42% when Gal-1 levels were forcely enhanced in RWP-1. Regarding Gli target genes, Cyclin-D2 levels were reduced to 60% when Gal-1 levels were depleted in PANC-1 cells. Col11A1 expression was increased 1.4 fold in PANC-1 with low Gal-1 and accordingly reduced to 40% when Gal-1 was overexpressed in RWP-1. PDGFD, Gadd45A and TGFBI were respectively reduced to a 50%, 60% or 67%, when Gal-1 was overexpressed in RWP-1 cells (Fig.114).

Upregulation of the reported Gli target gene Cyclin-D2 after Gal-1 overexpression, and unpublished results from M.E Fernandez-Zapico (personal communication), suggested that Gal-1 could be regulating Gli1 expression. To test that hypothesis *in vitro*, we checked whether Gli1 transcription and activity changed among different Gal-1 expressing systems. Luciferase activity was assessed after transient transfection of a construct containing a luciferase reporter cassette under the control of 8 Gli responding elements in RWP-1 cells with basal low Gal-1 levels (pcDNA3) or overexpressing the protein (Gal-1). Gal-1 overexpression resulted in a clearly enhanced Gli

driven luciferase activity (Fig.115), suggesting that the lectin could be involved in Gli transcription factor activation.

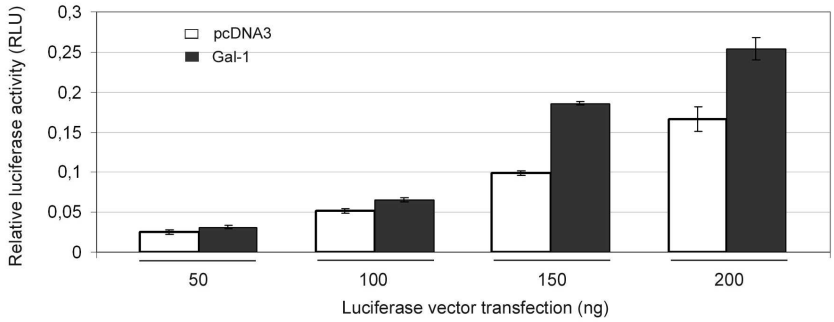

Figure 115. Gal-1 is involved in Gli transcription factor activation. RWP-1 cells with overexpressed Gal-1 levels (Gal-1) displayed a marked increase in Gli driven luciferase activity which was detected at different amounts of luciferase vector transfected (50-200 ng), although 150 and 200 ng showed improved sensibility.

Altogether, these data suggested that Gal-1 was related to Shh pathway modulation in pancreatic cancer cells.

3 DISCUSSION

**The important thing is not to stop questioning;
curiosity has its own reason for existing.**

Albert Einstein

3.1 SETTING OUR CONTRIBUTIONS INTO CONTEXT

Cancer is the second leading cause of death in developed countries, only after heart disease. Although the first data referring to cancer dates from the 4th century BCE with Hippocrates, it was not until the 19th century when the modern era of cancer research started[723]. Importantly, the start of the 21st century brought the description of the six essential cell physiology alterations dictating malignant growth[724]: self-sufficiency in growth signals, insensitivity to growth-inhibitory ones, evasion of apoptosis, limitless replicative potential, sustained angiogenesis and tissue invasion and metastasis. During the last decade, cancer research has moved its focus from oncogenes and tumor suppressor genes to depict a much more complex scenario to try to understand tumor development. Two additional cancer hallmarks have been later added to the initial list[725]: energy metabolism reprogramming and immune evasion, capturing the importance of the tumor microenvironment in tumor progression.

Although pancreatic cancer is not one of the neoplasms with highest incidence, it occupies the fourth place on the list of cancer related causes of death, as its mortality rate almost equals the number of diagnoses[18]. Several aspects have impaired improvement in pancreatic cancer dismal prognosis but the main reason is that patients do not show overt symptoms until very advanced stages, when the tumor has already metastasized, excessively delaying time of diagnosis and limiting surgery as a curative procedure. Pancreatic cancer research has been boycotted by different causes. Precursor lesions and cell types are rarely detected, so they are not frequently available for studies directed to better understand the molecular

events driving tumorigenesis and achieve biomarker identification. Still, if the neoplasm is detected at preliminary phases, several technical issues make pancreatic cancer studies really challenging. Some of the main problems are the inaccessibility of the organ for biopsy, the high amount of proteinases and nucleases present, which difficult tissue collection and manipulation, the extensive desmoplastic reaction, which hampers mutational analysis, and the lack of suitable animal models. An improved understanding of pancreatic cancer biology is essential to develop new therapies, which are more than urgent considering the low efficiency of current treatments. Although the tools are hard to use, pancreatic cancer researchers have been recently given the key ingredient required to believe in the near possibility to improve survival rates: time. A window of more than 15 years has been described between PDAC initiation and metastasis[25], bringing some motivation to overcome mentioned difficulties and pursue new biomarkers and targets for therapy.

In this regard, our group has joined efforts to functionally characterize, for the first time, Gal-1 importance in pancreatic cancer, with the intention to bring a new putative target in this dismal pathology. We have tried to delineate a pretty complete analysis of Gal-1 involvement in pancreatic cancer, using not only *in vitro* but also *in vivo* strategies. We have first centered our attention on analyzing *in vitro* Gal-1 involvement in tPA induced pathological effects. Once proven that Gal-1 is a *bona fide* functional tPA receptor and thinking of inhibitory strategies, we have also started the biochemical characterization of the interaction. In addition, our *in vivo* data have depicted a much wider range of effects for Gal-1 in

pancreatic cancer, which further highlight the lectin role in pancreatic tumor progression. We have also glimpsed at the molecular events that could be involved in Gal-1 mediated effects by performing microarray analyses. Altogether, our data strongly proposes Gal-1 as a promising candidate to design new pancreatic cancer therapies.

3.2 GAL-1: OUR MAIN CHARACTER

3.2.1 Gal-1: a Dice with Many Faces

Our data have always gone in the direction of considering *LGALS1* as an "oncogene", which is consistent with Gal-1 protein overexpression in many tumors and in particular, in pancreatic cancer. However, contradictory data outline a much more complex scenario in which Gal-1 physiochemical properties and cell context appear to be decisive to decide on a final biological outcome[600,601].

At physiological concentrations, Gal-1 exists as a mixture of a dimer and a monomer, which preserves glycan binding affinity, though lower[466,475]. Addressing the quaternary structure of Gal-1 in our experiments has been technically frustrated. In particular, when addressing Gal-1/tPA interaction, different functional complexes could exist taking into account that tPA has more than one glycosylation site suitable for galectin recognition. For instance a single monomeric Gal-1 could be binding a tPA molecule. Dimeric Gal-1 could be binding to two different tPA molecules or to two different glycosylation sites of a single tPA molecule. Indicative of the dimer existence is that the anti-Gal-1 rabbit polyclonal antibody recognizes a band around 30 KDa in pancreatic cancer cell extracts, which is also detected when only recombinant Gal-1 is loaded, excluding the possibility of non-specific antibody recognition. However, the predominant band observed, as expected due to strong reducing conditions, corresponds to 14 KDa, associated with the monomer conformation. SPR experiments are also far from reproducing an *in vivo* context. Still, discrepancy on dissociation

constants for monomeric and dimeric Gal-1 and glycans in the literature[466,726,727], does not allow us to at least identify the *in vitro* nature of the interaction according to the Kd=9.1 μM calculated. Absence of interaction with Gal-3, which in solution is basically monomeric[728], has been previously used to determine Gal-1 crosslinking requirements[488]. Thus, our data finding a much weaker interaction between tPA and Gal-3[421] might be insinuating that dimeric Gal-1 is more efficient for tPA recognition. However, special caution must be taken as monomeric Gal-3 can form aggregates acquiring similar functionality to dimeric Gal-1[729-731].

Protein concentration also represents a very important issue and can be responsible for triggering complete opposite effects, as observed with such an important protein in PDAC as K-Ras, which is able to induce both transformation[45,732] and senescence[733,734] depending on its concentration. Micromolar concentrations of recombinant Gal-1 must be used in *in vitro* experiments, making it difficult to determine whether observed phenotypes are really happening under physiological or pathological conditions. Moreover, cell surface and ECM depositon *in vivo* generates high local concentrations of the protein[467], what even more hampers the will to define functional Gal-1 amounts. In our experiments, we have bypassed this problem by using what we think is a more elegant approach than protein overexpression, which consists in assessing Gal-1 role by reducing its levels through siRNA mediated silencing.

Gal-1 biological outcomes also depend on its lectin dependent or independent behavior. Typically, Gal-1 intracellular functions rely exclusively on protein/protein interactions whereas extracellularly,

glycan recognition is predominant. Frequently, oxidized Gal-1, a form that lacks lectin activity[476], is chosen to investigate whether Gal-1 binds to the glycan or the protein fraction of its partner. Lectin requirement for Gal-1/tPA binding has been thoroughly addressed in the present study by two alternative approaches directed to tPA or Gal-1, reaching the same conclusion. Both tPA N-deglycosylation and lactose preincubation with the lectin[421], fully impaired tPA/Gal-1 interaction, indicating that protein/glycan recognition is essential.

Gal-1 is found in several cell compartments as well as in the ECM. Protein localization seems to be key to decide on galectins performance and partner interaction, as shown by the fact that cytoplasmic Gal-3 expression is implicated in proliferation, whereas nuclear Gal-3 induces cell cycle arrest[735]. Different cell systems have been proposed to study the effects of site-specific Gal-1. For instance, a colorectal cancer cell line that does not secrete Gal-1 has been used to study its intracellular functions[537]. A CHO mutant exists that does not add galactose residues on glycoproteins[736] and as a consequence, Gal-1 can not be cell surface retained, being all secreted[737].

3.2.2 Gal-1 in Tumor Progression

11 Galectin family members are expressed in humans and several members of the family have been involved in tumor progression[428,431,516]. Gal-1 and Gal-3 are by far the most well characterized galectins, as easily observed by typing them in pubmed data base. Whereas around 900 and 1500 entries are retrieved by Gal-1 and Gal-3, respectively, the number of articles

dramatically decreases to less than a hundred and even to less than ten for other members of the galectin family. Cancer research studies exclusively taking into account Gal-1 and Gal-3 might possibly lead to misinterpret conclusions[563]. Nevertheless, in pancreatic cancer, the situation is a little bit more manageable since only these two members of the protein family have been reported to be overexpressed. Although both proteins have high affinity for β-galactosides and indeed they share many interacting partners such as, laminin, fibronectin, integrins or CD45[738], a fine specificity level results in binding differences. Gal-1 shows high affinity for complex type N-glycans, whereas Gal-3 prefers repeating lactosamine units[425]. Binding site presentation is also involved in distinct specific partner recognition by Gal-1 and Gal-3. The nature of the glycosylation structures found in tPA (more suitable to Gal-1 carbohydrate preferences) might be responsible for Gal-1 specific recognition.

Gal-1 has been found to be overexpressed in many neoplasms and interestingly, it accumulates in the stroma of HCC[584], OSCC[571], thyroid[574], ovary[544], HNSCC[576], colon[585], prostate[580] and pancreatic cancers[582]. However, as it already happens in consistently downregulated molecules in cancer like E-cadherin, whose gain of function is reported in ovarian carcinoma[739], no universal generalizations can be stated for Gal-1, even in the context of pancreatic cancer[600,601]. Gal-1 expression and functions can be modulated by regulating transcription, but also by changing subcellular localization or by affecting its ligands expression and glycosylation, adding further levels of complexity. For example, in renal cell carcinomas, a decrease in Gal-1 binding sites with

unaltered Gal-1 protein expression seems to be responsible for increased aggressiveness[518]. Although many reports mention Gal-1 overrepresentation in tumors, few have addressed the molecular mechanisms triggering this event. In HCC, Gal-1 upregulation is due to promoter hypomethylation[455]. In contrast, in colorectal cancer cells, HIF-1α has been shown to bind to Gal-1 promoter and induce its expression under hypoxic conditions[586]. This possibility might be important in pancreatic cancer, taking into account its well established ischemic environment.

TNM (tumor, node, metastasis) system has been established by the AJCC (American Joint Committee on Cancer) to classify patients according to three categories: primary tumor size (T), the existence of affected lymph nodes (N), and the occurrence of metastasis (M). The information is summarized in an overall AJCC stage, which ranges from 1 to 4 (early to advanced stage). Gal-1 has been repeatedly found to be misregulated in pancreatic cancer[582,589,590], being overrepresented in poorly differentiated tumors. Interestingly, its expression levels correlated not only with histology but also with T stage, N stage and global AJCC stage of pancreatic cancer disease[590], suggesting that Gal-1 might also participate in tumor progression and that its presence does not seem to be a random event. Indeed, Gal-1 involvement in stepwise tumor development has been extensively reported, modulating many different aspects: influencing tumor cell growth[524], inducing T cells death[484], suppressing T-cell-derived-proinflammatory cytokine secretion[556], mediating cell/cell or cell/ECM adhesion[544,740], participating in angiogenesis[445] and promoting cancer cell migration[541,568]. Gal-1 did not appear in the list of genes consistently misregulated in

pancreatic cancer that were gathered in 12 core signaling pathways[87]. Notwithstanding, 54 of the genes found overexpressed encoded secreted or cell surface proteins, putative and already known Gal-1 binding targets, like laminin. Thus, Gal-1 overexpression might be involved in the functional outcome of these overrepresented molecules, playing a role in some of the key identified signaling pathways such as homophilic cell adhesion, integrin signaling and regulation of invasion[87]. Gal-1 could have been excluded from the reported list because this important global genomic analysis was based on tumoral epithelial cells, leaving out the stroma, whose population seems to be the one predominantly affected by Gal-1 increased levels.

Despite the fact that Gal-1 induced molecular mechanisms leading to tumor progression are not fully understood, several reports have shed some light in this issue. Gal-1 might be involved in so many different pathological effects due to its ability to interact with so many different partners in so many different situations. But, interestingly, Gal-1 has been linked to some of the most importantly altered proteins in pancreatic cancer. For instance, one of the best characterized Gal-1 effects in tumor progression is its involvement in Ras proper membrane anchorage, which happens intracellularly and is independent of Gal-1 lectin properties[499,525,528,529]. In fact, Gal-1 and Ras proteins share many characteristics, what confirms the relevance of their interaction. Gal-1[434,741] and Ras proteins[742-744] affect cell growth, apoptosis, cell adhesion, migration and metastasis. Besides, both Ras proteins[742-744] and Gal-1[434,741,745,746] can show contradictory effects depending on the cell context, being pro or antiapoptotic and regulating proliferation or senescence for

instance. Gal-1 is essential for Ras mediated Erk1/2 activation, cell proliferation and transformation. We have also defined a Gal-1 requirement in some of these events in our context, although we have not yet addressed Ras involvement. Interestingly, Gal-1 has been reported to be essential to modulate the strength and duration of Ras signaling activating Raf-Erk1/2 pathway but not PI3K[527,528]. Though less detailed, Gal-1 has been linked to other molecules important in pancreatic cancer. Gal-1 inhibition has been associated to increased p53[523], and p53 transfection downregulates Gal-1 expression[747], bringing more molecular hints on Gal-1 involvement in tumor progression. Some transcription factors have been reported to be Gal-1 modulated. Gal-1 modulates *BEX-2*[549], *ORP-150* and several other hypoxia-related genes involved in angiogenesis[550]. Gal-1 takes part in the induction of the tumor immune escape by regulating AP-1 expression[748]. But one of the best mechanisms described for Gal-1 involvement in tumor progression is its adhesion regulation, which is driven by its interaction with cell surface integrins and ECM proteins such as laminin and fibronectin. With these interplayers, Gal-1 is able to modulate cell/cell and cell/ECM interactions as desired. Gal-1 can favor cell migration from primary sites by binding to integrins and thus interfering with their physiological binding to the ECM. When required though, Gal-1 is able to form stronger interactions by crosslinking cell surface glycosylated proteins among them or with ECM proteins, resulting in tumoral cell establishment in secondary sites. Of particular interest is that tPA also binds to ECM proteins, including laminin and fibronectin[749].

3.3 BIOCHEMICAL CHARACTERIZATION OF GAL-1/ tPA INTERACTION DOMAINS

3.3.1 Glycans are Involved in tPA/Gal-1 Interaction

Our *in vitro* data (see section *2.2. Study of tPA/Gal-1 Interaction in vitro*) concluded that Gal-1 participated in many of the tPA-mediated pathological effects in pancreatic cancer cells and fibroblasts. Taking into account that Gal-1 was not expressed in normal pancreas, we thought that an efficient way to specifically target tPA effects in pancreatic cancer without disrupting its physiological functions, would be by impairing tPA interaction with Gal-1. Therefore, profound characterization of tPA/Gal-1 binding was required in order to design inhibitory peptides disrupting their interaction.

Using SPR we have shown that Gal-1 uses its lectin domain to recognize the N-glycans from tPA and we have identified carbohydrate chains attached to Asn184 as key participants of tPA/Gal-1 interaction. Structural data suggests that Asn448 could be also relevant in this regard, as well as protein/protein interactions, which could contribute to strengthen the interplay. Thereby, K2 and possibly the SP domain, have been identified to be involved in Gal-1 recognition. tPA interaction with several different proteins has been previously reported. K2 domain is responsible for NMDAR binding[750]. Yet, although tPA is composed of independent domains, frequently they cooperate to establish interactions and modulate tPA catalytic activity[338]. For instance, tPA binding to AnxA2 requires FN1 domain[751], although other parts of the protease

might be involved in the interaction[335,338]. Similarly to what we speculate for Gal-1/tPA interaction, the SP domain has been described to assist K2 to mediate tPA binding to melanoma cells[339]. Interestingly, these domains are known to harbor glycosylated chains suggesting that binding might be glycan mediated.

The dissociation constant for Gal-1/tPA interaction calculated by SPR, suggests a strong interaction between the CRD of Gal-1 and tPA glycosylated structures. N-glycans from cell surface glycoproteins are the major ligands for Gal-1 and Gal-3[752], although they also bind to mucins, proteoglycans and ECM[753,754]. The general rule is that Gal-1 recognizes independent lactosamine disaccharides with low affinity (Kd=50 μM)[461,465] but deeply increases avidity when presented in multiantennary repeating units (Kd=5 μM)[468] and when the lectin is surface bound to cell membranes or to the ECM[467]. However, as a matter of fact, Gal-1 is able to recognize only about 1/40 of the total N-glycans present in human serum glycoproteins[755], and around 1/8 of the sites supposed to be galectin specific. It is believed that part of Gal-1 specificity is mediated by additional binding sites recognizing more than the canonical galactose[489,756]. Thus, the particular structural context of galectin binding sites depicts a complex scenario and impairs stating generalizations. For instance, Gal-1 is able to induce T cell death by binding a glycan ligand without lactosamine units, that is very abundant but less preferred[757]. Normally though, Gal-1 recognition capacity is deeply influenced by specific conditions regarding carbohydrate content and linkage[461,466,758-760]. Minor alterations in N-glycan chains have been reported to influence Gal-1 binding in such a way that changes the overall biological outcome[600,761,762].

Cell type specific expression patterns of several proteins and their glycans can modulate different Gal-1 mediated effects[481,543,763]. Particular glycosylation structures are known to mask glycans to Gal-1, which impede Gal-1 induced T-lymphocyte[460,557,563,760,764-766] and cancer cell[767] death. For instance, in contrast to Th1 and Th17 cells, Th2 cells are protected from Gal-1 induced apoptosis by presenting α2-6 sialylation of cell surface glycoproteins[460].

Intringuingly, we have described that type I tPA, containing glycosylation at Asn184, is able to trigger intracellular signaling in a more efficient way, compared to type II tPA (see *Results*, section *2.1.2. Asn184 is Important for Gal-1/tPA Interaction*). We hypothesize that these results are, at least in part, due to optimal Gal-1 recognition, although further experiments will be necessary to support our hypothesis. Glycosylation at Asn184 in type I tPA avoids its conversion to two-chain tPA by plasmin, resulting in an isoform with decreased proteolytic acitivity[305]. Our data further separate the plasmin dependent and independent activities of tPA.

The crystallization of full length tPA has remained technically unfeasible possibly because of the presence of glycan chains and the high mobility of independent domains. Alternative strategies directed to deeply characterize the interaction domains between Gal-1 and tPA will open new avenues in the design and development of inhibitory strategies to block tPA effects in PDAC, contributing to improve its dismal prognosis.

3.3.2 tPA Glycosylation Pattern in Pancreatic Cell Lines

Studies focused on the carbohydrate moiety of proteins are methodologically complicated due to the extremely high diversity and flexibility of these structures. N-glycan content at one particular site is frequently miscellaneous. An example of this complexity is encountered in CD59, for which around 120 glycan chains have been reported[768]. In spite of this physiological marked heterogeneity, cancer progression and metastasis have been characterized by significant alterations of the carbohydrate signature. Besides, changes in glycosylation are presented not only by cancerous cells but also by cells surrounding the tumor[769]. This specific pattern of glycosylation linked to neoplasia might alter cell behavior in many different ways. As discussed above, distinctive glycosylation profiles favor or impede interactions with different proteins. Besides, glycosylation determines many of the main glycoprotein features, such as solubility and stability, among others.

tPA is a good example of a glycoprotein whose carbohydrates modulate many of its characteristics. For instance, glycans are largely responsible for regulating tPA clearance[324]. Besides, tPA catalytic activity is also tuned through the presence of glycosylated chains, providing specificity to the enzymatic reaction[305]. The string of AAs in a protein is determined by its nucleotide sequence whereas glycosylation depends on many different extrinsic and intrinsic variables. The final pattern of glycosylation shown by a glycoprotein is the result of the sum of many different factors. It does

not only depend on the cell type and its physiological state, but also on the culture media and incubating conditions.

Cell type specific N-glycosylation for tPA was previously described[295,297]. Our data regarding tPA pattern of glycosylation from different pancreatic cell lines are preliminary and require further evaluation. Nevertheless, glycan structures determined by MALDI-TOF MS (see *Results*, Fig.31) give a glimpse of a possible difference among pancreatic tumoral cells and HPDE cells, which share many properties in common with normal ductal epithelial cells[689,690]. For HPDE cells, lack of tPA secretion made us work with cell extracts instead of supernatants. Our data reporting lack of differences observed among RWP-1 tPA glycosylation in cell extracts or supernatants excludes the source of origin as a putative explanation for HPDE distinctive glycosylation structures. Instead, we hypothesize that the increase of core fucosylation observed in tPA from pancreatic tumoral cells might be due to a cancer specific glycosylation signature (see *Introduction*, section *1.5.2. Glycosylation in Cancer*).

Interestingly, galectins play an active role in translating the glycan code into different biological outcomes. Protein glycosylation alterations during tumor progression can lead to changes in membrane protein clustering and lectin binding conferring functional advantages to tumoral cells[770]. Galectins crosslink trasmembrane receptor glycoproteins at the cell surface forming lattices[472,771] and enhance their residency time[616,772,773], which results in increased intracellular signaling, cell migration and metastasis[627]. Once the tPA glycosylation pattern will be faithfully established, it would be very

interesting to try to assess Gal-1 interaction for each differently glycosylated tPA. In fact, our group has reported that tPA might display differences regarding protein binding in pancreatic tumoral cells and HPDE[420]. tPA induced Erk1/2 phosphorylation in HPDE was previously shown to be mediated by AnxA2[318]. We have also found that Gal-1 was involved in tPA induced Erk1/2 activation in this non-tumoral cell line, although our functional assays did not ensure direct protein/protein binding. Indeed, Gal-1 immunoprecipitation with endogenous tPA has just been proven in a pancreatic tumoral cell line[421]. It remains possible that Gal-1 selectivity as a tPA receptor in pancreatic cancer is modulated through the protease glycan profile.

3.4 STUDY OF tPA/GAL-1 INTERACTION IN VITRO

In vitro experiments have a series of limitations that must be at least well taken into account when interpreting results. The most general constraint is that bidimensional *in vitro* models can respond differently from tridimensional models regarding cell morphology and tumoral and stromal cell behavior[774-777]. A direct interaction between Gal-1 and tPA has been found by SPR. Type and densities of molecules have a definitive impact on the result and we are conscious that a positive response in an *in vitro* assay does not directly translate into a real *in vivo* interaction. However, immunoprecipitation experiments with recombinant tPA and pancreatic cancer cell lysates were performed in our group and identified Gal-1 in the bound fraction[421]. Besides, colocalization of these two proteins has been observed by confocal microscopy. Although these data are not discarding an indirect interaction, pull-down experiments with recombinant proteins proved that no other proteins are required for tPA/Gal-1 binding *in vitro*. All data gathered from our experiments match with a **direct interaction** between tPA and Gal-1.

We have found that **Gal-1** is **expressed and secreted** in most of the human pancreatic cell lines analyzed. These data are surprising considering that in human pancreatic cancer tissues, Gal-1 is basically found to be expressed in the stromal compartment. However, cancer cell lines sometimes differ from tissue cells on gene expression and pathway activation[778]. Furthermore, bearing in mind that Gal-1 is undetectable in confluent monolayers but observed in the tumor edge advancing front by IF in cell culture migration

experiments, it can also be possible that previous studies analyzing Gal-1 in human pancreatic tumors by IHC have skipped these particular areas[582]. Moreover, cell fixation has been linked to membrane blebs and vesicle release into the ECM, demanding special caution when interpreting protein localization from immunocytotechniques[779]. Gal-1 expression in fibroblasts is high, both intracellularly and in the secreted fraction, in agreement with the pathologic *in vivo* situation. tPA has been detected in some pancreatic transformed cell lines but not in fibroblasts. Regarding tPA detection, we decided to use WB analysis instead of zymography (frequently used to detect tPA proteolytic activity) considering that tPA might be important both in its catalytic and non-catalytic forms. tPA expression is not consistently found in all human pancreatic cancer cell lines as expected, once again detecting discrepancies with reported human data. Another important deviation comes from the observation that the HPDE cell line, which is an immortalized non-tumorigenic cell line, and should be thus considered as a normal ductal cell[689,690], expresses high Gal-1 and tPA levels (although the latter just endogenously). Importantly, no direct correlation between tPA and Gal-1 levels can be derived from our pancreatic cell lines. This might be consequence of the wide variety of functions that both proteins display both physiologically and pathologically, most of which are independent of tPA/Gal-1 interaction.

Gal-1 and tPA colocalize at the migration front in wound healing experiments and they are both involved in pancreatic and fibroblastic cell **invasion**. Similarly, uPA interacts with its main receptor (uPAR) to concentrate plasmin activity in the leading edge

of invading cells and in cell/cell junctions[780-782]. tPA/Gal-1 interaction might probably be involved in a similar mechanism driving invasion. Yet, we do not discard intracellular signaling to cooperate with tPA catalytic activity to result in cell migration and invasion, as tPA has been previously shown to induce MMP gene expression[417,783], which are found to be localized in the invasion front in epithelial cells[784]. Gal-1, but not its family member Gal-3, has been previously linked to *in vitro* stellate cell migration[535].

Previous *in vitro* data have described that pancreatic cancer cell invasion involves AnxA2 and is dependent on tPA proteolytic activity[415] whereas proliferation is not[318]. In fact, tPA is not the first protease to be disconnected from its proteolytic activity and be involved in intracellular signaling. uPA interacts with its receptor (uPAR) to mediate intracellular signaling[225,785-787], modulating cell proliferation, differentiation, adhesion and migration[788,789]. tPA proteolytic dependent or independent functions can be different according to the cellular context. Whereas in human fibroblasts and ECs, proteolytic activity is not involved in proliferation[790-792], in vascular smooth muscle cells[793], mouse fibroblasts[794] and hepatocytes[795], it is. In fact, the non-proteolytic tPA activities might be more important than what was previously thought and might well be cooperating with plasmin formation in fibroblast migration and invasion through MMP-9 upregulation[417]. In our project, we have not extensively addressed whether tPA interaction with Gal-1 is involved in proteolytic dependent or independent events. The only information we have regarding this issue is that PAI-1 inhibits tPA effects over fibroblast invasion in co-culture experiments (see *Results*,

Fig.43), which suggests that tPA catalytic activity might be required to trigger invasion.

We have also found that Gal-1 is involved in tPA induced **Erk1/2 activation** in pancreatic transformed cells and fibroblasts. Several facts lead us to suppose that in our assays with pancreatic cell lines and human fibroblasts, tPA might be displaying the previously mentioned catalytic dependent and independent dual behavior. On one hand, Gal-1 is able to activate tPA proteolytic activity (see *Introduction*, Fig.13C)[421] and on the other, Gal-1 is known to be involved in many cell signaling events leading to proliferative responses[522]. Moreover, our group has recently shown that non-catalytic tPA is able to trigger Gal-1 mediated Erk1/2 activation in microglia[796], further supporting the non-catalytic requirement for tPA induced proliferation. Still, detailed examination of how tPA behaves regarding Gal-1 interaction might be required considering the strong dependency of tPA upon context.

tPA has been involved in **intracellular signaling** through interaction with several different receptors such as AnxA2, EGFR[318], NMDAR[259] and LRP-1[417]. In this project, we have found that Gal-1 participates in tPA induced Erk1/2 activation and proliferation in pancreatic transformed cells and fibroblasts. We have focused our attention on Erk1/2 signaling pathway as previous results from our group reported a rapid and sustained Erk1/2 phosphorylation upon tPA treatment in pancreatic cell lines, whereas Jnk and p38 remained unaffected[318]. Moreover, with the help of Erk1/2 inhibitors, it was confirmed that the mitogenic tPA effects were due to this pathway activation. How tPA coupled with intracellular signaling was already

addressed in a previous report, finding several receptors to be participating in the event, such as AnxA2 and EGFR. Anti-AnxA2 antibodies blocked tPA binding to pancreatic cancer cells only partially, suggesting the existence of other receptors involved in transducing tPA signaling[318,415]. Adding Gal-1 in the story line opens new possible mechanisms. Gal-1 has been related to the Ras-Mek-Erk pathway and subsequent induced proliferation in several cell types, such as in mesenchymal stellate cells[535] and T-cells[746]. As mentioned earlier, Gal-1 is able to directly interact with Ras. However, this interaction occurs exclusively in the intracellular compartment, which would question tPA's role in the scenario, unless the possibility of multiple simultaneous Gal-1 units inside and outside the cell was considered. Alternatively, $\alpha_5\beta_1$ integrin interaction with ECM substrates has been described to be coupled to Ras-Mek-Erk pathway[797], and Gal-1 has been proposed to be upstream regulating the final outcome, though in this particular report, Gal-1 induces growth arrest[488]. Finding that inhibiting individual tPA receptors, such as AnxA2, EGFR or Gal-1 equally impairs signaling activation, raises the possibility of the existence of a multicomplex containing all these proteins, which would be responsible for these effects. For uPA, a multiprotein complex including EGFR and integrins has been previously described[798-800]. We hypothesize that EGFR, via Gal-1 interaction, might well be the key protein translating tPA extracellular effects inside the cell. Indeed, a pull-down experiment with recombinant tPA identified EGFR as a partner, and tPA could induce Erk1/2 activation only in CHO cells expressing EGFR but not in the ones that did not[318]. EGFR is a transmembrane protein with 11 potential N-glycosylation sites[801], which have been shown to be critical for its conformation and phosphorylation[770]. Intringuingly, it

has been reported that, galectin lattices are involved in EGFR recruitment in the cell membrane[773]. One possibility could be that dimeric Gal-1 could be interacting with EGFR through one of its carbohydrate binding pocket, while tPA could be occupying the second one. Still, these are just simple non-data supported lucubrations in our context, and biomolecular experiments should be performed to further clarify the real nature of the complex. Nevertheless, characterization of the multicomplex is biochemically complicated, as interactions might be transient, require particular conditions or additional proteins. EGFR is a major drug target in pancreatic cancer, hence identifying new partners to better understand the molecular mechanisms affected when blocking its functionality might be extremely of relevance.

How Gal-1 affects tPA induced **angiogenesis** in pancreatic cancer *in vitro* has been recently addressed with a doctoral thesis in our group[802]. In the present work, we have just tried to find out whether Anginex, an antiangiogenic peptide reported to bind to Gal-1[445], could be disrupting tPA/Gal-1 interaction. Our interest has focused on Anginex because of its potential in therapy as this peptide does not affect quiescent ECs in normal vasculature[693]. Gal-1 was identified as an Anginex partner by yeast two-hybrid analysis and its interaction was confirmed by double staining colocalization, NMR and SPR. Moreover, Anginex showed no effects in Gal-1 KO mice, validating the biological relevance of their interaction[445]. Therefore, we have taken Gal-1/Anginex binding for granted and we have tried to address tPA's role in this scenario. Surprisingly, we have found that Anginex is not only binding to tPA but also directly to the dextran matrix used for SPR experiments, as well as to many other

proteins assessed, giving extremely high non-specific responses. This peptide has been previously shown to form dimers and larger aggregates[445,697]. Thus, previous reported data in favor of Gal-1/Anginex interaction might be masking a possible indirect interaction, as the other techniques used did not exclusively point at protein/protein direct binding. Actually, alternative hypotheses concerning Anginex molecular mechanisms of action have appeared. Some authors support that Anginex might not act by blocking interactions between matrix and endothelial cell (EC) adhesion molecules but directly by affecting gene expression of adhesion molecules, such as integrins and CD44[693]. Different Anginex partners from Gal-1 have also been described, such as fibronectin[803] or anionic phospholipids[804]. Indeed, the cell membrane lipid structure itself has been described as being Anginex primary target[804].

Our *in vitro* data have proven that Gal-1 mediates tPA induced pathological effects in pancreatic cancer cells and fibroblasts. As tPA is not secreted by fibroblasts, we hypothesize that the protease realeased by pancreatic cancer cells could be exerting **paracrine effects** over this mesenchymal population through Gal-1. We have tried to directly address the study of these paracrine effects by subjecting fibroblasts to serum free conditioned medium from pancreatic cancer cells with different tPA secreting levels and analyzing their invasive capability. Although co-culture experiments present several innate limitations, such as the lack of an ECM and a complete environment, they get a little bit closer to the biological landscape. We are aware of the fact that the F88.2 cell line used comes from breast cancer and that fibroblasts from different origins display unique phenotypic features[805]. Moreover, in order to be

strict, pancreatic stellate cells (PSCs), which represent the predominant cell type in pancreatic tumors should be used. Nonetheless, we considered using F88.2 cells because PSCs are very difficult to isolate whereas the fibroblastic cell line used was readily available. An immortalized cell line of PSCs was established several years ago[806], and it would be very interesting to have the opportunity to address our questions in this context.

3.4.1 Model Proposed

In vitro data have demonstrated that Gal-1 is mediating many of the tPA induced pathological effects, being involved in migration, Erk1/2 activation, proliferation and invasion. Moreover, Gal-1 is acting as a functional tPA receptor not only in pancreatic epithelial cells but also in fibroblasts, suggesting that their interaction could be important in the so typical desmoplastic reaction. Thus we propose a model in which tPA secreted from pancreatic epithelial cells could act both in a paracrine and in an autocrine manner. In the latter, it would bind to Gal-1 in the cell surface of pancreatic tumoral cells triggering Erk1/2 activation and subsequent proliferation, as well as invasion. These events would be favoring tumor progression. On the other hand, tPA could bind in a paracrine fashion to Gal-1 from fibroblasts, what would induce the same events but in this mesenchymal cell line, leading to the desmoplastic reaction (Fig.116).

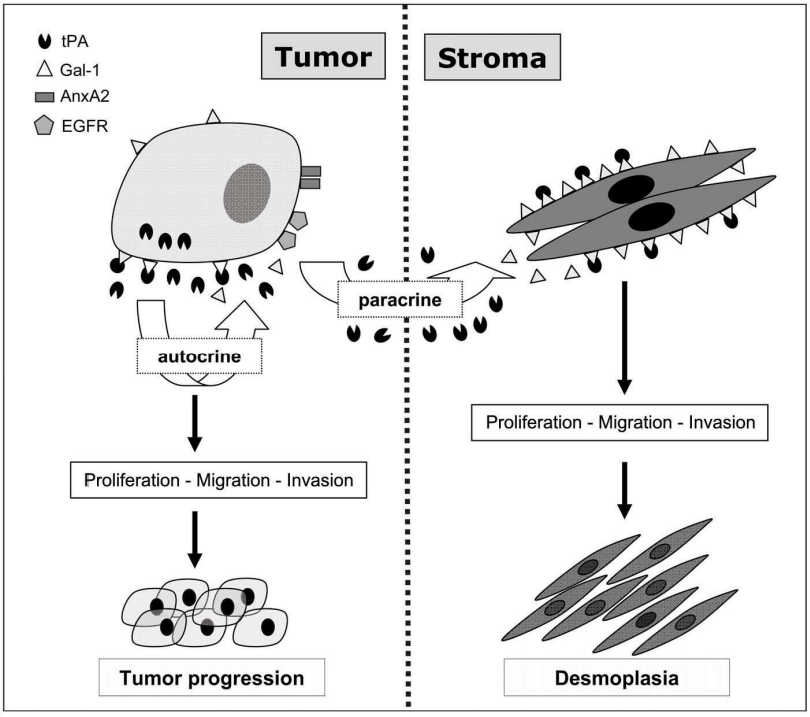

Figure 116. Gal-1 is acting as a functional tPA receptor in pancreatic cell lines and fibroblasts. Gal-1 in pancreatic cancer cells can activate Erk1/2, induce proliferation, migration and invasion by binding to tPA in an autocrine fashion. Gal-1 can also act in a paracrine fashion over fibroblasts, triggering the same pathological effects that could be involved in the desmoplastic reaction.

Gal-1 has been reported to be involved in other paracrine mechanisms leading to tumor progression, for instance in OSCC, where Gal-1 downregulation in fibroblasts impairs cancer cell invasion and migration[531]. Several reports have addressed the molecular mechanisms taking part in the interaction between cancer cells and the stroma. Still though, the paracrine events responsible for altering the behavior of fibroblasts and pancreatic cancer cells are not fully deciphered. Some of the players that have been reported to be relevant are Erk1/2, Akt[134], IL-1β and TGF-β[807], Mcp-1 and Ccl-2[531], Cox-2[39] and Sparc[808]. An even more tangled

situation might be real which could involve more cell populations in the stroma establishing additional paracrine mechanisms. Gal-1 has been reported to be endocytosed by T cells[809] and by ECs in culture, promoting Ras mediated Erk1/2 activation and stimulating their proliferation and migration[540].

3.5 STUDY OF GAL-1 RELEVANCE IN PDAC IN VIVO

3.5.1 Gal-1 Study in Mouse Pancreatic Cancer

Although we have provided some insights into the zebrafish model to study pancreatic cancer, our functional results rely exclusively on mouse models. Mice have been largely used to model human cancer but we must be aware of the differences that exist between genetically engineered mouse models and humans[155]. During life, humans undergo many more cell divisions than mice but the rodents' metabolic rate is seven times higher. Differences also exist concerning the cell types involved in tumor formation. Whereas mice spontaneously develop tumors in cells of mesenchymal tissues, humans frequently develop carcinomas. The molecular mechanisms involved in DNA stability are also playing a very important differential role among species. The retinoblastoma pathway modulates senescence in human fibroblasts whereas this role is overtaken by p53 in mice. Furthermore, murine cells have long telomeres and present constitutive telomerase expression. Nevertheless, mice represent faithful suitable models to study cancer as confirmed by the fact that cloning putative human oncogenes and deletion of candidate human tumor suppressor genes have the potential to induce cancer in transgenic mice. In fact, preclinical drug development is strongly dependent on studies performed in mouse models with transplanted tumors, which must be interpreted carefully as they do respond successfully to many chemotherapeutic agents[810-815].

Several gaps also exist between human and mouse pancreatic cancers in particular. The first difference resides in the grade of tumor differentiation. Whereas human PDAC is usually described as being moderate or poorly differentiated, many mouse models produce anaplastic carcinomas. Second, mouse models display multilineage differentiation including acinar features while human pancreatic cancers are frequently classified as ductal. Third, PanINs are often observed in humans but rarely in mice. Fourth, mice pancreatic tumors do show different tumoral nodules but human pancreatic cancer does not usually show multifocality. Finally, desmoplasia is one of the repetitive hallmarks in human pancreatic cancer, though it is many times unobserved in mouse models[170].

3.5.2 *In vivo* Role of Gal-1 in Pancreatic Cancer using Xenograft Models

Once proven that Gal-1 was clearly impairing some of the key events driving pancreatic progression *in vitro*, we wanted to address its importance *in vivo*. Our first attempt, establishing an interface between *in vitro* and *in vivo* analyses, centred on using xenografts, in which human pancreatic tumoral cell lines were injected in immunodeficient mice. The use of xenografts seemed convenient as a first aproximation because they are rapidly and easily established without requiring time consuming and expensive breeding and tumor latency is usually much shorter and reproducible compared to genetically engineered mice.

To accomplish Gal-1 stable downregulation, shRNA mediated silencing instead of siRNA was used in these experiments. 2 different sequences against Gal-1 mRNA were used to exclude off-target effects and cells were characterized before mice injection. Other studies directed to assess the importance of paracrine mechanisms in pancreatic cancer associated desmoplasia, have been successfully addressed with similar *in vivo* models[98].

Consistent to what was already published in different systems[554], Gal-1 *in vitro* downregulation does not affect cell proliferation. Although these data seem to enter in conflict with our previously described proliferation experiments with Gal-1 siRNA in pancreatic cancer cell lines, it must be noted that in that case only tPA induced proliferation is affected upon Gal-1 downregulation whereas basal proliferative levels are unaltered. Others have analyzed how Gal-1 modified proliferation taking into account the tumor microenvironment through *in vivo* studies. Importantly, they described that cells whose proliferation was unaffected *in vitro* by Gal-1 inhibition presented impaired proliferation rates *in vivo* due to Gal-1 immunosuppression activity[816]. In our system, we have also failed to detect significant differences in tumor growth *in vivo*. Nevertheless, in this mentioned report, Gal-1 blockade was achieved by using inhibitory disaccharides, which would completely affect Gal-1 functions, both in cancer cells and in the tumor stroma. In contrast, in our experiments, pancreatic cancer cells were exclusively affected by Gal-1 depletion, whereas the tumor microenvironment showed unperturbed Gal-1 levels, which might explain the lack of differences observed concerning proliferation.

In our results, although a trend is observed connecting Gal-1 depletion to reduced invasion, we have failed to detect significant differences (see *Results*, Fig.51), though in siRNA mediated silencing, alteration of Gal-1 levels *per se* affects pancreatic cancer cell invasion (see *Results*, Fig.38). Although the molecular mechanisms sequestering and degrading Gal-1 mRNA are common in both silencing techniques, we think that stable downregulation might differ from a transient one by offering cells the chance to adapt and overcome deficiencies derived from specific protein depletion. Moreover, we think that luciferase expression might influence PANC-1 cells significantly, as observed by subtle morphological differences of these cell lines *in vitro*. So, the possibility exists that PANC-1 and PANC-1_LUC cell line might behave discrepantly.

Following *in vivo* tumor progression through luciferin injection and bioluminescence detection was proven to be useful but tricky. Discrepant measures were obtained from day to day which impaired exact tumor progression tracking. Intraperitoneal injections to deliver luciferin might be one of the sources of variability[698] as well as this product loss of activity after freeze/thaw cycles.

The first subcutaneous experiment did not provide clues regarding Gal-1 importance in tumor progression. Surprisingly, control non-infected control cells behaved much differently from other cell types. This control cell line failed to develop tumors and due to the experiment technical details (all mice were injected with non-infected cells on the left flank and infected cells on the right) we had to sacrifice animals before non-infected cells could generate significant tumors. In fact, differences have been also observed regarding

anchorage independent growth between the two control groups (non-infected versus non-targeting shRNA). It is unclear to what extent infection affects the behavior of a tumoral cell line and why this effect depends on the experimental design. Nevertheless, we could still compare both groups with Gal-1 depleted levels to the control shRNA. No effect on tumor progression has been observed depending on Gal-1 levels of expression. Intraperitoneal injections generated tumors resembling the human pathologic environment, which were far more glandular and vascularized. In this case, a clearer trend linking the lack of Gal-1 to reduced tumor development could be glanced. However, the small number of animals per group used, combined to the high variability among them, may have hiden conclusions, as no significant differences have been detected regarding survival, metastasis, proliferation, angiogenesis or stroma formation. The lack of phenotype observed is probably consequence of the underestimation of the protein impact on the stromal compartment (which contained high host Gal-1 levels in all four animal groups). As previously mentioned, including the stroma contribution to pancreatic cancer in xenografts seems more than necessary to work with a proper *in vivo* model, considering Gal-1 importance in the tumor microenvironment. Several studies in pancreatic cancer have used the co-injection of pancreatic tumoral cells with human PSCs[134,135], achieving successful working models. Indeed, to be even stricter and reproduce the real biological landscape, all stromal cell types, including adipocytes, pericytes and ECs should be taken into account. Other groups have also realized that xenograft experiments to study Gal-1 present a key limitation due to the significance of Gal-1 in the stromal compartment and have tried to solve it. For example, direct co-

injection of CAFs with low Gal-1 levels with epithelial tumoral cells in nude mice has been reported, with the intention to target Gal-1 in the compartment where it is usually overrepresented[531]. Besides, it must be well taken into account that Gal-1 has been reported to be actively participating in tumor progression through its ability to allow tumors evade the immune response. Thereby, in xenografts, which are characterized by a deficient immune response, the effects of Gal-1 might also been disguised in this sense. Additionally, in our work we have also found that Gal-1 has a deep influence on the acinar to ductal differentiation occuring in Ela-1-myc mice developing pancreatic tumors. Thus, Gal-1 might not have such a remarkable role in xenograft tumors, which do not undergo acinar-ductal metaplasia and are far from resembling human pancreatic ductal adenocarcinomas.

3.5.3 *In vivo* Role of Gal-1 in Pancreatic Cancer using Transgenic Models: Ela-1-myc:Gal-1$^{-/-}$

As it has already been addressed in the former section, xenografts did present several inconvenients that suggested the use of improved *in vivo* models. Not only Gal-1 depletion could not be achieved but also tumor development in xenografts did not reproduce the typical pancreatic cancer stepwise progression. Thus, in order to define a more suitable system, we used the murine Ela-1-myc transgenic model, which presents several features that highlight its appropiateness to study pancreatic carcinogenesis. Although c-Myc has not been one of the classical referred key genes in pancreatic tumorigenesis, it is more evident everyday that it plays very relevant

roles in this pathology[191]. Ela-1-myc model is one of the few that is based exclusively on altering a single gene[62], which facilitates breeding and genotyping. Other advantages include short latency of tumor progression and the presence of ductal adenocarcinomas resembling human PDACs, a feature that has classically boycotted many of the emerging mouse models. Still, caution needs to be taken when translating results from mice to human, because in the Ela-1-myc model, all acinar cells express the c-Myc oncogene whereas, in human, only distinct cells acquire genetic alterations driving tumor progression.

To elaborate on Gal-1 importance in pancreatic tumor progression in the Ela-1-myc model we decided to cross this engineered mouse model with Gal-1 KO. This strategy offered a way to obtain total depletion of the protein in all cell types, which seemed to be required to understand Gal-1 importance on the whole process, considering the pleiotropic effects displayed by this protein. Interestingly, we have found several very important phenotypic effects linked to Gal-1 depletion or absence.

3.5.3.1 Gal-1 Haploinsufficiency in Pancreatic Cancer

Slight differences in genetic background did not affect tumor development in a very similar study performed in our group using the same Ela-1-myc model[418]. Yet, to avoid any possible source of variation and bearing in mind gene compensation, our initial intention was to compare Ela-1-myc:Gal-$1^{-/-}$ pancreatic progression to control Ela-1-myc:Gal-$1^{+/-}$ mice instead of Ela-1-myc:Gal-$1^{+/+}$.

This strategy would allow us to use animals from the same generation, faithfully maintaining a constant genetic background.

Nevertheless, Gal-1 haploinsufficiency in Ela-1-myc pancreatic tumor progression has been repeatedly observed in our experiments. Deletion of one single allele of Gal-1 has had a marked impact on survival, necrosis, hemorrhage, angiogenesis and proliferation of pancreatic tumors. Indeed, this scenario reflects the sensitive nature of all these processes to changes of Gal-1 levels. Despite not being the most common situation, our results are not the first ones to report that heterozygots can sometimes behave as homozygotes[817] and that tumor progression can be markedly hampered in heterozygosity[817-819]. In particular, in pancreatic cancer, *Tgfbr1* heterozygosity has been related to decreased pancreatic precursor lesion formation[820], and depletion of one allele of several tumor suppressor genes has been reported to steadily favor tumor progression[187,821,822]. Surprisingly, Ela-1-myc:Gal-1$^{+/-}$ mice do not behave exactly the same comparing its phenotype to wild type or KO animals. In some events, heterozygous mice display intermediate phenotypes whereas in others, their response is the same as Gal-1 KO mice. This lack of repetitive and consistent data regarding Gal-1 number of alleles expressed and overall functional outcome, might be due to distinct levels of Gal-1 expression in heterozygosity depending on the cell compartment, as it has been reported in other haploinsufficiencies[823,824].

Gal-1 protein quantification in pancreatic tumors to assess its levels in heterozygosity resulted challenging taking into account that acinar tumors displayed almost no Gal-1 expression. The scarce number of

tumors with ductal differentiation in Ela-1-myc:Gal-1$^{-/-}$ mice and tumor heterogeneity among animals demanded a suitable mesenchymal marker to be able to compare tumors and quantify Gal-1 depletion upon heterozygosity. Our first candidate was α-SMA but this possibility was discarded considering that this protein is only expressed in activated stromal cells and that Gal-1 has been reported to induce fibroblast activation and α-SMA expression[531]. In fact our data also showed that Gal-1 depletion correlates with decreased α-SMA staining. Consistent with previous data[127], we finally chose desmin as a loading control to ensure equal mesenchymal populations in pancreatic tumors.

As many others[823-826], we have observed a dramatic decrease of more than 50% on Gal-1 expression within heterozygosity. In fact, we had previously found a Gal-1 dose dependent effect in our *in vitro* studies, as Gal-1 siRNA mediated downregulation (without total depletion) significantly impairs tPA induced pathological effects. Besides, in xenografts, the lack of effects has been always linked to the importance of Gal-1 in the stromal compartment rather than to the reminiscent Gal-1 levels after downregulation. These data would suggest reconsideration of the studies that have directly used Gal-1 heterozygous mice as controls, without comparing them to the wild type counterpart[827-829]. Furthermore, it has been observed that depending on the cell tissue or compartment, heterozygosity can affect protein levels differently[823,824], which might explain why the effects observed in Ela-1-myc:Gal-1$^{+/-}$ are not always in accordance with Ela-1-myc:Gal-1$^{-/-}$ mice.

3.5.3.2 Ela-1-myc:Gal-1$^{-/-}$ Mice Tumor Formation and Survival

Previous data from our group reported a 10 day increase of **survival** in Ela-1-myc:tPA$^{-/-}$ mice compared to control mice[418], confirming tPA importance in pancreatic tumor progression. Still, in this manuscript we have detected a much more significant 21 days increase in survival, and this increase has been observed both in Ela-1-myc:Gal-1$^{+/-}$ and Ela-1-myc:Gal-1$^{-/-}$ mice. This relevant improvement depicts a wider and more important role for the lectin, partially dissociated from tPA activity. Thus, although Gal-1 might be mediating tPA induced pathological effects *in vivo*, it must be involved in several distinct events driving pancreatic carcinogenesis. As observed with the Ela-1-myc:tPA$^{-/-}$ study[418], the absence of Ela-1-myc:Gal-1$^{-/-}$ animals recovering normal life span might be intrinsic to the pancreatic transgenic model as it develops very aggressive tumors with a very complex environment and the single inactivation of a gene is not sufficient to impair total tumor development. In addition, at least concerning Gal-1 ability to trigger tPA induced pathological effects, it would not be until late stages of tumor progression (when tPA is expressed in ductal tumors), when Gal-1 depletion would become physiologically significant. Classically, ductal tumors are considered to be more aggressive. Although Ela-1-myc:Gal-1$^{+/+}$ mice (with more ductal tumors) die earlier, the intermediate phenotype shown by Ela-1-myc:Gal-1$^{+/-}$ regarding formation of acinar-ductal metaplasia (ADM) implies that survival (which is on average the same in Gal-1 heterozygous and KO tumors) is not a direct consequence of the type of tumor formed. The same tumor weight measured during necropsies in all three groups

suggests that animals may die when reaching a tumor size threshold that hamper animal life. Thus, Gal-1 heterozygous and KO mice would require more time for tumors to grow and so their survival would be higher. These data are coherent with the lower proliferation rate described for Ela-1-myc:Gal-$1^{+/-}$ and Ela-1-myc:Gal-$1^{-/-}$ (see *Results*, Fig.83). Interestingly, our data quantifying 40-60% of proliferation in mice ductal tumors shows higher proliferative indexes than what has been reported for human pancreatic cancer[25,703].

We are aware of the fact that our study lacks addressing the role of the **immune system** in pancreatic tumor progression, which is crucial considering Gal-1 reported effects in this compartment. Gal-1 suppresses secretion of proinflammatory cytokines[830] and inhibitory several functions in relation to activated T cells[467,484,552,553,831,832] and Gal-1 KO mice have been reported to display deficient B-cell development[509] and affect macrophage stimulation in response to inflammatory stimuli[510]. Although several data in different contexts have reported comparable tumor immune responses in Gal-1 wild type or KOs animals[445,540], this issue remains opened for further examination in our study. A Gal-1 effect favoring an immunosuppressive tumor environment would cooperate with the direct described Gal-1 effects on tumor progression to explain the strong correlation among aggressiveness and Gal-1 expression, similar to what has been reported in prostate carcinoma[580].

Although depending on the genetic background, Ela-1-myc mice are more or less predisposed to develop metastasis, this mouse model is

not one of the typical ones to study tumor spread to surrounding tissues[62,202]. Whether this is consequence of rapid tumor development in primary sites or if additional genetic alterations are required for metastasis, is not still clear. Due to the high amount of tumors involved in the study, automatically analyzing each possible organ presenting encroachment became unfeasible. Thus, only organs presenting macroscopic signs of invasion were examined. We have detected tumors attached to intestine, liver, kidney and spleen but barely identified real dissemination to those sites. What we have frequently encountered while studying pancreatic tumor histology are peripancreatic lymph node infiltrations by contiguity, present in more than 25% of tumors. Despite the fact that Ela-1-myc heterozygous and KO mice for Gal-1 show reduced percentage of animals affected by node infiltrations, significant differences among groups with different Gal-1 expression have not been found. Gal-1 has been extensively linked to tumor invasion and metastasis in several carcinogenic processes such as in HCC[584], breast cancer[579], neuroblastoma[587], OSCC[571] and lung adenocarcinomas[542]. Although in pancreatic cancer, Gal-1 expression does not correlate with M stage in AJCC classification[590], it does correlate with node infiltration, which has not been reproduced in our system. Still, we think that considering the inappropriateness of the system to study metastasis, we can not conclude that Gal-1 is not involved in tumor dissemination. Further Gal-1 studies in other animal models will help to properly address this issue. Moreover, the lack of differences detected concerning node infiltration might be explained because in all examined cases, invaded nodes have been found inside pancreatic tumors but not in distal sites. Therefore, this proximity together with tumor histologic analyses point at a direct tumor cell

invasion rather than blood vessel mediated tumor dissemination, process in which Gal-1 is believed to be taking part.

3.5.3.3 Gal-1 is Involved in Acinar to Ductal Metaplasia

Ela-1-myc model has been outlined in pancreatic cancer studies because of its ability to generate ductal lesions from c-Myc expressing acinar cells (Fig.117). Biphenotypic cells expressing markers of acinar and ductal differentiation are observed in Ela-1-myc lesions (see *Results*, Fig.70).

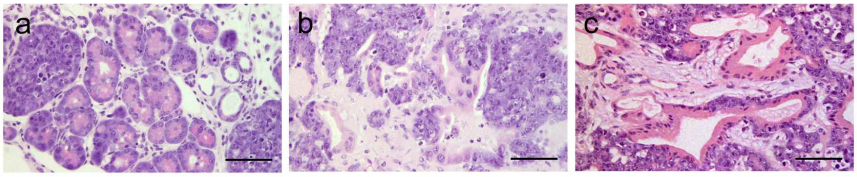

Figure 117. Ela-1-myc pancreatic tumoral progression and acinar ductal metaplasia. A) Normal acinar cells surrounded by nascent tumoral nodules with acinar features from an Ela-1-myc mouse sacrificed at early stages of tumoral progression. B) Compact acinar nodules start to lose their architecture and form glandular strcutres. C) Tumoral ducts presenting a mixture of cells with ductal and acinar features. Scale bars represent 100μm.

Considering that ductal cells are not the predominant cell type in the human normal pancreas but pancreatic tumors are frequently classified as ductal, this process of acinar to ductal metaplasia has been highlighted as one of the possible mechanisms triggering tumor initiation and progression. Still, although being one of the most supported hypotheses, this is not by far, the only one proposed. Pancreatic cells are known for their high plasticity characteristics and indeed, almost all of them have been reported to be feasible sources of pancreatic tumoral cells. Thus, not only acinar cells[46,47] but also centroacinar[48], progenitor[52], ductal[42-45] and islet cells[49-51] have been proposed to originate neoplasia[42,46,833]. Extensive data have

been used to characterize the mechanisms to explain how acinar cells are able to develop tubular complexes[174,834-840]. Acinar-ductal metaplasia has been identified and followed not only by *in vitro*[841] but also by *in vivo* lineage tracing[842], discarding possible in culture artifacts. Several animal models developing pancreatic tumors as a result of the expression of oncogenes under acinar specific promoters[61,176,843], and among them Ela-1-myc[62], have also brought evidences towards an acinar origin for pancreatic ductal adenocarcinoma. In fact, it is not clear yet whether acinar-ductal metaplasia represents a PanIN precursor or if it is itself a pancreatic cancer precursor event directly processing to PDAC[183].

One of the main novelties presented in this manuscript is the fact that Gal-1 is markedly involved in acinar to ductal metaplasia. Whereas 40% of Ela-1-myc:Gal-$1^{+/+}$ areas are classified as ductal, this percentage is significantly reduced to the half in Ela-1-myc:Gal-$1^{+/-}$ tumors, and even falls to the 10% in Ela-1-myc:Gal-$1^{-/-}$ ones. Taking into account that the process of acinar to ductal differentiation in Ela-1-myc tumors is favored with animal age, and that Ela-1-myc:Gal-$1^{+/-}$ and Ela-1-myc:Gal-$1^{-/-}$ life span is on average 20 days longer, the effect of Gal-1 impact in ADM is in fact even more important. For instance, in Ela-1-myc:tPA$^{-/-}$ study[418], a 8.2% increase in the ductal fraction was observed due to an increase in survival of 10 days. Thus, probably, if tumors from the three groups were analyzed in the same time point, differences observed according to Gal-1 levels would even be more dramatic, rarely finding ductal tumors in Ela-1-myc:Gal-$1^{-/-}$ mice. We can not rule out the possible error made by histologically classifying tumors according to one tissue slide but we tried to minimize the impact of this limitation by

preparing paraffin blocks to optimize the amount of tisse analyzed. Moreover, the distinctive nature of the tumors was clearly manifested macroscopically during necropsies as tumors from KO mice almost always presented typical acinar characteristics with extensive necrosis. Thus, we strongly believe that data collected are faithful and representative and that they claim for an essential role for the lectin to promote ADM.

We have not addressed the molecular mechanisms related to Gal-1 involvement in ADM. The percentage of ductal tumors remained unaffected upon tPA depletion in the same Ela-1-myc tumoral model[418], what implies that Gal-1 involvement in this event is totally unconnected to the protease. Few molecular reports have addressed the molecular mechanisms involved in ADM, which difficult filling the gap between Gal-1 and the observed phenotype.

One of the clue molecules involved in acinar to ductal reprogramming identified by genetic engineered animal models is, probably not by coincidence, the most generally altered gene in PDAC: K-Ras[72,188,189]. Several reports have shown that K-Ras can spontaneously induce ADM[47,57,188,189,844,845]. Additional events like tissue damage, inflammation or alteration on additional genes have enabled acceleration of acinar-ductal metaplasia. For instance, activated Gli[95], Notch[188] and TGF-α[846] or alterations in Smad4[186], Pten[183] and TGF-β[187] result in an increased ADM formation and subsequent tumor acceleration.

Moreover, the presence of ADM in wild type K-Ras scenarios, such as in our working Ela-1-myc model[847], suggests that additional

signaling events might induce this process *in vivo*. Another pillar in ADM data is sustained by growth factor signaling, including TGF-α and EGFR [840,848]. MMP-7 has also been identified as as a participant in ADM[837,849] through MMP-7 KO mice analysis. This protein is linked to metaplasia through its requirement for Notch activation and subsequent acinar dedifferentiation[849]. Notch activation has been observed in ADM[47] and it has been proven to be essential for ADM in the context of growth factor stimulation[188,839], although requiring K-Ras activation too. Other signaling pathways whose relevance in ADM has been proven include Akt[850], Pdx1 and Stat3[851], TGF-β[843] and Cox-2[852]. Several targets preventing ADM have also been detected by observing increased ADM formation in protein KO scenarios. In this direction, p53[175,177,181,182], and Pten[48] have been linked to this event. β-catenin[853] and Mist[845] have also been shown to impair ADM.

We have no data regarding how Gal-1 could be mediating ADM but we have contemplated several options. Although, as previously mentioned, Ela-1-myc tumors show wild type K-Ras expression[847], a strong possibility exists that Gal-1 cooperates with K-Ras mediated ADM. Gal-1 has been required for correct Ras membrane anchorage and Ras signaling, regulating the MAPK signal output[499,525,528], what would explain that Gal-1 deficient mice present difficulties in performing acinar to ductal differentiation. Another key pathway that emerges when trying to find explanation for Gal-1 induced ADM, taking into account the results here described, is Hedgehog (Hh). Increased Hh signaling has been shown to cooperate with K-Ras to promote PanIN formation[95] but also to induce itself the formation of tubular structures[93]. Thus, we think that

Gal-1 could be playing a dual role by stabilizing Ras on one hand and further activating Hh signaling on the other, thus optimizing their ability to induce cell transformation. Upon other feasible possibilities, we speculate that a putative Gal-1 partner, could be CD44, a cell surface glycoprotein that has been linked to ADM and is upregulated in human PDACs[183]. Another feature that has gathered our attention is that, bearing in mind that ductal tumors are much more vascularized than acinar ones, and that Gal-1 is involved in angiogenesis, it could be feasible that Gal-1 absence is impairing ADM through a deficient vascularization. However, the link between vascularization and ADM has not been well established, which makes necessary a deep study of this matter to understand Gal-1 effects. Intringuingly, Pten, which has been described to prevent ADM[48], downregulates HIF-1[854], which in turn induces VEGFR and PDGFR-β[855] expression, critically influencing angiogenesis of invasive PDACs. These data could be of relevance *in vivo* considering that HIF-1 has been reported to bind to Gal-1 promoter and induce its overexpression[586]. However in our working model, Gal-1 is absent, what suggests that Gal-1 inducing ADM and angiogenesis might be hypoxia/Pten independent. Although MMP-7 appears in our transcriptome analysis, its expression is found to be downregulated when Gal-1 is overexpressed in RWP-1 cells, which would point to the opposite direction. Still, we are aware that pancreatic tumoral cell lines are often far from reality and indeed, RWP-1 cells come from a pancreatic metastasis to the liver, which might explain some of the differences found regarding gene expression.

Interestingly, we have detected a strong correlation within the lack of Gal-1 and an increase in the **necrosis** found in pancreatic tumors.

Antiapoptotic functions directed to several tumor cell types have been classically assigned to a close family member of Gal-1, Gal-3, which has been extensively studied to outline its potential to increase chemotherapy mediated apoptosis[428,699-701,856-861]. Gal-1 literature related to tumor cell apoptosis is far less abundant and points towards the opposite direction. Gal-1 expression induces apoptosis in pancreatic cancer[600] and colorectal cancer cells[537]. Although the role of Gal-1 promoting activated T cell apoptosis is well established and documented, it is only in this cell line where an anti-apoptotic function for stromal secreted Gal-1 has been reported[862]. In fact, we do contemplate the strong possibility that the increase of necrosis seen in Ela-1-myc:Gal-$1^{+/-}$ and Ela-1-myc:Gal-$1^{-/-}$ tumors is a consequence of the architecture of the type of tumors formed rather than a direct Gal-1 consequence. Thus, Ela-1-myc:Gal-$1^{-/-}$ tumors, which are far more acinar and less vascularized, are more prone to present intratumoral necrosis.

3.5.3.4 Ela-1-myc:Gal-$1^{-/-}$ Tumor Characterization

Although not exclusive, Gal-1 staining is predominantly found in the **stroma** surrounding glandular structures in ductal tumors. These type of lesions resemble their human counterpart in that the most abundantly found cell type are cancer associated fibroblasts. Although their origin has not been perfectly traced, several hypotheses include local fibroblasts, bone marrow-derived progenitor cells, stellate cells or transdifferentiating epithelial cells[863], as possible cell line sources. The presence of Gal-1 in such an important cell type in pancreatic cancer, might explain why this protein appears to be key in tumor progression in the Ela-1-myc

mouse model, whereas its effects on xenografts are much less spectacular. Indeed, stromal fibroblasts have been shown to trigger tumor initiation, growth and metastatic spread[864-866]. We have quantified stroma formation in ductal tumors through α-SMA protein detection, which is found in myofibroblasts, vascular smooth muscle cells, pericytes and myoepithelial cells[111,867]. We have found a mild decrease in α-SMA protein levels in Ela-1-myc:Gal-1$^{-/-}$ ductal tumors. The distinctive trends observed within survival and stroma accumulation related to Gal-1 expression, have not allowed us to assume that the differences observed in animal life span are exclusively due to a reduced desmoplastic reaction in ductal tumors. Yet, we must be conscious that the small representation of ductal areas (rich in stromal compartment) in Gal-1 KO animals has hampered the analysis. Indeed, when we analyze all tumors, irrespective of their acinar or ductal nature, we find that the amount of stroma present in Ela-1-myc:Gal-1$^{+/-}$ falls significantly, an effect that is even be more dramatic in Ela-1-myc:Gal-1$^{-/-}$ mice (see *Results*, Fig.85B). Therefore, we have described for the first time in pancreatic cancer *in vivo*, that Gal-1 is able to modulate the amount of stroma formed. Previous reports linked Gal-1 to myofibroblast activation[531,533]. Although the mechanisms mediating this event are not fully understood, the names of several proteins have appeared in the field. For instance, Gal-1 has been hypothesized to control fibroblast activation by regulating Nox4 expression[868]. Besides, Gal-1 has been proposed as a downstream target of proteins involved in myofibroblast differentiation such as TGF-β1[869], endothelin-1 and PDGF[870]. Intringuingly, co-injection in nude mice of epithelial tumoral cells with Gal-1 depleted fibroblasts, has led to the identification of two additional molecules involved in metastasis:

Mcp-1/Ccl2[531]. Shh pathway has been extensively related to PSC activation[98]. In addition, although the link between Shh with Gal-1 has not yet been well characterized, our data pointing at a functional relationship between Gli and Gal-1 could help understanding their common role in such an important event in pancreatic cancer.

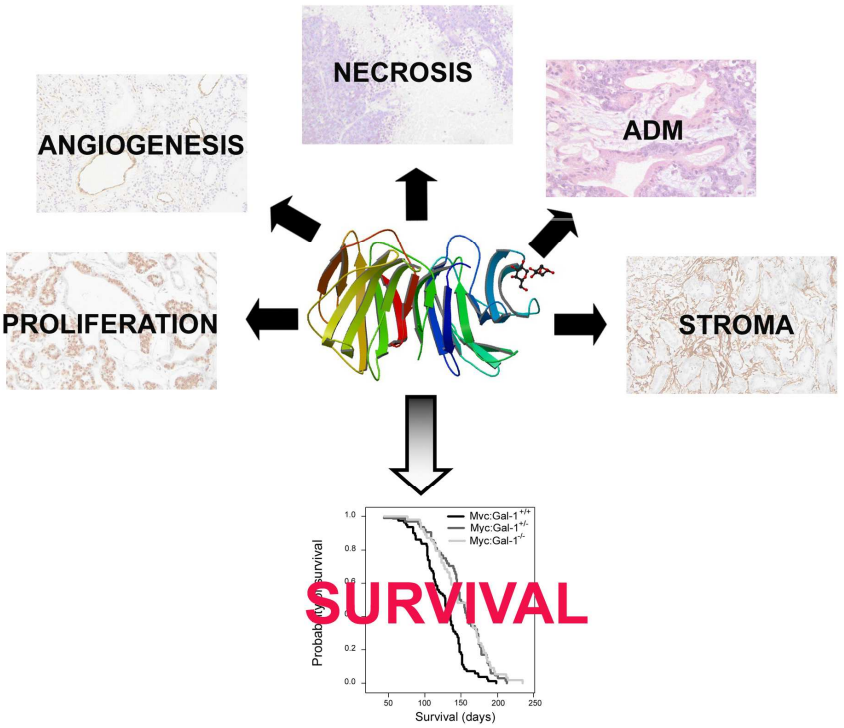

Figure 118. Gal-1 is involved in several events driving pancreatic tumor progression *in vivo*. We have identified Gal-1 to be involved in pancreatic tumoral cell proliferation, stroma formation, angiogenesis, necrosis and acinar to ductal metaplasia. Gal-1 might cooperate in all these events to finally have an overall effect upon survival.

Special blood supply requirements are essential for tumors to grow beyond a certain threshold[871]. In our transgenic mouse model, one of the most relevant phenotypes observed due to Gal-1 deficiency concerns **tumoral angiogenic network**. Supporting our data, Gal-1

depletion has been several times connected to deficiencies in tumor angiogenesis, highlighting its importance for proper blood vessel formation and overall tumor development[445,540,550]. Some of these previous reports have outlined the defects in blood vessel formation of Gal-1 KO animals compared to their wild type littermates, excluding heterozygots from the analysis[445,540]. However, Gal-1 downregulation is also reported to reduce blood vessel formation[550]. Interestingly, one of the main results of our work is the identification for the first time of Gal-1 haploinsufficiency in intratumoral angiogenesis by analyzing Gal-1 heterozygosis. Besides, once again, Gal-1 effect on ADM hides a more dramatic indirect effect of the lectin in angiogenesis (see *Results*, Fig.87C). Heterozygous and KO animals show fewer ductal areas (far more vascularized) than wild type mice. The fact that in ductal tumors, blood vessel network and stroma abundance follow the same trend, suggests that Gal-1 presence in this non-epithelial compartment could be responsible for EC activation and angiogenesis. In addition, we have found that Gal-1 expression seems to correlate well with the presence of intraperitoneal hemorrhages. Additional *in vivo* experiments to examine angiogenesis in pancreatic cancer are currently ongoing in our group. Several reports have focused on Gal-1 importance in tumor angiogenesis. Gal-1 modulates EC proliferation and migration[445,540]. In fact, ECs are known to suffer activation after internalizing Gal-1[540], proving the existence of further paracrine systems involving our lectin. Ras signaling and Erk1/2 activation have been involved in this process. Our group has also added tPA as a functional Gal-1 partner in *in vitro* angiogenesis[802]. Another protein reported to mediate Gal-1 effects on angiogenesis is NRP-1, whose interaction induced VEGFR phosphorylation[482]. One of the

outlined cell surface group of proteins involved in intracellular signaling triggering angiogenesis are integrins[872], well known glycoprotein partners of Gal-1. But different mechanisms are believed to join efforts towards a well supplied tumor environment. Gal-1 could participate in protease mediated activation of pro-angiogenic growth factors like VEGF, bFGF and others[124]. Besides, Gal-1 modulates the expression of several hypoxia-related genes implicated in angiogenesis[550].

In summary, these findings reveal that Gal-1 is a key protein involved in pancreatic tumor progression, regulating animal survival, acinar-ductal transformation, tumoral necrosis, proliferation, stroma formation and angiogenesis (Fig.118). We have identified Gal-1 heterozygosity as a tumor resistant genotype. The gene dosage-dependent effect observed for Gal-1 results very interesting for therapy, where reduction instead of complete inactivation of the protein might be a much more feasible approach. Although Gal-1 depletion in mice has been unrelated to important deficiencies[501], we can not predict the outcome of Gal-1 blockade in humans. The attractive possibility exists that haploinsufficiency of the gene might specifically affect pathological processes but not physiological ones, as it has already been described for other molecules[817]. The importance of Gal-1 in the stromal context is very appealing and again highlights Gal-1 as a promising target in pancreatic cancer. Stromal cells expressing Gal-1 are genetically more stable than tumoral cells and so they are less likely to develop drug resistance[873,874]. Indeed, the important reduction of ductal tumors and, respectively, of stromal component, observed after depleting a single copy of *Lgals1* gene, outlines hope towards an increased

response to chemotherapy, which would imply a major advance in pancreatic cancer treatment[134,875,876].

3.5.4 *In vivo* Role of Gal-1 in Pancreatic Cancer using Zebrafish Models

Zebrafish (*Danio rerio*) has gathered much attention concerning cancer studies and has timidly displaced the focus from rodent mouse models. Many advantages are responsible for zebrafish success in cancer research. Fertilization is external and experiments become easier and much more affordable as embryos develop more rapidly *in vitro* and are transparent. Moreover, gene expression alteration turns out to be straightforward and zebrafish cell lines have been established. Besides, zebrafish represent a system much closer to mammals compared to other typically used invertebrate animal models. *Danio rerio* has emerged as a suitable model to study pancreatic cancer[207]. Pancreas anatomy is pretty similar between zebrafish and mammals, with acini and ducts alike. Islets are organized comparably and zebrafish hormones can be even identified with antibodies raised to mammalian ones. Several conserved genes and orthologous signaling pathways have been reported to both control zebrafish and human pancreatic development.

Zebrafish has been previously used as a model to study Gal-1 importance in cancer and its convenience has been highlighted due to the less diversified repertoire of galectins compaired to its human counterpart[445]. DrGal1-L2 expression appears in zebrafish 12 hpf

and it is abundantly found in the notochord[442]. Nevertheless, we have been the first ones to address DrGal1-L2 expression in zebrafish pancreatic cancer, localizing the protein in the tumor stromal compartment in 2 different transgenic zebrafish models. This situation resembles what happens in human pancreatic tumors and stresses the significance of *Danio rerio* as a model to study Gal-1 in this pathology. Techniques to assess the functional relevance of DrGal1-L2 by knocking it down during tumoral development are still methodologically complicated. Nevertheless, reducing the protein levels during embryonic development is feasible and pretty efficient. As it will be described in the next section, pancreas development and pancreatic tumor progression seem to use in common several signaling pathways and the pattern of Gal-1 expression is shared in both scenarios. Therefore, protein deregulation in zebrafish development through morpholinos remains outstanding for future experiments and will bring more evidences in favor or against the appropiateness of *Danio rerio* as a model to characterize Gal-1 importance in pancreatic cancer.

3.5.5 Gal-1 in Mouse Pancreas Development

Many of the key events during development are also relevant in tumorigenic processes and indeed both phenomenon share several features such as common signaling pathway activation. Pancreatic tumorigenesis in particular is characterized by the reactivation of developmental signaling pathways such as Notch[839], Hh[877] or Wnt-β-catenin[72]. Besides, as it has been addressed above (see section *3.5.3.3. Gal-1 is Involved in Acinar to Ductal Metaplasia*), the process of acinar to ductal metaplasia is linked to the reexpression of

embryonic factors, which are kept active throughout PanIN and PDAC progression[878,879], suggesting that these pathways might be relevant for tumor initiation. Similarly to what is described in pancreatic cancer, in human embryogenesis, Gal-3 is basically localized in epithelial cells whereas Gal-1 is detected in the mesenchymal compartment[880].

Hence, we thought it could be interesting to analyze Gal-1 importance in pancreatic development. We have confirmed Gal-1 to be prominently detected in the mesenchyme surrounding pancreatic epithelium during embryogenesis. Indeed, Gal-1 potential to be one of the important orchestrators during pancreatic development has been based on its tissue localization. The mesenchyme is one of the main source of signals during pancreas formation, being actively involved in growth, proliferation and exocrine differentiation[881]. Many insights have been made concerning the molecular mechanisms involved in mesenchymal signaling during development. Still, additional proexocrine factors working via cell contact and diffusible proendocrine proteins secreted by the mesenchyme remain to be identified[5].

In order to study the effects of Gal-1 in pancreas development, partial or total depletion in mouse developing pancreas was achieved through siRNA mediated silencing or working with Gal-1 KO dorsal bud explants. Interestingly, and despite being preliminary data requiring further confirmation, we have found that Gal-1 absence seems to unbalance the normal proportion of pancreatic cell populations, in favor of a more prominent epithelial compartment at the expense of the stroma, and enhancing endocrine

tissue. Cell/cell adhesion seems to be key regulating pancreas maturation, a process to which Gal-1 has been extensively connected. Although Gal-1 role in pancreatic development had never been truly studied before, several known partners of the lectin, such as fibronectin and laminin-1, previously appeared in the field. In fact, laminin has been postulated as being one of the key molecules mediating the mesenchymal effects directed towards exocrine differentiation[881]. This protein, whose expression has been localized at the interface between pancreatic epithelium and the stroma[882], acts through interacting with integrins[14,883], a second group of molecules that have been tightly related to Gal-1. Interestingly, Hh signaling pathway inhibition results in decreased amounts of stroma in mouse pancreatic cancer[100]. Besides, Shh has been also involved in mesenchymal signaling events occurring during pancreatic organogenesis[93,884,885], which influence the overall endocrine and exocrine pancreatic cell populations. Considering that we present reasonable evidence linking Gal-1 and Hh signaling, we could speculate that Gal-1 effects observed during pancreatic development might be also Hh mediated.

Additional confirmation is required to understand the molecular mechanisms involved and to finally conclude the exact Gal-1 role in pancreatic development. For example, *in vitro* and *in vivo* experiments with the NIH3T3 cell line, which has been shown to be able to substitute the mesenchyme during pancreas formation, might be useful to further analyze to which extend Gal-1 is involved in pancreas growth and differentiation[881]. Our data provide feasible hints to open new perspectives towards the molecular mechanism that could be involved in pancreatic proliferation and

differentiation, by adding Gal-1 as a new functional player in these events.

3.6 DECIPHERING GAL-1 MOLECULAR MECHANISMS: TRANSCRIPTOME ANALYSIS

Previous reports in glioblastoma cell lines had previously studied the effects of Gal-1 downregulation on general gene expression[523,550], identifying targets classically involved in tumor progression. Similarly to what was described in these former studies, Gal-1 protein changes in PANC-1 and RWP-1 cells are translated into a vast amount of genes with altered expression. We are aware of the limitations of the results of our arrays, based on an *in vitro* cell system, which is genetically different from human pancreatic cancer cells. Yet, the fact that we have observed several genes whose alteration had been well established in pancreatic cancer before, outlines the biological importance of this type of studies. Furthermore, some of the identified proteins in these glioblastoma transcriptome analyses were also found to be altered in our pancreatic cancer cell line microarray, such as thrombospondin-1, β-catenin and integrin α_7. Besides, several families of proteins are also commonly disregulated upon Gal-1 deficiency such as tetraspanins, HSPAs and ADAMs (see *Supplementary information*). Reconfirmation of Gal-1 influencing their expression suggests a possible general mechanism relating the lectin with these targets. Nevertheless, we have also found several genes whose expression is altered in the opposite direction in glioblastoma cells or in pancreatic cells upon Gal-1 modulation. These data might be indicative of the context dependent effects of altering Gal-1 levels. Indeed, important differences are already observed between PANC-1 and RWP-1 differential transcriptomes with low or high Gal-1 levels. We must bear in mind that part of these discrepancies could be due to the

cell line origin. Whereas PANC-1 cells were directly obtained from a pancreatic tumor, RWP-1 cells came from a pancreatic liver metastasis. We have observed phenotypic differences among those cell lines as well. For instance, regarding migration, we show that decreased Gal-1 levels in PANC-1 cells impairs migration and mobility (see *Results*, section *2.4.2. Functional Effects of the Modulation of Gal-1 Expression Levels in Cultured Pancreatic Cancer Cells*). In contrast, RWP-1 cells with endogenous Gal-1 levels display reduced migration capacities compared to Gal-1 overexpressing RWP-1 cells. These data indicate once again, that Gal-1 can exert a positive or negative modulation of cell migration depending on protein levels and/or cellular contexts. In fact, clones forming distal metastasis display an altered genetic profile compared to the parental non-metastatic ones[25,26]. Still, our results fit with the previously mentioned ones in the sense that genes altered are also connected to ECM interaction, cell surface adhesion and angiogenesis.

Microarray data have depicted a possible molecular link between Gal-1 and Hh signaling pathway, two well known inducers of the desmoplastic reaction reported to be actively expressed in this compartment[97]. This relation has been later confirmed *in vitro,* as cells overexpressing Gal-1 show a marked increase in Gli driven transcription activation. Hh shares several functional features with what we have observed and what was reported for Gal-1 in pancreatic cancer. Similar to what we describe in the present work, paracrine mechanisms for Hh signaling pathway controlling the desmoplastic reaction have been reported[98,99]. For instance, Shh was shown to be involved in *in vitro* PSCs invasion and migration.

Moreover, as previously addressed (see section *3.5.5. Gal-1 in Mouse Pancreas Development*), Shh was involved in controlling the amount of stroma formed in pancreatic cancer[100]. We have just glanced at the intersection between Gal-1 and Hh through confirmation of some of the proteins of the Hh family whose expression was modulated after Gal-1 alteration levels in pancreatic cancer cells. Although Gli did not appear in our arrays, previous data from our collaborator M.E. Fernández-Zapico, suggested a possible direct effect of Gal-1 modulating expression of Gli levels in pancreatic cancer cells. We have confirmed these data, providing evidence towards how Gal-1 affects the expression of several Gli target genes. Indeed, the connection between Gal-1 and Gli might be independent of the canonical Hh signaling pathway. In pancreatic cancer cells, an alternative mechanism responsible for Gli transcription activation decoupled from upstream Hh pathway has been reported[92] (see *Introduction*, Fig.4). In this case, TGF-β and Ras, a well known Gal-1 interactor, are responsible for Gli expression, further strengthening our data observing Gal-1 induced Gli dependent transcription. Still, further experiments are required to study these options, as alternative mechanisms have already been described in the literature[886].

After all, we are conscious that this is just the beginning and that much more information can be derived from our transcriptome analysis. Once seen the clear phenotype after Gal-1 depletion *in vivo*, reevaluation of the data by looking to possible mediators of the observed effects (like angiogenesis, ADM, necrosis, stroma formation,…) could pinpoint putative molecular mechanisms involved. Besides, our functional studies highlight the importance of Gal-1 in

different cell populations from tumoral epithelial cells. Therefore, it would be very interesting to study the effects on gene expression after altering Gal-1 levels in cells from the tumor microenvironment.

3.7 GAL-1 & tPA IN PANCREATIC CANCER THERAPY

We have studied in depth the involvement of Gal-1 in pancreatic cancer both *in vitro* and *in vivo*, proving its importance in several aspects driving tumor progression. Our data suggest that Gal-1 is expressed both in pancreatic cancer cells and in fibroblasts, being involved in cell migration. Using siRNA mediated silencing, we have found that Gal-1 is involved in tPA induced Erk1/2 activation, proliferation and invasion in both previously mentioned cell types. Our *in vitro* data, adding new mechanisms and partners, help on tPA characterization in tumor progression, which has been largely focused on uPA[277]. The pleiotropic consequences of tPA/Gal-1 interaction indicate that these proteins could be well considered in pancreatic cancer therapy. Proteases seem to be suitable molecules for therapy because of their easy accessibility. However, their multiple important physiological functions in the organism and the existence of functional overlapping within different protease systems, have closely linked protease targeting to high toxicity and undesirable side effects. In our particular case, therapies directed to tPA could be pretty useful taking into account that uPA might be able to replace its family partner in many physiological functions as tPA deficient mice do not show critical deficiencies[279]. In addition, considering that tPA exerts many of its pathological effects by binding to cell surface receptors and that it is absent in the pancreas[360,361,410], higher specificity and reduced side effects could be achieved by exclusively inhibiting tPA interaction with a pancreas specific receptor. This idea guided our group to design a proteomic approach to identify a putative candidate and Gal-1 emerged as a strong possibility[420]. Gal-1 fulfills interesting requirements to be

considered for targeting such as not being expressed in normal pancreas[582], increasing drug selectivity. Moreover, the use of Gal-1 inhibitors is particularly appealing because Gal-1 KO mice are viable and fertile and do not show overt abnormalities[501], probably due to redundant functions from other members of the galectin family. However, we have biochemically shown that tPA interaction specifically occurs with Gal-1[421], what has been confirmed by the fact that inhibiting their interaction by siRNA mediated Gal-1 silencing, impairs tPA pathological events. Yet, our *in vivo* data, depict a much broader involvement of Gal-1 in pancreatic cancer, this time independently of tPA. Pancreatic tumor progression in Ela-1-myc mice is severely delayed after Gal-1 depletion. Interestingy, we have found that Gal-1 participates in acinar-ductal metaplasia. Besides, Gal-1 depletion is associated with increased necrosis indexes, decreased proliferation, stroma, and severly hampers angiogenesis. These phenotypes further highlight Gal-1 as an interesting target for pancreatic cancer therapy. Nevertheless, the dichotomous effects of Gal-1 must be well considered for efficient targeting, as depending on many intrinsic and extrinsic factors, the lectin can exert contrary effects (mitogenic or antiproliferative and pro or antiadhesive). That is so the case that even Gal-1 and Gal-1 mimetic compounds have been also proposed for anti-cancer therapy[488]. Thus, special attention must be paid concerning Gal-1 conformation, quaternary structure, oxidation state, concentration, subcellular localization, ability to establish protein/protein or protein/glycan interactions, target cell type, and presence of specific glycan receptors with certain glycosylation signatures, among others.

The importance of our findings regarding Gal-1 implications in the non-neoplastic cells is increased in the context of pancreatic cancer due to its characteristics. It has been reported that the huge stromal reaction accompanied with an important lack of angiogenesis impairs drug delivery and cause pancreatic cancer resistance[887,888]. The stroma has been shown to be decisive in tumor progression, which can be inhibited maintaining a normal context[109,889]. Different non-tumoral cells have been under the scope for therapy as they are more accessible to pharmacological agents and genetically stable, which makes them less prone to acquire resistance. Indeed, therapies targeting other molecules involved in the desmoplastic reaction and vasculature have proven to improve efficiency delivery of gemcitabine in a pancreatic mouse model[100], highlighting Gal-1 as a possible promising drug in this pathology. Interestingly, silencing Gal-1 results in increased chemotherapy toxicity in glioblastoma cell lines[747,890]. Gal-1 importance in the tumor microenvironment immunosuppression is also considered in treatment. As a matter of fact, Gal-1 inhibition as adjuvant with vaccine immunotherapy significantly reduces breast tumor progression in mice[816]. Gal-1 has been also considered as a biomarker in HNSCC[564] and in ovarian carcinoma, where its serum concentration is five-fold reduced[565] due to increased Gal-1 deposition on glycoproteins and the stroma[891].

Overall, this work provides strong evidences towards the importance of Gal-1 in pancreatic tumor progression both *in vitro* and *in vivo*. Our data add valuable knowledge to enable a better understanding of pancreatic cancer molecular biology. The strong phenotypes observed upon Gal-1 depletion, open the door to new therapeutic strategies targeting the lectin without interfering with its

physiological functions. Therefore, we stand for Gal-1 as a promising target for pancreatic cancer, which could delay or even revert tumoral progression in this devastating disease.

4 CONCLUSIONS

A new type of thinking is essential if mankind is to survive and move to higher levels.

Albert Einstein

1. Gal-1/tPA interaction is mediated by Gal-1 carbohydrate recognition domain and tPA N-glycan chains. In particular, glycosylation in tPA Asn184 is key for Gal-1 binding and tPA induced Erk1/2 activation.

2. Our preliminary glycosylation analysis indicate that tPA glycan structure might be different in tumoral versus non-tumoral pancreatic cell lines, suggesting different functionality.

3. Pancreatic ductal epithelial cells and fibroblasts express Gal-1, which is localized at the migration front and it is involved in tPA induced Erk1/2 activation and invasion *in vitro*.

4. The anti-angiogenic peptide Anginex, previously reported to bind specifically to Gal-1, recognizes non-specifically many different proteins, indicating that Gal-1/Anginex interaction requires further validation.

5. In xenograft models, downregulation of Gal-1 in tumoral pancreatic cells does not significantly affect tumor progression, highlighting the key contribution of Gal-1 in tumoral stroma.

6. In the Ela-1-myc model developing pancreatic tumors, Gal-1 partial or total loss of expression results in increased tumor necrosis, decreased pancreatic cell proliferation, stroma formation, and angiogenesis, and in a strong reduction in acinar-ductal metaplasia. Importantly, these effects are translated into a 20% increase in the life span of mice with reduced levels of Gal-1.

7. Zebrafish transgenic models developing pancreatic cancer (ptf1a:eGFP-K-Ras^{G12V} or ptf1a:GAL4/VP16 UAS:eGFP-K-Ras^{G12V}) display similar Gal-1 expression patterns than human PDA tumors, indicating that they are appropriate models to study Gal-1 role in this pathology.

8. During mouse pancreatic embryonic development, Gal-1 is expressed in the stroma and its levels seem to affect pancreas endocrine and exocrine compartment as well as stroma proliferation. These data indicate Gal-1 parallelisms between pancreatic development and tumors.

9. A transcriptome analysis by microarrays in pancreatic tumoral cell lines with different levels of Gal-1 indicates that this lectin regulates key genes related to tumoral progression, adhesion/migration molecules and several members of the Shh pathway.

5 MATERIALS & METHODS

It is a scale of proportions which makes the bad difficult and the good easy.

Albert Einstein

5.1 BIOCHEMICAL CHARACTERIZATION OF GAL-1/tPA INTERACTION

5.1.1 tPA N-Deglycosylation

1 µL of N-GlycosidaseF (PNGaseF) at 1000 U/µL was added to tPA in sodium phosphate buffer 50 mM pH 7.3 and incubation took place at 37°C for 24 h, gently agitating.

5.1.2 Protein/Peptide Purification

To separate, desalt and purify the protein fraction, the sample was first acidified with CF_3COOH (TFA) 0.1% and a reverse phase micro-column was used. A 20 µL narrow pipette tip (GELoader, eppendorf) was packed with POROS 20 R2 resin in CH_3CN. An equilibration step with 0.1% TFA preceeded sample application. Sample slowly moved through the column and the flow-through containing N-glycans collected. The column was washed twice with the same equilibration buffer and proteins or peptides were later eluted with CH_3CN:H_2O (80:20) 0.1% TFA (10-40 µL). Eluates were frozen and lyophilized overnight (ON) when necessary.

5.1.3 Glycan purification

To purify the glycan fraction, a graphitized carbon column was used. The column was packed with CH_3CN:H_2O (80:20) 0.1% TFA and conditioned with H_2O. Sample was applied and washed twice with H_2O. Elution followed with 50 µL CH_3CN:H_2O (80:20) 0.1% TFA. Eluates were frozen and lyophilized ON when necessary.

5.1.4 Protein, Peptide and Glycan MALDI-TOF MS

Adequate matrices are critical for mass accuracy and optimal resolution and depend on the nature of the biomolecule to analyze. For peptide analysis, the matrix used was alpha-cyano-4-hydroxycinnamic acid (20 mg/mL in CH_3CN:H_2O (70:30) 0.1% TFA), whereas for protein analysis we used sinapinic acid (10 mg/mL in CH_3CN:H_2O (50:50) 0.1% TFA) and for glycan studies, 2,5-dihydroxybenzoic acid was chosen. Samples were mixed with the proper matrix and applied to a polished stainless steel plate. MALDI-TOF MS analysis was performed on a Voyager-DETM STR Biospectrometry workstation (Applied Biosystems) equipped with a N_2 laser (337 nm). Mass scans were accumulated in the corresponding mass range (550-3500 Da for peptides, 10000-50000 Da for proteins and 1000-4000 Da for glycans). Recorded data were analyzed with Data ExplorerTM Software (Applied Biosystems).

5.1.5 Type I / II tPA Separation by Affinity Chromatography

6 g of Lysine Sepharose 4B resin were hydrated in MilliQ water (4 mL/resin). The resin was then washed with MilliQ water (200 mL/g resin) in order to remove the additives and was equilibrated for 1 h with the elution buffer (Na_2HPO_4 5 mM, NaH_2PO_4 5 mM, KSCN 0.15 M, Tween 80 0.001%, pH 8.0). The chromatography column (30X1 cm) was then packed with the hydrated resin and connected to a UV-visible detector and a recorder. Once the column was equilibrated with the above mentioned buffer (9 mL/h for 12 h) , 1 mg of tPA was injected in a final volume of 200 µL. Elution

proceeded 3 h with the equilibration buffer and was followed by a concentration gradient of L-Arg (0.025 M to 0.25 M, increasing 0.025 M per hour). Afterwards, 0.25 M of L-Arg was kept for 12 h and elution ended with 0.5 M for 10 h. Fractions were collected at 15 min intervals, lyophilized, and analyzed by WB and MALDI-TOF MS.

5.1.6 K2 and SP tPA Domain Constructs

For human Kringle 2 (K2) domain, we amplified the region corresponding to AAs 174 to 263 from pBS-htPA plasmid. However, the first Ser was changed to Pro in order to have a KpnI restriction site, and an XbaI restriction site was inserted at the 3' end, after a stop codon. The following primers were used. K2: Fw (GGT ACC TGA GGG AAA CAG TGA C), Rv (TCT AGA TCA GGT GGA GCA GGA). For the Serine Protease (SP) domain, we amplified the region corresponding to AAs 276 to 527 from pBS-htPA plasmid. In this mutant, though, the first two AAs (Ile-Lys) were changed to Val-Pro to include a KpnI restriction site and an XbaI restriction site was added after the stop codon in the reverse primer. The following primers were used: Fw (GGT ACC TGG AGG GCT CTT CGC C), Rv (TCA AGA TCA CGG TCG CAT GTT). Inserts were first cloned into pGEM-T easy vector (Promega) and later into pcDNA3/HisA vector for easier protein purification. Once in this mammalian expression vector, mutations were carried out in order to restore the correct AA sequence (K2: Pro176Ser; SP: Pro277Lys, Val276Ile). Moreover, mutations were also directed to change Cys395 by Ser in order to avoid the formation of incorrect disulfide bridges. Primers used for K2 mutagenesis were: GAT GAC GAT AAG GTA **T**CT GAG GGA AAC AGT GAC TGC. Primers for SP mutagenesis were: GAT GAC

GAT AAG **ATC** CCT GGA GGG CTC TTC GCC, GAC GAT GAC GAT AAG ATC **AAA** GGA GGG CTC TTC GCC, AGC GTG GTC CGC ACT GTG **A**GC CTT CCC CCG GCG. Mutagenesis was performed with the QuickChange Multi Site-Directed Mutagenesis kit (Qiagen). Clones were sequenced to find successful mutants.

5.1.7 CHO Expression of K2 and SP tPA Domains

CHO cells at 60% confluence were transfected with 100 ng of pcDNA3/HisA-htPA-K2, pcDNA3/HisA-htPA-SP or with the empty pcDNA3/HisA constructs by means of Lipofectamine and Plus reagents as described in section *5.2.6. Gal-1 Knockdown: Transfection with siRNA*. Cells were selected with G418 (Calbiochem) 1 mg/mL for a week. RNA extracts were prepared with GenElute Mammalian Total RNA MiniPrep kit (Sigma). One step RT-PCR (Qiagen) with 40 ng of RNA allowed construct detection of expression at the RNA level. A forward primer from the pcDNA3/HisA vector and a specific reverse primer for each construct were used. Primers: htPA-K2 construct: Fw (GCT AGC ATG ACT GGT GGA CAG), Rv (GCT GAC CCA TTC CCA AAG TA) which gave a 103 bp band; htPA-SP construct: Fw (TAG CAT GAC TGG TGG ACA GC), Rv (CAC TGC TTC CAG GAG AGG TT), which gave a 251 bp band.

5.1.8 Silver Staining

Supernatans and cell extracts were submitted to both Western blot (WB) and silver staining in parallel to identify proteins. Gel electrophoresis was performed with gels of 0.75 mm and 10% acrylamide. For silver staining, gels were fixed ON in 10%

CH_3COOH, 50% CH_3OH. Gels were washed three times in MilliQ water to rehydrate them and sensitized by incubating the gel with 0.1% of $Na_2S_2O_3$ for 2 min. Gels were washed twice in MilliQ water and incubated for 20 min in 0.1% silver nitrate solution. After washing twice, developing solution containing 3% Na_2CO_3, 3.36 mM formaldehyde was added and silver precipitation was stopped with 10% CH_3COOH when desired. The gel was rinsed with water and bands of interest were excised and chopped in small pieces. Gel particles were washed twice with water, dehydrated with CH_3CN and dried down in a vacuum centrifuge.

5.1.9 2-AB Glycan Derivatization

For protein reduction, gel pieces were swollen in 10 mM dithiothreitol (DTT), 0.1 M NH_4HCO_3 and incubated for 30 min at 56°C. Excess liquid was removed and gel pieces dehydrated and dried as previously described. For alkylation, 55 mM iodoacetamide 0.1 M was added and incubated for 30 min room temperature (RT) at dark. Gel particles were washed twice in 0.05 M Na_2HPO_4/NaH_2PO_4 pH 7.3 and subsequently dehydrated and dried in the vacuum centrifuge. Gel particles were rehydrated with 0.05 M Na_2HPO_4/NaH_2PO_4 pH 7.3 containing PNGaseF (Boehringer, 1 U per sample) and incubated 37°C ON. Excess liquid was recovered and gel particles were washed with MilliQ water. Gel particles were dehydrated with CH_3CN and all these supernatants were joined and lyophilized for later purification. Samples were resuspended in 40 µL of 0.1% TFA and applied to a graphitized carbon column for N-glycan purification. The column was washed with MilliQ water and carbohydrates were eluted in 80% CH_3CN, 0.1% TFA. After lyophilizing, samples were dried in a 60°C

oven for 1 h. For glycan labeling, samples were incubated with 10 µL of 2-aminobenzamide (2-AB) 0.35 M, $NaCNBH_3$ 1 M in DMSO:CH_3COOH 70:30 for 2 h at 65°C. Samples were spot on an acid-pretreated quartz filter (Whatman) and allowed to dry in a vacuum drier with P_2O_5 ON. Filters were washed with 10 mL of CH_3CN to remove the excess of 2-AB and glycans were eluted with 1.6 mL of MilliQ water. Samples were lyophilized ON.

5.1.10 HPLC

t (min)	% CH_3CN	Flow (µL/min)	Max pressure
0	80	500	400
100	45	500	400
105	0	300	400
107	0	300	400
115	80	500	400
118	80	500	400
125	80	500	400

Table 12. Mobile phase used during HPLC chromatography to detect 2-AB labeled glycans.

After derivatization, samples were finally diluted in 10 µL of 50% CH_3CN, 50% MilliQ water and later filtered with 0.22 µm, to be ready for HPLC and MS analysis. 2-DHB (2,5-dihydroxybenzoic acid) matrix was used for glycan MALDI-TOF MS. 5 µL of labeled glycan were injected. Normal phase chromatography was used for glycan analysis. The column used consisted of an Acquity UPLC BEH Amide 1.7 µm (particle size) (Waters), 3.0 (intern diameter) X 100 mm. The mobile phase consisted of a gradient of CH_3CN, AMFO (NH_4HCOO) 100 mM pH 4.4 (Tab.12).

Patrons used to identify peaks were: RNAseB (ribonuclease B); rePO (erythropoietin), bovine thyroglobulin, a/1-acidGP (alpha1-acidglycoprotein), dextran (previously hydrolised to quantify glucose units) and human chorionic gonadotropin (hCG) (Fig.119).

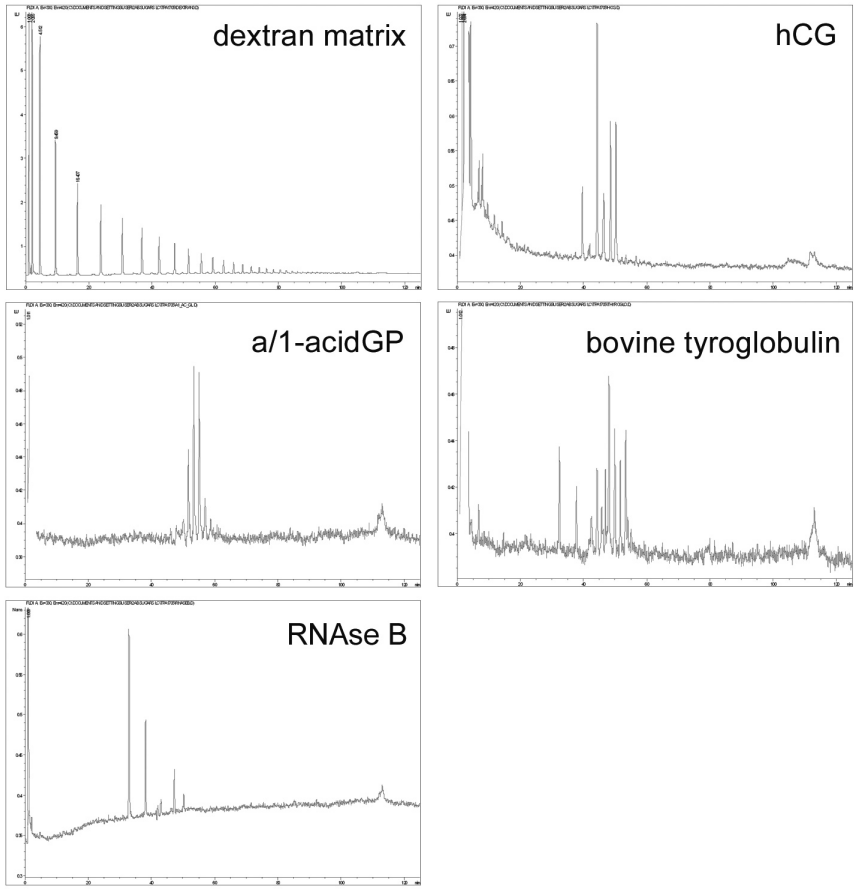

Figure 119. HPLC chromatogram of some the patrons used to calibrate and later identify tPA peaks.

Detection used the 2-AB derivatization. λ_{em}=320-360 nm and λ_{ex}=420 nm.

HPLC after sialidase and mannosidase treatment helped in identifying glycan structures. Ion exchange chromatography was

used to elucidate the number of sialic acid bound to glycosylated chains (Fig.120).

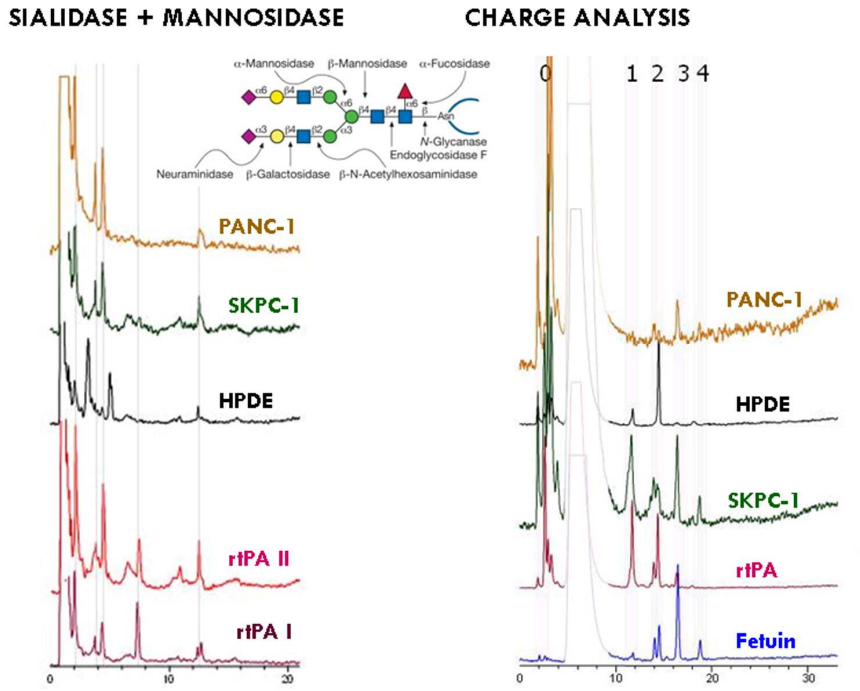

Figure 120. HPLC analysis from tPA after different reactions. This information provided further insights regarding linkage and glycan content.

5.1.11 Trypsin Digestion

For peptide identification, trypsin (60 ng/sample; 1:250 protease:protein) was added in 100 mM NH_4HCO_3 pH 7.8 and incubation was performed at 37°C ON. Peptides were recovered from the supernatant and gel particles were washed and dehydrated with CH_3CN. These fractions were joined, lyophilized and diluted in 10 µL of 0.1% TFA. Peptides were purified with POROS R2 chromatography and eluted in 10 µL of 80% CH_3CN 0.1% TFA for MS analysis.

5.2 STUDY OF tPA/GAL-1 INTERACTION IN VITRO

5.2.1 Cell Lines

The following human pancreatic cell lines were used: HPDE (Human pancreatic ductal cells immortalized with E6 and E7 papillomavirus genes[689]); PANC-1 (pancreatic epithelioid carcinoma cells[892]), and its variant PANC-1_LUC (kindly given by Dra.Fillat, CRG, Barcelona); SK-PC-1 and SK-PC-3 (exocrine pancreatic adenocarcinoma cells with an epithelial morphology[893]) and BxPC-3[894] . Cells derived from metastasis to other organs were also used as RWP-1[895] (epithelial cells from a pancreatic tumor metastasis in liver) and Hs766T[896] (from a lymph node metastasis of pancreatic cancer). A fibroblastic spontaneously immortalized cell line from a breast tumor was also used: F88.2. For virus generation, HEK293T cells[897] or Phoenix Ampho 293T cells[898] were used. Cells were cultured at 5% CO_2 and 37ºC stable temperature. DMEM (Gibco) supplemented with 10% FBS was normally used except for HPDE cells, whose medium was KSFM (Gibco) supplemented with EGF (0.2 ng/mL), BPE (25 µg/mL), sodium pyruvate (1 mM), penicillin (100 U/mL), streptomycin (100 µg/mL) and L-Gln (2 mM). For viral infections, a laboratory that obeys BioSafety Level 2 (BSL-2, P2) according to EU legislation was used.

5.2.2 Conditioned Medium Recovery and Protein Concentration

The absence of an established loading control in WB analysis when working with conditioned medium implied that the protocol for

supernatant collection had to be extremely invariable and reproducible. Cells were seeded in a 75 cm^2 plate and when reaching 70% confluence, cells were washed 3 times extensively with DMEM (without serum) and left in 5 mL of DMEM for 72 h. The conditioned medium was collected and centrifuged (1000 rpm, 5 min) in order to discard cell debris, and immediately frozen at -80°C for later concentration or concentrated directly, if necessary. To do so, Amicon filters (Millipore) were used (30 KDa for tPA, 10 KDa for htPA-SP domain, 3 KDa for htPA-K2 domain and empty pcDNA3/HisA). Supernatants were centrifuged at 4000 g until reducing the initial volume ten fold.

5.2.3 Cell Lysis and WB Analysis

Cells were directly lysed with Laemmli buffer 1X (2% SDS, 40% glycerol, 5% 2-mercaptoethanol, 0.005% bromophenol blue, 62.5 mM Tris HCl, pH 6.8) for total protein extraction. For serum free supernatants, Laemmli buffer 4X was added. Samples were boiled and centrifuged. Approximately 20 µg of protein were loaded per lane. Electrophoresis was performed with 10% acrylamide gels (15% for Gal-1), 1.5 h at 100 V. WB (1.5 h, 400 mA) allowed transferring proteins to a nitrocellulose membrane, which was then blocked for 1 h RT with TBS 0.1%Tween (TBS-T) 5% of fat milk. Primary incubation followed 1 h RT with mouse α-tubulin (1:10000, Sigma), rabbit α-PErk1/2 (1:750, Cell Signaling), rabbit α-Total Erk1/2 (1:1000, Upstate Laboratories), rabbit α-Gal-1 (1:1000, rabbit serum kindly provided by Dr. Gabius, Ludwig-Maximilians-University, Munich, Germany[489]), rabbit α-Gal-1 (1:1000, Sigma), goat α-Gal-1 (1:1000, R&D Systems), mouse α-tPA monoclonal antibodies 374-B, 373, and 387 (1:1000, American Diagnostica),

goat α-uPA polyclonal antibody 398 (1:500, American Diagnostica), mouse α-desmin (1:500, Dako). After washing with TBS-T, secondary antibodies were used: goat α-rabbit (0.15 mg/L), rabbit α-mouse (0.65 mg/L), or rabbit α-goat (0.25 mg/L) immunoglobulins conjugated to HRP (DakoCytomation). After washing, enhanced chemiluminescence (ECL) detection method (Pierce) was used to develop.

5.2.4 Cell Migration: Wound Healing Experiments

Cells were seeded over sterile coverslips placed in a 24 well plate and left in DMEM with 10% FBS until tight confluence (coverslips were precoated with 1% gelatine for HPDE cells). The wound was performed by detaching cells with a micropipette tip. Cells were washed once with DMEM 1% BSA or supplemented KSFM (for HPDE) and left to migrate (heal the wound) for different times (depending on the cell type: PANC-1: 48 h, SK-PC-1, HPDE: 24 h and RWP-1: 72 h) in 500 µL of DMEM 0.5% FBS or KSFM (for HPDE). Wound closure was quantified in RWP-1 cells using ImageJ software analysis.

5.2.5 Gal-1 and tPA Cytoimmunofluorescence

In wound healing experiments, coverslips were washed twice with DMEM 1% BSA and incubation with 40 µg/mL α-Gal-1 (a kind gift from Dr. Gabius, Ludwig-Maximilians-University, Munich, Germany[489]) was done *in vivo* (25 min at 37°C). After 3 more DMEM 1% BSA washes followed by 2 PBS washes, fixation was achieved with methanol at -20°C for 5 min over ice. Methanol was removed and coverslips were thoroughly washed with PBS. If the rest

of the procedure could not be continued immediately, coverslips were kept at this point in PBS 0.02% sodium azide. Blocking was performed in PBS 1% BSA at 37°C for 1 h. For double (tPA and Gal-1) immunofluorescence (IF), fixed cells were then incubated with α-tPA 373 (20 µg/mL in PBS 1% BSA) (American Diagnostica) for 1 h at 37°C. After three washes with PBS 1% BSA, fluorescent secondary antibodies were incubated (20 µL of anti-mouse Alexa-488 for tPA and α-rabbit Alexa-555 for Gal-1, both at 3.30 µg/mL) for 1 h 37°C. Finally coverslips were washed three times with PBS and once with MilliQ water and mounted over slides with Fluoromont-G (Southern Biotechnology Associates). Immunofluorescent images were acquired with Olympus BX61 microscope adapted to a camera fit with 494 nm (FITC) and 522 nm (TRITC) emission filters. For the competition control experiment, α-Gal-1 polyclonal antibody was co-incubated with the recombinant protein (1:5 respectively) in unpermeabilized living cells. For the time zero control experiment, α-Gal-1 was added 15 min before the wound and cells were fixed immediately after scratching.

5.2.6 Gal-1 Knockdown: Transfection with siRNA

40000 cells were seeded in a 24 well plate. Transfection was carried out at 40% confluence approximately with Gal-1 siRNA and an Irrelevant siRNA (SMARTpool® Reagents, Dharmacon) at 50 nM concentration using Lipofectamine and Plus reagents (Invitrogen). Non-transfected cells were treated with the same mixture without siRNA. For a 24 well: siRNA was well mixed with Opti-Mem (Gibco), and then Plus was added (1 µL of Plus per well) and pre-complexion took place for 15 min at RT. Afterwards, we combined pre-complexed siRNA with diluted Lipofectamine (1 µL per well), mixed

and incubated for 15 min RT. Dilution of the mixture was done with Opti-Mem until a final volume of 250 µL per well. Cells were washed twice with sterile PBS and the transfection mixture added. Incubation took place for 3 h at 37°C. Afterwards, cells were washed to remove the transfection mixture with DMEM 10% FBS and incubated with this fresh, complete medium to allow recovery.

5.2.7 tPA Induced Erk1/2 Activation

Tissue-type plasminogen activator (Actilyse®, Boehringer Ingelheim GmbH) was added at a final concentration of 20 µg/mL and incubated at 37°C for corresponding time (2,10 min). For the positive control, FBS was added at a final percentage of 5% and incubated for 2 min. Negative controls were left untreated. Cells were washed twice with PBS and frozen with liquid nitrogen and stored at -80°C or immediately processed for cell lysis and WB. For purified type I/II tPA experiments, the same concentration was applied.

5.2.8 Invasion Experiments

Cells were transfected with siRNA 3 days before invasion experiments when required. Cells were washed and resuspended in DMEM 1%BSA and seeded (10000-40000 depending on the cell line) over transwells with 8.0 µm polycarbonate membranes covered with matrigel (previously diluted 1:20 in PBS and dried ON under UV light). DMEM 10% FBS was added in the lower compartment and invasion followed for 72 h. For co-culture experiments, pancreatic cancer cells (40000 cells/well or 80000 cells/well of PANC-1 and SK-PC-1, respectively) were seeded in a T24 well

plate and they were left without serum for 48 h. Afterwards, F88.2 cells were seeded over matrigel and the filter placed over the appropriate conditioned medium. tPA and PAI-1 were added when necessary 3 h after F88.2 seeding at 20 μg/mL and 0.15 μM, respectively. To quantify invasion, cells that passed to the lower compartment were fixed with glutaraldehyde 1% for 10 min and stained with crystal violet 0.2%. Extraction followed with 10% CH_3COOH and absorbance at 590 nm was measured (Infinite™ 200 series, Tecan Trading AG).

5.2.9 Protein Immobilization over SPR Chips

For immobilization of proteins on a CM5 sensor chip, carboxyl groups of the dextran matrix were activated as esters by injecting a mixture of 0.025 M *N*-hydroxysuccinimide and 0.1 M 1-ethyl-3-(3-dimethylaminopropyl carbodiimide (7 min, 5 μL/min). Subsequently, analyte solutions (BSA, tPA, or uPA) at 10-75 μg/mL in 10 mM sodium acetate (pH 5.0) were flown across at 5 μL/min in 60 μL pulses until the desired immobilization level was achieved. Then, unreacted succinimide esters were neutralized with 1 M ethanolamine at pH 8.0 (7 min, 5 μL/min) followed by two NaCl pulses (0.5 min at 10 μL/min) to eliminate unbound protein. Finally, the surface was equilibrated with HBS-P (0.01 M HEPES, pH 7.4, 0.15 M NaCl, 0.005% Tween 20) buffer for 24 h (5 μL/min). Immobilization levels were 20000 RU for BSA (1 RU=1 pg), 12000 RU (for tPA and BSA) and 6500 RU for AnxA2. For N-deglycosylated tPA experiments, immobilization levels achieved were 16700 (BSA), 16500 (N-deglycosylated tPA) and 13000 (rtPA).

5.2.10 Binding Experiments by SPR

Recombinant Gal-1 at 500 nM in HBS-EP buffer (HBS + 3 mM EDTA, BIAcore) was used to confirm tPA binding at a flow rate of 20 µL/min for 3 min (association phase). In order to remove unbound molecules, the dissociation phase consisted of an injection of the same buffer (5 min, 20 µL/min). Surface regeneration was achieved with β-lactose (2 or 10 mM), NaCl pulses (1 M), glycine 10 mM at pH 2.5, as required. Signal stabilization with HBS-EP followed for 5 min, 10 µL/min, until the basal line corresponded to ±2 RU from the initial value. To assess how Anginex affected Gal-1 binding over tPA, Gal-1 was preincubated with Anginex (β-peptide25) or with the control β-peptide28 (synthesized at UPF Proteomics facility, Barcelona) at different concentrations (1-64 µM) for 15 min and the mixture was analyzed for tPA interaction. Otherwise, Anginex directly (1 µM) was passed over the dextran matrix with immobilized tPA. A BSA surface was used as a control for non-specific binding and differential curves (tPA-BSA) were obtained, when mentioned. Data were processed with the BIAevaluation software (V.4.0.1 from BIAcore).

5.3 STUDY OF GAL-1 RELEVANCE IN PDAC IN VIVO

5.3.1 Lentiviral Infection of Human Epithelial Tumoral Cells

HEK-293T cells were seeded at high confluence over polylysine covered plates. Cells were transfected with polyethylenimine (PEI) at 78 µg/mL with three lentiviral packing vectors (pRSV-rev, pHCMV-G, pMDLg/pRRE) and the vector containing Gal-1 shRNA (pLKO-1-puro vector, MissionRNAi, TRCN0000057423-427) or shCtl the non-targeting shRNA control provided by Sigma (SHC002). Another irrelevant shRNA was used (shCtl*), which targeted the murine Gys1 sequence, which did not overlap with any human sequence. Their supernatant was collected at 48 and 72 h, filtered (0.45 µm) and polybrene was added (8 µg/mL). Human pancreatic tumoral cells were infected at 60% confluence for 9 h, washed and left in DMEM 10% FBS. Selection was carried out with puromycin at 3 µg/mL. Interference efficiency was checked by WB analysis.

5.3.2 Gal-1 Downregulation in SK-PC-1 Cells

Gal-1 was downregulated in SK-PC-1 cells by lentiviral infection as previously described. Gal-1 efficiency downregulation was assessed by 5 different shRNA sequences targeting Gal-1 (Fig.121). As a control to later assess infection effects, parental non-infected cells (wt) were used and compared to cells infected with an irrelevant shRNA (shCtl*). Downregulation was maintained throughout passaging and after freeze/thaw cycles.

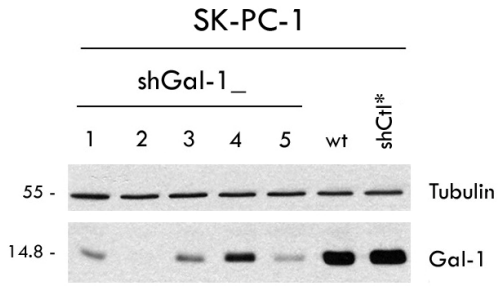

Figure 121. Gal-1 downregulation achieved by shRNA targeting Gal-1 in SK-PC-1 cells. Protein levels showing Gal-1 depletion 17 days after SK-PC-1 lentiviral infection carrying 5 different shRNA for Gal-1 (shGal-1_1,shGal-1_2, shGal-1_3, shGal-1_4, shGal-1_5). Cells were cultured with puromycin in order to achieve selection of positively infected cells. Tubulin levels are shown as the loading control.

5.3.3 RWP-1_LUC Cell Line Generation

Phoenix Ampho 293T cells at 20% confluence were transfected with PEI (78 µg/mL), 6.5 ng/µL pLHC-LUC vector (kindly provided by Dra.Fillat, CRG, Barcelona) in NaCl 150 mM (diluted 9 times before transfection in DMEM 10% FBS). RWP-1 cells were infected when at 20% confluence with Phoenix Ampho 293T supernatant with polybrene (8 µg/mL) after 0.45 µm filtration at 48, 60 and 72 h post transfection. Cells were selected with hygromicin 0.3 µg/mL for a week. 21 clones were isolated and their luciferase expressing levels characterized with Dual-Luciferase reporter system (Promega), normalizing values with their concentration determined by Bradford assay. Several clones expressing different luciferase levels were selected for *in vivo* analyses (Fig.122).

	RLU / (µg x s)
A	131876,4
B	31232,3
C	170480,6
D	212804,9
F	294161,4
H	66759,6
I	57038,3
J	165707,1
K	174551,7
L	1086392,0
M	358713,0
N	182907,0
O	229570,1
Q	129810,9
R	367977,5
S	262141,0
T	211543,8
U	83276,0
V	196539,0
W	118610,3
X	226878,5

Figure 122. RWP-1_LUC clones expressing different luciferase levels. Several clones were obtained and assessed for their luciferase expressing levels. L and M clones were picked up as high luciferase expressing clones, N and W were selected as medium and the B clone was chosen as a low luciferase expressing one.

5.3.4 MTT Proliferation Assays

Cell proliferation was determined by seeding 1000 cells per 0.32 cm^2 well in quintuplicates. Cell number was quantified periodically by adding MTT substrate (3-(4.5-dimethylthiazol-2-yl)-2.5-diphenyltetrazolium bromide, Sigma) at 1 mg/mL in DMEM for 4 h at 37°C and 5% CO_2. Absorbance at 570 nm was measured after extraction with 0.1 M HCl, 0.1% Triton X-100 in isopropanol.

5.3.5 Anchorage Independent Growth

5000 cells were seeded in 9.4 cm^2 plates in DMEM 0.3% Noble Agar over a compacter layer of DMEM 0.7% Noble Agar. DMEM 10% FBS was added on the top, supplementing every 48 h. Colony number was counted after 6 weeks, helping visualization with MTT staining (0.5 mg/mL, 4 h, 37°C).

5.3.6 BALB/c Nude Injection of Human Pancreatic Tumoral Cell Lines

PANC-1_LUC control or lentiviral infected cells were washed and resuspended in PBS in order to have 1 million cells in 100 µL. Subcutaneous injection was performed in both posterior flanks of the 6 week old BALB/c nude mice (200 µL/injection). Intraperitoneal injection was performed using same quantities.

5.3.7 Bioluminiscent Measures to Control Tumoral Progression in Xenografts

Tumoral progression was followed weekly by macroscopic observation of the animal as well as by measuring the bioluminescence emitted by luciferase-expressing tumoral cells injected. For this purpose, 100 µL of D-Luciferine (Xenogen) was injected intraperitoneally (16 mg luciferine/Kg). Image was taken after 12 min. Animals were anesthetized with isofluorane and bioluminescence measured for 5 min with IVIS 50 Imaging System (Xenogen). In order to follow tumor progression along time and be able to compare animals, images were all taken with 5 min exposition. However, shorter expositions were recorded when

saturated images appeared in order to quantify data. Animal recovery after anesthesia was carefully controlled. Animals were sacrificed when tumor perimeter reached 1 cm in the case of the subcutaneous tumors or when animals presented compromised general welfare, weakness or enlarged abdomen in intraperitoneal oens. In order to localize secondary sites different from the pancreas, luciferase was injected just before animal sacrifice and organ luminescence images were taken afterwards.

5.3.8 Immunohistochemistry

Formalin-fixed paraffin-embedded tissue blocks were sectioned at 5 µm for immunohistochemistry (IHC) analysis. Sections were deparaffined and antigen retrieval was performed with citrate buffer 0.01 M pH 6.0 at 120ºC for 10 min in a pressure cooker (all antibodies) or with pepsin 0.1% in HCl 0.1 M, 20 min 37ºC (only for von Willebrand Factor (vWF)). Endogenous peroxidase activity was quenched with H_2O_2 3% for 10 min and blocking was achieved with 5% FBS in PBS-T. Primary antibody incubation followed ON at 4ºC and the antibodies used were α-Gal-1 (1:100, kindly provided by Dr. Gabius, Ludwig-Maximilians-University, Munich, Germany[489]), α-Gal-1 (1:100, R&D Biosystems), α-Gal-1 (1:100, Sigma), α-luciferase (1:1000, Sigma), α-Ki67 (1:1000, Novo Castra), α-SMA, (1:400, Sigma), α-vWF (1:200, Neomarkers), α-DrGal1-L2 (1:100, kindly provided by Dr. Vasta, UMBI, Baltimore, MD), rabbit α-amylase (1:400) and rat α-CK19 (1:1000, TROMA 3). For the competition experiment, DrGal1-L2 antibody was pre-mixed with the recombinant DrGal1-L2 protein (kindly provided by Dr.Vasta, UMBI, Baltimore, MD) in a 1:10 ratio (antibody:protein) before adding it to slides. For negative controls, tissues were incubated with

a pre-immune serum. As secondary antibody, Envision+ reagent was applied (Dako), anti-rat HRP (1:200, Dako) or the DAKO LSAB + System HRP (for primary goat antibodies). Reactions were developed using 3,3'-diaminobenzidine (DAB) as chromogenic substrate. Sections were counterstained with hematoxylin, dehydrated, and mounted. For visualization, an Olympus BX61 microscope was used and images were acquired using cell^B software.

5.3.9 Animals

Animals were housed and fed as previously described[62,501]. Basically, animals were maintained in groups of four in ventilated cages with 12 h stable light cycles, with a temperature of 22±2°C and controlled moisture between 40-70%. Animals were fed *ad libitum* with complete feed. *5* week old immunodeficient female BALB/c mice were obtained from Charles River. Founder pairs of Ela-1-myc (C57BL/6 genetic background) were kindly providen by E.Sandgren (University of Wisconsin-Madison, Madison, WI). Male hetereozygous transgenic mice were mated to wild type C57BL/6 females to maintain the Ela-1-myc colony. Littermates were assessed for oncogene presence after weaning by DNA tail extraction and PCR analysis (see below). Gal-1 KO mice came from F. Poirier (Institute Jacques Monod, CNRS, Paris, France). To generate the Ela-1-myc:Gal-$1^{+/-}$ and Ela-1-myc:Gal-$1^{-/-}$ mice, we crossed the previously mentioned animals in the following manner: for the F1 generation, Ela-1-myc male mice were crossbred with female Gal-$1^{-/-}$ to obtain Ela-1-myc heterozygous for Gal-1 (Ela-1-$myc^{+/-}$:Gal-$1^{+/-}$, which represented 50% of the progeny). For the F2, Ela-1-$myc^{+/-}$:Gal-$1^{+/-}$ males from F1 were paired with Gal-$1^{-/-}$ KO female

mice to obtain transgenic mice KO for Gal-1 (Ela-1-myc$^{+/-}$:Gal-1$^{-/-}$, corresponding to 25% of the progeny). To generate the amount of animals required and work with Gal-1 pure genotype populations we crossed Ela-1-myc$^{+/-}$:Gal-1$^{-/-}$ mice with Gal-1 KO or with wild type C57BL/6 females to obtain the homozygous (Ela-1-myc$^{+/-}$:Gal-1$^{-/-}$) and heterozygous (Ela-1-myc$^{+/-}$:Gal-1$^{+/-}$) mice respectively (see *Results*, Fig.71). All procedures were approved by the CEEA (Ethical committee for animal experimentation).

5.3.10 Animal Genotyping

A tail fragment was collected after weaning, and 0.5 mL of extraction buffer was added (Tris HCl 20 mM, EDTA 5 mM, pH 8.0, SDS 0.5%, NaCl 200 mM, proteinase K (100 µg/mL, Dako) and samples were incubated at 55°C for 12 h with gentle agitation. To extract DNA, samples were centrifuged and the supernatant was mixed with 0.5 mL of isopropanol to precipitate DNA. Washing was achieved with 70% ethanol and the pellet was allowed to dry and resuspended in 200 µL of TE buffer (Tris HCl 10 mM, EDTA 1 mM pH 8.0). PCR reactions were performed with 0.5U EcoTaq Polymerase (Ecogen). For genotyping, the following primers were used: c-*Myc*: Fw (CAC CGC CTA CAT CCT GTC CAT TCA AGC) and Rv (TTA GGA CAA GGC TGG TGG GCA CTG), expecting a 200 bp band, *Lgals1*: Fw (CTC AGT GGC TAC ATC TGT AAA ATGG) and Rv (TTC TTT GAC ATT TGA ACC CTA TACC (3'neo) or TTC TTT GAC ATT TGA ACC CTA TACC (3'Gal)), expecting a 478 bp band for the wt allele or a 694 bp band for the targeted one. PCR conditions were as follows: after 2 min at 94°C, 35 cycles of denaturation at 94°C for 45 sec, annealing at 60°C for 1 min, extension at 72°C for 1 min

were carried out, followed by a final extension at 72ºC for 10 min. DNA bands were observed in a 2% agarose gel.

5.3.11 *In vivo* Survival Analysis and Sample Collection

Overall survival was calculated from the day of birth to spontaneous death or day of sacrifice determined by tumor size and ethical guidelines, taking into account animal weight loss, antalgic positions, weakness, reduced activity, ascites, jaundice or a palpable abdominal mass. Animals were sacrificed through cervical dislocation or, alternatively, by CO_2 asphyxiation. All procedures were CEEA approved. Tumors were weighted and measured through the largest 3 perpendicular diameters to estimate their volume. Major macroscopic features were annotated (shape, vascularization, consistence, color, localization…). General aspects were also registered such as splenomegaly, intraperitoneal hemorrages, tumor attachment to intestine or other organs, collapsed intestines… For histology, tumors were fixed in buffered formalin for 24 h, dehydrated and embedded in paraffin. Alternatively, tissue was also harvested in plastic molds (Tissue-Tek Cryomold, Sakura) with OCT embedding medium (Tissue-Tek, OCT Compound, Sakura) and directly frozen in 2-methylbutane at -80ºC. A sample for RNA preservation was also collected in RNAlater (Sigma). Tumors were analyzed by histological and IHC analysis.

5.3.12 Histopathological Tumor Analysis

Tumor sections were contrasted with hematoxylin and eosin staining and analyzed by Dr. Jessica Munné Collado and Dr. Mar Iglesias (Pathology Department, Hospital del Mar, Barcelona). Different

parameters were evaluated for each tumor such as the differentiation type (percentage of acinar and ductal components), node infiltration, necrosis, apoptosis and hemorrhage.

5.3.13 Immunohistochemistries and Quantification

Immunohistochemistries were performed as previously described. For xenograft studies, quantification was done by analyzing 20 images taken with a 20X objective per tumor, by means of ImageJ software. For proliferation staining, the area corresponding to positive nuclei for Ki67 and the total nuclei area (stained with hematoxylin) were measured. The percentage of cells proliferating was derived from relating these two values. To quantify both the stroma abundance and angiogenesis, we took 10 pictures with a 20X objective from the center of each tumor, and 10 more from the outer part (usually with more stroma and more vascularized). The percentual area positive for α-SMA for each tumor was obtained through the mean of these 20 values and corresponded to the percentage of stroma present in the tumor. To quantify angiogenesis by vWF staining, we counted the number of blood vessels with a diameter above 100 μm (macro blood vessels), between 50-100 μm (medium blood vessels), 25-50 μm (micro blood vessels) or single ECs. For Ela-1-myc:Gal-1 study, 10 pictures with the 10X objective were taken for quantification. ImageJ analysis was done as described except for vWF, in which overal positive area was quantified instead of blood vessel counting.

5.3.14 ptf1a:eGFP-K-Ras^{G12V}

This zebrafish model was established in Dr. Leach laboratory at Johns Hopkins University, in Baltimore, MD[82]. To generate it, recombinant engineering was used to modify a bacterial artificial chromosome (BAC) containing the *ptf1a* locus to obtain the transgenic constructs ptf1a:eGFP and ptf1a:eGFP-K-Ras^{G12V}. In this construct, K-Ras was fused to GFP to allow real time visualization of the cells expressing the oncogene. These transgenes (ptf1a:eGFP and ptf1a:eGFP-K-Ras^{G12V}) were injected into AB wild type embryos, at one cell stage and were crossed to generate F1, when adults. Through matings involving transgenic and wild type fish, 200 embryos were selected for GFP expression. This expression was assessed at different time points (1,2,3,6 and 9 months) and for each time, several animals were sacrificed to collect tumors and perform the histologic analysis.

5.3.15 Ptf1a: GAL4/VP16 UAS:eGFP-K-Ras^{G12V}

This zebrafish model was established in Dr. Leach laboratory at Johns Hopkins University, in Baltimore, MD. In the GAL4/UAS system, the transcription factor GAL4 bound to its target sequence UAS and activated the transcription of those genes fused to UAS. In order to even more amplify gene activation, GAL4 DNA binding domain was linked to VP16 activity. The main advantage of this system was that GAL4 gene and the gene fused to UAS were separated in two different transgenic lines to generate a binaric transgenic system. In the activator line (GAL4 DNA binding domain fused to VP16), *ptf1a* promoter drove gene expression. In the other line, UAS was fused to K-Ras, which remained silenced if GAL4/VP16 was absent. When

both lines were crossed, K-Ras was activated, following Ptf1a expression pattern.

5.3.16 Zebrafish Histology

For histologic analysis, formaldehyde 40% was abdominally injected in zebrafish and the whole animal was immersed in this buffer for 12 h. The abdominal cavity was dissected and embedded in 1% agarose to preserve tissue consistency before paraffin embedding. Alternatively, the tissue could be immersed in 30% sucrose and cryopreserved embedded in OCT.

5.3.17 ISH in Paraffin Embedded Zebrafish Tissue

Sections were deparaffined and fixed in 4% PFA (15 min, RT). Permeabilization was performed with proteinaseK at 1 µg/mL, which was inhibited by 2 mg/mL of glycine (5 min). Sections were again fixed for 15 min with 4% PFA. To block non-specific riboprobe binding, amino groups were acetyled with acetic anhydride 0.025% in 0.1 M triethanolamine for 10 min. Prehybridization was performed for 30 min at 65°C with 5X SSC, 50% formamide, 1% SDS, 50 µg/mL yeast tRNA and 50 µg/mL heparin. Hybridization took place for 12 h at 70°C (1:500 probe dilution). Unbound probe was washed with 50% formamide, 5X SSC, 1% SDS (5 min, 15 min, 30 min), 50% formamide, 2X SSC (2 X 15 min) and TBS-T (0.14 M NaCl, 2.7 mM KCl, 25 mM Tris, pH 7.5, 1% Tween20). Blocking was performed with TBS-T 1% BSA, 5% FBS, 0.5% Blocking reagent (Roche). For dioxigenin (DIG) recognition, tissue sections were incubated with an α-DIG conjugated to alkaline phosphatase (Roche, 1:2000 dilution), for 2 h. To remove non-specific binding, 6 washes

with TBS-T and 6 washes with the detection buffer (NTMT: 100 mM NaCl, 100 mM Tris pH 9.5, 50 mM $MgCl_2$, 1% Tween20, 2 mM levamisole) followed. For detection, BMPurple (Roche) was used for 12-72 h. Sections were dehydrated and mounted with histomount (Invitrogen).

5.3.18 ISH: Probe Generation

In situ hybridization (ISH) to detect Gal-1 RNA was preformed over paraffin embedded or cryopreserved 8 μm tissue sections. Primers to design DIG-labeled probes were: mGal-1 (sense 5'-TCT CAA ACC TGG GGA ATG TC-3', antisense 5'-CCT GGA AAG CAC AAG AGA GG -3' that gave rise to a *557* bp PCR fragment. Fragment amplification was performed through RT-PCR with the above mentioned primers and cloned into a TOPO-TA vector (Invitrogen), which allowed synthesis of the sense and antisense probes with T7 and Sp6 RNA polymerases, according to sequence orientation. For DrGal1-L2 probe generation, the whole sequence was used (405 bp). In this case, Dr.Vasta (UMBI, Baltimore, MD) kindly provided us with a pET30a(+) vector with DrGal1-L2 sequence cloned between EcoRI and NdeI restriction sites. This vector was digested with HindIII and XbaI and subsequently cloned into a TOPO-TA vector to obtain the sense and antisense probes. Similarly, for zebrafish trypsin, the complete sequence was used (405 bp). For riboprobe synthesis, we performed a PCR with M13 primers and *in vitro* transcription with DIG uracil labeled nucleotides followed at 37°C for 2 h. Probe was kept at -80°C and quality was analyzed by agarose gel before performing ISH.

5.3.19 Mouse Embryonic Pancreas Dissection

ON matings were arranged between male and female CD1, C57BL/6 or Gal-1 KO mice. A plug was indicative of pregnancy and noon of that day was treated as 0.5 days of gestation (E0.5). Embryonic pancreas was isolated under a dissecting microscope on day 13.5 14.5 or 19.5 of gestation. Early embryonic pancreas consisted of mesenchyme surrounding the inner epithelium. After *in vitro* growth, amylase-positive cells were typically localized in the exterior side of the epithelium, whereas endocrine cells were found in the central region.

5.3.20 siRNA Transfection in Dorsal Bud Explants

Dorsal bud explants were put inside PBS just after dissection. To prepare the transfection mixture, on one side, Lipofectamine (0.5 µL for each pancreas) was mixed with serum free medium (M-199 (Invitrogen) with 1% penicillin/streptomycin and 250 ng/µL fungi zone 1:100). On the other side, siRNA at 20 µM (0.25 µL of mouse Gal-1 siRNA or an irrelevant siRNA) was mixed with 12.25 µL of serum free M-199 supplemented as described above. After 5 min incubation, both mixtures were joined and left for 30 min. 25 µL drops were placed over a petri dish and dissected pancreas were carefully immersed. A wet chamber was created with PBS with the lower side of the petri dish. Transfection proceeded at 37°C for 24 h. Afterwards, pancreas were transferred to 0.4 µm filters (Millicell, Millipore) in T24 well plates with 10% FBS M-199. Medium was replaced every 48 h. 6 days after *in vitro* culture, dorsal bud explants were prepared for RNA extraction by immersing the tissue in RNA later for 24 h. For IF, pancreas were fixed with 10% PFA for

10 min, sedimented in 30% sucrose for 24 h and embedded in OCT blocks for sectioning.

5.3.21 Histoimmunofluorescence over Mouse Developing Pancreas

OCT sections stood at RT for 5 min and they were blocked with 0.2% Triton X-100, 10% FBS for 1 h, RT. Tissues were incubated with primary antibodies diluted in the blocking solution for 12 h at 4°C (Rabbit α-Glucagon (1:400), guinea pig α-insulin (1:400), rabbit α-amylase (1:300), rat α-E-Cadherin (1:400), rabbit α-CPA (1:400) (all of them kindly provided by Dr.Leach, JHU, Baltimore, MD), goat α-Gal-1 (1:400, R&D Biosystems)). Slides were washed with blocking solution and Alexa Fluor antibodies (Invitrogen) or antibodies conjugated to cyanine dyes (Cy2, Cy3, Cy5, Jackson Immunoresearch) were added, and incubation took place for 2 h, RT. After washing and DAPI (1:1000, 2 min) or Hoechst staining (1:10000, 3 min), coverslides were mounted with Fluoromont-G. Images were obtained with an Olympus BX61 microscope and the cell^B software analysis.

5.4 DECIPHERING GAL-1 MOLECULAR MECHANISMS: TRANSCRIPTOME ANALYSIS

5.4.1 Gal-1 Overexpression in RWP-1 Cells

RWP-1 cells at 60% confluence were transfected in T24 well plates with 250 ng of pcDNA3-Gal-1 or empty pcDNA3 with Lipofectamine and Plus reagents as previously described. Cells that incorporated DNA were selected with G418 1 mg/mL for 7 days. Clones were prepared by seeding 100 cells in p100 plates. When macroscopic, original single cell colonies were picked and trypsinized. 20 clones for Gal-1 overexpressing and control cells were selected, and assessed for Gal-1 protein levels by WB analysis. A clone (C.20, named Gal-1 in section *2. Results*) with very high Gal-1 levels was selected and compared to a control clone (C.23, named pcDNA3 in section *2. Results*).

5.4.2 BrdU Incorporation Analysis and IF Detection

Around 50000 cells were seeded over T24 sterile coverslips. BrdU at 40 μM was added and cells were incubated for 10 min at 37°C. Afterwards, cells were fixed in 2% PFA for 15 min and treated for 10 min with HCl 4 M. For pH neutralization, washes with PBS were performed. Permeabilization was achieved with 0.2% Triton in PBS for 5 min and blocking with 5% BSA, 0.1% Tween20 in PBS for 10 min. Coverslips were incubated with a mouse α-BrdU specific antibody (1:400, Santa Cruz Biotechnologies) for 1 h RT. Secondary antibody α-mouse Alexa Fluor 488 (Invitrogen) followed for 1 h. Finally, DAPI staining (0.25 μg/mL) for 3 min allowed nuclei

visualization. Coverslips were washed and mounted with Fluoromont-G and IF detected with an Olympus BX61 Microscope with its appropriate filters (DAPI filter with absorbance at 358 nm, and FITC at 494 nm). 10 fields per coverslip were used for quantification. The number of BrdU positive cells were manually counted and compared to total number of cells (DAPI positive) for each experiment. Quantification data were normalized to 1 in order to be able to compare between experiments.

5.4.3 Matrigel Adhesion

Matrigel (1:20 diluted in PBS) was used to coat T24 well plates for 2 h at 37°C and its surface was blocked with PBS 2% BSA for 2 h 37°C. Cells were trypsinized and washed with DMEM 1% BSA before counting. 150000 cells/well were seeded in triplicates. Attachment was allowed for 45 min at 37°C and supernatant carefully removed. To visualize adhered cells, MTT solution at 0.5 mg/mL was added and cells were incubated with this reagent for 2 h at 37°C. Medium was removed and images showing attached cells taken. To quantify, 150 µL of MTT extraction buffer was used (0.1 M HCl, 10% Triton X-100 in isopropanol) and absorbance read at 550 nm. In order to compare different experiments, data were normalized to 1.

5.4.4 Trypsin Lift Up Experiments

Trypsin was diluted 1:2 in PBS and trypsinization kinetics were followed for each cell line by means of an optic microscope.

5.4.5 Mobility Experiments: Time-Lapse Video Microscopy

10000 cells/well were seeded 24 h before the mobility assay in borosilicate coverglass 4 chamber plates (LabTek). Pictures were taken every 15 min for 10 h (5 fields/cell line) with a Zeiss Cell Observer HS microscope. Recorded trajectories were analyzed and the greatest linear distance was measured and quantified using Manual Tracking software for ImageJ. 25 cell trajectories per cell line were monitored. Mobility experiments were carried out in the Advanced Light Microscopy Unit (CRG, Barcelona).

5.4.6 RNA Extraction for Micoarray Analysis

RNA extraction from cell lysates was performed with RNeasy Plus Mini kit (Qiagen), having been previously purified with Qiashredder columns (Qiagen). Purity and integrity of the RNA were assessed by spectrophotometry and nanoelectrophoresis using the NanoDrop ND-1000 spectrophotometer (NanoDrop Technologies) and the Nano lab-on-a-chip assay for total eukaryotic RNA using Bioanalyzer 2100 (Agilent Technologies), respectively. Only samples with high purity (Abs260/280>2.0; Abs260/230>1.6) and high integrity (RNA integrity number (RIN) of 10) were subsequently used in microarray experiments.

5.4.7 Microarray Description

Microarray expression profiles were obtained using the Affymetrix Human Exon ST 1.0 arrays (Affymetrix) in IMIM's Microarray facility (Barcelona). This array allows analyzing 18708 genes from the

human genome. Specifically, the array contained 4 probes per exon, allowing detection of genetic variants due to alternative splicing. Thus, the array summarized approximately 40 probes per gene in a single level of expression result, representing all the transcripts derived from this gene. This high density array, which comprised over 5.5 million features, was the first-generation GeneChip Exon Array and allowed to analyze both gene expression and alternative splicing on the whole-genome scale on a single array. Briefly, 1 μg of total RNA from each sample was processed, labeled and hybridized to Affymetrix Human Exon ST 1.0 arrays according to the Affymetrix GeneChip Whole Transcript Sense Target Labeling Assay described below.

5.4.8 Microarray Analysis

First, a ribosomal RNA (rRNA) reduction was performed from the 1 μg of initial total RNA by using the RiboMinus Human/Mouse Transcriptome Isolation Kit (Invitrogen). Afterwards, double-stranded cDNA was synthesized with random hexamers tagged with a T7 promoter sequence and subsequently used as a template to produce many copies of cRNA though an *in vitro* transcription reaction, which was purified using the Affymetrix sample cleanup module. A second cycle of cDNA synthesis was performed, in which single-stranded DNA was generated through a random-primed reverse transcription using a dNTP mix containing dUTP. The RNA was hydrolyzed with RNase H and the cDNA purified. The cDNA was then fragmented by incubation with a combination of uracil DNA glycosylase (UDG) and apurinic/apyrimidinic endonuclease 1 (APE 1), which specifically recognized the unnatural dUTP residues and broke the DNA strand. Finally, the DNA was labeled by terminal sample deoxynucleotidyl

transferase (TdT) with the Affymetrix proprietary DNA Labeling Reagent that was covalently linked to biotin. 5.5 µg of the fragmented and biotinylated cDNA was added to a hybridization cocktail, loaded on a Human Exon 1.0 ST array and hybridized for 16 h at 45°C and 60 rpm in an Affymetrix GeneChip Oven 645. Following hybridization, the array was washed and stained in the Affymetrix GeneChip Fluidics.Station 450. The stained array was scanned using an Affymetrix GeneChip® Scanner 3000 7G, generating CEL files for each array. After quality control of raw data, it was background corrected, quantile-normalized and summarized to a gene-level using the robust multi-chip average (RMA) (Irizarry 2003) obtaining a total of 18708 transcript clusters, which roughly correspond to genes. Normalized data were then filtered to avoid noise created by non-expressed transcript clusters in the condition. Only transcripts over 75% of variance from total variance were considered for further analysis, which led to 4612 transcript clusters. Core annotations (version netaffx 29, human genome 18) were used to summarize data into transcript clusters. Linear Models for Microarray (LIMMA), a moderated t-statistics model, was used for detecting differentially expressed genes between the conditions in study. Correction for multiple comparisons was performed using false discovery rate and only genes with an adjusted p-value less than 0.05 were selected as significant.

5.4.9 Microarray Data Treatment

The first comparison performed was between non-infected PANC-1 cells (wt) versus PANC-1 cells infected with the scrambled shRNA (shCtl). Transcripts obtained in this comparison were subsequently deleted from the rest of the comparisons, as they corresponded to

transfection "technique controls". Common genes in comparisons PANC-1 (wt minus shCtl) / PANC-1 shGal-1_2 / PANC-1 shGal-1_5 and RWP1 pcDNA3 / RWP1 Gal-1, generated the final list. Hierarchical cluster analysis was also performed to see how data aggregated. All data analyses were performed in R (version 2.8.1) with packages aroma.affymetrix, Biobase, Affy, limma, genefilter. Ingenuity Pathway Analysis (Ingenuity Systems, version 8.5) was used to perform functional analysis of the results.

Data were processed through a second independent analysis (in collaboration with Dr. M. E. Fernandez-Zapico (Mayo Clinic, Rochester, NY), offering an alternative list of altered genes (named *Summary List* in *Supplementary Information*). Data pre-processing was as follows: the raw exon array probe level data were imported into Partek and processed using RMA (robust multi-array average) algorithms[899]. Once probe set expression was obtained, gene level data were obtained using mean method (mean of the all exon expressions). There were 17865 core genes. Following are the settings used: RMA background correction; core probe sets; quantile normalization; and median polish for data summarization. Gene level expression was calculated using mean of exons. The generated data were log2 transformed. ANOVA was used to detect singificantly altered genes in PANC-1 group and t test was used in RWP-1 group.

5.4.10 Reverse Transcription (RT) and Validation by qRT-PCR Analysis

Total RNA was extracted from cultured cells with the RNeasy kit (Qiagen) and first strand cDNA was prepared from RNA using random hexamer primers and the RevertAid first strand cDNA synthesis kit (Fermentas). Both HPRT and GAPDH were used to normalize cDNA inputs. qRT-PCR primers were designed with Oligo Perfect Designer (Invitrogen) and were as follows: ***GAPDH***: Fw (GCG TCT CTG CTC CTC CTG TT), Rv (CCA TGG TGT CTG AGC GAT GT); ***HPRT***: Fw (GGC CAG ACT TTG TTG GAT TTG), Rv (TGC GCT CAT CTT AGG CTT TGT); ***LGALS1***: Fw (CAG CAA CCT GAA TCT CAA ACC), Rv (AAA GAC AGC AAC AAC CTG TGC); ***TGFBR3***: Fw (TCA AGC CTG TCT TCA ACA CCT), Rv (GGC ACA CAC TTA GGC AAC TTC); ***FGFR2***: Fw (TGA TGC CAC AGA GAA AGA CCT), Rv (GTG CAG GCT CCA AGA AGA TTT); ***CDH1***: Fw (CAG TTG AGG ATC CAA TGG AGA), Rv (TCT GTC ATG GAA GGT GCT CTT); ***ERBB2***: Fw (GGG AAG AAT GGG GTC GTC AAA), Rv (CTC CTC CCT GGG GTG TCA AGT); ***FN1***: Fw (CTG CAG GTC CAG ATC AAA CA), Rv (TGA CTC TCT CCG CTT GGA TT); ***ITGAV***: Fw (CGT ATC TGC GGG ATG AAT CT), Rv (GGG TTG CAA GCC TGT TGT AT); ***THBS1***: Fw (AGA TGG CCA CCA GAA CAA TC), Rv (GTC ATC ATC GTG GTC ACA GG); ***PLAT***: Fw (ACC CAG ATC GAG ACT CAA AGC), Rv (GTC ACT GTT TCC CTC AGA GCA); ***PLAU***: Fw (GTT TGG CAC AAG CTG TGA GAT), Rv (GGG AAA TCA GCT TCA CAA CAG); ***PLAUR***: Fw (GCT TGT GGG AAG AAG GAG AAG), Rv (CTG GTG ATC TTC AAG CCA GTC); ***DISP1***: Fw (ACT CTT CTG ACG GCG TGA CTA), Rv (ATG GCT ATG GCA GGA TAC ACA); ***HHAT***: Fw (TGA AGT ACT TGG TGC TCT TTG G), Rv (GGT GAA ACT GAA CAT GGT GCT);

CCND2A: Fw (ATT ACC TGG ACC TGG TCT TGG), Rv (GCT GGT CTC TTT GAG TTT GGA); ***COL11A1***: Fw (AGG GTG ACA AGG GAG AAA ATG), Rv (CTA GGA CCT GGT TCA CCA TCA); ***PDGFD***: Fw (TGG AAC TGT CAA CTG GAG GTC), Rv (TCT ACC CCT CCT CCT GAT GTG); ***GADD45A***: Fw (GGA GGA AGT GCT CAG CAA AG), Rv (CAG GCA CAA CAC CAC GTT ATC); ***TGFBI***: Fw (TCA GGA AAG AGG GGA TGA ACT), Rv (TTG ATA GAC AGG GGC TAG TCG). 10 µL sample reactions for RT-qPCR were prepared with SybrGreen Master Mix (Applied Bioscience) and 25 ng of sample. RT-qPCR was performed in ABI7900HT (Applied Biosystems).

5.4.11 *In vitro* Luciferase Measure

50000 RWP-1 cells (control: a clone transfected with an empty pcDNA3) or RWP-1 Gal-1 cells (transfected with pcDNA3-Gal-1) were seeded over T24 plates. Cells were transfected with Lipofectamine and Plus reagent (as previously described) with 25, 50, 100 or 150 ng of the vector pδ51 Luc II containing 8 Gli responding elements. After 48 h, cells were lysed with passive lysis buffer (PLB) and Luciferase and Renilla activity were measured (Promega).

5.5 STATISTICAL ANALYSIS

Unless otherwise stated, values are expressed as the relative mean of three independent experiments and error bars represent ±SEM (standard error of the mean). When error bars are not present in column bars is because one representative experiment out of the three performed, is shown. Statistical analyses were performed with SPSS version 12.0 and GraphPad Prism 5 software. Statistical significance has been always considered when $p \leq 0.05$. Kaplan-Meier analyses were used for establishing survival curves and comparisons were performed using the log-rank test. To determine whether two quantitative variables differed significantly, the t test (when normally distributed) or Mann Whitney test (non-normally distributed) were applied. To compare more than two quantitative variables, Kruskal Wallis test (for non-normally distributed populations) was used. To model counts (such as the number of blood vessels when quantifying vWF IHCs), Poisson regression was applied to take into account the size and blood vessel distribution inside or around tumors. To compare qualitative dichotomic variables, Chi-square test was used. Unless otherwise stated, statistical analysis and given p values were calculated using the t test.

6 SUPPLEMENTARY INFORMATION

A new idea comes suddenly and in a rather intuitive way. But intuition is nothing but the outcome of earlier intellectual experience.

Albert Einstein

6.1 PANC-1 DATA

6.1.1 PANC-1 Ctl-shSC Compared to shGal-1_2

6.1.1.1 Gene Detailed Analysis in PANC-1 shGal-1_2

logFC	AveExpr	adj.P.Val	unlist.symbol	Gene description
1,976	**9,89512**	**6,83E-007**	**LGALS1**	**lectin, galactoside-binding, soluble, 1 (galectin 1)**
-1,176	8,11955	2,03E-006	EGR1	early growth response 1
-1,427	5,91314	0,0004492	FOS	v-fos FBJ murine osteosarcoma viral oncogene homolog
0,545	10,2068	0,0011297	STAT3	signal transducer and activator of transcription 3 (acute-phase response factor)
-0,632	6,50529	0,0011297	SCUBE3	signal peptide, CUB domain, EGF-like 3
1,08	8,58526	0,0011297	RAG1AP1	recombination activating gene 1 activating protein 1
0,695	6,57537	0,0011297	CXorf15	chromosome X open reading frame 15
-0,645	7,83887	0,0011297	CXCL1	chemokine (C-X-C motif) ligand 1 (melanoma growth stimulating activity, alpha)
-0,827	5,20039	0,0011297	EPHA7	EPH receptor A7
-0,53	9,43918	0,0011297	ITGA3	integrin, alpha 3 (antigen CD49C, alpha 3 subunit of VLA-3 receptor)
-0,684	5,40192	0,0011297	PLA2R1	phospholipase A2 receptor 1, 180kDa
0,656	8,01619	0,0011297	CAMK2N1	calcium/calmodulin-dependent protein kinase II inhibitor 1
-0,715	6,72835	0,0011567	CD82	CD82 molecule
-0,484	7,65456	0,002071	PODXL	podocalyxin-like
-0,489	8,04915	0,0022131	TNFAIP2	tumor necrosis factor, alpha-induced protein 2
0,803	7,90793	0,0025104	BTG3	BTG family, member 3
0,793	5,76297	0,0029685	C10orf83	chromosome 10 open reading frame 83
0,809	5,06027	0,0038771	BCAT1	branched chain aminotransferase 1, cytosolic
0,692	6,31344	0,0049831	GRK5	G protein-coupled receptor kinase 5
0,835	6,41487	0,0056472	C14orf147	chromosome 14 open reading frame 147
0,489	7,34779	0,0071826	CKMT1B	creatine kinase, mitochondrial 1B
-0,7	9,03415	0,0071826	PADI2	peptidyl arginine deiminase, type II
0,507	8,4015	0,0071826	NUP50	nucleoporin 50kDa
0,715	7,28358	0,0071826	RBM35A	RNA binding motif protein 35A
-0,566	**10,1062**	**0,0071826**	**TGFBI**	**transforming growth factor, beta-induced, 68kDa**
-0,9	5,89433	0,0072236	CCL2	chemokine (C-C motif) ligand 2
0,829	8,52906	0,0072236	PCNA	proliferating cell nuclear antigen
-0,527	7,55031	0,0072236	LOXL2	lysyl oxidase-like 2
0,541	5,61233	0,0072236	ASAM	adipocyte-specific adhesion molecule
-0,658	**6,63683**	**0,007456**	**THBS1**	**thrombospondin 1**
-0,592	7,32382	0,0079331	TSPAN1	tetraspanin 1
-0,396	8,03911	0,0087644	DKK3	dickkopf homolog 3 (Xenopus laevis)

logFC	AveExpr	adj.P.Val	unlist.symbol	Gene description
-0,416	**7,41412**	**0,009576**	**CDH1**	**cadherin 1, type 1, E-cadherin (epithelial)**
-0,602	5,64144	0,009576	RET	ret proto-oncogene
-0,6	4,89248	0,0096765	TMEM26	transmembrane protein 26
0,539	5,73415	0,0100717	BDH1	3-hydroxybutyrate dehydrogenase, type 1
-0,731	5,46013	0,0104582	C4A	complement component 4A (Rodgers blood group)
0,711	8,25361	0,0104582	RDX	radixin
-0,431	7,4048	0,0112725	FLJ20160	FLJ20160 protein
0,786	3,79154	0,0114837	SF3B4	splicing factor 3b, subunit 4, 49kDa
-0,596	5,42186	0,0121059	NRP2	neuropilin 2
-0,4	8,91649	0,0121059	CXXC5	CXXC finger 5
-0,496	7,66335	0,0121059	MRC2	mannose receptor, C type 2
0,56	6,96938	0,0121059	B4GALT6	UDP-Gal:betaGlcNAc beta 1,4- galactosyltransferase, polypeptide 6
0,501	7,56336	0,0124683	CKMT1A	creatine kinase, mitochondrial 1A (CKMT1A), nuclear gene encoding mitochondrial protein, mRNA
-0,842	7,73027	0,0124683	AK3L1	adenylate kinase 3-like 1
0,432	5,93714	0,0138637	PAPSS2	3'-phosphoadenosine 5'-phosphosulfate synthase 2
0,441	6,75217	0,0138637	DSC2	desmocollin 2
0,526	8,51226	0,0139732	LIMA1	LIM domain and actin binding 1
0,99	5,05254	0,0139732	TMEM156	transmembrane protein 156 (TMEM156), mRNA
0,467	7,28313	0,0151527	ETV4	ets variant gene 4 (E1A enhancer binding protein, E1AF)
0,424	10,6837	0,0151527	HIST1H2BF	histone cluster 1, H2bf
-0,563	4,89368	0,0151527	PGCP	plasma glutamate carboxypeptidase
-0,467	7,91411	0,0154586	FAM43A	family with sequence similarity 43, member A
0,437	5,78627	0,0154586	CAMK1D	calcium/calmodulin-dependent protein kinase ID
0,388	6,37017	0,0154586	IL6R	interleukin 6 receptor
0,456	7,2827	0,0154586	ENTPD4	ectonucleoside triphosphate diphosphohydrolase 4
-1,631	3,62485	0,0154586	SEMA3D	sema domain, immunoglobulin domain (Ig), short basic domain, secreted, (semaphorin) 3D
-0,625	6,27257	0,0154586	PON3	paraoxonase 3
-0,516	9,87804	0,0169155	CTSD	cathepsin D
0,384	8,30878	0,0191987	NF2	neurofibromin 2 (bilateral acoustic neuroma)
0,665	6,3973	0,0191987	OXNAD1	oxidoreductase NAD-binding domain containing 1
-0,669	5,65621	0,019865	CBLN2	cerebellin 2 precursor
0,403	7,73063	0,019865	PAK1	p21/Cdc42/Rac1-activated kinase 1 (STE20 homolog, yeast)
-0,507	6,18298	0,0213503	HMOX1	heme oxygenase (decycling) 1
0,533	5,02015	0,0213503	SCML1	sex comb on midleg-like 1 (Drosophila)
0,429	7,74867	0,0213503	STS-1	Cbl-interacting protein Sts-1
0,365	6,28606	0,0213903	PKP2	plakophilin 2
0,441	6,6596	0,0213903	OTUB2	OTU domain, ubiquitin aldehyde binding 2
-0,678	5,61421	0,0213903	SLC38A3	solute carrier family 38, member 3
-0,467	7,70203	0,0213903	P4HA2	procollagen-proline, 2-oxoglutarate 4-dioxygenase (proline 4-hydroxylase), alpha polypeptide II
0,389	7,60155	0,0215175	CTDSPL	CTD (carboxy-terminal domain, RNA polymerase II, polypeptide A) small phosphatase-like
-0,477	5,00709	0,02215	FAM134B	family with sequence similarity 134, member B

logFC	AveExpr	adj.P.Val	unlist.symbol	Gene description
0,433	7,27044	0,0224289	RBMS2	RNA binding motif, single stranded interacting protein 2
-0,529	7,1445	0,0224289	LAMC2	laminin, gamma 2
0,504	6,71076	0,0224289	MTHFS	5,10-methenyltetrahydrofolate synthetase (5-formyltetrahydrofolate cyclo-ligase)
-0,367	8,48684	0,0238258	SLC44A2	solute carrier family 44, member 2
-1,359	3,36239	0,0242264	OR10H3	olfactory receptor, family 10, subfamily H, member 3
-0,477	7,79235	0,0242264	CDKN1A	cyclin-dependent kinase inhibitor 1A (p21, Cip1)
0,463	6,8161	0,0242264	ZMAT3	zinc finger, matrin type 3
-0,349	7,9516	0,0242264	PLXND1	plexin D1
-0,495	4,22631	0,0242264	SEMA3E	sema domain, immunoglobulin domain (Ig), short basic domain, secreted, (semaphorin) 3E
-0,713	7,14873	0,0242264	BNIP3	BCL2/adenovirus E1B 19kDa interacting protein 3
-0,499	8,01029	0,0242264	NA	NA
-0,427	4,93902	0,0242264	PCDH7	protocadherin 7
-0,4	7,89275	0,0242264	HOXB8	homeobox B8
-0,612	5,32737	0,0246942	PTGS1	prostaglandin-endoperoxide synthase 1 (prostaglandin G/H synthase and cyclooxygenase)
-0,579	7,22944	0,0259917	ZFP36L1	zinc finger protein 36, C3H type-like 1
0,359	6,01814	0,0277366	AS3MT	arsenic (+3 oxidation state) methyltransferase
0,604	5,49369	0,0288293	RASGRF2	Ras protein-specific guanine nucleotide-releasing factor 2
-0,474	5,97828	0,0288293	ARNT2	aryl-hydrocarbon receptor nuclear translocator 2
0,435	6,01749	0,0290782	MAP7	microtubule-associated protein 7
-0,778	7,45822	0,0294154	ARRDC3	arrestin domain containing 3
0,54	8,37125	0,0300141	DDAH1	dimethylarginine dimethylaminohydrolase 1
0,503	4,23098	0,0316336	ZNF14	zinc finger protein 14
-0,704	4,78946	0,0325141	EDIL3	EGF-like repeats and discoidin I-like domains 3
0,603	6,87375	0,0339424	SCARNA8	small Cajal body-specific RNA 8
-0,735	4,74343	0,0345412	NA	NA
-0,368	6,2478	0,035263	FHL1	four and a half LIM domains 1
0,545	6,32494	0,035263	GPD1L	glycerol-3-phosphate dehydrogenase 1-like
0,352	4,81488	0,035263	NSUN7	NOL1/NOP2/Sun domain family, member 7
-0,504	9,67837	0,035263	SLC2A1	solute carrier family 2 (facilitated glucose transporter), member 1
0,33	7,50884	0,0355905	RAD54L2	RAD54-like 2 (S. cerevisiae)
0,496	8,1108	0,0355905	HMGA2	high mobility group AT-hook 2
0,427	8,25605	0,0359724	UHRF1	ubiquitin-like, containing PHD and RING finger domains, 1
-0,454	7,66872	0,0359724	JUNB	jun B proto-oncogene
-0,484	6,56913	0,0361786	ST6GALNAC2	ST6 (alpha-N-acetyl-neuraminyl-2,3-beta-galactosyl-1,3)-N-acetylgalactosaminide alpha-2,6-sialyltransferase 2
-0,399	7,0928	0,03618	GAS6	growth arrest-specific 6
-0,507	7,26761	0,0371594	FZD7	frizzled homolog 7 (Drosophila)
0,466	6,4548	0,0371594	LHFP	lipoma HMGIC fusion partner
-0,52	7,43972	0,0372422	CSF1	colony stimulating factor 1 (macrophage)
0,488	7,40221	0,0388956	MPP5	membrane protein, palmitoylated 5 (MAGUK p55 subfamily member 5)
0,555	6,58752	0,0405584	MAG1	lung cancer metastasis-associated protein
0,492	6,53742	0,0405584	SRGAP1	SLIT-ROBO Rho GTPase activating protein 1

logFC	AveExpr	adj.P.Val	unlist.symbol	Gene description
0,65	7,15154	0,0406998	FAM116A	family with sequence similarity 116, member A (FAM116A), mRNA
-0,375	4,47893	0,04488	LY75	lymphocyte antigen 75
-0,525	7,95407	0,04488	S100A3	S100 calcium binding protein A3
0,296	7,79018	0,04488	FOXQ1	forkhead box Q1
0,748	5,67653	0,04488	WDR76	WD repeat domain 76
0,324	7,93284	0,04488	INPP5A	inositol polyphosphate-5-phosphatase, 40kDa
-0,495	6,26509	0,04488	CDH2	cadherin 2, type 1, N-cadherin (neuronal)
-0,366	5,73616	0,0452547	KIAA1244	KIAA1244
-0,382	8,30489	0,0475279	C17orf70	chromosome 17 open reading frame 70
0,379	6,51186	0,0486003	CDS1	CDP-diacylglycerol synthase (phosphatidate cytidylyltransferase) 1

Table S1. List of genes significantly altered when Gal-1 was downregulated in PANC-1 with shGal-1_2 compared to control PANC-1 cells (data from non-infected cells with the genes found altered in the shCtl filtered). Genes are presented according to increasing adjusted p value until 0.05. The first column expresses the fold change in logarithmic units with base 2 (log FC). The second column gives the average expression and the third column the adjusted p value.

6.1.1.2 Pathway Analysis in PANC-1 shGal-1_2

Pathway	Set Size	Percent Up	NTk Stat	NTk q-value	NTk Rank	NEk* Stat	NEk* q-value	NEk* Rank
Extracellular Matrix / Adhesion Molecules	95	25	6.93	0.0000	2.0	3.88	0.0000	20.0
Cancer PathwayFinder	93	46	4.93	0.0000	21.0	4.17	0.0000	3.0
Signal Transduction PathwayFinder	94	35	5.22	0.0000	15.0	3.91	0.0000	16.0
Nitric Oxide	90	40	5.80	0.0000	10.0	3.87	0.0000	21.0
ECM-receptor interaction	81	17	6.79	0.0000	5.0	3.82	0.0000	30.0
Signal Transduction in Cancer	95	38	4.86	0.0000	23.0	3.85	0.0000	23.0
Tumor Metastasis	92	33	5.50	0.0000	11.0	3.75	0.0000	36.0
Sphingolipid metabolism	42	33	4.14	0.0000	42.0	3.96	0.0000	13.0
Lysosome	112	33	6.86	0.0000	3.0	3.65	0.0000	53.0

Pathway	Set Size	Percent Up	NTk Stat	NTk q-value	NTk Rank	NEk* Stat	NEk* q-value	NEk* Rank
Aminoacyl-tRNA synthetases	32	84	-5.48	0.0000	12.0	-3.69	0.0000	45.0
Frizzled signaling pathway	18	22	4.02	0.0000	48.0	3.95	0.0000	14.0
Axon guidance	125	38	4.86	0.0000	24.0	3.69	0.0000	44.0
Integrin complex	34	24	3.47	0.0000	66.0	4.08	0.0000	5.0
Osteogenesis	91	27	4.96	0.0000	20.0	3.65	0.0000	51.0
NFkB Signaling Pathway	92	38	3.50	0.0000	65.0	3.99	0.0000	10.0
Cardiovascular Disease	164	24	6.95	0.0000	1.0	3.49	0.0000	87.0
B Lymphocyte Cell Surface Molecules	11	18	3.09	0.0160	94.5	4.23	0.0000	2.0
Oxidoreductase activity, acting on NADH or NADPH	59	75	-5.34	0.0000	13.0	-3.49	0.0000	84.0
Nucleosome	56	79	-6.34	0.0000	8.0	-3.47	0.0000	92.0
Vascular endothelial growth factor receptor activity	14	21	3.09	0.0160	94.5	4.06	0.0000	7.0
Cells and Molecules involved in local acute inflammatory response	16	0	3.90	0.0000	56.0	3.65	0.0000	52.0
Wnt Signaling Pathway	96	36	4.26	0.0000	37.0	3.52	0.0000	76.0
Chromatin assembly	75	75	-6.39	0.0000	6.0	-3.42	0.0000	108.0
Oxidative phosphorylation	121	64	-4.99	0.0000	18.0	-3.45	0.0000	98.0
Adhesion and Diapedesis of Lymphocytes	13	23	3.09	0.0160	94.5	3.85	0.0000	24.0
RNA polymerase	25	80	-4.53	0.0000	32.0	-3.48	0.0000	88.0
Di-, tri-valent inorganic cation transporter activity	33	21	3.09	0.0160	94.5	3.77	0.0000	31.0
Glycosphingolipid metabolism	17	18	4.36	0.0000	35.0	3.47	0.0000	91.0
tRNA charging pathway	29	83	-3.09	0.0160	94.5	-3.76	0.0000	34.0
Nucleosome assembly	66	80	-6.81	0.0000	4.0	-3.34	0.0000	129.0
Methionine metabolism	16	69	-3.09	0.0160	94.5	-3.72	0.0000	39.0

Pathway	Set Size	Percent Up	NTk Stat	NTk q-value	NTk Rank	NEk* Stat	NEk* q-value	NEk* Rank
Transmembrane receptor protein tyrosine kinase activity	67	31	3.09	0.0160	94.5	3.71	0.0000	41.0
Endothelial Cell Biology	95	28	4.57	0.0000	31.0	3.39	0.0000	115.0
Cell adhesion molecules (CAMs)	125	18	6.28	0.0000	9.0	3.28	0.0000	140.0
Integrin-mediated signaling pathway	50	22	3.28	0.0000	70.0	3.50	0.0000	83.0
Downregulated of MTA-3 in ER-negative Breast Tumors	14	29	3.93	0.0000	53.0	3.43	0.0000	106.0
Transition metal ion transporter activity	18	22	2.88	0.0253	131.5	3.82	0.0000	29.0
Non-G-protein coupled 7TM receptor activity	11	18	2.88	0.0253	131.5	3.76	0.0000	32.0
N-Glycan degradation	16	25	4.65	0.0000	27.0	3.28	0.0000	139.0
Carboxypeptidase activity	38	26	4.34	0.0000	36.0	3.32	0.0000	133.0
G-Protein Coupled Receptors Signaling PathwayFinder	95	38	3.96	0.0000	51.0	3.38	0.0000	118.0
Monocyte differentiation	12	25	2.88	0.0253	131.5	3.74	0.0000	38.0
Cell-matrix adhesion	54	30	3.09	0.0160	94.5	3.51	0.0000	78.0
Cell-substrate adhesion	54	30	3.09	0.0160	94.5	3.51	0.0000	78.0
Glycolipid metabolism	21	29	2.88	0.0253	131.5	3.70	0.0000	42.0
Receptor complex	71	25	3.35	0.0000	67.0	3.42	0.0000	109.0
Pyrimidine metabolism	93	68	-4.89	0.0000	22.0	-3.23	0.0000	154.0
tRNA binding	13	100	-2.88	0.0253	131.5	-3.67	0.0000	47.0
Electron carrier activity	66	76	-5.22	0.0000	14.0	-3.21	0.0000	166.0
Homophilic cell adhesion	92	13	6.36	0.0000	7.0	3.18	0.0000	174.0

Table S2. List of pathways significantly altered when Gal-1 was downregulated in PANC-1 with shGal-1_2 compared to control PANC-1 cells (data from non-infected cells with the genes found altered in the shCtl filtered).

6.1.1.2.1 ECM/Adhesion Molecules

Probes	Mean_1	Mean_3	StDev_1	StDev_3	p-value
DCC	3.4	3.5	0.2	0.2	0.6217
SELP	3.6	3.7	0.3	0.2	0.5455
ITGA6	8.8	8.7	0.2	0.1	0.4659
MMP10	3.3	3.5	0.1	0.0	0.1299
MMP14	7.2	7.3	0.1	0.2	0.4430
ITGA4	3.2	3.2	0.1	0.1	0.5361
ITGAL	4.1	4.2	0.2	0.1	0.8055
ITGB6	3.3	3.3	0.2	0.1	0.6794
PLAT	**5.2**	**5.5**	**0.1**	**0.0**	**0.0116**
THBS1	**6.7**	**7.3**	**0.1**	**0.1**	**0.0017**
MMP2	**8.6**	**8.9**	**0.0**	**0.1**	**0.0088**
MMP15	6.0	6.0	0.1	0.1	0.3143
CASP8	6.3	6.2	0.1	0.1	0.7885
MMP3	3.4	3.5	0.2	0.1	0.4915
HPSE	5.0	4.8	0.2	0.1	0.0947
VCAM1	2.8	3.0	0.0	0.1	0.0968
ITGAX	4.7	4.8	0.1	0.1	0.4859
CTSL1	7.2	7.4	0.1	0.2	0.3944
MMP20	3.5	3.5	0.3	0.2	0.9114
ITGB5	9.9	9.8	0.1	0.0	0.2171
ICAM1	**8.3**	**8.6**	**0.0**	**0.0**	**0.0014**
ITGB7	4.9	5.0	0.2	0.1	0.4195
COL4A2	5.4	5.5	0.2	0.2	0.5671
TIMP2	8.3	8.3	0.1	0.1	0.6175
ITGA2	9.0	8.7	0.2	0.1	0.1697
CNTN1	2.8	2.8	0.1	0.2	0.8895
CD44	9.6	9.5	0.0	0.2	0.2867
MMP11	5.9	6.1	0.2	0.3	0.3902
CASP9	6.9	6.8	0.1	0.1	0.3408

Probes	Mean_1	Mean_3	StDev_1	StDev_3	p-value
CTSD	**10.5**	**11.0**	**0.1**	**0.0**	**0.0002**
TMPRSS4	4.0	4.1	0.2	0.2	0.5934
PLAU	8.7	8.9	0.1	0.1	0.0652
ITGA1	4.2	4.2	0.1	0.1	0.9930
THBS2	4.8	4.9	0.2	0.1	0.3323
TIMP1	10.5	10.6	0.1	0.0	0.2968
FN1	**4.1**	**4.3**	**0.0**	**0.1**	**0.0033**
MMP16	5.0	4.9	0.5	0.3	0.7173
MMP7	3.9	4.0	0.1	0.1	0.5744
MMP26	3.1	3.1	0.2	0.2	0.9552
MMP12	2.6	2.6	0.0	0.1	0.6210
CEACAM5	3.8	3.7	0.2	0.1	0.4556
CDH1	**6.7**	**7.1**	**0.1**	**0.1**	**0.0024**
ITGA11	4.4	4.5	0.2	0.2	0.6270
ITGA10	4.8	4.9	0.0	0.1	0.1407
LAMB1	8.2	8.4	0.1	0.0	0.1367
ITGB8	4.9	4.9	0.1	0.1	0.5095
CST3	**8.7**	**8.9**	**0.1**	**0.1**	**0.0351**
MMP24	5.5	5.6	0.1	0.1	0.3423
ITGAV	**9.6**	**10.0**	**0.2**	**0.0**	**0.0434**
ECM1	5.3	5.4	0.2	0.1	0.4760
CTNNB1	**9.5**	**8.9**	**0.2**	**0.1**	**0.0361**
ITGB3	7.2	7.2	0.1	0.1	0.4414
SELE	3.3	3.5	0.1	0.2	0.1832
THBS3	7.0	7.2	0.1	0.2	0.1977
CTSG	3.9	4.0	0.1	0.1	0.1985
MMP17	6.6	6.6	0.1	0.1	0.7467
CTNND2	4.9	5.0	0.2	0.1	0.5004
CTSB	9.3	9.4	0.0	0.0	0.0063
SPARC	10.0	10.0	0.2	0.1	0.6043

Probes	Mean_1	Mean_3	StDev_1	StDev_3	p-value
PLAUR	6.0	6.1	0.1	0.0	0.5651
ITGA5	8.3	8.4	0.0	0.1	0.1287
MGEA5	8.1	7.9	0.0	0.1	0.0662
ITGA9	**4.6**	**4.7**	**0.2**	**0.1**	**0.6449**
COL1A1	7.3	7.5	0.1	0.1	0.0798
TIMP3	4.7	4.9	0.1	0.1	0.0591
COL18A1	9.1	9.4	0.1	0.1	0.0189
MMP13	3.0	3.0	0.1	0.2	0.9891
SERPINB2	3.4	3.3	0.3	0.1	0.8078
SPP1	3.5	3.7	0.1	0.1	0.0815
ITGA2B	5.4	5.5	0.2	0.2	0.3931
ITGA8	3.1	3.2	0.2	0.1	0.6623
ITGAM	4.4	4.5	0.1	0.1	0.6165
NCAM1	4.2	4.3	0.1	0.2	0.5490
NRCAM	3.0	3.1	0.2	0.1	0.6418
CTNNAL1	7.6	7.3	0.2	0.4	0.2559
MMP27	3.0	3.1	0.1	0.2	0.5155
FGB	3.2	3.3	0.2	0.2	0.4964
ITGB2	5.8	6.0	0.2	0.1	0.1872
CTNND1	9.1	9.0	0.1	0.1	0.2415
LAMC1	8.4	8.3	0.1	0.1	0.5695
ITGA7	5.2	5.3	0.2	0.1	0.4986
MMP9	5.1	5.3	0.3	0.3	0.5461
SELL	3.1	3.0	0.2	0.0	0.6066
ITGB4	6.6	7.0	0.1	0.0	0.0061
ITGB1	9.7	9.7	0.1	0.1	0.7534
SERPINE1	10.1	10.4	0.0	0.1	0.1043
ITGA3	9.7	10.2	0.0	0.0	0.0003
ADAMTS8	5.9	5.9	0.2	0.3	0.9906
SERPINB5	2.5	2.7	0.2	0.0	0.1909

Probes	Mean_1	Mean_3	StDev_1	StDev_3	p-value
ADAMTS1	4.7	4.9	0.1	0.2	0.1456
VTN	5.0	5.0	0.2	0.2	0.8932
CAV1	9.5	9.4	0.1	0.1	0.4509
CTNNA1	9.1	9.1	0.0	0.1	0.7066
MMP1	3.7	3.7	0.2	0.1	0.9093
PECAM1	3.8	3.7	0.1	0.1	0.5786

Table S3. List of genes in the ECM/Adhesion Molecules (First to be altered in the S2 list) from PANC-1 control cells to shGal-1_2. Genes significantly altered ($p<0.05$) are highlighted in grey.

6.1.2 PANC-1 Ctl-shSC Compared to shGal-1_5

6.1.2.1 Gene detailed analysis in PANC-1 shGal-1_5

logFC	AveExpr	adj.P.Val	unlist.symbol	Gene description
-2,631	4,91453	2,94E-010	TRY6	trypsinogen C
1,686	6,17897	1,20E-009	KIAA0953	KIAA0953
2,303	5,47493	1,20E-009	ARHGEF6	Rac/Cdc42 guanine nucleotide exchange factor (GEF) 6
-2,55	6,47404	1,20E-009	AREG	amphiregulin (schwannoma-derived growth factor) (AREG), mRNA
-1,707	8,11955	3,89E-009	EGR1	early growth response 1
-2,609	6,47821	4,07E-009	EREG	epiregulin
1,965	6,00939	4,47E-009	TSPAN18	tetraspanin 18
1,549	**5,85564**	**4,47E-009**	**TGFBR3**	**transforming growth factor, beta receptor III**
1,462	5,74855	4,47E-009	SORBS1	sorbin and SH3 domain containing 1
1,564	8,79409	6,76E-009	ARRB1	arrestin, beta 1
-1,991	6,79946	7,17E-009	CES1	carboxylesterase 1 (monocyte/macrophage serine esterase 1)
1,373	5,55321	7,77E-009	CACNA1D	calcium channel, voltage-dependent, L type, alpha 1D subunit
2,585	7,76637	1,22E-008	EDG7	endothelial differentiation, lysophosphatidic acid G-protein-coupled receptor, 7
1,743	6,53218	1,64E-008	SH3BGRL2	SH3 domain binding glutamic acid-rich protein like 2
-1,415	5,18606	1,64E-008	TMC5	transmembrane channel-like 5
1,531	7,76228	2,19E-008	ATP2B4	ATPase, Ca++ transporting, plasma membrane 4
2,684	5,11517	3,29E-008	TSHZ3	teashirt zinc finger homeobox 3
-2,06	6,08834	4,03E-008	ANKRD1	ankyrin repeat domain 1 (cardiac muscle)
-2,213	4,63471	4,14E-008	TRY6	trypsinogen C
1,728	6,56913	4,42E-008	ST6GALNAC2	ST6 (alpha-N-acetyl-neuraminyl-2,3-beta-galactosyl-1,3)-N-acetylgalactosaminide alpha-2,6-sialyltransferase 2
1,356	5,35329	4,42E-008	ABCA1	ATP-binding cassette, sub-family A (ABC1), member 1

logFC	AveExpr	adj.P.Val	unlist.symbol	Gene description
2,057	5,81945	4,42E-008	KIAA1822L	KIAA1822-like
1,036	7,99398	4,42E-008	PTK7	PTK7 protein tyrosine kinase 7
-1,821	7,28358	4,67E-008	RBM35A	RNA binding motif protein 35A
1,58	6,25314	4,89E-008	ATP8B1	ATPase, Class I, type 8B, member 1
1,759	5,77531	5,99E-008	GJB2	gap junction protein, beta 2, 26kDa
1,587	5,80301	6,09E-008	GRIN2A	glutamate receptor, ionotropic, N-methyl D-aspartate 2A
1,506	8,20277	6,41E-008	OPN3	opsin 3 (encephalopsin, panopsin)
1,253	5,78627	6,79E-008	CAMK1D	calcium/calmodulin-dependent protein kinase ID
1,297	7,78241	6,79E-008	PRKAA2	protein kinase, AMP-activated, alpha 2 catalytic subunit
-2,202	4,39662	7,78E-008	CALB2	calbindin 2, 29kDa (calretinin)
-1,16	7,34779	8,24E-008	CKMT1B	creatine kinase, mitochondrial 1B
1,956	6,98065	1,17E-007	DEPDC6	DEP domain containing 6
-1,683	5,8503	1,37E-007	EXPH5	exophilin 5
1,691	6,44451	1,37E-007	NFATC2	nuclear factor of activated T-cells, cytoplasmic, calcineurin-dependent 2
1,404	8,93361	1,69E-007	SERINC5	serine incorporator 5
-1,512	6,98102	2,24E-007	DMKN	dermokine
1,194	6,89716	2,24E-007	SSBP3	single stranded DNA binding protein 3
1,664	5,412	2,27E-007	PLEKHH2	pleckstrin homology domain containing, family H (with MyTH4 domain) member 2
1,777	7,60324	2,45E-007	NEBL	nebulette
1,99	5,92126	2,90E-007	SLC2A12	solute carrier family 2 (facilitated glucose transporter), member 12
1,609	5,69391	3,20E-007	MXRA5	matrix-remodelling associated 5
1,368	8,14618	3,57E-007	GPR177	G protein-coupled receptor 177
1,221	6,86572	3,57E-007	EML1	echinoderm microtubule associated protein like 1
-1,183	7,56336	3,57E-007	CKMT1A	creatine kinase, mitochondrial 1A (CKMT1A), nuclear gene encoding mitochondrial protein, mRNA
-1,024	8,29767	3,68E-007	LSR	lipolysis stimulated lipoprotein receptor
1,043	5,9693	4,63E-007	RNF144B	ring finger 144B
0,92	7,9516	4,63E-007	PLXND1	plexin D1
-1,412	5,8439	4,63E-007	TRY6	trypsinogen C
1,164	8,45835	4,80E-007	SLC4A11	solute carrier family 4, sodium borate transporter, member 11
1,163	6,41168	4,80E-007	PELI1	pellino homolog 1 (Drosophila)
1,275	6,2221	4,89E-007	ADAMTS15	ADAM metallopeptidase with thrombospondin type 1 motif, 15
1,36	6,21375	5,22E-007	GABBR2	gamma-aminobutyric acid (GABA) B receptor, 2
0,949	**8,2146**	**5,35E-007**	**TOB1**	**transducer of ERBB2, 1**
1,094	7,02632	5,81E-007	TBC1D2B	TBC1 domain family, member 2B
-1,525	6,16613	6,08E-007	BSPRY	B-box and SPRY domain containing
-1,467	6,27257	6,08E-007	PON3	paraoxonase 3
1,271	7,02685	6,38E-007	SDK1	sidekick homolog 1, cell adhesion molecule (chicken)
-1,113	7,21414	7,02E-007	MAPK13	mitogen-activated protein kinase 13
1,254	7,17573	7,02E-007	AFAP1L2	actin filament associated protein 1-like 2
-1,34	5,09551	7,18E-007	THBD	thrombomodulin
-1,1	7,38395	7,46E-007	DUSP5	dual specificity phosphatase 5

logFC	AveExpr	adj.P.Val	unlist.symbol	Gene description
-1,278	4,53005	8,36E-007	ICA1	islet cell autoantigen 1, 69kDa
1,233	7,17663	8,71E-007	NUAK1	NUAK family, SNF1-like kinase, 1
1,081	4,78251	9,54E-007	GPR155	G protein-coupled receptor 155
1,081	**10,1062**	**9,55E-007**	**TGFBI**	**transforming growth factor, beta-induced, 68kDa**
1,009	6,74662	9,55E-007	ITPR2	inositol 1,4,5-triphosphate receptor, type 2
1,199	6,93852	1,02E-006	BHLHB3	basic helix-loop-helix domain containing, class B, 3
-1,305	8,18735	1,03E-006	IGFBP4	insulin-like growth factor binding protein 4
0,982	7,7511	1,03E-006	CTSH	cathepsin H
0,835	8,91649	1,08E-006	CXXC5	CXXC finger 5
1,114	4,30364	1,18E-006	BMP5	bone morphogenetic protein 5
0,884	6,31633	1,29E-006	USP18	ubiquitin specific peptidase 18
0,955	7,91962	1,33E-006	GLUL	glutamate-ammonia ligase (glutamine synthetase)
-1,059	6,04765	1,47E-006	LRRC16	leucine rich repeat containing 16
1,625	8,41753	1,50E-006	CD24	CD24 molecule
1,447	8,78937	1,51E-006	SLC6A6	solute carrier family 6 (neurotransmitter transporter, taurine), member 6
0,988	5,67356	1,58E-006	SYTL2	synaptotagmin-like 2
1,269	5,49875	1,88E-006	RAB30	RAB30, member RAS oncogene family
-0,853	7,84402	1,88E-006	DSG2	desmoglein 2
0,843	8,45053	1,90E-006	EFHD1	EF-hand domain family, member D1
1,281	6,88262	1,94E-006	TP53INP1	tumor protein p53 inducible nuclear protein 1
-1,512	5,77567	1,98E-006	TNS4	tensin 4
1,546	5,04776	2,29E-006	GJB6	gap junction protein, beta 6
1,306	7,00112	2,29E-006	HIG2	hypoxia-inducible protein 2
0,94	5,97645	2,55E-006	ST5	suppression of tumorigenicity 5
0,862	8,70903	2,76E-006	DUSP1	dual specificity phosphatase 1
-1,037	6,97427	2,92E-006	SUSD2	sushi domain containing 2
1,233	5,79513	2,92E-006	PTPN13	protein tyrosine phosphatase, non-receptor type 13 (APO-1/CD95 (Fas)-associated phosphatase)
1,203	5,28378	2,92E-006	SAMD9	sterile alpha motif domain containing 9
1,061	6,17758	3,01E-006	FOXN3	forkhead box N3
1,258	7,90106	3,07E-006	AYTL1	acyltransferase like 1
-1,035	7,29928	3,14E-006	OSBPL3	oxysterol binding protein-like 3
-0,898	5,73616	3,14E-006	KIAA1244	KIAA1244
-1,191	6,71519	3,33E-006	ST14	suppression of tumorigenicity 14 (colon carcinoma)
0,888	7,47228	3,41E-006	LGR4	leucine-rich repeat-containing G protein-coupled receptor 4
0,693	7,65456	3,45E-006	PODXL	podocalyxin-like
0,812	6,9868	3,63E-006	SLC16A2	solute carrier family 16, member 2 (monocarboxylic acid transporter 8)
1,223	6,68381	3,76E-006	EPB41	erythrocyte membrane protein band 4.1 (elliptocytosis 1, RH-linked)
1,243	6,10595	3,84E-006	FLVCR2	feline leukemia virus subgroup C cellular receptor family, member 2
0,878	8,52375	4,07E-006	NEU1	sialidase 1 (lysosomal sialidase)
1,393	7,60149	4,73E-006	PARP9	poly (ADP-ribose) polymerase family, member 9
1,044	7,82854	4,76E-006	GPR137B	G protein-coupled receptor 137B

logFC	AveExpr	adj.P.Val	unlist.symbol	Gene description
-1,04	5,47471	4,89E-006	FGD4	FYVE, RhoGEF and PH domain containing 4
0,775	6,51967	4,89E-006	SLC47A1	solute carrier family 47, member 1
0,98	7,42187	4,89E-006	SEMA3F	sema domain, immunoglobulin domain (Ig), short basic domain, secreted, (semaphorin) 3F
0,953	5,24697	4,89E-006	MAP2	microtubule-associated protein 2
0,749	8,02662	5,65E-006	TPCN1	two pore segment channel 1
0,988	5,45416	5,71E-006	FAM13A1	family with sequence similarity 13, member A1
-0,719	5,56307	5,83E-006	PCNXL2	pecanex-like 2 (Drosophila)
0,8	6,40481	5,86E-006	LFNG	LFNG O-fucosylpeptide 3-beta-N-acetylglucosaminyltransferase
0,967	5,61071	6,23E-006	PTGIS	prostaglandin I2 (prostacyclin) synthase
-1,504	6,93946	6,25E-006	MAL2	mal, T-cell differentiation protein 2
1,113	5,83244	6,41E-006	SLC44A4	solute carrier family 44, member 4
1,472	6,56516	6,41E-006	SSPN	sarcospan (Kras oncogene-associated gene)
1,178	**9,89512**	**6,90E-006**	**LGALS1**	**lectin, galactoside-binding, soluble, 1 (galectin 1)**
-0,827	6,42598	6,92E-006	SLC12A8	solute carrier family 12 (potassium/chloride transporters), member 8
0,811	7,50179	7,87E-006	HSPA2	heat shock 70kDa protein 2
1,001	6,3507	8,20E-006	TMPRSS2	transmembrane protease, serine 2
1,096	6,18446	8,66E-006	TRPS1	trichorhinophalangeal syndrome I
0,771	7,50067	8,69E-006	NID1	nidogen 1
0,589	9,48973	8,87E-006	CTSB	cathepsin B
-1,647	5,59708	8,88E-006	ANXA3	annexin A3
0,828	8,09843	8,94E-006	AFAP1	actin filament associated protein 1
1,261	7,3444	9,63E-006	CRABP2	cellular retinoic acid binding protein 2
1,116	7,35716	1,00E-005	CTBS	chitobiase, di-N-acetyl-
1,071	5,09865	1,04E-005	STAC	SH3 and cysteine rich domain
0,763	6,13815	1,07E-005	RECK	reversion-inducing-cysteine-rich protein with kazal motifs
0,813	7,60392	1,09E-005	TMEM2	transmembrane protein 2
-0,859	7,12711	1,10E-005	KLF5	Kruppel-like factor 5 (intestinal)
1,146	6,28856	1,18E-005	BMP7	bone morphogenetic protein 7 (osteogenic protein 1)
0,811	5,26339	1,18E-005	UNC5C	unc-5 homolog C (C. elegans)
0,882	6,55536	1,18E-005	EPHX1	epoxide hydrolase 1, microsomal (xenobiotic)
-0,79	4,39413	1,18E-005	COBLL1	COBL-like 1
-0,753	8,18457	1,19E-005	SERINC2	serine incorporator 2
-1,071	3,63821	1,31E-005	WDR69	WD repeat domain 69
1,134	7,48444	1,33E-005	HTRA1	HtrA serine peptidase 1
-1,303	5,43471	1,33E-005	ZNF165	zinc finger protein 165
0,724	5,93714	1,38E-005	PAPSS2	3'-phosphoadenosine 5'-phosphosulfate synthase 2
-1,754	6,52429	1,42E-005	MORC4	MORC family CW-type zinc finger 4
0,695	7,9184	1,49E-005	CD99L2	CD99 molecule-like 2
0,738	9,70008	1,55E-005	TMED10	transmembrane emp24-like trafficking protein 10 (yeast)
-1,43	4,9325	1,55E-005	HOOK1	hook homolog 1 (Drosophila)
1,325	5,89433	1,56E-005	CCL2	chemokine (C-C motif) ligand 2

logFC	AveExpr	adj.P.Val	unlist.symbol	Gene description
1,299	5,62466	1,60E-005	RGS2	regulator of G-protein signaling 2, 24kDa
-0,82	5,66077	1,61E-005	MYO1D	myosin ID
0,84	5,87224	1,65E-005	SLIT3	slit homolog 3 (Drosophila)
0,985	4,93998	1,65E-005	LRAP	leukocyte-derived arginine aminopeptidase
0,805	7,36539	1,65E-005	SPSB1	splA/ryanodine receptor domain and SOCS box containing 1
-1,707	7,93555	1,73E-005	TACSTD1	tumor-associated calcium signal transducer 1
-0,759	6,74586	1,75E-005	FUT8	fucosyltransferase 8 (alpha (1,6) fucosyltransferase)
1,198	5,25434	1,75E-005	C5orf13	chromosome 5 open reading frame 13
-0,818	5,73911	1,80E-005	ADAM19	ADAM metallopeptidase domain 19 (meltrin beta)
0,992	6,7064	1,80E-005	TRIB2	tribbles homolog 2 (Drosophila)
0,935	6,91123	1,89E-005	PGM2L1	phosphoglucomutase 2-like 1
1,305	7,95083	1,89E-005	TXNIP	thioredoxin interacting protein
1,218	6,22701	1,92E-005	MAML2	mastermind-like 2 (Drosophila)
0,99	4,91619	1,92E-005	EFEMP1	EGF-containing fibulin-like extracellular matrix protein 1
0,679	6,81751	1,95E-005	ALDH2	aldehyde dehydrogenase 2 family (mitochondrial)
0,841	3,70015	2,10E-005	ABCA5	ATP-binding cassette, sub-family A (ABC1), member 5
-0,613	7,80915	2,11E-005	FXYD5	FXYD domain containing ion transport regulator 5
-1,11	8,76844	2,11E-005	PEG10	paternally expressed 10
0,899	**5,386**	**2,11E-005**	**DISP1**	**dispatched homolog 1 (Drosophila)**
-1,007	5,62932	2,18E-005	GCH1	GTP cyclohydrolase 1 (dopa-responsive dystonia)
0,87	6,465	2,22E-005	ATXN1	ataxin 1
0,904	6,35299	2,27E-005	CNKSR3	CNKSR family member 3
-0,914	7,9428	2,34E-005	MYEOV	myeloma overexpressed gene (in a subset of t(11;14) positive multiple myelomas)
1,025	7,04636	2,35E-005	PARP14	poly (ADP-ribose) polymerase family, member 14
0,818	4,68229	2,35E-005	ATRNL1	attractin-like 1
-0,738	3,95126	2,35E-005	SLCO4C1	solute carrier organic anion transporter family, member 4C1
0,895	7,85678	2,46E-005	IGFBP2	insulin-like growth factor binding protein 2, 36kDa
1,353	5,32103	2,50E-005	CACNA2D1	calcium channel, voltage-dependent, alpha 2/delta subunit 1
0,81	6,27905	2,50E-005	CCNG2	cyclin G2
-0,935	7,41635	2,54E-005	SPINT1	serine peptidase inhibitor, Kunitz type 1
0,929	4,98412	2,58E-005	LCA5	Leber congenital amaurosis 5
0,872	7,69075	2,65E-005	NA	NA
0,619	9,62385	2,66E-005	ABCC1	ATP-binding cassette, sub-family C (CFTR/MRP), member 1
-0,929	6,02355	2,66E-005	LMO7	LIM domain 7
1,119	4,99503	2,70E-005	FLJ20035	hypothetical protein FLJ20035 (FLJ20035), mRNA
1,126	4,8352	2,78E-005	ASB9	ankyrin repeat and SOCS box-containing 9
1,21	6,23453	3,01E-005	ERO1LB	ERO1-like beta (S. cerevisiae)
1,02	4,23186	3,08E-005	PCDH20	protocadherin 20
0,884	5,87818	3,21E-005	ATP10D	ATPase, Class V, type 10D
0,677	9,01426	3,21E-005	ECE1	endothelin converting enzyme 1
-1,671	4,16426	3,24E-005	ASB4	ankyrin repeat and SOCS box-containing 4
0,612	7,18708	3,29E-005	BTRC	beta-transducin repeat containing

logFC	AveExpr	adj.P.Val	unlist.symbol	Gene description
0,957	7,66944	3,30E-005	IGF1R	insulin-like growth factor 1 receptor
0,715	8,19013	3,38E-005	KIRREL	kin of IRRE like (Drosophila)
0,798	6,41961	3,43E-005	KIAA0922	KIAA0922
1,185	7,35259	3,54E-005	CACHD1	cache domain containing 1
1,343	5,63648	3,68E-005	OASL	2'-5'-oligoadenylate synthetase-like
1,429	6,80574	3,73E-005	PDE5A	phosphodiesterase 5A, cGMP-specific
-0,773	7,1895	3,77E-005	CTGF	connective tissue growth factor
-0,604	7,79301	4,16E-005	NFKB2	nuclear factor of kappa light polypeptide gene enhancer in B-cells 2 (p49/p100)
0,615	6,01814	4,24E-005	AS3MT	arsenic (+3 oxidation state) methyltransferase
0,657	6,2478	4,24E-005	FHL1	four and a half LIM domains 1
-0,862	3,81223	4,28E-005	SGIP1	SH3-domain GRB2-like (endophilin) interacting protein 1
0,629	7,03045	4,33E-005	TMEM112	transmembrane protein 112
-1,105	5,47413	4,34E-005	CA2	carbonic anhydrase II
0,872	5,22162	4,63E-005	ZC3H6	zinc finger CCCH-type containing 6
-0,616	6,57545	5,00E-005	PRDM8	PR domain containing 8
0,815	5,19735	5,16E-005	PALLD	palladin, cytoskeletal associated protein
0,794	10,1459	5,18E-005	PERP	PERP, TP53 apoptosis effector
-0,87	5,85799	5,25E-005	DNAJC6	DnaJ (Hsp40) homolog, subfamily C, member 6
0,956	6,90869	5,42E-005	CYP1B1	cytochrome P450, family 1, subfamily B, polypeptide 1
0,713	8,45999	5,47E-005	IDH2	isocitrate dehydrogenase 2 (NADP+), mitochondrial
-0,97	6,57053	5,49E-005	SLC9A3	solute carrier family 9 (sodium/hydrogen exchanger), member 3
0,648	6,31239	5,64E-005	AMOTL1	angiomotin like 1
-1,168	5,94904	5,64E-005	IRF6	interferon regulatory factor 6
0,934	6,00226	5,67E-005	ITGB3	integrin, beta 3 (platelet glycoprotein IIIa, antigen CD61)
0,631	7,784	5,92E-005	TRAF3IP2	TRAF3 interacting protein 2
0,931	5,58127	5,98E-005	GRAMD3	GRAM domain containing 3
-0,685	7,27044	6,04E-005	RBMS2	RNA binding motif, single stranded interacting protein 2
1,216	7,35822	6,51E-005	IFITM1	interferon induced transmembrane protein 1 (9-27)
-0,92	7,76009	6,53E-005	FOSL1	FOS-like antigen 1
0,815	5,20039	6,92E-005	EPHA7	EPH receptor A7
-0,645	8,96714	7,10E-005	PPM2C	protein phosphatase 2C, magnesium-dependent, catalytic subunit
0,692	5,80881	7,10E-005	GTF2IRD2	GTF2I repeat domain containing 2
0,963	6,41781	7,20E-005	TOX2	TOX high mobility group box family member 2
0,783	7,77519	7,30E-005	HPS3	Hermansky-Pudlak syndrome 3
0,786	4,22631	7,30E-005	SEMA3E	sema domain, immunoglobulin domain (Ig), short basic domain, secreted, (semaphorin) 3E
0,811	4,95002	7,52E-005	ALS2CR8	amyotrophic lateral sclerosis 2 (juvenile) chromosome region, candidate 8
0,757	6,12593	7,56E-005	IFIT2	interferon-induced protein with tetratricopeptide repeats 2
0,725	6,52841	7,81E-005	VASN	vasorin
1,007	6,38613	7,83E-005	IL17RB	interleukin 17 receptor B
0,92	6,50921	7,87E-005	FAM107B	family with sequence similarity 107, member B (FAM107B), mRNA
0,66	7,8215	7,95E-005	TST	thiosulfate sulfurtransferase (rhodanese)

logFC	AveExpr	adj.P.Val	unlist.symbol	Gene description
0,74	8,00729	8,04E-005	EDARADD	EDAR-associated death domain
0,657	6,20759	8,08E-005	ROR2	receptor tyrosine kinase-like orphan receptor 2
0,753	7,56086	8,31E-005	SLC29A4	solute carrier family 29 (nucleoside transporters), member 4
0,718	7,62921	8,75E-005	GPX7	glutathione peroxidase 7
0,577	5,58284	8,83E-005	SLC4A8	solute carrier family 4, sodium bicarbonate cotransporter, member 8
0,961	5,93405	8,84E-005	C8orf37	chromosome 8 open reading frame 37
-0,536	9,04499	8,84E-005	IRAK1	interleukin-1 receptor-associated kinase 1
-0,933	5,58815	9,43E-005	SLC16A14	solute carrier family 16, member 14 (monocarboxylic acid transporter 14)
1,469	5,0674	9,86E-005	PLCL2	phospholipase C-like 2
0,748	8,0457	9,93E-005	TBC1D8	TBC1 domain family, member 8 (with GRAM domain)
-0,903	3,78253	0,0001018	SLC38A4	solute carrier family 38, member 4
0,889	6,32494	0,0001028	GPD1L	glycerol-3-phosphate dehydrogenase 1-like
0,543	9,55483	0,0001057	RHPN2	rhophilin, Rho GTPase binding protein 2
0,968	5,58729	0,0001071	TMEM47	transmembrane protein 47
-0,835	5,69527	0,0001083	ERBB3	v-erb-b2 erythroblastic leukemia viral oncogene homolog 3 (avian)
0,812	9,51758	0,0001089	SH3BGRL3	SH3 domain binding glutamic acid-rich protein like 3
0,581	4,9843	0,0001114	SP110	SP110 nuclear body protein
1,115	5,23736	0,0001128	NA	NA
1,423	6,46171	0,0001154	LIFR	leukemia inhibitory factor receptor alpha
1,139	5,98279	0,0001186	NAPE-PLD	N-acyl-phosphatidylethanolamine-hydrolyzing phospholipase D
0,766	7,89312	0,0001204	MLXIP	MLX interacting protein
0,648	5,8896	0,0001204	KRT15	keratin 15
0,486	7,3246	0,0001214	TSC22D1	TSC22 domain family, member 1
0,734	6,79441	0,0001214	ARHGEF3	Rho guanine nucleotide exchange factor (GEF) 3
0,673	7,13787	0,0001214	C11orf54	chromosome 11 open reading frame 54
0,53	8,81461	0,0001239	EPHB4	EPH receptor B4
0,928	7,01043	0,0001242	PIK3R3	phosphoinositide-3-kinase, regulatory subunit 3 (p55, gamma)
0,774	7,29674	0,0001249	RAB26	RAB26, member RAS oncogene family
0,712	6,10249	0,000125	DZIP1	DAZ interacting protein 1
0,8	8,36175	0,000125	LGALS8	lectin, galactoside-binding, soluble, 8 (galectin 8)
0,779	5,23665	0,0001271	SCNN1G	sodium channel, nonvoltage-gated 1, gamma
-0,993	7,28155	0,0001278	ALCAM	activated leukocyte cell adhesion molecule
0,851	6,64498	0,0001278	ARTS-1	type 1 tumor necrosis factor receptor shedding aminopeptidase regulator
0,867	7,21064	0,000129	SEMA3A	sema domain, immunoglobulin domain (Ig), short basic domain, secreted, (semaphorin) 3A
0,797	8,13395	0,0001318	ERGIC1	endoplasmic reticulum-golgi intermediate compartment (ERGIC) 1
0,57	7,528	0,0001318	ABLIM1	actin binding LIM protein 1
1,089	7,23574	0,0001318	HIST2H4B	histone cluster 2, H4b
-1,091	5,91314	0,0001328	FOS	v-fos FBJ murine osteosarcoma viral oncogene homolog
0,664	3,81073	0,0001328	C5	complement component 5
-0,613	**7,78972**	**0,0001362**	**PLAU**	**plasminogen activator, urokinase**
0,584	8,52625	0,0001362	SH3BGRL	SH3 domain binding glutamic acid-rich protein like

logFC	AveExpr	adj.P.Val	unlist.symbol	Gene description
-0,624	5,26893	0,0001395	RICH2	Rho-type GTPase-activating protein RICH2
0,69	8,15797	0,0001433	TNS3	tensin 3
-0,686	7,78838	0,0001453	ATF4	activating transcription factor 4 (tax-responsive enhancer element B67)
1,268	8,268	0,0001498	IFI6	interferon, alpha-inducible protein 6
0,712	6,9962	0,0001535	KCNMA1	potassium large conductance calcium-activated channel, subfamily M, alpha member 1
0,632	6,44829	0,0001535	THBS3	thrombospondin 3
-0,698	4,90581	0,0001535	EPB41L4A	erythrocyte membrane protein band 4.1 like 4A
0,882	4,46357	0,0001544	CTSO	cathepsin O
0,582	8,0583	0,0001567	KDELC2	KDEL (Lys-Asp-Glu-Leu) containing 2
1,232	7,61756	0,0001614	TRERF1	transcriptional regulating factor 1 (TRERF1), mRNA
1,067	5,21283	0,0001618	CCL5	chemokine (C-C motif) ligand 5
0,729	9,58541	0,0001632	CKB	creatine kinase, brain
0,77	6,69797	0,0001638	PPAP2A	phosphatidic acid phosphatase type 2A
-1,013	4,9268	0,0001639	SLAIN1	SLAIN motif family, member 1
0,721	5,64144	0,0001647	RET	ret proto-oncogene
-0,66	7,94868	0,0001723	STAM	signal transducing adaptor molecule (SH3 domain and ITAM motif) 1
0,649	6,50507	0,000175	ACSS1	acyl-CoA synthetase short-chain family member 1
0,59	7,36015	0,0001813	ABHD6	abhydrolase domain containing 6
0,543	7,01886	0,000182	LRRK1	leucine-rich repeat kinase 1
-0,962	5,51823	0,0001827	PADI1	peptidyl arginine deiminase, type I
0,6	8,19669	0,0001827	OSBPL10	oxysterol binding protein-like 10
0,867	6,54139	0,0001827	OLFML2A	olfactomedin-like 2A
0,571	7,61407	0,0001835	HOXC13	homeobox C13
1,055	4,16756	0,0001835	P2RY5	purinergic receptor P2Y, G-protein coupled, 5
-0,821	7,24501	0,0001836	SMOX	spermine oxidase
0,843	6,53552	0,0001883	DDX58	DEAD (Asp-Glu-Ala-Asp) box polypeptide 58
0,74	7,32041	0,000192	TSKU	tsukushin
-0,563	7,83887	0,000192	CXCL1	chemokine (C-X-C motif) ligand 1 (melanoma growth stimulating activity, alpha)
0,639	8,59865	0,0001924	TSPAN5	tetraspanin 5
0,7	8,38985	0,0001953	PSPH	phosphoserine phosphatase
1,022	8,74963	0,0001953	ATP1B1	ATPase, Na+/K+ transporting, beta 1 polypeptide
0,68	5,09991	0,000196	CACNB4	calcium channel, voltage-dependent, beta 4 subunit
-0,53	6,50529	0,000196	SCUBE3	signal peptide, CUB domain, EGF-like 3
1,109	6,58983	0,000197	GALM	galactose mutarotase (aldose 1-epimerase)
1,28	3,16606	0,0002024	TSPAN8	tetraspanin 8
-0,704	4,61247	0,0002024	NUP62CL	nucleoporin 62kDa C-terminal like
-0,7	5,69942	0,0002024	FAM84B	family with sequence similarity 84, member B
0,659	5,63883	0,0002095	PDK3	pyruvate dehydrogenase kinase, isozyme 3
0,793	5,27884	0,0002098	ATF7IP2	activating transcription factor 7 interacting protein 2
0,744	7,35262	0,00021	ACSL1	acyl-CoA synthetase long-chain family member 1
-0,628	6,06458	0,00021	C20orf42	chromosome 20 open reading frame 42

logFC	AveExpr	adj.P.Val	unlist.symbol	Gene description
0,769	7,49637	0,0002115	HAPLN3	hyaluronan and proteoglycan link protein 3
0,757	5,6517	0,0002136	ZEB1	zinc finger E-box binding homeobox 1
0,544	7,77803	0,0002141	IGF1R	insulin-like growth factor 1 receptor
0,586	4,47893	0,0002184	LY75	lymphocyte antigen 75
-0,603	8,20912	0,000219	IER3	immediate early response 3
0,952	7,07349	0,000224	RNF182	ring finger protein 182
0,856	9,0922	0,0002252	EML4	echinoderm microtubule associated protein like 4
1,667	6,38038	0,0002258	LXN	latexin
-0,636	5,33186	0,0002392	RALGPS2	Ral GEF with PH domain and SH3 binding motif 2
0,85	7,05436	0,0002413	TCF7L1	transcription factor 7-like 1 (T-cell specific, HMG-box)
0,493	5,95931	0,0002439	EPB41L4B	erythrocyte membrane protein band 4.1 like 4B
0,521	7,18734	0,0002491	GPATCH1	G patch domain containing 1
1,003	7,16018	0,0002515	USP46	ubiquitin specific peptidase 46
1,164	5,73244	0,0002538	CLK4	CDC-like kinase 4
0,94	5,99449	0,0002538	TMEM171	transmembrane protein 171
0,69	8,80222	0,0002603	CRIP2	cysteine-rich protein 2
1,067	5,75996	0,0002603	SCNN1B	sodium channel, nonvoltage-gated 1, beta (Liddle syndrome)
0,751	4,31487	0,0002607	SLC46A3	solute carrier family 46, member 3
0,574	7,14866	0,0002643	PLCE1	phospholipase C, epsilon 1
-0,553	9,11569	0,0002643	RPL23	ribosomal protein L23
1,382	4,77542	0,0002643	C5orf13	chromosome 5 open reading frame 13
0,801	5,26896	0,0002688	PLD1	phospholipase D1, phosphatidylcholine-specific
-0,666	5,52683	0,0002783	FST	follistatin
-0,556	7,35042	0,0002791	RFFL	ring finger and FYVE-like domain containing 1
0,749	6,42903	0,0002791	FAM46C	family with sequence similarity 46, member C
-1,054	4,40215	0,0002798	NA	NA
-0,638	6,35671	0,0002814	MLSTD1	male sterility domain containing 1
0,783	4,72108	0,0002868	CGNL1	cingulin-like 1
-0,94	4,58328	0,0002893	SERPINB5	serpin peptidase inhibitor, clade B (ovalbumin), member 5
-0,575	7,91411	0,0002904	FAM43A	family with sequence similarity 43, member A
-1,24	6,24359	0,0002952	CHAC1	ChaC, cation transport regulator homolog 1 (E. coli)
0,79	8,07061	0,0002983	VPS41	vacuolar protein sorting 41 homolog (S. cerevisiae)
0,7	6,55013	0,0003033	RASL11A	RAS-like, family 11, member A
0,903	5,56987	0,0003089	CREB3L1	cAMP responsive element binding protein 3-like 1
0,653	6,57814	0,0003089	PREX1	phosphatidylinositol 3,4,5-trisphosphate-dependent RAC exchanger 1
-0,541	4,73803	0,0003186	MTAP	methylthioadenosine phosphorylase
0,555	6,56649	0,0003326	ZDHHC14	zinc finger, DHHC-type containing 14
-0,989	4,19591	0,0003333	GALNT3	UDP-N-acetyl-alpha-D-galactosamine:polypeptide N-acetylgalactosaminyltransferase 3 (GalNAc-T3)
0,694	6,11667	0,0003426	FZD3	frizzled homolog 3 (Drosophila)
-1,062	5,91624	0,0003466	CLDN1	claudin 1
-0,594	6,4816	0,0003537	CENTA2	centaurin, alpha 2

logFC	AveExpr	adj.P.Val	unlist.symbol	Gene description
0,983	7,70312	0,0003609	TIA1	TIA1 cytotoxic granule-associated RNA binding protein
-0,8	7,09581	0,0003609	PRSS22	protease, serine, 22
0,401	10,8282	0,0003609	PSAP	prosaposin (variant Gaucher disease and variant metachromatic leukodystrophy)
-1,035	2,65294	0,0003609	FUT9	fucosyltransferase 9 (alpha (1,3) fucosyltransferase)
-0,812	6,55092	0,000365	UPP1	uridine phosphorylase 1
-0,619	4,15985	0,0003662	NPL	N-acetylneuraminate pyruvate lyase (dihydrodipicolinate synthase)
0,874	4,23525	0,0003674	GPR64	G protein-coupled receptor 64
0,547	7,55997	0,0003757	CHDH	choline dehydrogenase
0,556	5,38711	0,0003965	RCBTB2	regulator of chromosome condensation (RCC1) and BTB (POZ) domain containing protein 2
0,943	6,32176	0,0004008	ENC1	ectodermal-neural cortex (with BTB-like domain)
0,797	5,71845	0,0004139	GNAI1	guanine nucleotide binding protein (G protein), alpha inhibiting activity polypeptide 1
-0,723	3,64124	0,0004146	MTMR8	myotubularin related protein 8
0,622	8,32772	0,0004282	RCP9	calcitonin gene-related peptide-receptor component protein
-0,725	5,00217	0,0004303	SERPINB8	serpin peptidase inhibitor, clade B (ovalbumin), member 8
-0,511	6,89838	0,0004322	ARHGAP8	Rho GTPase activating protein 8
-0,548	6,69067	0,000457	CLMN	calmin (calponin-like, transmembrane)
0,526	7,35635	0,000457	PTGFRN	prostaglandin F2 receptor negative regulator
0,636	6,58359	0,0004627	CBR4	carbonyl reductase 4
0,873	7,10565	0,0004824	HOXC12	homeobox C12
0,738	5,62585	0,0004824	TMEM117	transmembrane protein 117 (TMEM117), mRNA
0,795	5,49844	0,0005003	TRIM6-TRIM34	tripartite motif-containing 6 and tripartite motif-containing 34
0,892	3,79029	0,0005078	KMO	kynurenine 3-monooxygenase (kynurenine 3-hydroxylase)
0,46	5,67074	0,0005226	ACACB	acetyl-Coenzyme A carboxylase beta
-0,437	8,78374	0,0005285	ARD1A	ARD1 homolog A, N-acetyltransferase (S. cerevisiae)
-0,966	4,63073	0,0005309	SLC27A2	solute carrier family 27 (fatty acid transporter), member 2
-0,521	5,67379	0,000534	MARCH9	membrane-associated ring finger (C3HC4) 9
0,618	8,64871	0,0005347	MXRA8	matrix-remodelling associated 8
-0,525	6,27841	0,0005347	WWC1	WW and C2 domain containing 1
-1,703	3,36239	0,0005517	OR10H3	olfactory receptor, family 10, subfamily H, member 3
1,355	7,03629	0,0005522	HIST2H4B	histone cluster 2, H4b
0,457	7,93284	0,0005657	INPP5A	inositol polyphosphate-5-phosphatase, 40kDa
0,613	7,67913	0,0005657	GLCCI1	glucocorticoid induced transcript 1
1,301	6,1607	0,0005774	HIST1H2BD	histone cluster 1, H2bd
0,776	7,29119	0,0005818	FAHD1	fumarylacetoacetate hydrolase domain containing 1
0,688	5,72489	0,0005918	MAP3K5	mitogen-activated protein kinase kinase kinase 5
0,66	4,42751	0,0005955	CPS1	carbamoyl-phosphate synthetase 1, mitochondrial
0,552	5,83487	0,0005955	GRHL3	grainyhead-like 3 (Drosophila)
0,53	7,69247	0,0005955	KCTD14	potassium channel tetramerisation domain containing 14
-0,762	7,94779	0,0006133	ZFP36	zinc finger protein 36, C3H type, homolog (mouse)
0,799	7,29821	0,0006135	CNOT6	CCR4-NOT transcription complex, subunit 6
-0,572	9,18208	0,0006135	LIPA	lipase A, lysosomal acid, cholesterol esterase (Wolman disease)

logFC	AveExpr	adj.P.Val	unlist.symbol	Gene description
0,817	5,61421	0,0006141	SLC38A3	solute carrier family 38, member 3
-0,591	4,974	0,0006345	NA	NA
-0,634	5,32011	0,0006345	GPR110	G protein-coupled receptor 110
0,567	6,67445	0,0006352	MGC24039	hypothetical protein MGC24039
-0,668	9,67837	0,0006352	SLC2A1	solute carrier family 2 (facilitated glucose transporter), member 1
-0,911	7,73027	0,0006451	AK3L1	adenylate kinase 3-like 1
0,596	7,47309	0,0006451	TP53I11	tumor protein p53 inducible protein 11
0,53	5,68565	0,0006451	HFE	hemochromatosis
-1,039	3,32227	0,000646	CCR2	chemokine (C-C motif) receptor 2
0,483	6,45896	0,0006512	CRYL1	crystallin, lambda 1
0,605	6,33772	0,0006518	ST6GAL1	ST6 beta-galactosamide alpha-2,6-sialyltranferase 1
-0,511	7,00589	0,0006518	LRRC61	leucine rich repeat containing 61
-0,752	7,34612	0,0006518	SIX3	SIX homeobox 3
0,782	8,07337	0,0006534	HIST2H2BE	histone cluster 2, H2be
0,838	6,70466	0,0006613	MSX2	msh homeobox 2
0,811	5,75972	0,0006667	ZNF597	zinc finger protein 597
0,816	8,14335	0,0006693	PLOD2	procollagen-lysine, 2-oxoglutarate 5-dioxygenase 2
0,611	6,0166	0,0006773	FAM81A	family with sequence similarity 81, member A
0,57	7,28613	0,0006777	KIAA1706	KIAA1706 protein
0,683	7,5445	0,0006802	PLCXD1	phosphatidylinositol-specific phospholipase C, X domain containing 1
0,652	7,3607	0,0006823	GPRC5B	G protein-coupled receptor, family C, group 5, member B
-0,652	8,1108	0,0006824	HMGA2	high mobility group AT-hook 2
-0,507	5,9563	0,0006869	CXCL3	chemokine (C-X-C motif) ligand 3
0,564	6,97404	0,0006906	CTHRC1	collagen triple helix repeat containing 1
0,645	7,90753	0,0007068	CHKA	choline kinase alpha
0,448	7,14924	0,0007068	COQ10A	coenzyme Q10 homolog A (S. cerevisiae)
0,782	4,95531	0,000723	PPP1R3C	protein phosphatase 1, regulatory (inhibitor) subunit 3C
0,49	7,06178	0,0007459	ANKRD25	ankyrin repeat domain 25
0,805	7,65601	0,0007459	TRIM24	tripartite motif-containing 24
0,566	6,3962	0,0007496	FANK1	fibronectin type III and ankyrin repeat domains 1
0,963	6,67364	0,0007496	TRPC1	transient receptor potential cation channel, subfamily C, member 1
-0,384	8,54168	0,0007507	EMD	emerin (Emery-Dreifuss muscular dystrophy)
0,856	6,74365	0,0007525	CHN1	chimerin (chimaerin) 1
0,628	6,70962	0,000765	ARSD	arylsulfatase D
-1,04	3,19386	0,000765	NUDT9P1	nudix (nucleoside diphosphate linked moiety X)-type motif 9 pseudogene 1
0,782	6,86719	0,000771	POLA1	polymerase (DNA directed), alpha 1
0,603	6,25902	0,000798	KIAA0831	KIAA0831 (KIAA0831), mRNA
0,51	5,40192	0,0007985	PLA2R1	phospholipase A2 receptor 1, 180kDa
0,633	6,69418	0,0007991	TMEM186	transmembrane protein 186 (TMEM186), mRNA
-0,611	6,29265	0,0008117	CDC42EP3	CDC42 effector protein (Rho GTPase binding) 3
-0,701	6,45713	0,0008189	GGTLA1	gamma-glutamyltransferase-like activity 1

logFC	AveExpr	adj.P.Val	unlist.symbol	Gene description
-0,648	8,11666	0,0008242	TESK1	testis-specific kinase 1
0,952	6,99348	0,0008721	COMMD10	COMM domain containing 10
0,626	6,72027	0,0008801	CFLAR	CASP8 and FADD-like apoptosis regulator
0,4	7,4805	0,0008801	DOCK1	dedicator of cytokinesis 1
0,705	8,1111	0,0008821	HS2ST1	heparan sulfate 2-O-sulfotransferase 1
0,858	10,068	0,0008994	TFRC	transferrin receptor (p90, CD71)
0,533	8,50528	0,0009168	MINPP1	multiple inositol polyphosphate histidine phosphatase, 1
-0,594	3,84094	0,0009168	PRKG2	protein kinase, cGMP-dependent, type II
0,494	8,0785	0,0009268	PTPRJ	protein tyrosine phosphatase, receptor type, J
-0,608	7,0901	0,0009268	HK2	hexokinase 2
-0,536	6,17263	0,0009595	NR4A1	nuclear receptor subfamily 4, group A, member 1
0,615	8,2525	0,0009662	GALNT7	UDP-N-acetyl-alpha-D-galactosamine:polypeptide N-acetylgalactosaminyltransferase 7 (GalNAc-T7)
0,569	8,39987	0,0009692	LAMB1	laminin, beta 1
0,549	5,86998	0,0010101	GALNT12	UDP-N-acetyl-alpha-D-galactosamine:polypeptide N-acetylgalactosaminyltransferase 12 (GalNAc-T12)
-0,791	7,86902	0,0010726	LIF	leukemia inhibitory factor (cholinergic differentiation factor)
0,758	7,84746	0,0010802	TSNAX	translin-associated factor X
-0,956	4,49031	0,0010906	SLCO1B3	solute carrier organic anion transporter family, member 1B3
-0,418	6,07207	0,0011049	AARSD1	alanyl-tRNA synthetase domain containing 1
0,734	6,20236	0,001116	CACNG4	calcium channel, voltage-dependent, gamma subunit 4
0,614	9,09116	0,001116	SFXN1	sideroflexin 1
0,469	7,0048	0,0011167	CCDC25	coiled-coil domain containing 25
-0,631	8,01249	0,0011286	ASNS	asparagine synthetase
0,874	3,4193	0,0011377	CALCRL	calcitonin receptor-like
-0,62	6,23044	0,0011488	DDIT3	DNA-damage-inducible transcript 3
-0,684	4,51135	0,0011495	MGC13057	hypothetical protein MGC13057
1,147	5,00846	0,0011599	KRCC1	lysine-rich coiled-coil 1
-0,471	7,05046	0,0011599	GPT2	glutamic pyruvate transaminase (alanine aminotransferase) 2
0,495	8,02434	0,0011765	CFL2	cofilin 2 (muscle)
0,623	8,59201	0,0011863	RNF130	ring finger protein 130
-0,47	5,26475	0,0011866	DCDC2	doublecortin domain containing 2
0,87	7,2866	0,0011866	DTX3L	deltex 3-like (Drosophila)
-0,7	**5,40825**	**0,0012144**	**CCND2**	**cyclin D2**
0,443	6,67406	0,0012164	B3GNT1	UDP-GlcNAc:betaGal beta-1,3-N-acetylglucosaminyltransferase 1
0,571	6,50684	0,0012164	RAB27B	RAB27B, member RAS oncogene family
1,173	3,61041	0,0012164	NA	NA
-0,591	9,23473	0,0012164	ANXA1	annexin A1
0,685	5,10933	0,0012353	ZNF607	zinc finger protein 607
-0,582	6,43932	0,0012373	ZNF503	zinc finger protein 503
0,786	6,44612	0,0012642	LIPH	lipase, member H
0,43	8,66376	0,0012642	SLC12A7	solute carrier family 12 (potassium/chloride transporters), member 7
0,709	3,07807	0,0012642	NA	NA

logFC	AveExpr	adj.P.Val	unlist.symbol	Gene description
-0,565	6,72309	0,001266	HAS3	hyaluronan synthase 3
0,572	**9,22777**	**0,0012692**	**ITGAV**	**integrin, alpha V (vitronectin receptor, alpha polypeptide, antigen CD51)**
0,483	5,84451	0,0012726	RNF128	ring finger protein 128
0,415	8,12343	0,0012726	GLCE	glucuronic acid epimerase
0,534	8,61033	0,0012817	C10orf104	chromosome 10 open reading frame 104
-0,622	6,10561	0,0012936	KRT81	keratin 81
-1,004	5,74065	0,0013024	OVOL2	ovo-like 2 (Drosophila)
-0,75	6,5069	0,0013073	PMAIP1	phorbol-12-myristate-13-acetate-induced protein 1
-0,484	6,6596	0,0013073	OTUB2	OTU domain, ubiquitin aldehyde binding 2
0,726	4,45743	0,0013128	IQCG	IQ motif containing G
0,761	8,01252	0,0013265	SKAP2	src kinase associated phosphoprotein 2
0,665	4,70581	0,0013265	DAB2	disabled homolog 2, mitogen-responsive phosphoprotein (Drosophila)
0,525	6,66194	0,0013311	ARSB	arylsulfatase B
0,553	5,22368	0,0013365	GUCY1A2	guanylate cyclase 1, soluble, alpha 2
0,716	5,26971	0,0013588	ZNF480	zinc finger protein 480
0,925	7,3897	0,0013739	SH3PXD2B	SH3 and PX domains 2B
1,01	4,29037	0,0013842	NA	NA
-0,698	6,7671	0,0014011	PCK2	phosphoenolpyruvate carboxykinase 2 (mitochondrial)
-0,385	7,10576	0,0014112	TNFRSF11A	tumor necrosis factor receptor superfamily, member 11a, NFKB activator
0,531	6,66265	0,0014301	ERCC4	excision repair cross-complementing rodent repair deficiency, complementation group 4
-0,66	4,2724	0,0014556	SLC22A15	solute carrier family 22 (organic cation transporter), member 15
-0,66	7,44975	0,0015084	CTSC	cathepsin C
0,49	6,10398	0,0015698	DSE	dermatan sulfate epimerase
0,37	6,72887	0,0015764	LRRC57	leucine rich repeat containing 57
-0,683	5,24811	0,0015764	GIPC2	GIPC PDZ domain containing family, member 2
0,487	9,06678	0,0015764	LITAF	lipopolysaccharide-induced TNF factor
1,039	4,78181	0,0015813	TMEM133	transmembrane protein 133
-0,467	3,8353	0,0016121	PTPRB	protein tyrosine phosphatase, receptor type, B
0,475	6,51186	0,0016289	CDS1	CDP-diacylglycerol synthase (phosphatidate cytidylyltransferase) 1
-0,455	7,74867	0,001642	STS-1	Cbl-interacting protein Sts-1
-0,814	6,48743	0,001645	SLC7A11	solute carrier family 7, (cationic amino acid transporter, y+ system) member 11
-0,471	6,60265	0,001645	C9orf25	chromosome 9 open reading frame 25
0,755	7,29401	0,0016721	OBSL1	obscurin-like 1
0,408	8,87614	0,0016968	ISYNA1	myo-inositol 1-phosphate synthase A1
0,781	6,7963	0,0017184	OSMR	oncostatin M receptor
0,752	8,27538	0,0017291	SLC12A2	solute carrier family 12 (sodium/potassium/chloride transporters), member 2
0,546	5,88538	0,0017485	ZNF75A	zinc finger protein 75a
0,455	6,08305	0,0017543	PER3	period homolog 3 (Drosophila)
0,507	6,34396	0,0017613	TAOK3	TAO kinase 3
1,093	5,43156	0,0017692	HIST2H2BF	histone cluster 2, H2bf
0,547	9,21635	0,00178	JAK1	Janus kinase 1 (a protein tyrosine kinase)

logFC	AveExpr	adj.P.Val	unlist.symbol	Gene description
-0,516	8,25604	0,00178	CLDN7	claudin 7
0,852	6,38621	0,00178	CX3CL1	chemokine (C-X3-C motif) ligand 1
0,61	7,358	0,00178	SAT1	spermidine/spermine N1-acetyltransferase 1
-1,191	5,38451	0,00178	FGFBP1	fibroblast growth factor binding protein 1
0,851	7,73388	0,0017831	BMPR2	bone morphogenetic protein receptor, type II (serine/threonine kinase)
0,817	5,94123	0,0017929	THY1	Thy-1 cell surface antigen
0,528	5,24319	0,0018012	PFTK1	PFTAIRE protein kinase 1
0,539	8,01951	0,001808	NCOA3	nuclear receptor coactivator 3
-0,547	8,68293	0,001825	CYR61	cysteine-rich, angiogenic inducer, 61
-0,564	5,04473	0,0018377	RNF212	ring finger protein 212
0,486	7,7775	0,0018462	PAPSS1	3'-phosphoadenosine 5'-phosphosulfate synthase 1
-0,639	7,6315	0,0018491	FABP5	fatty acid binding protein 5 (psoriasis-associated)
-0,734	5,77305	0,0018491	AMIGO2	adhesion molecule with Ig-like domain 2
0,528	7,03754	0,0018593	HBP1	HMG-box transcription factor 1
0,514	6,18327	0,0018594	GTF2IRD2	GTF2I repeat domain containing 2
0,488	6,90216	0,0018738	RAB6B	RAB6B, member RAS oncogene family
0,674	6,41487	0,0018961	C14orf147	chromosome 14 open reading frame 147
0,733	5,65328	0,0018991	GSTM2	glutathione S-transferase M2 (muscle)
-0,733	6,08074	0,0019211	BARX2	BARX homeobox 2
0,614	4,31406	0,001942	LOH11CR2A	loss of heterozygosity, 11, chromosomal region 2, gene A
0,662	5,32737	0,001942	PTGS1	prostaglandin-endoperoxide synthase 1 (prostaglandin G/H synthase and cyclooxygenase)
0,856	4,64577	0,001963	OAS2	2'-5'-oligoadenylate synthetase 2, 69/71kDa
1,085	4,73965	0,0019982	LRFN5	leucine rich repeat and fibronectin type III domain containing 5
-1,518	3,25894	0,0020163	NA	NA
0,428	5,92186	0,0020288	MYLIP	myosin regulatory light chain interacting protein
0,714	5,69659	0,0020288	TIAM2	T-cell lymphoma invasion and metastasis 2
0,561	7,3255	0,0021111	PLCXD1	phosphatidylinositol-specific phospholipase C, X domain containing 1
-0,646	6,5171	0,0021111	CXCL16	chemokine (C-X-C motif) ligand 16
0,639	7,75482	0,002149	YPEL5	yippee-like 5 (Drosophila)
0,358	6,76371	0,0022777	SVIL	supervillin
0,413	7,16644	0,0023185	CHST11	carbohydrate (chondroitin 4) sulfotransferase 11
0,82	8,29005	0,0023275	VDP	vesicle docking protein p115
0,524	4,89248	0,0023362	TMEM26	transmembrane protein 26
-0,767	4,06159	0,0023362	STK33	serine/threonine kinase 33
-0,494	5,26711	0,0023366	SLC7A2	solute carrier family 7 (cationic amino acid transporter, y+ system), member 2
-0,62	4,90236	0,002348	EGR3	early growth response 3
0,517	7,21111	0,0023648	MUC1	mucin 1, cell surface associated
-0,586	5,73972	0,0023684	NA	NA
0,433	6,34284	0,0023802	PLEKHA7	pleckstrin homology domain containing, family A member 7
-0,837	3,71948	0,0024121	GPR160	G protein-coupled receptor 160
0,416	6,72449	0,0024197	THSD4	thrombospondin, type I, domain containing 4

logFC	AveExpr	adj.P.Val	unlist.symbol	Gene description
-0,524	6,66333	0,0024197	UNC13D	unc-13 homolog D (C. elegans)
-0,604	5,24124	0,0024267	C6orf138	chromosome 6 open reading frame 138
-0,481	8,36959	0,002453	PYGL	phosphorylase, glycogen; liver (Hers disease, glycogen storage disease type VI)
-0,643	3,75226	0,0024628	MCTP2	multiple C2 domains, transmembrane 2
-0,408	6,72456	0,0024667	TCEAL4	transcription elongation factor A (SII)-like 4
0,343	9,19057	0,0024677	NME4	non-metastatic cells 4, protein expressed in
0,676	4,26333	0,0024717	DMC1	DMC1 dosage suppressor of mck1 homolog, meiosis-specific homologous recombination (yeast)
1,132	4,366	0,0024788	PCDHB14	protocadherin beta 14
1,013	5,74418	0,0025	PPM1L	protein phosphatase 1 (formerly 2C)-like
-0,583	3,62471	0,0025	ACADL	acyl-Coenzyme A dehydrogenase, long chain
0,467	7,38012	0,0025	CABLES1	Cdk5 and Abl enzyme substrate 1
0,696	6,78603	0,0025224	CDH3	cadherin 3, type 1, P-cadherin (placental)
0,53	6,13795	0,0025441	PLAGL1	pleiomorphic adenoma gene-like 1
-0,661	4,67456	0,0025605	GJB5	gap junction protein, beta 5 (GJB5), mRNA
0,576	6,50469	0,0025692	SEPT6	septin 6
-0,63	5,76182	0,0025847	LAMB3	laminin, beta 3
-0,412	7,205	0,00259	AP1G2	adaptor-related protein complex 1, gamma 2 subunit
0,822	6,87119	0,0026454	SSX2IP	synovial sarcoma, X breakpoint 2 interacting protein
0,532	6,46061	0,0026516	TENC1	tensin like C1 domain containing phosphatase (tensin 2)
0,645	5,3286	0,0026561	KITLG	KIT ligand
0,564	6,0528	0,0026968	PEX12	peroxisomal biogenesis factor 12
-0,78	4,52807	0,0026968	ESX1	ESX homeobox 1
-0,5	6,62013	0,0026968	TINAGL1	tubulointerstitial nephritis antigen-like 1
0,807	7,31133	0,0026968	STXBP5	syntaxin binding protein 5 (tomosyn)
0,39	8,98774	0,0026968	H1F0	H1 histone family, member 0
-0,973	3,94522	0,0026968	ABHD9	abhydrolase domain containing 9
0,603	7,79424	0,0027273	UXS1	UDP-glucuronate decarboxylase 1
0,395	9,14709	0,0027433	ITGB5	integrin, beta 5
0,471	7,77756	0,002748	DMPK	dystrophia myotonica-protein kinase
0,547	4,81039	0,00275	CECR2	cat eye syndrome chromosome region, candidate 2
0,835	5,5861	0,0027544	ARL15	ADP-ribosylation factor-like 15
-0,483	6,82711	0,0028251	RAD51L3	RAD51-like 3 (S. cerevisiae)
-0,684	6,62644	0,0028377	MARVELD3	MARVEL domain containing 3
-0,731	5,25266	0,0028534	NR4A2	nuclear receptor subfamily 4, group A, member 2
0,511	8,01029	0,0028534	NA	NA
0,398	9,06675	0,0028534	GNA12	guanine nucleotide binding protein (G protein) alpha 12
-0,548	6,79767	0,0028626	CD74	CD74 molecule, major histocompatibility complex, class II invariant chain
0,722	6,2674	0,0028932	RAI14	retinoic acid induced 14
0,613	4,94979	0,0029305	IL1R1	interleukin 1 receptor, type I
0,366	8,26628	0,0029305	FAM115A	KIAA0738 gene product (KIAA0738), mRNA
-0,639	5,56805	0,0029632	COBL	cordon-bleu homolog (mouse)

logFC	AveExpr	adj.P.Val	unlist.symbol	Gene description
-0,598	6,21863	0,002988	NFKBIZ	nuclear factor of kappa light polypeptide gene enhancer in B-cells inhibitor, zeta
0,518	4,42975	0,0029943	COL21A1	collagen, type XXI, alpha 1
0,387	8,44729	0,00301	STOM	stomatin
0,413	8,40637	0,00301	TTYH3	tweety homolog 3 (Drosophila)
0,392	7,82158	0,0030127	TGFBR1	transforming growth factor, beta receptor I (activin A receptor type II-like kinase, 53kDa)
-0,891	3,41535	0,0030233	NAP1L3	nucleosome assembly protein 1-like 3
0,523	6,34745	0,0030272	TMEM159	transmembrane protein 159
0,798	5,64477	0,0030761	SDC2	syndecan 2
-0,555	5,94868	0,003115	INHBA	inhibin, beta A
0,417	8,46772	0,0031152	LRP5	low density lipoprotein receptor-related protein 5
-0,524	9,05319	0,0031354	RPL27	ribosomal protein L27
0,501	6,57552	0,0031798	TBX2	T-box 2
0,433	6,5435	0,0031798	ATP8B3	ATPase, Class I, type 8B, member 3
-0,839	5,15541	0,0031882	DGCR14	DiGeorge syndrome critical region gene 14
0,661	4,83344	0,0031999	TCP11L2	t-complex 11 (mouse)-like 2
0,627	6,7435	0,0032043	TRIM23	tripartite motif-containing 23
-0,53	4,25005	0,0032446	MYO5B	myosin VB
-0,575	4,81391	0,0032565	ACOT12	acyl-CoA thioesterase 12
0,493	5,23283	0,0032565	TIAM1	T-cell lymphoma invasion and metastasis 1
0,723	6,9483	0,0034147	RBP1	retinol binding protein 1, cellular
0,36	9,39762	0,0034763	TKT	transketolase (Wernicke-Korsakoff syndrome)
0,54	7,1117	0,0035277	TARBP1	TAR (HIV-1) RNA binding protein 1
0,426	5,95456	0,0035368	ST3GAL3	ST3 beta-galactoside alpha-2,3-sialyltransferase 3
0,546	5,93148	0,0036003	ZNF420	zinc finger protein 420
-0,525	5,10345	0,0036307	SRPX	sushi-repeat-containing protein, X-linked
0,581	6,64705	0,0036595	PDP2	pyruvate dehydrogenase phosphatase isoenzyme 2
0,432	8,86015	0,003681	USP12	ubiquitin specific peptidase 12
-0,416	5,68429	0,0037152	IL28RA	interleukin 28 receptor, alpha (interferon, lambda receptor)
-0,578	6,42705	0,0037695	MPZL3	hypothetical protein LOC196264 (LOC196264), mRNA
0,588	7,39455	0,0037726	RABEP1	rabaptin, RAB GTPase binding effector protein 1
0,68	6,83832	0,0037805	KLHL24	kelch-like 24 (Drosophila)
0,51	8,00836	0,0038069	GNE	glucosamine (UDP-N-acetyl)-2-epimerase/N-acetylmannosamine kinase
-0,5	6,54569	0,0038069	TCEAL3	transcription elongation factor A (SII)-like 3
0,4	5,79991	0,0038185	FAM120C	family with sequence similarity 120C (FAM120C), mRNA
-0,537	4,80535	0,0038185	UST	uronyl-2-sulfotransferase
0,946	6,19292	0,0038737	ZNF322A	zinc finger protein 322A
0,683	6,78806	0,003896	TCEA3	transcription elongation factor A (SII), 3
0,556	6,81431	0,0039102	GARNL4	GTPase activating Rap/RanGAP domain-like 4
-0,889	3,6007	0,003935	FLJ13769	hypothetical protein FLJ13769
-0,584	4,62985	0,0039389	MARK1	MAP/microtubule affinity-regulating kinase 1
-0,507	6,68311	0,0039766	MGC4172	short-chain dehydrogenase/reductase

logFC	AveExpr	adj.P.Val	unlist.symbol	Gene description
0,816	7,04367	0,0039801	SCARNA4	small Cajal body-specific RNA 4
0,751	5,97127	0,0039821	UTRN	utrophin
0,549	6,18437	0,0039941	MANSC1	MANSC domain containing 1
-0,672	3,10374	0,0040305	DP58	cytosolic phosphoprotein DP58
-0,83	3,50859	0,0040394	VNN1	vanin 1
0,75	7,77985	0,0040933	PAM	peptidylglycine alpha-amidating monooxygenase
-1,102	3,17412	0,0041042	NA	NA
0,674	6,72568	0,0041242	HGSNAT	heparan-alpha-glucosaminide N-acetyltransferase
-0,589	3,88986	0,004165	RASGEF1B	RasGEF domain family, member 1B
0,88	6,87187	0,004165	REV3L	REV3-like, catalytic subunit of DNA polymerase zeta (yeast)
0,466	6,60076	0,0041675	PRRG1	proline rich Gla (G-carboxyglutamic acid) 1
0,513	7,16083	0,0041764	SERTAD2	SERTA domain containing 2
-0,496	5,95165	0,0042173	KCNMB4	potassium large conductance calcium-activated channel, subfamily M, beta member 4
0,638	6,94101	0,0042256	QPRT	quinolinate phosphoribosyltransferase (nicotinate-nucleotide pyrophosphorylase (carboxylating))
-0,848	3,55471	0,0042256	TLR6	toll-like receptor 6
-0,417	**6,84093**	**0,0042345**	**PLAUR**	**plasminogen activator, urokinase receptor**
-0,368	5,39715	0,0042345	RAPGEFL1	Rap guanine nucleotide exchange factor (GEF)-like 1
-0,638	5,53377	0,0042345	TLE4	transducin-like enhancer of split 4 (E(sp1) homolog, Drosophila)
-0,464	6,61416	0,0042666	ADCY7	adenylate cyclase 7
0,62	4,71371	0,0042666	ALOX5AP	arachidonate 5-lipoxygenase-activating protein
-0,671	3,69763	0,0042952	FAAH2	fatty acid amide hydrolase 2
0,351	8,62894	0,0042961	FBXO27	F-box protein 27
0,556	5,40835	0,0043095	C18orf37	chromosome 18 open reading frame 37
-0,315	9,43918	0,0043095	ITGA3	integrin, alpha 3 (antigen CD49C, alpha 3 subunit of VLA-3 receptor)
0,609	8,06345	0,0043251	PQLC3	PQ loop repeat containing 3
0,606	4,7525	0,0043866	CTNNA2	catenin (cadherin-associated protein), alpha 2
0,413	7,0928	0,0043866	GAS6	growth arrest-specific 6
0,519	5,04855	0,0043936	ZNF260	zinc finger protein 260
1,376	5,16941	0,0043936	SSTR5	somatostatin receptor 5
0,336	7,11594	0,0044535	RAPGEF1	Rap guanine nucleotide exchange factor (GEF) 1
0,435	7,39497	0,0044768	DECR2	2,4-dienoyl CoA reductase 2, peroxisomal
-0,373	7,23169	0,0045529	EHD1	EH-domain containing 1
-0,309	7,69363	0,0045529	FAM100B	family with sequence similarity 100, member B (FAM100B), mRNA
-0,731	4,21603	0,0045774	NA	NA
-0,327	8,07418	0,0045929	AXL	AXL receptor tyrosine kinase
-0,554	3,49975	0,0046277	SAMD12	sterile alpha motif domain containing 12
-0,666	5,69044	0,004673	CHST6	carbohydrate (N-acetylglucosamine 6-O) sulfotransferase 6
-0,585	5,44796	0,0047283	MAGED4B	melanoma antigen family D, 4B
0,657	5,46377	0,0047306	MB	myoglobin
0,56	6,27242	0,0047625	LRIG2	leucine-rich repeats and immunoglobulin-like domains 2
-0,314	7,79018	0,0047625	FOXQ1	forkhead box Q1

logFC	AveExpr	adj.P.Val	unlist.symbol	Gene description
-0,537	4,38861	0,0048487	NEDD9	neural precursor cell expressed, developmentally down-regulated 9
0,525	6,48799	0,0048487	CDKN2C	cyclin-dependent kinase inhibitor 2C (p18, inhibits CDK4)
0,555	7,95407	0,0048499	S100A3	S100 calcium binding protein A3
0,334	8,29559	0,0048499	UROS	uroporphyrinogen III synthase (congenital erythropoietic porphyria)
-0,563	4,80648	0,0048597	WNT16	wingless-type MMTV integration site family, member 16
0,543	7,23708	0,0048597	TFAP2A	transcription factor AP-2 alpha (activating enhancer binding protein 2 alpha)
0,607	5,39176	0,0048822	TFAP2C	transcription factor AP-2 gamma (activating enhancer binding protein 2 gamma)
-0,609	6,02905	0,0048824	LCN2	lipocalin 2 (oncogene 24p3)
-0,448	5,02299	0,0048995	HERC3	hect domain and RLD 3
-0,595	6,44743	0,0049227	LSM11	LSM11, U7 small nuclear RNA associated
0,401	7,28489	0,0049525	FLJ22662	hypothetical protein FLJ22662
-0,379	7,35075	0,0050186	TGM2	transglutaminase 2 (C polypeptide, protein-glutamine-gamma-glutamyltransferase)
-0,639	5,56179	0,0050443	ASPHD2	aspartate beta-hydroxylase domain containing 2
0,836	8,14969	0,0050598	MYO1B	myosin IB
0,749	5,61137	0,0050925	ZNF713	zinc finger protein 713
-0,373	7,33239	0,0050993	CREB3	cAMP responsive element binding protein 3
0,705	7,04372	0,0051423	ANKMY2	ankyrin repeat and MYND domain containing 2
0,752	5,82234	0,0051941	ZFP62	zinc finger protein 62 homolog (mouse)
0,551	8,95735	0,0052046	ITGA6	integrin, alpha 6
0,357	6,71918	0,0052046	CCNDBP1	cyclin D-type binding-protein 1
0,376	4,48356	0,0052066	RPS6KA5	ribosomal protein S6 kinase, 90kDa, polypeptide 5
0,403	9,90886	0,0052512	ECH1	enoyl Coenzyme A hydratase 1, peroxisomal
0,37	7,0961	0,005257	LTBP1	latent transforming growth factor beta binding protein 1
0,63	6,34148	0,0053278	C1orf63	chromosome 1 open reading frame 63
0,403	8,30489	0,0053796	C17orf70	chromosome 17 open reading frame 70
-0,386	5,24235	0,0054992	ACPL2	acid phosphatase-like 2
0,399	7,66335	0,0054992	MRC2	mannose receptor, C type 2
-0,392	7,07481	0,0054992	H2AFY2	H2A histone family, member Y2
0,611	6,01905	0,005508	RRAGB	Ras-related GTP binding B
0,782	5,20222	0,0055668	RHBDL2	rhomboid, veinlet-like 2 (Drosophila)
0,453	6,73762	0,0055668	CCDC77	coiled-coil domain containing 77
-0,878	2,99688	0,0055878	C6orf142	chromosome 6 open reading frame 142
0,58	7,15201	0,0056082	RIPK1	receptor (TNFRSF)-interacting serine-threonine kinase 1
0,561	5,53275	0,0056082	CTAGE6	CTAGE family, member 6
0,386	9,90634	0,0056404	SLC29A1	solute carrier family 29 (nucleoside transporters), member 1
-0,914	5,56163	0,0056699	FAM105A	family with sequence similarity 105, member A (FAM105A), mRNA
-0,407	6,04935	0,0057083	HOOK2	hook homolog 2 (Drosophila)
0,405	8,23856	0,0058033	NFIX	nuclear factor I/X (CCAAT-binding transcription factor)
0,455	7,71861	0,0058315	KIAA0182	KIAA0182
-0,48	5,62369	0,0058315	SULF2	sulfatase 2
0,559	7,40947	0,0058318	CRBN	cereblon

logFC	AveExpr	adj.P.Val	unlist.symbol	Gene description
0,45	5,21047	0,0059342	TNIK	TRAF2 and NCK interacting kinase
-0,486	4,5432	0,0059605	FBN2	fibrillin 2 (congenital contractural arachnodactyly)
0,535	7,16307	0,0059605	SP4	Sp4 transcription factor
0,445	7,06526	0,0060163	TNRC6A	trinucleotide repeat containing 6A
0,474	8,55734	0,006025	C16orf63	chromosome 16 open reading frame 63
-0,463	6,60742	0,00603	HSD17B1	hydroxysteroid (17-beta) dehydrogenase 1
-0,454	5,33455	0,0060331	ZNF365	zinc finger protein 365
0,356	8,44793	0,0060555	LGMN	legumain
0,835	6,2639	0,0060844	FAM13A1	family with sequence similarity 13, member A1
-0,484	4,10144	0,0060968	ST3GAL6	ST3 beta-galactoside alpha-2,3-sialyltransferase 6
-0,428	3,47625	0,0061171	C3orf15	chromosome 3 open reading frame 15
-0,44	8,00038	0,0061171	CARS	cysteinyl-tRNA synthetase
-0,725	3,98077	0,006176	NRXN1	neurexin 1
-0,537	4,39852	0,006176	SLC15A1	solute carrier family 15 (oligopeptide transporter), member 1
-0,469	5,94107	0,006176	HYI	hydroxypyruvate isomerase homolog (E. coli)
-0,391	8,83709	0,006176	OBFC2B	oligonucleotide/oligosaccharide-binding fold containing 2B
-0,424	4,59961	0,006176	TMTC2	transmembrane and tetratricopeptide repeat containing 2
0,782	4,96738	0,006176	NTN4	netrin 4
-0,569	7,2351	0,0062564	PLEK2	pleckstrin 2
0,547	4,68046	0,0062601	ZNF804A	zinc finger protein 804A
0,419	8,89978	0,0063331	LDB1	LIM domain binding 1
-0,361	4,94507	0,0063331	PTPRG	protein tyrosine phosphatase, receptor type, G
-0,543	7,33873	0,0063331	HSPC159	galectin-related protein
0,796	8,79448	0,0063331	UGDH	UDP-glucose dehydrogenase
-0,804	7,63091	0,0063331	NKX6-2	NK6 homeobox 2
0,709	8,30478	0,0063724	RAD50	RAD50 homolog (S. cerevisiae)
0,332	8,43561	0,0063734	HPCAL1	hippocalcin-like 1
-0,556	5,54327	0,0063941	PIB5PA	phosphatidylinositol (4,5) bisphosphate 5-phosphatase, A
-0,616	4,80837	0,0063941	TMEM163	transmembrane protein 163 (TMEM163), mRNA
-0,917	2,71404	0,0064008	C21orf114	chromosome 21 open reading frame 114
0,282	8,28596	0,0064008	PHF15	PHD finger protein 15
-0,683	5,94095	0,0064008	FGF5	fibroblast growth factor 5
-0,49	4,77752	0,0064008	CPE	carboxypeptidase E
0,315	6,97924	0,0064008	C14orf119	chromosome 14 open reading frame 119
0,445	8,30143	0,0064008	ZC3HAV1L	zinc finger CCCH-type, antiviral 1-like
0,528	5,46071	0,0064008	SLC25A18	solute carrier family 25 (mitochondrial carrier), member 18
0,392	8,3345	0,0064008	TMEPAI	transmembrane, prostate androgen induced RNA
0,292	8,03911	0,0064821	DKK3	dickkopf homolog 3 (Xenopus laevis)
0,664	5,72002	0,0065041	DBT	dihydrolipoamide branched chain transacylase E2
-0,362	7,89275	0,0065041	HOXB8	homeobox B8
-0,574	4,51094	0,0065927	GRB14	growth factor receptor-bound protein 14
0,484	7,0809	0,0066594	JUN	jun oncogene

logFC	AveExpr	adj.P.Val	unlist.symbol	Gene description
-0,631	4,20331	0,0066727	TRHDE	thyrotropin-releasing hormone degrading enzyme
0,488	5,33291	0,0066727	MEIS2	Meis homeobox 2
-0,333	6,78368	0,0067288	KIAA1804	mixed lineage kinase 4
-1,276	3,17807	0,0067508	NA	NA
0,505	6,96088	0,0068093	ZNF436	zinc finger protein 436
-0,429	9,41199	0,0068093	ERRFI1	ERBB receptor feedback inhibitor 1
0,89	4,75684	0,006924	RBM43	RNA binding motif protein 43
0,352	6,65774	0,006924	KIAA1754	KIAA1754 (KIAA1754), mRNA
0,7	6,57264	0,006927	CLK1	CDC-like kinase 1
0,429	5,50947	0,0069942	GPR176	G protein-coupled receptor 176
-0,636	4,96043	0,0070361	SLC16A6	solute carrier family 16, member 6 (monocarboxylic acid transporter 7)
-0,422	5,72312	0,0070361	CAMKV	CaM kinase-like vesicle-associated
1,001	6,28875	0,0070391	IFIT3	interferon-induced protein with tetratricopeptide repeats 3
-0,993	4,42212	0,0070391	FLJ44815	FLJ44815 protein
-0,528	6,07618	0,0070794	PLEKHG6	pleckstrin homology domain containing, family G (with RhoGef domain) member 6
0,402	5,6517	0,0070804	HOMEZ	homeobox and leucine zipper encoding
0,361	7,71921	0,0071552	TRIB1	tribbles homolog 1 (Drosophila)
0,371	6,44134	0,0072054	THNSL2	threonine synthase-like 2 (S. cerevisiae)
0,388	8,78875	0,0072084	ITFG3	integrin alpha FG-GAP repeat containing 3
0,533	6,52762	0,0072248	TUFT1	tuftelin 1
0,481	9,03415	0,007308	PADI2	peptidyl arginine deiminase, type II
-0,603	3,40422	0,0073263	VN1R1	vomeronasal 1 receptor 1
0,407	8,7519	0,0073496	FBXO17	F-box protein 17
-0,709	5,51356	0,0073496	MGST1	microsomal glutathione S-transferase 1
0,949	6,67583	0,007358	NA	NA
-0,87	3,06602	0,0074098	NA	NA
-0,454	4,65219	0,0074302	KIAA1727	KIAA1727 protein
0,401	7,93789	0,0074378	ABHD2	abhydrolase domain containing 2
-0,403	4,55853	0,0074424	TEC	tec protein tyrosine kinase
-0,555	4,84971	0,0074424	KIAA1324L	KIAA1324-like
0,713	7,58337	0,0074424	BAHCC1	BAH domain and coiled-coil containing 1
-0,598	5,19019	0,0074424	GALNT14	UDP-N-acetyl-alpha-D-galactosamine:polypeptide N-acetylgalactosaminyltransferase 14 (GalNAc-T14)
0,461	5,0282	0,0074424	BFSP1	beaded filament structural protein 1, filensin
-0,503	7,33845	0,0074442	DSP	desmoplakin
0,637	6,95757	0,0074462	C21orf66	chromosome 21 open reading frame 66
0,381	7,96278	0,007472	TAPBP	TAP binding protein (tapasin)
0,766	5,13285	0,0074979	LSAMP	limbic system-associated membrane protein
0,621	6,97322	0,0074979	CCDC126	coiled-coil domain containing 126
-0,723	5,67328	0,0075981	BEX2	brain expressed X-linked 2
-0,379	8,99777	0,0076037	RPL36	ribosomal protein L36
-0,585	6,89918	0,0076546	FLJ25801	hypothetical protein FLJ25801 (FLJ25801), mRNA

logFC	AveExpr	adj.P.Val	unlist.symbol	Gene description
0,407	6,28231	0,0076546	ANKH	ankylosis, progressive homolog (mouse)
-0,53	5,53023	0,0077011	FAM50B	family with sequence similarity 50, member B
-0,464	4,83816	0,0078119	FRAS1	Fraser syndrome 1
0,428	6,25005	0,0078122	ISGF3G	interferon-stimulated transcription factor 3, gamma 48kDa
-0,639	6,75197	0,0079388	ANTXR2	anthrax toxin receptor 2
-0,632	3,5276	0,0079959	IL1A	interleukin 1, alpha
0,346	7,2581	0,008012	NRP1	neuropilin 1
-0,276	7,78204	0,0080291	LARP6	La ribonucleoprotein domain family, member 6
0,505	4,85262	0,008037	LOC388335	similar to RIKEN cDNA A730055C05 gene
0,631	6,65551	0,0080619	CASD1	CAS1 domain containing 1
-0,556	4,76573	0,0080832	SRrp35	serine-arginine repressor protein (35 kDa)
0,812	7,1607	0,0081964	TBCE	tubulin folding cofactor E
-0,4	5,01073	0,008205	GLDC	glycine dehydrogenase (decarboxylating)
-0,511	7,55377	0,0082234	TSC22D2	TSC22 domain family, member 2
0,769	7,34004	0,0082554	NA	NA
-0,393	7,70203	0,0082682	P4HA2	procollagen-proline, 2-oxoglutarate 4-dioxygenase (proline 4-hydroxylase), alpha polypeptide II
-0,771	3,88062	0,0082738	HEY2	hairy/enhancer-of-split related with YRPW motif 2
1,104	6,72801	0,0082825	C1orf103	chromosome 1 open reading frame 103
-0,327	10,0914	0,0083387	PRDX5	peroxiredoxin 5
-0,457	7,32198	0,0084438	MERTK	c-mer proto-oncogene tyrosine kinase
-0,653	5,58945	0,0084438	VENTX	VENT homeobox homolog (Xenopus laevis)
-0,603	7,9515	0,0084438	MAP3K10	mitogen-activated protein kinase kinase kinase 10
0,376	5,70091	0,0084531	SHROOM3	shroom family member 3
-0,417	4,03353	0,0084829	PDE4D	phosphodiesterase 4D, cAMP-specific (phosphodiesterase E3 dunce homolog, Drosophila)
0,394	5,611	0,0084829	SGK	serum/glucocorticoid regulated kinase
0,436	6,33901	0,0084829	NPHP3	nephronophthisis 3 (adolescent)
0,388	9,13565	0,0084829	IFITM2	interferon induced transmembrane protein 2 (1-8D)
0,439	5,83142	0,0085037	DET1	de-etiolated homolog 1 (Arabidopsis)
0,44	5,14864	0,0085244	ITGB8	integrin, beta 8
0,573	6,30321	0,0085295	DENND4C	DENN/MADD domain containing 4C
0,746	6,95355	0,0085295	NA	NA
0,48	6,50545	0,0085295	MGST2	microsomal glutathione S-transferase 2
0,515	7,60762	0,0085406	LMAN2L	lectin, mannose-binding 2-like
-0,785	4,87984	0,00858	NRN1	neuritin 1
-0,663	3,49903	0,0086192	RGSL1	regulator of G-protein signaling like 1
0,441	5,02015	0,0086469	SCML1	sex comb on midleg-like 1 (Drosophila)
0,662	7,2888	0,0087465	MBD4	methyl-CpG binding domain protein 4
0,323	4,81488	0,0087556	NSUN7	NOL1/NOP2/Sun domain family, member 7
-0,544	4,59498	0,0088003	TC2N	tandem C2 domains, nuclear
-0,447	5,96913	0,0088306	MCOLN3	mucolipin 3
0,407	5,79516	0,008858	FLJ10986	hypothetical protein FLJ10986 (FLJ10986), mRNA

logFC	AveExpr	adj.P.Val	unlist.symbol	Gene description
-0,848	4,68043	0,0088608	GYPC	glycophorin C (Gerbich blood group)
0,439	6,7698	0,0088608	PSMB9	proteasome (prosome, macropain) subunit, beta type, 9 (large multifunctional peptidase 2)
0,63	6,66617	0,0089418	BVES	blood vessel epicardial substance
0,539	9,05385	0,0089418	CLDN4	claudin 4
-0,544	5,64771	0,008997	MYPN	myopalladin
0,365	7,84009	0,0090306	LRP6	low density lipoprotein receptor-related protein 6
-0,394	5,40379	0,0090306	MCC	mutated in colorectal cancers
0,629	8,03909	0,0090306	MTA3	metastasis associated 1 family, member 3
0,434	6,31344	0,0090495	GRK5	G protein-coupled receptor kinase 5
-0,45	5,75013	0,0090495	DPYSL3	dihydropyrimidinase-like 3
-0,638	4,8488	0,0090495	ALS2CR7	amyotrophic lateral sclerosis 2 (juvenile) chromosome region, candidate 7
0,62	7,30548	0,0091141	TMEM34	transmembrane protein 34
-0,502	4,59199	0,0091141	PDLIM3	PDZ and LIM domain 3
-0,74	4,43385	0,00917	TRIM36	tripartite motif-containing 36
0,47	8,88273	0,0091741	LIMS1	LIM and senescent cell antigen-like domains 1
0,574	6,99126	0,0091741	YTHDC2	YTH domain containing 2
0,395	7,41953	0,0091808	TCF7L2	transcription factor 7-like 2 (T-cell specific, HMG-box)
0,355	7,2827	0,009236	ENTPD4	ectonucleoside triphosphate diphosphohydrolase 4
-0,427	7,01657	0,0092418	GAN	giant axonal neuropathy (gigaxonin)
-0,593	3,21357	0,0092831	TDO2	tryptophan 2,3-dioxygenase
0,572	6,25287	0,0093289	NA	NA
0,28	9,76875	0,0093696	MFGE8	milk fat globule-EGF factor 8 protein
-0,34	7,28469	0,0093696	TPM1	tropomyosin 1 (alpha)
0,301	6,37017	0,0093962	IL6R	interleukin 6 receptor
-0,537	3,92545	0,0094385	BCL2A1	BCL2-related protein A1
0,457	6,03611	0,0094531	FBXO8	F-box protein 8
0,534	6,97396	0,0094655	ETNK1	ethanolamine kinase 1
0,805	8,02387	0,0094848	SFT2D2	SFT2 domain containing 2
0,304	7,28348	0,0095359	DTNB	dystrobrevin, beta
0,357	7,98025	0,0095359	TP53I3	tumor protein p53 inducible protein 3
0,362	6,14876	0,0095404	STX17	syntaxin 17
0,39	8,63962	0,0095563	TSPAN13	tetraspanin 13
0,53	5,74647	0,0095587	CCDC121	coiled-coil domain containing 121
0,542	6,78731	0,0095587	FGF2	fibroblast growth factor 2 (basic) (FGF2), mRNA
-0,903	3,57132	0,0095601	UNQ6125	hypothetical LOC442092
0,567	7,64296	0,0095767	ZAK	sterile alpha motif and leucine zipper containing kinase AZK
0,442	6,44461	0,0095783	ZNF318	zinc finger protein 318
0,31	6,30953	0,0096267	NA	NA
0,459	8,8792	0,0096759	ATF2	activating transcription factor 2
-0,418	5,16373	0,0096759	TSPAN12	tetraspanin 12
-0,733	3,51252	0,0096841	AMY2A	amylase, alpha 2A (pancreatic)

logFC	AveExpr	adj.P.Val	unlist.symbol	Gene description
-0,517	5,89317	0,0096841	HOXA9	homeobox A9
-1,08	3,80867	0,0096976	NA	NA
-1,437	4,15076	0,0097169	NA	NA
0,373	6,27002	0,0097335	SLC30A4	solute carrier family 30 (zinc transporter), member 4
-0,628	4,95501	0,0097335	LBH	limb bud and heart development homolog (mouse)
0,621	4,78946	0,0097651	EDIL3	EGF-like repeats and discoidin I-like domains 3
0,424	5,46212	0,0097845	RASSF5	Ras association (RalGDS/AF-6) domain family 5
0,61	6,9998	0,0098527	NCOA1	nuclear receptor coactivator 1
-0,783	5,77393	0,0098667	ID2	inhibitor of DNA binding 2, dominant negative helix-loop-helix protein
-0,498	4,56586	0,0098788	TMEM168	transmembrane protein 168
-0,769	5,24344	0,0099133	SCG2	secretogranin II (chromogranin C)
-0,751	5,36782	0,0099437	SLC7A4	solute carrier family 7 (cationic amino acid transporter, y+ system), member 4
-0,593	3,46351	0,010009	DPP4	dipeptidyl-peptidase 4 (CD26, adenosine deaminase complexing protein 2)
0,405	5,76868	0,010009	PIGB	phosphatidylinositol glycan anchor biosynthesis, class B
0,524	7,7091	0,0100178	ASS1	argininosuccinate synthetase 1
-0,921	2,48523	0,0100265	NA	NA
0,369	8,34404	0,0100506	RDH11	retinol dehydrogenase 11 (all-trans/9-cis/11-cis)
-0,552	6,43003	0,0100506	KCTD12	potassium channel tetramerisation domain containing 12
-0,407	6,0934	0,0100629	AFAP1L1	actin filament associated protein 1-like 1
-0,498	5,075	0,0101135	JAKMIP1	janus kinase and microtubule interacting protein 1
-0,317	6,82434	0,0101875	TBC1D4	TBC1 domain family, member 4
-0,551	6,19711	0,0102094	KLC3	kinesin light chain 3
-0,58	4,87694	0,0102094	OXSM	3-oxoacyl-ACP synthase, mitochondrial
-0,808	3,47588	0,010229	CCR5	chemokine (C-C motif) receptor 5
-0,336	5,30247	0,0102557	OSBPL6	oxysterol binding protein-like 6
-0,528	4,49907	0,010278	PCSK5	proprotein convertase subtilisin/kexin type 5
-0,381	6,63799	0,0103405	NRG1	neuregulin 1
0,378	8,38593	0,0103677	ECOP	EGFR-coamplified and overexpressed protein
-0,43	3,24536	0,0104629	ABCC9	ATP-binding cassette, sub-family C (CFTR/MRP), member 9
0,715	6,52998	0,0105178	PHACTR2	phosphatase and actin regulator 2
0,53	5,30438	0,0105579	OAS1	2',5'-oligoadenylate synthetase 1, 40/46kDa
0,346	8,67933	0,0105687	ATP6V1B2	ATPase, H+ transporting, lysosomal 56/58kDa, V1 subunit B2
-0,715	2,49208	0,0105732	OR4F5	olfactory receptor, family 4, subfamily F, member 5
-0,325	8,1929	0,0105874	RBM42	RNA binding motif protein 42
-0,559	3,50602	0,0105877	GPR87	G protein-coupled receptor 87
0,342	8,7811	0,010637	CPT1A	carnitine palmitoyltransferase 1A (liver)
-0,489	4,96473	0,0106446	SYK	spleen tyrosine kinase
0,296	7,12075	0,0106803	AK3	adenylate kinase 3
-0,334	4,2178	0,0106803	ABCC2	ATP-binding cassette, sub-family C (CFTR/MRP), member 2
0,417	7,0438	0,0106803	C10orf26	chromosome 10 open reading frame 26
0,436	5,50582	0,0106803	WIPF1	WAS/WASL interacting protein family, member 1

logFC	AveExpr	adj.P.Val	unlist.symbol	Gene description
-0,489	6,00054	0,0107216	MDFI	MyoD family inhibitor
-0,574	5,76866	0,0107389	WFDC2	WAP four-disulfide core domain 2
-1,07	3,55139	0,0107686	MGC15705	hypothetical protein MGC15705
0,369	7,63246	0,0107932	TNFRSF10B	tumor necrosis factor receptor superfamily, member 10b
0,487	7,86209	0,0109471	RNF38	ring finger protein 38
-0,272	8,05245	0,0110721	SLC9A7	solute carrier family 9 (sodium/hydrogen exchanger), member 7
0,262	6,45306	0,0110721	ULK2	unc-51-like kinase 2 (C. elegans)
-0,44	3,71022	0,0111308	AK7	adenylate kinase 7
-0,492	5,04591	0,0112357	KIAA0040	KIAA0040
0,32	7,51239	0,0112457	ANXA4	annexin A4
0,336	7,47683	0,0112554	VPS39	vacuolar protein sorting 39 homolog (S. cerevisiae)
0,345	8,00506	0,0113611	CCNT1	cyclin T1
-0,475	7,04343	0,0113947	GYLTL1B	glycosyltransferase-like 1B
-0,577	3,74278	0,0115639	RANBP17	RAN binding protein 17
-0,411	**6,43369**	**0,0115639**	**DISP2**	**dispatched homolog 2 (Drosophila)**
-0,431	6,00199	0,0116268	DEF6	differentially expressed in FDCP 6 homolog (mouse)
-0,449	5,76297	0,0116724	C10orf83	chromosome 10 open reading frame 83
-0,381	7,03232	0,0117029	SYDE1	synapse defective 1, Rho GTPase, homolog 1 (C. elegans)
-0,698	3,57143	0,0119467	ARHGDIB	Rho GDP dissociation inhibitor (GDI) beta
0,668	6,91074	0,012002	MRPS14	mitochondrial ribosomal protein S14
0,507	4,53327	0,0120304	ZNF605	zinc finger protein 605
-0,66	4,87822	0,012304	D4S234E	DNA segment on chromosome 4 (unique) 234 expressed sequence
0,292	7,54046	0,0123531	BCOR	BCL6 co-repressor
0,417	6,97555	0,0123666	TBCEL	tubulin folding cofactor E-like
0,31	10,6837	0,0123921	HIST1H2BF	histone cluster 1, H2bf
-0,449	8,99438	0,0123921	SLC3A2	solute carrier family 3 (activators of dibasic and neutral amino acid transport), member 2
0,505	6,30196	0,0124745	PRPF39	PRP39 pre-mRNA processing factor 39 homolog (S. cerevisiae)
-0,842	4,49334	0,0126668	RAB38	RAB38, member RAS oncogene family
-0,489	4,17433	0,0126835	PROM1	prominin 1
0,43	4,68254	0,0127179	P4HA3	procollagen-proline, 2-oxoglutarate 4-dioxygenase (proline 4-hydroxylase), alpha polypeptide III
0,362	7,14685	0,0127179	ALPP	alkaline phosphatase, placental (Regan isozyme)
0,52	6,22466	0,0128827	CORO2A	coronin, actin binding protein, 2A
0,528	5,99219	0,0128994	TTC21B	tetratricopeptide repeat domain 21B
1,122	7,14076	0,0128994	CYBRD1	cytochrome b reductase 1
0,524	7,87199	0,01292	PTPN14	protein tyrosine phosphatase, non-receptor type 14
-0,337	6,67881	0,0129342	AP1M2	adaptor-related protein complex 1, mu 2 subunit
0,42	4,441	0,0129482	KLHDC1	kelch domain containing 1
-0,438	4,91296	0,0129822	BCL11A	B-cell CLL/lymphoma 11A (zinc finger protein)
0,433	4,57449	0,0131131	TCBA1	T-cell lymphoma breakpoint associated target 1
0,525	8,00433	0,0131639	LZIC	leucine zipper and CTNNBIP1 domain containing
-0,424	5,48019	0,0132231	CXCL2	chemokine (C-X-C motif) ligand 2

logFC	AveExpr	adj.P.Val	unlist.symbol	Gene description
-0,383	5,88326	0,0132409	ARL10	ADP-ribosylation factor-like 10
0,297	6,83796	0,0132821	PLEKHF1	pleckstrin homology domain containing, family F (with FYVE domain) member 1
-0,445	4,99503	0,0132821	MAGEA12	melanoma antigen family A, 12
-0,377	7,84787	0,0133605	IGFBP6	insulin-like growth factor binding protein 6
-0,622	5,34236	0,0133605	KCNJ8	potassium inwardly-rectifying channel, subfamily J, member 8
-0,522	4,62834	0,0134341	PGBD5	piggyBac transposable element derived 5
-0,617	4,5896	0,0134341	TMEM74	transmembrane protein 74 (TMEM74), mRNA
-0,451	6,35758	0,0135029	EFNB1	ephrin-B1
0,655	5,30458	0,0135601	APOL6	apolipoprotein L, 6
0,756	6,07066	0,0135936	CD58	CD58 molecule
-0,351	5,1675	0,0136822	SNRPN	small nuclear ribonucleoprotein polypeptide N
0,602	7,87086	0,0139245	CTNNBIP1	catenin, beta interacting protein 1
0,374	8,1604	0,014097	CLCN3	chloride channel 3
0,321	9,83525	0,014097	DDX5	DEAD (Asp-Glu-Ala-Asp) box polypeptide 5
-0,336	6,83946	0,0141509	FLJ10769	hypothetical protein FLJ10769
-0,447	4,34075	0,0141509	TSPAN2	tetraspanin 2
0,393	6,12878	0,0142243	ANK1	ankyrin 1, erythrocytic
-0,459	6,34714	0,0142295	COCH	coagulation factor C homolog, cochlin (Limulus polyphemus)
-0,446	4,59073	0,0142507	PGM5	phosphoglucomutase 5
-0,438	8,40848	0,0142507	FAM50A	family with sequence similarity 50, member A
0,416	8,04309	0,0142638	ANTXR1	anthrax toxin receptor 1
-0,288	5,76875	0,0143306	KIAA0746	KIAA0746 protein (KIAA0746), mRNA
0,307	5,85599	0,0143392	MAN1A1	mannosidase, alpha, class 1A, member 1
-1,056	4,72179	0,0144838	TRDN	triadin
0,724	6,32641	0,0145664	TTC14	tetratricopeptide repeat domain 14
0,358	6,97956	0,0145664	TRERF1	transcriptional regulating factor 1
-0,444	6,78715	0,0148402	DENND2D	DENN/MADD domain containing 2D
0,43	7,70834	0,0148402	RBPJ	recombination signal binding protein for immunoglobulin kappa J region
0,37	7,79235	0,0150637	CDKN1A	cyclin-dependent kinase inhibitor 1A (p21, Cip1)
-0,887	4,41168	0,0150637	NA	NA
-1,093	2,6196	0,0150637	OR1L3	olfactory receptor, family 1, subfamily L, member 3
0,459	6,38011	0,0150637	ZNF84	zinc finger protein 84
0,425	6,51881	0,015072	GDA	guanine deaminase
0,308	7,78853	0,015072	JARID1A	jumonji, AT rich interactive domain 1A
0,303	8,53364	0,0150898	PARN	poly(A)-specific ribonuclease (deadenylation nuclease)
0,481	8,36853	0,0151117	EIF1AX	eukaryotic translation initiation factor 1A, X-linked
-0,586	5,16023	0,0151117	C1orf116	chromosome 1 open reading frame 116
-0,531	3,23678	0,0151468	NOSTRIN	nitric oxide synthase trafficker
-0,433	5,95908	0,0151495	CYFIP2	cytoplasmic FMR1 interacting protein 2
-1,01	3,85318	0,0151914	CLIC5	chloride intracellular channel 5
-0,372	5,32817	0,0152205	HPSE	heparanase

logFC	AveExpr	adj.P.Val	unlist.symbol	Gene description
-0,643	6,15466	0,0152205	TESC	tescalcin
-0,371	5,36093	0,0152598	EZH1	enhancer of zeste homolog 1 (Drosophila)
-0,452	6,85592	0,0152598	CHMP4C	chromatin modifying protein 4C
-0,432	4,94678	0,015319	VIL1	villin 1
0,53	6,05033	0,015319	ZNF566	zinc finger protein 566
0,355	6,25046	0,0154008	LOXL4	lysyl oxidase-like 4
-0,661	4,51541	0,0154419	CD69	CD69 molecule
0,428	7,78527	0,0154874	CTDSPL2	CTD (carboxy-terminal domain, RNA polymerase II, polypeptide A) small phosphatase like 2
0,301	8,92453	0,0156509	GALNT2	UDP-N-acetyl-alpha-D-galactosamine:polypeptide N-acetylgalactosaminyltransferase 2 (GalNAc-T2)
-0,28	8,30878	0,0157518	NF2	neurofibromin 2 (bilateral acoustic neuroma)
0,516	**6,9263**	**0,0157518**	**COL1A1**	**collagen, type I, alpha 1**
-0,436	3,82047	0,0158975	ATP12A	ATPase, H+/K+ transporting, nongastric, alpha polypeptide
0,416	8,168	0,0159862	SFRS5	splicing factor, arginine/serine-rich 5
-0,521	5,87192	0,0162486	FAM83F	family with sequence similarity 83, member F (FAM83F), mRNA
0,358	8,48197	0,0162603	SLC25A32	solute carrier family 25, member 32
0,426	7,23403	0,0162672	KIAA0999	KIAA0999 protein
0,288	7,64679	0,0162731	SLC44A1	solute carrier family 44, member 1
-0,842	4,70962	0,0163801	OR2T2	olfactory receptor, family 2, subfamily T, member 2
-0,279	8,48684	0,0164038	SLC44A2	solute carrier family 44, member 2
0,322	6,87468	0,0166773	ATF5	activating transcription factor 5
0,723	7,59826	0,0168676	NA	NA
-0,532	3,7514	0,0169059	LEMD1	LEM domain containing 1
0,524	9,05914	0,016948	HIAT1	hippocampus abundant transcript 1
-0,538	3,58469	0,016963	C1orf114	chromosome 1 open reading frame 114
-0,642	5,01603	0,0170643	MYCN	v-myc myelocytomatosis viral related oncogene, neuroblastoma derived (avian)
-0,284	7,37777	0,0171348	POLR2I	polymerase (RNA) II (DNA directed) polypeptide I, 14.5kDa
0,532	7,83143	0,0171348	PPP1R14A	protein phosphatase 1, regulatory (inhibitor) subunit 14A
0,515	7,82437	0,017146	PMS2	PMS2 postmeiotic segregation increased 2 (S. cerevisiae)
1,176	5,25388	0,0172544	RTN4RL1	reticulon 4 receptor-like 1
0,363	7,59533	0,0172682	MVP	major vault protein
-0,614	4,36603	0,0173529	LRAT	lecithin retinol acyltransferase (phosphatidylcholine--retinol O-acyltransferase)
0,606	8,25544	0,0173529	PIGX	phosphatidylinositol glycan anchor biosynthesis, class X
-1,162	5,29619	0,0173625	NA	NA
0,281	5,99543	0,0173945	PPFIBP2	PTPRF interacting protein, binding protein 2 (liprin beta 2)
0,422	7,44044	0,0174055	STIM2	stromal interaction molecule 2
0,478	4,67486	0,017553	DKFZp451M2119	hypothetical protein DKFZp451M2119
-0,458	5,09606	0,0175682	EPB41L3	erythrocyte membrane protein band 4.1-like 3
0,286	7,60155	0,0176057	CTDSPL	CTD (carboxy-terminal domain, RNA polymerase II, polypeptide A) small phosphatase-like
0,321	6,98943	0,0176837	TMEM44	transmembrane protein 44
0,536	6,84882	0,0176867	BAMBI	BMP and activin membrane-bound inhibitor homolog (Xenopus laevis)
-0,483	5,28076	0,0176867	TSPAN7	tetraspanin 7

logFC	AveExpr	adj.P.Val	unlist.symbol	Gene description
-0,775	5,50634	0,0176957	C20orf135	chromosome 20 open reading frame 135
-0,286	9,14094	0,0177203	SHMT2	serine hydroxymethyltransferase 2 (mitochondrial)
0,319	7,09255	0,0179182	TRIM21	tripartite motif-containing 21
0,375	5,1599	0,0179289	PRKD1	protein kinase D1
0,472	6,72915	0,017955	SNAPAP	SNAP-associated protein
0,386	8,06343	0,0180411	TMEM69	transmembrane protein 69
0,465	9,3657	0,0180569	POLR2B	polymerase (RNA) II (DNA directed) polypeptide B, 140kDa
-0,538	4,43356	0,0181496	BMPR1B	bone morphogenetic protein receptor, type IB
-0,623	3,4862	0,0182951	TNIP3	TNFAIP3 interacting protein 3
-0,398	4,97198	0,0182951	SLCO5A1	solute carrier organic anion transporter family, member 5A1
0,752	7,22801	0,0182951	SLU7	SLU7 splicing factor homolog (S. cerevisiae)
-0,589	6,31336	0,0183257	SFRP1	secreted frizzled-related protein 1
-0,348	5,25266	0,0184867	ITGA1	integrin, alpha 1
0,42	8,71951	0,0185288	IFITM3	interferon induced transmembrane protein 3 (1-8U)
-0,771	5,02632	0,01858	LCE4A	late cornified envelope 4A
0,559	7,67779	0,0185818	RNF103	ring finger protein 103
0,379	7,86837	0,0186421	SH3BP4	SH3-domain binding protein 4
-0,425	4,82066	0,0186421	PPM1K	protein phosphatase 1K (PP2C domain containing)
0,415	7,24258	0,0187018	PI4K2B	phosphatidylinositol 4-kinase type 2 beta
0,497	7,82743	0,0187746	HIST1H3H	histone cluster 1, H3h
0,634	7,4235	0,0187746	CSNK1G3	casein kinase 1, gamma 3
0,533	5,29658	0,0187746	DHX9	DEAH (Asp-Glu-Ala-His) box polypeptide 9
0,577	5,59335	0,0187746	AHSA2	AHA1, activator of heat shock 90kDa protein ATPase homolog 2 (yeast)
-0,334	10,964	0,0188699	RPL19	ribosomal protein L19
0,744	7,36663	0,0189864	PUS7	pseudouridylate synthase 7 homolog (S. cerevisiae)
-0,713	4,78419	0,0190088	RP13-36C9.6	cancer/testis antigen CT45-5
-0,904	2,60973	0,0190425	OR10X1	olfactory receptor, family 10, subfamily X, member 1
0,342	6,26932	0,0190425	GPR56	G protein-coupled receptor 56
0,352	7,11911	0,0190425	HSP90B1	heat shock protein 90kDa beta (Grp94), member 1
0,459	6,97825	0,0190425	C12orf30	chromosome 12 open reading frame 30
0,605	6,481	0,0190767	FAM92A1	family with sequence similarity 92, member A1
-0,538	4,59685	0,0191283	CAMK4	calcium/calmodulin-dependent protein kinase IV
-0,923	2,91854	0,0191283	MAS1	MAS1 oncogene
-0,446	3,79333	0,0191314	CSMD3	CUB and Sushi multiple domains 3
-0,455	3,8536	0,019146	SAGE1	sarcoma antigen 1
-0,368	6,08933	0,0191504	ZNF544	zinc finger protein 544
-0,296	8,15673	0,0191504	DYRK2	dual-specificity tyrosine-(Y)-phosphorylation regulated kinase 2
-0,996	3,48963	0,0191608	C21orf121	chromosome 21 open reading frame 121
0,946	7,37329	0,0191892	LOC401152	HCV F-transactivated protein 1
-0,503	5,8978	0,019296	OXCT1	3-oxoacid CoA transferase 1
0,427	6,70962	0,019296	TMEM135	transmembrane protein 135 (TMEM135), mRNA
0,391	5,48286	0,0193876	ZNF354C	zinc finger protein 354C

logFC	AveExpr	adj.P.Val	unlist.symbol	Gene description
-0,435	4,4873	0,0193876	ABHD12B	abhydrolase domain containing 12B
-0,423	6,44819	0,0193876	CRMP1	collapsin response mediator protein 1
0,336	7,70939	0,0194451	VPS53	vacuolar protein sorting 53 homolog (S. cerevisiae)
0,484	6,22215	0,0194639	PCAF	p300/CBP-associated factor
0,319	8,17548	0,0194639	PLEKHA1	pleckstrin homology domain containing, family A (phosphoinositide binding specific) member 1
-0,271	5,16383	0,0196238	BCAS2	breast carcinoma amplified sequence 2
-0,333	5,80096	0,0197179	MFSD2	major facilitator superfamily domain containing 2
-0,611	5,2124	0,0197647	CT45-1	cancer/testis antigen CT45-1 (CT45-1), mRNA
-0,336	5,71875	0,0198564	TMEM16A	transmembrane protein 16A
-0,306	5,80025	0,019946	MOSC1	MOCO sulphurase C-terminal domain containing 1
-0,896	4,19303	0,0200018	NA	NA
-0,807	4,42833	0,0200038	INHA	inhibin, alpha
0,472	7,06227	0,0200315	FKBP14	FK506 binding protein 14, 22 kDa
-0,502	4,8015	0,0200571	KIF5C	kinesin family member 5C
-0,315	8,40442	0,0200571	DUSP6	dual specificity phosphatase 6
0,434	4,82572	0,0200754	MDM1	Mdm4, transformed 3T3 cell double minute 1, p53 binding protein (mouse)
-0,409	6,79962	0,0200811	NA	NA
-0,359	6,18298	0,020108	HMOX1	heme oxygenase (decycling) 1
0,688	7,40189	0,020149	ALDOC	aldolase C, fructose-bisphosphate
-0,51	6,71782	0,0201934	PHLDA3	pleckstrin homology-like domain, family A, member 3
0,227	9,8346	0,0202825	CTSA	cathepsin A
-0,335	4,62303	0,0202825	CPA4	carboxypeptidase A4
0,388	6,3392	0,0203078	LMCD1	LIM and cysteine-rich domains 1
0,533	5,79971	0,0203179	SLC35B3	solute carrier family 35, member B3
-0,341	6,61973	0,0204138	ZC3H12A	zinc finger CCCH-type containing 12A
0,381	7,09011	0,0204918	ZBED5	zinc finger, BED-type containing 5
0,41	6,08714	0,020515	STK3	serine/threonine kinase 3 (STE20 homolog, yeast)
-0,444	5,59416	0,020515	COL17A1	collagen, type XVII, alpha 1
0,535	4,50835	0,0205545	SYCP2	synaptonemal complex protein 2
-0,575	4,79682	0,0206564	LGI3	leucine-rich repeat LGI family, member 3
-0,48	5,29658	0,0208021	NPR1	natriuretic peptide receptor A/guanylate cyclase A (atrionatriuretic peptide receptor A)
0,585	9,94552	0,0209848	CDV3	CDV3 homolog (mouse)
0,54	4,53965	0,0210457	FLI1	Friend leukemia virus integration 1
0,538	6,03815	0,0210457	SESN1	sestrin 1
0,8	5,47074	0,0210537	PBLD	phenazine biosynthesis-like protein domain containing
0,502	3,09207	0,0210822	ZMAT1	zinc finger, matrin type 1
0,482	6,97485	0,0212261	CACNG7	calcium channel, voltage-dependent, gamma subunit 7
-0,306	6,55537	0,0212758	PMM1	phosphomannomutase 1
0,365	8,03911	0,0212898	ARL5B	ADP-ribosylation factor-like 5B
0,343	4,75513	0,0213071	CLYBL	citrate lyase beta like
1,214	4,74839	0,0213345	LYRM7	Lyrm7 homolog (mouse)

logFC	AveExpr	adj.P.Val	unlist.symbol	Gene description
-0,446	5,96717	0,0213831	SPTBN2	spectrin, beta, non-erythrocytic 2
-1,928	3,9092	0,0215698	OR2M5	olfactory receptor, family 2, subfamily M, member 5
-0,268	6,7399	0,0215821	LIMK2	LIM domain kinase 2
-0,458	4,25205	0,0216464	SEMA6A	sema domain, transmembrane domain (TM), and cytoplasmic domain, (semaphorin) 6A
0,575	6,13499	0,021676	ZNF322A	zinc finger protein 322A
-0,459	4,32433	0,0217043	MBNL3	muscleblind-like 3 (Drosophila)
0,384	8,48222	0,0217388	NIPA1	Non imprinted in Prader-Willi/Angelman syndrome 1
-0,865	2,82199	0,0217769	OR5K2	olfactory receptor, family 5, subfamily K, member 2
-0,273	6,64766	0,0218488	ATG4A	ATG4 autophagy related 4 homolog A (S. cerevisiae)
0,264	7,52639	0,0218488	PEX10	peroxisome biogenesis factor 10
0,729	5,97922	0,0218524	ELMOD2	ELMO/CED-12 domain containing 2
0,671	5,93327	0,0218524	PGAP1	GPI deacylase
-0,435	5,00043	0,0218733	ARHGAP22	Rho GTPase activating protein 22
0,341	7,50362	0,0218733	MARCH8	membrane-associated ring finger (C3HC4) 8
-0,341	4,51991	0,0218755	CADPS2	Ca2+-dependent activator protein for secretion 2
0,392	6,45959	0,0220713	C2orf34	chromosome 2 open reading frame 34
0,582	5,78063	0,0220713	KCTD1	potassium channel tetramerisation domain containing 1
0,263	7,2845	0,0220899	SNX19	sorting nexin 19
0,417	7,04299	0,0221067	C6orf145	chromosome 6 open reading frame 145
-1,122	3,32157	0,0221403	NA	NA
-0,999	3,11088	0,0221432	NODAL	nodal homolog (mouse)
-0,62	3,75959	0,0222618	KBTBD8	kelch repeat and BTB (POZ) domain containing 8
-0,388	4,86117	0,0224089	SPTB	spectrin, beta, erythrocytic (includes spherocytosis, clinical type I)
-0,475	8,19999	0,0224433	UACA	uveal autoantigen with coiled-coil domains and ankyrin repeats
0,268	10,5322	0,02246	CD9	CD9 molecule
0,466	7,78547	0,022599	ALPPL2	alkaline phosphatase, placental-like 2
-0,397	6,75807	0,022599	GRTP1	growth hormone regulated TBC protein 1
-0,37	6,27177	0,0226244	ID2	inhibitor of DNA binding 2, dominant negative helix-loop-helix protein
-0,485	5,70949	0,0226705	MAFF	v-maf musculoaponeurotic fibrosarcoma oncogene homolog F (avian)
0,38	7,08272	0,0227247	ASRGL1	asparaginase like 1
0,512	5,59792	0,0228283	SCML2	sex comb on midleg-like 2 (Drosophila)
0,574	8,284	0,0228612	IL6ST	interleukin 6 signal transducer (gp130, oncostatin M receptor)
0,412	7,47564	0,0228813	DDEF1	development and differentiation enhancing factor 1
0,523	6,60713	0,0230197	SOBP	sine oculis binding protein homolog (Drosophila)
0,391	6,86319	0,0230596	STK38L	serine/threonine kinase 38 like
-0,484	5,50923	0,0230596	ARHGEF4	Rho guanine nucleotide exchange factor (GEF) 4
0,272	7,60329	0,0230596	LOC89944	hypothetical protein BC008326
-0,377	5,65492	0,0230596	ULBP2	UL16 binding protein 2
-0,724	4,28987	0,0231409	GALNT3	UDP-N-acetyl-alpha-D-galactosamine:polypeptide N-acetylgalactosaminyltransferase 3 (GalNAc-T3)
-0,373	7,31139	0,0231495	CHPF	chondroitin polymerizing factor
0,545	8,2401	0,0231495	TAF7	TAF7 RNA polymerase II, TATA box binding protein (TBP)-associated factor, 55kDa

logFC	AveExpr	adj.P.Val	unlist.symbol	Gene description
-0,916	4,65147	0,0232524	HLA-DQA2	major histocompatibility complex, class II, DQ alpha 2
-0,397	5,77528	0,0233083	MAGEA2B	melanoma antigen family A, 2B
-0,337	6,75533	0,0233703	NA	NA
0,474	8,377	0,0234019	HSD17B11	hydroxysteroid (17-beta) dehydrogenase 11
0,44	8,54476	0,0234019	GRPEL1	GrpE-like 1, mitochondrial (E. coli)
0,392	4,6376	0,023423	BNC2	basonuclin 2
0,451	6,87112	0,0234367	S100PBP	S100P binding protein
0,279	8,0905	0,0234773	KIAA1967	KIAA1967
-0,321	4,22904	0,0236024	KIAA1622	KIAA1622
0,538	6,0494	0,0237333	QKI	quaking homolog, KH domain RNA binding (mouse)
-0,492	4,1493	0,0237522	FREM2	FRAS1 related extracellular matrix protein 2
-0,563	3,55535	0,0237733	MGC48628	similar to KIAA1680 protein
-0,463	3,88818	0,0238745	ENPEP	glutamyl aminopeptidase (aminopeptidase A)
0,635	3,75131	0,0238745	PCDHB8	protocadherin beta 8
0,34	6,86632	0,0239019	TMEM53	transmembrane protein 53
0,399	8,37125	0,0239814	DDAH1	dimethylarginine dimethylaminohydrolase 1
-0,433	5,94846	0,0240039	C10orf116	chromosome 10 open reading frame 116
-0,364	5,56313	0,0240302	NA	NA
-0,737	2,91452	0,024036	RNASE2	ribonuclease, RNase A family, 2 (liver, eosinophil-derived neurotoxin)
-0,63	5,80494	0,0243506	FUT1	fucosyltransferase 1 (galactoside 2-alpha-L-fucosyltransferase, H blood group)
0,612	4,23743	0,0243506	C6orf65	chromosome 6 open reading frame 65
-0,431	5,14147	0,0244118	CORO2B	coronin, actin binding protein, 2B
-0,501	3,21998	0,0244118	NA	NA
0,814	2,92422	0,0244669	NA	NA
0,615	8,78389	0,0244669	EIF1AP1	eukaryotic translation initiation factor 1A pseudogene 1
-0,451	4,14276	0,0244669	RARB	retinoic acid receptor, beta
-0,486	5,51739	0,0244669	MAGED4B	melanoma antigen family D, 4B
-0,584	5,03208	0,0245195	VSNL1	visinin-like 1
-0,353	6,9755	0,0245195	SPHK1	sphingosine kinase 1
-0,33	6,79875	0,0245782	B4GALNT1	beta-1,4-N-acetyl-galactosaminyl transferase 1
-0,29	6,46241	0,0245782	TRIM35	tripartite motif-containing 35
0,459	7,45571	0,0245878	SCP2	sterol carrier protein 2
0,363	7,25416	0,0246638	PMS2CL	PMS2-C terminal-like
-0,501	4,92634	0,0246772	REEP1	receptor accessory protein 1
-0,308	7,39754	0,0248416	LOC57228	small trans-membrane and glycosylated protein
0,388	7,42244	0,0249815	STRN3	striatin, calmodulin binding protein 3
0,422	3,83293	0,0250584	ZNF665	zinc finger protein 665
-0,467	3,85756	0,0250584	TRAM1L1	translocation associated membrane protein 1-like 1
0,49	7,54719	0,0252642	AAK1	AP2 associated kinase 1
0,614	6,78472	0,0253131	C4orf16	chromosome 4 open reading frame 16
0,394	8,42106	0,0253131	MPV17	MpV17 mitochondrial inner membrane protein

logFC	AveExpr	adj.P.Val	unlist.symbol	Gene description
0,218	6,73276	0,0253131	KIAA1600	KIAA1600 (KIAA1600), mRNA
0,452	5,10363	0,0253131	NA	NA
-0,531	5,1937	0,0256422	MGC45491	hypothetical protein MGC45491
-0,389	6,1391	0,0258422	TMEM98	transmembrane protein 98
-0,548	5,53075	0,026131	GAP43	growth associated protein 43
-0,431	4,38391	0,0261788	CTTNBP2	cortactin binding protein 2
0,427	6,55187	0,0262301	VPS8	vacuolar protein sorting 8 homolog (S. cerevisiae)
1,059	4,17902	0,0262454	LOC63920	transposon-derived Buster3 transposase-like
-0,482	5,09314	0,026354	ATP2C2	ATPase, Ca++ transporting, type 2C, member 2
-0,557	3,90517	0,0265015	ZNF533	zinc finger protein 533
0,298	8,00348	0,0265496	TGOLN2	trans-golgi network protein 2
-0,407	3,88381	0,0265496	DSG4	desmoglein 4
0,431	4,88811	0,0266353	TTLL7	tubulin tyrosine ligase-like family, member 7
-0,839	2,85215	0,0266752	OR4K1	olfactory receptor, family 4, subfamily K, member 1
-0,55	4,69414	0,0266752	FUT2	fucosyltransferase 2 (secretor status included)
-0,557	6,20371	0,0267301	HPGD	hydroxyprostaglandin dehydrogenase 15-(NAD)
-0,484	4,62353	0,0267498	SLC1A1	solute carrier family 1 (neuronal/epithelial high affinity glutamate transporter, system Xag), member 1
0,251	7,78894	0,0267952	LONP2	lon peptidase 2, peroxisomal
0,662	7,91315	0,0268598	PTCD3	Pentatricopeptide repeat domain 3
-0,354	3,71004	0,0268598	CR2	complement component (3d/Epstein Barr virus) receptor 2
0,434	8,13392	0,0269065	WDR36	WD repeat domain 36
-0,449	4,57133	0,0269237	HERC6	hect domain and RLD 6
0,507	6,84517	0,0269237	SNAPC5	small nuclear RNA activating complex, polypeptide 5, 19kDa
-0,608	5,7177	0,0269895	BIRC3	baculoviral IAP repeat-containing 3
-0,541	5,68146	0,0270052	OVOL1	ovo-like 1(Drosophila)
0,707	4,61037	0,0270802	DPY19L2P2	dpy-19-like 2 pseudogene 2 (C. elegans)
-0,45	3,29248	0,027106	CNTN1	contactin 1
0,987	6,70411	0,0272293	VANGL1	vang-like 1 (van gogh, Drosophila)
-0,353	5,70467	0,0272957	C7orf41	chromosome 7 open reading frame 41
-0,401	6,84013	0,0272957	ACP6	acid phosphatase 6, lysophosphatidic
-0,968	4,18176	0,0272957	ACP5	acid phosphatase 5, tartrate resistant
-0,599	7,91488	0,0273504	NA	NA
0,395	6,53378	0,0275032	TNKS	tankyrase, TRF1-interacting ankyrin-related ADP-ribose polymerase
-1,009	3,41485	0,0275133	TAS2R40	taste receptor, type 2, member 40
0,653	6,72668	0,0275494	ARSK	arylsulfatase family, member K
0,226	8,35205	0,0275503	MARCKS	myristoylated alanine-rich protein kinase C substrate
0,54	7,37369	0,0276054	RAB23	RAB23, member RAS oncogene family
-0,621	6,14017	0,0276574	KRT23	keratin 23 (histone deacetylase inducible)
-0,445	4,84488	0,0276725	KIAA1305	KIAA1305
0,627	7,77822	0,0277217	TMCO1	transmembrane and coiled-coil domains 1
0,717	6,94918	0,0277217	CCDC88A	coiled-coil domain containing 88A

logFC	AveExpr	adj.P.Val	unlist.symbol	Gene description
-0,517	4,55372	0,0277436	CYP2J2	cytochrome P450, family 2, subfamily J, polypeptide 2
-0,321	5,00709	0,0277503	FAM134B	family with sequence similarity 134, member B
0,492	8,06971	0,0277717	SEMA3C	sema domain, immunoglobulin domain (Ig), short basic domain, secreted, (semaphorin) 3C
-0,421	3,23041	0,0277967	LRRC6	leucine rich repeat containing 6
0,363	8,08423	0,0279439	EPAS1	endothelial PAS domain protein 1
-0,339	6,39338	0,028022	HECA	headcase homolog (Drosophila)
-0,411	5,81474	0,028022	DOC2B	double C2-like domains, beta
0,303	7,25714	0,0280601	SCMH1	sex comb on midleg homolog 1 (Drosophila)
-0,41	4,65359	0,0282282	CCDC136	coiled-coil domain containing 136
-0,462	6,2434	0,0282583	WNT11	wingless-type MMTV integration site family, member 11
-0,366	3,68607	0,0284439	C6orf174	chromosome 6 open reading frame 174
-0,698	6,03961	0,0284439	IL8	interleukin 8
0,659	6,77922	0,0284992	ATG10	ATG10 autophagy related 10 homolog (S. cerevisiae)
0,59	7,58767	0,0285051	RNF146	ring finger protein 146
-0,259	6,66257	0,0285051	B3GNTL1	UDP-GlcNAc:betaGal beta-1,3-N-acetylglucosaminyltransferase-like 1
-0,361	4,90695	0,0286112	UCHL1	ubiquitin carboxyl-terminal esterase L1 (ubiquitin thiolesterase)
0,256	7,37081	0,0286112	IFT122	intraflagellar transport 122 homolog (Chlamydomonas)
-0,31	8,07833	0,0286616	MEX3C	mex-3 homolog C (C. elegans)
0,305	6,16257	0,0286748	LOC152485	hypothetical protein LOC152485
-0,371	5,83062	0,0288739	BMP4	bone morphogenetic protein 4
0,327	7,3412	0,0289549	APLP1	amyloid beta (A4) precursor-like protein 1
0,363	7,26177	0,0289549	FAM80A	family with sequence similarity 80, member A
-0,392	3,40237	0,0290216	WDR52	WD repeat domain 52
-0,418	5,06238	0,0290216	AK5	adenylate kinase 5
0,607	8,75082	0,0292056	RANBP2	RAN binding protein 2
0,421	5,83806	0,0292301	ZNF570	zinc finger protein 570
0,607	7,57627	0,0292865	SKIL	SKI-like oncogene
-0,473	4,71028	0,0293811	FLJ37396	hypothetical protein FLJ37396
-0,535	5,87105	0,0295033	HOXA6	homeobox A6
-0,52	4,69734	0,0295068	TTC22	tetratricopeptide repeat domain 22
0,318	3,85323	0,0295771	RPL24	ribosomal protein L24
-0,494	2,59857	0,0296296	KLRA1	killer cell lectin-like receptor subfamily A, member 1
-0,498	5,5693	0,0296296	GLS2	glutaminase 2 (liver, mitochondrial)
-0,729	2,37629	0,0296958	NA	NA
-0,6	5,05254	0,0297692	TMEM156	transmembrane protein 156 (TMEM156), mRNA
-0,577	5,16643	0,0300262	SRGN	serglycin
-0,432	4,0348	0,0302705	WDR17	WD repeat domain 17
-0,496	4,30931	0,0302705	NR3C2	nuclear receptor subfamily 3, group C, member 2
0,347	6,55061	0,0303543	ZNF302	zinc finger protein 302
0,222	8,04915	0,0303543	TNFAIP2	tumor necrosis factor, alpha-induced protein 2
0,274	7,31633	0,0305645	RASSF8	Ras association (RalGDS/AF-6) domain family 8 (RASSF8), mRNA

logFC	AveExpr	adj.P.Val	unlist.symbol	Gene description
0,31	8,35363	0,030587	TCF25	transcription factor 25 (basic helix-loop-helix)
-0,716	3,50352	0,0307406	OR8B12	olfactory receptor, family 8, subfamily B, member 12
0,271	6,79704	0,0308711	ACSS2	acyl-CoA synthetase short-chain family member 2
-0,379	4,62557	0,0310656	SYTL4	synaptotagmin-like 4 (granuphilin-a)
-0,465	2,90436	0,031069	LST-3TM12	organic anion transporter LST-3b
-0,537	6,17258	0,031146	CBLC	Cas-Br-M (murine) ecotropic retroviral transforming sequence c
0,257	4,31287	0,031146	DNAH5	dynein, axonemal, heavy chain 5
-0,692	4,25893	0,0312323	SPRR2A	small proline-rich protein 2A
0,378	6,57373	0,0312429	DMN	desmuslin
-0,447	4,14287	0,0312429	FAM13C1	family with sequence similarity 13, member C1
-0,777	3,05924	0,0313082	NA	NA
0,552	4,0232	0,0313217	NTS	neurotensin
-0,448	4,55828	0,0313884	7A5	putative binding protein 7a5
0,329	9,4347	0,0314138	WWTR1	WW domain containing transcription regulator 1
-0,347	6,94925	0,0314138	SLC45A3	solute carrier family 45, member 3
0,417	5,92291	0,031513	PRTFDC1	phosphoribosyl transferase domain containing 1
0,475	5,40587	0,031597	GSTM3	glutathione S-transferase M3 (brain)
0,417	5,33983	0,0317047	NA	NA
-0,354	6,02312	0,0317047	GPR161	G protein-coupled receptor 161
0,911	7,82255	0,0317047	HIST1H3A	histone cluster 1, H3a
-0,29	7,48497	0,0317949	CUTC	cutC copper transporter homolog (E. coli)
0,377	8,48736	0,0319573	TTRAP	TRAF and TNF receptor associated protein
-0,495	5,15861	0,0319836	RP3-377H14.5	hypothetical protein FLJ35429
0,368	7,98726	0,032005	RECQL	RecQ protein-like (DNA helicase Q1-like)
0,38	7,14548	0,0321164	DDHD2	DDHD domain containing 2
0,616	7,00286	0,0321164	ATR	ataxia telangiectasia and Rad3 related
0,299	7,21908	0,0321378	ELF1	E74-like factor 1 (ets domain transcription factor)
0,505	6,8241	0,0321772	C3orf64	chromosome 3 open reading frame 64
-0,426	6,28407	0,0325237	MGC10334	hypothetical protein MGC10334
-0,315	5,1221	0,0325598	ARG2	arginase, type II
-0,346	5,85898	0,0325598	DFFB	DNA fragmentation factor, 40kDa, beta polypeptide (caspase-activated DNase)
-0,595	3,6865	0,0327133	NA	NA
-0,396	5,87404	0,0327133	RCSD1	RCSD domain containing 1
-0,78	4,21664	0,0327133	FLJ45831	FLJ45831 protein (FLJ45831), mRNA
0,445	4,62876	0,0327266	RGN	regucalcin (senescence marker protein-30)
-0,8	2,41227	0,0327953	OR4F16	olfactory receptor, family 4, subfamily F, member 16
-0,382	5,04104	0,0328638	MAOB	monoamine oxidase B
-0,294	10,6648	0,0329402	MT1L	metallothionein 1L (gene/pseudogene)
0,526	6,59886	0,0329402	DLEU1	deleted in lymphocytic leukemia, 1
0,66	6,72951	0,0330087	WASF1	WAS protein family, member 1
0,376	5,49244	0,033011	MTCP1	mature T-cell proliferation 1
-0,431	5,70389	0,0331147	NOV	nephroblastoma overexpressed gene

logFC	AveExpr	adj.P.Val	unlist.symbol	Gene description
-0,241	7,43083	0,0335493	FVT1	follicular lymphoma variant translocation 1
0,413	7,37699	0,0335815	HOXC10	homeobox C10
0,449	6,66344	0,033615	LPHN2	latrophilin 2
-0,499	6,07567	0,0337896	KIAA1161	KIAA1161 (KIAA1161), mRNA
-0,618	2,92537	0,0338329	CST9	cystatin 9 (testatin)
-0,602	6,53474	0,0338496	PCSK1N	proprotein convertase subtilisin/kexin type 1 inhibitor
-0,343	3,25495	0,0338675	EML5	echinoderm microtubule associated protein like 5
-0,801	4,1539	0,0340353	FAM47B	family with sequence similarity 47, member B (FAM47B), mRNA
0,428	7,37329	0,0341395	CEPT1	choline/ethanolamine phosphotransferase 1
-0,363	6,84427	0,0341395	SLC26A11	solute carrier family 26, member 11
-0,485	5,25612	0,0341395	RP13-36C9.1	cancer/testis antigen CT45
0,506	6,1933	0,0343735	TMEM67	transmembrane protein 67
0,242	9,76061	0,034387	ARPC1B	actin related protein 2/3 complex, subunit 1B, 41kDa
-0,497	6,14771	0,0344293	RUNX3	runt-related transcription factor 3
-0,247	6,8299	0,0346738	IKBKG	inhibitor of kappa light polypeptide gene enhancer in B-cells, kinase gamma
-0,455	5,67335	0,0347504	RAB3B	RAB3B, member RAS oncogene family
-0,276	6,11495	0,0348841	ADRBK2	adrenergic, beta, receptor kinase 2
-0,404	6,06323	0,0350744	MCF2L	MCF.2 cell line derived transforming sequence-like
-0,392	3,83028	0,0351952	FLJ21511	hypothetical protein FLJ21511 (FLJ21511), mRNA
-0,241	5,89706	0,0352131	RAB11FIP1	RAB11 family interacting protein 1 (class I)
0,615	6,14461	0,0356794	PDGFC	platelet derived growth factor C
-0,269	8,7469	0,0357975	RHOG	ras homolog gene family, member G (rho G)
0,238	5,10569	0,0358051	ZNF559	zinc finger protein 559
0,353	7,64181	0,0358956	ARFIP1	ADP-ribosylation factor interacting protein 1 (arfaptin 1)
-0,434	5,3731	0,0363711	PRSS12	protease, serine, 12 (neurotrypsin, motopsin)
-0,461	7,7845	0,0363977	C11orf68	chromosome 11 open reading frame 68
-0,439	4,25744	0,0364001	MUC13	mucin 13, cell surface associated
-0,488	5,59557	0,0366599	SNTB1	syntrophin, beta 1 (dystrophin-associated protein A1, 59kDa, basic component 1)
-0,29	7,44631	0,0366599	REEP4	receptor accessory protein 4
-0,444	7,48436	0,0367017	ID3	inhibitor of DNA binding 3, dominant negative helix-loop-helix protein
-0,77	3,0098	0,0367017	OR7G1	olfactory receptor, family 7, subfamily G, member 1
0,383	3,26293	0,0367145	ZNF382	zinc finger protein 382
-0,304	7,94686	0,0368461	MAPKAPK3	mitogen-activated protein kinase-activated protein kinase 3
0,469	5,23749	0,0368685	SERPINF1	serpin peptidase inhibitor, clade F (alpha-2 antiplasmin, pigment epithelium derived factor), member 1
-0,432	5,43997	0,0370456	NELL2	NEL-like 2 (chicken)
0,568	7,2272	0,0371115	STXBP3	syntaxin binding protein 3
-0,51	3,82604	0,0373009	SERPINB7	serpin peptidase inhibitor, clade B (ovalbumin), member 7
-0,426	4,83949	0,0374416	NMU	neuromedin U
-0,265	7,63162	0,0376254	HABP4	hyaluronan binding protein 4
-0,226	7,37651	0,0377995	NA	NA
-0,576	6,89895	0,0378642	RAET1L	retinoic acid early transcript 1L

logFC	AveExpr	adj.P.Val	unlist.symbol	Gene description
0,386	7,93975	0,0378642	EIF5A2	eukaryotic translation initiation factor 5A2
-1,334	3,47291	0,0378642	FMO1	flavin containing monooxygenase 1
-0,633	4,15024	0,0378655	FGF9	fibroblast growth factor 9 (glia-activating factor)
0,508	6,01007	0,0379014	BAZ2B	bromodomain adjacent to zinc finger domain, 2B
-0,324	7,71713	0,0381302	FBRS	fibrosin (FBRS), mRNA
0,455	8,29244	0,0381302	OSTM1	osteopetrosis associated transmembrane protein 1
-0,432	7,51055	0,0382048	KRT6A	keratin 6A
0,373	8,16244	0,038206	AKAP12	A kinase (PRKA) anchor protein (gravin) 12
0,339	4,86028	0,038234	RAPGEF5	Rap guanine nucleotide exchange factor (GEF) 5
-0,259	8,18307	0,0383036	TUBB2B	tubulin, beta 2B
-0,373	3,8816	0,0383925	SLC16A4	solute carrier family 16, member 4 (monocarboxylic acid transporter 5)
-0,38	5,18153	0,0385199	NA	NA
-0,739	2,75001	0,0385199	PMCHL2	pro-melanin-concentrating hormone-like 2
0,627	7,63878	0,0386769	SLC35A5	solute carrier family 35, member A5
-0,428	4,35295	0,0387085	DSG3	desmoglein 3 (pemphigus vulgaris antigen)
-0,22	7,65973	0,0387365	CXorf40A	chromosome X open reading frame 40A
0,381	8,69527	0,0387774	GSR	glutathione reductase
-1,227	4,76754	0,0392929	STX11	syntaxin 11
0,479	4,1577	0,0395408	RAB39	RAB39, member RAS oncogene family
-0,372	4,78403	0,039689	HS6ST2	heparan sulfate 6-O-sulfotransferase 2
-0,558	5,76981	0,0397359	EPS8L3	EPS8-like 3
-0,248	7,85964	0,0399	VPS18	vacuolar protein sorting 18 homolog (S. cerevisiae)
0,388	5,88025	0,0400555	ADAL	adenosine deaminase-like
0,475	6,7992	0,0400555	MRPL44	mitochondrial ribosomal protein L44
-0,197	9,87086	0,0401399	SCARNA12	small Cajal body-specific RNA 12
0,315	6,87479	0,0401777	SPG11	spastic paraplegia 11 (autosomal recessive)
0,288	10,1249	0,0401777	SLC25A6	solute carrier family 25 (mitochondrial carrier; adenine nucleotide translocator), member 6
0,575	8,47242	0,0402327	SF3B5	splicing factor 3b, subunit 5, 10kDa
0,441	6,77437	0,0402327	BRIP1	BRCA1 interacting protein C-terminal helicase 1
0,328	8,99691	0,0402327	CUTA	cutA divalent cation tolerance homolog (E. coli)
-0,438	5,8516	0,0402327	RASAL1	RAS protein activator like 1 (GAP1 like)
0,673	4,62666	0,0402765	TF	transferrin
-0,445	5,64434	0,0403771	ARMCX1	armadillo repeat containing, X-linked 1
0,316	8,42412	0,0405097	NPAS2	neuronal PAS domain protein 2
-0,574	4,67656	0,0405097	DLX5	distal-less homeobox 5
-0,409	3,42899	0,0405236	LOC51336	mesenchymal stem cell protein DSCD28
0,625	10,4321	0,0405236	HIST1H2AL	histone cluster 1, H2al
0,332	6,61138	0,0406647	ZKSCAN5	zinc finger with KRAB and SCAN domains 5
-0,507	5,05476	0,0408914	ABHD7	abhydrolase domain containing 7
0,436	7,76606	0,0408914	CD46	CD46 molecule, complement regulatory protein
-0,424	4,06738	0,0409856	ZPLD1	zona pellucida-like domain containing 1

logFC	AveExpr	adj.P.Val	unlist.symbol	Gene description
-0,474	4,32554	0,0410061	PDE4B	phosphodiesterase 4B, cAMP-specific (phosphodiesterase E4 dunce homolog, Drosophila)
-0,461	4,01813	0,0410422	TMEM16D	transmembrane protein 16D
-0,732	2,39448	0,0410422	MGC24103	hypothetical protein MGC24103
0,346	6,82908	0,041087	HEBP1	heme binding protein 1
-0,916	3,13555	0,041087	TAAR6	trace amine associated receptor 6
0,371	7,22944	0,041087	ZFP36L1	zinc finger protein 36, C3H type-like 1
0,52	4,5584	0,041087	RARRES3	retinoic acid receptor responder (tazarotene induced) 3
-0,772	3,34916	0,0412454	EPHA5	EPH receptor A5
-0,581	4,03862	0,0415409	LOC654433	hypothetical LOC654433
0,233	7,1761	0,0415409	DNASE1L1	deoxyribonuclease I-like 1
0,317	6,76972	0,0416066	PRAF2	PRA1 domain family, member 2
0,703	4,66127	0,0416692	NA	NA
-0,371	6,99325	0,0416771	FSD1	fibronectin type III and SPRY domain containing 1
0,564	5,01154	0,041759	RHOBTB1	Rho-related BTB domain containing 1
0,894	5,29888	0,041999	NMI	N-myc (and STAT) interactor
0,421	4,08115	0,041999	ZNF253	zinc finger protein 253
0,353	7,63511	0,041999	ZBTB44	zinc finger and BTB domain containing 44
-0,33	7,34525	0,041999	KATNB1	katanin p80 (WD repeat containing) subunit B 1
-0,399	3,94068	0,0423378	CADPS	Ca2+-dependent secretion activator
-0,688	5,45129	0,0423501	MUM1L1	melanoma associated antigen (mutated) 1-like 1
0,422	9,24068	0,0423552	SLC16A1	solute carrier family 16, member 1 (monocarboxylic acid transporter 1)
-0,419	4,66021	0,042419	HUNK	hormonally upregulated Neu-associated kinase
-0,518	4,26544	0,0424378	IL12A	interleukin 12A (natural killer cell stimulatory factor 1, cytotoxic lymphocyte maturation factor 1, p35)
0,303	4,53667	0,0424735	ZNF565	zinc finger protein 565
0,201	7,86586	0,0424735	FBXW4	F-box and WD repeat domain containing 4
0,472	4,80913	0,0424735	HOXA11	homeobox A11
0,415	7,09644	0,0424735	VAMP2	vesicle-associated membrane protein 2 (synaptobrevin 2)
-0,352	4,08685	0,0424735	DOCK8	dedicator of cytokinesis 8
0,923	5,7809	0,0425412	NA	NA
0,605	6,96891	0,0426591	NA	NA
-0,423	3,63354	0,0426836	ENPP5	ectonucleotide pyrophosphatase/phosphodiesterase 5 (putative function)
-0,787	3,22967	0,0427892	FAM112A	family with sequence similarity 112, member A
-0,388	6,94526	0,0428595	FLJ20489	hypothetical protein FLJ20489 (FLJ20489), mRNA
0,266	7,02477	0,0428609	TRIM68	tripartite motif-containing 68
0,555	5,92899	0,0429598	EVI5	ecotropic viral integration site 5
-1,124	3,32916	0,0429617	CX62	connexin 62
-0,403	5,16263	0,04309	GREM1	gremlin 1, cysteine knot superfamily, homolog (Xenopus laevis)
-0,412	5,31177	0,0431081	SLFN5	schlafen family member 5
0,305	7,69059	0,0431081	RERE	arginine-glutamic acid dipeptide (RE) repeats
-0,445	3,29433	0,0431081	FLJ21062	hypothetical protein FLJ21062
-0,266	10,9637	0,0431081	RPL9	ribosomal protein L9

logFC	AveExpr	adj.P.Val	unlist.symbol	Gene description
-0,587	5,73992	0,0431345	GPR92	G protein-coupled receptor 92
-0,618	4,91874	0,0431787	NA	NA
-0,822	5,82985	0,0431787	OR2T12	olfactory receptor, family 2, subfamily T, member 12
-0,223	7,54645	0,0431921	NA	NA
0,606	5,784	0,0432816	N4BP2	Nedd4 binding protein 2
-0,658	5,28038	0,0437886	FLJ32575	hypothetical protein FLJ32575
0,301	6,40115	0,0439038	EID2B	EP300 interacting inhibitor of differentiation 2B
0,426	6,25909	0,0439038	EYA3	eyes absent homolog 3 (Drosophila)
0,632	6,58017	0,0439038	SLC35A1	solute carrier family 35 (CMP-sialic acid transporter), member A1
-0,763	3,57224	0,0439038	PBOV1	prostate and breast cancer overexpressed 1
0,478	7,78245	0,0439038	PPAT	phosphoribosyl pyrophosphate amidotransferase
-0,407	3,20157	0,043905	SLCO1A2	solute carrier organic anion transporter family, member 1A2
0,243	8,20444	0,0442617	SLC20A2	solute carrier family 20 (phosphate transporter), member 2
0,319	5,42186	0,0443638	NRP2	neuropilin 2
-0,837	4,87261	0,0444448	GSDM1	gasdermin 1
0,46	6,1087	0,0446369	AGL	amylo-1, 6-glucosidase, 4-alpha-glucanotransferase (glycogen debranching enzyme, glycogen storage disease type III)
0,492	5,44883	0,0446369	ICAM4	intercellular adhesion molecule 4 (Landsteiner-Wiener blood group)
-0,381	5,83114	0,0446369	ITGA7	integrin, alpha 7
-0,285	7,4387	0,0446369	TAZ	tafazzin (cardiomyopathy, dilated 3A (X-linked); endocardial fibroelastosis 2; Barth syndrome)
0,31	8,22588	0,0446369	CRIP1	cysteine-rich protein 1 (intestinal)
0,339	9,2624	0,0446761	POLR2L	polymerase (RNA) II (DNA directed) polypeptide L, 7.6kDa
0,733	7,37699	0,0447561	EIF2AK2	eukaryotic translation initiation factor 2-alpha kinase 2
0,38	4,39631	0,0448807	ZNF583	zinc finger protein 583
0,341	4,55511	0,045228	ChGn	chondroitin beta1,4 N-acetylgalactosaminyltransferase
-0,444	6,09751	0,045228	SLC16A10	solute carrier family 16, member 10 (aromatic amino acid transporter)
0,295	8,12126	0,0456421	USP9X	ubiquitin specific peptidase 9, X-linked
0,218	6,66429	0,0460707	ABTB2	ankyrin repeat and BTB (POZ) domain containing 2
0,335	7,80482	0,0460707	DYRK1B	dual-specificity tyrosine-(Y)-phosphorylation regulated kinase 1B
0,306	7,69514	0,0462367	CIRBP	cold inducible RNA binding protein
-0,724	3,56498	0,0463027	PHLDB2	pleckstrin homology-like domain, family B, member 2
0,284	9,10123	0,0464288	GSN	gelsolin (amyloidosis, Finnish type)
-0,274	7,0947	0,0465034	TSSC4	tumor suppressing subtransferable candidate 4
-0,494	7,45822	0,04658	ARRDC3	arrestin domain containing 3
0,359	7,62315	0,0466302	FNDC3B	fibronectin type III domain containing 3B
0,319	6,2287	0,0468425	BEGAIN	brain-enriched guanylate kinase-associated homolog (rat)
0,545	6,0281	0,0469226	FAM101A	family with sequence similarity 101, member A
0,475	5,72735	0,0470055	HOXA2	homeobox A2
0,466	7,17069	0,0472945	SMARCAD1	SWI/SNF-related, matrix-associated actin-dependent regulator of chromatin, subfamily a, containing DEAD/H box 1
0,274	6,57024	0,0473015	ZNF395	zinc finger protein 395
0,515	5,84741	0,0473032	D21S2089E	D21S2089E
0,384	7,66472	0,047428	GLB1	galactosidase, beta 1

logFC	AveExpr	adj.P.Val	unlist.symbol	Gene description
0,46	9,87126	0,047428	NA	NA
-0,51	3,12037	0,0475234	RLN2	relaxin 2
-0,656	2,64173	0,0477346	FSD1L	fibronectin type III and SPRY domain containing 1-like
-0,388	4,04443	0,0477346	SORCS1	sortilin-related VPS10 domain containing receptor 1
-0,339	6,1241	0,047735	NKD1	naked cuticle homolog 1 (Drosophila)
0,29	7,32382	0,0478034	TSPAN1	tetraspanin 1
0,403	8,42739	0,0478086	GNL3	guanine nucleotide binding protein-like 3 (nucleolar)
0,241	6,62458	0,0478283	CTPS2	CTP synthase II (CTPS2), transcript variant 1, mRNA; CTP synthase II (CTPS2), transcript variant 2, mRNA
-0,224	7,66282	0,0480054	STAT5B	signal transducer and activator of transcription 5B
0,798	5,47644	0,0480546	HAS2	hyaluronan synthase 2
-0,485	4,77749	0,0481498	PPP1R1C	protein phosphatase 1, regulatory (inhibitor) subunit 1C
-0,363	4,99893	0,0481706	GPC6	glypican 6
0,494	7,92973	0,0481706	SLC30A9	solute carrier family 30 (zinc transporter), member 9
0,407	5,81933	0,0481706	JAM3	junctional adhesion molecule 3
0,508	8,28956	0,0482223	CD109	CD109 molecule
0,411	8,70414	0,0483352	HEXB	hexosaminidase B (beta polypeptide)
0,319	4,23098	0,0483352	ZNF14	zinc finger protein 14
0,222	6,99024	0,04836	AP4B1	adaptor-related protein complex 4, beta 1 subunit
0,832	5,72725	0,0484419	MIA3	melanoma inhibitory activity family, member 3
0,31	5,63106	0,0485421	DDX59	DEAD (Asp-Glu-Ala-Asp) box polypeptide 59
0,521	7,45864	0,0486988	FNBP1L	formin binding protein 1-like
-0,283	5,02261	0,0489326	BIK	BCL2-interacting killer (apoptosis-inducing)
-0,497	4,5256	0,0489385	KCNJ11	potassium inwardly-rectifying channel, subfamily J, member 11
-0,362	6,44345	0,0489477	ACVR2B	activin A receptor, type IIB
0,244	7,41017	0,049121	SBF2	SET binding factor 2
0,411	6,96928	0,049121	KIF13A	kinesin family member 13A
0,387	8,82502	0,049121	WDR26	WD repeat domain 26
-0,345	4,87402	0,049121	ACTBL1	ACTBL1 protein
0,385	6,87375	0,049121	SCARNA8	small Cajal body-specific RNA 8
0,348	8,95334	0,0491544	ARHGEF12	Rho guanine nucleotide exchange factor (GEF) 12
-0,348	6,83098	0,0491977	ROR1	receptor tyrosine kinase-like orphan receptor 1
0,413	7,8613	0,0491977	PTPRK	protein tyrosine phosphatase, receptor type, K
0,517	5,81871	0,0491977	C10orf10	chromosome 10 open reading frame 10
0,537	6,35472	0,0493848	ZNF35	zinc finger protein 35
0,443	5,17886	0,0493848	KRBA2	KRAB-A domain containing 2
-0,511	6,91709	0,0495035	LOC25845	hypothetical LOC25845
-0,659	5,31243	0,0495572	KRTAP10-11	keratin associated protein 10-11
0,48	7,43575	0,0495724	EXOSC3	exosome component 3
-0,614	3,64316	0,0495724	NA	NA
-0,549	5,50279	0,0495724	C18orf24	chromosome 18 open reading frame 24
-0,42	3,86299	0,0495861	TRPC3	transient receptor potential cation channel, subfamily C, member 3
-0,745	2,3554	0,0495911	OR5AS1	olfactory receptor, family 5, subfamily AS, member 1

logFC	AveExpr	adj.P.Val	unlist.symbol	Gene description
-0,465	5,77477	0,0498931	LTK	leukocyte tyrosine kinase
-0,829	4,04083	0,0498988	NA	NA
0,266	8,51389	0,0498988	PRAME	preferentially expressed antigen in melanoma
-0,364	6,2535	0,0499637	LOC348262	hypothetical protein LOC348262
-0,781	6,55145	0,0499653	LOC389458	hypothetical gene supported by BC031661

(In previous page) Table S4. List of genes significantly altered when Gal-1 was downregulated in PANC-1 with shGal-1_5 compared to control PANC-1 cells (data from non-infected cells with the genes found altered in the shCtl filtered). Genes are presened according to increasing adjusted p value until 0.05. The first column expresses the fold change in logarithmic units with base 2 (log FC). The second column gives the average expression and the third column the adjusted p value.

6.1.2.2 Pathway analysis PANC-1 in shGal-1_5

Pathway	Set Size	Percent Up	NTk Stat	NTk q-value	NTk Rank	NEk* Stat	NEk* q-value	NEk* Rank
Lipid raft	13	46	-5.60	0.0000	4.0	-4.57	0.0000	1.0
Cholesterol metabolism	63	44	-6.32	0.0000	2.0	-4.54	0.0000	3.0
Sterol metabolism	69	48	-6.57	0.0000	1.0	-4.53	0.0000	5.0
ABC transporters - General	43	40	-5.31	0.0000	6.0	-4.56	0.0000	2.0
Lipid transporter activity	65	45	-6.03	0.0000	3.0	-4.41	0.0000	26.0
Insulin receptor signaling pathway	19	63	-2.88	0.0622	60.5	-4.51	0.0000	12.0
Insulin signaling pathway	135	47	-3.09	0.0451	35.5	-4.35	0.0000	41.0
Vascular endothelial growth factor receptor activity	14	36	-2.88	0.0622	60.5	-4.45	0.0000	21.0
Lysosome	112	55	-3.09	0.0451	35.5	-4.28	0.0000	55.0
Fatty acid biosynthesis	49	49	-2.75	0.0822	76.5	-4.48	0.0000	16.0
Rho guanyl-nucleotide exchange factor activity	11	64	-3.09	0.0451	35.5	-4.28	0.0000	57.0
Carbon-oxygen lyase activity	56	50	-3.09	0.0451	35.5	-4.24	0.0000	62.0

Pathway	Set Size	Percent Up	NTk Stat	NTk q-value	NTk Rank	NEk* Stat	NEk* q-value	NEk* Rank
Hydro-lyase activity	47	45	-2.88	0.0622	60.5	-4.38	0.0000	37.0
Fatty acid beta-oxidation	14	71	-3.09	0.0451	35.5	-4.23	0.0000	64.0
Phosphatidylinositol signaling system	99	54	-2.88	0.0622	60.5	-4.35	0.0000	42.0
cAMP / Ca2+ Signaling PathwayFinder	94	21	5.55	0.0000	5.0	4.09	0.0000	99.0
Fatty acid metabolism	50	64	-3.09	0.0451	35.5	-4.17	0.0000	73.0
NFkB activation by Nontypeable Hemophilus influenzae	24	50	-2.58	0.0959	105.5	-4.53	0.0000	6.0
Positive regulation of cytokine biosynthesis	21	10	3.09	0.0451	35.5	4.16	0.0000	78.0
Valine, leucine and isoleucine degradation	51	76	-5.13	0.0000	7.0	-4.05	0.0000	109.0
p38 MAPK Signaling Pathway	32	62	-2.58	0.0959	105.5	-4.49	0.0000	14.0
Human Cytomegalovirus and Map Kinase Pathways	13	54	-2.58	0.0959	105.5	-4.48	0.0000	15.0
Fatty acid oxidation	21	57	-2.65	0.0885	93.0	-4.41	0.0000	29.0
CTCF First Multivalent Nuclear Factor	18	67	-2.58	0.0959	105.5	-4.41	0.0000	27.0
Control of skeletal myogenesis by HDAC calcium/calmodulin-dependent kinase (CaMK)	18	56	-2.51	0.0972	123.0	-4.52	0.0000	10.0
Limonene and pinene degradation	28	61	-2.58	0.0959	105.5	-4.39	0.0000	35.0
Carboxylesterase activity	19	26	2.65	0.0885	93.0	4.29	0.0000	53.0
Serine esterase activity	19	26	2.65	0.0885	93.0	4.29	0.0000	53.0

Pathway	Set Size	Percent Up	NTk Stat	NTk q-value	NTk Rank	NEk* Stat	NEk* q-value	NEk* Rank
ALK in cardiac myocytes	34	62	-2.75	0.0822	76.5	-4.14	0.0000	82.0
beta-Alanine metabolism	27	52	-2.46	0.1096	135.0	-4.43	0.0000	25.0
TCA cycle -- aerobic respiration	18	83	-2.65	0.0885	93.0	-4.21	0.0000	67.0
Superpathway of glyoxylate bypass TCA	18	83	-2.65	0.0885	93.0	-4.21	0.0000	67.0
Carboxylic acid biosynthesis	57	46	-2.51	0.0972	123.0	-4.38	0.0000	38.0
Organic acid biosynthesis	57	46	-2.51	0.0972	123.0	-4.38	0.0000	38.0
Carbonate dehydratase activity	17	18	-2.75	0.0822	76.5	-4.13	0.0000	85.0
Butanoate metabolism	52	65	-2.88	0.0622	60.5	-4.09	0.0000	101.0
Cysteine-type endopeptidase activity	97	55	-3.09	0.0451	35.5	-3.99	0.0000	130.0
Lysine degradation	60	67	-2.88	0.0622	60.5	-4.06	0.0000	106.0
One-carbon compound metabolism	32	34	-2.51	0.0972	123.0	-4.34	0.0000	45.0
Phosphoinositide binding	58	55	-2.51	0.0972	123.0	-4.31	0.0000	48.0
Cell-matrix junction	11	36	-2.33	0.1168	176.5	-4.54	0.0000	4.0
Positive regulation of cellular biosynthesis	25	12	2.88	0.0622	60.5	4.00	0.0000	124.0
Cell cycle checkpoint	41	71	-2.75	0.0822	76.5	-4.04	0.0000	111.0
Regulation of cytokine biosynthesis	34	12	3.09	0.0451	35.5	3.93	0.0000	152.0
Notch signaling pathway	42	62	-2.58	0.0959	105.5	-4.13	0.0000	86.0
Cytokine metabolism	37	14	3.09	0.0451	35.5	3.92	0.0000	157.0
Keratinocyte differentiation	12	25	2.46	0.0988	143.5	4.30	0.0000	50.0
Huntington's disease	30	60	-2.33	0.1168	176.5	-4.47	0.0000	17.0

Pathway	Set Size	Percent Up	NTk Stat	NTk q-value	NTk Rank	NEk* Stat	NEk* q-value	NEk* Rank
Phospholipid-translocating ATPase activity	12	58	-2.51	0.0972	123.0	-4.17	0.0000	71.0
Aminophospholipid transporter activity	12	58	-2.51	0.0972	123.0	-4.17	0.0000	71.0

Table S5. List of pathways significantly altered when Gal-1 was downregulated in PANC-1 with shGal-1_5 compared to control PANC-1 cells (data from non-infected cells with the genes found altered in the shCtl filtered).

6.1.3 PANC-1 Summary List: Gene Detailed Analysis

p value	FC	Gene Symbol	Gene_assignment
5,03E-05	3,82	SEMA3D	NM_152754 // SEMA3D // sema domain, immunoglobulin domain (Ig), short basic doma
2,69E-03	2,90	OR10H3	NM_013938 // OR10H3 // olfactory receptor, family 10, subfamily H, member 3 // 1
5,33E-05	2,88	CP	NM_000096 // CP // ceruloplasmin (ferroxidase) // 3q23-q25 // 1356 /// ENST00000
2,38E-04	2,65	FOS	NM_005252 // FOS // v-fos FBJ murine osteosarcoma viral oncogene homolog // 14q2
4,08E-06	2,53	EGR1	NM_001964 // EGR1 // early growth response 1 // 5q31.1 // 1958 /// ENST000002399
2,06E-02	2,10	TRDN	NM_006073 // TRDN // triadin // 6q22-q23 // 10345 /// ENST00000334268 // TRDN //
1,01E-03	2,02	CCL2	NM_002982 // CCL2 // chemokine (C-C motif) ligand 2 // 17q11.2-q12 // 6347 /// E
2,67E-02	1,97	PTX3	NM_002852 // PTX3 // pentraxin-related gene, rapidly induced by IL-1 beta // 3q2
9,11E-03	1,96	LBH	NM_030915 // LBH // limb bud and heart development homolog (mouse) // 2p23.1 //
2,22E-02	1,88	NDRG1	NM_006096 // NDRG1 // N-myc downstream regulated gene 1 // 8q24.3 // 10397 /// E
4,75E-02	1,88	STX19	NM_001001850 // STX19 // syntaxin 19 // 3q11 // 415117 /// ENST00000315099 // ST
9,60E-03	1,84	FLJ33360	BC132707 // FLJ33360 // FLJ33360 protein // 5p15.31 // 401172 /// AK090679 // FL
6,89E-05	1,82	EPHA7	NM_004440 // EPHA7 // EPH receptor A7 // 6q16.1 // 2045 /// ENST00000369303 // E
9,38E-04	1,81	NAP1L3	NM_004538 // NAP1L3 // nucleosome assembly protein 1-like 3 // Xq21.3-q22 // 467
3,03E-02	1,80	TM7SF4	NM_030788 // TM7SF4 // transmembrane 7 superfamily member 4 // 8q23 // 81501 ///
4,17E-04	1,80	CXCL1	NM_001511 // CXCL1 // chemokine (C-X-C motif) ligand 1 (melanoma growth stimulat
1,13E-02	1,75	NRN1	NM_016588 // NRN1 // neuritin 1 // 6p25.1 // 51299 /// ENST00000244766 // NRN1 /
6,70E-03	1,74	BNIP3	NM_004052 // BNIP3 // BCL2/adenovirus E1B 19kDa interacting protein 3 // 10q26.3
7,42E-03	1,72	EDIL3	NM_005711 // EDIL3 // EGF-like repeats and discoidin I-like domains 3 // 5q14 //
4,88E-04	1,72	C4B	NM_001002029 // C4B // complement component 4B (Childo blood group) // 6p21.3 //
2,21E-02	1,72	SIX3	NM_005413 // SIX3 // SIX homeobox 3 // 2p16-p21 // 6496 /// ENST00000260653 // S
1,13E-02	1,71	OR51S1	NM_001004758 // OR51S1 // olfactory receptor, family 51, subfamily S, member 1 /
1,51E-04	1,71	PLA2R1	NM_007366 // PLA2R1 // phospholipase A2 receptor 1, 180kDa // 2q23-q24 // 22925
1,57E-02	1,70	TF	NM_001063 // TF // transferrin // 3q22.1 // 7018 /// ENST00000264998 // TF // tr

p value	FC	Gene Symbol	Gene_assignment
4,90E-02	1,70	KCNJ2	NM_000891 // KCNJ2 // potassium inwardly-rectifying channel, subfamily J, member
1,21E-02	1,69	ARRDC3	NM_020801 // ARRDC3 // arrestin domain containing 3 // 5q14.3 // 57561 /// ENST0
3,86E-03	1,67	PFKFB4	NM_004567 // PFKFB4 // 6-phosphofructo-2-kinase/fructose-2,6-biphosphatase 4 //
1,99E-02	1,67	PDK1	NM_002610 // PDK1 // pyruvate dehydrogenase kinase, isozyme 1 // 2q31.1 // 5163
5,65E-04	1,66	CBLN2	NM_182511 // CBLN2 // cerebellin 2 precursor // 18q22.3 // 147381 /// ENST000002
1,13E-02	1,66	C6orf117	NM_138409 // C6orf117 // chromosome 6 open reading frame 117 // 6q14.3 // 112609
1,54E-03	**1,65**	**THBS1**	**NM_003246 // THBS1 // thrombospondin 1 // 15q15 // 7057 /// ENST00000260356 // T**
4,57E-03	1,65	PTGS1	NM_000962 // PTGS1 // prostaglandin-endoperoxide synthase 1 (prostaglandin G/H s
1,50E-02	1,64	PADI3	NM_016233 // PADI3 // peptidyl arginine deiminase, type III // 1p36.13 // 51702
5,97E-04	1,64	ANKRD22	NM_144590 // ANKRD22 // ankyrin repeat domain 22 // 10q23.31 // 118932 /// ENST0
2,06E-03	1,61	YPEL1	NM_013313 // YPEL1 // yippee-like 1 (Drosophila) // 22q11.2 // 29799 /// ENST000
1,98E-04	1,60	CD82	NM_002231 // CD82 // CD82 molecule // 11p11.2 // 3732 /// NM_001024844 // CD82 /
4,84E-02	1,60	BGN	NM_001711 // BGN // biglycan // Xq28 // 633 /// ENST00000331595 // BGN // biglyc
2,37E-02	1,60	C6orf124	NM_001042508 // C6orf124 // chromosome 6 open reading frame 124 // 6q27 // 65348
1,31E-02	1,60		---
1,31E-03	1,60	EGLN3	NM_022073 // EGLN3 // egl nine homolog 3 (C. elegans) // 14q13.1 // 112399 /// E
5,65E-04	1,59	PADI2	NM_007365 // PADI2 // peptidyl arginine deiminase, type II // 1p36.13 // 11240 /
1,53E-05	1,58	L1CAM	NM_000425 // L1CAM // L1 cell adhesion molecule // Xq28 // 3897 /// NM_024003 //
1,29E-02	1,58	GPNMB	NM_001005340 // GPNMB // glycoprotein (transmembrane) nmb // 7p15 // 10457 /// N
4,87E-02	1,58		---
1,13E-04	1,58	SCUBE3	NM_152753 // SCUBE3 // signal peptide, CUB domain, EGF-like 3 // 6p21.3 // 22266
7,47E-03	1,58	ZFP36L1	NM_004926 // ZFP36L1 // zinc finger protein 36, C3H type-like 1 // 14q22-q24 //
4,90E-04	1,58	RET	NM_020975 // RET // ret proto-oncogene // 10q11.2 // 5979 /// NM_020630 // RET /
3,60E-03	1,57	IL2RA	NM_000417 // IL2RA // interleukin 2 receptor, alpha // 10p15-p14 // 3559 /// ENS
1,33E-02	1,57	RAMP1	NM_005855 // RAMP1 // receptor (G protein-coupled) activity modifying protein 1
1,44E-04	1,56		---
4,77E-06	1,56	TNC	NM_002160 // TNC // tenascin C (hexabrachion) // 9q33 // 3371 /// ENST0000035076
1,93E-03	1,56	ENO2	NM_001975 // ENO2 // enolase 2 (gamma, neuronal) // 12p13 // 2026 /// ENST000002
1,44E-03	1,56	PGCP	NM_016134 // PGCP // plasma glutamate carboxypeptidase // 8q22.2 // 10404 /// EN
5,61E-03	1,55	SLIT1	NM_003061 // SLIT1 // slit homolog 1 (Drosophila) // 10q23.3-q24 // 6585 /// ENS
2,90E-02	1,55	CD1E	NM_030893 // CD1E // CD1e molecule // 1q22-q23 // 913 /// NM_001042583 // CD1E /
1,65E-02	1,55	PON3	NM_000940 // PON3 // paraoxonase 3 // 7q21.3 // 5446 /// ENST00000265627 // PON3
6,60E-04	1,55	SLFN11	NM_001104587 // SLFN11 // schlafen family member 11 // 17q12 // 91607 /// NM_001
2,64E-02	1,54		---
6,20E-03	1,54	PLSCR4	NM_020353 // PLSCR4 // phospholipid scramblase 4 // 3q24 // 57088 /// ENST000003
3,57E-05	1,54	TMEM26	NM_178505 // TMEM26 // transmembrane protein 26 // 10q21.2 // 219623 /// ENST000
1,34E-02	1,53	PACS2	NM_001100913 // PACS2 // phosphofurin acidic cluster sorting protein 2 // 14q32.
1,33E-03	1,52	TSPAN1	NM_005727 // TSPAN1 // tetraspanin 1 // 1p34.1 // 10103 /// ENST00000372003 // T
1,88E-03	1,52	CSF1	NM_000757 // CSF1 // colony stimulating factor 1 (macrophage) // 1p21-p13 // 143
1,42E-04	1,52	SLCO4A1	NM_016354 // SLCO4A1 // solute carrier organic anion transporter family, member
1,99E-02	1,52	SLITRK6	NM_032229 // SLITRK6 // SLIT and NTRK-like family, member 6 // 13q31.1 // 84189

p value	FC	Gene Symbol	Gene_assignment
3,71E-03	1,52	TMEM47	NM_031442 // TMEM47 // transmembrane protein 47 // Xp11.4 // 83604 /// ENST00000
2,05E-02	1,51	UBL5	NM_024292 // UBL5 // ubiquitin-like 5 // 19p13.3 // 59286 /// NM_001048241 // UB
5,58E-03	1,51	C1orf34	NM_001080494 // C1orf34 // chromosome 1 open reading frame 34 // 1p32.3 // 22996
1,55E-03	**1,51**	**TGFBI**	**NM_000358 // TGFBI // transforming growth factor, beta-induced, 68kDa // 5q31 //**
1,03E-03	1,51	AKR1C3	NM_003739 // AKR1C3 // aldo-keto reductase family 1, member C3 (3-alpha hydroxys
3,22E-02	1,51	KCNK3	NM_002246 // KCNK3 // potassium channel, subfamily K, member 3 // 2p23 // 3777 /
5,39E-03	1,50	C20orf200	NM_152757 // C20orf200 // chromosome 20 open reading frame 200 // 20q13.33 // 25
3,95E-03	1,50	NRP2	NM_201266 // NRP2 // neuropilin 2 // 2q33.3 // 8828 /// NM_003872 // NRP2 // neu
1,26E-03	1,50	VIT	NM_053276 // VIT // vitrin // 2p22-p21 // 5212 /// ENST00000379242 // VIT // vit
1,41E-02	1,50	C12orf27	ENST00000315185 // C12orf27 // chromosome 12 open reading frame 27 // 12q24.31 /
2,48E-02	1,49	KRTAP3-1	NM_031958 // KRTAP3-1 // keratin associated protein 3-1 // 17q12-q21 // 83896 //
7,96E-05	1,49	TNFAIP2	NM_006291 // TNFAIP2 // tumor necrosis factor, alpha-induced protein 2 // 14q32
7,35E-03	1,49	TNFSF10	NM_003810 // TNFSF10 // tumor necrosis factor (ligand) superfamily, member 10 //
1,50E-02	1,49	P4HA1	NM_000917 // P4HA1 // procollagen-proline, 2-oxoglutarate 4-dioxygenase (proline
3,12E-03	1,48	C10orf107	BC041932 // C10orf107 // chromosome 10 open reading frame 107 // 10q21.2 // 2196
2,89E-02	1,48	AGT	NM_000029 // AGT // angiotensinogen (serpin peptidase inhibitor, clade A, member
1,03E-02	1,48	SLC38A3	NM_006841 // SLC38A3 // solute carrier family 38, member 3 // 3p21.3 // 10991 //
1,71E-02	1,48	DEFB132	NM_207469 // DEFB132 // defensin, beta 32 // 20p13 // 400830 /// ENST00000382376
1,35E-02	1,48	WDR78	NM_024763 // WDR78 // WD repeat domain 78 // 1p31.3 // 79819 /// NM_207014 // WD
1,79E-02	1,47	C7orf41	NM_152793 // C7orf41 // chromosome 7 open reading frame 41 // 7p15.1 // 222166 /
2,30E-04	1,47	LOXL2	NM_002318 // LOXL2 // lysyl oxidase-like 2 // 8p21.3-p21.2 // 4017 /// ENST00000
4,34E-02	1,47	DPY19L2P2	NR_003561 // DPY19L2P2 // dpy-19-like 2 pseudogene 2 (C. elegans) // 7q22.1 // 3
4,75E-02	1,47	THSD3	NM_199265 // THSD3 // thrombospondin, type I, domain containing 3 // 14q24.3 //
1,24E-03	1,47	CDKN1A	NM_078467 // CDKN1A // cyclin-dependent kinase inhibitor 1A (p21, Cip1) // 6p21.
1,75E-02	1,47	ID3	NM_002167 // ID3 // inhibitor of DNA binding 3, dominant negative helix-loop-hel
2,14E-02	1,47	KLHL24	NM_017644 // KLHL24 // kelch-like 24 (Drosophila) // 3q27.1 // 54800 /// ENST000
3,73E-03	1,47	LAMC2	NM_005562 // LAMC2 // laminin, gamma 2 // 1q25-q31 // 3918 /// NM_018891 // LAMC
1,71E-03	1,46	GRN	NM_002087 // GRN // granulin // 17q21.32 // 2896 /// ENST00000053867 // GRN // g
4,01E-02	1,46		---
1,87E-02	1,46	AMIGO2	NM_181847 // AMIGO2 // adhesion molecule with Ig-like domain 2 // 12q13.11 // 34
2,78E-02	1,46	HGF	NM_000601 // HGF // hepatocyte growth factor (hepapoietin A; scatter factor) //
2,51E-03	**1,46**	**PDGFD**	**NM_025208 // PDGFD // platelet derived growth factor D // 11q22.3 // 80310 /// N**
3,37E-04	1,46	FAM134B	NM_001034850 // FAM134B // family with sequence similarity 134, member B // 5p15
1,30E-02	1,45	DRD2	NM_000795 // DRD2 // dopamine receptor D2 // 11q23 // 1813 /// NM_016574 // DRD2
1,30E-03	**1,45**	**HHAT**	**NM_018194 // HHAT // hedgehog acyltransferase // 1q32 // 55733 /// NM_001122834**
2,40E-05	1,45	ITGA3	NM_002204 // ITGA3 // integrin, alpha 3 (antigen CD49C, alpha 3 subunit of VLA-3
6,68E-03	1,45	C1QL2	NM_182528 // C1QL2 // complement component 1, q subcomponent-like 2 // 2q14.2 //
1,28E-02	1,44	NECAB1	NM_022351 // NECAB1 // N-terminal EF-hand calcium binding protein 1 // 8q21.3 //
1,33E-02	1,44	PCDHB16	NM_020957 // PCDHB16 // protocadherin beta 16 // 5q31 // 57717 /// ENST000003610
4,23E-02	1,43	NAT8	NM_003960 // NAT8 // N-acetyltransferase 8 // 2p13.1-p12 // 9027 /// NM_016347 /
2,86E-03	1,43	HMOX1	NM_002133 // HMOX1 // heme oxygenase (decycling) 1 // 22q12|22q13.1 // 3162 ///

p value	FC	Gene Symbol	Gene_assignment
1,43E-04	1,43	PODXL	NM_001018111 // PODXL // podocalyxin-like // 7q32-q33 // 5420 /// NM_005397 // P
1,20E-03	1,42	CDH2	NM_001792 // CDH2 // cadherin 2, type 1, N-cadherin (neuronal) // 18q11.2 // 100
1,27E-03	1,42	ST6GALNAC2	NM_006456 // ST6GALNAC2 // ST6 (alpha-N-acetyl-neuraminyl-2,3-beta-galactosyl-1,
4,65E-04	1,42	KLF10	NM_005655 // KLF10 // Kruppel-like factor 10 // 8q22.2 // 7071 /// NM_001032282
2,11E-02	1,42	ADRA1D	NM_000678 // ADRA1D // adrenergic, alpha-1D-, receptor // 20p13 // 146 /// ENST0
1,59E-02	1,42	GJB5	NM_005268 // GJB5 // gap junction protein, beta 5, 31.1kDa // 1p35.1 // 2709 ///
7,57E-03	1,42	DKFZP564O0823	NM_015393 // DKFZP564O0823 // DKFZP564O0823 protein // 4q13.3-q21.3 // 25849 ///
4,04E-05	1,42	MRC2	NM_006039 // MRC2 // mannose receptor, C type 2 // 17q23.2 // 9902 /// ENST00000
4,41E-05	**1,42**	**GADD45A**	**NM_001924 // GADD45A // growth arrest and DNA-damage-inducible, alpha // 1p31.2-**
2,81E-02	1,42	C2orf51	NM_152670 // C2orf51 // chromosome 2 open reading frame 51 // 2p11.2 // 200523 /
2,03E-02	1,42	C20orf160	NM_080625 // C20orf160 // chromosome 20 open reading frame 160 // 20q11.2 // 140
6,65E-03	1,42	SLC2A1	NM_006516 // SLC2A1 // solute carrier family 2 (facilitated glucose transporter)
4,50E-03	1,42	PFKL	NM_001002021 // PFKL // phosphofructokinase, liver // 21q22.3 // 5211 /// NM_002
6,76E-03	1,42	NFKBIZ	NM_031419 // NFKBIZ // nuclear factor of kappa light polypeptide gene enhancer i
1,23E-03	1,42	FAM43A	NM_153690 // FAM43A // family with sequence similarity 43, member A // 3q29 // 1
1,93E-02	1,41	TLR3	NM_003265 // TLR3 // toll-like receptor 3 // 4q35 // 7098 /// ENST00000296795 //
3,39E-02	1,41	CLDN16	NM_006580 // CLDN16 // claudin 16 // 3q28 // 10686 /// ENST00000264734 // CLDN16
7,13E-03	1,41	KLF6	NM_001300 // KLF6 // Kruppel-like factor 6 // 10p15 // 1316 /// ENST00000173785
7,20E-03	1,41	S1PR4	NM_003775 // S1PR4 // sphingosine-1-phosphate receptor 4 // 19p13.3 // 8698 ///
3,73E-02	1,41	TMEM141	NM_032928 // TMEM141 // transmembrane protein 141 // 9q34.3 // 85014 /// ENST000
5,29E-04	1,41	SEMA3E	NM_012431 // SEMA3E // sema domain, immunoglobulin domain (Ig), short basic doma
2,35E-03	1,41	SLC39A8	NM_022154 // SLC39A8 // solute carrier family 39 (zinc transporter), member 8 //
3,52E-02	1,41	NHEDC1	NM_001100874 // NHEDC1 // Na+/H+ exchanger domain containing 1 // 4q24 // 150159
3,77E-03	1,41	P2RX4	NM_002560 // P2RX4 // purinergic receptor P2X, ligand-gated ion channel, 4 // 12
4,19E-02	1,41	OR10J1	NM_012351 // OR10J1 // olfactory receptor, family 10, subfamily J, member 1 // 1
3,76E-02	1,41	CSPG4	NM_001897 // CSPG4 // chondroitin sulfate proteoglycan 4 // 15q24.2 // 1464 ///
2,46E-02	1,40	TMEM98	NM_015544 // TMEM98 // transmembrane protein 98 // 17q11.2 // 26022 /// NM_00103
8,36E-03	1,40	SLC5A7	NM_021815 // SLC5A7 // solute carrier family 5 (choline transporter), member 7 /
9,37E-03	1,40	CTSF	NM_003793 // CTSF // cathepsin F // 11q13 // 8722 /// ENST00000310325 // CTSF //
6,79E-03	1,40	RECK	NM_021111 // RECK // reversion-inducing-cysteine-rich protein with kazal motifs
1,25E-02	1,40	DEPDC6	NM_022783 // DEPDC6 // DEP domain containing 6 // 8q24.12 // 64798 /// ENST00000
5,65E-04	1,40	FLJ20160	NM_017694 // FLJ20160 // FLJ20160 protein // 2q32.2 // 54842 /// ENST00000392328
4,74E-04	1,40	CTSD	NM_001909 // CTSD // cathepsin D // 11p15.5 // 1509 /// ENST00000236671 // CTSD
3,61E-04	1,40	SH3BP2	NM_001122681 // SH3BP2 // SH3-domain binding protein 2 // 4p16.3 // 6452 /// NM_
4,04E-02	1,40	BMP8A	NM_181809 // BMP8A // bone morphogenetic protein 8a // 1p34.2 // 353500 /// ENST
8,91E-03	1,40	FOSB	NM_006732 // FOSB // FBJ murine osteosarcoma viral oncogene homolog B // 19q13.3
3,40E-03	1,39	P4HA2	NM_004199 // P4HA2 // procollagen-proline, 2-oxoglutarate 4-dioxygenase (proline
4,79E-02	1,39		---
4,09E-02	1,39	C14orf132	BC042922 // C14orf132 // chromosome 14 open reading frame 132 // 14q32.2 // 5696
3,86E-03	1,39	SDC3	NM_014654 // SDC3 // syndecan 3 // 1pter-p22.3 // 9672 /// ENST00000339394 // SD

p value	FC	Gene Symbol	Gene_assignment
1,03E-04	1,39	HEXA	NM_000520 // HEXA // hexosaminidase A (alpha polypeptide) // 15q23-q24 // 3073 /
2,74E-02	1,39	TXNIP	NM_006472 // TXNIP // thioredoxin interacting protein // 1q21.1 // 10628 /// ENS
3,73E-02	1,38	ZNF578	NM_001099694 // ZNF578 // zinc finger protein 578 // 19q13.41 // 147660 /// BC10
6,26E-03	1,38	PLCD4	NM_032726 // PLCD4 // phospholipase C, delta 4 // 2q35 // 84812 /// ENST00000251
1,42E-02	1,38	FZD7	NM_003507 // FZD7 // frizzled homolog 7 (Drosophila) // 2q33 // 8324 /// ENST000
3,48E-02	1,38	RAB17	NM_022449 // RAB17 // RAB17, member RAS oncogene family // 2q37.3 // 64284 /// E
3,63E-02	1,38	WSB1	NM_015626 // WSB1 // WD repeat and SOCS box-containing 1 // 17q11.1 // 26118 ///
1,08E-02	1,38	C6orf206	BC029519 // C6orf206 // chromosome 6 open reading frame 206 // 6p21.1 // 221421
1,77E-03	1,38	ARNT2	NM_014862 // ARNT2 // aryl-hydrocarbon receptor nuclear translocator 2 // 15q24
4,76E-02	1,37	VPREB1	NM_007128 // VPREB1 // pre-B lymphocyte gene 1 // 22q11.2|22q11.22 // 7441 /// E
1,81E-03	1,37	PTHLH	NM_198965 // PTHLH // parathyroid hormone-like hormone // 12p12.1-p11.2 // 5744
3,75E-02	1,37	NKAIN4	NM_152864 // NKAIN4 // Na+/K+ transporting ATPase interacting 4 // 20q13.33 // 1
1,49E-02	**1,37**	**ITGAV**	**NM_002210 // ITGAV // integrin, alpha V (vitronectin receptor, alpha polypeptide**
2,83E-02	1,37	PCDH20	NM_022843 // PCDH20 // protocadherin 20 // 13q21 // 64881 /// ENST00000397986 //
2,46E-02	1,37	SCUBE2	NM_020974 // SCUBE2 // signal peptide, CUB domain, EGF-like 2 // 11p15.3 // 5775
1,41E-02	1,37	C1orf162	BC017973 // C1orf162 // chromosome 1 open reading frame 162 // 1p13.2 // 128346
5,01E-04	1,37	PLXNA3	NM_017514 // PLXNA3 // plexin A3 // Xq28 // 55558 /// ENST00000369682 // PLXNA3
2,38E-02	1,37	ADFP	NM_001122 // ADFP // adipose differentiation-related protein // 9p22.1 // 123 //
1,94E-02	1,36	TRIM16	NM_006470 // TRIM16 // tripartite motif-containing 16 // 17p11.2 // 10626 /// NM
1,90E-02	1,36	WNT10A	NM_025216 // WNT10A // wingless-type MMTV integration site family, member 10A //
5,01E-03	1,36	GPRC5C	NM_022036 // GPRC5C // G protein-coupled receptor, family C, group 5, member C /
3,33E-02	1,36	KCNS3	NM_002252 // KCNS3 // potassium voltage-gated channel, delayed-rectifier, subfam
4,58E-03	1,36	TNIP2	NM_024309 // TNIP2 // TNFAIP3 interacting protein 2 // 4p16.3 // 79155 /// ENST0
4,60E-03	1,36	LY75	NM_002349 // LY75 // lymphocyte antigen 75 // 2q24 // 4065 /// NM_014880 // CD30
2,79E-02	1,36	S100A13	NM_001024210 // S100A13 // S100 calcium binding protein A13 // 1q21 // 6284 ///
9,39E-04	1,36	CREG1	NM_003851 // CREG1 // cellular repressor of E1A-stimulated genes 1 // 1q24 // 88
9,85E-03	**1,36**	**COL11A1**	**NM_001854 // COL11A1 // collagen, type XI, alpha 1 // 1p21 // 1301 /// NM_080629**
3,53E-02	1,35	KIAA0776	BC036379 // KIAA0776 // KIAA0776 // 6q16.1 // 23376 /// BC028608 // KIAA0776 //
1,69E-03	1,35	SLITRK2	NM_032539 // SLITRK2 // SLIT and NTRK-like family, member 2 // Xq27.3 // 84631 /
2,26E-03	1,35	HPCAL1	NM_002149 // HPCAL1 // hippocalcin-like 1 // 2p25.1 // 3241 /// NM_134421 // HPC
3,16E-02	1,35	MAP6	NM_207577 // MAP6 // microtubule-associated protein 6 // 11q13.5 // 4135 /// NM_
1,12E-03	**1,35**	**CDH1**	**NM_004360 // CDH1 // cadherin 1, type 1, E-cadherin (epithelial) // 16q22.1 // 9**
6,37E-03	1,35	JUNB	NM_002229 // JUNB // jun B proto-oncogene // 19p13.2 // 3726 /// ENST00000302754
4,88E-02	1,35	DPY19L2P2	NR_003561 // DPY19L2P2 // dpy-19-like 2 pseudogene 2 (C. elegans) // 7q22.1 // 3
4,56E-02	-1,35	ISCA2	NM_194279 // ISCA2 // iron-sulfur cluster assembly 2 homolog (S. cerevisiae) //
2,02E-02	-1,35	ZNF767	NM_024910 // ZNF767 // zinc finger family member 767 // 7q36.1 // 79970 /// ENST
1,53E-02	-1,35	E2F8	NM_024680 // E2F8 // E2F transcription factor 8 // 11p15.1 // 79733 /// ENST0000
1,97E-03	-1,35	KLHL4	NM_019117 // KLHL4 // kelch-like 4 (Drosophila) // Xq21.3 // 56062 /// NM_057162
2,30E-02	-1,35	FSIP1	NM_152597 // FSIP1 // fibrous sheath interacting protein 1 // 15q14 // 161835 //
3,16E-02	-1,35	UHRF1	NM_001048201 // UHRF1 // ubiquitin-like, containing PHD and RING finger domains,
1,37E-02	-1,35	RND2	NM_005440 // RND2 // Rho family GTPase 2 // 17q21 // 8153 /// ENST00000225973 //

p value	FC	Gene Symbol	Gene_assignment
6,53E-04	-1,35	PAK1	NM_002576 // PAK1 // p21/Cdc42/Rac1-activated kinase 1 (STE20 homolog, yeast) //
6,32E-03	-1,36	ASNS	NM_133436 // ASNS // asparagine synthetase // 7q21.3 // 440 /// NM_183356 // ASN
2,02E-03	-1,36	ZNF81	NM_007137 // ZNF81 // zinc finger protein 81 // Xp11.23 // 347344 /// ENST000003
2,55E-02	-1,36	PTPN2	NM_002828 // PTPN2 // protein tyrosine phosphatase, non-receptor type 2 // 18p11
5,19E-03	-1,36	GNA13	NM_006572 // GNA13 // guanine nucleotide binding protein (G protein), alpha 13 /
1,08E-02	-1,36	FLJ16165	NM_001004318 // FLJ16165 // purple acid phosphatase long form // 19q13.2 // 3909
3,28E-04	-1,36	LAMA4	NM_001105206 // LAMA4 // laminin, alpha 4 // 6q21 // 3910 /// NM_002290 // LAMA4
1,82E-02	-1,36	ARNTL2	NM_020183 // ARNTL2 // aryl hydrocarbon receptor nuclear translocator-like 2 //
2,62E-02	-1,36	MGAT4A	NM_012214 // MGAT4A // mannosyl (alpha-1,3-)-glycoprotein beta-1,4-N-acetylgluco
4,12E-02	-1,36	CHN1	NM_001822 // CHN1 // chimerin (chimaerin) 1 // 2q31-q32.1 // 1123 /// NM_0010252
2,12E-02	-1,36	PLEKHH2	NM_172069 // PLEKHH2 // pleckstrin homology domain containing, family H (with My
2,83E-02	-1,36	EFHC2	NM_025184 // EFHC2 // EF-hand domain (C-terminal) containing 2 // Xp11.3 // 8025
4,23E-02	-1,36	KMO	NM_003679 // KMO // kynurenine 3-monooxygenase (kynurenine 3-hydroxylase) // 1q4
3,30E-03	-1,36	ZMAT3	NM_022470 // ZMAT3 // zinc finger, matrin type 3 // 3q26.3-q27 // 64393 /// NM_1
4,83E-02	-1,36		---
8,27E-03	-1,36	TFAM	NM_003201 // TFAM // transcription factor A, mitochondrial // 10q21 // 7019 ///
9,63E-03	-1,36	TMED8	NM_213601 // TMED8 // transmembrane emp24 protein transport domain containing 8
1,81E-02	-1,36	WDR89	NM_080666 // WDR89 // WD repeat domain 89 // 14q23.2 // 112840 /// NM_001008726
4,09E-02	-1,36	S100PBP	NM_022753 // S100PBP // S100P binding protein // 1p35.1 // 64766 /// ENST0000037
4,21E-02	-1,36	SYT1	NM_005639 // SYT1 // synaptotagmin I // 12cen-q21 // 6857 /// ENST00000393240 //
2,32E-03	-1,36	ZNF804A	NM_194250 // ZNF804A // zinc finger protein 804A // 2q32.1 // 91752 /// ENST0000
2,76E-03	-1,36	TNRC6C	NM_018996 // TNRC6C // trinucleotide repeat containing 6C // 17q25.3 // 57690 //
1,94E-03	-1,37	LHFP	NM_005780 // LHFP // lipoma HMGIC fusion partner // 13q12 // 10186 /// ENST00000
3,26E-03	-1,37	ZNF287	NM_020653 // ZNF287 // zinc finger protein 287 // 17p11.2 // 57336 /// ENST00000
7,25E-04	-1,37	MICAL2	NM_014632 // MICAL2 // microtubule associated monoxygenase, calponin and LIM dom
4,98E-02	-1,37	LCORL	NM_153686 // LCORL // ligand dependent nuclear receptor corepressor-like // 4p15
1,93E-03	-1,37	DNAJB1	NM_006145 // DNAJB1 // DnaJ (Hsp40) homolog, subfamily B, member 1 // 19p13.2 //
2,16E-02	-1,37	ACTR3B	NM_020445 // ACTR3B // ARP3 actin-related protein 3 homolog B (yeast) // 7q36.1
5,33E-03	-1,37	HMGA2	NM_003483 // HMGA2 // high mobility group AT-hook 2 // 12q15 // 8091 /// NM_0034
4,02E-02	-1,37	MAML2	NM_032427 // MAML2 // mastermind-like 2 (Drosophila) // 11q21 // 84441 /// ENST0
3,52E-02	-1,37	EXOC2	NM_018303 // EXOC2 // exocyst complex component 2 // 6p25.3 // 55770 /// ENST000
2,85E-02	-1,37	MCM10	NM_182751 // MCM10 // minichromosome maintenance complex component 10 // 10p13 /
1,10E-03	-1,37	OTUB2	NM_023112 // OTUB2 // OTU domain, ubiquitin aldehyde binding 2 // 14q32.13 // 78
3,59E-02	-1,37	HES7	NM_032580 // HES7 // hairy and enhancer of split 7 (Drosophila) // 17p13.1 // 84
3,99E-03	-1,37	ANKRD44	NM_153697 // ANKRD44 // ankyrin repeat domain 44 // 2q33.1 // 91526 /// ENST0000
3,74E-03	-1,37	SAE1	NM_005500 // SAE1 // SUMO1 activating enzyme subunit 1 // 19q13.32 // 10055 ///
1,44E-04	-1,38	NSUN7	NM_024677 // NSUN7 // NOL1/NOP2/Sun domain family, member 7 // 4p14 // 79730 ///
3,72E-02	-1,38	NTN4	NM_021229 // NTN4 // netrin 4 // 12q22-q23 // 59277 /// ENST00000343702 // NTN4
3,79E-02	-1,38	RAD51AP1	NM_006479 // RAD51AP1 // RAD51 associated protein 1 // 12p13.2-p13.1 // 10635 //
4,66E-02	-1,38	C18orf24	NM_001039535 // C18orf24 // chromosome 18 open reading frame 24 // 18q21.1 // 22
4,18E-03	-1,38	SRGAP1	NM_020762 // SRGAP1 // SLIT-ROBO Rho GTPase activating protein 1 // 12q14.2 // 5

p value	FC	Gene Symbol	Gene_assignment
1,09E-02	-1,38	GINS1	NM_021067 // GINS1 // GINS complex subunit 1 (Psf1 homolog) // 20p11.21 // 9837
1,74E-02	-1,38	ARHGAP19	NM_032900 // ARHGAP19 // Rho GTPase activating protein 19 // 10q24.1 // 84986 //
4,35E-02	-1,38	CROT	NM_021151 // CROT // carnitine O-octanoyltransferase // 7q21.1 // 54677 /// ENST
1,03E-02	-1,38	BNC2	NM_017637 // BNC2 // basonuclin 2 // 9p22.3-p22.2 // 54796 /// ENST00000380672 /
4,28E-02	-1,38	IGF2BP2	NM_006548 // IGF2BP2 // insulin-like growth factor 2 mRNA binding protein 2 // 3
3,59E-02	-1,38	FLI1	NM_002017 // FLI1 // Friend leukemia virus integration 1 // 11q24.1-q24.3 // 231
3,85E-02	-1,38	KIAA0408	NM_014702 // KIAA0408 // KIAA0408 // 6q22.33 // 9729 /// NM_001012279 // C6orf17
4,92E-04	-1,38	KBTBD6	NM_152903 // KBTBD6 // kelch repeat and BTB (POZ) domain containing 6 // 13q14.1
3,98E-04	-1,38	PHKB	NM_001031835 // PHKB // phosphorylase kinase, beta // 16q12-q13 // 5257 /// NM_0
2,22E-03	-1,38	RAB22A	NM_020673 // RAB22A // RAB22A, member RAS oncogene family // 20q13.32 // 57403 /
3,06E-03	-1,38	DDIT3	NM_004083 // DDIT3 // DNA-damage-inducible transcript 3 // 12q13.1-q13.2 // 1649
7,41E-04	-1,38	MT1DP	NR_003658 // MT1DP // metallothionein 1D (pseudogene) // 16q13 // 326343 /// NM_
1,31E-02	-1,39	SSH2	NM_033389 // SSH2 // slingshot homolog 2 (Drosophila) // 17q11.2 // 85464 /// EN
4,24E-02	-1,39	PDP2	NM_020786 // PDP2 // pyruvate dehydrogenase phosphatase isoenzyme 2 // 16q22.1 /
1,53E-02	-1,39	TUBD1	NM_016261 // TUBD1 // tubulin, delta 1 // 17q23.1 // 51174 /// ENST00000325752 /
7,91E-04	-1,39	LIMA1	NM_001113546 // LIMA1 // LIM domain and actin binding 1 // 12q13 // 51474 /// NM
1,22E-04	-1,39	IL6R	NM_000565 // IL6R // interleukin 6 receptor // 1q21 // 3570 /// NM_181359 // IL6
1,72E-03	-1,39	MLLT11	NM_006818 // MLLT11 // myeloid/lymphoid or mixed-lineage leukemia (trithorax hom
1,61E-02	-1,39	FDX1	NM_004109 // FDX1 // ferredoxin 1 // 11q22 // 2230 /// ENST00000260270 // FDX1 /
5,49E-04	-1,39	HLCS	NM_000411 // HLCS // holocarboxylase synthetase (biotin-(proprionyl-Coenzyme A-c
1,04E-02	-1,39	SCML1	NM_001037540 // SCML1 // sex comb on midleg-like 1 (Drosophila) // Xp22.2-p22.1
5,15E-03	-1,39	NDUFA12	NM_018838 // NDUFA12 // NADH dehydrogenase (ubiquinone) 1 alpha subcomplex, 12 /
2,28E-02	-1,39	ZNF616	NM_178523 // ZNF616 // zinc finger protein 616 // 19q13.33 // 90317 /// ENST0000
1,14E-02	-1,39	DMC1	NM_007068 // DMC1 // DMC1 dosage suppressor of mck1 homolog, meiosis-specific ho
4,67E-04	-1,40	DSC2	NM_004949 // DSC2 // desmocollin 2 // 18q12.1 // 1824 /// NM_024422 // DSC2 // d
2,40E-03	-1,40	ETV4	NM_001986 // ETV4 // ets variant gene 4 (E1A enhancer binding protein, E1AF) //
3,00E-02	-1,40	PYGO1	NM_015617 // PYGO1 // pygopus homolog 1 (Drosophila) // 15q21.1 // 26108 /// ENS
3,69E-03	-1,40	MID1	NM_000381 // MID1 // midline 1 (Opitz/BBB syndrome) // Xp22 // 4281 /// NM_03329
3,08E-02	-1,40	FASTKD3	NM_024091 // FASTKD3 // FAST kinase domains 3 // 5p15.3-p15.2 // 79072 /// ENST0
4,60E-02	-1,40	C3orf34	BC007827 // C3orf34 // chromosome 3 open reading frame 34 // 3q29 // 84984 /// A
7,58E-03	-1,40	DOCK4	NM_014705 // DOCK4 // dedicator of cytokinesis 4 // 7q31.1 // 9732 /// ENST00000
3,77E-02	-1,40	DUSP12	NM_007240 // DUSP12 // dual specificity phosphatase 12 // 1q21-q22 // 11266 ///
1,84E-03	-1,40	MAP7	NM_003980 // MAP7 // microtubule-associated protein 7 // 6q23.3 // 9053 /// ENST
1,15E-02	-1,41	ZNF204	NR_002722 // ZNF204 // zinc finger protein 204 (pseudogene) // 6p21.3 // 7754 //
7,50E-03	-1,41	MPP5	NM_022474 // MPP5 // membrane protein, palmitoylated 5 (MAGUK p55 subfamily memb
2,24E-04	-1,41	ZNF185	NM_007150 // ZNF185 // zinc finger protein 185 (LIM domain) // Xq28 // 7739 ///
1,89E-02	-1,41	ARNT	NM_001668 // ARNT // aryl hydrocarbon receptor nuclear translocator // 1q21 // 4
2,06E-05	-1,41	KIAA0515	NM_013318 // KIAA0515 // KIAA0515 // 9q34.13 // 84726 /// ENST00000357304 // KIA
6,64E-05	-1,41	MAP3K15	NM_001001671 // MAP3K15 // mitogen-activated protein kinase kinase kinase 15 //
3,33E-02	-1,42	NAPEPLD	NM_001122838 // NAPEPLD // N-acyl phosphatidylethanolamine phospholipase D // 7q
2,48E-02	-1,42	DBT	NM_001918 // DBT // dihydrolipoamide branched chain transacylase E2 // 1p31 // 1

p value	FC	Gene Symbol	Gene_assignment
8,35E-04	-1,42	RBMS3	NM_001003793 // RBMS3 // RNA binding motif, single stranded interacting protein
1,85E-02	-1,42	RNF182	NM_152737 // RNF182 // ring finger protein 182 // 6p23 // 221687 /// ENST0000031
6,94E-04	-1,42	DNAJA3	NM_005147 // DNAJA3 // DnaJ (Hsp40) homolog, subfamily A, member 3 // 16p13.3 //
2,85E-02	-1,42	CHAC2	NM_001008708 // CHAC2 // ChaC, cation transport regulator homolog 2 (E. coli) //
2,43E-02	-1,42	DDAH1	NM_012137 // DDAH1 // dimethylarginine dimethylaminohydrolase 1 // 1p22 // 23576
1,74E-02	-1,42	ERLIN1	NM_006459 // ERLIN1 // ER lipid raft associated 1 // 10q21-q22 // 10613 /// NM_0
4,57E-03	-1,42	C16orf75	BC039361 // C16orf75 // chromosome 16 open reading frame 75 // 16p13.13 // 11602
6,76E-03	-1,43	ETFA	NM_000126 // ETFA // electron-transfer-flavoprotein, alpha polypeptide (glutaric
4,92E-02	-1,43	HIST1H3C	NM_003531 // HIST1H3C // histone cluster 1, H3c // 6p21.3 // 8352 /// ENST000003
2,98E-02	-1,43	KRT81	NM_002281 // KRT81 // keratin 81 // 12q13 // 3887 /// ENST00000327741 // KRT81 /
7,29E-03	-1,44	CXorf57	BC011483 // CXorf57 // chromosome X open reading frame 57 // Xq22.3 // 55086 ///
2,70E-03	-1,44	KIAA0101	NM_014736 // KIAA0101 // KIAA0101 // 15q22.31 // 9768 /// NM_001029989 // KIAA01
2,43E-02	-1,44	ATAD5	NM_024857 // ATAD5 // ATPase family, AAA domain containing 5 // 17q11.2 // 79915
1,56E-03	-1,44	PHGDH	NM_006623 // PHGDH // phosphoglycerate dehydrogenase // 1p12 // 26227 /// ENST00
1,74E-06	-1,45	STAT3	NM_139276 // STAT3 // signal transducer and activator of transcription 3 (acute-
4,36E-02	-1,45	C20orf121	NM_024331 // C20orf121 // chromosome 20 open reading frame 121 // 20q13.12 // 79
2,61E-03	-1,45	RHCG	NM_016321 // RHCG // Rh family, C glycoprotein // 15q25 // 51458 /// ENST0000026
1,37E-02	-1,45	ZNF382	NM_032825 // ZNF382 // zinc finger protein 382 // 19q13.12 // 84911 /// ENST0000
9,34E-03	-1,45	INTS6	NM_012141 // INTS6 // integrator complex subunit 6 // 13q14.12-q14.2 // 26512 //
7,65E-03	-1,45	AK3	NM_016282 // AK3 // adenylate kinase 3 // 9p24.1-p24.3 // 50808 /// ENST00000381
7,02E-03	-1,45	HIST1H2BM	NM_003521 // HIST1H2BM // histone cluster 1, H2bm // 6p22-p21.3 // 8342 /// ENST
4,45E-02	-1,45	SRGN	NM_002727 // SRGN // serglycin // 10q22.1 // 5552 /// ENST00000242465 // SRGN //
6,88E-03	-1,46	C17orf85	NM_018553 // C17orf85 // chromosome 17 open reading frame 85 // 17p13.2 // 55421
4,81E-02	-1,46	EEA1	NM_003566 // EEA1 // early endosome antigen 1 // 12q22 // 8411 /// ENST000003223
1,90E-02	-1,46	CDC2	NM_001786 // CDC2 // cell division cycle 2, G1 to S and G2 to M // 10q21.1 // 98
4,67E-02	-1,46	FLRT3	NM_198391 // FLRT3 // fibronectin leucine rich transmembrane protein 3 // 20p11
1,16E-03	-1,46	GPD1L	NM_015141 // GPD1L // glycerol-3-phosphate dehydrogenase 1-like // 3p22.3 // 231
2,63E-02	-1,46	C12orf24	NM_013300 // C12orf24 // chromosome 12 open reading frame 24 // 12q24.11 // 2990
4,14E-02	-1,47	COMMD10	NM_016144 // COMMD10 // COMM domain containing 10 // 5q23.1 // 51397 /// ENST000
6,05E-03	-1,47	ACTR6	NM_022496 // ACTR6 // ARP6 actin-related protein 6 homolog (yeast) // 12q23.1 //
3,34E-02	-1,47	FANCM	NM_020937 // FANCM // Fanconi anemia, complementation group M // 14q21.3 // 5769
3,39E-02	-1,47	DEFB128	NM_001037732 // DEFB128 // defensin, beta 128 // 20p13 // 245939 /// ENST0000033
1,13E-02	-1,47	NUDT5	NM_014142 // NUDT5 // nudix (nucleoside diphosphate linked moiety X)-type motif
2,53E-02	-1,47	PRO0628	ENST00000327069 // PRO0628 // Putative uncharacterized protein PRO0628 // 20q12
2,02E-03	-1,47	DEPDC7	NM_001077242 // DEPDC7 // DEP domain containing 7 // 11p13 // 91614 /// NM_13916
1,18E-03	-1,48	B4GALT6	NM_004775 // B4GALT6 // UDP-Gal:betaGlcNAc beta 1,4- galactosyltransferase, poly
5,18E-03	-1,48	FAM111A	NM_022074 // FAM111A // family with sequence similarity 111, member A // 11q12.1
1,52E-02	-1,48	NEDD4	NM_006154 // NEDD4 // neural precursor cell expressed, developmentally down-regu
3,03E-05	-1,48	RDX	NM_002906 // RDX // radixin // 11q23 // 5962 /// ENST00000343115 // RDX // radix
2,33E-03	-1,48	POLR3F	NM_006466 // POLR3F // polymerase (RNA) III (DNA directed) polypeptide F, 39 kDa

p value	FC	Gene Symbol	Gene_assignment
2,29E-02	-1,49	GLIS3	NM_001042413 // GLIS3 // GLIS family zinc finger 3 // 9p24.2 // 169792 /// NM_15
2,70E-03	-1,49	LYSMD1	NM_212551 // LYSMD1 // LysM, putative peptidoglycan-binding, domain containing 1
1,24E-02	-1,49	ZNF14	NM_021030 // ZNF14 // zinc finger protein 14 // 19p13.3-p13.2 // 7561 /// ENST00
2,68E-02	-1,49	CTNNB1	NM_001904 // CTNNB1 // catenin (cadherin-associated protein), beta 1, 88kDa // 3
1,22E-02	-1,50	ACOT12	NM_130767 // ACOT12 // acyl-CoA thioesterase 12 // 5q14.1 // 134526 /// ENST0000
2,06E-04	-1,50	KIAA0515	NM_013318 // KIAA0515 // KIAA0515 // 9q34.13 // 84726 /// NR_002914 // SNORD62A
9,57E-03	-1,50	ELMOD1	NM_018712 // ELMOD1 // ELMO/CED-12 domain containing 1 // 11q22.3 // 55531 /// E
8,13E-05	-1,51	TRPA1	NM_007332 // TRPA1 // transient receptor potential cation channel, subfamily A,
7,07E-03	-1,51	RASGRF2	NM_006909 // RASGRF2 // Ras protein-specific guanine nucleotide-releasing factor
7,22E-03	-1,51	AGPAT9	NM_032717 // AGPAT9 // 1-acylglycerol-3-phosphate O-acyltransferase 9 // 4q21.23
3,10E-02	-1,51	ZNF491	NM_152356 // ZNF491 // zinc finger protein 491 // 19p13.2 // 126069 /// ENST0000
3,77E-02	-1,51	PXK	NM_017771 // PXK // PX domain containing serine/threonine kinase // 3p14.3 // 54
2,98E-02	-1,52	PBK	NM_018492 // PBK // PDZ binding kinase // 8p21.2 // 55872 /// ENST00000301905 //
3,29E-03	-1,52	KLHL2	NM_007246 // KLHL2 // kelch-like 2, Mayven (Drosophila) // 4q21.2 // 11275 /// E
3,62E-02	-1,52	C1orf104	BC131614 // C1orf104 // chromosome 1 open reading frame 104 // 1q22 // 284618 //
2,13E-02	-1,52	PRIM1	NM_000946 // PRIM1 // primase, DNA, polypeptide 1 (49kDa) // 12q13 // 5557 /// E
1,19E-02	-1,52	BCL2A1	NM_001114735 // BCL2A1 // BCL2-related protein A1 // 15q24.3 // 597 /// NM_00404
3,42E-04	-1,53	KLHL13	NM_033495 // KLHL13 // kelch-like 13 (Drosophila) // Xq23-q24 // 90293 /// ENST0
9,57E-04	-1,53	FRMD6	NM_001042481 // FRMD6 // FERM domain containing 6 // 14q22.1 // 122786 /// NM_15
2,42E-03	-1,53	PDHX	NM_003477 // PDHX // pyruvate dehydrogenase complex, component X // 11p13 // 805
5,13E-03	-1,53	UPK1B	NM_006952 // UPK1B // uroplakin 1B // 3q13.3-q21 // 7348 /// ENST00000264234 //
2,01E-03	-1,53	DHX33	NM_020162 // DHX33 // DEAH (Asp-Glu-Ala-His) box polypeptide 33 // 17p13.2 // 56
1,99E-03	-1,54	SETD8	NM_020382 // SETD8 // SET domain containing (lysine methyltransferase) 8 // 12q2
2,64E-02	-1,54	HIST1H4B	NM_003544 // HIST1H4B // histone cluster 1, H4b // 6p21.3 // 8366 /// ENST000003
4,92E-03	-1,55	EXO1	NM_130398 // EXO1 // exonuclease 1 // 1q42-q43 // 9156 /// NM_006027 // EXO1 //
2,64E-03	-1,55	SCARNA8	NR_003009 // SCARNA8 // small Cajal body-specific RNA 8 // 9p22.1 // 677776 ///
1,09E-02	-1,55	C7orf46	BC042034 // C7orf46 // chromosome 7 open reading frame 46 // 7p15.3 // 340277 //
2,92E-02	-1,56	TLR6	NM_006068 // TLR6 // toll-like receptor 6 // 4p14 // 10333 /// ENST00000381950 /
2,04E-02	-1,56	AKR1B10	NM_020299 // AKR1B10 // aldo-keto reductase family 1, member B10 (aldose reducta
1,02E-04	-1,58	ASAM	NM_024769 // ASAM // adipocyte-specific adhesion molecule // 11q24.1 // 79827 //
3,14E-02	-1,58	RIG	U32331 // RIG // regulated in glioma // 11p15.1 // 10530
6,82E-05	-1,58	DCTN5	NM_032486 // DCTN5 // dynactin 5 (p25) // 16p12.1 // 84516 /// ENST00000300087 /
1,22E-02	-1,58	MCEE	NM_032601 // MCEE // methylmalonyl CoA epimerase // 2p13.3 // 84693 /// ENST0000
2,34E-02	-1,58	MOCS2	NM_176806 // MOCS2 // molybdenum cofactor synthesis 2 // 5q11 // 4338 /// NM_004
1,93E-03	-1,59	CAMK2N1	NM_018584 // CAMK2N1 // calcium/calmodulin-dependent protein kinase II inhibitor
1,89E-02	-1,59	UAP1	NM_003115 // UAP1 // UDP-N-acteylglucosamine pyrophosphorylase 1 // 1q23.3 // 66
2,06E-02	-1,59	EXTL2	NM_001439 // EXTL2 // exostoses (multiple)-like 2 // 1p21 // 2135 /// NM_0010330
3,93E-04	-1,60	FAM129A	NM_052966 // FAM129A // family with sequence similarity 129, member A // 1q25 //
2,05E-02	-1,61	TGDS	NM_014305 // TGDS // TDP-glucose 4,6-dehydratase // 13q32.1 // 23483 /// ENST000
1,51E-02	-1,61	PEX11B	NM_003846 // PEX11B // peroxisomal biogenesis factor 11B // 1q21.1 // 8799 /// E
2,01E-02	-1,61	DLEU2	NR_002612 // DLEU2 // deleted in lymphocytic leukemia, 2 // 13q14.3 // 8847 ///

p value	FC	Gene Symbol	Gene_assignment
3,67E-02	-1,61	COQ3	NM_017421 // COQ3 // coenzyme Q3 homolog, methyltransferase (S. cerevisiae) // 6
9,37E-04	-1,61	CXorf15	NM_018360 // CXorf15 // chromosome X open reading frame 15 // Xp22.2 // 55787 //
3,35E-02	-1,61	FLJ45139	ENST00000380931 // FLJ45139 // FLJ45139 protein // 21q22.2 // 400867 /// AK12708
2,81E-02	-1,62	FAM111B	AY457926 // FAM111B // family with sequence similarity 111, member B // 11q12.1
2,47E-03	-1,62	PCNA	NM_002592 // PCNA // proliferating cell nuclear antigen // 20pter-p12 // 5111 //
2,62E-03	-1,62	RAB39	NM_017516 // RAB39 // RAB39, member RAS oncogene family // --- // 54734 /// ENST
1,31E-02	-1,62	OXNAD1	NM_138381 // OXNAD1 // oxidoreductase NAD-binding domain containing 1 // 3p25-p2
1,55E-02	-1,63	HIST1H2AH	NM_080596 // HIST1H2AH // histone cluster 1, H2ah // 6p21.33 // 85235 /// ENST00
2,76E-03	-1,63	C1orf128	NM_020362 // C1orf128 // chromosome 1 open reading frame 128 // 1p36.11 // 57095
2,67E-02	-1,64	FAM116A	BC040291 // FAM116A // family with sequence similarity 116, member A // 3p14.3 /
4,07E-02	-1,64	RPL41	NM_001035267 // RPL41 // ribosomal protein L41 // 12q13 // 6171 /// NM_021104 //
8,03E-03	-1,64	RBM35A	NM_017697 // RBM35A // RNA binding motif protein 35A // 8q22.1 // 54845 /// NM_0
2,89E-02	-1,65	ATP6V1E2	NM_080653 // ATP6V1E2 // ATPase, H+ transporting, lysosomal 31kDa, V1 subunit E2
9,23E-03	-1,68	IL18	NM_001562 // IL18 // interleukin 18 (interferon-gamma-inducing factor) // 11q22.
1,17E-02	-1,68	WDR76	NM_024908 // WDR76 // WD repeat domain 76 // 15q15.3 // 79968 /// ENST0000026379
5,11E-03	-1,69	EMP1	NM_001423 // EMP1 // epithelial membrane protein 1 // 12p12.3 // 2012 /// ENST00
4,30E-03	-1,69	LOC727817	XM_001125873 // LOC727817 // hypothetical LOC727817 // --- // 727817
7,79E-04	-1,69	BDH1	NM_203314 // BDH1 // 3-hydroxybutyrate dehydrogenase, type 1 // 3q29 // 622 ///
1,39E-02	-1,69	SLC30A6	NM_017964 // SLC30A6 // solute carrier family 30 (zinc transporter), member 6 //
2,40E-02	-1,70	FLJ14327	AK024389 // FLJ14327 // hypothetical protein FLJ14327 // 16q23.2 // 79972
3,66E-02	-1,71	HIST1H1T	NM_005323 // HIST1H1T // histone cluster 1, H1t // 6p21.3 // 3010 /// ENST000003
2,03E-04	-1,71	C15orf15	NM_016304 // C15orf15 // chromosome 15 open reading frame 15 // 15q21 // 51187 /
4,21E-02	-1,73	WASF1	NM_003931 // WASF1 // WAS protein family, member 1 // 6q21-q22 // 8936 /// NM_00
1,73E-02	-1,74	LYPLA1	NM_006330 // LYPLA1 // lysophospholipase I // 8q11.23 // 10434 /// ENST000003169
1,50E-03	-1,74	GRK5	NM_005308 // GRK5 // G protein-coupled receptor kinase 5 // 10q24-qter // 2869 /
2,67E-02	-1,76	SRP9	NM_003133 // SRP9 // signal recognition particle 9kDa // 1q42.12 // 6726 /// BC0
2,14E-02	-1,76	FGF5	NM_004464 // FGF5 // fibroblast growth factor 5 // 4q21 // 2250 /// NM_033143 //
3,68E-03	-1,77	C10orf83	NM_178832 // C10orf83 // chromosome 10 open reading frame 83 // 10q24.1 // 11881
2,11E-03	-1,85	C14orf147	NM_138288 // C14orf147 // chromosome 14 open reading frame 147 // 14q13.1 // 171
6,54E-04	-1,86	FAM71D	NM_173526 // FAM71D // family with sequence similarity 71, member D // 14q23.3 /
9,95E-04	-1,87	BCAT1	NM_005504 // BCAT1 // branched chain aminotransferase 1, cytosolic // 12pter-q12
1,21E-03	-1,88	TMEM156	NM_024943 // TMEM156 // transmembrane protein 156 // 4p14 // 80008 /// ENST00000
1,04E-02	-1,88	ZNF681	NM_138286 // ZNF681 // zinc finger protein 681 // 19p12 // 148213 /// ENST000003
7,90E-03	-1,94	PLCZ1	NM_033123 // PLCZ1 // phospholipase C, zeta 1 // 12p12.3 // 89869 /// ENST000002
1,06E-05	-1,95	BTG3	NM_006806 // BTG3 // BTG family, member 3 // 21q21.1-q21.2 // 10950 /// ENST0000
9,59E-03	-1,96	FAM54A	NM_001099286 // FAM54A // family with sequence similarity 54, member A // 6q23.3
2,65E-02	-1,98	HIST1H2BC	NM_003526 // HIST1H2BC // histone cluster 1, H2bc // 6p21.3 // 8347 /// ENST0000
1,86E-02	-1,98	RGS17	NM_012419 // RGS17 // regulator of G-protein signaling 17 // 6q25.3 // 26575 ///
1,28E-04	-2,15	RAG1AP1	NM_018845 // RAG1AP1 // recombination activating gene 1 activating protein 1 //
2,25E-02	-2,33	KRTAP9-3	NM_031962 // KRTAP9-3 // keratin associated protein 9-3 // 17q12-q21 // 83900 //
3,63E-03	-2,46	PRR4	NM_001098538 // PRR4 // proline rich 4 (lacrimal) // 12p13 // 11272 /// NM_00625

p value	FC	Gene Symbol	Gene_assignment
3,52E-02	-2,63	HIST1H4L	NM_003546 // HIST1H4L // histone cluster 1, H4l // 6p22-p21.3 // 8368 /// ENST00
6,38E-08	**-4,49**	**LGALS1**	**NM_002305 // LGALS1 // lectin, galactoside-binding, soluble, 1 (galectin 1) // 2**

Table S6. List of genes significantly altered when Gal-1 was downregulated in PANC-1 compared to control cells (data from non-infected cells with the genes found altered in the shCtl filtered). Fold change (FC) is given in positive values (upper part of the table) when the gene is upregulated in knocked down cells (opposite direction of Gal-1). These genes are ordered by increasing p value until p=0.05. In the lower part of the table, FC is negative and p values are decreasing. These genes showed decreased expression when Gal-1 was downregulated (same direction as Gal-1). The first column shows p values.

6.2 RWP-1 DATA

6.2.1 Gene Detailed Analysis in RWP-1 Group

logFC	AveExpr	adj.P.Val	unlist.symbol	Gene description
-3,1085	7,8388699	2,91E-012	CXCL1	chemokine (C-X-C motif) ligand 1 (melanoma growth stimulating activity, alpha)
-2,7824	5,3614412	2,68E-011	TNFAIP3	tumor necrosis factor, alpha-induced protein 3
-2,9519	5,4801912	1,57E-010	CXCL2	chemokine (C-X-C motif) ligand 2
-1,9896	5,7195835	1,57E-010	MITF	microphthalmia-associated transcription factor
-3,4235	6,029052	1,98E-010	LCN2	lipocalin 2 (oncogene 24p3)
-2,0532	5,9563014	4,52E-010	CXCL3	chemokine (C-X-C motif) ligand 3
-2,7859	5,9135908	1,70E-009	HLA-DPA1	major histocompatibility complex, class II, DP alpha 1
-2,4919	5,2450362	4,77E-009	SERPINA3	serpin peptidase inhibitor, clade A (alpha-1 antiproteinase, antitrypsin), member 3
-1,8741	8,425175	5,40E-009	NFKBIA	nuclear factor of kappa light polypeptide gene enhancer in B-cells inhibitor, alpha
-3,3197	5,717696	1,37E-008	BIRC3	baculoviral IAP repeat-containing 3
-1,9331	6,0330673	1,38E-008	IL32	interleukin 32
-3,8445	4,0652303	8,58E-008	GPR15	G protein-coupled receptor 15
2,2195	7,488583	2,98E-007	HMGN4	high mobility group nucleosomal binding domain 4
2,7105	4,3283582	2,98E-007	CALB1	calbindin 1, 28kDa
-2,1668	4,5717698	5,99E-007	MMP7	matrix metallopeptidase 7 (matrilysin, uterine)
-1,6725	8,7297242	5,99E-007	TM4SF18	transmembrane 4 L six family member 18
-0,988	7,7930137	7,53E-007	NFKB2	nuclear factor of kappa light polypeptide gene enhancer in B-cells 2 (p49/p100)
-1,4467	6,7976742	9,41E-007	CD74	CD74 molecule, major histocompatibility complex, class II invariant chain
-1,6608	**6,0737383**	**1,00E-006**	**PLAT**	**plasminogen activator, tissue**
-1,7918	4,1493018	1,33E-006	FREM2	FRAS1 related extracellular matrix protein 2
-1,2041	6,6197334	1,33E-006	ZC3H12A	zinc finger CCCH-type containing 12A
-0,9183	5,7485471	1,33E-006	SORBS1	sorbin and SH3 domain containing 1
2,0161	3,9807685	1,73E-006	NRXN1	neurexin 1
-1,2262	7,4796915	1,90E-006	INS-IGF2	insulin- insulin-like growth factor 2
-1,2695	6,7698031	2,16E-006	PSMB9	proteasome (prosome, macropain) subunit, beta type, 9 (large multifunctional peptidase 2)
1,7275	4,9604253	2,82E-006	SLC16A6	solute carrier family 16, member 6 (monocarboxylic acid transporter 7)
-0,9863	5,3532921	2,94E-006	ABCA1	ATP-binding cassette, sub-family A (ABC1), member 1
-0,8481	6,6348578	2,94E-006	OAS3	2'-5'-oligoadenylate synthetase 3, 100kDa
-0,773	8,0491473	3,67E-006	TNFAIP2	tumor necrosis factor, alpha-induced protein 2
-1,4117	4,1743279	4,30E-006	PROM1	prominin 1
-1,4618	4,324335	4,32E-006	MBNL3	muscleblind-like 3 (Drosophila)
-1,112	4,6938251	5,15E-006	ACSL5	acyl-CoA synthetase long-chain family member 5
0,8987	7,2581026	5,51E-006	NRP1	neuropilin 1
-1,3812	6,4208611	5,66E-006	IGFBP3	insulin-like growth factor binding protein 3
1,3656	**5,4082545**	**6,05E-006**	**CCND2**	**cyclin D2**
-1,9409	4,9345281	6,05E-006	HLA-DRA	major histocompatibility complex, class II, DR alpha

logFC	AveExpr	adj.P.Val	unlist.symbol	Gene description
1,5228	5,4353924	6,79E-006	CTH	cystathionase (cystathionine gamma-lyase)
-1,4652	4,1149905	9,09E-006	RGS5	regulator of G-protein signaling 5
1,3496	5,3012083	9,09E-006	COL6A3	collagen, type VI, alpha 3
-1,7718	5,4896342	9,40E-006	HLA-DMA	major histocompatibility complex, class II, DM alpha
-1,6767	4,7002991	9,40E-006	SERPINB2	serpin peptidase inhibitor, clade B (ovalbumin), member 2
0,903	5,6735604	9,64E-006	SYTL2	synaptotagmin-like 2
-1,1556	5,0497559	1,13E-005	SERPINA1	serpin peptidase inhibitor, clade A (alpha-1 antiproteinase, antitrypsin), member 1
-1,3245	5,2807566	1,25E-005	TSPAN7	tetraspanin 7
-0,9311	4,2290402	1,32E-005	KIAA1622	KIAA1622
-0,871	6,659599	1,55E-005	OTUB2	OTU domain, ubiquitin aldehyde binding 2
-1,1842	3,7203601	1,69E-005	ESM1	endothelial cell-specific molecule 1
-1,273	3,9406787	1,90E-005	CADPS	Ca2+-dependent secretion activator
-2,0073	6,0396108	2,27E-005	IL8	interleukin 8
0,6372	7,1619379	4,61E-005	MLPH	melanophilin
-0,9636	7,144497	4,61E-005	LAMC2	laminin, gamma 2
-0,9711	4,5431968	5,36E-005	FBN2	fibrillin 2 (congenital contractural arachnodactyly)
-0,9341	5,3201087	5,36E-005	GPR110	G protein-coupled receptor 110
-0,8419	5,5514489	5,85E-005	MAP3K8	mitogen-activated protein kinase kinase kinase 8
-0,6536	8,0170018	6,16E-005	APOBEC3B	apolipoprotein B mRNA editing enzyme, catalytic polypeptide-like 3B
-0,6101	6,7637051	6,28E-005	SVIL	supervillin
-1,4011	6,5898279	6,57E-005	GALM	galactose mutarotase (aldose 1-epimerase)
-0,5755	6,9753633	7,09E-005	IRAK2	interleukin-1 receptor-associated kinase 2
-0,7388	6,7402969	7,55E-005	DOCK9	dedicator of cytokinesis 9
0,6904	7,5753697	0,000100491	LTBP2	latent transforming growth factor beta binding protein 2
-0,7067	5,9320656	0,000100491	SEC14L2	SEC14-like 2 (S. cerevisiae)
1,281	5,7257994	0,000111089	XYLT1	xylosyltransferase I
0,6862	7,719212	0,000119465	TRIB1	tribbles homolog 1 (Drosophila)
1,25	5,3486839	0,000133444	ZNF83	zinc finger protein 83
-1,2729	5,9043109	0,000150017	MPZL2	myelin protein zero-like 2
-1,2624	5,4989863	0,000153626	HLA-DPB1	major histocompatibility complex, class II, DP beta 1
-0,6773	6,9402832	0,000163892	BACH1	BTB and CNC homology 1, basic leucine zipper transcription factor 1
-1,6743	4,2589295	0,000176705	SPRR2A	small proline-rich protein 2A
-1,7103	4,6927299	0,000209027	NA	NA
1,3949	5,0740034	0,00024702	RGS4	regulator of G-protein signaling 4
-0,6981	6,4116829	0,00024702	PELI1	pellino homolog 1 (Drosophila)
-0,6755	7,9627778	0,000266038	TAPBP	TAP binding protein (tapasin)
-1,0727	5,4717042	0,00028454	ZNF738	zinc finger protein 738
-1,202	5,4024704	0,000291916	CIITA	class II, major histocompatibility complex, transactivator
1,5475	3,610408	0,000382126	NA	NA
-0,5702	7,1664354	0,000587136	CHST11	carbohydrate (chondroitin 4) sulfotransferase 11
0,7759	6,4740418	0,000587136	AREG	amphiregulin (schwannoma-derived growth factor) (AREG), mRNA

logFC	AveExpr	adj.P.Val	unlist.symbol	Gene description
-0,6051	7,1908146	0,000628701	OPTN	optineurin
0,5786	7,7602185	0,000733338	GPC1	glypican 1
-0,7322	7,0873592	0,000755018	ETS1	v-ets erythroblastosis virus E26 oncogene homolog 1 (avian)
-1,2013	3,5085862	0,000781826	VNN1	vanin 1
-0,5804	**7,7897209**	**0,000829615**	**PLAU**	**plasminogen activator, urokinase**
-0,5962	8,3677705	0,000914797	RIPK4	receptor-interacting serine-threonine kinase 4
0,8073	**9,8951242**	**0,000914797**	**LGALS1**	**lectin, galactoside-binding, soluble, 1 (galectin 1)**
-0,7142	3,9029447	0,000932562	ANKRD22	ankyrin repeat domain 22
-0,5287	5,9371448	0,000942659	PAPSS2	3'-phosphoadenosine 5'-phosphosulfate synthase 2
0,9006	5,2311207	0,00101209	PRF1	perforin 1 (pore forming protein)
0,7984	3,8838059	0,00101209	DSG4	desmoglein 4
-0,7116	4,7439352	0,001030805	NAV3	neuron navigator 3
0,4637	8,0741806	0,0010987	AXL	AXL receptor tyrosine kinase
-1,0536	4,5201487	0,001108939	TMEM45B	transmembrane protein 45B
-0,8716	5,9519055	0,001332684	ZNF626	zinc finger protein 626
-0,6426	4,8870502	0,001332684	KIAA1217	KIAA1217
-0,4746	7,0868291	0,001332684	EPDR1	ependymin related protein 1 (zebrafish)
0,7379	5,815431	0,001362636	TNFRSF19	tumor necrosis factor receptor superfamily, member 19
-0,5668	**6,8409339**	**0,001445629**	**PLAUR**	**plasminogen activator, urokinase receptor**
-0,5554	5,6477344	0,001455072	ZNF114	zinc finger protein 114
0,608	8,5122635	0,001593621	LIMA1	LIM domain and actin binding 1
-0,8082	5,9592845	0,001671025	RNF43	ring finger protein 43
-0,5123	8,735049	0,001751225	TSPAN15	tetraspanin 15
-0,677	5,7501335	0,001756086	DPYSL3	dihydropyrimidinase-like 3
-0,5684	8,5838771	0,001822373	PES1	pescadillo homolog 1, containing BRCT domain (zebrafish)
0,5815	4,6822903	0,001944136	ATRNL1	attractin-like 1
0,8512	5,5182332	0,001944136	PADI1	peptidyl arginine deiminase, type I
0,4942	8,1195451	0,002104449	EGR1	early growth response 1
-0,4892	5,4699368	0,002104449	HKR1	GLI-Kruppel family member HKR1
-0,9237	4,1675596	0,002133503	P2RY5	purinergic receptor P2Y, G-protein coupled, 5
0,7861	5,1198284	0,002514673	GALNT5	UDP-N-acetyl-alpha-D-galactosamine:polypeptide N-acetylgalactosaminyltransferase 5 (GalNAc-T5)
-0,7732	7,6032381	0,002722464	NEBL	nebulette
0,8855	7,9200013	0,003133568	STRN	striatin, calmodulin binding protein
0,4385	5,7687491	0,003199361	KIAA0746	KIAA0746 protein (KIAA0746), mRNA
-0,3981	8,6519001	0,003243241	RAB31	RAB31, member RAS oncogene family
-0,8596	3,527602	0,003514785	IL1A	interleukin 1, alpha
-0,4567	7,7780311	0,003763873	IGF1R	insulin-like growth factor 1 receptor
-0,7882	4,0452765	0,003763873	SPRR3	small proline-rich protein 3
-0,7153	4,9590996	0,003940758	OVOS2	ovostatin 2
-0,9056	6,4746413	0,003940758	SPRR2B	small proline-rich protein 2B
-1,0452	3,6865028	0,003940758	NA	NA

logFC	AveExpr	adj.P.Val	unlist.symbol	Gene description
0,6462	4,9467782	0,00412009	VIL1	villin 1
-0,4727	8,8625482	0,004200658	ETS2	v-ets erythroblastosis virus E26 oncogene homolog 2 (avian)
-0,7032	5,8345777	0,004202238	AKR1CL2	aldo-keto reductase family 1, member C-like 2
-0,4268	6,3163328	0,004522619	USP18	ubiquitin specific peptidase 18
-0,7915	3,1037379	0,004522619	DP58	cytosolic phosphoprotein DP58
-0,5928	11,23243	0,004535331	TM4SF1	transmembrane 4 L six family member 1
-0,4779	7,1139025	0,004535331	STAT5A	signal transducer and activator of transcription 5A
-0,4027	6,2860628	0,004546018	PKP2	plakophilin 2
-0,5469	5,5094749	0,004712265	GPR176	G protein-coupled receptor 176
0,6602	3,8816022	0,004737342	SLC16A4	solute carrier family 16, member 4 (monocarboxylic acid transporter 5)
-0,5311	5,0226132	0,004737342	BIK	BCL2-interacting killer (apoptosis-inducing)
0,4355	7,5279989	0,004737342	ABLIM1	actin binding LIM protein 1
0,4665	6,342835	0,004975514	PLEKHA7	pleckstrin homology domain containing, family A member 7
0,5786	8,1556478	0,005146411	ADORA2B	adenosine A2b receptor
0,7054	4,5181208	0,005253921	ATP8A2	ATPase, aminophospholipid transporter-like, Class I, type 8A, member 2
-0,7922	7,0818058	0,005406861	CPOX	coproporphyrinogen oxidase
-0,464	8,0785045	0,005655858	PTPRJ	protein tyrosine phosphatase, receptor type, J
0,5408	5,5268275	0,005906553	FST	follistatin
-1,1087	4,613534	0,006120064	GPR110	G protein-coupled receptor 110
-0,6856	5,5518467	0,006407106	CYP24A1	cytochrome P450, family 24, subfamily A, polypeptide 1
-0,6878	4,5158507	0,006407106	SLC16A9	solute carrier family 16, member 9 (monocarboxylic acid transporter 9)
-0,8607	3,8260445	0,006407106	SERPINB7	serpin peptidase inhibitor, clade B (ovalbumin), member 7
-0,5823	6,5667024	0,006847016	NFXL1	nuclear transcription factor, X-box binding-like 1
-0,6767	7,2350997	0,006988285	PLEK2	pleckstrin 2
0,6246	5,4117155	0,007006195	F3	coagulation factor III (thromboplastin, tissue factor)
0,5809	9,0341455	0,007571315	PADI2	peptidyl arginine deiminase, type II
-0,393	7,2123991	0,007682061	PPARD	peroxisome proliferator-activated receptor delta
-0,401	7,3477917	0,007798641	CKMT1B	creatine kinase, mitochondrial 1B
-0,3669	7,3423302	0,007867492	BACE2	beta-site APP-cleaving enzyme 2
-0,4442	5,419086	0,008119493	GBGT1	globoside alpha-1,3-N-acetylgalactosaminyltransferase 1
1,1142	4,5911494	0,008119493	PTGER2	prostaglandin E receptor 2 (subtype EP2), 53kDa
-0,6087	3,7772982	0,00849053	PLCB4	phospholipase C, beta 4
-0,4146	7,983349	0,008807274	KIAA1618	KIAA1618
-1,0716	4,2719408	0,00911596	NA	NA
-0,9466	5,2783805	0,00954548	SPRR1B	small proline-rich protein 1B (cornifin)
-0,7141	4,0083268	0,01002482	ZNF321	zinc finger protein 321
-0,607	8,9048279	0,01042767	CLDND1	claudin domain containing 1
0,8033	5,5307503	0,010469673	GAP43	growth associated protein 43
-0,8111	5,0600934	0,010746934	SGPP2	sphingosine-1-phosphate phosphotase 2
-0,4515	6,064583	0,011639904	C20orf42	chromosome 20 open reading frame 42
1,1045	5,3845131	0,011639904	FGFBP1	fibroblast growth factor binding protein 1

logFC	AveExpr	adj.P.Val	unlist.symbol	Gene description
-0,6516	5,1626308	0,011639904	GREM1	gremlin 1, cysteine knot superfamily, homolog (Xenopus laevis)
-0,397	7,3093508	0,011639904	PIH1D1	PIH1 domain containing 1
-1,056	3,904318	0,011979631	OTUD6A	OTU domain containing 6A
-0,4991	6,0165997	0,012062715	FAM81A	family with sequence similarity 81, member A
-0,7077	5,7853103	0,012121994	FLJ90757	hypothetical protein LOC440465
-0,4392	6,8837271	0,012994242	ZNF468	zinc finger protein 468
-0,4179	7,09255	0,013346364	TRIM21	tripartite motif-containing 21
-0,6165	5,3838186	0,013354363	TIFA	TRAF-interacting protein with a forkhead-associated domain
0,7602	7,7798518	0,013857081	PAM	peptidylglycine alpha-amidating monooxygenase
0,6823	3,9834704	0,014372835	SLC44A5	solute carrier family 44, member 5
0,6606	5,975048	0,014439274	OSR1	odd-skipped related 1 (Drosophila)
-0,3636	8,8761396	0,014543484	ISYNA1	myo-inositol 1-phosphate synthase A1
-0,6204	4,5856395	0,01521022	C1orf88	chromosome 1 open reading frame 88
-0,3635	10,091412	0,01655035	PRDX5	peroxiredoxin 5
0,6437	4,0673788	0,016609519	ZPLD1	zona pellucida-like domain containing 1
-0,5061	6,0235493	0,017272637	LMO7	LIM domain 7
-0,7288	9,153934	0,017288952	B2M	beta-2-microglobulin
-0,4121	8,3344961	0,018120791	TMEPAI	transmembrane, prostate androgen induced RNA
-0,3219	8,071139	0,018417879	SNX15	sorting nexin 15
-0,4137	7,5633561	0,018417879	CKMT1A	creatine kinase, mitochondrial 1A (CKMT1A), nuclear gene encoding mitochondrial protein, mRNA
-0,3699	6,2477972	0,018675463	FHL1	four and a half LIM domains 1
-0,3782	7,3507523	0,019337164	TGM2	transglutaminase 2 (C polypeptide, protein-glutamine-gamma-glutamyltransferase)
-0,3993	8,0981379	0,021011015	RNF213	ring finger protein 213
-0,3704	5,786273	0,021192739	CAMK1D	calcium/calmodulin-dependent protein kinase ID
-0,4224	7,1895045	0,021381986	CTGF	connective tissue growth factor
-0,4537	5,2104667	0,021381986	TNIK	TRAF2 and NCK interacting kinase
-0,3495	6,9868044	0,021381986	SLC16A2	solute carrier family 16, member 2 (monocarboxylic acid transporter 8)
-0,6235	8,089847	0,022499573	PLAC8	placenta-specific 8
-0,3367	8,4505266	0,023226893	EFHD1	EF-hand domain family, member D1
-0,6338	5,6733484	0,023226893	RAB3B	RAB3B, member RAS oncogene family
0,4381	6,1259279	0,023226893	IFIT2	interferon-induced protein with tetratricopeptide repeats 2
-0,5555	6,0883356	0,02394805	ANKRD1	ankyrin repeat domain 1 (cardiac muscle)
0,4459	6,3804177	0,02394805	TSHZ1	teashirt zinc finger homeobox 1
-0,3657	8,1830685	0,024343148	TUBB2B	tubulin, beta 2B
-0,5025	7,6694397	0,025342823	IGF1R	insulin-like growth factor 1 receptor
-0,4645	6,3474494	0,025855613	TMEM159	transmembrane protein 159
-1,0153	3,4100085	0,025978547	TAS2R13	taste receptor, type 2, member 13
-0,3922	6,5281635	0,027852879	EFNB2	ephrin-B2
-0,5294	4,8064809	0,028069413	WNT16	wingless-type MMTV integration site family, member 16
-0,5069	6,6449814	0,028069413	ARTS-1	type 1 tumor necrosis factor receptor shedding aminopeptidase regulator
-0,7078	5,91624	0,028679966	CLDN1	claudin 1

logFC	AveExpr	adj.P.Val	unlist.symbol	Gene description
-0,3272	9,6307146	0,029106186	PYGB	phosphorylase, glycogen; brain
-0,3732	4,1861096	0,029223998	ANK3	ankyrin 3, node of Ranvier (ankyrin G)
0,4505	4,9005774	0,029481018	C20orf19	chromosome 20 open reading frame 19
-0,6135	3,8629899	0,029481018	TRPC3	transient receptor potential cation channel, subfamily C, member 3
0,7256	5,0320841	0,029481018	VSNL1	visinin-like 1
-0,6105	5,5259641	0,031262344	QPCT	glutaminyl-peptide cyclotransferase (glutaminyl cyclase)
-0,3652	6,2075872	0,031490114	ROR2	receptor tyrosine kinase-like orphan receptor 2
0,3072	5,5532125	0,031490114	CACNA1D	calcium channel, voltage-dependent, L type, alpha 1D subunit
-0,6032	5,310406	0,031490114	EHF	ets homologous factor
-0,3534	7,3163273	0,031490114	RASSF8	Ras association (RalGDS/AF-6) domain family 8 (RASSF8), mRNA
-0,4282	5,4254524	0,031987428	PDE9A	phosphodiesterase 9A
-0,3295	5,2758434	0,031997227	ZNF234	zinc finger protein 234
0,544	5,226522	0,032030291	C1orf176	chromosome 1 open reading frame 176
0,3712	7,0928	0,03295964	GAS6	growth arrest-specific 6
0,852	6,1836081	0,034472951	DIRAS3	DIRAS family, GTP-binding RAS-like 3
-0,4492	5,7337015	0,034766695	DNER	delta/notch-like EGF repeat containing
-0,3602	6,1149459	0,034766695	ADRBK2	adrenergic, beta, receptor kinase 2
0,2734	7,6545554	0,035460806	PODXL	podocalyxin-like
-0,4479	6,7202691	0,03572823	CFLAR	CASP8 and FADD-like apoptosis regulator
-0,2691	7,7820418	0,03572823	LARP6	La ribonucleoprotein domain family, member 6
-0,4934	6,4301238	0,03572823	GATM	glycine amidinotransferase (L-arginine:glycine amidinotransferase)
0,5899	3,7913914	0,036002895	ITGB6	integrin, beta 6
0,3664	6,5317369	0,036002895	MAP3K14	mitogen-activated protein kinase kinase kinase 14
-0,7166	7,6175552	0,037232644	TRERF1	transcriptional regulating factor 1 (TRERF1), mRNA
0,5703	6,7863401	0,037266724	HIST1H3F	histone cluster 1, H3f
0,3093	7,4048049	0,037699059	FLJ20160	FLJ20160 protein
0,6385	4,750546	0,038496046	GZMB	granzyme B (granzyme 2, cytotoxic T-lymphocyte-associated serine esterase 1)
-0,4213	6,3283141	0,04040263	PRDM1	PR domain containing 1, with ZNF domain
0,5312	4,7215578	0,040525674	IGFL2	IGF-like family member 2
0,3965	7,3238246	0,040563832	TSPAN1	tetraspanin 1
-0,7174	2,4920786	0,040787276	OR4F5	olfactory receptor, family 4, subfamily F, member 5
-0,8454	4,5720668	0,041254194	PI3	peptidase inhibitor 3, skin-derived (SKALP)
-0,3029	8,1234308	0,041254194	GLCE	glucuronic acid epimerase
-0,4601	6,5046887	0,041803713	SEPT6	septin 6
-0,4965	5,3803807	0,041818643	ZFP30	zinc finger protein 30 homolog (mouse)
-0,4704	4,9511654	0,042254514	C14orf138	chromosome 14 open reading frame 138
-0,293	9,5548302	0,042687355	RHPN2	rhophilin, Rho GTPase binding protein 2
0,8585	5,994978	0,042687355	SYP	synaptophysin
0,4355	4,8381566	0,04299006	FRAS1	Fraser syndrome 1
-0,9201	5,8745894	0,043381866	HLA-DMB	major histocompatibility complex, class II, DM beta
0,552	4,25744	0,04414797	MUC13	mucin 13, cell surface associated

logFC	AveExpr	adj.P.Val	unlist.symbol	Gene description
0,5447	4,5582762	0,044631168	7A5	putative binding protein 7a5
-0,411	10,172784	0,044631168	HSPB1	heat shock 27kDa protein 1
-0,3582	9,098206	0,045647984	PDLIM1	PDZ and LIM domain 1 (elfin)
0,3362	6,6423874	0,046268581	PLXNB1	plexin B1
0,5395	7,2815452	0,046407785	ALCAM	activated leukocyte cell adhesion molecule
0,5429	4,3327036	0,046407785	DCLK1	doublecortin-like kinase 1

Table S7. List of genes significantly altered when Gal-1 was upregulated in RWP-1 compared to control RWP-1 cells, ordered according to increasing adjusted p value until 0.05. The first column expresses the fold change (expression in RWP-1 Gal-1/Ctl) in logarithmic units with base 2 (log FC). The second column gives the average expression and the third column the adjusted p value.

6.2.2 Pathway Analysis in RWP-1 Group

Pathway	Set Size	Percent Up	NTk Stat	NTk q-value	NTk Rank	NEk* Stat	NEk* q-value	NEk* Rank
MHC class II receptor activity	12	92	-20.65	0.0000	1.0	-4.52	0.0000	3.0
antigen presentation, exogenous antigen	12	92	-20.65	0.0000	1.0	-4.52	0.0000	3.0
antigen processing, exogenous antigen via MHC class II	12	92	-20.65	0.0000	1.0	-4.52	0.0000	3.0
CD40L Signaling Pathway	13	69	-10.33	0.0000	7.0	-4.51	0.0000	4.0
TNFR2 Signaling Pathway	16	69	-9.54	0.0000	8.0	-4.47	0.0000	9.0
NF-kB Signaling Pathway	21	67	-8.81	0.0000	9.0	-4.48	0.0000	8.0
antigen processing	28	86	-16.00	0.0000	2.0	-4.42	0.0000	18.0
Epithelial cell signaling in Helicobacter pylori infection	44	57	-8.02	0.0000	13.0	-4.46	0.0000	12.0

Pathway	Set Size	Percent Up	NTk Stat	NTk q-value	NTk Rank	NEk* Stat	NEk* q-value	NEk* Rank
antigen presentation	40	80	-12.32	0.0000	3.0	-4.40	0.0000	23.0
Chaperones modulate interferon Signaling Pathway	16	69	-8.48	0.0000	11.0	-4.41	0.0000	19.0
Type I diabetes mellitus	39	74	-10.76	0.0000	6.0	-4.37	0.0000	29.0
IL 5 Signaling Pathway	10	80	-7.72	0.0000	15.0	-4.41	0.0000	20.0
Antigen processing and presentation	72	74	-12.31	0.0000	4.0	-4.30	0.0000	39.0
HIV-I Nef negative effector of Fas and TNF	50	66	-7.80	0.0000	14.0	-4.35	0.0000	31.0
Apoptosis	91	60	-6.62	0.0000	25.0	-4.40	0.0000	21.0
Erythropoietin mediated neuroprotection through NF-kB	10	70	-10.84	0.0000	5.0	-4.24	0.0000	44.0
Cadmium induces DNA synthesis and proliferation in macrophages	14	71	-7.15	0.0000	21.0	-4.35	0.0000	35.0
Signal Transduction in Cancer	95	60	-7.37	0.0000	19.0	-4.32	0.0000	37.0
Chemokine activity	45	60	-7.65	0.0000	17.0	-4.28	0.0000	42.0
Chemokine receptor binding	45	60	-7.65	0.0000	17.0	-4.28	0.0000	42.0
Negative regulation of MAPK activity	16	62	3.72	0.0000	50.0	4.46	0.0000	13.0
Role of Mitochondria in Apoptotic Signaling	21	90	-8.53	0.0000	10.0	-4.11	0.0000	59.0
G-protein-coupled receptor binding	53	57	-7.02	0.0000	23.0	-4.22	0.0000	47.0
NFkB Signaling Pathway	92	70	-7.25	0.0000	20.0	-4.16	0.0000	53.0
Nitric Oxide	90	61	-5.77	0.0000	33.0	-4.29	0.0000	40.0

Pathway	Set Size	Percent Up	NTk Stat	NTk q-value	NTk Rank	NEk* Stat	NEk* q-value	NEk* Rank
Neuropeptides VIP and PACAP inhibit the apoptosis of activated T cells	13	69	-3.09	0.0337	60.0	-4.45	0.0000	14.0
Response to pathogen	24	71	-6.55	0.0000	26.0	-4.19	0.0000	50.0
Inactivation of MAPK activity	15	67	3.67	0.0000	51.0	4.37	0.0000	28.0
Aspartic-type endopeptidase activity	10	60	-2.88	0.0538	75.0	-4.49	0.0000	5.0
B Lymphocyte Cell Surface Molecules	11	55	-2.88	0.0538	75.0	-4.49	0.0000	7.0
Signal Transduction PathwayFinder	94	67	-7.66	0.0000	16.0	-4.09	0.0000	68.0
Hydrolase activity, acting on carbon-nitrogen (but not peptide) bonds, in linear amidines	10	30	2.88	0.0538	75.0	4.47	0.0000	10.0
NFkB activation by Nontypeable Hemophilus influenzae	24	50	-2.88	0.0538	75.0	-4.47	0.0000	11.0
Influence of Ras and Rho proteins on G1 to S Transition	24	67	-3.09	0.0337	60.0	-4.35	0.0000	34.0
Negative regulation of apoptosis	134	62	-5.76	0.0000	34.0	-4.11	0.0000	61.0
Vascular endothelial growth factor receptor activity	14	36	4.26	0.0000	48.0	4.20	0.0000	48.0
The 4-1BB-dependent immune response	16	81	-8.45	0.0000	12.0	-3.99	0.0000	85.0
Signal transduction through IL1R	28	61	-2.65	0.0833	97.5	-4.53	0.0000	1.0
Anti-apoptosis	116	62	-5.37	0.0000	39.0	-4.11	0.0000	60.0
Negative regulation of programmed cell death	135	62	-5.79	0.0000	32.0	-4.09	0.0000	67.0

Pathway	Set Size	Percent Up	NTk Stat	NTk q-value	NTk Rank	NEk* Stat	NEk* q-value	NEk* Rank
Regulation of viral life cycle	10	70	-2.75	0.0772	84.5	-4.43	0.0000	15.0
Lck and Fyn tyrosine kinases in initiation of TCR Activation	12	50	-2.65	0.0833	97.5	-4.53	0.0000	2.0
Acetylation and Deacetylation of RelA in The Nucleus	13	62	-2.88	0.0538	75.0	-4.38	0.0000	25.0
ATM Signaling Pathway	19	79	-6.29	0.0000	28.0	-4.07	0.0000	73.0
Viral genome replication	20	50	-2.88	0.0538	75.0	-4.37	0.0000	27.0
Fibrinolysis Pathway	10	60	-2.88	0.0538	75.0	-4.36	0.0000	30.0
Th1/Th2 Differentiation	20	80	-6.27	0.0000	29.0	-4.04	0.0000	77.0
Negative regulation of protein import into nucleus	10	70	-2.88	0.0538	75.0	-4.35	0.0000	32.0
Negative regulation of transcription factor import into nucleus	10	70	-2.88	0.0538	75.0	-4.35	0.0000	32.0
Cytoplasmic sequestering of transcription factor	10	70	-2.88	0.0538	75.0	-4.35	0.0000	32.0

Table S8. List of pathways significantly altered when Gal-1 was upregulated in RWP-1 compared to control RWP-1 cells.

6.2.3 RWP-1 Summary List: Gene Detailed Analysis

p value	FC	Gene Symbol	Gene_assignment
2,24E-05	9,49	CALB1	NM_004929 // CALB1 // calbindin 1, 28kDa // 8q21.3-q22.1 // 793 /// ENST00000265
1,73E-03	5,06	HMGN4	NM_006353 // HMGN4 // high mobility group nucleosomal binding domain 4 // 6p21.3
9,44E-04	4,54	NRXN1	NM_004801 // NRXN1 // neurexin 1 // 2p16.3 // 9378 /// NM_138735 // NRXN1 // neu
3,61E-04	3,26	C4orf18	BC043193 // C4orf18 // chromosome 4 open reading frame 18 // 4q32.1 // 51313 ///
7,80E-04	3,15	CTH	NM_001902 // CTH // cystathionase (cystathionine gamma-lyase) // 1p31.1 // 1491
1,39E-03	2,99	ZNF83	NM_001105549 // ZNF83 // zinc finger protein 83 // 19q13.3 // 55769 /// NR_00393
8,50E-04	2,95	S100A14	NM_020672 // S100A14 // S100 calcium binding protein A14 // 1q21.3 // 57402 ///
2,56E-03	2,86	SLC16A6	NM_004694 // SLC16A6 // solute carrier family 16, member 6 (monocarboxylic acid
1,37E-04	**2,79**	**CCND2**	**NM_001759 // CCND2 // cyclin D2 // 12p13 // 894 /// ENST00000261254 // CCND2 //**
1,71E-03	2,71	COL6A3	NM_004369 // COL6A3 // collagen, type VI, alpha 3 // 2q37 // 1293 /// NM_057164
7,72E-05	2,57	RGS4	NM_001102445 // RGS4 // regulator of G-protein signaling 4 // 1q23.3 // 5999 ///
2,64E-04	2,48	XYLT1	NM_022166 // XYLT1 // xylosyltransferase I // 16p12.3 // 64131 /// ENST000002613
3,01E-02	2,25	OR52B4	NM_001005161 // OR52B4 // olfactory receptor, family 52, subfamily B, member 4 /
3,89E-04	2,21	HHLA3	NM_007071 // HHLA3 // HERV-H LTR-associating 3 // 1p31.1 // 11147 /// NM_0010366
5,24E-03	2,16	PTGER2	NM_000956 // PTGER2 // prostaglandin E receptor 2 (subtype EP2), 53kDa // 14q22
5,22E-04	2,11	NPC2	NM_006432 // NPC2 // Niemann-Pick disease, type C2 // 14q24.3 // 10577 /// NM_00
3,04E-02	2,11	OSTbeta	NM_178859 // OSTbeta // organic solute transporter beta // 15q22.31 // 123264 //
9,55E-04	2,08	PRF1	NM_005041 // PRF1 // perforin 1 (pore forming protein) // 10q22 // 5551 /// NM_0
9,93E-04	2,06	SYTL2	NM_206927 // SYTL2 // synaptotagmin-like 2 // 11q14 // 54843 /// NM_206928 // SY
1,44E-03	2,04	FGFBP1	NM_005130 // FGFBP1 // fibroblast growth factor binding protein 1 // 4p16-p15 //
1,58E-03	2,03	DSG4	NM_177986 // DSG4 // desmoglein 4 // 18q12.1 // 147409 /// ENST00000308128 // DS
4,25E-02	2,03	GSTTP1	NR_003081 // GSTTP1 // glutathione S-transferase theta pseudogene 1 // 22q12 //
5,34E-03	1,98	GZMB	NM_004131 // GZMB // granzyme B (granzyme 2, cytotoxic T-lymphocyte-associated s
3,76E-03	1,93	PADI1	NM_013358 // PADI1 // peptidyl arginine deiminase, type I // 1p36.13 // 29943 //
7,38E-03	1,92	KRTAP5-2	NM_001004325 // KRTAP5-2 // keratin associated protein 5-2 // 11p15.5 // 440021
2,56E-02	1,90	SYP	NM_003179 // SYP // synaptophysin // Xp11.23-p11.22 // 6855 /// ENST00000376303
2,72E-02	1,90	HIST1H2BA	NM_170610 // HIST1H2BA // histone cluster 1, H2ba // 6p22.2 // 255626 /// ENST00
2,31E-02	1,90	DEFA5	NM_021010 // DEFA5 // defensin, alpha 5, Paneth cell-specific // 8pter-p21 // 16
2,43E-02	1,86	RPL31	NM_001099693 // RPL31 // ribosomal protein L31 // 2q11.2 // 6160 /// NM_00109857
3,78E-02	1,86	TOM1L2	NM_001033551 // TOM1L2 // target of myb1-like 2 (chicken) // 17p11.2 // 146691 /
3,38E-03	1,85	STC1	NM_003155 // STC1 // stanniocalcin 1 // 8p21-p11.2 // 6781 /// ENST00000290271 /
1,17E-03	1,83	DIRAS3	NM_004675 // DIRAS3 // DIRAS family, GTP-binding RAS-like 3 // 1p31 // 9077 ///
9,75E-03	1,82	GALNT5	NM_014568 // GALNT5 // UDP-N-acetyl-alpha-D-galactosamine:polypeptide N-acetylga
6,26E-03	1,82	STRN	NM_003162 // STRN // striatin, calmodulin binding protein // 2p22-p21 // 6801 //
2,43E-02	1,81	KRTAP5-6	NM_001012416 // KRTAP5-6 // keratin associated protein 5-6 // 11p15.5 // 440023
3,10E-02	1,80	MUSP1	AF384996 // MUSP1 // MUSP1 // 16q24.1 // 100131952 /// ENST00000326395 // MUSP1
9,11E-05	1,80	NRP1	NM_003873 // NRP1 // neuropilin 1 // 10p12 // 8829 /// NM_001024628 // NRP1 // n
1,55E-02	1,79	IFIT2	NM_001547 // IFIT2 // interferon-induced protein with tetratricopeptide repeats

p value	FC	Gene Symbol	Gene_assignment
2,07E-05	1,78	KRT13	NM_153490 // KRT13 // keratin 13 // 17q12-q21.2 // 3860 /// NM_002274 // KRT13 /
2,15E-04	1,77	VIL1	NM_007127 // VIL1 // villin 1 // 2q35-q36 // 7429 /// ENST00000392114 // VIL1 //
1,68E-02	1,76	HIST1H2BK	ENST00000396891 // HIST1H2BK // histone cluster 1, H2bk // 6p21.33 // 85236 ///
1,06E-02	1,76	PPP1R2P3	NR_002168 // PPP1R2P3 // protein phosphatase 1, regulatory (inhibitor) subunit 2
5,62E-04	1,75	RHOBTB3	NM_014899 // RHOBTB3 // Rho-related BTB domain containing 3 // 5q15 // 22836 ///
4,58E-04	1,74	SLC16A4	NM_004696 // SLC16A4 // solute carrier family 16, member 4 (monocarboxylic acid
2,18E-04	1,72	LTBP2	NM_000428 // LTBP2 // latent transforming growth factor beta binding protein 2 /
1,42E-02	1,71	PDE1C	NM_005020 // PDE1C // phosphodiesterase 1C, calmodulin-dependent 70kDa // 7p15.1
2,85E-02	1,71	GEMIN8	DQ224033 // GEMIN8 // gem (nuclear organelle) associated protein 8 // Xp22.2 //
1,89E-03	1,70	PAM	NM_000919 // PAM // peptidylglycine alpha-amidating monooxygenase // 5q14-q21 //
1,04E-02	1,70	GPR19	NM_006143 // GPR19 // G protein-coupled receptor 19 // 12p12.3 // 2842 /// ENST0
2,23E-02	1,70	WFS1	NM_006005 // WFS1 // Wolfram syndrome 1 (wolframin) // 4p16 // 7466 /// ENST0000
8,07E-03	1,69	GAP43	NM_002045 // GAP43 // growth associated protein 43 // 3q13.1-q13.2 // 2596 /// E
1,83E-03	1,69	KCNJ8	NM_004982 // KCNJ8 // potassium inwardly-rectifying channel, subfamily J, member
5,80E-04	1,68	ZPLD1	NM_175056 // ZPLD1 // zona pellucida-like domain containing 1 // 3q12.3 // 13136
1,67E-02	1,68	C22orf28	BC016707 // C22orf28 // chromosome 22 open reading frame 28 // 22q12 // 51493 //
8,29E-03	1,67	B3GALT1	NM_020981 // B3GALT1 // UDP-Gal:betaGlcNAc beta 1,3-galactosyltransferase, polyp
8,01E-05	1,67	TNFRSF19	NM_148957 // TNFRSF19 // tumor necrosis factor receptor superfamily, member 19 /
2,47E-03	1,66	ATP8A2	NM_016529 // ATP8A2 // ATPase, aminophospholipid transporter-like, class I, type
1,66E-02	-1,65	ANKRD34B	NM_001004441 // ANKRD34B // ankyrin repeat domain 34B // 5q14.1 // 340120 /// EN
1,39E-04	-1,66	PLEK2	NM_016445 // PLEK2 // pleckstrin 2 // 14q23.3 // 26499 /// ENST00000216446 // PL
1,35E-02	-1,66	C9orf30	AY598327 // C9orf30 // chromosome 9 open reading frame 30 // 9q31.1 // 91283 ///
1,03E-02	**-1,66**	**PLAU**	**NM_002658 // PLAU // plasminogen activator, urokinase // 10q24 // 5328 /// ENST0**
1,08E-03	-1,66	FGF13	NM_004114 // FGF13 // fibroblast growth factor 13 // Xq26.3 // 2258 /// NM_03364
4,72E-02	-1,67	DEFB118	NM_054112 // DEFB118 // defensin, beta 118 // 20q11.1-q11.22 // 117285 /// ENST0
1,19E-03	-1,68	C1R	NM_001733 // C1R // complement component 1, r subcomponent // 12p13 // 715 /// A
2,47E-02	-1,68	NEBL	NM_006393 // NEBL // nebulette // 10p12 // 10529 /// NM_213569 // NEBL // nebule
9,16E-04	-1,69	SGPP2	NM_152386 // SGPP2 // sphingosine-1-phosphate phosphotase 2 // 2q36.1 // 130367
3,30E-02	-1,69	C7orf58	NM_024913 // C7orf58 // chromosome 7 open reading frame 58 // 7q31.31 // 79974 /
1,94E-02	-1,69	BIRC2	NM_001166 // BIRC2 // baculoviral IAP repeat-containing 2 // 11q22 // 329 /// EN
2,86E-02	-1,71	OR13C2	NM_001004481 // OR13C2 // olfactory receptor, family 13, subfamily C, member 2 /
2,07E-03	-1,71	IGF2	NM_000612 // IGF2 // insulin-like growth factor 2 (somatomedin A) // 11p15.5 //
2,14E-03	-1,71	CTSS	NM_004079 // CTSS // cathepsin S // 1q21 // 1520 /// ENST00000368985 // CTSS //
2,29E-02	-1,72	P2RY5	NM_005767 // P2RY5 // purinergic receptor P2Y, G-protein coupled, 5 // 13q14 //
1,61E-02	-1,73	FGF17	NM_003867 // FGF17 // fibroblast growth factor 17 // 8p21 // 8822 /// ENST000003
3,17E-03	-1,74	RNF43	NM_017763 // RNF43 // ring finger protein 43 // 17q22 // 54894 /// ENST000003762
7,85E-03	-1,74	CPOX	NM_000097 // CPOX // coproporphyrinogen oxidase // 3q12 // 1371 /// ENST00000264
4,45E-02	-1,74	LTB	NM_002341 // LTB // lymphotoxin beta (TNF superfamily, member 3) // 6p21.3 // 40
1,96E-02	-1,74	LOC100128508	AF370407 // LOC100128508 // PP12100 // 5p15.2 // 100128508 /// XM_001724076 // L
1,41E-02	-1,75	DKFZP434P211	NR_003714 // DKFZP434P211 // POM121-like protein // 22q11.22 // 29774 /// AY3589

p value	FC	Gene Symbol	Gene_assignment
2,68E-03	-1,76	HLA-DMB	NM_002118 // HLA-DMB // major histocompatibility complex, class II, DM beta // 6
4,16E-03	-1,76	TAPBP	NM_172208 // TAPBP // TAP binding protein (tapasin) // 6p21.3 // 6892 /// NM_003
2,83E-02	-1,79	NEUROD1	NM_002500 // NEUROD1 // neurogenic differentiation 1 // 2q32 // 4760 /// ENST000
1,77E-03	-1,80	RAC2	NM_002872 // RAC2 // ras-related C3 botulinum toxin substrate 2 (rho family, sma
3,35E-02	-1,80	DEFB128	NM_001037732 // DEFB128 // defensin, beta 128 // 20p13 // 245939 /// ENST0000033
9,72E-03	-1,80	LSDP5	NM_001013706 // LSDP5 // lipid storage droplet protein 5 // 19p13.3 // 440503 //
3,71E-04	-1,81	TNFAIP2	NM_006291 // TNFAIP2 // tumor necrosis factor, alpha-induced protein 2 // 14q32
4,66E-02	-1,82	ISLR	NM_005545 // ISLR // immunoglobulin superfamily containing leucine-rich repeat /
1,67E-03	-1,84	OTUB2	NM_023112 // OTUB2 // OTU domain, ubiquitin aldehyde binding 2 // 14q32.13 // 78
8,11E-04	-1,84	PI3	NM_002638 // PI3 // peptidase inhibitor 3, skin-derived (SKALP) // 20q12-q13 //
9,67E-04	-1,85	MAP3K8	NM_005204 // MAP3K8 // mitogen-activated protein kinase kinase kinase 8 // 10p11
2,53E-02	-1,87	SOX14	NM_004189 // SOX14 // SRY (sex determining region Y)-box 14 // 3q22-q23 // 8403
3,54E-05	-1,88	ANXA6	NM_001155 // ANXA6 // annexin A6 // 5q32-q34 // 309 /// NM_004033 // ANXA6 // an
2,92E-05	-1,89	NFKB2	NM_001077494 // NFKB2 // nuclear factor of kappa light polypeptide gene enhancer
3,71E-02	-1,90	ZNF321	NM_203307 // ZNF321 // zinc finger protein 321 // 19q13.41 // 399669 /// ENST000
1,25E-03	-1,92	SERPINA1	NM_001002236 // SERPINA1 // serpin peptidase inhibitor, clade A (alpha-1 antipro
9,70E-05	-1,92	TNIP1	NM_006058 // TNIP1 // TNFAIP3 interacting protein 1 // 5q32-q33.1 // 10318 /// E
1,52E-03	-1,93	FLJ90757	BC110822 // FLJ90757 // hypothetical protein LOC440465 // 17q25.3 // 440465 ///
4,60E-03	-1,93	IFNGR1	NM_000416 // IFNGR1 // interferon gamma receptor 1 // 6q23.3 // 3459 /// ENST000
3,12E-02	-1,94	SERPINB7	NM_003784 // SERPINB7 // serpin peptidase inhibitor, clade B (ovalbumin), member
4,26E-02	-1,94	IFNA21	NM_002175 // IFNA21 // interferon, alpha 21 // 9p22 // 3452 /// NM_002175 // IFN
8,95E-04	-1,95	KIAA1622	NM_058237 // KIAA1622 // KIAA1622 // 14q32.13 // 57718 /// NM_020958 // KIAA1622
1,89E-04	-1,96	LAMC2	NM_005562 // LAMC2 // laminin, gamma 2 // 1q25-q31 // 3918 /// NM_018891 // LAMC
2,34E-04	-1,97	FBN2	NM_001999 // FBN2 // fibrillin 2 (congenital contractural arachnodactyly) // 5q2
6,10E-03	-1,98	HLA-DQA2	NM_020056 // HLA-DQA2 // major histocompatibility complex, class II, DQ alpha 2
8,63E-05	-2,00	SORBS1	NM_001034954 // SORBS1 // sorbin and SH3 domain containing 1 // 10q23.3-q24.1 //
1,72E-02	-2,01	CSF2	NM_000758 // CSF2 // colony stimulating factor 2 (granulocyte-macrophage) // 5q3
4,57E-03	-2,02	TNFRSF9	NM_001561 // TNFRSF9 // tumor necrosis factor receptor superfamily, member 9 //
1,60E-02	-2,03	RPP21	NM_024839 // RPP21 // ribonuclease P/MRP 21kDa subunit // 6p21.33 // 79897 /// E
3,89E-02	-2,04	PCDHB6	NM_018939 // PCDHB6 // protocadherin beta 6 // 5q31 // 56130 /// ENST00000231136
2,05E-02	-2,04	FLJ45248	AK127183 // FLJ45248 // FLJ45248 protein // 8q22.3 // 401472
4,24E-02	-2,08	PIGH	NM_004569 // PIGH // phosphatidylinositol glycan anchor biosynthesis, class H //
1,12E-02	-2,08	MPZL2	NM_144765 // MPZL2 // myelin protein zero-like 2 // 11q24 // 10205 /// NM_005797
2,31E-03	-2,09	TMEM45B	NM_138788 // TMEM45B // transmembrane protein 45B // 11q24.3 // 120224 /// ENST0
2,92E-03	-2,10	C3orf14	AF236158 // C3orf14 // chromosome 3 open reading frame 14 // 3p14.2 // 57415 ///
3,26E-02	-2,13	IFNA7	NM_021057 // IFNA7 // interferon, alpha 7 // 9p22 // 3444 /// NM_002172 // IFNA1
5,69E-04	-2,15	OAS3	NM_006187 // OAS3 // 2'-5'-oligoadenylate synthetase 3, 100kDa // 12q24.2 // 494
1,97E-04	-2,17	SDC4	NM_002999 // SDC4 // syndecan 4 // 20q12 // 6385 /// ENST00000372733 // SDC4 //
3,34E-04	-2,17	ABCA1	NM_005502 // ABCA1 // ATP-binding cassette, sub-family A (ABC1), member 1 // 9q3
1,01E-04	-2,17	ACSL5	NM_016234 // ACSL5 // acyl-CoA synthetase long-chain family member 5 // 10q25.1-
5,83E-03	-2,19	PLAC8	NM_016619 // PLAC8 // placenta-specific 8 // 4q21.22 // 51316 /// ENST0000031150

p value	FC	Gene Symbol	Gene_assignment
1,26E-03	-2,22	GPR110	NM_025048 // GPR110 // G protein-coupled receptor 110 // 6p12.3 // 266977 /// NM
4,63E-02	-2,25	OTUD6A	NM_207320 // OTUD6A // OTU domain containing 6A // Xq13.1 // 139562 /// ENST0000
2,55E-03	-2,26	ZNF738	BC034499 // ZNF738 // zinc finger protein 738 // 19p12 // 148203 /// AK291002 //
3,80E-02	-2,33	PSG8	NM_182707 // PSG8 // pregnancy specific beta-1-glycoprotein 8 // 19q13.31 // 440
3,94E-04	-2,40	VNN1	NM_004666 // VNN1 // vanin 1 // 6q23-q24 // 8876 /// ENST00000367928 // VNN1 //
3,36E-02	-2,40	SPRR2D	NM_006945 // SPRR2D // small proline-rich protein 2D // 1q21-q22 // 6703 /// NM_
2,13E-05	-2,44	IGF2	NM_000612 // IGF2 // insulin-like growth factor 2 (somatomedin A) // 11p15.5 //
9,55E-04	-2,49	RGS5	NM_003617 // RGS5 // regulator of G-protein signaling 5 // 1q23.1 // 8490 /// EN
2,30E-03	-2,50	GPR110	NM_153840 // GPR110 // G protein-coupled receptor 110 // 6p12.3 // 266977 /// EN
3,38E-04	-2,54	PROM1	NM_006017 // PROM1 // prominin 1 // 4p15.32 // 8842 /// ENST00000265014 // PROM1
1,70E-03	-2,56	HLA-DQA1	NM_002122 // HLA-DQA1 // major histocompatibility complex, class II, DQ alpha 1
1,49E-04	-2,57	CD74	NM_001025159 // CD74 // CD74 molecule, major histocompatibility complex, class I
4,75E-05	-2,57	MBNL3	NM_018388 // MBNL3 // muscleblind-like 3 (Drosophila) // Xq26.2 // 55796 /// NM_
2,89E-04	-2,63	HLA-DMA	NM_006120 // HLA-DMA // major histocompatibility complex, class II, DM alpha //
7,33E-04	-2,66	ESM1	NM_007036 // ESM1 // endothelial cell-specific molecule 1 // 5q11.2 // 11082 ///
1,02E-05	-2,69	CADPS	NM_003716 // CADPS // Ca2+-dependent secretion activator // 3p14.2 // 8618 /// N
7,52E-05	-2,71	CIITA	NM_000246 // CIITA // class II, major histocompatibility complex, transactivator
1,58E-05	-2,71	SPRR1B	NM_003125 // SPRR1B // small proline-rich protein 1B (cornifin) // 1q21-q22 // 6
9,85E-05	-2,76	IGFBP3	NM_001013398 // IGFBP3 // insulin-like growth factor binding protein 3 // 7p13-p
1,17E-03	-2,78	PSMB9	NM_002800 // PSMB9 // proteasome (prosome, macropain) subunit, beta type, 9 (lar
6,68E-03	-2,80	GALM	NM_138801 // GALM // galactose mutarotase (aldose 1-epimerase) // 2p22.1 // 1305
2,27E-04	-2,90	TM4SF18	NM_138786 // TM4SF18 // transmembrane 4 L six family member 18 // 3q25.1 // 1164
2,43E-04	-2,98	TSPAN7	NM_004615 // TSPAN7 // tetraspanin 7 // Xp11.4 // 7102 /// ENST00000378482 // TS
1,87E-04	**-3,15**	**PLAT**	**NM_000930 // PLAT // plasminogen activator, tissue // 8p12 // 5327 /// NM_033011**
1,22E-05	-3,18	SERPINB2	NM_002575 // SERPINB2 // serpin peptidase inhibitor, clade B (ovalbumin), member
2,22E-04	-3,20	HLA-DPB1	NM_002121 // HLA-DPB1 // major histocompatibility complex, class II, DP beta 1 /
4,85E-03	-3,45	CXCL2	NM_002089 // CXCL2 // chemokine (C-X-C motif) ligand 2 // 4q21 // 2920 /// ENST0
1,42E-05	-3,56	ZC3H12A	NM_025079 // ZC3H12A // zinc finger CCCH-type containing 12A // 1p34.3 // 80149
1,11E-04	-3,58	HLA-DRA	NM_019111 // HLA-DRA // major histocompatibility complex, class II, DR alpha //
1,96E-05	-3,63	NFKBIA	NM_020529 // NFKBIA // nuclear factor of kappa light polypeptide gene enhancer i
2,48E-05	-3,78	CXCL3	NM_002090 // CXCL3 // chemokine (C-X-C motif) ligand 3 // 4q21 // 2921 /// ENST0
1,51E-05	-3,85	FREM2	NM_207361 // FREM2 // FRAS1 related extracellular matrix protein 2 // 13q13.3 //
8,13E-04	-3,96	IL8	NM_000584 // IL8 // interleukin 8 // 4q13-q21 // 3576 /// ENST00000307407 // IL8
4,60E-06	-4,00	MITF	NM_006722 // MITF // microphthalmia-associated transcription factor // 3p14.2-p1
2,22E-05	-4,33	MMP7	NM_002423 // MMP7 // matrix metallopeptidase 7 (matrilysin, uterine) // 11q21-q2
8,98E-05	-4,46	IL32	NM_001012631 // IL32 // interleukin 32 // 16p13.3 // 9235 /// NM_004221 // IL32
1,13E-06	-6,26	CXCL1	NM_001511 // CXCL1 // chemokine (C-X-C motif) ligand 1 (melanoma growth stimulat
9,95E-05	-6,35	SERPINA3	NM_001085 // SERPINA3 // serpin peptidase inhibitor, clade A (alpha-1 antiprotei
1,63E-06	-6,40	HLA-DPA1	NM_033554 // HLA-DPA1 // major histocompatibility complex, class II, DP alpha 1
1,65E-05	-6,41	TNFAIP3	NM_006290 // TNFAIP3 // tumor necrosis factor, alpha-induced protein 3 // 6q23 /
2,82E-03	-7,44	SPRR2A	NM_005988 // SPRR2A // small proline-rich protein 2A // 1q21-q22 // 6700 /// ENS

p value	FC	Gene Symbol	Gene_assignment
5,47E-05	-11,21	LCN2	NM_005564 // LCN2 // lipocalin 2 // 9q34 // 3934 /// ENST00000373017 // LCN2 //
4,77E-05	-13,60	BIRC3	NM_001165 // BIRC3 // baculoviral IAP repeat-containing 3 // 11q22 // 330 /// NM
1,82E-04	-15,18	GPR15	NM_005290 // GPR15 // G protein-coupled receptor 15 // 3q11.2-q13.1 // 2838 ///

Table S9. List of genes significantly altered when Gal-1 was overexpressed in RWP-1 compared to control cells (MFZ list). Fold change (FC) is given in positive values (upper part of the table) when the gene was upregulated in transfected cells with high Gal-1 levels (same direction as Gal-1). These genes are ordered by increasing p value until p=0.05. In the lower part of the table, FC is negative and p values are decreasing. These genes showed decreased expression when Gal-1 was overexpressed (opposite direction as Gal-1). The first column shows p values.

6.3 INTERSECTED LIST PANC-1/RWP-1

6.3.1 Gene Detailed Analysis: Genes Regulated in the Same Direction as Gal-1

PANC-1 Ctl/sh_5	PANC-1 Ctl/sh_2	RWP-1 Gal-1/Ctl	adj.P.Val	unlist. symbol	Gene description
1,55	**0,17**	**0,25**	**6,91E-009**	**TGFBR3**	**transforming growth factor, beta receptor III**
1,37	0,31	0,31	1,90E-008	CACNA1D	calcium channel, voltage-dependent, L type, alpha 1D subunit
1,18	**1,98**	**0,81**	**7,50E-008**	**LGALS1**	**lectin, galactoside-binding, soluble, 1**
1,58	0,32	0,08	1,73E-007	ATP8B1	ATPase, class I, type 8B, member 1
1,51	0,25	0,07	1,98E-007	OPN3	opsin 3
1,30	0,21	0,13	1,98E-007	PRKAA2	protein kinase, AMP-activated, alpha 2 catalytic subunit
1,69	0,08	0,14	2,26E-007	NFATC2	nuclear factor of activated T-cells, cytoplasmic, calcineurin-dependent 2
0,99	0,13	0,90	2,43E-007	SYTL2	synaptotagmin-like 2
1,66	0,38	0,02	8,83E-007	PLEKHH2	pleckstrin homology domain containing, family H (with MyTH4 domain) member 2
0,95	**0,05**	**0,14**	**9,13E-007**	**TOB1**	**transducer of ERBB2, 1**
1,09	0,07	0,01	1,14E-006	TBC1D2B	TBC1 domain family, member 2B
1,37	0,32	0,22	1,19E-006	GPR177	G protein-coupled receptor 177
1,27	0,01	0,10	2,59E-006	RAB30	RAB30, member RAS oncogene family
1,25	0,29	0,04	2,64E-006	AFAP1L2	actin filament associated protein 1-like 2
1,23	0,05	0,14	4,85E-006	PTPN13	protein tyrosine phosphatase, non-receptor type 13 (APO-1/CD95 (Fas)-associated phosphatase)
1,20	0,05	0,13	4,97E-006	SAMD9	sterile alpha motif domain containing 9
1,55	0,16	0,19	5,00E-006	GJB6	gap junction protein, beta 6, 30kDa
1,26	0,07	0,07	5,74E-006	LPCAT2	lysophosphatidylcholine acyltransferase 2
0,35	0,26	0,90	6,46E-006	NRP1	neuropilin 1
0,94	0,12	0,03	6,72E-006	ST5	suppression of tumorigenicity 5
0,75	0,15	0,23	1,32E-005	TPCN1	two pore segment channel 1
0,77	0,02	0,09	1,38E-005	NID1	nidogen 1
1,22	0,36	0,07	1,76E-005	EPB41	erythrocyte membrane protein band 4.1 (elliptocytosis 1, RH-linked)
1,12	0,16	0,29	2,15E-005	CTBS	chitobiase, di-N-acetyl-
0,83	0,12	0,03	2,51E-005	AFAP1	actin filament associated protein 1
0,87	0,01	0,27	2,97E-005	C4orf34	chromosome 4 open reading frame 34
0,62	0,02	0,16	3,65E-005	ABCC1	ATP-binding cassette, sub-family C (CFTR/MRP), member 1
1,35	0,06	0,31	3,65E-005	CACNA2D1	calcium channel, voltage-dependent, alpha 2/delta subunit 1
0,80	0,00	0,22	3,91E-005	KIAA0922	KIAA0922
0,69	0,10	0,03	3,91E-005	CD99L2	CD99 molecule-like 2
0,76	0,01	0,44	3,95E-005	IFIT2	interferon-induced protein with tetratricopeptide repeats 2
0,71	0,00	0,14	4,53E-005	KIRREL	kin of IRRE like (Drosophila)
0,94	0,20	0,15	6,01E-005	PGM2L1	phosphoglucomutase 2-like 1

PANC-1 Ctl/sh_5	PANC-1 Ctl/sh_2	RWP-1 Gal-1/Ctl	adj.P.Val	unlist. symbol	Gene description
0,93	0,14	0,06	7,67E-005	LCA5	Leber congenital amaurosis 5
0,57	0,17	0,44	7,77E-005	ABLIM1	**actin binding LIM protein 1**
0,90	**0,28**	**0,13**	**9,33E-005**	**DISP1**	**dispatched homolog 1 (Drosophila)**
0,82	0,11	0,22	0,000103335	PALLD	palladin, cytoskeletal associated protein
1,34	0,18	0,03	0,000103335	OASL	2'-5'-oligoadenylate synthetase-like
0,81	0,08	0,15	0,000155264	ALS2CR8	amyotrophic lateral sclerosis 2 (juvenile) chromosome region, candidate 8
0,16	0,55	0,05	0,000157571	STAT3	signal transducer and activator of transcription 3 (acute-phase response factor)
0,40	0,08	1,25	0,000159752	ZNF83	zinc finger protein 83
0,11	0,53	0,61	0,000164232	LIMA1	LIM domain and actin binding 1
0,96	0,18	0,01	0,000178575	CYP1B1	cytochrome P450, family 1, subfamily B, polypeptide 1
0,80	0,01	0,02	0,000216718	ERGIC1	endoplasmic reticulum-golgi intermediate compartment (ERGIC) 1
0,93	0,13	0,25	0,000263687	PIK3R3	phosphoinositide-3-kinase, regulatory subunit 3 (gamma)
0,96	0,32	0,24	0,000270217	TOX2	TOX high mobility group box family member 2
0,58	0,03	0,10	0,000278594	KDELC2	KDEL (Lys-Asp-Glu-Leu) containing 2
1,09	0,52	0,51	0,000326368	HIST2H4A	histone cluster 2, H4a
0,70	0,06	0,21	0,000335743	PSPH	phosphoserine phosphatase
0,43	0,03	0,47	0,000356476	PLEKHA7	pleckstrin homology domain containing, family A member 7
0,58	0,13	0,11	0,00037878	SP110	SP110 nuclear body protein
1,47	0,35	0,02	0,000395649	PLCL2	phospholipase C-like 2
0,67	0,13	0,01	0,000423833	C11orf54	chromosome 11 open reading frame 54
1,28	0,09	0,12	0,000451004	TSPAN8	tetraspanin 8
0,74	0,03	0,32	0,000541354	TMEM117	transmembrane protein 117
0,89	0,54	0,03	0,000566449	GPD1L	glycerol-3-phosphate dehydrogenase 1-like
1,14	0,50	0,21	0,000593122	NAPEPLD	N-acyl phosphatidylethanolamine phospholipase D
1,12	0,45	0,10	0,000620011	C3orf34	chromosome 3 open reading frame 34
0,56	0,00	0,09	0,000645108	RCBTB2	regulator of chromosome condensation (RCC1) and BTB (POZ) domain containing protein 2
0,90	0,05	0,11	0,000649431	CREB3L1	cAMP responsive element binding protein 3-like 1
0,94	0,15	0,40	0,000687864	ENC1	ectodermal-neural cortex (with BTB-like domain)
0,69	0,34	0,36	0,000741826	FZD3	frizzled homolog 3 (Drosophila)
0,86	0,21	0,19	0,000797538	EML4	echinoderm microtubule associated protein like 4
1,16	0,47	0,43	0,000858757	CLK4	CDC-like kinase 4
0,59	0,19	0,04	0,000910256	ABHD6	abhydrolase domain containing 6
0,75	0,15	0,10	0,000915638	SLC46A3	solute carrier family 46, member 3
0,52	0,12	0,02	0,001001662	GPATCH1	G patch domain containing 1
0,62	0,02	0,05	0,001034434	MXRA8	matrix-remodelling associated 8
1,15	0,17	0,71	0,001104106	KRCC1	lysine-rich coiled-coil 1
0,53	0,01	0,20	0,001113608	MINPP1	multiple inositol polyphosphate histidine phosphatase, 1
1,36	0,51	0,68	0,001148378	HIST2H4A	histone cluster 2, H4a
0,68	0,31	0,02	0,001181566	CACNB4	calcium channel, voltage-dependent, beta 4 subunit
0,55	0,12	0,07	0,001228683	ZDHHC14	zinc finger, DHHC-type containing 14

PANC-1 Ctl/sh_5	PANC-1 Ctl/sh_2	RWP-1 Gal-1/Ctl	adj.P.Val	unlist. symbol	Gene description
0,80	0,04	0,19	0,001350862	TRIM24	tripartite motif-containing 24
0,02	0,13	0,90	0,001477167	PRF1	perforin 1 (pore forming protein)
0,68	0,04	0,03	0,001535862	PLCXD1	phosphatidylinositol-specific phospholipase C, X domain containing 1
0,98	0,39	0,15	0,00184136	TIA1	TIA1 cytotoxic granule-associated RNA binding protein
1,30	0,25	0,16	0,001934551	HIST1H2BD	histone cluster 1, H2bd
0,76	0,01	0,22	0,001989483	SKAP2	src kinase associated phosphoprotein 2
0,60	0,19	0,20	0,002059095	ST6GAL1	ST6 beta-galactosamide alpha-2,6-sialyltranferase 1
0,71	0,08	0,15	0,002107186	HS2ST1	heparan sulfate 2-O-sulfotransferase 1
0,14	0,54	0,06	0,002216085	ASAM	adipocyte-specific adhesion molecule
0,63	0,10	0,11	0,002308364	TMEM186	transmembrane protein 186
0,80	0,22	0,16	0,002318081	CNOT6	CCR4-NOT transcription complex, subunit 6
0,87	0,03	0,02	0,002399777	DTX3L	deltex 3-like (Drosophila)
0,89	0,38	0,02	0,002884185	KMO	kynurenine 3-monooxygenase (kynurenine 3-hydroxylase)
0,86	0,15	0,11	0,002912251	TFRC	transferrin receptor (p90, CD71)
0,84	0,29	0,16	0,002998421	MSX2	msh homeobox 2
0,86	0,48	0,19	0,003601844	CHN1	chimerin (chimaerin) 1
0,48	0,38	0,19	0,003609218	CDS1	CDP-diacylglycerol synthase (phosphatidate cytidylyltransferase) 1
0,54	0,01	0,03	0,003641547	NCOA3	nuclear receptor coactivator 3
0,81	0,32	0,00	0,003699096	ZNF597	zinc finger protein 597
0,45	0,22	0,03	0,004161902	COQ10A	coenzyme Q10 homolog A (S. cerevisiae)
0,82	0,23	0,58	0,004194662	SCARNA4	small Cajal body-specific RNA 4
0,49	0,34	0,14	0,004327025	CFL2	cofilin 2 (muscle)
0,36	0,46	0,17	0,004391048	ENTPD4	ectonucleoside triphosphate diphosphohydrolase 4
0,82	0,04	0,20	0,004394119	USO1	USO1 homolog, vesicle docking protein (yeast)
1,09	0,16	0,30	0,0044076	HIST2H2BF	histone cluster 2, H2bf
0,72	0,13	0,05	0,004660502	ZNF480	zinc finger protein 480
0,44	0,53	0,23	0,004882679	SCML1	sex comb on midleg-like 1 (Drosophila)
0,95	0,50	0,07	0,004991617	COMMD10	COMM domain containing 10
0,79	0,26	0,20	0,004998447	LIPH	lipase, member H
0,55	0,24	0,38	0,005125291	MANSC1	MANSC domain containing 1
1,01	0,04	0,14	0,005171513	PPM1L	protein phosphatase 1 (formerly 2C)-like
0,81	0,01	0,05	0,005356872	STXBP5	syntaxin binding protein 5 (tomosyn)
0,61	0,21	0,07	0,005407902	SFXN1	sideroflexin 1
0,60	0,07	0,22	0,005422475	UXS1	UDP-glucuronate decarboxylase 1
0,32	0,79	0,04	0,005590971	FAM71D	family with sequence similarity 71, member D
0,23	0,24	0,62	0,005696913	F3	coagulation factor III (thromboplastin, tissue factor)
0,73	0,12	0,09	0,00622799	GSTM2	glutathione S-transferase mu 2 (muscle)
1,13	0,13	0,15	0,006789317	PCDHB14	protocadherin beta 14
0,44	0,21	0,02	0,006907557	B3GNT1	UDP-GlcNAc:betaGal beta-1,3-N-acetylglucosaminyltransferase 1
0,49	0,19	0,10	0,007132731	DSE	dermatan sulfate epimerase
0,73	0,32	0,03	0,007386988	IQCG	IQ motif containing G

PANC-1 Ctl/sh_5	PANC-1 Ctl/sh_2	RWP-1 Gal-1/Ctl	adj.P.Val	unlist. symbol	Gene description
0,40	0,04	0,00	0,007936219	GNA12	guanine nucleotide binding protein (G protein) alpha 12
0,40	0,02	0,03	0,008572953	FAM120C	family with sequence similarity 120C
1,38	0,05	0,31	0,008681055	SSTR5	somatostatin receptor 5
0,12	0,50	0,15	0,008859344	MTHFS	5,10-methenyltetrahydrofolate synthetase (5-formyltetrahydrofolate cyclo-ligase)
0,62	0,11	0,40	0,009460402	CCDC126	coiled-coil domain containing 126
0,43	0,08	0,08	0,009867328	ATP8B3	ATPase, class I, type 8B, member 3
0,53	0,01	0,04	0,010241495	CDKN2C	cyclin-dependent kinase inhibitor 2C (p18, inhibits CDK4)
0,82	0,20	0,08	0,010261102	SSX2IP	synovial sarcoma, X breakpoint 2 interacting protein
0,40	0,05	0,14	0,010553684	PLBD1	phospholipase B domain containing 1
0,55	0,11	0,24	0,010899576	ITGA6	integrin, alpha 6
0,64	0,16	0,02	0,010899576	KITLG	KIT ligand
0,30	0,66	0,09	0,011091387	OXNAD1	oxidoreductase NAD-binding domain containing 1
0,56	0,40	0,30	0,011209146	FAM115C	family with sequence similarity 115, member C
0,54	0,07	0,17	0,011209146	TFAP2A	transcription factor AP-2 alpha (activating enhancer binding protein 2 alpha)
0,78	0,34	0,48	0,011312601	NTN4	netrin 4
0,64	0,01	0,23	0,011652785	C21orf66	chromosome 21 open reading frame 66
0,59	0,10	0,06	0,011994606	RABEP1	rabaptin, RAB GTPase binding effector protein 1
0,58	0,02	0,00	0,012438349	RIPK1	receptor (TNFRSF)-interacting serine-threonine kinase 1
0,72	0,25	0,13	0,012480226	RAI14	retinoic acid induced 14
0,08	0,33	0,14	0,012570465	RAD54L2	RAD54-like 2 (S. cerevisiae)
0,54	0,08	0,20	0,013243679	SP4	Sp4 transcription factor
0,40	0,54	0,16	0,013538153	DDAH1	dimethylarginine dimethylaminohydrolase 1
0,63	0,32	0,16	0,013830507	TRIM23	tripartite motif-containing 23
1,00	0,03	0,18	0,014847627	IFIT3	interferon-induced protein with tetratricopeptide repeats 3
0,28	0,04	0,09	0,014847627	PHF15	PHD finger protein 15
0,25	0,46	0,07	0,015667593	ZMAT3	zinc finger, matrin type 3
0,47	0,26	0,45	0,015820302	FKBP14	FK506 binding protein 14, 22 kDa
0,40	0,24	0,21	0,017066457	ABHD2	abhydrolase domain containing 2
0,36	0,17	0,04	0,017868101	TKT	transketolase
0,24	0,07	0,45	0,017868101	NCRNA00153	non-protein coding RNA 153
0,57	0,01	0,11	0,017868101	DENND4C	DENN/MADD domain containing 4C
0,48	0,02	0,12	0,017922325	MGST2	microsomal glutathione S-transferase 2
0,56	0,09	0,09	0,018175512	CRBN	cereblon
0,55	0,25	0,06	0,018180254	ZNF420	zinc finger protein 420
0,77	0,02	0,10	0,018186278	RBMS1	RNA binding motif, single stranded interacting protein 1
0,52	0,20	0,12	0,018319744	ZNF260	zinc finger protein 260
0,95	0,42	0,11	0,01916535	ZNF322A	zinc finger protein 322A
0,35	0,36	0,09	0,019769793	CCNT1	cyclin T1
0,56	0,22	0,08	0,020329651	INO80C	INO80 complex subunit C
0,30	0,01	0,57	0,020380493	HIST1H3F	histone cluster 1, H3f

PANC-1 Ctl/sh_5	PANC-1 Ctl/sh_2	RWP-1 Gal-1/Ctl	adj.P.Val	unlist. symbol	Gene description
0,66	0,44	0,25	0,020634905	DBT	dihydrolipoamide branched chain transacylase E2
0,56	0,25	0,13	0,020901308	LRIG2	leucine-rich repeats and immunoglobulin-like domains 2
0,63	0,05	0,17	0,020990032	MTA3	metastasis associated 1 family, member 3
0,42	0,32	0,42	0,021178122	RIMBP3	RIMS binding protein 3
0,70	0,46	0,27	0,021294953	CLK1	CDC-like kinase 1
0,75	0,47	0,17	0,021551442	ZFP62	zinc finger protein 62 homolog (mouse)
0,71	0,23	0,21	0,022749524	RAD50	RAD50 homolog (S. cerevisiae)
0,95	0,13	0,01	0,023074342	HEG1	HEG homolog 1 (zebrafish)
0,62	0,26	0,31	0,023273435	TMEM184C	transmembrane protein 184C
0,22	0,22	0,16	0,02344141	FAM160B1	family with sequence similarity 160, member B1
0,24	0,18	0,54	0,023464571	DEM1	defects in morphology 1 homolog (S. cerevisiae)
0,84	0,34	0,10	0,024256507	MYO1B	myosin IB
0,42	0,03	0,18	0,024747834	ANTXR1	anthrax toxin receptor 1
0,72	0,44	0,48	0,024866809	TTC14	tetratricopeptide repeat domain 14
0,40	0,17	0,05	0,025331021	ECH1	enoyl Coenzyme A hydratase 1, peroxisomal
0,83	0,32	0,18	0,025581134	FAM13A	family with sequence similarity 13, member A
0,72	0,06	0,39	0,025778539	CENPO	centromere protein O
0,26	0,08	0,21	0,025956858	SNX19	sorting nexin 19
0,16	0,49	0,08	0,026249852	SRGAP1	SLIT-ROBO Rho GTPase activating protein 1
0,48	0,23	0,13	0,02768879	JUN	jun oncogene
0,44	0,27	0,02	0,029245682	TNRC6A	trinucleotide repeat containing 6A
0,50	0,32	0,27	0,029334419	PRPF39	PRP39 pre-mRNA processing factor 39 homolog (S. cerevisiae)
0,63	0,21	0,21	0,030512305	BVES	blood vessel epicardial substance
0,66	0,27	0,22	0,031782097	MBD4	methyl-CpG binding domain protein 4
0,48	0,44	0,47	0,032119122	HOXA2	homeobox A2
0,01	0,38	0,04	0,032468644	ADAT2	adenosine deaminase, tRNA-specific 2, TAD2 homolog (S. cerevisiae)
0,57	0,21	0,19	0,03261465	YTHDC2	YTH domain containing 2
0,39	0,36	0,12	0,03261465	ANK1	ankyrin 1, erythrocytic
1,10	0,40	0,28	0,032670142	C1orf103	chromosome 1 open reading frame 103
0,71	0,09	0,05	0,033117387	PHACTR2	phosphatase and actin regulator 2
0,38	0,10	0,06	0,033135828	SHROOM3	shroom family member 3
0,58	0,08	0,30	0,03328561	AHSA2	AHA1, activator of heat shock 90kDa protein ATPase homolog 2 (yeast)
0,44	0,08	0,11	0,033634416	WIPF1	WAS/WASL interacting protein family, member 1
0,40	0,08	0,00	0,034476306	TCF7L2	transcription factor 7-like 2 (T-cell specific, HMG-box)
0,60	0,05	0,12	0,034599219	CTNNBIP1	catenin, beta interacting protein 1
0,48	0,22	0,32	0,036133648	KAT2B	K(lysine) acetyltransferase 2B
0,42	0,07	0,17	0,036180725	SFRS5	splicing factor, arginine/serine-rich 5
0,54	0,03	0,25	0,036212476	SESN1	sestrin 1
0,51	0,01	0,12	0,036383733	PMS2	PMS2 postmeiotic segregation increased 2 (S. cerevisiae)
0,14	**0,18**	**0,27**	**0,036433553**	**FGFR2**	**fibroblast growth factor receptor 2**

PANC-1 Ctl/sh_5	PANC-1 Ctl/sh_2	RWP-1 Gal-1/Ctl	adj.P.Val	unlist. symbol	Gene description
0,37	0,13	0,10	0,036604246	SLC30A4	solute carrier family 30 (zinc transporter), member 4
0,36	0,04	0,22	0,037066128	PMS2CL	PMS2 C-terminal like pseudogene
0,54	0,41	0,07	0,037083726	SPATA5	spermatogenesis associated 5
0,29	0,06	0,30	0,037434563	CYP51A1	cytochrome P450, family 51, subfamily A, polypeptide 1
0,40	0,03	0,25	0,037761368	TNKS	tankyrase, TRF1-interacting ankyrin-related ADP-ribose polymerase
0,74	0,02	0,16	0,040359041	PUS7	pseudouridylate synthase 7 homolog (S. cerevisiae)
0,32	0,02	0,25	0,041213458	PRAF2	PRA1 domain family, member 2
0,37	0,14	0,04	0,041260947	LRP6	low density lipoprotein receptor-related protein 6
0,44	0,17	0,09	0,041311895	ZNF318	zinc finger protein 318
0,52	0,25	0,21	0,041738582	PTPN14	protein tyrosine phosphatase, non-receptor type 14
0,32	0,10	0,13	0,041804837	DDX5	DEAD (Asp-Glu-Ala-Asp) box polypeptide 5
0,43	0,09	0,16	0,042743946	KIAA0999	KIAA0999 protein
0,53	0,30	0,07	0,044284277	ETNK1	ethanolamine kinase 1
0,66	0,79	0,08	0,044292075	WASF1	WAS protein family, member 1
0,57	0,24	0,07	0,044586655	ZAK	sterile alpha motif and leucine zipper containing kinase AZK
0,42	0,27	0,21	0,046608188	PI4K2B	phosphatidylinositol 4-kinase type 2 beta
0,18	0,15	0,48	0,048580214	RUNX2	runt-related transcription factor 2
0,43	0,12	0,12	0,049279296	RBPJ	recombination signal binding protein for immunoglobulin kappa J region
0,47	0,12	0,19	0,049283901	POLR2B	polymerase (RNA) II (DNA directed) polypeptide B, 140kDa
0,37	0,18	0,01	0,049900528	RDH11	retinol dehydrogenase 11 (all-trans/9-cis/11-cis)

Table S10. List of genes significantly altered in the same direction as Gal-1 was (downregulated when Gal-1 levels were low in PANC-1 and upregulated when Gal-1 levels were high in RWP-1), when intersecting PANC-1 and RWP-1 lists, ordered according to increasing adjusted p value until 0.05. The first three columns express the fold change in logarithmic units with base 2 (FC = 2^column). The first column compared PANC-1 Ctl (which had already been filtered with the shCtl data) with PANC-1 shGal-1_5; the second compared PANC-1 Ctl with shGal-1_2; and the third compared RWP-1 Gal-1 with RWP-1 Ctl cells.

6.3.2 Gene Detailed Analysis: Genes Regulated in the Opposite Direction to Gal-1

PANC-1 Ctl/sh_5	PANC-1 Ctl/sh_2	RWP-1 Gal-1/Ctl	adj.P.Val	unlist. symbol	Gene description
-0,56	-0,64	-3,11	3,20E-011	CXCL1	chemokine (C-X-C motif) ligand 1 (melanoma growth stimulating activity, alpha)
-0,25	-0,15	-2,78	2,78E-010	TNFAIP3	tumor necrosis factor, alpha-induced protein 3
-2,63	-0,15	-0,02	2,78E-010	PRSS2	protease, serine, 2 (trypsin 2)
-0,42	-0,21	-2,95	1,03E-009	CXCL2	chemokine (C-X-C motif) ligand 2
-0,61	-0,15	-3,42	1,21E-009	LCN2	lipocalin 2
-0,51	-0,29	-2,05	2,29E-009	CXCL3	chemokine (C-X-C motif) ligand 3
-0,09	-0,02	-2,79	8,77E-009	HLA-DPA1	major histocompatibility complex, class II, DP alpha 1
-0,20	-0,24	-1,87	2,19E-008	NFKBIA	nuclear factor of kappa light polypeptide gene enhancer in B-cells inhibitor, alpha
-2,06	-0,11	-0,56	4,00E-008	ANKRD1	ankyrin repeat domain 1 (cardiac muscle)
-0,08	-0,05	-1,93	5,92E-008	IL32	interleukin 32
-2,21	-0,19	-0,08	6,64E-008	PRSS1	protease, serine, 1 (trypsin 1)
-2,20	0,00	-0,19	1,01E-007	CALB2	calbindin 2
-0,54	-0,06	-3,84	2,28E-007	GPR15	G protein-coupled receptor 15
-0,60	-0,10	-0,99	2,58E-007	NFKB2	nuclear factor of kappa light polypeptide gene enhancer in B-cells 2 (p49/p100)
-1,41	-0,09	-0,23	8,33E-007	PRSS3	protease, serine, 3
-1,10	-0,02	-0,25	1,01E-006	DUSP5	dual specificity phosphatase 5
-0,55	-0,22	-1,45	1,14E-006	CD74	CD74 molecule, major histocompatibility complex, class II invariant chain
-1,34	-0,06	-0,01	1,28E-006	THBD	thrombomodulin
-1,52	-0,31	-0,25	1,97E-006	BSPRY	B-box and SPRY domain containing
-0,19	**-0,29**	**-1,66**	**2,08E-006**	**PLAT**	**plasminogen activator, tissue**
-0,49	-0,11	-1,79	2,12E-006	FREM2	FRAS1 related extracellular matrix protein 2
-0,34	-0,12	-1,20	2,12E-006	ZC3H12A	zinc finger CCCH-type containing 12A
-1,06	-0,02	-0,03	2,20E-006	LRRC16A	leucine rich repeat containing 16A
-1,11	-0,25	0,00	2,56E-006	MAPK13	mitogen-activated protein kinase 13
-1,31	-0,23	-0,06	3,17E-006	IGFBP4	insulin-like growth factor binding protein 4
-0,49	-0,06	-1,41	5,29E-006	PROM1	prominin 1
-1,19	-0,05	-0,14	5,68E-006	ST14	suppression of tumorigenicity 14 (colon carcinoma)
-0,35	-0,37	-1,38	9,09E-006	IGFBP3	insulin-like growth factor binding protein 3
-1,04	-0,35	-0,02	1,50E-005	SUSD2	sushi domain containing 2
-0,48	-0,10	-1,32	1,60E-005	TSPAN7	tetraspanin 7
-0,32	-0,02	-0,93	1,68E-005	PPP4R4	protein phosphatase 4, regulatory subunit 4
-0,90	-0,37	-0,13	1,69E-005	KIAA1244	KIAA1244
-0,63	-0,25	-0,93	1,70E-005	GPR110	G protein-coupled receptor 110
-0,12	-0,28	-1,16	2,17E-005	SERPINA 1	serpin peptidase inhibitor, clade A (alpha-1 antiproteinase, antitrypsin), member 1
-0,61	-0,04	-0,23	2,58E-005	FXYD5	FXYD domain containing ion transport regulator 5
-0,31	-0,53	-0,96	2,63E-005	LAMC2	laminin, gamma 2

PANC-1 Ctl/sh_5	PANC-1 Ctl/sh_2	RWP-1 Gal-1/Ctl	adj.P.Val	unlist. symbol	Gene description
-0,76	-0,04	-0,17	2,71E-005	FUT8	fucosyltransferase 8 (alpha (1,6) fucosyltransferase)
-0,40	-0,14	-1,27	2,88E-005	CADPS	Ca++-dependent secretion activator
-0,70	-0,25	-2,01	2,97E-005	IL8	interleukin 8
-0,61	**-0,15**	**-0,58**	**3,05E-005**	**PLAU**	**plasminogen activator, urokinase**
-0,74	-0,06	-0,25	3,14E-005	SLCO4C1	solute carrier organic anion transporter family, member 4C1
-0,49	-0,12	-0,97	3,27E-005	FBN2	fibrillin 2
-1,67	-0,29	-0,47	7,71E-005	ASB4	ankyrin repeat and SOCS box-containing 4
-1,17	-0,02	-0,13	8,88E-005	IRF6	interferon regulatory factor 6
-1,10	-0,09	-0,15	8,93E-005	CA2	carbonic anhydrase II
-0,15	-0,02	-0,74	0,000125988	DOCK9	dedicator of cytokinesis 9
-0,62	-0,12	-0,06	0,000165596	PRDM8	PR domain containing 8
-0,83	-0,13	-1,20	0,000166471	VNN1	vanin 1
-0,07	-0,11	-0,71	0,0001787	SEC14L2	SEC14-like 2 (S. cerevisiae)
-0,28	0,00	-1,26	0,00022233	HLA-DPB1	major histocompatibility complex, class II, DP beta 1
-0,29	-0,22	-1,27	0,000226989	MPZL2	myelin protein zero-like 2
-0,42	**-0,05**	**-0,57**	**0,000253585**	**PLAUR**	**plasminogen activator, urokinase receptor**
-0,56	-0,04	-0,26	0,000320108	RFFL	ring finger and FYVE-like domain containing 1
-0,38	-0,06	-1,20	0,000331432	CIITA	class II, major histocompatibility complex, transactivator
-0,28	-0,15	-1,71	0,000356905	HLA-DRB5	major histocompatibility complex, class II, DR beta 5
-0,21	-0,01	-1,07	0,000434626	ZNF738	zinc finger protein 738
-0,19	-0,40	-0,71	0,000455542	ANKRD22	ankyrin repeat domain 22
-0,54	-0,19	-0,05	0,000457838	IRAK1	interleukin-1 receptor-associated kinase 1
-0,57	-0,47	-0,28	0,000461669	FAM43A	family with sequence similarity 43, member A
-0,45	-0,12	-0,68	0,000528362	DPYSL3	dihydropyrimidinase-like 3
-0,17	-0,22	-0,61	0,00056655	OPTN	optineurin
-0,64	-0,20	-0,30	0,000617418	FAR2	fatty acyl CoA reductase 2
-0,63	-0,06	-0,86	0,000625459	IL1A	interleukin 1, alpha
-0,62	0,00	-0,07	0,00063381	NPL	N-acetylneuraminate pyruvate lyase (dihydrodipicolinate synthase)
-0,73	-0,06	-0,28	0,000637784	SERPINB8	serpin peptidase inhibitor, clade B (ovalbumin), member 8
-0,67	-0,31	-0,79	0,000717262	ANKRD34B	ankyrin repeat domain 34B
-0,54	-0,18	-0,26	0,000721299	MTAP	methylthioadenosine phosphorylase
-1,04	-0,12	-0,21	0,000876845	FUT9	fucosyltransferase 9 (alpha (1,3) fucosyltransferase)
-0,81	-0,14	-0,24	0,000919875	UPP1	uridine phosphorylase 1
-0,37	-0,16	-1,05	0,001089378	TMEM45B	transmembrane protein 45B
-0,42	-0,11	-0,24	0,001538936	AARSD1	alanyl-tRNA synthetase domain containing 1
-0,59	-0,10	-0,15	0,001632745	C8orf47	chromosome 8 open reading frame 47
-0,60	-0,13	-1,05	0,001682353	HLA-DQA1	major histocompatibility complex, class II, DQ alpha 1
-1,70	-1,36	-0,33	0,001739156	OR10H3	olfactory receptor, family 10, subfamily H, member 3
-0,33	-0,04	-0,36	0,001814984	PRDX5	peroxiredoxin 5

PANC-1 Ctl/sh_5	PANC-1 Ctl/sh_2	RWP-1 Gal-1/Ctl	adj.P.Val	unlist. symbol	Gene description
-0,61	-0,03	-0,08	0,001859929	HK2	hexokinase 2
-0,72	-0,24	-0,08	0,00201688	MTMR8	myotubularin related protein 8
-0,56	-0,13	-0,53	0,002034966	WNT16	wingless-type MMTV integration site family, member 16
-0,59	-0,27	-0,02	0,002091349	ADAP2	ArfGAP with dual PH domains 2
-0,79	-0,09	-0,22	0,002299683	LIF	leukemia inhibitory factor (cholinergic differentiation factor)
-0,73	-0,53	-0,47	0,002318081	AMIGO2	adhesion molecule with Ig-like domain 2
-0,28	-0,17	-0,53	0,00269932	BIK	BCL2-interacting killer (apoptosis-inducing)
-0,62	-0,03	-0,06	0,002705046	KRT81	keratin 81
-0,54	-0,29	-0,22	0,002983223	NR4A1	nuclear receptor subfamily 4, group A, member 1
-0,75	-0,48	-0,02	0,003504588	SIX3	SIX homeobox 3
-0,57	-0,15	-1,11	0,003534264	GPR110	G protein-coupled receptor 110
-0,59	-0,15	-0,09	0,003596994	PRKG2	protein kinase, cGMP-dependent, type II
-0,65	-0,18	-0,06	0,00367229	TESK1	testis-specific kinase 1
-0,68	-0,06	-0,01	0,004023062	GIPC2	GIPC PDZ domain containing family, member 2
-0,40	-0,03	-0,65	0,004045393	GREM1	gremlin 1, cysteine knot superfamily, homolog (Xenopus laevis)
-1,04	-0,45	-0,07	0,004373637	NUDT9P1	nudix (nucleoside diphosphate linked moiety X)-type motif 9 pseudogene 1
-0,63	-0,10	-0,29	0,004391048	LAMB3	laminin, beta 3
-0,70	-0,28	-0,01	0,0045941	GGT5	gamma-glutamyltransferase 5
-0,54	-0,24	-0,43	0,004598851	NEDD9	neural precursor cell expressed, developmentally down-regulated 9
-0,14	-0,14	-0,48	0,004598851	STAT5A	signal transducer and activator of transcription 5A
-0,47	-0,08	-0,09	0,004737556	PTPRB	protein tyrosine phosphatase, receptor type, B
-0,15	-0,08	-0,79	0,004937905	SPRR3	small proline-rich protein 3
-0,77	-0,04	-0,12	0,005048677	STK33	serine/threonine kinase 33
-0,13	-0,16	-0,91	0,005250401	SPRR2B	small proline-rich protein 2B
-0,49	-0,78	-0,53	0,005420148	ARRDC3	arrestin domain containing 3
-0,50	-0,15	-0,95	0,005475938	SPRR1B	small proline-rich protein 1B (cornifin)
-0,64	-0,10	-0,06	0,005791275	FABP5	fatty acid binding protein 5 (psoriasis-associated)
-0,47	-0,14	-0,12	0,005988348	C9orf25	chromosome 9 open reading frame 25
-0,41	-0,04	-0,10	0,006177277	AP1G2	adaptor-related protein complex 1, gamma 2 subunit
-0,41	-0,31	-0,81	0,006616426	SGPP2	sphingosine-1-phosphate phosphotase 2
0,00	-0,02	-0,59	0,006892509	TM4SF1	transmembrane 4 L six family member 1
-0,39	-0,47	-0,12	0,007148333	P4HA2	prolyl 4-hydroxylase, alpha polypeptide II
-0,54	-0,09	-0,24	0,007240515	UST	uronyl-2-sulfotransferase
-0,52	-0,08	-0,07	0,007415557	UNC13D	unc-13 homolog D (C. elegans)
-0,56	-0,14	-0,06	0,007512084	RNF212	ring finger protein 212
-0,42	-0,02	-0,07	0,008149415	IL28RA	interleukin 28 receptor, alpha (interferon, lambda receptor)
-0,40	-0,07	-1,07	0,008151383	HLA-DRB1	major histocompatibility complex, class II, DR beta 1
-0,37	-0,11	-0,21	0,008161517	EHD1	EH-domain containing 1
-1,52	-0,92	-0,42	0,008253773	IGKV3D-15	immunoglobulin kappa variable 3D-15 (gene/pseudogene)

PANC-1 Ctl/sh_5	PANC-1 Ctl/sh_2	RWP-1 Gal-1/Ctl	adj.P.Val	unlist. symbol	Gene description
-0,50	-0,06	-0,16	0,008260815	TCEAL3	transcription elongation factor A (SII)-like 3
-0,26	-0,16	-0,37	0,008445547	TUBB2B	tubulin, beta 2B
-0,64	-0,02	-0,12	0,008632367	TLE4	transducin-like enhancer of split 4 (E(sp1) homolog, Drosophila)
-0,31	-0,04	-0,13	0,008657511	FAM100B	family with sequence similarity 100, member B
-0,68	-0,12	-0,13	0,008681055	MARVELD 3	MARVEL domain containing 3
-0,92	-0,03	-0,42	0,008698408	NA	NA
-0,08	-0,18	-0,40	0,008736904	PIH1D1	PIH1 domain containing 1
-0,52	-0,10	-0,18	0,008899128	SRPX	sushi-repeat-containing protein, X-linked
-0,36	-0,40	-0,04	0,00892441	HOXB8	homeobox B8
-0,78	-0,71	-0,51	0,009045943	NRN1	neuritin 1
-0,48	-0,26	-0,16	0,009063734	PYGL	phosphorylase, glycogen, liver
-0,42	-0,04	-0,61	0,009099734	TRPC3	transient receptor potential cation channel, subfamily C, member 3
-0,56	-0,18	-0,21	0,009260216	INHBA	inhibin, beta A
-0,89	-0,69	-0,20	0,009981212	NAP1L3	nucleosome assembly protein 1-like 3
-0,01	-0,45	-0,12	0,010110157	JUNB	jun B proto-oncogene
-0,84	-0,35	-0,19	0,010735005	GPR160	G protein-coupled receptor 160
-0,03	-0,01	-0,39	0,011091387	PPARD	peroxisome proliferator-activated receptor delta
-0,67	-0,11	-0,18	0,011341615	FAAH2	fatty acid amide hydrolase 2
-0,48	-0,16	-0,10	0,011812812	RAD51L3	RAD51-like 3 (S. cerevisiae)
-0,89	-0,12	-0,05	0,011843955	NA	NA
-0,57	-0,23	-0,44	0,013538153	WFDC2	WAP four-disulfide core domain 2
-0,84	-0,23	-0,01	0,013810004	DGCR14	DiGeorge syndrome critical region gene 14
-0,45	-0,03	-0,31	0,013933781	PGM5	phosphoglucomutase 5
-0,42	-0,39	-0,10	0,013987403	TMTC2	transmembrane and tetratricopeptide repeat containing 2
-0,46	-0,14	-0,42	0,015218436	SAGE1	sarcoma antigen 1
-0,38	-0,10	-0,20	0,015448556	RPL36	ribosomal protein L36
-0,20	-0,05	-0,37	0,015868763	ANK3	ankyrin 3, node of Ranvier (ankyrin G)
-0,88	-0,18	-0,25	0,015957922	C6orf142	chromosome 6 open reading frame 142
-0,48	-0,15	-0,19	0,016690837	SULF2	sulfatase 2
-0,41	-0,16	-0,17	0,016692098	HOOK2	hook homolog 2 (Drosophila)
-0,35	-0,01	-0,30	0,017159301	SPHK1	sphingosine kinase 1
-0,56	-0,03	-0,14	0,017590837	SRrp35	serine-arginine repressor protein (35 kDa)
-0,41	-0,07	-0,22	0,017868101	AFAP1L1	actin filament associated protein 1-like 1
-0,34	-0,14	-0,61	0,018051225	QPCT	glutaminyl-peptide cyclotransferase
-0,60	-0,13	-0,03	0,018757234	LSM11	LSM11, U7 small nuclear RNA associated
-0,59	-0,03	-0,18	0,018807617	TDO2	tryptophan 2,3-dioxygenase
-0,53	-0,13	-0,20	0,019553054	PLEKHG6	pleckstrin homology domain containing, family G (with RhoGef domain) member 6
-0,38	-0,12	-0,43	0,019704514	HCP5	HLA complex P5
-0,63	-0,52	-0,30	0,01980116	LBH	limb bud and heart development homolog (mouse)
-0,46	0,00	-0,85	0,020329651	PI3	peptidase inhibitor 3, skin-derived

PANC-1 Ctl/sh_5	PANC-1 Ctl/sh_2	RWP-1 Gal-1/Ctl	adj.P.Val	unlist. symbol	Gene description
-0,57	-0,15	-0,65	0,020374262	DLX5	distal-less homeobox 5
-0,42	-0,17	-0,17	0,021474414	CAMKV	CaM kinase-like vesicle-associated
-0,44	-0,09	-0,23	0,021570074	AK7	adenylate kinase 7
-0,28	-0,07	-0,20	0,022216293	POLR2I	polymerase (RNA) II (DNA directed) polypeptide I, 14.5kDa
-0,49	-0,13	-0,27	0,022456022	KIAA0040	KIAA0040
-0,05	-0,04	-0,32	0,023273435	SNX15	sorting nexin 15
-0,19	-0,27	-0,60	0,023299135	EHF	ets homologous factor
-0,32	-0,52	-0,08	0,025996404	CSF1	colony stimulating factor 1 (macrophage)
-0,43	-0,18	-0,10	0,026052071	C3orf15	chromosome 3 open reading frame 15
-0,77	-0,20	-0,24	0,026075264	HEY2	hairy/enhancer-of-split related with YRPW motif 2
-0,11	-0,30	-1,02	0,026249852	TAS2R13	taste receptor, type 2, member 13
-0,59	-0,05	-0,05	0,028187521	DPP4	dipeptidyl-peptidase 4
-0,48	-0,17	-0,04	0,028187521	ST3GAL6	ST3 beta-galactoside alpha-2,3-sialyltransferase 6
-0,41	-0,07	-0,27	0,028522575	PLD6	phospholipase D family, member 6
-0,50	-0,06	-0,53	0,028603968	KCNJ11	potassium inwardly-rectifying channel, subfamily J, member 11
-0,31	-0,35	-0,09	0,02874286	DUSP6	dual specificity phosphatase 6
-0,47	-0,18	-0,05	0,028919842	HYI	hydroxypyruvate isomerase homolog (E. coli)
-0,38	-0,31	-0,15	0,029245682	SYDE1	synapse defective 1, Rho GTPase, homolog 1 (C. elegans)
-0,70	-0,03	-0,02	0,029974374	ARHGDIB	Rho GDP dissociation inhibitor (GDI) beta
-0,60	-0,15	0,00	0,030302391	GALNT14	UDP-N-acetyl-alpha-D-galactosamine:polypeptide N-acetylgalactosaminyltransferase 14 (GalNAc-T14)
-0,48	-0,14	-0,40	0,03055	SLC1A1	solute carrier family 1 (neuronal/epithelial high affinity glutamate transporter, system Xag), member 1
-0,22	-0,30	-0,11	0,030631746	GALNAC4S-6ST	B cell RAG associated protein
-0,43	-0,05	-0,10	0,031217572	DEF6	differentially expressed in FDCP 6 homolog (mouse)
-0,55	-0,17	-0,21	0,031217572	KLC3	kinesin light chain 3
-1,28	-0,54	-0,19	0,03180981	C15orf49	chromosome 15 open reading frame 49
-0,18	-0,29	-0,17	0,031925307	SEMA4B	sema domain, immunoglobulin domain (Ig), transmembrane domain (TM) and short cytoplasmic domain, (semaphorin) 4B
-0,53	-0,15	-0,06	0,032468644	FAM50B	family with sequence similarity 50, member B
-0,48	-0,28	-0,35	0,033299845	UACA	uveal autoantigen with coiled-coil domains and ankyrin repeats
-0,40	-0,29	-0,92	0,033533822	HLA-DMB	major histocompatibility complex, class II, DM beta
-0,92	-0,15	-0,09	0,033562622	NA	NA
-0,99	-0,41	-0,05	0,034352911	C17orf102	chromosome 17 open reading frame 102
-0,32	-0,10	-0,38	0,034599219	C13orf18	chromosome 13 open reading frame 18
-0,92	-0,49	-0,68	0,035248924	HLA-DQA2	major histocompatibility complex, class II, DQ alpha 2
-0,65	-0,26	-0,14	0,035597932	VENTX	VENT homeobox homolog (Xenopus laevis)
-0,07	-0,37	-0,14	0,035800257	RNPEPL1	arginyl aminopeptidase (aminopeptidase B)-like 1
-0,55	-0,10	-0,02	0,036180725	KCTD12	potassium channel tetramerisation domain containing 12
-0,44	-0,07	-0,18	0,036609932	ATP12A	ATPase, H+/K+ transporting, nongastric, alpha polypeptide

PANC-1 Ctl/sh_5	PANC-1 Ctl/sh_2	RWP-1 Gal-1/Ctl	adj.P.Val	unlist. symbol	Gene description
-0,51	-0,35	-0,32	0,036637262	PHLDA3	pleckstrin homology-like domain, family A, member 3
-0,41	-0,15	-0,41	0,03740116	SLFN5	schlafen family member 5
-0,81	-0,37	-0,28	0,037616688	CCR5	chemokine (C-C motif) receptor 5
-0,84	-0,14	-0,19	0,037761368	RAB38	RAB38, member RAS oncogene family
-0,73	-0,43	-0,60	0,037849882	NA	NA
-0,34	-0,10	-0,05	0,038394736	TPM1	tropomyosin 1 (alpha)
-0,42	-0,15	0,00	0,038978785	PDE4D	phosphodiesterase 4D, cAMP-specific (phosphodiesterase E3 dunce homolog, Drosophila)
-0,34	-0,21	-0,61	0,039383718	HS3ST3A1	heparan sulfate (glucosamine) 3-O-sulfotransferase 3A1
-0,22	-0,17	-0,34	0,039839461	WDR18	WD repeat domain 18
-0,33	-0,01	-0,37	0,039942144	MAOA	monoamine oxidase A
-0,40	-0,21	-0,50	0,04031201	KLK10	kallikrein-related peptidase 10
-0,49	-0,14	-0,10	0,041211113	SYK	spleen tyrosine kinase
-0,44	-0,10	-0,12	0,041213458	BCL11A	B-cell CLL/lymphoma 11A (zinc finger protein)
-0,85	-0,38	-0,08	0,042311704	GYPC	glycophorin C (Gerbich blood group)
-0,11	-0,01	-0,36	0,042686751	PDLIM1	PDZ and LIM domain 1
-0,35	-0,06	-0,05	0,044255239	SNRPN	small nuclear ribonucleoprotein polypeptide N
-0,27	-0,16	-0,27	0,044882647	OGDHL	oxoglutarate dehydrogenase-like
-0,40	-0,04	-0,10	0,045269144	SLCO5A1	solute carrier organic anion transporter family, member 5A1
-0,23	-0,23	-0,14	0,045470696	GALNAC4S-6ST	B cell RAG associated protein
-0,48	-0,12	-0,01	0,046201909	GYLTL1B	glycosyltransferase-like 1B
-0,05	-0,48	-0,15	0,046314877	GPNMB	glycoprotein (transmembrane) nmb
-0,04	-0,30	-0,06	0,048069236	FAM102A	family with sequence similarity 102, member A
-0,50	-0,19	-0,02	0,048192342	JAKMIP1	Janus kinase and microtubule interacting protein 1
-0,22	-0,04	-0,21	0,048302723	SLC25A39	solute carrier family 25, member 39
-0,45	-0,07	-0,47	0,04842011	IL23A	interleukin 23, alpha subunit p19
-0,45	-0,14	-0,32	0,048979727	FAM13C	family with sequence similarity 13, member C
-0,64	-0,16	-0,17	0,049567403	TESC	tescalcin
-0,61	-0,16	-0,22	0,049567403	LRAT	lecithin retinol acyltransferase (phosphatidylcholine--retinol O-acyltransferase)
-0,23	-0,03	-0,20	0,04958438	ILK	integrin-linked kinase
-0,64	-0,38	-0,28	0,04964759	MYCN	v-myc myelocytomatosis viral related oncogene, neuroblastoma derived (avian)
-0,62	-0,21	-0,16	0,04964759	TMEM74	transmembrane protein 74

Table S11. List of genes significantly altered in the opposite direction of Gal-1 (upregulated when Gal-1 levels were low in PANC-1 and downregulated when Gal-1 levels were high in RWP-1), when intersecting PANC-1 and RWP-1 lists, ordered according to increasing adjusted p value until 0.05. The first three columns express the fold change in logarithmic units with base 2 (FC = 2^column). The first column compared PANC-1 Ctl (which had already been filtered with the shCtl data) with PANC-1 shGal-1_5; the second compared PANC-1 Ctl with shGal-1_2; and the third compared RWP-1 Gal-1 with RWP-1 Ctl cells.

ABBREVIATIONS

The following criteria has been applied for nomenclature: Mice gene symbols are shown in italics, with only the first letter in uppercase and the remaining letters in lowercase (Ej. *Ras*), according to Mouse Genome Informatics (MGI). Human genes are italicized, with all letters in uppercase (Ej. *RAS*), according to HUGO Gene Nomenclature Committee (HGNC). For zebrafish, genes are written in italics and lowercase (Ej. *ras*), according to Zebrafish Model Organism Database (ZFIN). When generally referring to proteins, capitals are used just for the first letter (Ej. Shh), unless for those proteins in which capital letters are normally used (Ej. TGF-β).

2-AB	2-aminobenzamide
2-DE	bidimensional electrophoresis
α	anti-
AAs	aminoacids
Abs	absorbance
ADM	acinar-ductal metaplasia
AJCC	American Joint Committee on Cancer
AnxA2	annexin A2
AP-1	activator protein-1
Arf	ADP Ribosylation Factors
BCE	before common era
Bcl2	B-cell lymphoma 2
BEH	bridged ethyl hybrid
BEX-2	brain expressed X-linked gene
b-FGF	basic FGF
BPE	bovine pituitary extract
BRCA	breast cancer
BrdU	bromodeoxyuridine
BSA	bovine serum albumin
CA	cancer antigen
CAF	carcinoma associated fibroblasts
CD	cluster of differentiation
Cdc52	cell division control protein 52
CDKN2A	cyclin-dependent kinase inhibitor 2A

CEA	carcinoembryonic antigen
CEEA	ethical committee for animal experimentation
CHO	chinese hamster ovary
CINC-1	cytokine-induced neutrophil chemoattractant-1
CK	cytokeratin
CKAP	cytoskeletal associated protein
CM	conditioned medium
Col11A1	collagen type11 alpha 1
COX-2	cyclooxygenase-2
CRD	carbohydrate recognition domain
CTGF	connective tissue growth factor)
Ctl	control
Ctrl	control
DAPI	5',6-diamidino-2-phenylindole
DIG	digoxigenin
Disp1	dispatched homolg protein
DMEM	Dulbecco's Modified Eagle's Medium
DPC5	deleted in pancreatic cancer, locus 5
E	embryonic day
E-cad	E-cadherin
ECM	extracellular matrix
EGF	epidermal growth factor
EGFR	epidermal growth factor receptor
Ela	elastase
EMT	epithelial to mesenchymal transition
ER	endoplasmatic reticulum
Erk	extracellular signal-regulated kinases
F	filial
FBS	fetal bovine serum
FDA	food and drug administration
FGF	fibroblast growth factor
FLD	postcolumn fluorescence derivatization
FN1	fibronectin type I
FOXN1	forkhead box protein N1
Fw	forward
GA	golgi apparatus
Gal	galactose
Gal-1	Galectin-1
GalNAc	*N*-acetylgalactosamine
GFP	green fluorescence protein
GH	growth hormone
Glc	glucose
GlcNAc	*N*-acetlyglucosamine

GlcNAcT, MGAT5	*N*-acetylglucosaminyltransferase V
GM1	monosialotetrahexosylganglioside
H&E	hematoxylin and eosin
HBG	human brain Galectin-1-binding
HCC	hepatocellular carcinoma
Hes-1	hairy and enhancer of split 1
HGF	hepatocyte growth factor
Hh	Hedgehog
Hhat	Hedgehog acetyltransferase
HIF	hypoxia-inducible factors
HNSCC	head and neck squamous cell carcinoma
HPDE	human pancreatic ductal epithelial
HPLC	high performance liquid chromatography
H-Ras	Harvey rat sarcoma viral oncogene homolog
HRP	horseradish peroxidase
HUVEC	human Umbilical Vein Endothelial Cells
IF	immunofluorescence
IFN	interferon
IGF1	insulin-like growth factor 1
IHC	immunohistochemistry
IL	interleukin
INB	bone infiltration
INK5A	inhibitor of cyclin-dependent kinase 5
INM	muscle infiltration
IP	intraperitoneal
IPMN	intraductal papillary mucinous neoplasm
ISH	*in situ* hybridisation
Jnk	c-Jun N terminal kinase
K	kringle
KD	knockdown
KO	knockout
K-Ras	Kirsten rat sarcoma viral oncogene homolog
KSFM	keratinocyte serum-free medium
LacNAc	*N*-acetylactosamine
LAMP	lysosomal-associated membrane protein
LRP	lipoprotein receprot-related protein
Luc	luciferase
MALDI-TOF	matrix assisted laser desorption/ionization- time of flight
Man	mannose
MCN	mucinous cystic neoplasm
MCP-1	monocyte chemoattractant protein-1
MHC	major histocompatibility complex

MMP	matrix metalloproteinases
MO	morpholino
mRNA	messenger ribonucleic acid
MS	mass spectrometry
MTT	3-(5.5-dimethylthiazol-2-yl)-2.5-diphenyltetrazolium bromide
Muc	mucin
myc	myelocytomatosis oncogene
NF-κB	nuclear factor kappa B
NMDAR	*N*-methyl-D-aspartate receptor
NMR	nuclear magnetic resonance
Nox5	NADPH oxidase 5
NRP-1	neuropilin-1
ON	overnight
ORP	oxygen regulated protein
OSCC	oral Squamous Cell Carcinoma
PAI	plasminogen activator inhibitor
PanIN	pancreatic intraepithelial neoplasia
PBS	phosphate-buffered saline
PCR	polymerase chain reaction
PDAC	pancreatic ductal adenocarcinoma
PDGF	platelet-derived growth factors
Pdx1	pancreatic and duodenal homeobox 1
PEI	polyethylenimine
PFA	paraformaldehyde
Pg	plasminogen
PI3K	phosphoinositide 3 kinase
PMF	peptide mass fingerprint
PNGaseF	peptide N-glycosidase F
PP cells	pancreatic polypeptide cells
PSC	pancreatic stellate cells
Ptch	patched
Pten	phosphatase and tensin homolog
PTF1	pancreas transcription factor 1
RhoA	Ras homolog gene family, member A
RNA	ribonculeic acid
Rnase	ribonuclease
rProtein	recombinant protein
RT	room temperature
RT-qPCR	real time quantitative PCR
RU	resonance units
Rv	reverse
SC	subcutaneous

SCID	severe combined immunodeficiency
SDF-1	stromal cell-derived factor-1
SDS	sodium dodecyl sulfate
SEM	standard error of the mean
Shh	sonic Hedgehog
shRNA	short hairpin RNA
siRNA	small interference RNA
Sle	sialyl lewis antigen
SMA	smooth muscle actin
SMAD5	Sowjetische Militäradministration in Deutschland 5
Smo	smoothened
SP	serine protease
SPARC	secreted protein acidic and rich in cysteine
SPR	surface plasmon resonance
SV50	simian vacuolating virus 50
TBS	tris-buffered saline
TBS-T	TBS 0.1% Tween
TCR	T cell receptor
TF	transcription factor
TFA	trifluoroacetic acid
TGF	transforming growth factor
TGFBI	transforming growth factor beta-induced
TIMP	tissue inhibitor of metalloproteinases
TNF	tumor necrosis factor
TNFR	tumor necrosis factor receptor
TNM	tumor node metastasis
tPA	tissue plasminogen activator
Trkb	neurotrophic tyrosine kinase receptor
TVA	receptor for ASLV virus subgroup A
UAS	upstream activation sequence
uPA	urokinase plasminogen activator
uPAR	uPA receptor
UPLC	ultra performance liquid chromatography
UV	ultraviolet
VEGF	vascular endothelial growth factor
VP16	viral protein 16
vWF	von Willebrand factor
WB	Western blot
wt	wild type

AMINOACID NOMENCLATURE AND SYMBOLISM

According to IUPAC-IUB Joint Commission on Biochemical Nomenclature (JCBN).

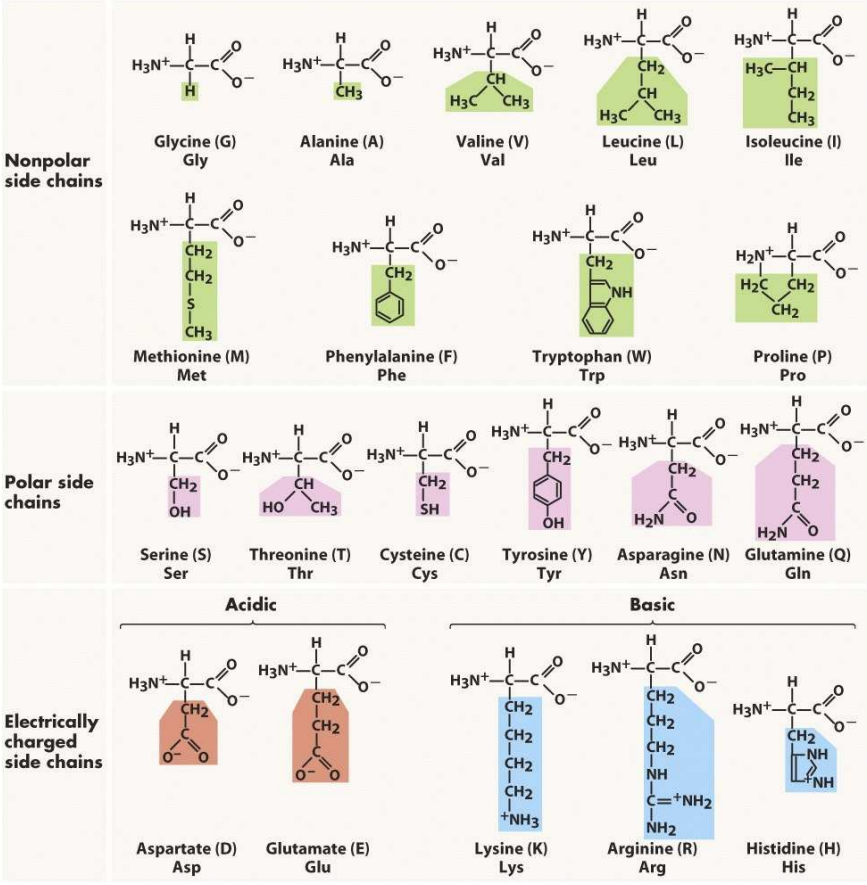

Figure 123. AA structures and most accepted symbolism. Extracted from [900].

REFERENCES

Nothing truly valuable arises from ambition or from a mere sense of duty; it stems rather from love and devotion towards men and towards objective things.

Albert Einstein

Reference List

1. Hezel,A.F., Kimmelman,A.C., Stanger,B.Z., Bardeesy,N. & DePinho,R.A. Genetics and biology of pancreatic ductal adenocarcinoma. *Genes Dev.* **20**, 1218-1249 (2006).

2. Stanger,B.Z. & Dor,Y. Dissecting the cellular origins of pancreatic cancer. *Cell Cycle* **5**, 43-46 (2006).

3. Edlund,H. Pancreatic organogenesis--developmental mechanisms and implications for therapy. *Nat. Rev. Genet.* **3**, 524-532 (2002).

4. Kim,S.K. & MacDonald,R.J. Signaling and transcriptional control of pancreatic organogenesis. *Curr. Opin. Genet. Dev.* **12**, 540-547 (2002).

5. Gittes,G.K. Developmental biology of the pancreas: a comprehensive review. *Dev. Biol.* **326**, 4-35 (2009).

6. Hebrok,M., Kim,S.K. & Melton,D.A. Notochord repression of endodermal Sonic hedgehog permits pancreas development. *Genes Dev.* **12**, 1705-1713 (1998).

7. Offield,M.F. *et al.* PDX-1 is required for pancreatic outgrowth and differentiation of the rostral duodenum. *Development* **122**, 983-995 (1996).

8. Kawaguchi,Y. *et al.* The role of the transcriptional regulator Ptf1a in converting intestinal to pancreatic progenitors. *Nat. Genet.* **32**, 128-134 (2002).

9. Slack,J.M. Developmental biology of the pancreas. *Development* **121**, 1569-1580 (1995).

10. Esni,F. *et al.* Notch inhibits Ptf1 function and acinar cell differentiation in developing mouse and zebrafish pancreas. *Development* **131**, 4213-4224 (2004).

11. Murtaugh,L.C. & Melton,D.A. Genes, signals, and lineages in pancreas development. *Annu. Rev. Cell Dev. Biol.* **19**, 71-89 (2003).

12. Kim,S.K., Hebrok,M. & Melton,D.A. Notochord to endoderm signaling is required for pancreas development. *Development* **124**, 4243-4252 (1997).

13. Scharfmann,R. Control of early development of the pancreas in rodents and humans: implications of signals from the mesenchyme. *Diabetologia* **43**, 1083-1092 (2000).

14. Gittes,G.K., Galante,P.E., Hanahan,D., Rutter,W.J. & Debase,H.T. Lineage-specific morphogenesis in the developing pancreas: role of mesenchymal factors. *Development* **122**, 439-447 (1996).

15. Miralles,F., Czernichow,P. & Scharfmann,R. Follistatin regulates the relative proportions of endocrine versus exocrine tissue during pancreatic development. *Development* **125**, 1017-1024 (1998).

16. Kloeppel,G., Luettges,J., Zamboni,G. & Scarpa,A. Exocrine Pancreas Cancer. The European Pancreatic Cancer-Research Cooperative. Gress TM,N.J.L.N.R.F. (ed.), pp. 62-83 (2005).

17. Hruban,R.H., Pitman,M.B. & Klimstra,D.S. Tumors of the Pancreas (AFIP Atlas of Tumor Pathology). Washington D.C (2007).

18. Jemal,A., Siegel,R., Xu,J. & Ward,E. Cancer statistics, 2010. *CA Cancer J. Clin.* **60**, 277-300 (2010).

19. American Cancer Society. Cancer Facts & Figures. Atlanta, GA (2010).

20. Hidalgo,M. Pancreatic cancer. *N. Engl. J. Med.* **362**, 1605-1617 (2010).

21. Wang,Z. *et al.* Pancreatic cancer: understanding and overcoming chemoresistance. *Nat. Rev. Gastroenterol. Hepatol.* **8**, 27-33 (2011).

22. Yachida,S. & Iacobuzio-Donahue,C.A. The pathology and genetics of metastatic pancreatic cancer. *Arch. Pathol. Lab Med.* **133**, 413-422 (2009).

23. Embuscado,E.E. *et al.* Immortalizing the complexity of cancer metastasis: genetic features of lethal metastatic pancreatic cancer obtained from rapid autopsy. *Cancer Biol. Ther.* **4**, 548-554 (2005).

24. Disibio,G. & French,S.W. Metastatic patterns of cancers: results from a large autopsy study. *Arch. Pathol. Lab Med.* **132**, 931-939 (2008).

25. Yachida,S. *et al.* Distant metastasis occurs late during the genetic evolution of pancreatic cancer. *Nature* **467**, 1114-1117 (2010).

26. Campbell,P.J. *et al.* The patterns and dynamics of genomic instability in metastatic pancreatic cancer. *Nature* **467**, 1109-1113 (2010).

27. Izeradjene,K. & Hingorani,S.R. Targets, trials, and travails in pancreas cancer. *J. Natl. Compr. Canc. Netw.* **5**, 1042-1053 (2007).

28. Moore,M.J. *et al.* Erlotinib plus gemcitabine compared with gemcitabine alone in patients with advanced pancreatic cancer: a phase III trial of

the National Cancer Institute of Canada Clinical Trials Group. *J. Clin. Oncol.* **25,** 1960-1966 (2007).

29. Wong,H.H. & Lemoine,N.R. Pancreatic cancer: molecular pathogenesis and new therapeutic targets. *Nat. Rev. Gastroenterol. Hepatol.* **6,** 412-422 (2009).

30. Philip,P.A. *et al.* Phase III study comparing gemcitabine plus cetuximab versus gemcitabine in patients with advanced pancreatic adenocarcinoma: Southwest Oncology Group-directed intergroup trial S0205. *J. Clin. Oncol.* **28,** 3605-3610 (2010).

31. Van Cutsem,E. *et al.* Phase III trial of bevacizumab in combination with gemcitabine and erlotinib in patients with metastatic pancreatic cancer. *J. Clin. Oncol.* **27,** 2231-2237 (2009).

32. Stathis,A. & Moore,M.J. Advanced pancreatic carcinoma: current treatment and future challenges. *Nat. Rev. Clin. Oncol.* **7,** 163-172 (2010).

33. Li,J., Merl,M.Y. & Saif,M.W. Any second-line therapy for advanced pancreatic cancer? Highlights from the "2010 ASCO Gastrointestinal Cancers Symposium". Orlando, FL, USA. January 22-24, 2010. *JOP.* **11,** 151-153 (2010).

34. Kim,R. FOLFIRINOX: a new standard treatment for advanced pancreatic cancer? *Lancet Oncol.* **12,** 8-9 (2011).

35. Trouilloud,I. *et al.* Medical treatment of pancreatic cancer: New hopes after 10years of gemcitabine. *Clin. Res. Hepatol. Gastroenterol.* **35,** 364-374 (2011).

36. Rowland-Goldsmith,M.A. *et al.* Soluble type II transforming growth factor-beta receptor attenuates expression of metastasis-associated genes and suppresses pancreatic cancer cell metastasis. *Mol. Cancer Ther.* **1,** 161-167 (2002).

37. Fukasawa,M. & Korc,M. Vascular endothelial growth factor-trap suppresses tumorigenicity of multiple pancreatic cancer cell lines. *Clin. Cancer Res.* **10,** 3327-3332 (2004).

38. Aikawa,T., Gunn,J., Spong,S.M., Klaus,S.J. & Korc,M. Connective tissue growth factor-specific antibody attenuates tumor growth, metastasis, and angiogenesis in an orthotopic mouse model of pancreatic cancer. *Mol. Cancer Ther.* **5,** 1108-1116 (2006).

39. Sato,N., Maehara,N. & Goggins,M. Gene expression profiling of tumor-stromal interactions between pancreatic cancer cells and stromal fibroblasts. *Cancer Res.* **64,** 6950-6956 (2004).

40. Bardeesy,N. & DePinho,R.A. Pancreatic cancer biology and genetics. *Nat. Rev. Cancer* **2,** 897-909 (2002).

41. Meszoely,I.M., Means,A.L., Scoggins,C.R. & Leach,S.D. Developmental aspects of early pancreatic cancer. *Cancer J.* **7,** 242-250 (2001).

42. Hruban,R.H., Wilentz,R.E. & Kern,S.E. Genetic progression in the pancreatic ducts. *Am. J Pathol.* **156,** 1821-1825 (2000).

43. Moskaluk,C.A., Hruban,R.H. & Kern,S.E. p16 and K-ras gene mutations in the intraductal precursors of human pancreatic adenocarcinoma. *Cancer Res.* **57,** 2140-2143 (1997).

44. Kloppel,G. & Longnecker,D.S. Hyperplastic and metaplastic changes in pancreatic ducts: nomenclature and preneoplastic potential. *Ann. N. Y. Acad. Sci.* **880,** 66-73 (1999).

45. Lee,K.E. & Bar-Sagi,D. Oncogenic KRas suppresses inflammation-associated senescence of pancreatic ductal cells. *Cancer Cell* **18,** 448-458 (2010).

46. Scarpelli,D.G., Rao,M.S. & Reddy,J.K. Are acinar cells involved in the pathogenesis of ductal adenocarcinoma of the pancreas? *Cancer Cells* **3,** 275-277 (1991).

47. Zhu,L., Shi,G., Schmidt,C.M., Hruban,R.H. & Konieczny,S.F. Acinar cells contribute to the molecular heterogeneity of pancreatic intraepithelial neoplasia. *Am. J. Pathol.* **171,** 263-273 (2007).

48. Stanger,B.Z. *et al.* Pten constrains centroacinar cell expansion and malignant transformation in the pancreas. *Cancer Cell* **8,** 185-195 (2005).

49. Pour,P.M. *et al.* Experimental evidence for the origin of ductal-type adenocarcinoma from the islets of Langerhans. *Am. J. Pathol.* **150,** 2167-2180 (1997).

50. Yoshida,T. & Hanahan,D. Murine pancreatic ductal adenocarcinoma produced by in vitro transduction of polyoma middle T oncogene into the islets of Langerhans. *Am. J. Pathol.* **145,** 671-684 (1994).

51. Pour,P.M. The role of Langerhans islets in pancreatic ductal adenocarcinoma. *Front Biosci.* **2,** d271-d282 (1997).

52. Carriere,C., Seeley,E.S., Goetze,T., Longnecker,D.S. & Korc,M. The Nestin progenitor lineage is the compartment of origin for pancreatic intraepithelial neoplasia. *Proc. Natl. Acad. Sci. U. S. A* **104,** 4437-4442 (2007).

53. Grippo,P.J., Nowlin,P.S., Demeure,M.J., Longnecker,D.S. & Sandgren,E.P. Preinvasive pancreatic neoplasia of ductal phenotype induced by acinar cell targeting of mutant Kras in transgenic mice. *Cancer Res.* **63**, 2016-2019 (2003).

54. Brembeck,F.H. *et al.* The mutant K-ras oncogene causes pancreatic periductal lymphocytic infiltration and gastric mucous neck cell hyperplasia in transgenic mice. *Cancer Res.* **63**, 2005-2009 (2003).

55. Ray,K.C. *et al.* Epithelial tissues have varying degrees of susceptibility to kras-initiated tumorigenesis in a mouse model. *PLoS. One.* **6**, e16786 (2011).

56. Hingorani,S.R. *et al.* Preinvasive and invasive ductal pancreatic cancer and its early detection in the mouse. *Cancer Cell* **4**, 437-450 (2003).

57. Guerra,C. *et al.* Chronic pancreatitis is essential for induction of pancreatic ductal adenocarcinoma by K-Ras oncogenes in adult mice. *Cancer Cell* **11**, 291-302 (2007).

58. Hall,P.A. & Lemoine,N.R. Rapid acinar to ductal transdifferentiation in cultured human exocrine pancreas. *J. Pathol.* **166**, 97-103 (1992).

59. Vila,M.R., Lloreta,J. & Real,F.X. Normal human pancreas cultures display functional ductal characteristics. *Lab Invest* **71**, 423-431 (1994).

60. Wagner,M. *et al.* Transgenic overexpression of amphiregulin induces a mitogenic response selectively in pancreatic duct cells. *Gastroenterology* **122**, 1898-1912 (2002).

61. Sandgren,E.P., Luetteke,N.C., Palmiter,R.D., Brinster,R.L. & Lee,D.C. Overexpression of TGF alpha in transgenic mice: induction of epithelial hyperplasia, pancreatic metaplasia, and carcinoma of the breast. *Cell* **61**, 1121-1135 (1990).

62. Sandgren,E.P., Quaife,C.J., Paulovich,A.G., Palmiter,R.D. & Brinster,R.L. Pancreatic tumor pathogenesis reflects the causative genetic lesion. *Proc. Natl. Acad. Sci. U. S. A* **88**, 93-97 (1991).

63. Everhart,J. & Wright,D. Diabetes mellitus as a risk factor for pancreatic cancer. A meta-analysis. *JAMA* **273**, 1605-1609 (1995).

64. Fuchs,C.S. *et al.* A prospective study of cigarette smoking and the risk of pancreatic cancer. *Arch. Intern. Med.* **156**, 2255-2260 (1996).

65. Gapstur,S.M. *et al.* Abnormal glucose metabolism and pancreatic cancer mortality. *JAMA* **283**, 2552-2558 (2000).

66. Michaud,D.S. *et al.* Physical activity, obesity, height, and the risk of pancreatic cancer. *JAMA* **286**, 921-929 (2001).

67. Berrington,d.G., Sweetland,S. & Spencer,E. A meta-analysis of obesity and the risk of pancreatic cancer. *Br. J. Cancer* **89**, 519-523 (2003).

68. Amundadottir,L.T. *et al.* Cancer as a complex phenotype: pattern of cancer distribution within and beyond the nuclear family. *PLoS. Med.* **1**, e65 (2004).

69. Klein,A.P. *et al.* Prospective risk of pancreatic cancer in familial pancreatic cancer kindreds. *Cancer Res.* **64**, 2634-2638 (2004).

70. Hruban,R.H., Goggins,M., Parsons,J. & Kern,S.E. Progression model for pancreatic cancer. *Clin. Cancer Res.* **6**, 2969-2972 (2000).

71. Bardeesy,N., Sharpless,N.E., DePinho,R.A. & Merlino,G. The genetics of pancreatic adenocarcinoma: a roadmap for a mouse model. *Semin. Cancer Biol.* **11**, 201-218 (2001).

72. Morris,J.P., Wang,S.C. & Hebrok,M. KRAS, Hedgehog, Wnt and the twisted developmental biology of pancreatic ductal adenocarcinoma. *Nat. Rev. Cancer* **10**, 683-695 (2010).

73. Hruban,R.H. *et al.* Pancreatic intraepithelial neoplasia: a new nomenclature and classification system for pancreatic duct lesions. *Am. J. Surg. Pathol.* **25**, 579-586 (2001).

74. Hruban,R.H. *et al.* An illustrated consensus on the classification of pancreatic intraepithelial neoplasia and intraductal papillary mucinous neoplasms. *Am. J. Surg. Pathol.* **28**, 977-987 (2004).

75. Maitra,A., Fukushima,N., Takaori,K. & Hruban,R.H. Precursors to invasive pancreatic cancer. *Adv. Anat. Pathol.* **12**, 81-91 (2005).

76. Brugge,W.R., Lauwers,G.Y., Sahani,D., Fernandez-del Castillo,C. & Warshaw,A.L. Cystic neoplasms of the pancreas. *N. Engl. J. Med.* **351**, 1218-1226 (2004).

77. Hruban,R.H., Wilentz,R.E. & Maitra,A. Identification and analysis of precursors to invasive pancreatic cancer. *Methods Mol. Med.* **103**, 1-13 (2005).

78. Kern,S. *et al.* A white paper: the product of a pancreas cancer think tank. *Cancer Res.* **61**, 4923-4932 (2001).

79. Hruban,R.H. *et al.* K-ras oncogene activation in adenocarcinoma of the human pancreas. A study of 82 carcinomas using a combination of mutant-enriched polymerase chain reaction analysis and allele-specific oligonucleotide hybridization. *Am. J. Pathol.* **143**, 545-554 (1993).

80. Almoguera,C. *et al.* Most human carcinomas of the exocrine pancreas contain mutant c-K-ras genes. *Cell* **53,** 549-554 (1988).

81. Tuveson,D.A. & Hingorani,S.R. Ductal pancreatic cancer in humans and mice. *Cold Spring Harb. Symp. Quant. Biol.* **70,** 65-72 (2005).

82. Park,S.W. *et al.* Oncogenic KRAS induces progenitor cell expansion and malignant transformation in zebrafish exocrine pancreas. *Gastroenterology* **134,** 2080-2090 (2008).

83. Rozenblum,E. *et al.* Tumor-suppressive pathways in pancreatic carcinoma. *Cancer Res.* **57,** 1731-1734 (1997).

84. Boschman,C.R., Stryker,S., Reddy,J.K. & Rao,M.S. Expression of p53 protein in precursor lesions and adenocarcinoma of human pancreas. *Am. J. Pathol.* **145,** 1291-1295 (1994).

85. Wilentz,R.E. *et al.* Loss of expression of Dpc4 in pancreatic intraepithelial neoplasia: evidence that DPC4 inactivation occurs late in neoplastic progression. *Cancer Res.* **60,** 2002-2006 (2000).

86. Luttges,J. *et al.* Allelic loss is often the first hit in the biallelic inactivation of the p53 and DPC4 genes during pancreatic carcinogenesis. *Am. J. Pathol.* **158,** 1677-1683 (2001).

87. Jones,S. *et al.* Core signaling pathways in human pancreatic cancers revealed by global genomic analyses. *Science* **321,** 1801-1806 (2008).

88. Pasca,d.M. & Hebrok,M. Hedgehog signalling in cancer formation and maintenance. *Nat. Rev. Cancer* **3,** 903-911 (2003).

89. Jacob,L. & Lum,L. Deconstructing the hedgehog pathway in development and disease. *Science* **318,** 66-68 (2007).

90. Lauth,M. & Toftgard,R. Non-canonical activation of GLI transcription factors: implications for targeted anti-cancer therapy. *Cell Cycle* **6,** 2458-2463 (2007).

91. Fernandez-Zapico,M.E. Primers on molecular pathways GLI: more than just Hedgehog? *Pancreatology.* **8,** 227-229 (2008).

92. Nolan-Stevaux,O. *et al.* GLI1 is regulated through Smoothened-independent mechanisms in neoplastic pancreatic ducts and mediates PDAC cell survival and transformation. *Genes Dev.* **23,** 24-36 (2009).

93. Thayer,S.P. *et al.* Hedgehog is an early and late mediator of pancreatic cancer tumorigenesis. *Nature* **425,** 851-856 (2003).

94. Feldmann,G. *et al.* Blockade of hedgehog signaling inhibits pancreatic cancer invasion and metastases: a new paradigm for combination therapy in solid cancers. *Cancer Res.* **67,** 2187-2196 (2007).

95. Pasca,d.M. *et al.* Hedgehog/Ras interactions regulate early stages of pancreatic cancer. *Genes Dev.* **20,** 3161-3173 (2006).

96. Yauch,R.L. *et al.* A paracrine requirement for hedgehog signalling in cancer. *Nature* **455,** 406-410 (2008).

97. Tian,H. *et al.* Hedgehog signaling is restricted to the stromal compartment during pancreatic carcinogenesis. *Proc. Natl. Acad. Sci. U. S. A* **106,** 4254-4259 (2009).

98. Bailey,J.M. *et al.* Sonic hedgehog promotes desmoplasia in pancreatic cancer. *Clin. Cancer Res.* **14,** 5995-6004 (2008).

99. Bailey,J.M., Mohr,A.M. & Hollingsworth,M.A. Sonic hedgehog paracrine signaling regulates metastasis and lymphangiogenesis in pancreatic cancer. *Oncogene* **28,** 3513-3525 (2009).

100. Olive,K.P. *et al.* Inhibition of Hedgehog signaling enhances delivery of chemotherapy in a mouse model of pancreatic cancer. *Science* **324,** 1457-1461 (2009).

101. Paget,S. The distribution of secondary growths in cancer of the breast. 1889. *Cancer Metastasis Rev.* **8,** 98-101 (1989).

102. Fidler,I.J. The pathogenesis of cancer metastasis: the 'seed and soil' hypothesis revisited. *Nat. Rev. Cancer* **3,** 453-458 (2003).

103. McAllister,S.S. & Weinberg,R.A. Tumor-host interactions: a far-reaching relationship. *J. Clin. Oncol.* **28,** 4022-4028 (2010).

104. Marx,J. Cancer biology. All in the stroma: cancer's Cosa Nostra. *Science* **320,** 38-41 (2008).

105. Chu,G.C., Kimmelman,A.C., Hezel,A.F. & DePinho,R.A. Stromal biology of pancreatic cancer. *J. Cell Biochem.* **101,** 887-907 (2007).

106. Mahadevan,D. & Von Hoff,D.D. Tumor-stroma interactions in pancreatic ductal adenocarcinoma. *Mol. Cancer Ther.* **6,** 1186-1197 (2007).

107. Hernandez-Munoz,I., Skoudy,A., Real,F.X. & Navarro,P. Pancreatic ductal adenocarcinoma: cellular origin, signaling pathways and stroma contribution. *Pancreatology.* **8,** 462-469 (2008).

108. Mueller,M.M. & Fusenig,N.E. Friends or foes - bipolar effects of the tumour stroma in cancer. *Nat. Rev. Cancer* **4,** 839-849 (2004).

109. Bissell,M.J. & Radisky,D. Putting tumours in context. *Nat. Rev. Cancer* **1**, 46-54 (2001).

110. Ikushima,H. & Miyazono,K. TGFbeta signalling: a complex web in cancer progression. *Nat. Rev. Cancer* **10**, 415-424 (2010).

111. Ronnov-Jessen,L., Petersen,O.W. & Bissell,M.J. Cellular changes involved in conversion of normal to malignant breast: importance of the stromal reaction. *Physiol Rev.* **76**, 69-125 (1996).

112. Tlsty,T.D. & Hein,P.W. Know thy neighbor: stromal cells can contribute oncogenic signals. *Curr. Opin. Genet. Dev.* **11**, 54-59 (2001).

113. Kalluri,R. & Zeisberg,M. Fibroblasts in cancer. *Nat. Rev. Cancer* **6**, 392-401 (2006).

114. Orimo,A. & Weinberg,R.A. Stromal fibroblasts in cancer: a novel tumor-promoting cell type. *Cell Cycle* **5**, 1597-1601 (2006).

115. Sieuwerts,A.M. *et al.* Urokinase-type-plasminogen-activator (uPA) production by human breast (myo) fibroblasts in vitro: influence of transforming growth factor-beta(1) (TGF beta(1)) compared with factor(s) released by human epithelial-carcinoma cells. *Int. J. Cancer* **76**, 829-835 (1998).

116. Sato,T. *et al.* Tumor-stromal cell contact promotes invasion of human uterine cervical carcinoma cells by augmenting the expression and activation of stromal matrix metalloproteinases. *Gynecol. Oncol.* **92**, 47-56 (2004).

117. Bhowmick,N.A., Neilson,E.G. & Moses,H.L. Stromal fibroblasts in cancer initiation and progression. *Nature* **432**, 332-337 (2004).

118. Tlsty,T.D. Stromal cells can contribute oncogenic signals. *Semin. Cancer Biol.* **11**, 97-104 (2001).

119. Bhowmick,N.A. *et al.* TGF-beta signaling in fibroblasts modulates the oncogenic potential of adjacent epithelia. *Science* **303**, 848-851 (2004).

120. Kuperwasser,C. *et al.* Reconstruction of functionally normal and malignant human breast tissues in mice. *Proc. Natl. Acad. Sci. U. S. A* **101**, 4966-4971 (2004).

121. Mueller,M.M. & Fusenig,N.E. Tumor-stroma interactions directing phenotype and progression of epithelial skin tumor cells. *Differentiation* **70**, 486-497 (2002).

122. Patocs,A. *et al.* Breast-cancer stromal cells with TP53 mutations and nodal metastases. *N. Engl. J. Med.* **357**, 2543-2551 (2007).

123. Korc,M. Pancreatic cancer-associated stroma production. *Am. J. Surg.* **194**, S84-S86 (2007).

124. Coussens,L.M. & Werb,Z. Inflammation and cancer. *Nature* **420**, 860-867 (2002).

125. Whitcomb,D.C. & Pogue-Geile,K. Pancreatitis as a risk for pancreatic cancer. *Gastroenterol. Clin. North Am.* **31**, 663-678 (2002).

126. Whitcomb,D.C. Inflammation and Cancer V. Chronic pancreatitis and pancreatic cancer. *Am. J. Physiol Gastrointest. Liver Physiol* **287**, G315-G319 (2004).

127. Omary,M.B., Lugea,A., Lowe,A.W. & Pandol,S.J. The pancreatic stellate cell: a star on the rise in pancreatic diseases. *J. Clin. Invest* **117**, 50-59 (2007).

128. Jaster,R. Molecular regulation of pancreatic stellate cell function. *Mol. Cancer* **3**, 26 (2004).

129. Apte,M.V. *et al.* Desmoplastic reaction in pancreatic cancer: role of pancreatic stellate cells. *Pancreas* **29**, 179-187 (2004).

130. Haber,P.S. *et al.* Activation of pancreatic stellate cells in human and experimental pancreatic fibrosis. *Am. J. Pathol.* **155**, 1087-1095 (1999).

131. Aoki,H. *et al.* Existence of autocrine loop between interleukin-6 and transforming growth factor-beta1 in activated rat pancreatic stellate cells. *J. Cell Biochem.* **99**, 221-228 (2006).

132. Ohuchida,K. *et al.* Radiation to stromal fibroblasts increases invasiveness of pancreatic cancer cells through tumor-stromal interactions. *Cancer Res.* **64**, 3215-3222 (2004).

133. Qian,L.W. *et al.* Co-cultivation of pancreatic cancer cells with orthotopic tumor-derived fibroblasts: fibroblasts stimulate tumor cell invasion via HGF secretion whereas cancer cells exert a minor regulative effect on fibroblasts HGF production. *Cancer Lett.* **190**, 105-112 (2003).

134. Hwang,R.F. *et al.* Cancer-associated stromal fibroblasts promote pancreatic tumor progression. *Cancer Res.* **68**, 918-926 (2008).

135. Vonlaufen,A. *et al.* Pancreatic stellate cells: partners in crime with pancreatic cancer cells. *Cancer Res.* **68**, 2085-2093 (2008).

136. Joyce,J.A. Therapeutic targeting of the tumor microenvironment. *Cancer Cell* **7**, 513-520 (2005).

137. Jain,R.K. Normalization of tumor vasculature: an emerging concept in antiangiogenic therapy. *Science* **307**, 58-62 (2005).

138. Micke,P. & Ostman,A. Tumour-stroma interaction: cancer-associated fibroblasts as novel targets in anti-cancer therapy? *Lung Cancer* **45** Suppl 2, S163-S175 (2004).

139. Sandler,A.B., Johnson,D.H. & Herbst,R.S. Anti-vascular endothelial growth factor monoclonals in non-small cell lung cancer. *Clin. Cancer Res.* **10**, 4258s-4262s (2004).

140. Gonda,T.A., Varro,A., Wang,T.C. & Tycko,B. Molecular biology of cancer-associated fibroblasts: can these cells be targeted in anti-cancer therapy? *Semin. Cell Dev. Biol.* **21**, 2-10 (2010).

141. Arteaga,C.L. Inhibition of TGFbeta signaling in cancer therapy. *Curr. Opin. Genet. Dev.* **16**, 30-37 (2006).

142. Pour,P.M. Modification of tumor development in the pancreas. *Prog. Exp. Tumor Res.* **33**, 108-131 (1991).

143. Longnecker,D.S. Animal model of human disease. Carcinoma of the pancreas in azaserine-treated rats. *Am. J. Pathol.* **105**, 94-96 (1981).

144. Bockman,D.E. Cells of origin of pancreatic cancer: experimental animal tumors related to human pancreas. *Cancer* **47**, 1528-1534 (1981).

145. Rivenson,A., Hoffmann,D., Prokopczyk,B., Amin,S. & Hecht,S.S. Induction of lung and exocrine pancreas tumors in F344 rats by tobacco-specific and Areca-derived N-nitrosamines. *Cancer Res.* **48**, 6912-6917 (1988).

146. Schuller,H.M., Jorquera,R., Reichert,A. & Castonguay,A. Transplacental induction of pancreas tumors in hamsters by ethanol and the tobacco-specific nitrosamine 4-(methylnitrosamino)-1-(3-pyridyl)-1-butanone. *Cancer Res.* **53**, 2498-2501 (1993).

147. Longnecker,D.S., Roebuck,B.D., Kuhlmann,E.T. & Curphey,T.J. Induction of pancreatic carcinomas in rats with N-nitroso(2-hydroxypropyl)(2-oxopropyl)amine: histopathology. *J. Natl. Cancer Inst.* **74**, 209-217 (1985).

148. Reddy,J.K. & Rao,M.S. Pancreatic adenocarcinoma in inbred guinea pigs induced by n-methyl-N-nitrosourea. *Cancer Res.* **35**, 2269-2277 (1975).

149. Furukawa,F. *et al.* Induction of pancreatic tumors in male Syrian golden hamsters by intraperitoneal N-methyl-N-nitrosourea injection. *Pancreas* **7**, 153-158 (1992).

150. Grippo,P.J. & Sandgren,E.P. Modeling pancreatic cancer in animals to address specific hypotheses. *Methods Mol. Med.* **103**, 217-243 (2005).

151. Longnecker D. Clues from experimental models in Pancreatic Cancer: Pathogenesis, Diagnosis and Treatment. Torowa, NJ (1998).

152. Ding,Y., Cravero,J.D., Adrian,K. & Grippo,P. Modeling pancreatic cancer in vivo: from xenograft and carcinogen-induced systems to genetically engineered mice. *Pancreas* **39**, 283-292 (2010).

153. Van Dyke,T. & Jacks,T. Cancer modeling in the modern era: progress and challenges. *Cell* **108**, 135-144 (2002).

154. Balmain,A. Cancer as a complex genetic trait: tumor susceptibility in humans and mouse models. *Cell* **108**, 145-152 (2002).

155. Rangarajan,A. & Weinberg,R.A. Opinion: Comparative biology of mouse versus human cells: modelling human cancer in mice. *Nat. Rev. Cancer* **3**, 952-959 (2003).

156. Fidler,I.J. Rationale and methods for the use of nude mice to study the biology and therapy of human cancer metastasis. *Cancer Metastasis Rev.* **5**, 29-49 (1986).

157. Bosma,M.J. & Carroll,A.M. The SCID mouse mutant: definition, characterization, and potential uses. *Annu. Rev. Immunol.* **9**, 323-350 (1991).

158. Hotz,H.G. *et al.* An orthotopic nude mouse model for evaluating pathophysiology and therapy of pancreatic cancer. *Pancreas* **26**, e89-e98 (2003).

159. Loukopoulos,P. *et al.* Orthotopic transplantation models of pancreatic adenocarcinoma derived from cell lines and primary tumors and displaying varying metastatic activity. *Pancreas* **29**, 193-203 (2004).

160. Suemizu,H. *et al.* Identification of a key molecular regulator of liver metastasis in human pancreatic carcinoma using a novel quantitative model of metastasis in NOD/SCID/gammacnull (NOG) mice. *Int. J. Oncol.* **31**, 741-751 (2007).

161. Tarbe,N. *et al.* Transcriptional profiling of cell lines derived from an orthotopic pancreatic tumor model reveals metastasis-associated genes. *Anticancer Res.* **21**, 3221-3228 (2001).

162. Niedergethmann,M. *et al.* Gene expression profiling of liver metastases and tumour invasion in pancreatic cancer using an orthotopic SCID mouse model. *Br. J. Cancer* **97**, 1432-1440 (2007).

163. Lee,S.O. *et al.* Inactivation of the orphan nuclear receptor TR3/Nur77 inhibits pancreatic cancer cell and tumor growth. *Cancer Res.* **70,** 6824-6836 (2010).

164. Tran Cao,H.S. *et al.* Metronomic gemcitabine in combination with sunitinib inhibits multisite metastasis and increases survival in an orthotopic model of pancreatic cancer. *Mol. Cancer Ther.* **9,** 2068-2078 (2010).

165. Bachem,M.G. *et al.* Pancreatic carcinoma cells induce fibrosis by stimulating proliferation and matrix synthesis of stellate cells. *Gastroenterology* **128,** 907-921 (2005).

166. Neesse,A. *et al.* Pancreatic stellate cells potentiate proinvasive effects of SERPINE2 expression in pancreatic cancer xenograft tumors. *Pancreatology.* **7,** 380-385 (2007).

167. Schneiderhan,W. *et al.* Pancreatic stellate cells are an important source of MMP-2 in human pancreatic cancer and accelerate tumor progression in a murine xenograft model and CAM assay. *J. Cell Sci.* **120,** 512-519 (2007).

168. Tseng,W.W. *et al.* Development of an orthotopic model of invasive pancreatic cancer in an immunocompetent murine host. *Clin. Cancer Res.* **16,** 3684-3695 (2010).

169. Leach,S.D. Mouse models of pancreatic cancer: the fur is finally flying! *Cancer Cell* **5,** 7-11 (2004).

170. Hruban,R.H. *et al.* Pathology of genetically engineered mouse models of pancreatic exocrine cancer: consensus report and recommendations. *Cancer Res.* **66,** 95-106 (2006).

171. Swift,G.H., Hammer,R.E., MacDonald,R.J. & Brinster,R.L. Tissue-specific expression of the rat pancreatic elastase I gene in transgenic mice. *Cell* **38,** 639-646 (1984).

172. Quaife,C.J., Pinkert,C.A., Ornitz,D.M., Palmiter,R.D. & Brinster,R.L. Pancreatic neoplasia induced by ras expression in acinar cells of transgenic mice. *Cell* **48,** 1023-1034 (1987).

173. Ornitz,D.M., Hammer,R.E., Messing,A., Palmiter,R.D. & Brinster,R.L. Pancreatic neoplasia induced by SV40 T-antigen expression in acinar cells of transgenic mice. *Science* **238,** 188-193 (1987).

174. Wagner,M., Luhrs,H., Kloppel,G., Adler,G. & Schmid,R.M. Malignant transformation of duct-like cells originating from acini in transforming growth factor transgenic mice. *Gastroenterology* **115,** 1254-1262 (1998).

175. Greten,F.R. *et al.* TGF alpha transgenic mice. A model of pancreatic cancer development. *Pancreatology.* **1,** 363-368 (2001).

176. Jhappan,C. *et al.* TGF alpha overexpression in transgenic mice induces liver neoplasia and abnormal development of the mammary gland and pancreas. *Cell* **61,** 1137-1146 (1990).

177. Wagner,M. *et al.* A murine tumor progression model for pancreatic cancer recapitulating the genetic alterations of the human disease. *Genes Dev.* **15,** 286-293 (2001).

178. Lewis,B.C., Klimstra,D.S. & Varmus,H.E. The c-myc and PyMT oncogenes induce different tumor types in a somatic mouse model for pancreatic cancer. *Genes Dev.* **17,** 3127-3138 (2003).

179. Tuveson,D.A. *et al.* Mist1-KrasG12D knock-in mice develop mixed differentiation metastatic exocrine pancreatic carcinoma and hepatocellular carcinoma. *Cancer Res.* **66,** 242-247 (2006).

180. Aguirre,A.J. *et al.* Activated Kras and Ink4a/Arf deficiency cooperate to produce metastatic pancreatic ductal adenocarcinoma. *Genes Dev.* **17,** 3112-3126 (2003).

181. Hingorani,S.R. *et al.* Trp53R172H and KrasG12D cooperate to promote chromosomal instability and widely metastatic pancreatic ductal adenocarcinoma in mice. *Cancer Cell* **7,** 469-483 (2005).

182. Bardeesy,N. *et al.* Both p16(Ink4a) and the p19(Arf)-p53 pathway constrain progression of pancreatic adenocarcinoma in the mouse. *Proc. Natl. Acad. Sci. U. S. A* **103,** 5947-5952 (2006).

183. Hill,R. *et al.* PTEN loss accelerates KrasG12D-induced pancreatic cancer development. *Cancer Res.* **70,** 7114-7124 (2010).

184. Izeradjene,K. *et al.* Kras(G12D) and Smad4/Dpc4 haploinsufficiency cooperate to induce mucinous cystic neoplasms and invasive adenocarcinoma of the pancreas. *Cancer Cell* **11,** 229-243 (2007).

185. Bardeesy,N. *et al.* Smad4 is dispensable for normal pancreas development yet critical in progression and tumor biology of pancreas cancer. *Genes Dev.* **20,** 3130-3146 (2006).

186. Kojima,K. *et al.* Inactivation of Smad4 accelerates Kras(G12D)-mediated pancreatic neoplasia. *Cancer Res.* **67,** 8121-8130 (2007).

187. Ijichi,H. *et al.* Aggressive pancreatic ductal adenocarcinoma in mice caused by pancreas-specific blockade of transforming growth factor-beta signaling in cooperation with active Kras expression. *Genes Dev.* **20,** 3147-3160 (2006).

188. De La,O.J. *et al.* Notch and Kras reprogram pancreatic acinar cells to ductal intraepithelial neoplasia. *Proc. Natl. Acad. Sci. U. S. A* **105**, 18907-18912 (2008).

189. Habbe,N. *et al.* Spontaneous induction of murine pancreatic intraepithelial neoplasia (mPanIN) by acinar cell targeting of oncogenic Kras in adult mice. *Proc. Natl. Acad. Sci. U. S. A* **105**, 18913-18918 (2008).

190. Prochownik,E.V. c-Myc: linking transformation and genomic instability. *Curr. Mol. Med.* **8**, 446-458 (2008).

191. Skoudy,A., Hernandez-Munoz,I. & Navarro,P. Pancreatic Ductal Adenocarcinoma and Transcription Factors: Role of c-Myc. *J. Gastrointest. Cancer* **42**, 76-84 (2011).

192. Mahlamaki,E.H. *et al.* Frequent amplification of 8q24, 11q, 17q, and 20q-specific genes in pancreatic cancer. *Genes Chromosomes. Cancer* **35**, 353-358 (2002).

193. Schleger,C., Verbeke,C., Hildenbrand,R., Zentgraf,H. & Bleyl,U. c-MYC activation in primary and metastatic ductal adenocarcinoma of the pancreas: incidence, mechanisms, and clinical significance. *Mod. Pathol.* **15**, 462-469 (2002).

194. Yamada,H. *et al.* Amplifications of both c-Ki-ras with a point mutation and c-myc in a primary pancreatic cancer and its metastatic tumors in lymph nodes. *Jpn. J. Cancer Res.* **77**, 370-375 (1986).

195. Sakorafas,G.H. *et al.* Oncogenes in cancer of the pancreas. *Eur. J. Surg. Oncol.* **21**, 251-253 (1995).

196. Zojer,N. *et al.* Chromosomal imbalances in primary and metastatic pancreatic carcinoma as detected by interphase cytogenetics: basic findings and clinical aspects. *Br. J. Cancer* **77**, 1337-1342 (1998).

197. Li,Y.J., Wei,Z.M., Meng,Y.X. & Ji,X.R. Beta-catenin up-regulates the expression of cyclinD1, c-myc and MMP-7 in human pancreatic cancer: relationships with carcinogenesis and metastasis. *World J. Gastroenterol.* **11**, 2117-2123 (2005).

198. Armengol,G. *et al.* DNA copy number changes and evaluation of MYC, IGF1R, and FES amplification in xenografts of pancreatic adenocarcinoma. *Cancer Genet. Cytogenet.* **116**, 133-141 (2000).

199. Han,H. *et al.* Identification of differentially expressed genes in pancreatic cancer cells using cDNA microarray. *Cancer Res.* **62**, 2890-2896 (2002).

200. Silverman,J.A., Kuhlmann,E.T., Zurlo,J., Yager,J.D. & Longnecker,D.S. Expression of c-myc, c-raf-1, and c-Ki-ras in azaserine-induced pancreatic carcinomas and growing pancreas in rats. *Mol. Carcinog.* **3**, 379-386 (1990).

201. Calvo,E.L., Dusetti,N.J., Cadenas,M.B., Dagorn,J.C. & Iovanna,J.L. Changes in gene expression during pancreatic regeneration: activation of c-myc and H-ras oncogenes in the rat pancreas. *Pancreas* **6**, 150-156 (1991).

202. Liao,D.J. *et al.* Characterization of pancreatic lesions from MT-tgf alpha, Ela-myc and MT-tgf alpha/Ela-myc single and double transgenic mice. *J. Carcinog.* **5**, 19 (2006).

203. Liao,J.D. *et al.* Histological complexities of pancreatic lesions from transgenic mouse models are consistent with biological and morphological heterogeneity of human pancreatic cancer. *Histol. Histopathol.* **22**, 661-676 (2007).

204. Keleg,S., Buchler,P., Ludwig,R., Buchler,M.W. & Friess,H. Invasion and metastasis in pancreatic cancer. *Mol. Cancer* **2**, 14 (2003).

205. Thakur,A., Bollig,A., Wu,J. & Liao,D.J. Gene expression profiles in primary pancreatic tumors and metastatic lesions of Ela-c-myc transgenic mice. *Mol. Cancer* **7**, 11 (2008).

206. Stoletov,K. & Klemke,R. Catch of the day: zebrafish as a human cancer model. *Oncogene* **27**, 4509-4520 (2008).

207. Yee,N.S. & Pack,M. Zebrafish as a model for pancreatic cancer research. *Methods Mol. Med.* **103**, 273-298 (2005).

208. Hajjar,K.A. & Krishnan,S. Annexin II: a mediator of the plasmin/plasminogen activator system. *Trends Cardiovasc. Med.* **9**, 128-138 (1999).

209. Raum,D. *et al.* Synthesis of human plasminogen by the liver. *Science* **208**, 1036-1037 (1980).

210. Hajjar,K.A. & Nachman,R.L. Endothelial cell-mediated conversion of Glu-plasminogen to Lys- plasminogen. Further evidence for assembly of the fibrinolytic system on the endothelial cell surface. *J Clin. Invest* **82**, 1769-1778 (1988).

211. Markus,G., Evers,J.L. & Hobika,G.H. Comparison of some properties of native (Glu) and modified (Lys) human plasminogen. *J. Biol. Chem.* **253**, 733-739 (1978).

212. Hoylaerts,M., Rijken,D.C., Lijnen,H.R. & Collen,D. Kinetics of the activation of plasminogen by human tissue plasminogen activator. Role of fibrin. *J. Biol. Chem.* **257**, 2912-2919 (1982).

213. Robbins,K.C., Summaria,L., Hsieh,B. & Shah,R.J. The peptide chains of human plasmin. Mechanism of activation of human plasminogen to plasmin. *J. Biol. Chem.* **242**, 2333-2342 (1967).

214. Forsgren,M., Raden,B., Israelsson,M., Larsson,K. & Heden,L.O. Molecular cloning and characterization of a full-length cDNA clone for human plasminogen. *FEBS Lett.* **213**, 254-260 (1987).

215. Collen,D. & Lijnen,H.R. Basic and clinical aspects of fibrinolysis and thrombolysis. *Blood* **78**, 3114-3124 (1991).

216. Blasi,F. Proteolysis, cell adhesion, chemotaxis, and invasiveness are regulated by the u-PA-u-PAR-PAI-1 system. *Thromb. Haemost.* **82**, 298-304 (1999).

217. Blasi,F. Urokinase and urokinase receptor: a paracrine/autocrine system regulating cell migration and invasiveness. *Bioessays* **15**, 105-111 (1993).

218. Steffens,G.J., Gunzler,W.A., Otting,F., Frankus,E. & Flohe,L. The complete amino acid sequence of low molecular mass urokinase from human urine. *Hoppe Seylers. Z. Physiol Chem.* **363**, 1043-1058 (1982).

219. Buko,A.M. *et al.* Characterization of a posttranslational fucosylation in the growth factor domain of urinary plasminogen activator. *Proc. Natl. Acad. Sci. U. S. A* **88**, 3992-3996 (1991).

220. Kasai,S., Arimura,H., Nishida,M. & Suyama,T. Proteolytic cleavage of single-chain pro-urokinase induces conformational change which follows activation of the zymogen and reduction of its high affinity for fibrin. *J. Biol. Chem.* **260**, 12377-12381 (1985).

221. Kasai,S., Arimura,H., Nishida,M. & Suyama,T. Primary structure of single-chain pro-urokinase. *J. Biol. Chem.* **260**, 12382-12389 (1985).

222. Bernik,M.B. & Kwaan,H.C. Plasminogen activator activity in cultures from human tissues. An immunological and histochemical study. *J. Clin. Invest* **48**, 1740-1753 (1969).

223. Beqaj,S., Shah,A.M. & Ryan,J.M. Identification of cells responsible for urokinase-type plasminogen activator synthesis and secretion in human diploid kidney cell cultures. *In Vitro Cell Dev. Biol. Anim* **40**, 102-107 (2004).

224. Prager,G.W., Breuss,J.M., Steurer,S., Mihaly,J. & Binder,B.R. Vascular endothelial growth factor (VEGF) induces rapid prourokinase (pro-uPA)

activation on the surface of endothelial cells. *Blood* **103**, 955-962 (2004).

225. Andreasen,P.A., Kjoller,L., Christensen,L. & Duffy,M.J. The urokinase-type plasminogen activator system in cancer metastasis: a review. *Int. J Cancer* **72**, 1-22 (1997).

226. Ellis,V., Behrendt,N. & Dano,K. Plasminogen activation by receptor-bound urokinase. A kinetic study with both cell-associated and isolated receptor. *J. Biol. Chem.* **266**, 12752-12758 (1991).

227. Blasi,F. & Carmeliet,P. uPAR: a versatile signalling orchestrator. *Nat. Rev. Mol. Cell Biol.* **3**, 932-943 (2002).

228. Nykjaer,A. *et al.* Recycling of the urokinase receptor upon internalization of the uPA:serpin complexes. *EMBO J.* **16**, 2610-2620 (1997).

229. Hajjar,K.A. Cellular receptors in the regulation of plasmin generation. *Thromb. Haemost.* **74**, 294-301 (1995).

230. Kruithof,E.K., Tran-Thang,C., Ransijn,A. & Bachmann,F. Demonstration of a fast-acting inhibitor of plasminogen activators in human plasma. *Blood* **64**, 907-913 (1984).

231. Sprengers,E.D. & Kluft,C. Plasminogen activator inhibitors. *Blood* **69**, 381-387 (1987).

232. Kruithof,E.K., Baker,M.S. & Bunn,C.L. Biological and clinical aspects of plasminogen activator inhibitor type 2. *Blood* **86**, 4007-4024 (1995).

233. Espana,F. *et al.* Evidence for the regulation of urokinase and tissue type plasminogen activators by the serpin, protein C inhibitor, in semen and blood plasma. *Thromb. Haemost.* **70**, 989-994 (1993).

234. Osterwalder,T., Contartese,J., Stoeckli,E.T., Kuhn,T.B. & Sonderegger,P. Neuroserpin, an axonally secreted serine protease inhibitor. *EMBO J.* **15**, 2944-2953 (1996).

235. Silverman,G.A. *et al.* The serpins are an expanding superfamily of structurally similar but functionally diverse proteins. Evolution, mechanism of inhibition, novel functions, and a revised nomenclature. *J. Biol. Chem.* **276**, 33293-33296 (2001).

236. Redlitz,A., Tan,A.K., Eaton,D.L. & Plow,E.F. Plasma carboxypeptidases as regulators of the plasminogen system. *J. Clin. Invest* **96**, 2534-2538 (1995).

237. Sasaki,T., Morita,T. & Iwanaga,S. Identification of the plasminogen-binding site of human alpha 2-plasmin inhibitor. *J. Biochem. (Tokyo)* **99**, 1699-1705 (1986).

238. Collen,D. On the regulation and control of fibrinolysis. Edward Kowalski Memorial Lecture. *Thromb. Haemost.* **43**, 77-89 (1980).

239. Aoki,N., Moroi,M. & Tachiya,K. Effects of alpha2-plasmin inhibitor on fibrin clot lysis. Its comparison with alpha2-macroglobulin. *Thromb. Haemost.* **39**, 22-31 (1978).

240. Wang,W., Boffa,M.B., Bajzar,L., Walker,J.B. & Nesheim,M.E. A study of the mechanism of inhibition of fibrinolysis by activated thrombin-activable fibrinolysis inhibitor. *J. Biol. Chem.* **273**, 27176-27181 (1998).

241. Miles,L.A. *et al.* Role of cell-surface lysines in plasminogen binding to cells: identification of alpha-enolase as a candidate plasminogen receptor. *Biochemistry* **30**, 1682-1691 (1991).

242. Redlitz,A., Fowler,B.J., Plow,E.F. & Miles,L.A. The role of an enolase-related molecule in plasminogen binding to cells. *Eur. J. Biochem.* **227**, 407-415 (1995).

243. Cesarman,G.M., Guevara,C.A. & Hajjar,K.A. An endothelial cell receptor for plasminogen/tissue plasminogen activator (t-PA). II. Annexin II-mediated enhancement of t-PA-dependent plasminogen activation. *J Biol. Chem.* **269**, 21198-21203 (1994).

244. Lottenberg,R. *et al.* Cloning, sequence analysis, and expression in Escherichia coli of a streptococcal plasmin receptor. *J. Bacteriol.* **174**, 5204-5210 (1992).

245. Parkkinen,J. & Rauvala,H. Interactions of plasminogen and tissue plasminogen activator (t-PA) with amphoterin. Enhancement of t-PA-catalyzed plasminogen activation by amphoterin. *J. Biol. Chem.* **266**, 16730-16735 (1991).

246. Gonzalez-Gronow,M., Gawdi,G. & Pizzo,S.V. Characterization of the plasminogen receptors of normal and rheumatoid arthritis human synovial fibroblasts. *J. Biol. Chem.* **269**, 4360-4366 (1994).

247. Miles,L.A., Dahlberg,C.M., Levin,E.G. & Plow,E.F. Gangliosides interact directly with plasminogen and urokinase and may mediate binding of these fibrinolytic components to cells. *Biochemistry* **28**, 9337-9343 (1989).

248. Vassalli,J.D., Sappino,A.P. & Belin,D. The plasminogen activator/plasmin system. *J Clin. Invest* **88**, 1067-1072 (1991).

249. HE,C.S. *et al*. Tissue cooperation in a proteolytic cascade activating human interstitial collagenase. *Proc. Natl. Acad. Sci. U. S. A* **86**, 2632-2636 (1989).

250. Rifkin,D.B. *et al*. Growth factor control of extracellular proteolysis. *Cell Differ. Dev.* **32**, 313-318 (1990).

251. Dano,K. *et al*. Plasminogen activators, tissue degradation, and cancer. *Adv. Cancer Res.* **44**, 139-266 (1985).

252. Carmeliet,P. *et al*. Urokinase-generated plasmin activates matrix metalloproteinases during aneurysm formation. *Nat. Genet.* **17**, 439-444 (1997).

253. Mars,W.M., Zarnegar,R. & Michalopoulos,G.K. Activation of hepatocyte growth factor by the plasminogen activators uPA and tPA. *Am. J Pathol.* **143**, 949-958 (1993).

254. Houck,K.A., Leung,D.W., Rowland,A.M., Winer,J. & Ferrara,N. Dual regulation of vascular endothelial growth factor bioavailability by genetic and proteolytic mechanisms. *J Biol. Chem.* **267**, 26031-26037 (1992).

255. Collen,D. The plasminogen (fibrinolytic) system. *Thromb. Haemost.* **82**, 259-270 (1999).

256. Tissue plasminogen activator for acute ischemic stroke. The National Institute of Neurological Disorders and Stroke rt-PA Stroke Study Group. *N. Engl. J. Med.* **333**, 1581-1587 (1995).

257. Ingall,T.J. *et al*. Findings from the reanalysis of the NINDS tissue plasminogen activator for acute ischemic stroke treatment trial. *Stroke* **35**, 2418-2424 (2004).

258. Opdenakker,G. & Van Damme,J. Cytokines and proteases in invasive processes: molecular similarities between inflammation and cancer. *Cytokine* **4**, 251-258 (1992).

259. Medina M.G. *et al*. Tissue plasminogen activator mediates amyloid-induced neurotoxicity via Erk1/2 activation. *EMBO J.* **24**, 1706-1716 (2005).

260. Benchenane,K., Lopez-Atalaya,J.P., Fernandez-Monreal,M., Touzani,O. & Vivien,D. Equivocal roles of tissue-type plasminogen activator in stroke-induced injury. *Trends Neurosci.* **27**, 155-160 (2004).

261. Caplan,L.R. Thrombolysis 2004: the good, the bad, and the ugly. *Rev. Neurol. Dis.* **1**, 16-26 (2004).

262. Yepes,M., Roussel,B.D., Ali,C. & Vivien,D. Tissue-type plasminogen activator in the ischemic brain: more than a thrombolytic. *Trends Neurosci.* **32,** 48-55 (2009).

263. Carmeliet,P. & Collen,D. Development and disease in proteinase-deficient mice: role of the plasminogen, matrix metalloproteinase and coagulation system. *Thromb. Res.* **91,** 255-285 (1998).

264. Chapman,H.A. Plasminogen activators, integrins, and the coordinated regulation of cell adhesion and migration. *Curr. Opin. Cell Biol.* **9,** 714-724 (1997).

265. Blasi,F. uPA, uPAR, PAI-1: key intersection of proteolytic, adhesive and chemotactic highways? *Immunol. Today* **18,** 415-417 (1997).

266. Romer,J. *et al.* Plasminogen and wound healing. *Nat. Med.* **2,** 725 (1996).

267. Friedman,G.C. & Seeds,N.W. Tissue plasminogen activator expression in the embryonic nervous system. *Brain Res. Dev. Brain Res.* **81,** 41-49 (1994).

268. Seeds,N.W., Basham,M.E. & Haffke,S.P. Neuronal migration is retarded in mice lacking the tissue plasminogen activator gene. *Proc. Natl. Acad. Sci. U. S. A* **96,** 14118-14123 (1999).

269. Seeds,N.W. *et al.* Plasminogen activators and plasminogen activator inhibitors in neural development. *Ann. N. Y. Acad. Sci.* **667,** 32-40 (1992).

270. Bugge,T.H., Flick,M.J., Daugherty,C.C. & Degen,J.L. Plasminogen deficiency causes severe thrombosis but is compatible with development and reproduction. *Genes Dev.* **9,** 794-807 (1995).

271. Feinberg,R.F. *et al.* Plasminogen activator inhibitor types 1 and 2 in human trophoblasts. PAI-1 is an immunocytochemical marker of invading trophoblasts. *Lab Invest* **61,** 20-26 (1989).

272. Gyetko,M.R. *et al.* Urokinase is required for the pulmonary inflammatory response to Cryptococcus neoformans. A murine transgenic model. *J. Clin. Invest* **97,** 1818-1826 (1996).

273. Hamsten,A., Eriksson,P., Karpe,F. & Silveira,A. Relationships of thrombosis and fibrinolysis to atherosclerosis. *Curr. Opin. Lipidol.* **5,** 382-389 (1994).

274. Tyagi,S.C. Extracellular matrix dynamics in heart failure: a prospect for gene therapy. *J. Cell Biochem.* **68,** 403-410 (1998).

275. Bacharach,E., Itin,A. & Keshet,E. In vivo patterns of expression of urokinase and its inhibitor PAI-1 suggest a concerted role in regulating physiological angiogenesis. *Proc. Natl. Acad. Sci. U. S. A* **89**, 10686-10690 (1992).

276. McMahon,B. & Kwaan,H.C. The plasminogen activator system and cancer. *Pathophysiol. Haemost. Thromb.* **36**, 184-194 (2008).

277. Kwaan,H.C. & McMahon,B. The role of plasminogen-plasmin system in cancer. *Cancer Treat. Res.* **148**, 43-66 (2009).

278. Tomooka,S., Border,W.A., Marshall,B.C. & Noble,N.A. Glomerular matrix accumulation is linked to inhibition of the plasmin protease system. *Kidney Int.* **42**, 1462-1469 (1992).

279. Carmeliet,P. *et al.* Physiological consequences of loss of plasminogen activator gene function in mice. *Nature* **368**, 419-424 (1994).

280. Carmeliet,P. *et al.* Biological effects of disruption of the tissue-type plasminogen activator, urokinase-type plasminogen activator, and plasminogen activator inhibitor-1 genes in mice. *Ann. N. Y. Acad. Sci.* **748**, 367-381 (1995).

281. Ploplis,V.A. *et al.* Effects of disruption of the plasminogen gene on thrombosis, growth, and health in mice. *Circulation* **92**, 2585-2593 (1995).

282. Pennica,D. *et al.* Cloning and expression of human tissue-type plasminogen activator cDNA in E. coli. *Nature* **301**, 214-221 (1983).

283. van Zonneveld,A.J., Veerman,H. & Pannekoek,H. Autonomous functions of structural domains on human tissue-type plasminogen activator. *Proc. Natl. Acad. Sci. U. S. A* **83**, 4670-4674 (1986).

284. Ny,T., Elgh,F. & Lund,B. The structure of the human tissue-type plasminogen activator gene: correlation of intron and exon structures to functional and structural domains. *Proc. Natl. Acad. Sci. U. S. A* **81**, 5355-5359 (1984).

285. Nordt,T.K. & Bode,C. Thrombolysis: newer thrombolytic agents and their role in clinical medicine. *Heart* **89**, 1358-1362 (2003).

286. Downing,A.K. *et al.* Solution structure of the fibrin binding finger domain of tissue-type plasminogen activator determined by 1H nuclear magnetic resonance. *J. Mol. Biol.* **225**, 821-833 (1992).

287. Smith,B.O., Downing,A.K., Driscoll,P.C., Dudgeon,T.J. & Campbell,I.D. The solution structure and backbone dynamics of the fibronectin type I and epidermal growth factor-like pair of modules of tissue-type plasminogen activator. *Structure.* **3**, 823-833 (1995).

288. Byeon,I.J., Kelley,R.F. & Llinas,M. Kringle-2 domain of the tissue-type plasminogen activator. 1H-NMR assignments and secondary structure. *Eur. J. Biochem.* **197**, 155-165 (1991).

289. Byeon,I.J. & Llinas,M. Solution structure of the tissue-type plasminogen activator kringle 2 domain complexed to 6-aminohexanoic acid an antifibrinolytic drug. *J. Mol. Biol.* **222**, 1035-1051 (1991).

290. de Vos,A.M. *et al.* Crystal structure of the kringle 2 domain of tissue plasminogen activator at 2.4-A resolution. *Biochemistry* **31**, 270-279 (1992).

291. Renatus,M. *et al.* Lysine 156 promotes the anomalous proenzyme activity of tPA: X-ray crystal structure of single-chain human tPA. *EMBO J.* **16**, 4797-4805 (1997).

292. Renatus,M. *et al.* Structural mapping of the active site specificity determinants of human tissue-type plasminogen activator. Implications for the design of low molecular weight substrates and inhibitors. *J. Biol. Chem.* **272**, 21713-21719 (1997).

293. Lamba,D. *et al.* The 2.3 A crystal structure of the catalytic domain of recombinant two- chain human tissue-type plasminogen activator. *J Mol. Biol.* **258**, 117-135 (1996).

294. Pohl,G., Kallstrom,M., Bergsdorf,N., Wallen,P. & Jornvall,H. Tissue plasminogen activator: peptide analyses confirm an indirectly derived amino acid sequence, identify the active site serine residue, establish glycosylation sites, and localize variant differences. *Biochemistry* **23**, 3701-3707 (1984).

295. Parekh,R.B. *et al.* Cell-type-specific and site-specific N-glycosylation of type I and type II human tissue plasminogen activator. *Biochemistry* **28**, 7644-7662 (1989).

296. Spellman,M.W. *et al.* Carbohydrate structures of human tissue plasminogen activator expressed in Chinese hamster ovary cells. *J. Biol. Chem.* **264**, 14100-14111 (1989).

297. Wittwer,A.J. *et al.* Effects of N-glycosylation on in vitro activity of Bowes melanoma and human colon fibroblast derived tissue plasminogen activator. *Biochemistry* **28**, 7662-7669 (1989).

298. Howard,S.C., Wittwer,A.J. & Welply,J.K. Oligosaccharides at each glycosylation site make structure-dependent contributions to biological properties of human tissue plasminogen activator. *Glycobiology* **1**, 411-418 (1991).

299. Berg,D.T., Burck,P.J., Berg,D.H. & Grinnell,B.W. Kringle glycosylation in a modified human tissue plasminogen activator improves functional properties. *Blood* **81**, 1312-1322 (1993).

300. Hansen,L., Blue,Y., Barone,K., Collen,D. & Larsen,G.R. Functional effects of asparagine-linked oligosaccharide on natural and variant human tissue-type plasminogen activator. *J. Biol. Chem.* **263**, 15713-15719 (1988).

301. Harris,R.J., Leonard,C.K., Guzzetta,A.W. & Spellman,M.W. Tissue plasminogen activator has an O-linked fucose attached to threonine-61 in the epidermal growth factor domain. *Biochemistry* **30**, 2311-2314 (1991).

302. Chan,A.L. *et al.* A novel sialylated N-acetylgalactosamine-containing oligosaccharide is the major complex-type structure present in Bowes melanoma tissue plasminogen activator. *Glycobiology* **1**, 173-185 (1991).

303. Wittwer,A.J. & Howard,S.C. Glycosylation at Asn-184 inhibits the conversion of single-chain to two-chain tissue-type plasminogen activator by plasmin. *Biochemistry* **29**, 4175-4180 (1990).

304. Ranby,M. Studies on the kinetics of plasminogen activation by tissue plasminogen activator. *Biochim. Biophys. Acta* **704**, 461-469 (1982).

305. Mori,K., Dwek,R.A., Downing,A.K., Opdenakker,G. & Rudd,P.M. The activation of type 1 and type 2 plasminogen by type I and type II tissue plasminogen activator. *J. Biol. Chem.* **270**, 3261-3267 (1995).

306. Levin,E.G. & del Zoppo,G.J. Localization of tissue plasminogen activator in the endothelium of a limited number of vessels. *Am. J. Pathol.* **144**, 855-861 (1994).

307. Sappino,A.P. *et al.* Extracellular proteolysis in the adult murine brain. *J Clin. Invest* **92**, 679-685 (1993).

308. Davies,B.J., Pickard,B.S., Steel,M., Morris,R.G. & Lathe,R. Serine proteases in rodent hippocampus. *J Biol. Chem.* **273**, 23004-23011 (1998).

309. Teesalu,T., Kulla,A., Asser,T., Koskiniemi,M. & Vaheri,A. Tissue plasminogen activator as a key effector in neurobiology and neuropathology. *Biochem. Soc. Trans.* **30**, 183-189 (2002).

310. Krystosek,A. & Seeds,N.W. Peripheral neurons and Schwann cells secrete plasminogen activator. *J. Cell Biol.* **98**, 773-776 (1984).

311. Rogove,A.D., Siao,C., Keyt,B., Strickland,S. & Tsirka,S.E. Activation of microglia reveals a non-proteolytic cytokine function for tissue

plasminogen activator in the central nervous system. *J Cell Sci.* **112** (Pt 22), 4007-4016 (1999).

312. Schmidt,E. *et al.* Elevated expression and release of tissue-type, but not urokinase-type, plasminogen activator after binding of autoantibodies to bullous pemphigoid antigen 180 in cultured human keratinocytes. *Clin. Exp. Immunol.* **135**, 497-504 (2004).

313. Chen,C.S., Lyons-Giordano,B., Lazarus,G.S. & Jensen,P.J. Differential expression of plasminogen activators and their inhibitors in an organotypic skin coculture system. *J. Cell Sci.* **106** (Pt 1), 45-53 (1993).

314. Hashimoto,K., Horikoshi,T., Nishioka,K., Yoshikawa,K. & Carter,D.M. Plasminogen activator secreted by cultured human melanocytes. *Br. J. Dermatol.* **115**, 205-209 (1986).

315. Rijken,D.C. & Collen,D. Purification and characterization of the plasminogen activator secreted by human melanoma cells in culture. *J. Biol. Chem.* **256**, 7035-7041 (1981).

316. Neuman,T., Stephens,R.W., Salonen,E.M., Timmusk,T. & Vaheri,A. Induction of morphological differentiation of human neuroblastoma cells is accompanied by induction of tissue-type plasminogen activator. *J. Neurosci. Res.* **23**, 274-281 (1989).

317. Amin,W., Karlan,B.Y. & Littlefield,B.A. Glucocorticoid sensitivity of OVCA 433 human ovarian carcinoma cells: inhibition of plasminogen activators, cell growth, and morphological alterations. *Cancer Res.* **47**, 6040-6045 (1987).

318. Ortiz-Zapater,E. *et al.* Tissue plasminogen activator induces pancreatic cancer cell proliferation by a non-catalytic mechanism that requires extracellular signal-regulated kinase 1/2 activation through epidermal growth factor receptor and annexin A2. *Am. J. Pathol.* **170**, 1573-1584 (2007).

319. Otter,M., Kuiper,J., van Berkel,T.J. & Rijken,D.C. Mechanisms of tissue-type plasminogen activator (tPA) clearance by the liver. *Ann. N. Y. Acad. Sci.* **667**, 431-442 (1992).

320. Collen,D. *et al.* Biological properties of human tissue-type plasminogen activator obtained by expression of recombinant DNA in mammalian cells. *J. Pharmacol. Exp. Ther.* **231**, 146-152 (1984).

321. Orth,K., Madison,E.L., Gething,M.J., Sambrook,J.F. & Herz,J. Complexes of tissue-type plasminogen activator and its serpin inhibitor plasminogen-activator inhibitor type 1 are internalized by means of the low density lipoprotein receptor-related protein/alpha 2-

macroglobulin receptor. *Proc. Natl. Acad. Sci. U. S. A* **89**, 7422-7426 (1992).

322. Ahern,T.J. *et al.* Site-directed mutagenesis in human tissue-plasminogen activator. Distinguishing sites in the amino-terminal region required for full fibrinolytic activity and rapid clearance from the circulation. *J. Biol. Chem.* **265**, 5540-5545 (1990).

323. Otter,M., Barrett-Bergshoeff,M.M. & Rijken,D.C. Binding of tissue-type plasminogen activator by the mannose receptor. *J. Biol. Chem.* **266**, 13931-13935 (1991).

324. Hajjar,K.A. & Reynolds,C.M. alpha-Fucose-mediated binding and degradation of tissue-type plasminogen activator by HepG2 cells. *J Clin. Invest* **93**, 703-710 (1994).

325. de Vries,C., Veerman,H., Nesheim,M.E. & Pannekoek,H. Kinetic characterization of tissue-type plasminogen activator (t-PA) and t-PA deletion mutants. *Thromb. Haemost.* **65**, 280-285 (1991).

326. Bennett,W.F. *et al.* High resolution analysis of functional determinants on human tissue-type plasminogen activator. *J. Biol. Chem.* **266**, 5191-5201 (1991).

327. Bakker,A.H., Weening-Verhoeff,E.J. & Verheijen,J.H. The role of the lysyl binding site of tissue-type plasminogen activator in the interaction with a forming fibrin clot. *J. Biol. Chem.* **270**, 12355-12360 (1995).

328. Salonen,E.M. *et al.* Plasminogen and tissue-type plasminogen activator bind to immobilized fibronectin. *J. Biol. Chem.* **260**, 12302-12307 (1985).

329. Moser,T.L., Enghild,J.J., Pizzo,S.V. & Stack,M.S. The extracellular matrix proteins laminin and fibronectin contain binding domains for human plasminogen and tissue plasminogen activator. *J. Biol. Chem.* **268**, 18917-18923 (1993).

330. Stack,M.S. & Pizzo,S.V. Modulation of tissue plasminogen activator-catalyzed plasminogen activation by synthetic peptides derived from the amino-terminal heparin binding domain of fibronectin. *J. Biol. Chem.* **268**, 18924-18928 (1993).

331. Stack,M.S., Gray,R.D. & Pizzo,S.V. Modulation of murine B16F10 melanoma plasminogen activator production by a synthetic peptide derived from the laminin A chain. *Cancer Res.* **53**, 1998-2004 (1993).

332. Reilly,T.M., Whitfield,M.D., Taylor,D.S. & Timmermans,P.B. Binding of tissue plasminogen activator to cultured human fibroblasts. *Thromb. Haemost.* **61**, 454-458 (1989).

333. Hajjar,K.A., Hamel,N.M., Harpel,P.C. & Nachman,R.L. Binding of tissue plasminogen activator to cultured human endothelial cells. *J Clin. Invest* **80**, 1712-1719 (1987).

334. Sanzo,M.A., Howard,S.C., Wittwer,A.J. & Cochrane,H.M. Binding of tissue plasminogen activator to human aortic endothelial cells. *Biochem. J.* **269**, 475-482 (1990).

335. Barnathan,E.S. *et al*. Tissue-type plasminogen activator binding to human endothelial cells. Evidence for two distinct binding sites. *J. Biol. Chem.* **263**, 7792-7799 (1988).

336. Ellis,V. & Whawell,S.A. Vascular smooth muscle cells potentiate plasmin generation by both urokinase and tissue plasminogen activator-dependent mechanisms: evidence for a specific tissue-type plasminogen activator receptor on these cells. *Blood* **90**, 2312-2322 (1997).

337. Bizik,J., Lizonova,A., Stephens,R.W., Grofova,M. & Vaheri,A. Plasminogen activation by t-PA on the surface of human melanoma cells in the presence of alpha 2-macroglobulin secretion. *Cell Regul.* **1**, 895-905 (1990).

338. Sinniger,V., Merton,R.E., Fabregas,P., Felez,J. & Longstaff,C. Regulation of tissue plasminogen activator activity by cells. Domains responsible for binding and mechanism of stimulation. *J. Biol. Chem.* **274**, 12414-12422 (1999).

339. Bizik,J., Trancikova,D., Felnerova,D., Verheijen,J.H. & Vaheri,A. Spatial orientation of tissue-type plasminogen activator bound at the melanoma cell surface. *Biochem. Biophys. Res. Commun.* **239**, 322-328 (1997).

340. Hajjar,K.A., Jacovina,A.T. & Chacko,J. An endothelial cell receptor for plasminogen/tissue plasminogen activator. I. Identity with annexin II. *J Biol. Chem.* **269**, 21191-21197 (1994).

341. Yeatman,T.J., Updyke,T.V., Kaetzel,M.A., Dedman,J.R. & Nicolson,G.L. Expression of annexins on the surfaces of non-metastatic and metastatic human and rodent tumor cells. *Clin. Exp. Metastasis* **11**, 37-44 (1993).

342. Falcone,D.J., Borth,W., Khan,K.M. & Hajjar,K.A. Plasminogen-mediated matrix invasion and degradation by macrophages is dependent on surface expression of annexin II. *Blood* **97**, 777-784 (2001).

343. MacLeod,T.J., Kwon,M., Filipenko,N.R. & Waisman,D.M. Phospholipid-associated annexin A2-S100A10 heterotetramer and its subunits: characterization of the interaction with tissue plasminogen activator, plasminogen, and plasmin. *J Biol. Chem.* **278**, 25577-25584 (2003).

344. Waisman,D.M. Annexin II tetramer: structure and function. *Mol. Cell Biochem.* **149-150**, 301-322 (1995).

345. Brownstein,C., Falcone,D.J., Jacovina,A. & Hajjar,K.A. A mediator of cell surface-specific plasmin generation. *Ann. N. Y. Acad. Sci.* **947**, 143-155 (2001).

346. Ma,A.S., Bell,D.J., Mittal,A.A. & Harrison,H.H. Immunocytochemical detection of extracellular annexin II in cultured human skin keratinocytes and isolation of annexin II isoforms enriched in the extracellular pool. *J Cell Sci.* **107 (Pt 7)**, 1973-1984 (1994).

347. Jacovina,A.T. *et al.* Neuritogenesis and the nerve growth factor-induced differentiation of PC-12 cells requires annexin II-mediated plasmin generation. *J Biol. Chem.* **276**, 49350-49358 (2001).

348. Ling,Q. *et al.* Annexin II regulates fibrin homeostasis and neoangiogenesis in vivo. *J. Clin. Invest* **113**, 38-48 (2004).

349. Hajjar,K.A. *et al.* Tissue plasminogen activator binding to the annexin II tail domain. Direct modulation by homocysteine. *J Biol. Chem.* **273**, 9987-9993 (1998).

350. Johnsson,N., Marriott,G. & Weber,K. p36, the major cytoplasmic substrate of src tyrosine protein kinase, binds to its p11 regulatory subunit via a short amino-terminal amphiphatic helix. *EMBO J* **7**, 2435-2442 (1988).

351. Roda,O. *et al.* New Insights into the tPA-Annexin A2 Interaction. Is Annexin a2 Cys8 the sole requirement for this association? *J Biol. Chem.* **278**, 5702-5709 (2003).

352. Merenmies,J., Pihlaskari,R., Laitinen,J., Wartiovaara,J. & Rauvala,H. 30-kDa heparin-binding protein of brain (amphoterin) involved in neurite outgrowth. Amino acid sequence and localization in the filopodia of the advancing plasma membrane. *J. Biol. Chem.* **266**, 16722-16729 (1991).

353. Hurtado,M. *et al.* Activation of the epidermal growth factor signalling pathway by tissue plasminogen activator in pancreas cancer cells. *Gut* **56**, 1266-1274 (2007).

354. Hembrough,T.A., Li,L. & Gonias,S.L. Cell-surface cytokeratin 8 is the major plasminogen receptor on breast cancer cells and is required for the accelerated activation of cell-associated plasminogen by tissue-type plasminogen activator. *J. Biol. Chem.* **271**, 25684-25691 (1996).

355. Kralovich,K.R. *et al.* Characterization of the binding sites for plasminogen and tissue-type plasminogen activator in cytokeratin 8 and cytokeratin 18. *J. Protein Chem.* **17**, 845-854 (1998).

356. Nakajima,K. *et al.* Plasminogen binds specifically to alpha-enolase on rat neuronal plasma membrane. *J. Neurochem.* **63**, 2048-2057 (1994).

357. Razzaq,T.M. *et al.* Functional regulation of tissue plasminogen activator on the surface of vascular smooth muscle cells by the type-II transmembrane protein p63 (CKAP4). *J. Biol. Chem.* **278**, 42679-42685 (2003).

358. Menell,J.S. *et al.* Annexin II and bleeding in acute promyelocytic leukemia. *N. Engl. J Med.* **340**, 994-1004 (1999).

359. Vishwanatha,J.K., Chiang,Y., Kumble,K.D., Hollingsworth,M.A. & Pour,P.M. Enhanced expression of annexin II in human pancreatic carcinoma cells and primary pancreatic cancers. *Carcinogenesis* **14**, 2575-2579 (1993).

360. Paciucci,R., Tora,M., Diaz,V.M. & Real,F.X. The plasminogen activator system in pancreas cancer: role of t-PA in the invasive potential in vitro. *Oncogene* **16**, 625-633 (1998).

361. Paciucci,R. *et al.* Isolation of tissue-type plasminogen activator, cathepsin H, and non- specific cross-reacting antigen from SK-PC-1 pancreas cancer cells using subtractive hybridization. *FEBS Lett.* **385**, 72-76 (1996).

362. Hembrough,T.A., Kralovich,K.R., Li,L. & Gonias,S.L. Cytokeratin 8 released by breast carcinoma cells in vitro binds plasminogen and tissue-type plasminogen activator and promotes plasminogen activation. *Biochem. J.* **317 (Pt 3)**, 763-769 (1996).

363. Kwaan,H.C. The plasminogen-plasmin system in malignancy. *Cancer Metastasis Rev.* **11**, 291-311 (1992).

364. Noel,A. *et al.* Emerging roles for proteinases in cancer. *Invasion Metastasis* **17**, 221-239 (1997).

365. Fischer,K. *et al.* Urokinase induces proliferation of human ovarian cancer cells: characterization of structural elements required for growth factor function. *FEBS Lett.* **438**, 101-105 (1998).

366. Andreasen,P.A., Egelund,R. & Petersen,H.H. The plasminogen activation system in tumor growth, invasion, and metastasis. *Cell Mol. Life Sci.* **57**, 25-40 (2000).

367. Liotta,L.A., Steeg,P.S. & Stetler-Stevenson,W.G. Cancer metastasis and angiogenesis: an imbalance of positive and negative regulation. *Cell* **64**, 327-336 (1991).

368. Almholt,K. *et al.* Reduced metastasis of transgenic mammary cancer in urokinase-deficient mice. *Int. J. Cancer* **113**, 525-532 (2005).

369. Dano,K. *et al*. Cancer invasion and tissue remodeling--cooperation of protease systems and cell types. *APMIS* **107**, 120-127 (1999).

370. Collen,D. & Lijnen,H.R. Thrombolytic agents. *Thromb. Haemost.* **93**, 627-630 (2005).

371. Melchor,J.P. & Strickland,S. Tissue plasminogen activator in central nervous system physiology and pathology. *Thromb. Haemost.* **93**, 655-660 (2005).

372. Dass,K., Ahmad,A., Azmi,A.S., Sarkar,S.H. & Sarkar,F.H. Evolving role of uPA/uPAR system in human cancers. *Cancer Treat. Rev.* **34**, 122-136 (2008).

373. Hildenbrand,R., Allgayer,H., Marx,A. & Stroebel,P. Modulators of the urokinase-type plasminogen activation system for cancer. *Expert. Opin. Investig. Drugs* **19**, 641-652 (2010).

374. Ulisse,S., Baldini,E., Sorrenti,S. & D'Armiento,M. The urokinase plasminogen activator system: a target for anti-cancer therapy. *Curr. Cancer Drug Targets.* **9**, 32-71 (2009).

375. Ploug,M. *et al*. Peptide-derived antagonists of the urokinase receptor. affinity maturation by combinatorial chemistry, identification of functional epitopes, and inhibitory effect on cancer cell intravasation. *Biochemistry* **40**, 12157-12168 (2001).

376. Hsu,D.W., Efird,J.T. & Hedley-Whyte,E.T. Prognostic role of urokinase-type plasminogen activator in human gliomas. *Am. J Pathol.* **147**, 114-123 (1995).

377. Nielsen,B.S., Sehested,M., Timshel,S., Pyke,C. & Dano,K. Messenger RNA for urokinase plasminogen activator is expressed in myofibroblasts adjacent to cancer cells in human breast cancer. *Lab Invest* **74**, 168-177 (1996).

378. Verspaget,H.W., Sier,C.F., Ganesh,S., Griffioen,G. & Lamers,C.B. Prognostic value of plasminogen activators and their inhibitors in colorectal cancer. *Eur J Cancer* **31A**, 1105-1109 (1995).

379. Gutierrez,L.S. *et al*. Tumor development is retarded in mice lacking the gene for urokinase-type plasminogen activator or its inhibitor, plasminogen activator inhibitor-1. *Cancer Res.* **60**, 5839-5847 (2000).

380. Hildenbrand,R. *et al*. The urokinase-system--role of cell proliferation and apoptosis. *Histol. Histopathol.* **23**, 227-236 (2008).

381. Alfano,D. *et al*. The urokinase plasminogen activator and its receptor: role in cell growth and apoptosis. *Thromb. Haemost.* **93**, 205-211 (2005).

382. Mazar,A.P., Henkin,J. & Goldfarb,R.H. The urokinase plasminogen activator system in cancer: implications for tumor angiogenesis and metastasis. *Angiogenesis.* **3,** 15-32 (1999).

383. Min,H.Y. *et al.* Urokinase receptor antagonists inhibit angiogenesis and primary tumor growth in syngeneic mice. *Cancer Res.* **56,** 2428-2433 (1996).

384. Ossowski,L. & Reich,E. Antibodies to plasminogen activator inhibit human tumor metastasis. *Cell* **35,** 611-619 (1983).

385. Yu,H.R. & Schultz,R.M. Relationship between secreted urokinase plasminogen activator activity and metastatic potential in murine B16 cells transfected with human urokinase sense and antisense genes. *Cancer Res.* **50,** 7623-7633 (1990).

386. Nielsen,B.S. *et al.* Urokinase plasminogen activator is localized in stromal cells in ductal breast cancer. *Lab Invest* **81,** 1485-1501 (2001).

387. Frandsen,T.L. *et al.* Direct evidence of the importance of stromal urokinase plasminogen activator (uPA) in the growth of an experimental human breast cancer using a combined uPA gene-disrupted and immunodeficient xenograft model. *Cancer Res.* **61,** 532-537 (2001).

388. Pyke,C. *et al.* Urokinase-type plasminogen activator is expressed in stromal cells and its receptor in cancer cells at invasive foci in human colon adenocarcinomas. *Am. J. Pathol.* **138,** 1059-1067 (1991).

389. Usher,P.A. *et al.* Expression of urokinase plasminogen activator, its receptor and type-1 inhibitor in malignant and benign prostate tissue. *Int. J. Cancer* **113,** 870-880 (2005).

390. Takeuchi,Y. *et al.* Expression of plasminogen activators and their inhibitors in human pancreatic carcinoma: immunohistochemical study. *Am. J Gastroenterol.* **88,** 1928-1933 (1993).

391. Nielsen,A. *et al.* Significant overexpression of urokinase-type plasminogen activator in pancreatic adenocarcinoma using real-time quantitative reverse transcription polymerase chain reaction. *J. Gastroenterol. Hepatol.* **20,** 256-263 (2005).

392. Harvey,S.R. *et al.* Evaluation of urinary plasminogen activator, its receptor, matrix metalloproteinase-9, and von Willebrand factor in pancreatic cancer. *Clin. Cancer Res.* **9,** 4935-4943 (2003).

393. Cantero,D. *et al.* Enhanced expression of urokinase plasminogen activator and its receptor in pancreatic carcinoma. *Br. J. Cancer* **75,** 388-395 (1997).

394. Wang,W., Abbruzzese,J.L., Evans,D.B. & Chiao,P.J. Overexpression of urokinase-type plasminogen activator in pancreatic adenocarcinoma is regulated by constitutively activated RelA. *Oncogene* **18**, 4554-4563 (1999).

395. Hildenbrand,R. *et al.* Amplification of the urokinase-type plasminogen activator receptor (uPAR) gene in ductal pancreatic carcinomas identifies a clinically high-risk group. *Am. J. Pathol.* **174**, 2246-2253 (2009).

396. Friess,H. *et al.* Enhanced urokinase plasminogen activation in chronic pancreatitis suggests a role in its pathogenesis. *Gastroenterology* **113**, 904-913 (1997).

397. Xue,A., Xue,M., Jackson,C. & Smith,R.C. Suppression of urokinase plasminogen activator receptor inhibits proliferation and migration of pancreatic adenocarcinoma cells via regulation of ERK/p38 signaling. *Int. J. Biochem. Cell Biol.* **41**, 1731-1738 (2009).

398. Sawai,H. *et al.* Interleukin-1alpha enhances the aggressive behavior of pancreatic cancer cells by regulating the alpha6beta1-integrin and urokinase plasminogen activator receptor expression. *BMC. Cell Biol.* **7**, 8 (2006).

399. Tan,X., Egami,H., Nozawa,F., Abe,M. & Baba,H. Analysis of the invasion-metastasis mechanism in pancreatic cancer: involvement of plasmin(ogen) cascade proteins in the invasion of pancreatic cancer cells. *Int. J. Oncol.* **28**, 369-374 (2006).

400. Bauer,T.W. *et al.* Targeting of urokinase plasminogen activator receptor in human pancreatic carcinoma cells inhibits c-Met- and insulin-like growth factor-I receptor-mediated migration and invasion and orthotopic tumor growth in mice. *Cancer Res.* **65**, 7775-7781 (2005).

401. Buchler,P. *et al.* Transcriptional regulation of urokinase-type plasminogen activator receptor by hypoxia-inducible factor 1 is crucial for invasion of pancreatic and liver cancer. *Neoplasia.* **11**, 196-206 (2009).

402. He,Y. *et al.* Interaction between cancer cells and stromal fibroblasts is required for activation of the uPAR-uPA-MMP-2 cascade in pancreatic cancer metastasis. *Clin. Cancer Res.* **13**, 3115-3124 (2007).

403. Mimura,K., Sueishi,K., Yasunaga,C. & Tanaka,K. Fibrinolysis activity promotes tumor invasiveness of B16 melanoma cell lines through a reconstituted gel matrix. *Invasion Metastasis* **12**, 24-34 (1992).

404. Sugiura,Y. *et al.* The plasminogen-plasminogen activator (PA) system in neuroblastoma: role of PA inhibitor-1 in metastasis. *Cancer Res.* **59**, 1327-1336 (1999).

405. Tiberio,A. *et al.* Retinoic acid-enhanced invasion through reconstituted basement membrane by human SK-N-SH neuroblastoma cells involves membrane-associated tissue-type plasminogen activator. *Int. J Cancer* **73**, 740-748 (1997).

406. Wilson,E.L., Jacobs,P. & Dowdle,E.B. The secretion of plasminogen activators by human myeloid leukemic cells in vitro. *Blood* **61**, 568-574 (1983).

407. De,P.G. *et al.* Expression of urokinase-type plasminogen activator (u-PA), u-PA receptor, and tissue-type PA messenger RNAs in human hepatocellular carcinoma. *Cancer Res.* **58**, 2234-2239 (1998).

408. Moser,T.L. *et al.* Secretion of extracellular matrix-degrading proteinases is increased in epithelial ovarian carcinoma. *Int. J. Cancer* **56**, 552-559 (1994).

409. Saito,K. *et al.* The concentration of tissue plasminogen activator and urokinase in plasma and tissues of patients with ovarian and uterine tumors. *Thromb. Res.* **58**, 355-366 (1990).

410. Ryu,B. *et al.* Relationships and differentially expressed genes among pancreatic cancers examined by large-scale serial analysis of gene expression. *Cancer Res.* **62**, 819-826 (2002).

411. Duffy,M.J. *et al.* Tissue-type plasminogen activator, a new prognostic marker in breast cancer. *Cancer Res.* **48**, 1348-1349 (1988).

412. Grondahl-Hansen,J., Bach,F. & Munkholm-Larsen,P. Tissue-type plasminogen activator in plasma from breast cancer patients determined by enzyme-linked immunosorbent assay. *Br. J. Cancer* **61**, 412-414 (1990).

413. Nordengren,J., Casslen,B., Gustavsson,B., Einarsdottir,M. & Willen,R. Discordant expression of mRNA and protein for urokinase and tissue plasminogen activators (u-PA, t-PA) in endometrial carcinoma. *Int. J. Cancer* **79**, 195-201 (1998).

414. Ortiz-Zapater,E. *et al.* Key contribution of CPEB4-mediated translational control to pancreatic cancer progression. 2011. In revision in *Nature Medicine*.

415. Diaz,V.M., Hurtado,M., Thomson,T.M., Reventos,J. & Paciucci,R. Specific interaction of tissue-type plasminogen activator (t-PA) with annexin II on the membrane of pancreatic cancer cells activates plasminogen and promotes invasion in vitro. *Gut* **53**, 993-1000 (2004).

416. Diaz,V.M., Planaguma,J., Thomson,T.M., Reventos,J. & Paciucci,R. Tissue plasminogen activator is required for the growth, invasion, and

angiogenesis of pancreatic tumor cells. *Gastroenterology* **122**, 806-819 (2002).

417. Hu,K. *et al.* Tissue-type plasminogen activator acts as a cytokine that triggers intracellular signal transduction and induces matrix metalloproteinase-9 gene expression. *J. Biol. Chem.* **281**, 2120-2127 (2006).

418. Aguilar S *et al.* Tissue plasminogen activator in murine exocrine pancreas cancer: selective expression in ductal tumors and contribution to cancer progression. *Am. J Pathol.* **165**, 1129-1139 (2004).

419. Ahmed,M., Forsberg,J. & Bergsten,P. Protein profiling of human pancreatic islets by two-dimensional gel electrophoresis and mass spectrometry. *J. Proteome. Res.* **4**, 931-940 (2005).

420. Roda,O. *et al.* A proteomic approach to the identification of new tPA receptors in pancreatic cancer cells. *Proteomics.* **6**, S36-S41 (2006).

421. Roda,O. *et al.* Galectin-1 is a novel functional receptor for tissue plasminogen activator in pancreatic cancer. *Gastroenterology* **136**, 1379-5 (2009).

422. Houzelstein,D. *et al.* Phylogenetic analysis of the vertebrate galectin family. *Mol. Biol. Evol.* **21**, 1177-1187 (2004).

423. Cooper,D.N. Galectinomics: finding themes in complexity. *Biochim. Biophys. Acta* **1572**, 209-231 (2002).

424. Barondes,S.H. *et al.* Galectins: a family of animal beta-galactoside-binding lectins. *Cell* **76**, 597-598 (1994).

425. Hirabayashi,J. *et al.* Oligosaccharide specificity of galectins: a search by frontal affinity chromatography. *Biochim. Biophys. Acta* **1572**, 232-254 (2002).

426. Rini,J.M. & Lobsanov,Y.D. New animal lectin structures. *Curr. Opin. Struct. Biol.* **9**, 578-584 (1999).

427. Leffler,H., Carlsson,S., Hedlund,M., Qian,Y. & Poirier,F. Introduction to galectins. *Glycoconj. J.* **19**, 433-440 (2004).

428. Yang,R.Y., Rabinovich,G.A. & Liu,F.T. Galectins: structure, function and therapeutic potential. *Expert. Rev. Mol. Med.* **10**, e17 (2008).

429. Hirabayashi,J. & Kasai,K. The family of metazoan metal-independent beta-galactoside-binding lectins: structure, function and molecular evolution. *Glycobiology* **3**, 297-304 (1993).

430. Vasta,G.R. Roles of galectins in infection. *Nat. Rev. Microbiol.* **7**, 424-438 (2009).

431. Danguy,A., Camby,I. & Kiss,R. Galectins and cancer. *Biochim. Biophys. Acta* **1572**, 285-293 (2002).

432. van den,B.F., Califice,S. & Castronovo,V. Expression of galectins in cancer: a critical review. *Glycoconj. J.* **19**, 537-542 (2004).

433. Lahm,H. *et al*. Tumor galectinology: insights into the complex network of a family of endogenous lectins. *Glycoconj. J.* **20**, 227-238 (2004).

434. Hughes,R.C. Secretion of the galectin family of mammalian carbohydrate-binding proteins. *Biochim. Biophys. Acta* **1473**, 172-185 (1999).

435. Nickel,W. The mystery of nonclassical protein secretion. A current view on cargo proteins and potential export routes. *Eur. J. Biochem.* **270**, 2109-2119 (2003).

436. Seelenmeyer,C., Stegmayer,C. & Nickel,W. Unconventional secretion of fibroblast growth factor 2 and galectin-1 does not require shedding of plasma membrane-derived vesicles. *FEBS Lett.* **582**, 1362-1368 (2008).

437. Hughes,R.C. Galectins as modulators of cell adhesion. *Biochimie* **83**, 667-676 (2001).

438. Rabinovich,G.A., Toscano,M.A., Ilarregui,J.M. & Rubinstein,N. Shedding light on the immunomodulatory properties of galectins: novel regulators of innate and adaptive immune responses. *Glycoconj. J.* **19**, 565-573 (2004).

439. Almkvist,J. & Karlsson,A. Galectins as inflammatory mediators. *Glycoconj. J.* **19**, 575-581 (2004).

440. Vasta,G.R., Ahmed,H., Du,S. & Henrikson,D. Galectins in teleost fish: Zebrafish (Danio rerio) as a model species to address their biological roles in development and innate immunity. *Glycoconj. J.* **21**, 503-521 (2004).

441. Colnot,C., Fowlis,D., Ripoche,M.A., Bouchaert,I. & Poirier,F. Embryonic implantation in galectin 1/galectin 3 double mutant mice. *Dev. Dyn.* **211**, 306-313 (1998).

442. Ahmed,H., Du,S.J., O'Leary,N. & Vasta,G.R. Biochemical and molecular characterization of galectins from zebrafish (Danio rerio): notochord-specific expression of a prototype galectin during early embryogenesis. *Glycobiology* **14**, 219-232 (2004).

443. Liao,D.I., Kapadia,G., Ahmed,H., Vasta,G.R. & Herzberg,O. Structure of S-lectin, a developmentally regulated vertebrate beta-galactoside-binding protein. *Proc. Natl. Acad. Sci. U. S. A* **91**, 1428-1432 (1994).

444. Ahmed,H., Du,S.J. & Vasta,G.R. Knockdown of a galectin-1-like protein in zebrafish (Danio rerio) causes defects in skeletal muscle development. *Glycoconj. J.* **26**, 277-283 (2009).

445. Thijssen,V.L. *et al.* Galectin-1 is essential in tumor angiogenesis and is a target for antiangiogenesis therapy. *Proc. Natl. Acad. Sci. U. S. A* **103**, 15975-15980 (2006).

446. Gitt,M.A. & Barondes,S.H. Evidence that a human soluble beta-galactoside-binding lectin is encoded by a family of genes. *Proc. Natl. Acad. Sci. U. S. A* **83**, 7603-7607 (1986).

447. Abbott,W.M. & Feizi,T. Evidence that the 14 kDa soluble beta-galactoside-binding lectin in man is encoded by a single gene. *Biochem. J.* **259**, 291-294 (1989).

448. Couraud,P.O. *et al.* Molecular cloning, characterization, and expression of a human 14-kDa lectin. *J. Biol. Chem.* **264**, 1310-1316 (1989).

449. Mehrabian,M. *et al.* Two members of the S-lac lectin gene family, LGALS1 and LGALS2, reside in close proximity on human chromosome 22q12-q13. *Genomics* **15**, 418-420 (1993).

450. Salvatore,P., Contursi,C., Benvenuto,G., Bruni,C.B. & Chiariotti,L. Characterization and functional dissection of the galectin-1 gene promoter. *FEBS Lett.* **373**, 159-163 (1995).

451. De Gregorio,E., Chiariotti,L. & Di Nocera,P.P. The overlap of Inr and TATA elements sets the use of alternative transcriptional start sites in the mouse galectin-1 gene promoter. *Gene* **268**, 215-223 (2001).

452. Camby,I., Le Mercier,M., Lefranc,F. & Kiss,R. Galectin-1: a small protein with major functions. *Glycobiology* **16**, 137R-157R (2006).

453. Gillenwater,A. *et al.* Modulation of galectin-1 content in human head and neck squamous carcinoma cells by sodium butyrate. *Int. J. Cancer* **75**, 217-224 (1998).

454. Chiariotti,L., Salvatore,P., Frunzio,R. & Bruni,C.B. Galectin genes: regulation of expression. *Glycoconj. J.* **19**, 441-449 (2004).

455. Kondoh,N. *et al.* Activation of Galectin-1 gene in human hepatocellular carcinoma involves methylation-sensitive complex formations at the transcriptional upstream and downstream elements. *Int. J. Oncol.* **23**, 1575-1583 (2003).

456. Benvenuto,G. *et al*. Cell-specific transcriptional regulation and reactivation of galectin-1 gene expression are controlled by DNA methylation of the promoter region. *Mol. Cell Biol.* **16**, 2736-2743 (1996).

457. Bourne,Y. *et al*. Crosslinking of mammalian lectin (galectin-1) by complex biantennary saccharides. *Nat. Struct. Biol.* **1**, 863-870 (1994).

458. Morris,S. *et al*. Quaternary solution structures of galectins-1, -3, and -7. *Glycobiology* **14**, 293-300 (2004).

459. Lopez-Lucendo,M.F. *et al*. Growth-regulatory human galectin-1: crystallographic characterisation of the structural changes induced by single-site mutations and their impact on the thermodynamics of ligand binding. *J. Mol. Biol.* **343**, 957-970 (2004).

460. Toscano,M.A. *et al*. Differential glycosylation of TH1, TH2 and TH-17 effector cells selectively regulates susceptibility to cell death. *Nat. Immunol.* **8**, 825-834 (2007).

461. Ahmad,N., Gabius,H.J., Sabesan,S., Oscarson,S. & Brewer,C.F. Thermodynamic binding studies of bivalent oligosaccharides to galectin-1, galectin-3, and the carbohydrate recognition domain of galectin-3. *Glycobiology* **14**, 817-825 (2004).

462. Wang,J.L., Gray,R.M., Haudek,K.C. & Patterson,R.J. Nucleocytoplasmic lectins. *Biochim. Biophys. Acta* **1673**, 75-93 (2004).

463. Elola,M.T., Chiesa,M.E., Alberti,A.F., Mordoh,J. & Fink,N.E. Galectin-1 receptors in different cell types. *J. Biomed. Sci.* **12**, 13-29 (2005).

464. Scott,K. & Zhang,J. Partial identification by site-directed mutagenesis of a cell growth inhibitory site on the human galectin-1 molecule. *BMC. Cell Biol.* **3**, 3 (2002).

465. Schwarz,F.P., Ahmed,H., Bianchet,M.A., Amzel,L.M. & Vasta,G.R. Thermodynamics of bovine spleen galectin-1 binding to disaccharides: correlation with structure and its effect on oligomerization at the denaturation temperature. *Biochemistry* **37**, 5867-5877 (1998).

466. Leppanen,A., Stowell,S., Blixt,O. & Cummings,R.D. Dimeric galectin-1 binds with high affinity to alpha2,3-sialylated and non-sialylated terminal N-acetyllactosamine units on surface-bound extended glycans. *J. Biol. Chem.* **280**, 5549-5562 (2005).

467. He,J. & Baum,L.G. Presentation of galectin-1 by extracellular matrix triggers T cell death. *J. Biol. Chem.* **279**, 4705-4712 (2004).

468. Symons,A., Cooper,D.N. & Barclay,A.N. Characterization of the interaction between galectin-1 and lymphocyte glycoproteins CD45 and Thy-1. *Glycobiology* **10,** 559-563 (2000).

469. Dam,T.K. & Brewer,C.F. Effects of clustered epitopes in multivalent ligand-receptor interactions. *Biochemistry* **47,** 8470-8476 (2008).

470. Sacchettini,J.C., Baum,L.G. & Brewer,C.F. Multivalent protein-carbohydrate interactions. A new paradigm for supermolecular assembly and signal transduction. *Biochemistry* **40,** 3009-3015 (2001).

471. Garner,O.B. & Baum,L.G. Galectin-glycan lattices regulate cell-surface glycoprotein organization and signalling. *Biochem. Soc. Trans.* **36,** 1472-1477 (2008).

472. Lee,R.T. & Lee,Y.C. Affinity enhancement by multivalent lectin-carbohydrate interaction. *Glycoconj. J.* **17,** 543-551 (2000).

473. Lundquist,J.J. & Toone,E.J. The cluster glycoside effect. *Chem. Rev.* **102,** 555-578 (2002).

474. Rabinovich,G.A., Toscano,M.A., Jackson,S.S. & Vasta,G.R. Functions of cell surface galectin-glycoprotein lattices. *Curr. Opin. Struct. Biol.* **17,** 513-520 (2007).

475. Cho,M. & Cummings,R.D. Galectin-1, a beta-galactoside-binding lectin in Chinese hamster ovary cells. I. Physical and chemical characterization. *J. Biol. Chem.* **270,** 5198-5206 (1995).

476. Outenreath,R.L. & Jones,A.L. Influence of an endogenous lectin substrate on cultured dorsal root ganglion cells. *J. Neurocytol.* **21,** 788-795 (1992).

477. Zhou,Q. & Cummings,R.D. L-14 lectin recognition of laminin and its promotion of in vitro cell adhesion. *Arch. Biochem. Biophys.* **300,** 6-17 (1993).

478. Andre,S. *et al.* Galectins-1 and -3 and their ligands in tumor biology. Non-uniform properties in cell-surface presentation and modulation of adhesion to matrix glycoproteins for various tumor cell lines, in biodistribution of free and liposome-bound galectins and in their expression by breast and colorectal carcinomas with/without metastatic propensity. *J. Cancer Res. Clin. Oncol.* **125,** 461-474 (1999).

479. Moiseeva,E.P., Javed,Q., Spring,E.L. & de Bono,D.P. Galectin 1 is involved in vascular smooth muscle cell proliferation. *Cardiovasc. Res.* **45,** 493-502 (2000).

480. Moiseeva,E.P., Williams,B. & Samani,N.J. Galectin 1 inhibits incorporation of vitronectin and chondroitin sulfate B into the

extracellular matrix of human vascular smooth muscle cells. *Biochim. Biophys. Acta* **1619**, 125-132 (2003).

481. Gu,M., Wang,W., Song,W.K., Cooper,D.N. & Kaufman,S.J. Selective modulation of the interaction of alpha 7 beta 1 integrin with fibronectin and laminin by L-14 lectin during skeletal muscle differentiation. *J. Cell Sci.* **107 (Pt 1)**, 175-181 (1994).

482. Hsieh,S.H. *et al.* Galectin-1, a novel ligand of neuropilin-1, activates VEGFR-2 signaling and modulates the migration of vascular endothelial cells. *Oncogene* **27**, 3746-3753 (2008).

483. Pace,K.E., Hahn,H.P., Pang,M., Nguyen,J.T. & Baum,L.G. CD7 delivers a pro-apoptotic signal during galectin-1-induced T cell death. *J. Immunol.* **165**, 2331-2334 (2000).

484. Perillo,N.L., Pace,K.E., Seilhamer,J.J. & Baum,L.G. Apoptosis of T cells mediated by galectin-1. *Nature* **378**, 736-739 (1995).

485. Walzel,H., Schulz,U., Neels,P. & Brock,J. Galectin-1, a natural ligand for the receptor-type protein tyrosine phosphatase CD45. *Immunol. Lett.* **67**, 193-202 (1999).

486. Fajka-Boja,R. *et al.* Receptor tyrosine phosphatase, CD45 binds galectin-1 but does not mediate its apoptotic signal in T cell lines. *Immunol. Lett.* **82**, 149-154 (2002).

487. Pace,K.E., Lee,C., Stewart,P.L. & Baum,L.G. Restricted receptor segregation into membrane microdomains occurs on human T cells during apoptosis induced by galectin-1. *J. Immunol.* **163**, 3801-3811 (1999).

488. Fischer,C. *et al.* Galectin-1 interacts with the {alpha}5{beta}1 fibronectin receptor to restrict carcinoma cell growth via induction of p21 and p27. *J. Biol. Chem.* **280**, 37266-37277 (2005).

489. Kopitz,J., von,R.C., Burchert,M., Cantz,M. & Gabius,H.J. Galectin-1 is a major receptor for ganglioside GM1, a product of the growth-controlling activity of a cell surface ganglioside sialidase, on human neuroblastoma cells in culture. *J. Biol. Chem.* **273**, 11205-11211 (1998).

490. Kopitz,J. *et al.* Negative regulation of neuroblastoma cell growth by carbohydrate-dependent surface binding of galectin-1 and functional divergence from galectin-3. *J. Biol. Chem.* **276**, 35917-35923 (2001).

491. Tinari,N. *et al.* Glycoprotein 90K/MAC-2BP interacts with galectin-1 and mediates galectin-1-induced cell aggregation. *Int. J. Cancer* **91**, 167-172 (2001).

492. Chadli,A., LeCaer,J.P., Bladier,D., Joubert-Caron,R. & Caron,M. Purification and characterization of a human brain galectin-1 ligand. *J. Neurochem.* **68**, 1640-1647 (1997).

493. Seelenmeyer,C., Wegehingel,S., Lechner,J. & Nickel,W. The cancer antigen CA125 represents a novel counter receptor for galectin-1. *J. Cell Sci.* **116**, 1305-1318 (2003).

494. Ohannesian,D.W., Lotan,D. & Lotan,R. Concomitant increases in galectin-1 and its glycoconjugate ligands (carcinoembryonic antigen, lamp-1, and lamp-2) in cultured human colon carcinoma cells by sodium butyrate. *Cancer Res.* **54**, 5992-6000 (1994).

495. Mahanthappa,N.K., Cooper,D.N., Barondes,S.H. & Schwarting,G.A. Rat olfactory neurons can utilize the endogenous lectin, L-14, in a novel adhesion mechanism. *Development* **120**, 1373-1384 (1994).

496. Park,J.W., Voss,P.G., Grabski,S., Wang,J.L. & Patterson,R.J. Association of galectin-1 and galectin-3 with Gemin4 in complexes containing the SMN protein. *Nucleic Acids Res.* **29**, 3595-3602 (2001).

497. Vyakarnam,A., Dagher,S.F., Wang,J.L. & Patterson,R.J. Evidence for a role for galectin-1 in pre-mRNA splicing. *Mol. Cell Biol.* **17**, 4730-4737 (1997).

498. Gauthier,L., Rossi,B., Roux,F., Termine,E. & Schiff,C. Galectin-1 is a stromal cell ligand of the pre-B cell receptor (BCR) implicated in synapse formation between pre-B and stromal cells and in pre-BCR triggering. *Proc. Natl. Acad. Sci. U. S. A* **99**, 13014-13019 (2002).

499. Paz,A., Haklai,R., Elad-Sfadia,G., Ballan,E. & Kloog,Y. Galectin-1 binds oncogenic H-Ras to mediate Ras membrane anchorage and cell transformation. *Oncogene* **20**, 7486-7493 (2001).

500. Laderach,D.J. *et al.* Dissecting the signal transduction pathways triggered by galectin-glycan interactions in physiological and pathological settings. *IUBMB. Life* **62**, 1-13 (2010).

501. Poirier,F. & Robertson,E.J. Normal development of mice carrying a null mutation in the gene encoding the L14 S-type lectin. *Development* **119**, 1229-1236 (1993).

502. Poirier,F., Timmons,P.M., Chan,C.T., Guenet,J.L. & Rigby,P.W. Expression of the L14 lectin during mouse embryogenesis suggests multiple roles during pre- and post-implantation development. *Development* **115**, 143-155 (1992).

503. Lindenberg,S., Kimber,S.J. & Kallin,E. Carbohydrate binding properties of mouse embryos. *J. Reprod. Fertil.* **89**, 431-439 (1990).

504. Cooper,D.N. & Barondes,S.H. Evidence for export of a muscle lectin from cytosol to extracellular matrix and for a novel secretory mechanism. *J. Cell Biol.* **110**, 1681-1691 (1990).

505. Chan,J. *et al.* Galectin-1 induces skeletal muscle differentiation in human fetal mesenchymal stem cells and increases muscle regeneration. *Stem Cells* **24**, 1879-1891 (2006).

506. Puche,A.C., Poirier,F., Hair,M., Bartlett,P.F. & Key,B. Role of galectin-1 in the developing mouse olfactory system. *Dev. Biol.* **179**, 274-287 (1996).

507. Regan,L.J., Dodd,J., Barondes,S.H. & Jessell,T.M. Selective expression of endogenous lactose-binding lectins and lactoseries glycoconjugates in subsets of rat sensory neurons. *Proc. Natl. Acad. Sci. U. S. A* **83**, 2248-2252 (1986).

508. Blois,S.M. *et al.* A pivotal role for galectin-1 in fetomaternal tolerance. *Nat. Med.* **13**, 1450-1457 (2007).

509. Espeli,M., Mancini,S.J., Breton,C., Poirier,F. & Schiff,C. Impaired B-cell development at the pre-BII-cell stage in galectin-1-deficient mice due to inefficient pre-BII/stromal cell interactions. *Blood* **113**, 5878-5886 (2009).

510. Barrionuevo,P. *et al.* A novel function for galectin-1 at the crossroad of innate and adaptive immunity: galectin-1 regulates monocyte/macrophage physiology through a nonapoptotic ERK-dependent pathway. *J. Immunol.* **178**, 436-445 (2007).

511. Norling,L.V., Sampaio,A.L., Cooper,D. & Perretti,M. Inhibitory control of endothelial galectin-1 on in vitro and in vivo lymphocyte trafficking. *FASEB J.* **22**, 682-690 (2008).

512. Liu,S.D. *et al.* Endogenous galectin-1 enforces class I-restricted TCR functional fate decisions in thymocytes. *Blood* **112**, 120-130 (2008).

513. Liu,S.D. *et al.* Galectin-1 tunes TCR binding and signal transduction to regulate CD8 burst size. *J. Immunol.* **182**, 5283-5295 (2009).

514. Drickamer,K. Two distinct classes of carbohydrate-recognition domains in animal lectins. *J. Biol. Chem.* **263**, 9557-9560 (1988).

515. Leffler,H. & Barondes,S.H. Specificity of binding of three soluble rat lung lectins to substituted and unsubstituted mammalian beta-galactosides. *J. Biol. Chem.* **261**, 10119-10126 (1986).

516. Liu,F.T. & Rabinovich,G.A. Galectins as modulators of tumour progression. *Nat. Rev. Cancer* **5**, 29-41 (2005).

517. Rabinovich,G.A. *et al*. Galectins and their ligands: amplifiers, silencers or tuners of the inflammatory response? *Trends Immunol*. **23**, 313-320 (2002).

518. Francois,C. *et al*. Galectin-1 and galectin-3 binding pattern expression in renal cell carcinomas. *Am. J. Clin. Pathol*. **112**, 194-203 (1999).

519. John,C.M., Leffler,H., Kahl-Knutsson,B., Svensson,I. & Jarvis,G.A. Truncated galectin-3 inhibits tumor growth and metastasis in orthotopic nude mouse model of human breast cancer. *Clin. Cancer Res*. **9**, 2374-2383 (2003).

520. Zou,J., Glinsky,V.V., Landon,L.A., Matthews,L. & Deutscher,S.L. Peptides specific to the galectin-3 carbohydrate recognition domain inhibit metastasis-associated cancer cell adhesion. *Carcinogenesis* **26**, 309-318 (2005).

521. Sorme,P. *et al*. Design and synthesis of galectin inhibitors. *Methods Enzymol*. **363**, 157-169 (2003).

522. Scott,K. & Weinberg,C. Galectin-1: a bifunctional regulator of cellular proliferation. *Glycoconj. J*. **19**, 467-477 (2004).

523. Camby,I. *et al*. Galectin-1 knocking down in human U87 glioblastoma cells alters their gene expression pattern. *Biochem. Biophys. Res. Commun*. **335**, 27-35 (2005).

524. Yamaoka,K. *et al*. Expression of galectin-1 mRNA correlates with the malignant potential of human gliomas and expression of antisense galectin-1 inhibits the growth of 9 glioma cells. *J. Neurosci. Res*. **59**, 722-730 (2000).

525. Belanis,L., Plowman,S.J., Rotblat,B., Hancock,J.F. & Kloog,Y. Galectin-1 is a novel structural component and a major regulator of h-ras nanoclusters. *Mol. Biol. Cell* **19**, 1404-1414 (2008).

526. Prior,I.A., Muncke,C., Parton,R.G. & Hancock,J.F. Direct visualization of Ras proteins in spatially distinct cell surface microdomains. *J. Cell Biol*. **160**, 165-170 (2003).

527. Elad-Sfadia,G., Haklai,R., Ballan,E., Gabius,H.J. & Kloog,Y. Galectin-1 augments Ras activation and diverts Ras signals to Raf-1 at the expense of phosphoinositide 3-kinase. *J. Biol. Chem*. **277**, 37169-37175 (2002).

528. Rotblat,B. *et al*. H-Ras nanocluster stability regulates the magnitude of MAPK signal output. *PLoS. One*. **5**, e11991 (2010).

529. Rotblat,B. *et al.* Galectin-1(L11A) predicted from a computed galectin-1 farnesyl-binding pocket selectively inhibits Ras-GTP. *Cancer Res.* **64,** 3112-3118 (2004).

530. Kristensen,D.B. *et al.* Proteome analysis of rat hepatic stellate cells. *Hepatology* **32,** 268-277 (2000).

531. Wu,M.H. *et al.* Targeting Galectin-1 in Carcinoma-Associated Fibroblasts Inhibits Oral Squamous Cell Carcinoma Metastasis by Downregulating MCP-1/CCL2 Expression. *Clin. Cancer Res.* **17,** 1306-1316 (2011).

532. Masamune,A. *et al.* Galectin-1 induces chemokine production and proliferation in pancreatic stellate cells. *Am. J. Physiol Gastrointest. Liver Physiol* **290,** G729-G736 (2006).

533. Fitzner,B. *et al.* Galectin-1 is an inductor of pancreatic stellate cell activation. *Cell Signal.* **17,** 1240-1247 (2005).

534. Sanford,G.L. & Harris-Hooker,S. Stimulation of vascular cell proliferation by beta-galactoside specific lectins. *FASEB J.* **4,** 2912-2918 (1990).

535. Maeda,N. *et al.* Stimulation of proliferation of rat hepatic stellate cells by galectin-1 and galectin-3 through different intracellular signaling pathways. *J. Biol. Chem.* **278,** 18938-18944 (2003).

536. Andersen,H., Jensen,O.N., Moiseeva,E.P. & Eriksen,E.F. A proteome study of secreted prostatic factors affecting osteoblastic activity: galectin-1 is involved in differentiation of human bone marrow stromal cells. *J. Bone Miner. Res.* **18,** 195-203 (2003).

537. Satelli,A. & Rao,U.S. Galectin-1 is silenced by promoter hypermethylation and its re-expression induces apoptosis in human colorectal cancer cells. *Cancer Lett.* **301,** 38-46 (2011).

538. Adams,L., Scott,G.K. & Weinberg,C.S. Biphasic modulation of cell growth by recombinant human galectin-1. *Biochim. Biophys. Acta* **1312,** 137-144 (1996).

539. Vas,V. *et al.* Biphasic effect of recombinant galectin-1 on the growth and death of early hematopoietic cells. *Stem Cells* **23,** 279-287 (2005).

540. Thijssen,V.L. *et al.* Tumor cells secrete galectin-1 to enhance endothelial cell activity. *Cancer Res.* **70,** 6216-6224 (2010).

541. Camby,I. *et al.* Galectin-1 modulates human glioblastoma cell migration into the brain through modifications to the actin cytoskeleton

and levels of expression of small GTPases. *J. Neuropathol. Exp. Neurol.* **61**, 585-596 (2002).

542. Wu,M.H. *et al.* Galectin-1-mediated tumor invasion and metastasis, up-regulated matrix metalloproteinase expression, and reorganized actin cytoskeletons. *Mol. Cancer Res.* **7**, 311-318 (2009).

543. Moiseeva,E.P., Spring,E.L., Baron,J.H. & de Bono,D.P. Galectin 1 modulates attachment, spreading and migration of cultured vascular smooth muscle cells via interactions with cellular receptors and components of extracellular matrix. *J. Vasc. Res.* **36**, 47-58 (1999).

544. van den,B.F. *et al.* Galectin-1 accumulation in the ovary carcinoma peritumoral stroma is induced by ovary carcinoma cells and affects both cancer cell proliferation and adhesion to laminin-1 and fibronectin. *Lab Invest* **83**, 377-386 (2003).

545. Glinsky,V.V., Huflejt,M.E., Glinsky,G.V., Deutscher,S.L. & Quinn,T.P. Effects of Thomsen-Friedenreich antigen-specific peptide P-30 on beta-galactoside-mediated homotypic aggregation and adhesion to the endothelium of MDA-MB-435 human breast carcinoma cells. *Cancer Res.* **60**, 2584-2588 (2000).

546. Clausse,N., van den,B.F., Waltregny,D., Garnier,F. & Castronovo,V. Galectin-1 expression in prostate tumor-associated capillary endothelial cells is increased by prostate carcinoma cells and modulates heterotypic cell-cell adhesion. *Angiogenesis.* **3**, 317-325 (1999).

547. Rabinovich,G.A. Galectin-1 as a potential cancer target. *Br. J. Cancer* **92**, 1188-1192 (2005).

548. Thijssen,V.L., Hulsmans,S. & Griffioen,A.W. The galectin profile of the endothelium: altered expression and localization in activated and tumor endothelial cells. *Am. J. Pathol.* **172**, 545-553 (2008).

549. Le Mercier,M. *et al.* Galectin 1 proangiogenic and promigratory effects in the Hs683 oligodendroglioma model are partly mediated through the control of BEX2 expression. *Neoplasia.* **11**, 485-496 (2009).

550. Le Mercier,M. *et al.* Knocking down galectin 1 in human hs683 glioblastoma cells impairs both angiogenesis and endoplasmic reticulum stress responses. *J. Neuropathol. Exp. Neurol.* **67**, 456-469 (2008).

551. Zou,W. Immunosuppressive networks in the tumour environment and their therapeutic relevance. *Nat. Rev. Cancer* **5**, 263-274 (2005).

552. Chung,C.D., Patel,V.P., Moran,M., Lewis,L.A. & Miceli,M.C. Galectin-1 induces partial TCR zeta-chain phosphorylation and antagonizes processive TCR signal transduction. *J. Immunol.* **165**, 3722-3729 (2000).

553. Blaser,C. *et al.* Beta-galactoside-binding protein secreted by activated T cells inhibits antigen-induced proliferation of T cells. *Eur. J. Immunol.* **28**, 2311-2319 (1998).

554. Rubinstein,N. *et al.* Targeted inhibition of galectin-1 gene expression in tumor cells results in heightened T cell-mediated rejection; A potential mechanism of tumor-immune privilege. *Cancer Cell* **5**, 241-251 (2004).

555. Rabinovich,G.A. *et al.* Recombinant galectin-1 and its genetic delivery suppress collagen-induced arthritis via T cell apoptosis. *J. Exp. Med.* **190**, 385-398 (1999).

556. Rabinovich,G.A. *et al.* Specific inhibition of T-cell adhesion to extracellular matrix and proinflammatory cytokine secretion by human recombinant galectin-1. *Immunology* **97**, 100-106 (1999).

557. Galvan,M., Tsuboi,S., Fukuda,M. & Baum,L.G. Expression of a specific glycosyltransferase enzyme regulates T cell death mediated by galectin-1. *J. Biol. Chem.* **275**, 16730-16737 (2000).

558. Salatino,M. *et al.* Galectin-1 as a potential therapeutic target in autoimmune disorders and cancer. *Expert. Opin. Biol. Ther.* **8**, 45-57 (2008).

559. Lefranc,F., Brotchi,J. & Kiss,R. Possible future issues in the treatment of glioblastomas: special emphasis on cell migration and the resistance of migrating glioblastoma cells to apoptosis. *J. Clin. Oncol.* **23**, 2411-2422 (2005).

560. Ingrassia,L. *et al.* Anti-galectin compounds as potential anti-cancer drugs. *Curr. Med. Chem.* **13**, 3513-3527 (2006).

561. Nangia-Makker,P., Conklin,J., Hogan,V. & Raz,A. Carbohydrate-binding proteins in cancer, and their ligands as therapeutic agents. *Trends Mol. Med.* **8**, 187-192 (2002).

562. Andre,S. *et al.* Wedgelike glycodendrimers as inhibitors of binding of mammalian galectins to glycoproteins, lactose maxiclusters, and cell surface glycoconjugates. *Chembiochem.* **2**, 822-830 (2001).

563. Lahm,H. *et al.* Comprehensive galectin fingerprinting in a panel of 61 human tumor cell lines by RT-PCR and its implications for diagnostic and therapeutic procedures. *J. Cancer Res. Clin. Oncol.* **127**, 375-386 (2001).

564. Saussez,S. *et al*. The determination of the levels of circulating galectin-1 and -3 in HNSCC patients could be used to monitor tumor progression and/or responses to therapy. *Oral Oncol.* **44**, 86-93 (2008).

565. Allen,H.J., Sharma,A., Ahmed,H., Piver,M.S. & Gamarra,M. Galaptin and galaptin-binding glycoconjugates in serum and effusions of carcinoma patients. *Tumour. Biol.* **14**, 360-368 (1993).

566. Demydenko,D. & Berest,I. Expression of galectin-1 in malignant tumors. *Exp. Oncol.* **31**, 74-79 (2009).

567. Wollina,U. *et al*. Galectin fingerprinting by immuno- and lectin histochemistry in cutaneous lymphoma. *J. Cancer Res. Clin. Oncol.* **128**, 103-110 (2002).

568. Rorive,S. *et al*. Galectin-1 is highly expressed in human gliomas with relevance for modulation of invasion of tumor astrocytes into the brain parenchyma. *Glia* **33**, 241-255 (2001).

569. Camby,I. *et al*. Galectins are differentially expressed in supratentorial pilocytic astrocytomas, astrocytomas, anaplastic astrocytomas and glioblastomas, and significantly modulate tumor astrocyte migration. *Brain Pathol.* **11**, 12-26 (2001).

570. Shimonishi,T. *et al*. Expression of endogenous galectin-1 and galectin-3 in intrahepatic cholangiocarcinoma. *Hum. Pathol.* **32**, 302-310 (2001).

571. Chiang,W.F. *et al*. Overexpression of galectin-1 at the tumor invasion front is associated with poor prognosis in early-stage oral squamous cell carcinoma. *Oral Oncol.* **44**, 325-334 (2008).

572. Hittelet,A. *et al*. Upregulation of galectins-1 and -3 in human colon cancer and their role in regulating cell migration. *Int. J. Cancer* **103**, 370-379 (2003).

573. Nagy,N. *et al*. Refined prognostic evaluation in colon carcinoma using immunohistochemical galectin fingerprinting. *Cancer* **97**, 1849-1858 (2003).

574. Xu,X.C., el Naggar,A.K. & Lotan,R. Differential expression of galectin-1 and galectin-3 in thyroid tumors. Potential diagnostic implications. *Am. J. Pathol.* **147**, 815-822 (1995).

575. van den Brule,F.A. *et al*. Expression of the 67-kD laminin receptor, galectin-1, and galectin-3 in advanced human uterine adenocarcinoma. *Hum. Pathol.* **27**, 1185-1191 (1996).

576. Gillenwater,A., Xu,X.C., el-Naggar,A.K., Clayman,G.L. & Lotan,R. Expression of galectins in head and neck squamous cell carcinoma. *Head Neck* **18**, 422-432 (1996).

577. Szoke,T. *et al.* Prognostic significance of endogenous adhesion/growth-regulatory lectins in lung cancer. *Oncology* **69**, 167-174 (2005).

578. Cindolo,L. *et al.* galectin-1 and galectin-3 expression in human bladder transitional-cell carcinomas. *Int. J. Cancer* **84**, 39-43 (1999).

579. Jung,E.J. *et al.* Galectin-1 expression in cancer-associated stromal cells correlates tumor invasiveness and tumor progression in breast cancer. *Int. J. Cancer* **120**, 2331-2338 (2007).

580. van den Brule,F.A., Waltregny,D. & Castronovo,V. Increased expression of galectin-1 in carcinoma-associated stroma predicts poor outcome in prostate carcinoma patients. *J. Pathol.* **193**, 80-87 (2001).

581. Allen,H.J. *et al.* Role of galaptin in ovarian carcinoma adhesion to extracellular matrix in vitro. *J. Cell Biochem.* **43**, 43-57 (1990).

582. Berberat,P.O. *et al.* Comparative analysis of galectins in primary tumors and tumor metastasis in human pancreatic cancer. *J. Histochem. Cytochem.* **49**, 539-549 (2001).

583. Zhong,L.P. *et al.* Overexpression of Galectin-1 is negatively correlated with pathologic differentiation grade in oral squamous cell carcinoma. *J. Cancer Res. Clin. Oncol.* **136**, 1527-1535 (2010).

584. Spano,D. *et al.* Galectin-1 and its involvement in hepatocellular carcinoma aggressiveness. *Mol. Med.* **16**, 102-115 (2010).

585. Sanjuan,X. *et al.* Differential expression of galectin 3 and galectin 1 in colorectal cancer progression. *Gastroenterology* **113**, 1906-1915 (1997).

586. Zhao,X.Y. *et al.* Hypoxia inducible factor-1 mediates expression of galectin-1: the potential role in migration/invasion of colorectal cancer cells. *Carcinogenesis* **31**, 1367-1375 (2010).

587. Cimmino,F. *et al.* Galectin-1 is a major effector of TrkB-mediated neuroblastoma aggressiveness. *Oncogene* **28**, 2015-2023 (2009).

588. Schaffert,C., Pour,P.M. & Chaney,W.G. Localization of galectin-3 in normal and diseased pancreatic tissue. *Int. J. Pancreatol.* **23**, 1-9 (1998).

589. Grutzmann,R. *et al.* Gene expression profiling of microdissected pancreatic ductal carcinomas using high-density DNA microarrays. *Neoplasia.* **6**, 611-622 (2004).

590. Chung,J.C., Oh,M.J., Choi,S.H. & Bae,C.D. Proteomic analysis to identify biomarker proteins in pancreatic ductal adenocarcinoma. *ANZ. J. Surg.* **78**, 245-251 (2008).

591. Terris,B. *et al*. Characterization of gene expression profiles in intraductal papillary-mucinous tumors of the pancreas. *Am. J. Pathol.* **160**, 1745-1754 (2002).

592. Senapati,S. *et al*. Novel interaction of MUC4 and galectin: potential pathobiological implications for metastasis in lethal pancreatic cancer. *Clin. Cancer Res.* (2010).

593. Shimamura,T. *et al*. Clinicopathological significance of galectin-3 expression in ductal adenocarcinoma of the pancreas. *Clin. Cancer Res.* **8**, 2570-2575 (2002).

594. Jiang,H.B., Xu,M. & Wang,X.P. Pancreatic stellate cells promote proliferation and invasiveness of human pancreatic cancer cells via galectin-3. *World J. Gastroenterol.* **14**, 2023-2028 (2008).

595. Sanchez-Ruderisch,H. *et al*. Tumor suppressor p16 INK4a: Downregulation of galectin-3, an endogenous competitor of the pro-anoikis effector galectin-1, in a pancreatic carcinoma model. *FEBS J.* **277**, 3552-3563 (2010).

596. Pan,S. *et al*. Quantitative proteomics investigation of pancreatic intraepithelial neoplasia. *Electrophoresis* **30**, 1132-1144 (2009).

597. Iacobuzio-Donahue,C.A. *et al*. Highly expressed genes in pancreatic ductal adenocarcinomas: a comprehensive characterization and comparison of the transcription profiles obtained from three major technologies. *Cancer Res.* **63**, 8614-8622 (2003).

598. Shen,J., Person,M.D., Zhu,J., Abbruzzese,J.L. & Li,D. Protein expression profiles in pancreatic adenocarcinoma compared with normal pancreatic tissue and tissue affected by pancreatitis as detected by two-dimensional gel electrophoresis and mass spectrometry. *Cancer Res.* **64**, 9018-9026 (2004).

599. Wang,L. *et al*. Galectin-1 and galectin-3 in chronic pancreatitis. *Lab Invest* **80**, 1233-1241 (2000).

600. Andre,S. *et al*. Tumor suppressor p16INK4a--modulator of glycomic profile and galectin-1 expression to increase susceptibility to carbohydrate-dependent induction of anoikis in pancreatic carcinoma cells. *FEBS J.* **274**, 3233-3256 (2007).

601. Kuramitsu,Y. *et al*. Identification of up- and down-regulated proteins in gemcitabine-resistant pancreatic cancer cells using two-dimensional gel

electrophoresis and mass spectrometry. *Anticancer Res.* **30**, 3367-3372 (2010).

602. Choufani,G. *et al.* The levels of expression of galectin-1, galectin-3, and the Thomsen-Friedenreich antigen and their binding sites decrease as clinical aggressiveness increases in head and neck cancers. *Cancer* **86**, 2353-2363 (1999).

603. Apweiler,R., Hermjakob,H. & Sharon,N. On the frequency of protein glycosylation, as deduced from analysis of the SWISS-PROT database. *Biochim. Biophys. Acta* **1473**, 4-8 (1999).

604. Spiro,R.G. Protein glycosylation: nature, distribution, enzymatic formation, and disease implications of glycopeptide bonds. *Glycobiology* **12**, 43R-56R (2002).

605. Hakomori,S. Glycosylation defining cancer malignancy: new wine in an old bottle. *Proc. Natl. Acad. Sci. U. S. A* **99**, 10231-10233 (2002).

606. Spillmann,D. & Burger,M.M. Carbohydrate-carbohydrate interactions in adhesion. *J. Cell Biochem.* **61**, 562-568 (1996).

607. Gahmberg,C.G. & Tolvanen,M. Why mammalian cell surface proteins are glycoproteins. *Trends Biochem. Sci.* **21**, 308-311 (1996).

608. Varki,A. Biological roles of oligosaccharides: all of the theories are correct. *Glycobiology* **3**, 97-130 (1993).

609. Freeze,H.H. & Aebi,M. Altered glycan structures: the molecular basis of congenital disorders of glycosylation. *Curr. Opin. Struct. Biol.* **15**, 490-498 (2005).

610. Kornfeld,R. & Kornfeld,S. Assembly of asparagine-linked oligosaccharides. *Annu. Rev. Biochem.* **54**, 631-664 (1985).

611. Lowe,J.B. & Marth,J.D. A genetic approach to Mammalian glycan function. *Annu. Rev. Biochem.* **72**, 643-691 (2003).

612. Schachter,H. The joys of HexNAc. The synthesis and function of N- and O-glycan branches. *Glycoconj. J.* **17**, 465-483 (2000).

613. Varki,A. *et al.* Essentials of Glycobiology. (2009).

614. Jones,J., Krag,S.S. & Betenbaugh,M.J. Controlling N-linked glycan site occupancy. *Biochim. Biophys. Acta* **1726**, 121-137 (2005).

615. Sasai,K., Ikeda,Y., Fujii,T., Tsuda,T. & Taniguchi,N. UDP-GlcNAc concentration is an important factor in the biosynthesis of beta1,6-branched oligosaccharides: regulation based on the kinetic properties

of N-acetylglucosaminyltransferase V. *Glycobiology* **12,** 119-127 (2002).

616. Lau,K.S. *et al*. Complex N-glycan number and degree of branching cooperate to regulate cell proliferation and differentiation. *Cell* **129,** 123-134 (2007).

617. Feizi,T. Demonstration by monoclonal antibodies that carbohydrate structures of glycoproteins and glycolipids are onco-developmental antigens. *Nature* **314,** 53-57 (1985).

618. Lau,K.S. & Dennis,J.W. N-Glycans in cancer progression. *Glycobiology* **18,** 750-760 (2008).

619. Dennis,J.W., Granovsky,M. & Warren,C.E. Glycoprotein glycosylation and cancer progression. *Biochim. Biophys. Acta* **1473,** 21-34 (1999).

620. Ludwig,J.A. & Weinstein,J.N. Biomarkers in cancer staging, prognosis and treatment selection. *Nat. Rev. Cancer* **5,** 845-856 (2005).

621. Fuster,M.M. & Esko,J.D. The sweet and sour of cancer: glycans as novel therapeutic targets. *Nat. Rev. Cancer* **5,** 526-542 (2005).

622. Dube,D.H. & Bertozzi,C.R. Glycans in cancer and inflammation--potential for therapeutics and diagnostics. *Nat. Rev. Drug Discov.* **4,** 477-488 (2005).

623. Dall'Olio,F. The sialyl-alpha2,6-lactosaminyl-structure: biosynthesis and functional role. *Glycoconj. J.* **17,** 669-676 (2000).

624. Seales,E.C. *et al*. Hypersialylation of beta1 integrins, observed in colon adenocarcinoma, may contribute to cancer progression by up-regulating cell motility. *Cancer Res.* **65,** 4645-4652 (2005).

625. Picco,G. *et al*. Over-expression of ST3Gal-I promotes mammary tumorigenesis. *Glycobiology* **20,** 1241-1250 (2010).

626. Ogata,S.I., Muramatsu,T. & Kobata,A. New structural characteristic of the large glycopeptides from transformed cells. *Nature* **259,** 580-582 (1976).

627. Partridge,E.A. *et al*. Regulation of cytokine receptors by Golgi N-glycan processing and endocytosis. *Science* **306,** 120-124 (2004).

628. Fernandes,B., Sagman,U., Auger,M., Demetrio,M. & Dennis,J.W. Beta 1-6 branched oligosaccharides as a marker of tumor progression in human breast and colon neoplasia. *Cancer Res.* **51,** 718-723 (1991).

629. Kannagi,R. Molecular mechanism for cancer-associated induction of sialyl Lewis X and sialyl Lewis A expression-The Warburg effect revisited. *Glycoconj. J.* **20,** 353-364 (2004).

630. Shimodaira,K. *et al.* Carcinoma-associated expression of core 2 beta-1,6-N-acetylglucosaminyltransferase gene in human colorectal cancer: role of O-glycans in tumor progression. *Cancer Res.* **57,** 5201-5206 (1997).

631. Herscovics,A. Importance of glycosidases in mammalian glycoprotein biosynthesis. *Biochim. Biophys. Acta* **1473,** 96-107 (1999).

632. Ohtsubo,K. & Marth,J.D. Glycosylation in cellular mechanisms of health and disease. *Cell* **126,** 855-867 (2006).

633. Beum,P.V., Bastola,D.R. & Cheng,P.W. Mucin biosynthesis: epidermal growth factor downregulates core 2 enzymes in a human airway adenocarcinoma cell line. *Am. J. Respir. Cell Mol. Biol.* **29,** 48-56 (2003).

634. Higai,K., Miyazaki,N., Azuma,Y. & Matsumoto,K. Interleukin-1beta induces sialyl Lewis X on hepatocellular carcinoma HuH-7 cells via enhanced expression of ST3Gal IV and FUT VI gene. *FEBS Lett.* **580,** 6069-6075 (2006).

635. Campbell,B.J., Yu,L.G. & Rhodes,J.M. Altered glycosylation in inflammatory bowel disease: a possible role in cancer development. *Glycoconj. J.* **18,** 851-858 (2001).

636. Peracaula,R., Barrabes,S., Sarrats,A., Rudd,P.M. & de Llorens,R. Altered glycosylation in tumours focused to cancer diagnosis. *Dis. Markers* **25,** 207-218 (2008).

637. Girnita,L. *et al.* Inhibition of N-linked glycosylation down-regulates insulin-like growth factor-1 receptor at the cell surface and kills Ewing's sarcoma cells: therapeutic implications. *Anticancer Drug Des* **15,** 67-72 (2000).

638. Komatsu,M., Jepson,S., Arango,M.E., Carothers Carraway,C.A. & Carraway,K.L. Muc4/sialomucin complex, an intramembrane modulator of ErbB2/HER2/Neu, potentiates primary tumor growth and suppresses apoptosis in a xenotransplanted tumor. *Oncogene* **20,** 461-470 (2001).

639. Yoshimura,M., Ihara,Y., Matsuzawa,Y. & Taniguchi,N. Aberrant glycosylation of E-cadherin enhances cell-cell binding to suppress metastasis. *J. Biol. Chem.* **271,** 13811-13815 (1996).

640. Seidenfaden,R., Krauter,A., Schertzinger,F., Gerardy-Schahn,R. & Hildebrandt,H. Polysialic acid directs tumor cell growth by controlling

heterophilic neural cell adhesion molecule interactions. *Mol. Cell Biol.* **23**, 5908-5918 (2003).

641. Lin,S., Kemmner,W., Grigull,S. & Schlag,P.M. Cell surface alpha 2,6 sialylation affects adhesion of breast carcinoma cells. *Exp. Cell Res.* **276**, 101-110 (2002).

642. Guo,H.B., Lee,I., Kamar,M., Akiyama,S.K. & Pierce,M. Aberrant N-glycosylation of beta1 integrin causes reduced alpha5beta1 integrin clustering and stimulates cell migration. *Cancer Res.* **62**, 6837-6845 (2002).

643. Kannagi,R., Izawa,M., Koike,T., Miyazaki,K. & Kimura,N. Carbohydrate-mediated cell adhesion in cancer metastasis and angiogenesis. *Cancer Sci.* **95**, 377-384 (2004).

644. Kim,Y.J., Borsig,L., Varki,N.M. & Varki,A. P-selectin deficiency attenuates tumor growth and metastasis. *Proc. Natl. Acad. Sci. U. S. A* **95**, 9325-9330 (1998).

645. Borsig,L., Wong,R., Hynes,R.O., Varki,N.M. & Varki,A. Synergistic effects of L- and P-selectin in facilitating tumor metastasis can involve non-mucin ligands and implicate leukocytes as enhancers of metastasis. *Proc. Natl. Acad. Sci. U. S. A* **99**, 2193-2198 (2002).

646. Zhao,Y.Y. *et al.* Functional roles of N-glycans in cell signaling and cell adhesion in cancer. *Cancer Sci.* **99**, 1304-1310 (2008).

647. Glithero,A. *et al.* Crystal structures of two H-2Db/glycopeptide complexes suggest a molecular basis for CTL cross-reactivity. *Immunity.* **10**, 63-74 (1999).

648. Demetriou,M., Nabi,I.R., Coppolino,M., Dedhar,S. & Dennis,J.W. Reduced contact-inhibition and substratum adhesion in epithelial cells expressing GlcNAc-transferase V. *J. Cell Biol.* **130**, 383-392 (1995).

649. Granovsky,M. *et al.* Suppression of tumor growth and metastasis in Mgat5-deficient mice. *Nat. Med.* **6**, 306-312 (2000).

650. Dennis,J.W., Pawling,J., Cheung,P., Partridge,E. & Demetriou,M. UDP-N-acetylglucosamine:alpha-6-D-mannoside beta1,6 N-acetylglucosaminyltransferase V (Mgat5) deficient mice. *Biochim. Biophys. Acta* **1573**, 414-422 (2002).

651. Buckhaults,P., Chen,L., Fregien,N. & Pierce,M. Transcriptional regulation of N-acetylglucosaminyltransferase V by the src oncogene. *J. Biol. Chem.* **272**, 19575-19581 (1997).

652. Chen,L., Zhang,W., Fregien,N. & Pierce,M. The her-2/neu oncogene stimulates the transcription of N-acetylglucosaminyltransferase V and

expression of its cell surface oligosaccharide products. *Oncogene* **17**, 2087-2093 (1998).

653. Guo,H.B., Zhang,Q.S. & Chen,H.L. Effects of H-ras and v-sis overexpression on N-acetylglucosaminyltransferase V and metastasis-related phenotypes in human hepatocarcinoma cells. *J. Cancer Res. Clin. Oncol.* **126**, 263-270 (2000).

654. Zhao,J., Qiu,W., Simeone,D.M. & Lubman,D.M. N-linked glycosylation profiling of pancreatic cancer serum using capillary liquid phase separation coupled with mass spectrometric analysis. *J. Proteome. Res.* **6**, 1126-1138 (2007).

655. Okuyama,N. *et al.* Fucosylated haptoglobin is a novel marker for pancreatic cancer: a detailed analysis of the oligosaccharide structure and a possible mechanism for fucosylation. *Int. J. Cancer* **118**, 2803-2808 (2006).

656. Lacunza,I., Kremmer,T., Diez-Masa,J.C., Sanz,J. & de Frutos,M. Comparison of alpha-1-acid glycoprotein isoforms from healthy and cancer patients by capillary IEF. *Electrophoresis* **28**, 4447-4451 (2007).

657. Li,C. *et al.* Pancreatic cancer serum detection using a lectin/glyco-antibody array method. *J. Proteome. Res.* **8**, 483-492 (2009).

658. Wu,Y.M., Nowack,D.D., Omenn,G.S. & Haab,B.B. Mucin glycosylation is altered by pro-inflammatory signaling in pancreatic-cancer cells. *J. Proteome. Res.* **8**, 1876-1886 (2009).

659. Rustgi,A.K. Pancreatic cancer: novel approaches to diagnosis and therapy. *Gastroenterology* **129**, 1344-1347 (2005).

660. Maupin,K.A. *et al.* Glycogene expression alterations associated with pancreatic cancer epithelial-mesenchymal transition in complementary model systems. *PLoS. One.* **5**, e13002 (2010).

661. Wigmore,S.J. *et al.* Cytokine regulation of constitutive production of interleukin-8 and -6 by human pancreatic cancer cell lines and serum cytokine concentrations in patients with pancreatic cancer. *Int. J. Oncol.* **21**, 881-886 (2002).

662. Fearon,K.C. *et al.* Pancreatic cancer as a model: inflammatory mediators, acute-phase response, and cancer cachexia. *World J. Surg.* **23**, 584-588 (1999).

663. Goonetilleke,K.S. & Siriwardena,A.K. Systematic review of carbohydrate antigen (CA 19-9) as a biochemical marker in the diagnosis of pancreatic cancer. *Eur. J. Surg. Oncol.* **33**, 266-270 (2007).

664. Ferrone,C.R. *et al.* Perioperative CA19-9 levels can predict stage and survival in patients with resectable pancreatic adenocarcinoma. *J. Clin. Oncol.* **24,** 2897-2902 (2006).

665. Boeck,S., Stieber,P., Holdenrieder,S., Wilkowski,R. & Heinemann,V. Prognostic and therapeutic significance of carbohydrate antigen 19-9 as tumor marker in patients with pancreatic cancer. *Oncology* **70,** 255-264 (2006).

666. Dalgleish,A.G. Tumour markers in malignancies. CA19.9 is useful in several cancers. *BMJ* **321,** 380 (2000).

667. Magnani,J.L., Steplewski,Z., Koprowski,H. & Ginsburg,V. Identification of the gastrointestinal and pancreatic cancer-associated antigen detected by monoclonal antibody 19-9 in the sera of patients as a mucin. *Cancer Res.* **43,** 5489-5492 (1983).

668. Aubert,M. *et al.* Peritoneal colonization by human pancreatic cancer cells is inhibited by antisense FUT3 sequence. *Int. J. Cancer* **88,** 558-565 (2000).

669. Aubert,M. *et al.* Restoration of alpha(1,2) fucosyltransferase activity decreases adhesive and metastatic properties of human pancreatic cancer cells. *Cancer Res.* **60,** 1449-1456 (2000).

670. Mann,D.V., Edwards,R., Ho,S., Lau,W.Y. & Glazer,G. Elevated tumour marker CA19-9: clinical interpretation and influence of obstructive jaundice. *Eur. J. Surg. Oncol.* **26,** 474-479 (2000).

671. Chang,C.Y. *et al.* Low efficacy of serum levels of CA 19-9 in prediction of malignant diseases in asymptomatic population in Taiwan. *Hepatogastroenterology* **53,** 1-4 (2006).

672. Kim,J.E. *et al.* Clinical usefulness of carbohydrate antigen 19-9 as a screening test for pancreatic cancer in an asymptomatic population. *J. Gastroenterol. Hepatol.* **19,** 182-186 (2004).

673. Riker,A., Libutti,S.K. & Bartlett,D.L. Advances in the early detection, diagnosis, and staging of pancreatic cancer. *Surg. Oncol.* **6,** 157-169 (1997).

674. Reddi,K.K. & Holland,J.F. Elevated serum ribonuclease in patients with pancreatic cancer. *Proc. Natl. Acad. Sci. U. S. A* **73,** 2308-2310 (1976).

675. Weickmann,J.L., Olson,E.M. & Glitz,D.G. Immunological assay of pancreatic ribonuclease in serum as an indicator of pancreatic cancer. *Cancer Res.* **44,** 1682-1687 (1984).

676. Kurihara,M. *et al*. Radioimmunoassay for human pancreatic ribonuclease and measurement of serum immunoreactive pancreatic ribonuclease in patients with malignant tumors. *Cancer Res.* **44**, 2240-2243 (1984).

677. Peracaula,R. *et al*. Glycosylation of human pancreatic ribonuclease: differences between normal and tumor states. *Glycobiology* **13**, 227-244 (2003).

678. Barrabes,S. *et al*. Glycosylation of serum ribonuclease 1 indicates a major endothelial origin and reveals an increase in core fucosylation in pancreatic cancer. *Glycobiology* **17**, 388-400 (2007).

679. Kim,Y.S. *et al*. Lex and Ley antigen expression in human pancreatic cancer. *Cancer Res.* **48**, 475-482 (1988).

680. Sarrats,A. *et al*. Glycosylation of liver acute-phase proteins in pancreatic cancer and chronic pancreatitis. *Proteomics. Clin. Appl.* **4**, 432-448 (2010).

681. Kim,H.J. & Kim,H.J. Glycosylation variant analysis of recombinant human tissue plasminogen activator produced in urea-cycle-enzyme-expressing Chinese hamster ovary (CHO) cell line. *J. Biosci. Bioeng.* **102**, 447-451 (2006).

682. Bergum,P.W. & Gardell,S.J. Vampire bat salivary plasminogen activator exhibits a strict and fastidious requirement for polymeric fibrin as its cofactor, unlike human tissue-type plasminogen activator. A kinetic analysis. *J. Biol. Chem.* **267**, 17726-17731 (1992).

683. Bringmann,P. *et al*. Structural features mediating fibrin selectivity of vampire bat plasminogen activators. *J. Biol. Chem.* **270**, 25596-25603 (1995).

684. Hokke,C.H. *et al*. Sialylated carbohydrate chains of recombinant human glycoproteins expressed in Chinese hamster ovary cells contain traces of N-glycolylneuraminic acid. *FEBS Lett.* **275**, 9-14 (1990).

685. Debeljak,N., Feldman,L., Davis,K.L., Komel,R. & Sytkowski,A.J. Variability in the immunodetection of His-tagged recombinant proteins. *Anal. Biochem.* **359**, 216-223 (2006).

686. Wu,S.L. The use of sequential high-performance liquid chromatography and capillary zone electrophoresis to separate the glycosylated peptides from recombinant tissue plasminogen activator to a detailed level of microheterogeneity. *Anal. Biochem.* **253**, 85-97 (1997).

687. Jaques,A.J., Opdenakker,G., Rademacher,T.W., Dwek,R.A. & Zamze,S.E. The glycosylation of Bowes melanoma tissue plasminogen activator: lectin mapping, reaction with anti-L2/HNK-1 antibodies and

the presence of sulphated/glucuronic acid containing glycans. *Biochem. J.* **316 (Pt 2),** 427-437 (1996).

688. Zamze,S. *et al.* A family of novel, acidic N-glycans in Bowes melanoma tissue plasminogen activator have L2/HNK-1-bearing antennae, many with sulfation of the fucosylated chitobiose core. *Eur. J. Biochem.* **268,** 4063-4078 (2001).

689. Furukawa,T. *et al.* Long-term culture and immortalization of epithelial cells from normal adult human pancreatic ducts transfected by the E6E7 gene of human papilloma virus 16. *Am. J. Pathol.* **148,** 1763-1770 (1996).

690. Ouyang,H. *et al.* Immortal human pancreatic duct epithelial cell lines with near normal genotype and phenotype. *Am. J Pathol.* **157,** 1623-1631 (2000).

691. Jung,T.Y. *et al.* Role of galectin-1 in migration and invasion of human glioblastoma multiforme cell lines. *J. Neurosurg.* **109,** 273-284 (2008).

692. van Beijnum,J.R. & Griffioen,A.W. In silico analysis of angiogenesis associated gene expression identifies angiogenic stage related profiles. *Biochim. Biophys. Acta* **1755,** 121-134 (2005).

693. Griffioen,A.W. *et al.* Anginex, a designed peptide that inhibits angiogenesis. *Biochem. J.* **354,** 233-242 (2001).

694. van der Schaft,D.W. *et al.* The designer anti-angiogenic peptide anginex targets tumor endothelial cells and inhibits tumor growth in animal models. *FASEB J.* **16,** 1991-1993 (2002).

695. Dings,R.P. *et al.* Anti-tumor activity of the novel angiogenesis inhibitor anginex. *Cancer Lett.* **194,** 55-66 (2003).

696. Dings,R.P., Yokoyama,Y., Ramakrishnan,S., Griffioen,A.W. & Mayo,K.H. The designed angiostatic peptide anginex synergistically improves chemotherapy and antiangiogenesis therapy with angiostatin. *Cancer Res.* **63,** 382-385 (2003).

697. Arroyo,M.M. & Mayo,K.H. NMR solution structure of the angiostatic peptide anginex. *Biochim. Biophys. Acta* **1774,** 645-651 (2007).

698. Miner,N.A., Koehler,J. & Greenaway,L. Intraperitoneal injection of mice. *Appl. Microbiol.* **17,** 250-251 (1969).

699. Cheong,T.C., Shin,J.Y. & Chun,K.H. Silencing of galectin-3 changes the gene expression and augments the sensitivity of gastric cancer cells to chemotherapeutic agents. *Cancer Sci.* **101,** 94-102 (2010).

700. Kim,H.R., Lin,H.M., Biliran,H. & Raz,A. Cell cycle arrest and inhibition of anoikis by galectin-3 in human breast epithelial cells. *Cancer Res.* **59**, 4148-4154 (1999).

701. Akahani,S., Nangia-Makker,P., Inohara,H., Kim,H.R. & Raz,A. Galectin-3: a novel antiapoptotic molecule with a functional BH1 (NWGR) domain of Bcl-2 family. *Cancer Res.* **57**, 5272-5276 (1997).

702. Takenaka,Y. *et al.* Malignant transformation of thyroid follicular cells by galectin-3. *Cancer Lett.* **195**, 111-119 (2003).

703. Klein,W.M., Hruban,R.H., Klein-Szanto,A.J. & Wilentz,R.E. Direct correlation between proliferative activity and dysplasia in pancreatic intraepithelial neoplasia (PanIN): additional evidence for a recently proposed model of progression. *Mod. Pathol.* **15**, 441-447 (2002).

704. Criswell,T.L., Dumont,N., Barnett,J.V. & Arteaga,C.L. Knockdown of the transforming growth factor-beta type III receptor impairs motility and invasion of metastatic cancer cells. *Cancer Res.* **68**, 7304-7312 (2008).

705. Konig,A., Fernandez-Zapico,M.E. & Ellenrieder,V. Primers on molecular pathways--the NFAT transcription pathway in pancreatic cancer. *Pancreatology.* **10**, 416-422 (2010).

706. Zhang,Y. *et al.* Antitumor activity of epidermal growth factor receptor-related protein is mediated by inactivation of ErbB receptors and nuclear factor-kappaB in pancreatic cancer. *Cancer Res.* **66**, 1025-1032 (2006).

707. Watanabe,N. *et al.* Recombinant human tumor necrosis factor causes regression in patients with advanced malignancies. *Oncology* **51**, 360-365 (1994).

708. Fujioka,S. *et al.* Function of nuclear factor kappaB in pancreatic cancer metastasis. *Clin. Cancer Res.* **9**, 346-354 (2003).

709. Komoto,M. *et al.* HER2 overexpression correlates with survival after curative resection of pancreatic cancer. *Cancer Sci.* **100**, 1243-1247 (2009).

710. Larbouret,C. *et al.* Combined cetuximab and trastuzumab are superior to gemcitabine in the treatment of human pancreatic carcinoma xenografts. *Ann. Oncol.* **21**, 98-103 (2010).

711. Hall,P.A. *et al.* The c-erb B-2 proto-oncogene in human pancreatic cancer. *J. Pathol.* **161**, 195-200 (1990).

712. Day,J.D. *et al.* Immunohistochemical evaluation of HER-2/neu expression in pancreatic adenocarcinoma and pancreatic intraepithelial neoplasms. *Hum. Pathol.* **27**, 119-124 (1996).

713. Pryczynicz,A., Guzinska-Ustymowicz,K., Kemona,A. & Czyzewska,J. Expression of the E-cadherin-catenin complex in patients with pancreatic ductal adenocarcinoma. *Folia Histochem. Cytobiol.* **48**, 128-133 (2010).

714. Maier,H.J. *et al.* NF-kappaB promotes epithelial-mesenchymal transition, migration and invasion of pancreatic carcinoma cells. *Cancer Lett.* **295**, 214-228 (2010).

715. Nomura,S. *et al.* FGF10/FGFR2 signal induces cell migration and invasion in pancreatic cancer. *Br. J. Cancer* **99**, 305-313 (2008).

716. Yan,Z., Deng,X. & Friedman,E. Oncogenic Ki-ras confers a more aggressive colon cancer phenotype through modification of transforming growth factor-beta receptor III. *J. Biol. Chem.* **276**, 1555-1563 (2001).

717. Gordon,K.J., Dong,M., Chislock,E.M., Fields,T.A. & Blobe,G.C. Loss of type III transforming growth factor beta receptor expression increases motility and invasiveness associated with epithelial to mesenchymal transition during pancreatic cancer progression. *Carcinogenesis* **29**, 252-262 (2008).

718. Gatza,C.E., Oh,S.Y. & Blobe,G.C. Roles for the type III TGF-beta receptor in human cancer. *Cell Signal.* **22**, 1163-1174 (2010).

719. Takahashi,K., Ikeo,K., Gojobori,T. & Tanifuji,M. Local function of urokinase receptor at the adhesion contact sites of a metastatic tumor cell. *Thromb. Res. Suppl* **10**, 55-61 (1990).

720. Burke,R. *et al.* Dispatched, a novel sterol-sensing domain protein dedicated to the release of cholesterol-modified hedgehog from signaling cells. *Cell* **99**, 803-815 (1999).

721. Tian,H., Jeong,J., Harfe,B.D., Tabin,C.J. & McMahon,A.P. Mouse Disp1 is required in sonic hedgehog-expressing cells for paracrine activity of the cholesterol-modified ligand. *Development* **132**, 133-142 (2005).

722. Yoon,J.W. *et al.* Gene expression profiling leads to identification of GLI1-binding elements in target genes and a role for multiple downstream pathways in GLI1-induced cell transformation. *J. Biol. Chem.* **277**, 5548-5555 (2002).

723. Weinstein,I.B. & Case,K. The history of Cancer Research: introducing an AACR Centennial series. *Cancer Res.* **68**, 6861-6862 (2008).

724. Hanahan,D. & Weinberg,R.A. The hallmarks of cancer. *Cell* **100**, 57-70 (2000).

725. Hanahan,D. & Weinberg,R.A. Hallmarks of cancer: the next generation. *Cell* **144**, 646-674 (2011).

726. Cooper,D.N. & Barondes,S.H. God must love galectins; he made so many of them. *Glycobiology* **9**, 979-984 (1999).

727. Giudicelli,V. *et al.* Is human galectin-1 activity modulated by monomer/dimer equilibrium? *Glycobiology* **7**, viii-viix (1997).

728. Ahmad,N. *et al.* Galectin-3 precipitates as a pentamer with synthetic multivalent carbohydrates and forms heterogeneous cross-linked complexes. *J. Biol. Chem.* **279**, 10841-10847 (2004).

729. Hsu,D.K., Zuberi,R.I. & Liu,F.T. Biochemical and biophysical characterization of human recombinant IgE-binding protein, an S-type animal lectin. *J. Biol. Chem.* **267**, 14167-14174 (1992).

730. Massa,S.M., Cooper,D.N., Leffler,H. & Barondes,S.H. L-29, an endogenous lectin, binds to glycoconjugate ligands with positive cooperativity. *Biochemistry* **32**, 260-267 (1993).

731. Ochieng,J. *et al.* Structure-function relationship of a recombinant human galactoside-binding protein. *Biochemistry* **32**, 4455-4460 (1993).

732. Tuveson,D.A. *et al.* Endogenous oncogenic K-ras(G12D) stimulates proliferation and widespread neoplastic and developmental defects. *Cancer Cell* **5**, 375-387 (2004).

733. Serrano,M., Lin,A.W., McCurrach,M.E., Beach,D. & Lowe,S.W. Oncogenic ras provokes premature cell senescence associated with accumulation of p53 and p16INK4a. *Cell* **88**, 593-602 (1997).

734. Lowe,S.W., Cepero,E. & Evan,G. Intrinsic tumour suppression. *Nature* **432**, 307-315 (2004).

735. Califice,S., Castronovo,V., Bracke,M. & van den,B.F. Dual activities of galectin-3 in human prostate cancer: tumor suppression of nuclear galectin-3 vs tumor promotion of cytoplasmic galectin-3. *Oncogene* **23**, 7527-7536 (2004).

736. Stanley,P., Sundaram,S. & Sallustio,S. A subclass of cell surface carbohydrates revealed by a CHO mutant with two glycosylation mutations. *Glycobiology* **1**, 307-314 (1991).

737. Cho,M. & Cummings,R.D. Galectin-1, a beta-galactoside-binding lectin in Chinese hamster ovary cells. II. Localization and biosynthesis. *J. Biol. Chem.* **270**, 5207-5212 (1995).

738. Stillman,B.N. *et al.* Galectin-3 and galectin-1 bind distinct cell surface glycoprotein receptors to induce T cell death. *J. Immunol.* **176,** 778-789 (2006).

739. Auersperg,N. *et al.* E-cadherin induces mesenchymal-to-epithelial transition in human ovarian surface epithelium. *Proc. Natl. Acad. Sci. U. S. A* **96,** 6249-6254 (1999).

740. Grassadonia,A. *et al.* 90K (Mac-2 BP) and galectins in tumor progression and metastasis. *Glycoconj. J.* **19,** 551-556 (2004).

741. Perillo,N.L., Marcus,M.E. & Baum,L.G. Galectins: versatile modulators of cell adhesion, cell proliferation, and cell death. *J. Mol. Med.* **76,** 402-412 (1998).

742. Bar-Sagi,D. & Hall,A. Ras and Rho GTPases: a family reunion. *Cell* **103,** 227-238 (2000).

743. Downward,J. Ras signalling and apoptosis. *Curr. Opin. Genet. Dev.* **8,** 49-54 (1998).

744. Shields,J.M., Pruitt,K., McFall,A., Shaub,A. & Der,C.J. Understanding Ras: 'it ain't over 'til it's over'. *Trends Cell Biol.* **10,** 147-154 (2000).

745. Allione,A., Wells,V., Forni,G., Mallucci,L. & Novelli,F. Beta-galactoside-binding protein (beta GBP) alters the cell cycle, up-regulates expression of the alpha- and beta-chains of the IFN-gamma receptor, and triggers IFN-gamma-mediated apoptosis of activated human T lymphocytes. *J. Immunol.* **161,** 2114-2119 (1998).

746. Vespa,G.N. *et al.* Galectin-1 specifically modulates TCR signals to enhance TCR apoptosis but inhibit IL-2 production and proliferation. *J. Immunol.* **162,** 799-806 (1999).

747. Puchades,M. *et al.* Proteomic investigation of glioblastoma cell lines treated with wild-type p53 and cytotoxic chemotherapy demonstrates an association between galectin-1 and p53 expression. *J. Proteome. Res.* **6,** 869-875 (2007).

748. Juszczynski,P. *et al.* The AP1-dependent secretion of galectin-1 by Reed Sternberg cells fosters immune privilege in classical Hodgkin lymphoma. *Proc. Natl. Acad. Sci. U. S. A* **104,** 13134-13139 (2007).

749. Goldfinger,L.E., Stack,M.S. & Jones,J.C. Processing of laminin-5 and its functional consequences: role of plasmin and tissue-type plasminogen activator. *J. Cell Biol.* **141,** 255-265 (1998).

750. Lopez-Atalaya,J.P. *et al.* Toward safer thrombolytic agents in stroke: molecular requirements for NMDA receptor-mediated neurotoxicity. *J. Cereb. Blood Flow Metab* **28,** 1212-1221 (2008).

751. Beebe,D.P., Miles,L.A. & Plow,E.F. A linear amino acid sequence involved in the interaction of t-PA with its endothelial cell receptor. *Blood* **74**, 2034-2037 (1989).

752. Patnaik,S.K. *et al*. Complex N-glycans are the major ligands for galectin-1, -3, and -8 on Chinese hamster ovary cells. *Glycobiology* **16**, 305-317 (2006).

753. Kinlough,C.L., Poland,P.A., Bruns,J.B., Harkleroad,K.L. & Hughey,R.P. MUC1 membrane trafficking is modulated by multiple interactions. *J. Biol. Chem.* **279**, 53071-53077 (2004).

754. He,J. & Baum,L.G. Galectin interactions with extracellular matrix and effects on cellular function. *Methods Enzymol.* **417**, 247-256 (2006).

755. Kita,Y. *et al*. Quantitative glycomics of human whole serum glycoproteins based on the standardized protocol for liberating N-glycans. *Mol. Cell Proteomics.* **6**, 1437-1445 (2007).

756. Siebert,H.C. *et al*. Unique conformer selection of human growth-regulatory lectin galectin-1 for ganglioside GM1 versus bacterial toxins. *Biochemistry* **42**, 14762-14773 (2003).

757. Hernandez,J.D. *et al*. Galectin-1 binds different CD43 glycoforms to cluster CD43 and regulate T cell death. *J. Immunol.* **177**, 5328-5336 (2006).

758. Di Virgilio,S., Glushka,J., Moremen,K. & Pierce,M. Enzymatic synthesis of natural and 13C enriched linear poly-N-acetyllactosamines as ligands for galectin-1. *Glycobiology* **9**, 353-364 (1999).

759. Stowell,S.R. *et al*. Human galectin-1 recognition of poly-N-acetyllactosamine and chimeric polysaccharides. *Glycobiology* **14**, 157-167 (2004).

760. Amano,M., Galvan,M., He,J. & Baum,L.G. The ST6Gal I sialyltransferase selectively modifies N-glycans on CD45 to negatively regulate galectin-1-induced CD45 clustering, phosphatase modulation, and T cell death. *J. Biol. Chem.* **278**, 7469-7475 (2003).

761. Gabius,H.J., Siebert,H.C., Andre,S., Jimenez-Barbero,J. & Rudiger,H. Chemical biology of the sugar code. *Chembiochem.* **5**, 740-764 (2004).

762. Andre,S. *et al*. Determination of modulation of ligand properties of synthetic complex-type biantennary N-glycans by introduction of bisecting GlcNAc in silico, in vitro and in vivo. *Eur. J. Biochem.* **271**, 118-134 (2004).

763. Sturm,A. *et al.* Human galectin-2: novel inducer of T cell apoptosis with distinct profile of caspase activation. *J. Immunol.* **173**, 3825-3837 (2004).

764. Nguyen,J.T. *et al.* CD45 modulates galectin-1-induced T cell death: regulation by expression of core 2 O-glycans. *J. Immunol.* **167**, 5697-5707 (2001).

765. Roberts,A.A. *et al.* Galectin-1-mediated apoptosis in mycosis fungoides: the roles of CD7 and cell surface glycosylation. *Mod. Pathol.* **16**, 543-551 (2003).

766. Liu,F.T. & Rabinovich,G.A. Galectins: regulators of acute and chronic inflammation. *Ann. N. Y. Acad. Sci.* **1183**, 158-182 (2010).

767. Valenzuela,H.F. *et al.* O-glycosylation regulates LNCaP prostate cancer cell susceptibility to apoptosis induced by galectin-1. *Cancer Res.* **67**, 6155-6162 (2007).

768. Rudd,P.M. *et al.* The glycosylation of the complement regulatory protein, human erythrocyte CD59. *Adv. Exp. Med. Biol.* **435**, 153-162 (1998).

769. Rabinovich,G.A. & Toscano,M.A. Turning 'sweet' on immunity: galectin-glycan interactions in immune tolerance and inflammation. *Nat. Rev. Immunol.* **9**, 338-352 (2009).

770. Fernandes,H., Cohen,S. & Bishayee,S. Glycosylation-induced conformational modification positively regulates receptor-receptor association: a study with an aberrant epidermal growth factor receptor (EGFRvIII/DeltaEGFR) expressed in cancer cells. *J. Biol. Chem.* **276**, 5375-5383 (2001).

771. Brewer,C.F., Miceli,M.C. & Baum,L.G. Clusters, bundles, arrays and lattices: novel mechanisms for lectin-saccharide-mediated cellular interactions. *Curr. Opin. Struct. Biol.* **12**, 616-623 (2002).

772. Demetriou,M., Granovsky,M., Quaggin,S. & Dennis,J.W. Negative regulation of T-cell activation and autoimmunity by Mgat5 N-glycosylation. *Nature* **409**, 733-739 (2001).

773. Lajoie,P. *et al.* Plasma membrane domain organization regulates EGFR signaling in tumor cells. *J. Cell Biol.* **179**, 341-356 (2007).

774. Weaver,V.M. *et al.* Reversion of the malignant phenotype of human breast cells in three-dimensional culture and in vivo by integrin blocking antibodies. *J. Cell Biol.* **137**, 231-245 (1997).

775. Yamada,K.M. & Cukierman,E. Modeling tissue morphogenesis and cancer in 3D. *Cell* **130**, 601-610 (2007).

776. Kenny,H.A., Krausz,T., Yamada,S.D. & Lengyel,E. Use of a novel 3D culture model to elucidate the role of mesothelial cells, fibroblasts and extra-cellular matrices on adhesion and invasion of ovarian cancer cells to the omentum. *Int. J. Cancer* **121**, 1463-1472 (2007).

777. Nelson,C.M. & Bissell,M.J. Modeling dynamic reciprocity: engineering three-dimensional culture models of breast architecture, function, and neoplastic transformation. *Semin. Cancer Biol.* **15**, 342-352 (2005).

778. Ertel,A., Verghese,A., Byers,S.W., Ochs,M. & Tozeren,A. Pathway-specific differences between tumor cell lines and normal and tumor tissue cells. *Mol. Cancer* **5**, 55 (2006).

779. Scott,R.E. Plasma membrane vesiculation: a new technique for isolation of plasma membranes. *Science* **194**, 743-745 (1976).

780. Estreicher,A., Muhlhauser,J., Carpentier,J.L., Orci,L. & Vassalli,J.D. The receptor for urokinase type plasminogen activator polarizes expression of the protease to the leading edge of migrating monocytes and promotes degradation of enzyme inhibitor complexes. *J. Cell Biol.* **111**, 783-792 (1990).

781. Yamamoto,M. *et al.* Expression and localization of urokinase-type plasminogen activator in human astrocytomas in vivo. *Cancer Res.* **54**, 3656-3661 (1994).

782. Limongi,P. *et al.* Biosynthesis and apical localization of the urokinase receptor in polarized MDCK epithelial cells. *FEBS Lett.* **369**, 207-211 (1995).

783. Wang,X. *et al.* Lipoprotein receptor-mediated induction of matrix metalloproteinase by tissue plasminogen activator. *Nat Med* **9**, 1313-1316 (2003).

784. Yamamoto,H. *et al.* Expression of matrix metalloproteinases and tissue inhibitors of metalloproteinases in human pancreatic adenocarcinomas: clinicopathologic and prognostic significance of matrilysin expression. *J. Clin. Oncol.* **19**, 1118-1127 (2001).

785. Konakova,M., Hucho,F. & Schleuning,W.D. Downstream targets of urokinase-type plasminogen-activator-mediated signal transduction. *Eur J Biochem.* **253**, 421-429 (1998).

786. Christow,S.P. *et al.* Urokinase activates calcium-dependent potassium channels in U937 cells via calcium release from intracellular stores. *Eur. J. Biochem.* **265**, 264-272 (1999).

787. Nguyen,D.H., Hussaini,I.M. & Gonias,S.L. Binding of urokinase-type plasminogen activator to its receptor in MCF-7 cells activates

extracellular signal-regulated kinase 1 and 2 which is required for increased cellular motility. *J. Biol. Chem.* **273**, 8502-8507 (1998).

788. Blasi,F. & Carmeliet,P. uPAR: a versatile signalling orchestrator. *Nat. Rev Mol. Cell Biol.* **3**, 932-943 (2002).

789. Yebra,M., Goretzki,L., Pfeifer,M. & Mueller,B.M. Urokinase-type plasminogen activator binding to its receptor stimulates tumor cell migration by enhancing integrin-mediated signal transduction. *Exp. Cell Res.* **250**, 231-240 (1999).

790. Maupas-Schwalm,F. *et al.* The sphingomyelin/ceramide pathway is involved in ERK1/2 phosphorylation, cell proliferation, and uPAR overexpression induced by tissue-type plasminogen activator. *FASEB J.* **18**, 1398-1400 (2004).

791. De Petro,G., Copeta,A. & Barlati,S. Urokinase-type and tissue-type plasminogen activators as growth factors of human fibroblasts. *Exp. Cell Res.* **213**, 286-294 (1994).

792. Welling,T.H., Huber,T.S., Messina,L.M. & Stanley,J.C. Tissue plasminogen activator increases canine endothelial cell proliferation rate through a plasmin-independent, receptor-mediated mechanism. *J Surg. Res.* **66**, 36-42 (1996).

793. Yang,Z., Eton,D., Zheng,F., Livingstone,A.S. & Yu,H. Effect of tissue plasminogen activator on vascular smooth muscle cells. *J. Vasc. Surg.* **42**, 532-538 (2005).

794. Fredriksson,L., Li,H., Fieber,C., Li,X. & Eriksson,U. Tissue plasminogen activator is a potent activator of PDGF-CC. *EMBO J.* **23**, 3793-3802 (2004).

795. Akao,M. *et al.* Plasminogen activator-plasmin system potentiates the proliferation of hepatocytes in primary culture. *Thromb. Res.* **107**, 169-174 (2002).

796. Pineda,D. *et al.* Tissue plasminogen activator (tPA) induces microglial inflammation via a non-catalytic molecular mechanism involving activation of MAPKs and AKT signalling pathways and AnnexinA2 and Galectin-1 receptors. 2011. In revision in *Glia.*

797. Stupack,D.G. Integrins as a distinct subtype of dependence receptors. *Cell Death. Differ.* **12**, 1021-1030 (2005).

798. Liu,D., Aguirre,G.J., Estrada,Y. & Ossowski,L. EGFR is a transducer of the urokinase receptor initiated signal that is required for in vivo growth of a human carcinoma. *Cancer Cell* **1**, 445-457 (2002).

799. Jo,M., Thomas,K.S., O'Donnell,D.M. & Gonias,S.L. Epidermal growth factor receptor-dependent and -independent cell-signaling pathways originating from the urokinase receptor. *J. Biol. Chem.* **278**, 1642-1646 (2003).

800. Monaghan-Benson,E. & McKeown-Longo,P.J. Urokinase-type plasminogen activator receptor regulates a novel pathway of fibronectin matrix assembly requiring Src-dependent transactivation of epidermal growth factor receptor. *J. Biol. Chem.* **281**, 9450-9459 (2006).

801. Ullrich,A. *et al.* Human epidermal growth factor receptor cDNA sequence and aberrant expression of the amplified gene in A431 epidermoid carcinoma cells. *Nature* **309**, 418-425 (1984).

802. Mohan R. Angiogenesis and Pancreatic Cancer: a role for tissue plasminogen activator (tPA). 2011. Doctoral Thesis. Universitat Pompeu Fabra.

803. Akerman,M.E., Pilch,J., Peters,D. & Ruoslahti,E. Angiostatic peptides use plasma fibronectin to home to angiogenic vasculature. *Proc. Natl. Acad. Sci. U. S. A* **102**, 2040-2045 (2005).

804. Pilch,J. *et al.* The anti-angiogenic peptide anginex disrupts the cell membrane. *J. Mol. Biol.* **356**, 876-885 (2006).

805. Chang,H.Y. *et al.* Diversity, topographic differentiation, and positional memory in human fibroblasts. *Proc. Natl. Acad. Sci. U. S. A* **99**, 12877-12882 (2002).

806. Jesnowski,R. *et al.* Immortalization of pancreatic stellate cells as an in vitro model of pancreatic fibrosis: deactivation is induced by matrigel and N-acetylcysteine. *Lab Invest* **85**, 1276-1291 (2005).

807. Aoki,H. *et al.* Autocrine loop between TGF-beta1 and IL-1beta through Smad3- and ERK-dependent pathways in rat pancreatic stellate cells. *Am. J. Physiol Cell Physiol* **290**, C1100-C1108 (2006).

808. Sato,N. *et al.* SPARC/osteonectin is a frequent target for aberrant methylation in pancreatic adenocarcinoma and a mediator of tumor-stromal interactions. *Oncogene* **22**, 5021-5030 (2003).

809. Fajka-Boja,R. *et al.* Co-localization of galectin-1 with GM1 ganglioside in the course of its clathrin- and raft-dependent endocytosis. *Cell Mol. Life Sci.* **65**, 2586-2593 (2008).

810. Bruns,C.J. *et al.* Effect of the vascular endothelial growth factor receptor-2 antibody DC101 plus gemcitabine on growth, metastasis and angiogenesis of human pancreatic cancer growing orthotopically in nude mice. *Int. J. Cancer* **102**, 101-108 (2002).

811. Shimamura,T. *et al*. Interleukin-4 cytotoxin therapy synergizes with gemcitabine in a mouse model of pancreatic ductal adenocarcinoma. *Cancer Res.* **67**, 9903-9912 (2007).

812. Verma,A. *et al*. Therapeutic significance of elevated tissue transglutaminase expression in pancreatic cancer. *Clin. Cancer Res.* **14**, 2476-2483 (2008).

813. Duan,J.X. *et al*. Potent and highly selective hypoxia-activated achiral phosphoramidate mustards as anticancer drugs. *J. Med. Chem.* **51**, 2412-2420 (2008).

814. Melisi,D. *et al*. LY2109761, a novel transforming growth factor beta receptor type I and type II dual inhibitor, as a therapeutic approach to suppressing pancreatic cancer metastasis. *Mol. Cancer Ther.* **7**, 829-840 (2008).

815. Schultz,R.M. *et al*. Evaluation of new anticancer agents against the MIA PaCa-2 and PANC-1 human pancreatic carcinoma xenografts. *Oncol. Res.* **5**, 223-228 (1993).

816. Stannard,K.A. *et al*. Galectin inhibitory disaccharides promote tumour immunity in a breast cancer model. *Cancer Lett.* **299**, 95-110 (2010).

817. DeBusk,L.M., Boelte,K., Min,Y. & Lin,P.C. Heterozygous deficiency of delta-catenin impairs pathological angiogenesis. *J. Exp. Med.* **207**, 77-84 (2010).

818. De Andrea,M. *et al*. Keratinocyte-specific stat3 heterozygosity impairs development of skin tumors in human papillomavirus 8 transgenic mice. *Cancer Res.* **70**, 7938-7948 (2010).

819. Hulit,J. *et al*. Cyclin D1 genetic heterozygosity regulates colonic epithelial cell differentiation and tumor number in ApcMin mice. *Mol. Cell Biol.* **24**, 7598-7611 (2004).

820. Adrian,K. *et al*. Tgfbr1 haploinsufficiency inhibits the development of murine mutant Kras-induced pancreatic precancer. *Cancer Res.* **69**, 9169-9174 (2009).

821. Alberici,P. *et al*. Smad4 haploinsufficiency: a matter of dosage. *Pathogenetics.* **1**, 2 (2008).

822. Morton,J.P. *et al*. LKB1 haploinsufficiency cooperates with Kras to promote pancreatic cancer through suppression of p21-dependent growth arrest. *Gastroenterology* **139**, 586-97, 597 (2010).

823. Shih,N.Y. *et al*. Congenital nephrotic syndrome in mice lacking CD2-associated protein. *Science* **286**, 312-315 (1999).

824. Heermann,S., Opazo,F., Falkenburger,B., Krieglstein,K. & Spittau,B. Aged Tgfbeta2/Gdnf double-heterozygous mice show no morphological and functional alterations in the nigrostriatal system. *J. Neural Transm.* **117**, 719-727 (2010).

825. Li,J., Houseknecht,K.L., Stenbit,A.E., Katz,E.B. & Charron,M.J. Reduced glucose uptake precedes insulin signaling defects in adipocytes from heterozygous GLUT4 knockout mice. *FASEB J.* **14**, 1117-1125 (2000).

826. Luo,Y., Wang,Y., Kuang,S.Y., Chiang,Y.H. & Hoffer,B. Decreased level of Nurr1 in heterozygous young adult mice leads to exacerbated acute and long-term toxicity after repeated methamphetamine exposure. *PLoS. One.* **5**, e15193 (2010).

827. Imaizumi,Y. *et al.* Galectin-1 is expressed in early-type neural progenitor cells and down-regulates neurogenesis in the adult hippocampus. *Mol. Brain* **4**, 7 (2011).

828. Sakaguchi,M. *et al.* Regulation of adult neural progenitor cells by Galectin-1/beta1 Integrin interaction. *J. Neurochem.* **113**, 1516-1524 (2010).

829. Sakaguchi,M. *et al.* A carbohydrate-binding protein, Galectin-1, promotes proliferation of adult neural stem cells. *Proc. Natl. Acad. Sci. U. S. A* **103**, 7112-7117 (2006).

830. Rabinovich,G.A. *et al.* Specific inhibition of lymphocyte proliferation and induction of apoptosis by CLL-I, a beta-galactoside-binding lectin. *J. Biochem. (Tokyo)* **122**, 365-373 (1997).

831. Rabinovich,G.A. *et al.* Activated rat macrophages produce a galectin-1-like protein that induces apoptosis of T cells: biochemical and functional characterization. *J. Immunol.* **160**, 4831-4840 (1998).

832. Rabinovich,G.A. *et al.* Induction of allogenic T-cell hyporesponsiveness by galectin-1-mediated apoptotic and non-apoptotic mechanisms. *Cell Death. Differ.* **9**, 661-670 (2002).

833. Bockman,D.E. *et al.* Origin and development of the precursor lesions in experimental pancreatic cancer in rats. *Lab Invest* **83**, 853-859 (2003).

834. Willemer,S. & Adler,G. Histochemical and ultrastructural characteristics of tubular complexes in human acute pancreatitis. *Dig. Dis. Sci.* **34**, 46-55 (1989).

835. Bockman,D.E., Boydston,W.R. & Anderson,M.C. Origin of tubular complexes in human chronic pancreatitis. *Am. J. Surg.* **144**, 243-249 (1982).

836. Tokoro,T., Tezel,E., Nagasaka,T., Kaneko,T. & Nakao,A. Differentiation of acinar cells into acinoductular cells in regenerating rat pancreas. *Pancreatology*. **3**, 487-496 (2003).

837. Crawford,H.C., Scoggins,C.R., Washington,M.K., Matrisian,L.M. & Leach,S.D. Matrix metalloproteinase-7 is expressed by pancreatic cancer precursors and regulates acinar-to-ductal metaplasia in exocrine pancreas. *J Clin. Invest* **109**, 1437-1444 (2002).

838. Schmid,R.M. Acinar-to-ductal metaplasia in pancreatic cancer development. *J Clin. Invest* **109**, 1403-1404 (2002).

839. Miyamoto,Y. *et al*. Notch mediates TGF alpha-induced changes in epithelial differentiation during pancreatic tumorigenesis. *Cancer Cell* **3**, 565-576 (2003).

840. Means,A.L. *et al*. Pancreatic epithelial plasticity mediated by acinar cell transdifferentiation and generation of nestin-positive intermediates. *Development* **132**, 3767-3776 (2005).

841. Wells,W.A. Is transdifferentiation in trouble? *J. Cell Biol.* **157**, 15-18 (2002).

842. Strobel,O. *et al*. In vivo lineage tracing defines the role of acinar-to-ductal transdifferentiation in inflammatory ductal metaplasia. *Gastroenterology* **133**, 1999-2009 (2007).

843. Bottinger,E.P. *et al*. Expression of a dominant-negative mutant TGF-beta type II receptor in transgenic mice reveals essential roles for TGF-beta in regulation of growth and differentiation in the exocrine pancreas. *EMBO J.* **16**, 2621-2633 (1997).

844. Murtaugh,L.C. & Leach,S.D. A case of mistaken identity? Nonductal origins of pancreatic "ductal" cancers. *Cancer Cell* **11**, 211-213 (2007).

845. Shi,G. *et al*. Loss of the acinar-restricted transcription factor Mist1 accelerates Kras-induced pancreatic intraepithelial neoplasia. *Gastroenterology* **136**, 1368-1378 (2009).

846. Siveke,J.T. *et al*. Concomitant pancreatic activation of Kras(G12D) and Tgfa results in cystic papillary neoplasms reminiscent of human IPMN. *Cancer Cell* **12**, 266-279 (2007).

847. Schaeffer,B.K., Terhune,P.G. & Longnecker,D.S. Pancreatic carcinomas of acinar and mixed acinar/ductal phenotypes in Ela-1-myc transgenic mice do not contain c-K-ras mutations. *Am. J Pathol.* **145**, 696-701 (1994).

848. Blaine,S.A. *et al*. Adult pancreatic acinar cells give rise to ducts but not endocrine cells in response to growth factor signaling. *Development* **137**, 2289-2296 (2010).

849. Sawey,E.T., Johnson,J.A. & Crawford,H.C. Matrix metalloproteinase 7 controls pancreatic acinar cell transdifferentiation by activating the Notch signaling pathway. *Proc. Natl. Acad. Sci. U. S. A* **104**, 19327-19332 (2007).

850. Elghazi,L. *et al*. Regulation of pancreas plasticity and malignant transformation by Akt signaling. *Gastroenterology* **136**, 1091-1103 (2009).

851. Miyatsuka,T. *et al*. Persistent expression of PDX-1 in the pancreas causes acinar-to-ductal metaplasia through Stat3 activation. *Genes Dev*. **20**, 1435-1440 (2006).

852. Colby,J.K. *et al*. Progressive metaplastic and dysplastic changes in mouse pancreas induced by cyclooxygenase-2 overexpression. *Neoplasia*. **10**, 782-796 (2008).

853. Morris,J.P., Cano,D.A., Sekine,S., Wang,S.C. & Hebrok,M. Beta-catenin blocks Kras-dependent reprogramming of acini into pancreatic cancer precursor lesions in mice. *J. Clin. Invest* **120**, 508-520 (2010).

854. Zhong,H. *et al*. Modulation of hypoxia-inducible factor 1alpha expression by the epidermal growth factor/phosphatidylinositol 3-kinase/PTEN/AKT/FRAP pathway in human prostate cancer cells: implications for tumor angiogenesis and therapeutics. *Cancer Res*. **60**, 1541-1545 (2000).

855. Thorarinsdottir,H.K. *et al*. Protein expression of platelet-derived growth factor receptor correlates with malignant histology and PTEN with survival in childhood gliomas. *Clin. Cancer Res*. **14**, 3386-3394 (2008).

856. Liu,F.T., Patterson,R.J. & Wang,J.L. Intracellular functions of galectins. *Biochim. Biophys. Acta* **1572**, 263-273 (2002).

857. Lin,H.M., Moon,B.K., Yu,F. & Kim,H.R. Galectin-3 mediates genistein-induced G(2)/M arrest and inhibits apoptosis. *Carcinogenesis* **21**, 1941-1945 (2000).

858. Yang,R.Y., Hsu,D.K. & Liu,F.T. Expression of galectin-3 modulates T-cell growth and apoptosis. *Proc. Natl. Acad. Sci. U. S. A* **93**, 6737-6742 (1996).

859. Yoshii,T. *et al*. Galectin-3 phosphorylation is required for its anti-apoptotic function and cell cycle arrest. *J. Biol. Chem*. **277**, 6852-6857 (2002).

860. Wongkham,S. *et al.* Suppression of galectin-3 expression enhances apoptosis and chemosensitivity in liver fluke-associated cholangiocarcinoma. *Cancer Sci.* **100**, 2077-2084 (2009).

861. Yu,F., Finley,R.L., Jr., Raz,A. & Kim,H.R. Galectin-3 translocates to the perinuclear membranes and inhibits cytochrome c release from the mitochondria. A role for synexin in galectin-3 translocation. *J. Biol. Chem.* **277**, 15819-15827 (2002).

862. Endharti,A.T., Zhou,Y.W., Nakashima,I. & Suzuki,H. Galectin-1 supports survival of naive T cells without promoting cell proliferation. *Eur. J. Immunol.* **35**, 86-97 (2005).

863. Anderberg,C. & Pietras,K. On the origin of cancer-associated fibroblasts. *Cell Cycle* **8**, 1461-1462 (2009).

864. Anderberg,C. *et al.* Paracrine signaling by platelet-derived growth factor-CC promotes tumor growth by recruitment of cancer-associated fibroblasts. *Cancer Res.* **69**, 369-378 (2009).

865. Karnoub,A.E. *et al.* Mesenchymal stem cells within tumour stroma promote breast cancer metastasis. *Nature* **449**, 557-563 (2007).

866. Camps,J.L. *et al.* Fibroblast-mediated acceleration of human epithelial tumor growth in vivo. *Proc. Natl. Acad. Sci. U. S. A* **87**, 75-79 (1990).

867. Tomasek,J.J., Gabbiani,G., Hinz,B., Chaponnier,C. & Brown,R.A. Myofibroblasts and mechano-regulation of connective tissue remodelling. *Nat. Rev. Mol. Cell Biol.* **3**, 349-363 (2002).

868. Almkvist,J., Dahlgren,C., Leffler,H. & Karlsson,A. Activation of the neutrophil nicotinamide adenine dinucleotide phosphate oxidase by galectin-1. *J. Immunol.* **168**, 4034-4041 (2002).

869. Wynn,T.A. Cellular and molecular mechanisms of fibrosis. *J. Pathol.* **214**, 199-210 (2008).

870. Shi-Wen,X. *et al.* Endothelin-1 promotes myofibroblast induction through the ETA receptor via a rac/phosphoinositide 3-kinase/Akt-dependent pathway and is essential for the enhanced contractile phenotype of fibrotic fibroblasts. *Mol. Biol. Cell* **15**, 2707-2719 (2004).

871. Folkman,J., Watson,K., Ingber,D. & Hanahan,D. Induction of angiogenesis during the transition from hyperplasia to neoplasia. *Nature* **339**, 58-61 (1989).

872. Jain,R.K. Molecular regulation of vessel maturation. *Nat. Med.* **9**, 685-693 (2003).

873. Sporn,M.B. & Suh,N. Chemoprevention of cancer. *Carcinogenesis* **21**, 525-530 (2000).

874. Kerbel,R.S. A cancer therapy resistant to resistance. *Nature* **390**, 335-336 (1997).

875. Miyamoto,H. *et al*. Tumor-stroma interaction of human pancreatic cancer: acquired resistance to anticancer drugs and proliferation regulation is dependent on extracellular matrix proteins. *Pancreas* **28**, 38-44 (2004).

876. Muerkoster,S. *et al*. Tumor stroma interactions induce chemoresistance in pancreatic ductal carcinoma cells involving increased secretion and paracrine effects of nitric oxide and interleukin-1beta. *Cancer Res.* **64**, 1331-1337 (2004).

877. Berman,D.M. *et al*. Widespread requirement for Hedgehog ligand stimulation in growth of digestive tract tumours. *Nature* **425**, 846-851 (2003).

878. Jensen,J.N. *et al*. Recapitulation of elements of embryonic development in adult mouse pancreatic regeneration. *Gastroenterology* **128**, 728-741 (2005).

879. Siveke,J.T. *et al*. Notch signaling is required for exocrine regeneration after acute pancreatitis. *Gastroenterology* **134**, 544-555 (2008).

880. van den Brule,F.A. *et al*. Differential expression of galectin-1 and galectin-3 during first trimester human embryogenesis. *Dev. Dyn.* **209**, 399-405 (1997).

881. Li,Z. *et al*. Multifaceted pancreatic mesenchymal control of epithelial lineage selection. *Dev. Biol.* **269**, 252-263 (2004).

882. Hisaoka,M., Haratake,J. & Hashimoto,H. Pancreatic morphogenesis and extracellular matrix organization during rat development. *Differentiation* **53**, 163-172 (1993).

883. Crisera,C.A. *et al*. Expression and role of laminin-1 in mouse pancreatic organogenesis. *Diabetes* **49**, 936-944 (2000).

884. Apelqvist,A., Ahlgren,U. & Edlund,H. Sonic hedgehog directs specialised mesoderm differentiation in the intestine and pancreas. *Curr. Biol.* **7**, 801-804 (1997).

885. Kawahira,H., Scheel,D.W., Smith,S.B., German,M.S. & Hebrok,M. Hedgehog signaling regulates expansion of pancreatic epithelial cells. *Dev. Biol.* **280**, 111-121 (2005).

886. Ji,Z., Mei,F.C., Xie,J. & Cheng,X. Oncogenic KRAS activates hedgehog signaling pathway in pancreatic cancer cells. *J. Biol. Chem.* **282,** 14048-14055 (2007).

887. Tredan,O., Galmarini,C.M., Patel,K. & Tannock,I.F. Drug resistance and the solid tumor microenvironment. *J. Natl. Cancer Inst.* **99,** 1441-1454 (2007).

888. Minchinton,A.I. & Tannock,I.F. Drug penetration in solid tumours. *Nat. Rev. Cancer* **6,** 583-592 (2006).

889. Bissell,M.J. *et al.* Tissue structure, nuclear organization, and gene expression in normal and malignant breast. *Cancer Res.* **59,** 1757-1763s (1999).

890. Le Mercier,M. *et al.* Evidence of galectin-1 involvement in glioma chemoresistance. *Toxicol. Appl. Pharmacol.* **229,** 172-183 (2008).

891. Dias-Baruffi,M. *et al.* Dimeric galectin-1 induces surface exposure of phosphatidylserine and phagocytic recognition of leukocytes without inducing apoptosis. *J. Biol. Chem.* **278,** 41282-41293 (2003).

892. Lieber,M., Mazzetta,J., Nelson-Rees,W., Kaplan,M. & Todaro,G. Establishment of a continuous tumor-cell line (panc-1) from a human carcinoma of the exocrine pancreas. *Int. J. Cancer* **15,** 741-747 (1975).

893. Vila,M.R. *et al.* New pancreas cancers cell lines that represent distinct stages of ductal differentiation. *Lab Invest* **72,** 395-404 (1995).

894. Tan,M.H. *et al.* Characterization of a new primary human pancreatic tumor line. *Cancer Invest* **4,** 15-23 (1986).

895. Dexter,D.L. *et al.* Establishment and characterization of two human pancreatic cancer cell lines tumorigenic in athymic mice. *Cancer Res.* **42,** 2705-2714 (1982).

896. Schmidt,M., Deschner,E.E., Thaler,H.T., Clements,L. & Good,R.A. Gastrointestinal cancer studies in the human to nude mouse heterotransplant system. *Gastroenterology* **72,** 829-837 (1977).

897. Pear,W.S., Nolan,G.P., Scott,M.L. & Baltimore,D. Production of high-titer helper-free retroviruses by transient transfection. *Proc. Natl. Acad. Sci. U. S. A* **90,** 8392-8396 (1993).

898. Kinsella,T.M. & Nolan,G.P. Episomal vectors rapidly and stably produce high-titer recombinant retrovirus. *Hum. Gene Ther.* **7,** 1405-1413 (1996).

899. Irizarry,R.A. *et al*. Exploration, normalization, and summaries of high density oligonucleotide array probe level data. *Biostatistics*. **4**, 249-264 (2003).

900. Freeman S, Hamilton H & et al. Biological Science. Upper Saddle River, N.J (2005).